VOL.29 NO.5
MAY
2026

AJSTR
of Scientific and Technological Reports

ASEAN JOURNAL

of Scientific and Technological Report





ISSN 2773-8752 (online)



ASEAN
Journal of Scientific and Technological Reports
Online ISSN:2773-8752

ASEAN Journal of Scientific and Technological Reports (AJSTR)

Name ASEAN Journal of Scientific and Technological Reports (AJSTR)

Owner Thaksin University

Advisory Board Assoc. Prof. Dr. Nathapong Chitniratna
(President of Thaksin University, Thailand)
Assoc. Prof. Dr. Samak Kaewsuksaeng
(Vice President for Reserach and Innovation, Thaksin University, Thailand)
Assoc. Prof. Dr. Samak Kaewsuksaeng
(Acting Director of Reserach and Innovation, Thaksin University, Thailand)

Editor-in-Chief Assoc. Prof. Dr. Sompong O-Thong, Mahidol University, Thailand

Associate Editor

1. Prof. Dr. Jompob Waewsak, Thaksin University, Thailand
2. Assoc. Prof. Dr. Samak Kaewsuksaeng, Thaksin University, Thailand

Session Editors

1. Prof. Dr. Rattana Jariyaboon, Prince of Songkla University, Thailand
2. Assoc. Prof. Dr. Jakkree Boonlakhorn, Thaksin University, Thailand
3. Assoc. Prof. Dr. Supawadee Thawaro, Nakhon Si Thammarat Rajabhat University, Thailand
4. Assoc. Prof. Dr. Surapon Boonlue, King Mongkut's University of Technology Thonburi, Thailand
5. Assoc. Prof. Dr. Warangkana Jutidamrongphan, Prince of Songkla University, Thailand
6. Asst. Prof. Dr. Aungkana Jattamart, Rajamangala University of Technology Rattanakosin, Thailand
7. Asst. Prof. Dr. Suphada Kiriratnikom, Thaksin University, Thailand
8. Dr. Pawadee Hamtanon, Thaksin University, Thailand

Editor Board

1. Amir Sada Khan, American University of Sharjah, United Arab Emirates
2. Chart Chiemchaisri, Kasetsart University,Thailand
3. Chen-Yeon Chu, Feng Chia University, Taiwan
4. Dariusz Jakobczak, National University, Pakistan
5. Ganjar Samudro, Universitas Diponegoro, Indonesia
6. Ghulam Murtaza, Government College University Lahore, Pakistan
7. Hidenari Yasui, University of Kitakyushu, Japan
8. Jatuporn Kaew-On, Thaksin University, Thailand
9. José Antonio Álvarez-Bermejo, University of Almeria, Spain
10. Jutamas Kumchai, Chiang Mai University, Thailand
11. Karun Thongprajukaew, Prince of Songkla University, Thailand
12. Marchee T. Picardal, Cebu Normal University, Philippines
13. Nares Chimres, Thaksin University, Thailand
14. Nasser Ahmed, Kyushu University, Japan
15. Noppamas Pukkhem, Thaksin University, Thailand
16. Peer Mohamed Abdul, Universiti Kebangsaan Malaysia, Malaysia
17. Prasong Kessaratikoon, Thaksin University, Thailand
18. Prawit Kongjan, Prince of Songkla University, Thailand
19. Sappasith Klomklao, Thaksin University, Thailand
20. Shahrul Isamail, Universiti Malaysia Terengganu, Malaysia
21. Supawadee Theerathammakorn, Sukhothai Thammatirat Open University, Thailand
22. Tharith Sriv, Royal University of Phnom Penh, Cambodia
23. Tjokorda Gde Tirta Nindhia, Udayana University in Bali, Indonesia
24. Tsuyoshi Imai, Yamaguchi University, Japan
25. Visit Boonchom, Thaksin University, Thailand
26. Win Win Myo, University of Information Technology, Myanmar
27. Yves Gagnon, University of Moncton, Canada
28. Zairi Ismael Rizman, Universiti Teknologi MARA, Malaysia

Staff: Journal Management Division

Miss Kanyanat Liadrak, Thaksin University, Thailand

Contact Us Institute of Research and Innovation, Thaksin University
222 M. 2 Ban-Prao sub-district, Pa-Pra-Yom district, Phaᵒhalung province, Thailand
Tel. 0 7460 9600 # 7258, 09 1070 0916, 08 1540 7304, E-mail: aseanjstr@tsu.ac.th

List of Contents

Logistical Packaging Evaluation in Automotive Supply Chains: A Multicriteria Decision-Making Approach with Industry Evidence **e260934**
Qian Huang, Ruixue Li, Noppakun Sangkhiew, and Shunichi Ohmori

Synthesis and Characterization of Carboxymethyl Cellulose from Sugarcane Bagasse Cellulose Using Physical and Chemical Pretreatments **e261176**
Adulsman Sukkaew, Sasamol Phasuk, and Pannraphat Takolpuckdee

Sweetness and Antioxidant Indices of Mango (*Mangifera indica* cv. *Nam Dok Mai Sithong*) using Red–Green–Blue and Near-Infrared Images **e261814**
Supawadee Theerathammakorn, Parichat Dittakit, and Chawan Koopipat

Influence of Different Solvents on Antioxidant Properties, Total Phenolics, and Flavonoids from *Piper betle* Leaves **e261613**
Nattawoot Rattanathamwat, Supharat Duanyai, Korakoj Pethassanayothin, Wachirasak Kienwong, Julalak Jarujutarat, Janyawan Janyatham, Pasit Tinnam, Piya Rontlaong, and Atchara Kaewnoi

Process Optimization and Quality Characteristics of Sheet-Type Puffed Rice from Glutinous and Pathum Thani Rice Flour **e262055**
Pracha Bunyawanichakul, Krissadang Sookramoon, and Manunya Khamwachirapitak

Carbohydrate Interfaces in Plant-Fungal Interactions: A Scoping Review **e262552**
Noor Azlina Mohd Nayan, Nur Maisarah Sarizan, and Muhammad Mukram Mohamed Mackeen

Bridging IT and OT: Cybersecurity Risks, Zero-Trust Solutions, and Industrial Resilience in Oil & Gas Downstream **e262008**
Santanu Purohit

The Development of a Web Application for Tracking Bedridden Patients by Village Health Volunteers **e261927**
Phatnutsooda Jaruteerapan, Nitchanan Kawiwangsakul, Maikam Tantipatum, Issadaporn Srisutham, Netnapa Wongla, and Sittisuk Pimmee

Fish Diversity and Fish Community Structure in Wang Nong Reservoir, Nakhon Phanom Province, Thailand **e261014**
Nattanan Tiengtam, and Adithepchaikarn Pachanawan

Bayesian Meta-Ensemble of Stacked Long Short-Term Memory Convolutional Neural Networks for Detection of AI-Generated Text under Uncertainty **e261582**
Nirawit Kanthachai, and Prompong Sugunnasil

The Influence of *Helicobacter pylori* Infection on Hepatic Enzymes, Inflammatory Markers, and Hematological Parameters in Patients with Gastritis **e261801**
Wasan A. Wahab Alsiadi, Malak A. Al-Yawer, and Rana H. k. Al-Rubaye

The Effect of Developed Blenderized Diet Formula on Physical Features **e256663**
Pachsiree Khwannimit, and Piyanuch Maitreegorn

Development of Microbial Bioremediation Products from Mixed Bacterial Consortia for Fat Degradation in Wastewater **e264475**
Pongsak Noparat

List of Contents

Chia Seed Extract Attenuates Streptozotocin-Induced Pancreatic Beta-Cell Dysfunction in Diabetic Rats: Evidence from Functional and Oxidative Stress Biomarkers **e263641**
Ennas Mohamed Majhwol

Gastroprotective Effects of Purslane (*Portulaca oleracea* L.) Ethanolic Extract Against Aspirin-Induced Gastric Ulcer: Modulation of Oxidative Stress, Inflammatory Mediators, and EGFR Signaling in Rats **e263937**
Zahraa Haidar Jawad, and Hussein Abbas Salman

Synergistic Carbon-Biodiversity Gains in Diversified Rubber Agroforestry Systems, Southern Thailand **e261871**
Uraiwan Tongkaemkaew, Suchawadee Bowchauy, Benchawan Bua-Khwan, Kamolpatara Kasikam, Robbe Verhofste, Michael Commons, Chooi Lin Phooi, Elisa Azura Azman, and Roslan Ismail

Association Between Vitamin D3 Status, Blood Pressure, and Lipid Profiles in Hypertensive Patients **e263938**
Wisam Abdan Wawi Al Abdullah, Najlaa O. H. Aljubury, and Shurooq Hussein Jaber Al-Jebur

Prevalence and Antimicrobial Resistance of Multidrug- Resistant *Salmonella* spp. in Retail Chicken Outlets in Phatthalung, Thailand **e264714**
Chaisit Niyasom, and Panadda Promjun

Design of a Knowledge-Based System for Economic Plants: A Case Study of Thailand **e260716**
Amphaphorn Leelamanotham, Prachasan Vaenthaison, Navinda Suetrong, Porntip Rodpon, and Promporn Poowadin

Development of an IoT Smart Learning Board Innovation to Enhance IoT and Coding Skills for Sustainable Secondary Education in Thailand **e264365**
Naphat Keawpibal, Grit Tongkhundam, Nantharat Phruksaphithak, Krisda Suwankarn, Sarunwich Bussaba, Worawat Sooksai, and Visit Boonchom



ASEAN
Journal of Scientific and Technological Reports
Online ISSN:2773-8752

ASEAN
Journal of Scientific and Technological Reports
Online ISSN:2773-8752

Research article

Logistical Packaging Evaluation in Automotive Supply Chains: A Multicriteria Decision-Making Approach with Industry Evidence

Qian Huang[1], Ruixue Li[2], Noppakun Sangkhiew[3], and Shunichi Ohmori[4]

[1] Department of Business Design and Management, Waseda University, Tokyo, Japan
[2] Faculty of Business Administration, Hosei University, Tokyo, Japan
[3] Faculty of Engineering and Industrial Technology, Silpakorn University, Nakhon Pathom, 73000, Thailand
[4] Department of Industrial and Management Systems Engineering, Waseda University, Tokyo, Japan
* Correspondence: huangqian@akane.waseda.jp

Citation:
Huang, Q.; Li, R.; Sangkhiew, N.; Ohmori, S. Logistical packaging evaluation in automotive supply chains: A multicriteria decision-making approach with industry evidence *ASEAN J. Sci. Tech. Report.* **2026**, *29*(5), e260934. https://doi.org/10.55164/ajstr.v29i5.260934

Article history:
Received: August 20, 2025
Revised: February 21, 2026
Accepted: March 8, 2026
Available online: April 26, 2026

Publisher's Note:
This article is published and distributed under the terms of the Thaksin University.

Abstract: The selection of packaging containers is a critical component of the global automotive industry's logistics strategy, influencing operational efficiency and environmental sustainability. This study proposes a multicriteria decision-making approach using the Analytic Hierarchy Process to evaluate packaging container alternatives for knock-down parts logistics. A key contribution of the study is the development of practical evaluation criteria derived from expert interviews, structured into five key dimensions. Evaluations were conducted in two stages: company-wide and origin–destination specific. Survey data from six Japanese automotive companies were analyzed using a unified group approach to ensure consistency. The importance of the evaluation criteria across companies was compared using the results to identify preferred container alternatives under each scenario. Additionally, actual container usage data were compared with the model outcomes to validate the findings. The analysis revealed diverse corporate strategies and highlighted the gap between model-based rational choices and real-world practices. Notably, many firms adopt returnable containers at levels exceeding model recommendations. For outer packaging, the actual returnable-to-one-way ratio exceeded the model-based ratio for five out of six companies, with differences ranging, suggesting that environmental initiatives, such as promoting reusable assets, play a central role in decision-making. The proposed model is a structured, practical tool to support container selection decisions, providing insights into the trade-offs among logistics performance, environmental goals, and operational realities.

Keywords: Returnable containers; decision support; AHP; environmental strategy; Japanese automotive industry

1. Introduction

Packaging containers are crucial for manufacturing companies. Not only do they protect products from damage and maintain their quality, but they also reduce supply chain operating costs and ensure a seamless flow[1]. The unit price of packaging containers was previously relatively fixed and proportional to the quantity used. Today, selecting packaging containers involves more complex factors, including initial investment, operational costs, post-use

disposal, and environmental considerations. This means taking a longer-term perspective and integrating packaging container choices into the business strategy. For example, when considering a wide range of options, one-way and returnable containers each have their pros and cons, making the decision challenging for many manufacturing companies. One-way containers, while initially lower in cost and simplifying logistics by eliminating the need for return shipments, generate waste and contribute to environmental deterioration.

Conversely, returnable containers require a higher initial investment and additional logistical processes for return and cleaning. However, returnable containers offer long-term cost savings and demonstrate measurable environmental and potential economic benefits over one-way containers [2]. The choice between these container types depends on many factors. By carefully weighing these factors and examining the trade-offs between cost, convenience, and environmental impact, organizations can make informed decisions to optimize their logistics packaging strategy. This enhances operational efficiency and aligns with corporate social responsibility policies, contributing to a more sustainable future.

Globalization is inevitable, especially in the automotive industry. With their numerous components, cars source parts from regions worldwide, showing the extensive and complex nature of supply chains. For instance, an automobile engine might originate in Germany, its transmission in Japan, and its components, such as glass and electrical systems, in Asian countries or other regions. This global production model entails multifaceted challenges and considerations when selecting packaging containers for automotive components. Global supply chains are prominent in Japan's automotive industry. Japanese automakers typically procure components from around the world and assemble them into final products. In this process, the choice of packaging containers for knock-down (KD) components is essential. Due to the need to consider the circumstances of different countries and regions, various packaging containers are required to address other situations. However, for manufacturing companies, too much variety in packaging containers can be challenging to manage. Therefore, evaluating and comparing containers to determine which are optimal is essential.

Multicriteria decision-making (MCDM) is a decision-making approach that involves multiple alternatives, each evaluated based on several criteria or factors considered simultaneously. This method is highly accurate and is frequently employed by scientists in various fields, including business, engineering, environmental science, public policy, and healthcare [3-4]. In supply chain management, MCDM techniques are widely applied in various decision-making tasks, including supply chain risk assessment, supplier selection, and transportation selection [5-8]. Several MCDM approaches have gained prominence in supply chain contexts owing to their effectiveness in handling complex decision-making scenarios. Overall, the flexibility and adaptability of MCDM methods make it an essential tool for supply chain professionals seeking to make balanced, data-driven, and context-sensitive decisions in an increasingly complex and dynamic global environment. This study will take the Japanese automotive industry as an example and employ an MCDM approach to evaluate each packaging alternative. This methodology will comprehensively consider factors such as packaging expenses, logistics costs, environmental impact, and component features to determine the optimal packaging container selection strategy. Through such research, valuable insights and guidance can be provided to the automotive industry and other multinational manufacturing sectors to address packaging challenges arising from globalization.

Despite the critical role of packaging container selection in KD logistics, systematic research addressing this specific context remains scarce. Prior studies have relied on experience-based methods or single-cost optimization models, which fail to capture the multi-dimensional trade-offs inherent in global supply chains. Simulation and optimization approaches, while valuable, often rely on simplified assumptions and overlook key factors such as operational ease at overseas sites, alignment with environmental strategies, and the practical challenges of managing inner and outer packaging combinations across borders. Furthermore, the complexity of KD logistics, involving long-distance transportation, reverse logistics for returnable containers, and diverse destination country conditions, makes packaging decisions particularly challenging yet under-researched. To address this gap, this study proposes a multi-criteria decision-making framework using AHP, with evaluation criteria derived directly from expert interviews in the automotive industry. By incorporating both company-wide and origin-destination specific evaluations, this research

provides a systematic, practice-grounded approach to packaging container selection that reflects the complex realities of global KD operations.

2. Literature Review

Multi-criteria decision-making (MCDM) is a sub-discipline of operations research that explicitly evaluates multiple conflicting criteria in decision-making. MCDM methods are designed to support decision-makers when faced with trade-offs among objectives, such as cost versus environmental impact or efficiency versus flexibility. Common MCDM approaches include the Analytic Hierarchy Process (AHP), Technique for Order Preference by Similarity to Ideal Solution (TOPSIS), and Analytic Network Process (ANP). These methods share a common structure: identifying alternatives, defining evaluation criteria, determining criteria weights, and ranking alternatives based on their overall performance. In supply chain management, MCDM has been widely applied to supplier selection, location choice, and investment strategy.

In recent years, the choice of packaging containers in the automotive industry has become increasingly critical, driven by rapid component changes and environmental considerations. As the industry shifts from traditional gasoline-powered vehicles to electric and fuel cell vehicles, automotive component performance and shapes have undergone significant changes, driving related changes in packaging container choices. Automotive component suppliers, assembly plants, and logistics companies are working to adapt to this evolving landscape. However, decision-making in this area has primarily relied on empirical methods rather than systematic approaches. While several articles emphasize the importance of packaging container selection, these decisions still lack systematic evaluation methods [9]. Relying solely on experience is insufficient to keep pace with these rapid changes, as experience comes from trial and error. New methods that go beyond experiential-based decision-making are being explored. For example, using data analysis, simulations, and optimization algorithms, engineering-based computational methods now determine and select the best automotive packaging containers.

By leveraging these advanced techniques, the automotive industry can adapt more swiftly to changes and optimize packaging solutions more efficiently and effectively [10-11]. Some studies have focused on the operational level of containers. Na et al. [12] calculated the optimal number of containers and the total cost optimization of packaging. Cildoz et al. [13] developed a software tool that uses statistical and optimization methods to help decision-makers select the most suitable container for each part. Some research has explored selecting multiple packaging containers and comparing them through simulations to assess their effectiveness [14]. Modeling enables comparison of various packaging systems [15]. While simulation and modeling methods offer advantages for evaluating packaging containers, they also have limitations. These methods often rely on assumptions and simplified models that may not accurately reflect the complex conditions of the supply chain. Additionally, they frequently overlook several key factors in packaging selection, focusing on efficiency measures, such as total cost. To provide a comprehensive overview of existing research on packaging container selection, we summarize key studies and their methodological approaches in Table 1.

Table 1. Summary of existing studies on packaging container selection

Study	Focus Area	Methodology
Twede and Clarke, 2004 [9]	Reusable packaging systems	Conceptual framework
Mollenkopf et al., 2005 [10]	Reusable packaging viability	Relative cost approach
Silva et al., 2013 [11]	One-way vs. returnable packaging	Case study
Na et al. 2019 [12]	Container quantity optimization	Optimization model
Cildoz et al. 2024 [13]	Container selection for parts	Statistical optimization and software tool
Pålsson et al., 2013 [14]	Packaging system selection	Simulation
Škerlič and Muha, 2020 [15]	Packaging life cycle management	Modeling approach

Thus, this study adopts an MCDM approach, enabling the comprehensive consideration of various factors, such as initial investment, logistics efficiency, operational cost, and environmental impact. This comprehensive evaluation allows for a better understanding of the strengths and weaknesses of different packaging container selection schemes. MCDM offers advantages over simulation and modeling methods by considering factors beyond cost and involving stakeholders in the decision-making process. This approach provides a robust framework for selecting packaging containers in the automotive industry, ensuring well-informed decisions based on a comprehensive understanding of relevant factors. This summary highlights that while previous studies have contributed valuable insights, most focus on cost optimization or single-dimensional analysis. Few studies adopt a multi-criteria approach that integrates expert judgment across multiple dimensions, and none specifically address the KD logistics context with both company-wide and destination-specific evaluations.

3. Application of MCDM

This section provides a detailed explanation of the methodology employed, focusing on modeling performance criteria to select containers used in parts supply for automotive manufacturers. Figure 1 illustrates the overall AHP evaluation framework adopted in this study. The framework consists of four main phases: (1) identification of evaluation criteria through expert interviews, (2) pairwise comparisons of criteria to determine their relative weights, (3) pairwise comparisons of packaging alternatives against each criterion, and (4) synthesis of results to obtain final priority scores for each alternative. The following sections detail each step of this process. Section 3.1 describes the survey participants, Section 3.2.1 defines the evaluation targets, Section 3.2.2 explains the criteria identification process, and Section 3.2.3 presents the unified group approach used to aggregate expert judgments.

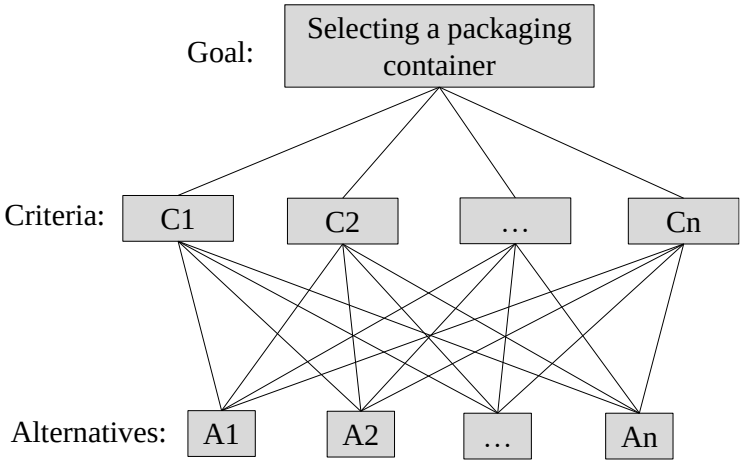


Figure 1. The AHP evaluation framework.

3.1 Survey participants

The analysis centers on multinational car/truck manufacturers that sell globally. These companies primarily operate parts manufacturing plants in Japan, China, and Southeast Asia, exporting parts to Asia, the United States, and Europe. While initially using one-way containers for component transportation, there has been a shift toward the use of returnable containers in recent years due to environmental considerations. Consequently, workshops between industry and academia have been organized to discuss container selection. These Japanese multinational automotive manufacturers have different departments that select packing containers (Table 2). To maintain the confidentiality of the firms, each automotive manufacturer is referred to as Companies A–F. Our study evaluates packaging containers for transporting components from Japanese KD factories to overseas assembly plants.

Table 2. Logistics experts for the interview and survey.

Department	Job Title
Supply Chain Procurement Department	Department Manager
Production and Logistics Department	Senior Engineer
Parts Logistics Department–Packaging	Director
Manufacturing Management Department	Director
The Logistics Planning Department's Parts Logistics Group	Primary contact
Purchasing Management Department	Section chief
Logistics Management Department, Packaging Management Section	Staff member

3.2 Evaluation method

The Analytic Hierarchy Process (AHP) is a decision-making technique that we employ to evaluate packaging containers for KD automotive components. While several MCDM methods exist, AHP was specifically chosen for this study for three primary reasons. First, given the manageable number of alternatives (four packaging combinations), AHP's pairwise comparison approach is more straightforward and less computationally intensive than methods such as TOPSIS, which are designed to rank larger sets of alternatives based on their distance from ideal solutions. Second, a core objective of this research is not only to identify preferred packaging options but also to quantify the relative importance of the five evaluation criteria from the perspective of different companies. AHP is particularly adept at deriving these weights through pairwise comparisons, providing crucial insights into each firm's strategic priorities. Third, AHP's 1-9 scale is highly suitable for processing the qualitative and semi-quantitative judgments elicited from logistics experts, effectively translating their expertise into a structured analytical framework. This method helps prioritize and select suitable containers by considering various criteria. We initially identify criteria relevant to packaging container selection. We then conduct pairwise comparisons to determine the relative importance of these criteria. Subsequently, different types of packaging containers are evaluated against each criterion through pairwise comparisons (Figure 1). By applying AHP, decision-makers can systematically assess and prioritize packaging container options based on their compatibility with the unique requirements of KD automotive component transportation. This structured approach ensures informed decision-making and optimizes packaging solutions for efficient, effective supply chain operations.

3.2.1 Evaluation target

The subjects of evaluation are the candidate packaging options for shipping KD components, including the choice between one-way and returnable containers, as well as inner and outer packaging (Figure 2, Table 3). One-way containers are designed for one-way use and are typically disposed of after delivery, whereas returnable containers, intended for multiple trips, are returned to the sender after use. Inner containers are the packaging used directly around components, while outer containers are the packaging used to transport multiple inner containers.



(Outer) (Inner)

Figure 2. Example of outer and inner containers.

Table 3. Packaging container alternatives

Alternative	Outer	Inner	Abbreviation
(1)	Returnable	Returnable	R-R
(2)	Returnable	One-way	R-O
(3)	One-way	Returnable	O-R
(4)	One-way	One-way	O-O

3.2.2 Identification criteria

To identify relevant criteria for evaluating packaging containers, we conducted interviews with six automotive companies, each represented by at least one logistics expert from the departments listed in Table 2. The interview questions were developed based on an initial literature review and discussions with academic logistics experts. To ensure content validity, the questions were pilot-tested with two packaging logistics professionals from the automotive industry. Based on their feedback, minor adjustments were made to improve clarity and relevance. The final set of seven questions was then used in the face-to-face interviews. This pilot testing process helped ensure that the questions effectively captured the key dimensions of packaging container selection in KD logistics.

The interview topics are as follows:

Question 1: How are containers selected for the international transportation of specific production parts once the decision to supply them to overseas locations has been made?

Question 2: Ratio of one-way containers to returnable containers, along with changes over time and reasons for the changes.

Question 3: Differences in the use of cushioning materials (such as dunnage and attachments) and work hours between one-way and returnable containers.

Question 4: Differences in container types based on part categories and shipping regions.

Question 5: Correspondence between one-way and returnable containers and generic versus dedicated containers.

Question 6: Differences in purchasing strategies between one-way and returnable containers.

Question 7: Disposal guidelines for one-way containers at destination sites.

Through face-to-face interviews with personnel from the packaging departments of automotive companies, as well as insights from academic logistics experts, we derived the following preliminary criteria, as outlined in Table 4.

Table 4. Preliminary criteria extracted from interviews.

Preliminary Criteria
Container Conversion, Return Mechanism, Transportation Lead Time, Part Size, Linkage to Production Lines, Purchasing Cost, Transportation burden, Disposal Cost, Management Cost, Residual Value, Initial Investment, Purchase Price, Container Management Cost, Ease of Purchase/Lease, Convenience of Return Scheme, Return Lead Time, Return Freight, Annual Turnover Rate, Container Durability, Distance, Load Capacity, Packing Efficiency, Ease of Disassembly, Ease of Identification, Line Deployment Ease, Usage of Packaging Material

Our analysis of the preliminary criteria identified the following five main criteria.

Criteria 1: Container procurement ease

This term refers to items associated with the purchase and use of packaging within a specific period, including packaging costs and various management issues, such as storage, inspection, inventory, maintenance, repair, and replenishment.

Criteria 2: Container transportation burden

This includes the costs of container transportation, return, and transfer, as well as other transportation activities. Factors include transportation distance, lead time, container size, weight, compression ratio, tariffs, and return loads.

Criteria 3: Total operational ease

This includes loading and unloading operations in the logistics process, the efficiency of removing parts from the packaging, the efficiency of connecting (discharging) to the production line, the effort required to dismantle, fold, and reassemble packaging, and the transfer work required when packaging conversion is needed.

Criteria 4: Product-specific correspondence

This refers to the ability to adapt to the characteristics and properties of shipped products, such as shape, size, weight, and volume fluctuations, within a specific period.

Criteria 5: International site feasibility

This refers to whether the overseas base (parts shipping destination) can smoothly manage, store, and return the packaging, and the difficulties involved in establishing and maintaining the system and scheme for this purpose.

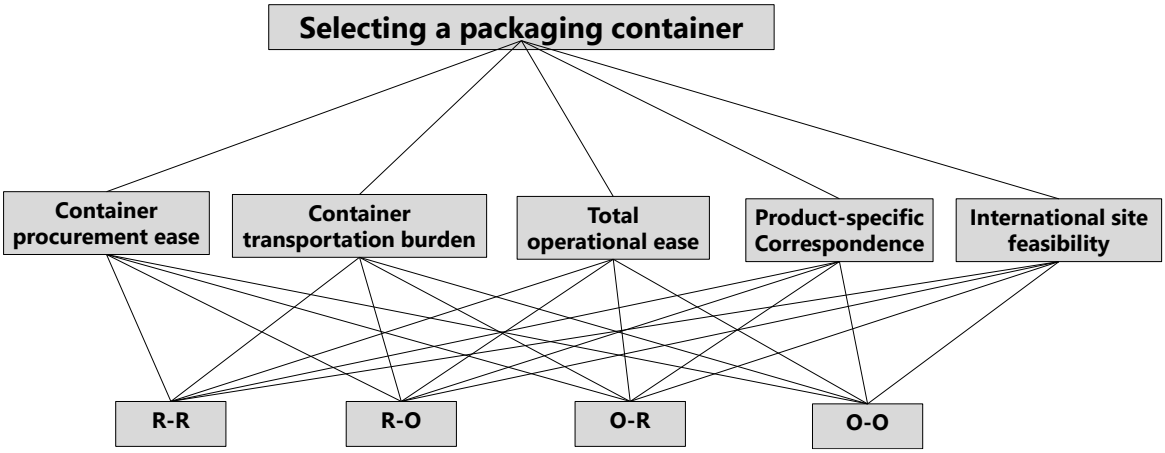


Figure 3. The proposed AHP framework.

The consolidation of the 26 preliminary criteria into five main dimensions was not an arbitrary decision but the result of an iterative, data-driven process. Through systematic content analysis of the interview transcripts, the preliminary criteria naturally clustered into five distinct thematic groups based on semantic similarity and underlying decision logic (Figure 3). To test the robustness of this structure, we evaluated alternative dimensional configurations, including four-dimensional and six-dimensional solutions. The four-dimensional solution resulted in overly broad categories that merged distinct concepts, for example, combining procurement costs with transportation costs, which experts consistently treat as separate considerations in practice. Conversely, the six-dimension solution produced overly granular categories, such as splitting "operational ease" into disassembly ease and line-side deployment ease, which experts found redundant and artificial in real-world decision-making. The proposed five-dimensional structure was then validated through follow-up consultation with the same logistics experts (Table 2). They confirmed that the five dimensions comprehensively capture all key decision factors without significant conceptual overlap, accurately reflecting their actual decision-making process. Additionally, from a methodological perspective, five dimensions provide an optimal balance for AHP-based pairwise comparisons, requiring 10 comparisons, thereby minimizing cognitive burden on respondents while maintaining sufficient analytical granularity. This design choice contributed to the consistency ratios observed in the evaluation results (Tables 5-10).

3.2.3 A unified group approach

The AHP questionnaire is answered by logistics professionals responsible for the logistics of the KD automotive components. Participants are presented with a series of questions structured around the five criteria mentioned above, which are the basis for evaluating four alternative packaging options. Participants are tasked with providing pairwise comparisons between the requirements and alternatives, expressing their judgments on the relative importance or preference of each criterion and the suitability of each alternative. However, participants' answers from the same company to business questions in a survey may be highly

inconsistent. To eliminate these biases and obtain a consistent value, we propose a unified group approach that assigns weights to each group member's answers. We began by comparing the criteria pairwise. The 20 logistics experts responsible for KD automotive component logistics across six automotive companies completed the criteria comparisons independently. We then used a unified group approach to eliminate bias, resulting in a unified comparison value for each company to calculate the weighted mean of the criteria comparisons, which can be expressed mathematically as follows. Let n represent the number of logistics experts from each company. For each company i and criterion j, the unified criteria comparison value U_i^j is calculated as the weighted mean of the individual logistics experts' comparisons as follows:

$$U_i^j = \frac{1}{n}\sum_{p=1}^{n} C_{ip}^j,$$

where
U_i^j is the unified criteria comparison value for Company i of criteria j, and
C_{ip}^j represents the criteria comparison value for Company i and logistics experts p of criteria j.

The term C_{ip}^j represents the pairwise comparison score given by logistics expert p from Company i for criterion j. In the AHP questionnaire, experts were asked to compare each pair of criteria using Saaty's 1-9 scale, where 1 indicates equal importance, and 9 indicates extreme importance of one criterion over the other. For each expert, these pairwise comparisons formed a comparison matrix, from which the priority vector was derived using the eigenvalue method. The C_{ip}^jvalues used in the unified group approach are the normalized priority scores for each criterion from each expert's individual comparison matrix. Furthermore, the AHP method, from obtaining the evaluation values from questionnaire surveys to obtaining the weights between criteria and between alternatives, involves the following steps: data collection; bias elimination; normalization; calculation of criteria weights; calculation of alternative weights; consistency check; adjustment and iteration; and final weight assignment.

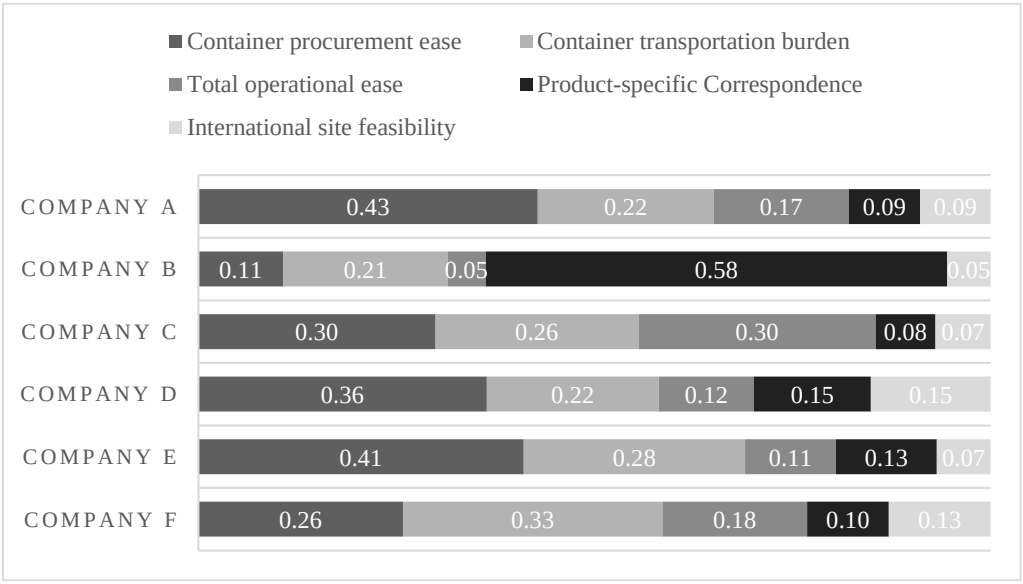


Figure 4. Results of the criteria weights

4. Results and Discussion

4.1 First round of evaluation

We have compiled the evaluation results in Figures 4 and Tables 5–10. From the results of different companies, we have gathered the following insights.

Table 5. Evaluation results for Company A.

Results	Criteria 1	Criteria 2	Criteria 3	Criteria 4	Criteria 5
R-R	0.63	0.39	0.53	0.49	0.41
R-O	0.15	0.33	0.21	0.26	0.30
O-R	0.15	0.14	0.19	0.13	0.17
O-O	0.07	0.14	0.07	0.12	0.12
(C.I.)	0.04	0.05	0.09	0.04	0.06
Weights	0.43	0.22	0.17	0.09	0.09

Table 6. Evaluation results for Company B.

Results	Criteria 1	Criteria 2	Criteria 3	Criteria 4	Criteria 5
R-R	0.04	0.05	0.08	0.05	0.26
R-O	0.30	0.56	0.28	0.26	0.57
O-R	0.10	0.11	0.21	0.11	0.06
O-O	0.56	0.28	0.42	0.58	0.12
(C.I.)	0.10	0.05	0.04	0.03	0.04
Weights	0.11	0.21	0.05	0.58	0.05

Table 7. Evaluation results for Company C.

Results	Criteria 1	Criteria 2	Criteria 3	Criteria 4	Criteria 5
R-R	0.52	0.06	0.48	0.07	0.36
R-O	0.32	0.20	0.28	0.23	0.25
O-R	0.05	0.18	0.14	0.07	0.10
O-O	0.11	0.56	0.11	0.62	0.29
(C.I.)	0.14	0.07	0.07	0.08	0.02
Weights	0.30	0.26	0.30	0.08	0.07

Table 8. Evaluation results for Company D.

Results	Criteria 1	Criteria 2	Criteria 3	Criteria 4	Criteria 5
R-R	0.18	0.02	0.07	0.01	0.02
R-O	0.13	0.03	0.03	0.03	0.03
O-R	0.03	0.04	0.01	0.03	0.02
O-O	0.02	0.13	0.01	0.08	0.09
(C.I.)	0.02	0.06	0.08	0.03	0.02
Weights	0.36	0.22	0.12	0.15	0.15

Table 9. Evaluation results for Company E.

Results	Criteria 1	Criteria 2	Criteria 3	Criteria 4	Criteria 5
R-R	0.16	0.13	0.05	0.03	0.00
R-O	0.18	0.07	0.01	0.03	0.02
O-R	0.04	0.05	0.01	0.03	0.01
O-O	0.04	0.02	0.04	0.03	0.04
(C.I.)	0.01	0.13	0.11	0.00	0.04
Weights	0.41	0.28	0.11	0.13	0.07

Table 10. Evaluation results for Company F.

Results	Criteria 1	Criteria 2	Criteria 3	Criteria 4	Criteria 5
R-R	0.62	0.61	0.70	0.61	0.61
R-O	0.24	0.27	0.20	0.22	0.23
O-R	0.10	0.05	0.06	0.09	0.06
O-O	0.05	0.06	0.04	0.08	0.10
(C.I.)	0.10	0.09	0.14	0.07	0.13
Weights	0.26	0.33	0.18	0.10	0.13

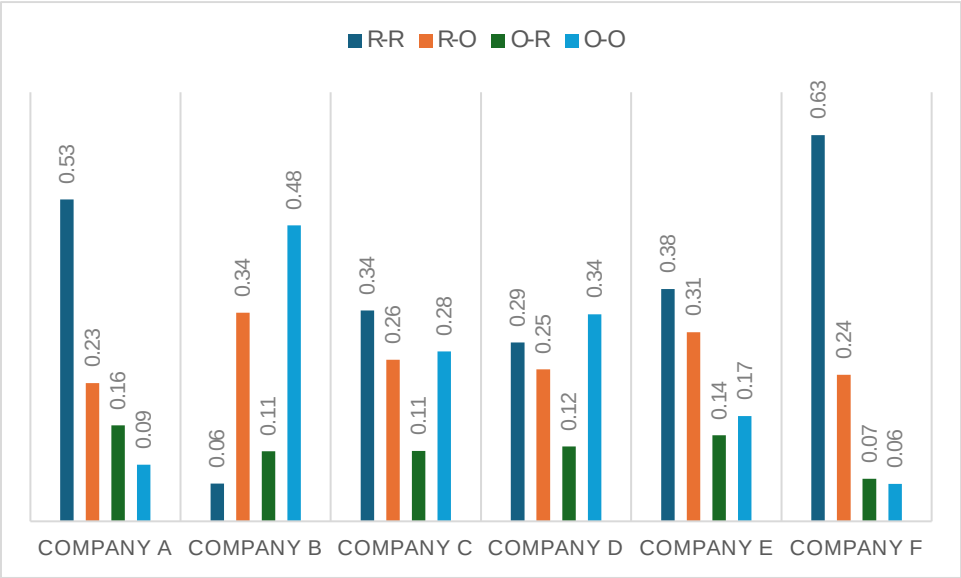


Figure 5. Results of alternative weights (1st round)

(1) Company A: Consistency in Favoring Returnable Packaging

The prioritization of ease in container procurement is notably higher for Company A (0.43) compared to other companies, indicating strategic foresight and a long-term perspective. This reflects a strong emphasis on the overall effort required for container procurement and use, as well as on environmental factors, including waste disposal and recycling costs. Among the alternatives, the highest composite evaluation score is observed for the returnable outer and inner packaging option (i.e., returnable–returnable, R-R: 0.53), indicating a strong preference for the R-R option among packaging logistics experts, partly influenced by the emphasis on ease of container procurement. This alignment underscores the high consistency in prioritizing alternatives that feature returnable containers for both inner and outer packaging.

(2) Company B: Emphasizing Container Compatibility in Packaging Strategy

For Company B, the prioritization of product-specific correspondence is notably higher (0.58) than for other companies. This suggests that the KD components in this automotive firm have a wide variety of shapes and sizes. Consequently, logistics experts place greater emphasis on how to accommodate these varied components effectively. In terms of alternative evaluations, the highest composite score also aligns with this emphasis, with one-way outer packaging with one-way inner packaging (O-O: 0.48) option receiving the highest rating.

(3) Companies C, D, and E: One-way external packaging and returnable internal packaging are inefficient

Three cost-efficiency criteria exhibit relatively similar evaluation values for Companies C, D, and E (Container procurement ease: 0.30/ 0.36/ 0.41; Container transportation burden: 0.26/ 0.22/ 0.28; Total operational ease: 0.30/ 0.12/ 0.11). Additionally, the comprehensive evaluation values of the three alternatives are close, particularly for the one-way external packaging and the returnable internal packaging (O-R: 0.11/0.12/0.14). This suggests that the logistics experts at Companies C, D, and E do not prefer the packaging

approach, as it may adversely affect critical criteria, such as ease of container procurement, container transportation burden, and overall operational ease.

(4) Company F: How to reduce the cost of container return and transfer while still using returnable inner and outer packaging?

In the case of Company F, it is notable that although the three cost-related criteria (container procurement ease: 0.26; container transportation burden: 0.33; total operational ease: 0.18) are relatively consistent with those of Companies C, D, and E, the final evaluation values of the alternatives indicate a completely different preference. Among the other options, the highest score is for returnable outer packaging and returnable inner packaging (R-R: 0.63). This reveals a strong consensus among the company's logistics experts on the use of returnable inner and outer packaging, resulting in a rating exceeding 0.63. However, they are also concerned about the weight of container transportation, including the cost of container return and transfer, compared with the use of returnable inner and outer packaging. Consequently, through partial weight offsetting, the composite evaluation value for returnable inner and outer packaging remains at 0.63.

4.2 Second evaluation round

This study carried out two rounds of evaluation tasks between January and May 2024, involving logistics personnel responsible for KD parts packaging configuration at six Japanese automotive companies. The first round focused on evaluating packaging container selection at the company-wide level for all KD parts (Figure 5), while the second round involved assessments based on specific overseas destinations, simulating container selection for KD parts shipments to particular international sites, referred to as origin–destination (OD)-specified evaluations (Figure 6).

In both rounds, participants conducted pairwise comparisons per the AHP method, comprising pairwise comparisons between evaluation criteria and among packaging alternatives under each criterion.

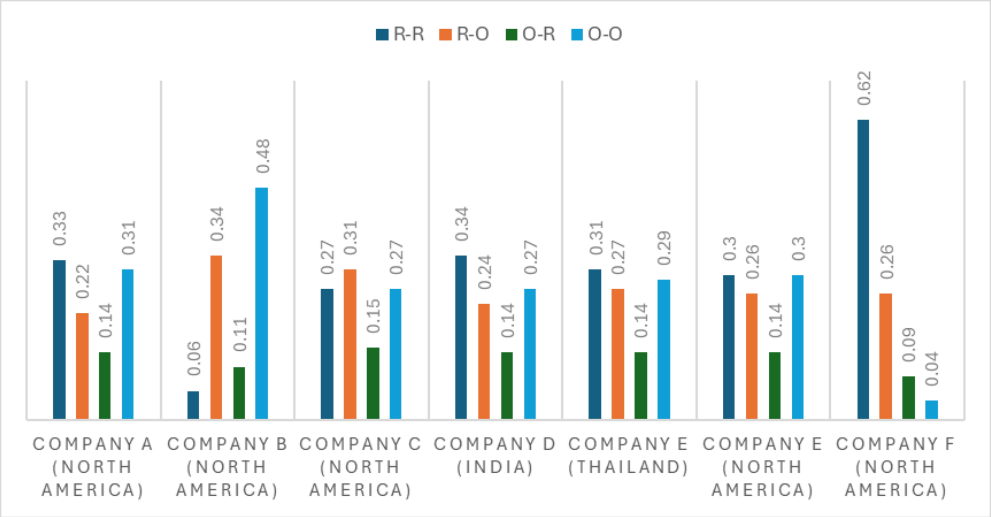


Figure 6. Results of alternative weights (2nd round)

After aggregating and processing the evaluation data, no significant differences were observed in the overall evaluation scores of the alternatives between the first (company-wide evaluation) and second rounds (OD-specified evaluation) for all companies, except for Company A. Additionally, many internal stakeholders at each company stated that the calculated evaluation scores could be effectively utilized as a rational basis for packaging container selection. These responses indicated a consensus about the validity and practical applicability of the proposed model.

(1) Interpretation of the Differences in Company A's Results:

In contrast with the other companies, a significant discrepancy was observed in Company A's evaluation results between the first and second rounds. This difference reveals two key insights:

First, selecting packaging containers in Company A appears to be more influenced by the conditions and agreements with overseas destinations. Depending on whether the receiving site has a system in place for

managing and returning containers, the choice between returnable and one-way containers may change accordingly. In such cases, the decision is made by coordinating with the receiving location, leading to variations in preference across destinations.

Second, compared to the other companies, Company A may not have a company-wide standardized strategy for selecting packaging containers. While other firms demonstrated greater consistency between the two rounds—suggesting that internal standardization and unified policies are already in place—Company A's approach appears more flexible. This flexibility may also be considered a strength, however, as it allows the company to adapt more effectively to the diverse conditions of international sites.

(2) Impact of North American Destinations on Returnable Container Preferences

In addition to Company A, four other companies (Companies B, C, E, and F) specified North America as their OD in the second evaluation round. Among them, only Company B showed no significant difference between the first and second rounds, likely because it ships its KD components exclusively to North America.

A notable trend was observed among the other three companies: evaluation scores for the R-R packaging option decreased when North America was specified as the destination, suggesting that returnable containers are less feasible in North American operations. One possible reason for this decline is the long distance between Japan and North America, which may result in longer return times for returnable containers. This logistical challenge might reduce the practicality and cost-effectiveness of using returnable containers for North American routes, thereby contributing to the lower preference in the OD-specific evaluations.

5. Actual Container Usage Versus AHP-Based Evaluation: A Comparative Analysis

A comparative analysis of the AHP model's comprehensive evaluation scores and each company's actual container usage data revealed several notable findings. Despite the variations across companies, the R/O ratio (the ratio of returnable to one-way containers) derived from the evaluation scores for outer packaging was significantly lower than the actual R/O ratio observed in FY2023 (as shown in Figures 7 and 8). For inner packaging, except for Companies A and D, which have hardly adopted returnable containers, the evaluation-based R/O ratios of the other companies are lower than their actual R/O ratios (measured by volume).

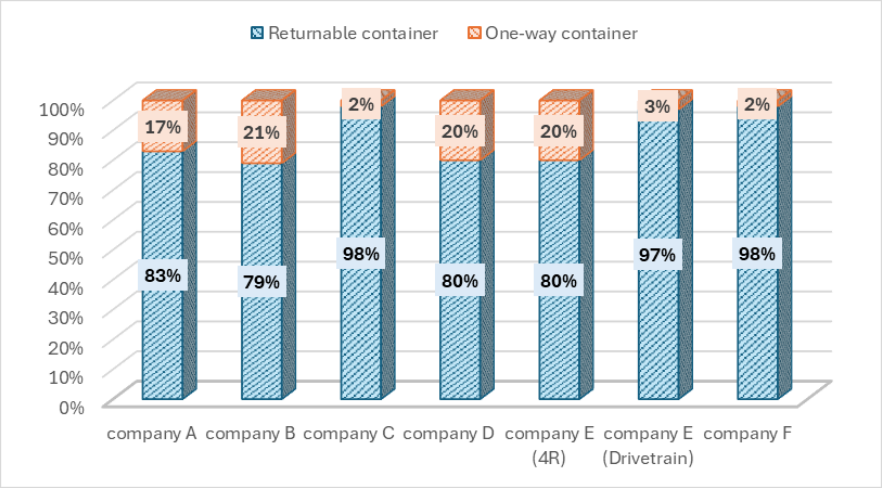
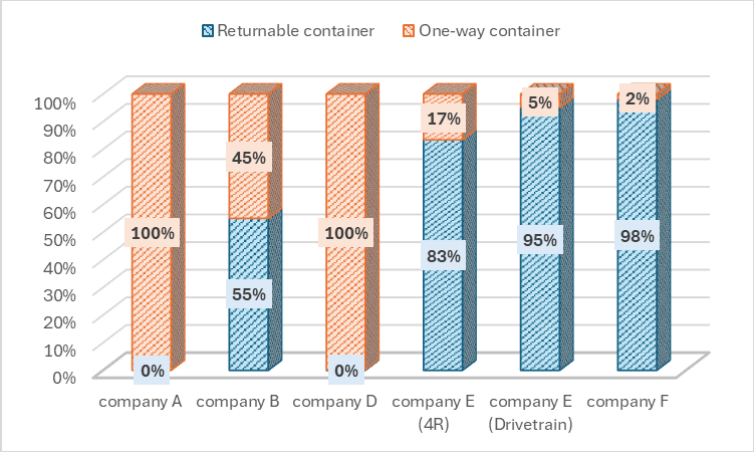


Figure 7. R/O ratio of outer packaging (by volume, FY2023 actual data)

It should be noted that the evaluation scores derived from the AHP model and the actual usage data represent inherently different dimensions. Thus, a direct comparison is not entirely appropriate. Typically, if R-R and Returnable Outer + One-way Inner (R-O) rank first and second, respectively, in the evaluation of outer packaging, it is reasonable that the actual usage ratio of returnable containers would exceed the ratio implied by the evaluation scores. However, among the five companies other than Company F, the R-R and R-O options did not necessarily occupy the top two positions in the evaluation rankings, although their actual R/O ratios for outer packaging exceeded those based on the evaluation scores. A similar trend was observed in the use of inner packaging across all companies, except for Companies A and D. These discrepancies between the

evaluation results and actual practices suggest that the number of returnable containers used in actual operations—particularly for outer packaging—substantially exceeds the rational level calculated by the evaluation model. The same discrepancy exists for inner packaging in most companies, again excluding Companies A and D.

Figure 8. R/O ratio of inner packaging (by volume, FY2023 actual data)



Assuming the evaluation model developed in this study is valid, these findings suggest that, based on the assumptions and criteria weights embedded in our AHP model, returnable containers are not always ranked as the economically optimal choice. It is important to clarify that this conclusion reflects model-based rationality, i.e., the outcome of a multi-criteria prioritization process, rather than an assessment of actual financial profitability. Due to the lack of detailed cost data, this study does not evaluate the real-world financial returns of each packaging option. Instead, the term "economic non-optimality" here refers to the lower priority assigned to returnable containers within the model's preference structure, given the participating companies' strategic weights on criteria such as procurement ease, transportation burden, and international site feasibility. Why, then, do Japanese automotive manufacturers continue to use a higher-than-optimal number of returnable containers, even when such a practice is not necessarily economically rational? The answer likely lies in each company's basic container selection policies and the ownership model of the containers. According to the interviews, most companies follow a standard policy of using returnable containers for both outer and inner packaging, except for Companies B and D (see Table 11). Furthermore, all returnable containers are purchased and owned outright by the companies themselves; they do not use rental or container-sharing schemes. This suggests that these companies may be emphasizing environmental management and promoting reusable packaging aligned with the principles of green transformation (GX) instead of prioritizing short-term cost efficiency. Additionally, under such policies, companies have made significant investments in returnable containers, resulting in a large stock of such assets. To maintain and improve asset utilization rates, there is a strong incentive to deploy returnable containers. Consequently, companies utilize returnable containers in volumes that exceed the levels considered optimal by the model, contributing to the discrepancies between evaluation scores and actual usage data. Nevertheless, determining whether prioritizing returnable containers within environmental management frameworks sacrifices economic rationality remains beyond the scope of this study. Due to the lack of available cost data, a detailed analysis of this point is not feasible. Future research should explore this matter further.

Table 11. Intercompany comparison of container selection and management systems (face-to-face interview)

Policy Area		Company A	Company B	Company C	Company D	Company E	Company F
Basic Policy on Container Use	Outer	Primarily uses returnable containers (R-containers)	Selects R or O containers based on logistics cost targets	Primarily uses R-containers; O-containers are used for new destinations	Primarily uses R-containers	Primarily uses R-containers	Primarily uses generic R-containers (e.g., steel pallets)
	Inner	Primarily uses one-way containers (O-containers)	Mainly uses existing R-containers	Heavy items use R-containers by default; compares R and O based on cost and workability	Primarily uses O-containers	Decides between R and O depending on the destination	Primarily uses generic R-containers (e.g., Orion containers)
Responsible Organization for Container Selection		KD plant	Plant logistics group	KD logistics group	Logistics department	Logistics department at the shipping site	Logistics department at the receiving site
Ownership and Procurement of Returnable Containers		Purchased and owned in-house	Purchased and owned in-house	Purchased and owned in-house	Purchased and owned in-house	Purchased and owned in-house	Purchased and owned in-house

6. Conclusion

This study evaluated packaging containers for KD automotive parts using an MCDM approach and environmentally friendly alternatives in a real-world case. We applied the AHP methodology and conducted interviews and surveys with logistics experts from six Japanese automotive companies. Key evaluation criteria were identified through qualitative interviews and structured into a five-factor framework. A unified group approach was used to assess the criteria and packaging alternatives comprehensively. Because verbal discussions typically lack consistency and traceability, our approach quantifies expert perceptions, enabling a more objective and visual comparison across alternatives. This was used to develop a decision-support tool for logistics and packaging managers. From an applied perspective, the main contribution of this study is its AHP-based evaluation model designed to assist decision makers in selecting optimal KD packaging containers under complex trade-offs. Theoretically, this research confirms that multiple interrelated factors influence the choice between returnable and one-way containers, and that cost considerations do not solely drive the selection logic. The study also revealed a unique causal chain among Japanese automotive firms: as part of their GX initiatives, companies have actively promoted the use of returnable containers and invested in company-specific R-container assets. Over time, this has led to the internalization of proprietary R-container stocks, strengthening the incentive to continue using them, even when, based on the multi-criteria preference structure of our model, such choices are not ranked as economically optimal. This finding highlights the distinction between model-based rationality and actual corporate practice, where environmental strategies and asset utilization considerations play a central role. Future research should refine group weighting mechanisms and aggregate results across companies to derive industry-wide preferences. Such insights could support future standardization efforts for KD logistics packaging.

7. Acknowledgments

This work was supported by JSPS KAKENHI (Grant Number 23K01655, Grant Number 23K13518). Furthermore, we would like to express our gratitude to the Japan Automobile Logistics Research Association for their consistent support throughout this research.

Author Contributions: Li, R and Huang, Q conceptualized the study and supervised the model development; Li, R collected and organized the empirical data; Huang, Q and Ohmori, S contributed to model refinement and experimental analysis; Sangkhiew, N reviewed the literature and supported the background formulation. All authors read and approved the final manuscript.

Funding: This work was supported by JSPS KAKENHI (Grant Number 23K01655, Grant Number 23K13518) and Hosei University, Waseda University, Japan.

Conflicts of Interest: The authors declare no conflict of interest.

References

[1] Rubert, C. K.; De Carvalho, C. P.; De Almeida, M. da G. D.; De Barros, J. G. M.; Sampaio, N. A. de S. Development of automotive packaging by applying the QFD method. *Rev. Gest. Secret.* **2023**, *14*(6), 10527–10548. https://doi.org/10.7769/gesec.v14i6.2391

[2] Coelho, P. M.; Corona, B.; Klooster, R.; Worrell, E. Sustainability of reusable packaging—Current situation and trends. *Resour. Conserv. Recycl. X* **2020**, *6*, 100037. https://doi.org/10.1016/j.rcrx.2020.100037

[3] Taherdoost, H.; Madanchian, M. Multi-criteria decision making (MCDM) methods and concepts. *Encyclopedia* **2023**, *3*(1), 77–87. https://doi.org/10.3390/encyclopedia3010006

[4] Tarnanidis, T.; Papathanasiou, J.; Mareschal, B.; Vlachopoulou, M. MCDM review in marketing and managerial decisions: Practical implications and future research. *Manag. Sci. Lett.* **2025**, *15*(1), 45–54. https://doi.org/10.5267/j.msl.2024.3.004

[5] Momena, A. F.; Gazi, K. H.; Rahaman, M.; Sobczak, A.; Salahshour, S.; Mondal, S. P.; Ghosh, A. Ranking and challenges of supply chain companies using MCDM methodology. *Logistics* **2024**, *8*(3), 87. https://doi.org/10.3390/logistics8030087

[6] Moktadir, M. A.; Paul, S. K.; Bai, C.; Santibanez Gonzalez, E. D. R. The current and future states of MCDM methods in sustainable supply chain risk assessment. *Environ. Dev. Sustain.* **2024**, *27*(3), 7435–7480. https://doi.org/10.1007/s10668-023-04200-1

[7] Wang, C.-N.; Le, T. Q.; Chang, K.-H.; Dang, T.-T. Measuring road transport sustainability using MCDM-based entropy objective weighting method. *Symmetry* **2022**, *14*(5), 1033. https://doi.org/10.3390/sym14051033

[8] Khan, S.; Khan, M. I.; Haleem, A.; Jami, A. R. Prioritising the risks in Halal food supply chain: An MCDM approach. *J. Islam. Mark.* **2022**, *13*(1), 45–65. https://doi.org/10.1108/jima-10-2018-0206

[9] Twede, D.; Clarke, R. Supply chain issues in reusable packaging. *J. Mark. Channels* **2004**, *12*(1), 7–26. https://doi.org/10.1300/J049v12n01_02

[10] Mollenkopf, D.; Closs, D.; Twede, D.; Lee, S.; Burgess, G. Assessing the viability of reusable packaging: A relative cost approach. *J. Bus. Logist.* **2005**, *26*(1), 169–197. https://doi.org/10.1002/j.2158-1592.2005.tb00198.x

[11] Silva, D. A. L.; Santos Renó, G. W.; Sevegnani, G.; Sevegnani, T. B.; Serra Truzzi, O. M. Comparison of one-way and returnable packaging: A case study of reverse logistics in Brazil. *J. Clean. Prod.* **2013**, *47*, 377–387. https://doi.org/10.1016/j.jclepro.2012.07.057

[12] Na, B.; Sim, M. K.; Lee, W. J. An optimal purchase decision of reusable packaging in the automotive industry. *Sustainability* **2019**, *11*(23), 6579. https://doi.org/10.3390/su11236579

[13] Cildoz, M.; Mateo, P. M.; Alonso, M. T.; Parreño, F.; Alvarez-Valdes, R.; Mallor, F. The optimal container selection problem for parts transportation in the automotive sector. *Expert Syst. Appl.* **2024**, *247*, 123321. https://doi.org/10.1016/j.eswa.2024.123321

[14] Pålsson, H.; Finnsgård, C.; Wänström, C. Selection of packaging systems in supply chains from a sustainability perspective: The case of Volvo. *Packag. Technol. Sci.* **2013**, *26*(5), 289–310. https://doi.org/10.1002/pts.1979

[15] Škerlič, S.; Muha, R. A model for managing packaging in the product life cycle in the automotive industry. *Sustainability* **2020**, *12*(22), 9431. https://doi.org/10.3390/su12229431

ASEAN
Journal of Scientific and Technological Reports
Online ISSN:2773-8752

Research article

Synthesis and Characterization of Carboxymethyl Cellulose from Sugarcane Bagasse Cellulose Using Physical and Chemical Pretreatments

Adulsman Sukkaew[1, 2], Sasamol Phasuk[2], and Pannraphat Takolpuckdee[2*]

[1] Faculty of Sciences Technology and Agriculture, Yala Rajabhat University, Yala, 95000, Thailand
[2] Faculty of Science and Technology, Valaya Alongkorn Rajabhat University under the Royal Patronage, Pathum Thani, 13180, Thailand
* Correspondence: pannraphat@vru.ac.th

Citation:
Sukkaew, A.; Phasuk , S.; Takolpuckdee , P. Synthesis and characterization of carboxymethyl cellulose from sugarcane bagasse cellulose using physical and chemical pretreatments. *ASEAN J. Sci. Tech. Report.* **2026**, *26*(5), e261176. https://doi.org/10.55164/ajstr.v26i5.261176

Article history:
Received: September 8, 2025
Revised: February 13, 2026
Accepted: March 11, 2026
Available online: April 26, 2026

Publisher's Note:
This article is published and distributed under the terms of the Thaksin University.

Abstract: This study investigates the optimization of carboxymethyl cellulose (CMC) synthesis from sugarcane bagasse cellulose through combined physical and chemical pretreatments. Bagasse, an abundant lignocellulosic byproduct of sugarcane juice extraction, underwent a sequential combination of heating, alkali treatment, and chloroacetic acid modification to obtain CMC. The synthesized CMC was characterized for degree of substitution (DS), viscosity, surface morphology, and functional group composition. Viscosity analysis was increased from 1.02 cP (0% w/v) to 6,770.35 cP (2.5% w/v), demonstrating excellent thickening properties suitable for various industrial applications. The DS value of 0.94 ± 0.21 indicated a high degree of hydroxyl substitution by carboxymethyl groups. Scanning electron microscopy (SEM) revealed a highly porous, roughened surface structure, reflecting the removal of lignin and hemicellulose during pretreatment. Fourier Transform Infrared Spectroscopy (FTIR) confirmed the successful incorporation of carboxymethyl groups, with distinct peaks at 1613 cm^{-1} (C=O stretching) and 1152 cm^{-1} (C–O–C stretching). The results demonstrate that optimized pretreatment conditions enhance cellulose purity and reactivity, yielding high-quality CMC with desirable physicochemical properties. This approach offers a sustainable pathway for valorizing agricultural waste into high-value biopolymers with potential applications in the food, pharmaceutical, and cosmetic industries.

Keywords: Carboxymethyl cellulose; sugarcane bagasse; physical pretreatment; chemical modification

1. Introduction

The southernmost provinces of Thailand are predominantly agricultural regions, generating high annual yields that serve as the main source of income and livelihood for local farmers. However, over the past decade, agricultural production has declined, leading to economic losses and daily hardships for farmers. Although government agencies have attempted to revitalize the agricultural economy through various mechanisms and policies, success has been limited. In response, new policies promoting integrated farming have been introduced to increase farmers' income opportunities and economic stability. The promoted crops include banana, durian, cassava, and sugarcane—each offering continuous economic value. Notably, sugarcane can be cultivated year-round and serves as a lignocellulosic raw material composed primarily of cellulose (45–55%), hemicellulose (20–30%), lignin

(15–29%), and extractives (1–5%) [1-3, 5]. During the month of Ramadan each year, in regions where the local population is predominantly Muslim and observes fasting, fresh sugarcane juice is widely consumed and regarded as a highly popular beverage. This seasonal demand leads to a significant increase in sugarcane consumption and results in large quantities of bagasse waste. Bagasse, a fibrous residue from the sugarcane juice extraction process, is highly flammable and primarily composed of carbon, hydrogen, oxygen, and nitrogen [7, 10, 14-16].

Bagasse can be utilized in various ways, such as producing briquette fuel, charcoal briquettes, concrete blocks, renewable energy in the form of bioethanol and biogas, and construction materials. However, research related to extracting carboxymethyl cellulose (CMC) from bagasse remains limited, and further product development is needed. Improving extraction methods begins with pretreating bagasse to obtain high-quality cellulose and hemicellulose, which is therefore an important step. Although previous studies have reported the synthesis of CMC from sugarcane bagasse, limited attention has been given to optimizing pretreatment conditions to improve cellulose quality and their impact on the physicochemical properties of the synthesized CMC. Therefore, this study focuses on improving the pretreatment process to obtain high-purity cellulose and evaluating its suitability for producing CMC with desirable functional properties [3]. Cellulose and Hemicellulose are water-insoluble polysaccharides composed of glucose units, similar to starch. Cellulose molecules are arranged in straight chains without branching, and hydrogen bonding between hydroxyl and oxygen groups results in high crystallinity, superior strength, and greater structural stability compared to starch. Carboxymethyl cellulose is an important material across various industries, including the pharmaceutical industry, where it is used as a binder in tablet production and as a thickening agent in liquid formulations. The food industry uses them as thickeners, texture enhancers, and stabilizers in emulsions. The cosmetic industry has potential as a natural alternative to synthetic thickeners and texture modifiers. However, research in this context remains limited [4-7]. The conversion of lignocellulosic biomass into value-added products, including cellulose and carboxymethyl cellulose (CMC), requires the development of cost-effective processing methods. This process involves several critical stages, including pretreatment of lignocellulosic materials to remove lignin and hemicellulose, isolation and purification of cellulose, and subsequent chemical modification to synthesize CMC. Each stage must be carefully designed to ensure process efficiency, product quality, and scalability. So, it is essential to establish an optimized approach to enhance the effectiveness of biomass conversion and also minimize production costs. The development of cost-effective and efficient methodologies is particularly important for enabling the sustainable utilization of lignocellulosic resources and supporting their potential application in industrial and environmental sectors [11, 19, 21-24]. Therefore, the objective of this study is to explore a novel approach for synthesizing carboxymethyl cellulose using cellulose derived from the pretreatment of sugarcane bagasse. This process aims to develop and create added value to agricultural waste, coresponding for promising strategy for both economic development and sustainable resource use.

2. Materials and Methods

2.1 Synthesis of CMC from Bagasse-Derived Cellulose by Physical and Chemical Pretreatment

Carboxymethyl cellulose (CMC) was synthesized from bagasse cellulose following the method of Kaewprachu et al. (2022), with slight modifications. Briefly, 5 g of purified cellulose was placed into a 250 mL glass beaker. 8 g of Chloroacetic acid was dissolved in 20 mL of isopropanol and added to the cellulose. Subsequently, 40 mL of 40% NaOH solution was slowly added under continuous stirring to initiate the alkalization and etherification reactions. The mixture was then soaked for 30 minutes, covered with aluminum foil, and heated at 55 °C for 3.5 hours. The liquid was filtered out, and the remaining cellulose was washed with 40 mL of 70% methanol, neutralized with 10% citric acid solution, and further washed with 40 mL of 70% ethanol, soaking for 10 minutes each time, for a total of 5 washes. The sample was then dried at 55 °C for 24 hours to obtain CMC powder, which was stored in an airtight desiccator container for further analysis, including CMC yield (1), viscosity measurement, and degree of substitution [4, 8-12, 17]. scanning electron microscopy (SEM), and Fourier-transform infrared spectroscopy (FT-IR). All experiments were conducted in triplicate.

$$\text{Yield (\%)} = \frac{W_{\text{dry CMC}}}{W_{\text{initial cellulose}}} \times 100 \quad (1)$$

Where:
$W_{\text{dry CMC}}$ = weight of dried synthesized CMC
$W_{\text{initial cellulose}}$ = weight of starting cellulose

2.2 Viscosity Testing of Synthesized CMC

CMC solutions were prepared at concentrations ranging from 0.5 to 2.5% w/v by gradually dispersing the CMC powder into distilled water under moderate stirring using a magnetic stirrer (Magnetic Stirrer; IKA, model C-MAG HS 9). Stir until the solution becomes homogeneous and allow it to hydrate for 2 hours. Adjust the test temperature to 25.0 ± 0.1 °C using a temperature-controlled water bath (Water Bath; Memmert, model WNB 9). Viscosity measurements were performed using a Brookfield rotational viscometer (Model DV2T LV, Brookfield Engineering Laboratories, USA) equipped with LV spindle No. 3. The spindle rotation speed was set to 60 rpm, maintaining torque within the recommended range of 10–90%. Record the apparent viscosity (cP) once the reading stabilizes, and repeat the measurement at least three times. [13-15].

2.3 Sample Preparation and Determination of Degree of Substitution (DS) of CMC

The CMC sample was dried at 60 °C for 12 hours, then cooled in a desiccator. Approximately 0.5 g of the CMC sample was accurately weighed and dispersed in 50 mL of distilled water. Then, 25 mL of 0.1 M hydrochloric acid (HCl) was added to convert the sodium carboxymethyl groups into their acid form, and the mixture was treated with 20 mL of 0.1 N hydrochloric acid (HCl) to convert the $–COO^-Na^+$ groups into –COOH. The mixture was stirred and heated at 65 ± 5 °C for 15 minutes, followed by the addition of ethanol to precipitate the CMC. The precipitate was filtered and washed with ethanol until free of sodium salts. The precipitate was then redispersed in a known volume of distilled water and titrated with 0.1 N NaOH to the phenolphthalein indicator, turning faint pink and persisting for at least 30 seconds. The volume of NaOH used for the sample (V_{sample}) and for a blank (V_{blank}, prepared under the same conditions without CMC) were recorded. The content of $–CH_2COONa$ per gram of sample (A) was calculated using formula (2). [16-20, 22]

$$A = \frac{(V_{Sample} - V_{Blank})\ X\ N_{NaOH} X 80}{m} \quad (2)$$

where N_{NaOH} is the normality of NaOH (N), 80 is the molar mass of $–CH_2COONa$ (g/mol), and m is the sample mass (g). The Degree of Substitution (DS) was then calculated using formula (3).

$$DS = \frac{162\ X\ A}{(58\ X\ 1000) - (80\ X\ A)} \quad (3)$$

where A is milliequivalents of carboxymethyl groups per gram of sample; 162 is the molar mass of the anhydroglucose unit (g/mol), 58 is the molar mass of $–CH_2COO–$ (g/mol), and 80 is the molar mass of $–CH_2COONa$ (g/mol). The results were reported as the mean ± standard deviation from at least three replicates.

2.4 Structural Characteristics of CMC from Pretreated Bagasse Observed by Scanning Electron Microscopy

Morphological changes of sugarcane bagasse during processing were examined by scanning electron microscopy (SEM; Model JSM-5800, JEOL, Japan or equivalent). Dried samples, including raw bagasse, extracted cellulose (after pretreatment), and synthesized CMC, were mounted on aluminum stubs using conductive carbon tape. Samples were sputter-coated with a thin gold layer (~5–10 nm) to reduce charging during imaging. SEM observation was performed at an accelerating voltage of 15–20 kV. Micrographs were captured at multiple magnifications (3,000× for overall fiber morphology and 50,000× for surface microstructure). The magnification and scale bar for each image are shown directly on the micrograph [18, 21, 24-26].

2.5 Functional Group Analysis of Carboxymethyl Cellulose (CMC) Using Fourier Transform Infrared Spectroscopy (FTIR)

The synthesized CMC samples were dried at 60 °C for 24 hours and sieved through an 80-mesh screen to ensure uniform particle size. Approximately 2.00 mg of dried CMC sample was accurately weighed and thoroughly mixed with 98.00 mg of dry spectroscopic-grade potassium bromide (KBr), corresponding to a 2.00 wt% sample-to-KBr ratio. The mixture was finely ground in an agate mortar and pestle and compressed into a transparent pellet under constant pressure using a hydraulic press. FTIR spectra were recorded using a Bruker Tensor II Fourier Transform Infrared Spectrometer (Bruker Optics GmbH, Germany). Measurements were conducted over the spectral range of 4000–400 cm^{-1} with a resolution of 4 cm^{-1} and 32 scans per sample. Background spectra were recorded using pure KBr under identical conditions before sample analysis. All measurements were performed at ambient temperature (25 ± 2 °C). The obtained spectra were analyzed to identify characteristic functional groups and confirm the successful substitution of hydroxyl groups by carboxymethyl groups on the cellulose backbone. [17, 25-27]

3. Results and Discussion

When testing viscosity at concentrations ranging from 0 to 2.5% (w/v), it was found that the viscosity values of CMC solutions at various concentrations could be used to evaluate changes in viscosity as the CMC concentration increased. The experimental results showed that the viscosity of the CMC solution increased significantly with increasing concentration, from an initial value of 1.02 ± 0.58 cP at 0% (w/v) (pure water) to 6,770.35 ± 325.21 cP at 2.5% (w/v). Low-concentration solutions (0.1–0.5% w/v) exhibited viscosities of 5.53–88.25 cP, indicating a relatively moderate increase. However, as the CMC concentration entered the medium range (0.6–1.5% w/v), viscosity increased sharply from 147.53 ± 21.25 cP to 1,284.77 ± 135.21 cP, reflecting the formation of more interconnected polymer structures, which progressively increased flow resistance. At higher concentrations (1.6–2.5% w/v), viscosity rose rapidly and markedly, ranging from 1,682.08 ± 111.52 cP to 6,770.35 ± 286.36 cP (Figure 1). This rapid increase suggests that the longer the time, the more complex the structures formed in the solution, hence the greater the flow resistance. CMC solutions are well known to exhibit pseudoplastic (shear-thinning) behavior, where apparent viscosity decreases with increasing shear rate due to alignment of polymer chains in the direction of flow. In this study, viscosity was measured at a fixed rotational speed; therefore, the values reported represent apparent viscosity under defined shear conditions. Future work will include rheological characterization across a range of shear rates to fully evaluate non-Newtonian flow behavior. Thus, CMC has great thickening ability and can control liquid viscosity. Thus, it can be used in the cosmetics, agriculture, food, and pharmaceutical industries that require defined viscosity. The higher the CMC concentration, the easier viscosity control is for the intended application. The DS value obtained in this study (0.94 ± 0.21) falls within the typical range reported for commercial CMC products. Food-grade CMC generally has DS values between 0.6 and 0.95, while technical-grade CMC ranges from 0.7 to 1.2. Previous studies on bagasse-derived CMC have reported DS values ranging from approximately 0.65 to 1.10, depending on synthesis conditions. The DS value obtained in this study is therefore comparable to both commercial and biomass-derived CMC, indicating successful etherification and confirming bagasse as a viable raw material for CMC production. [19, 22-24].

To analyze the degree of substitution of the CMC (carboxymethyl cellulose) sample, 1 g of CMC was diluted to 100 mL with distilled water. Then 25 mL of standardized hydrochloric acid (HCl, 0.1 M) was added to the CMC, which converted the carboxymethyl groups (–CH_2COONa) to carboxylic acid groups (–CH_2COOH). The suspension was heated to 60–70 °C for 30 minutes to ensure that all carboxymethyl groups were substituted, then cooled. After that, the mixture was titrated with NaOH by adding drops of NaOH solution until the endpoint was reached. The volume of titrated NaOH solution was then used to determine the number of NaOH moles, equivalent to the carboxymethyl groups present in the CMC sample. The degree of substitution for the sample was determined to be 0.94 ± 0.21, which means that the extent of the substitution of carboxymethyl groups (–CH_2COOH) with hydroxyl groups (–OH) in the CMC sample was 0.94 ± 0.21. Shown as Figures 2 and 3.

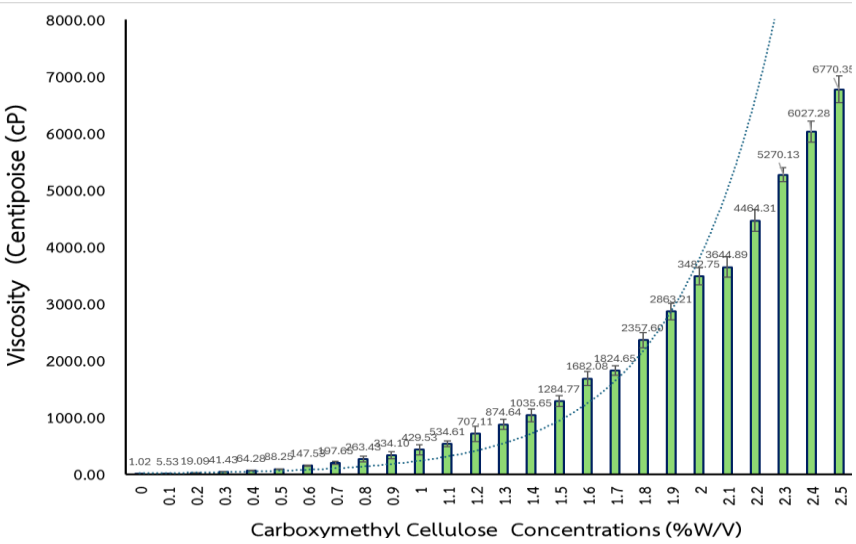


Figure 1. Apparent viscosity of synthesized CMC solutions at different concentrations (0–2.5% w/v). Values represent mean ± SD (n = 3).

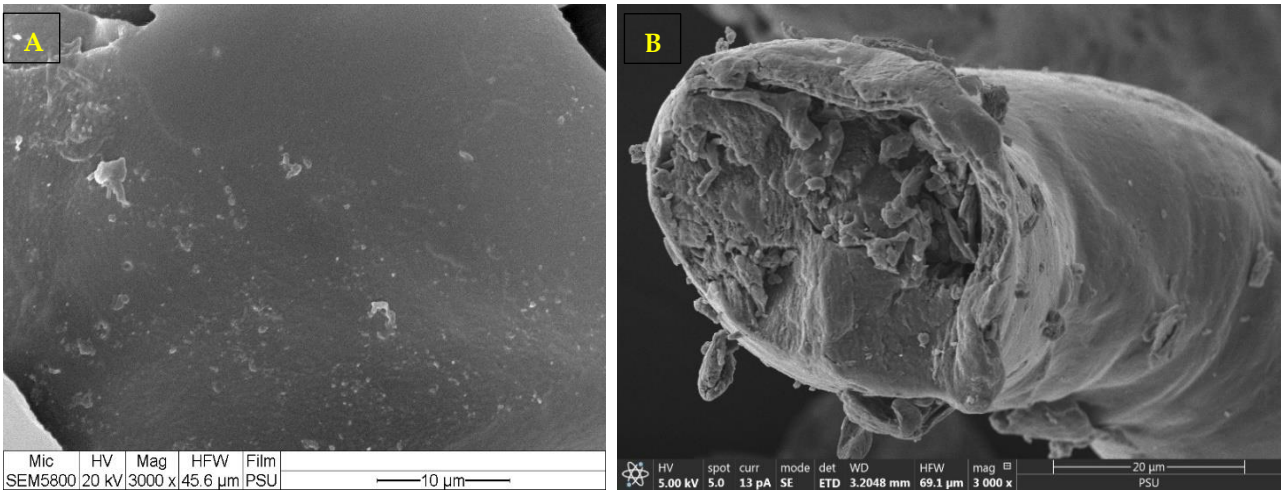


Figure 2. Morphological Characteristics of A) Before Synthesized, B) Synthesized Cellulose from Bagasse Observed by Scanning Electron Microscopy (SEM)

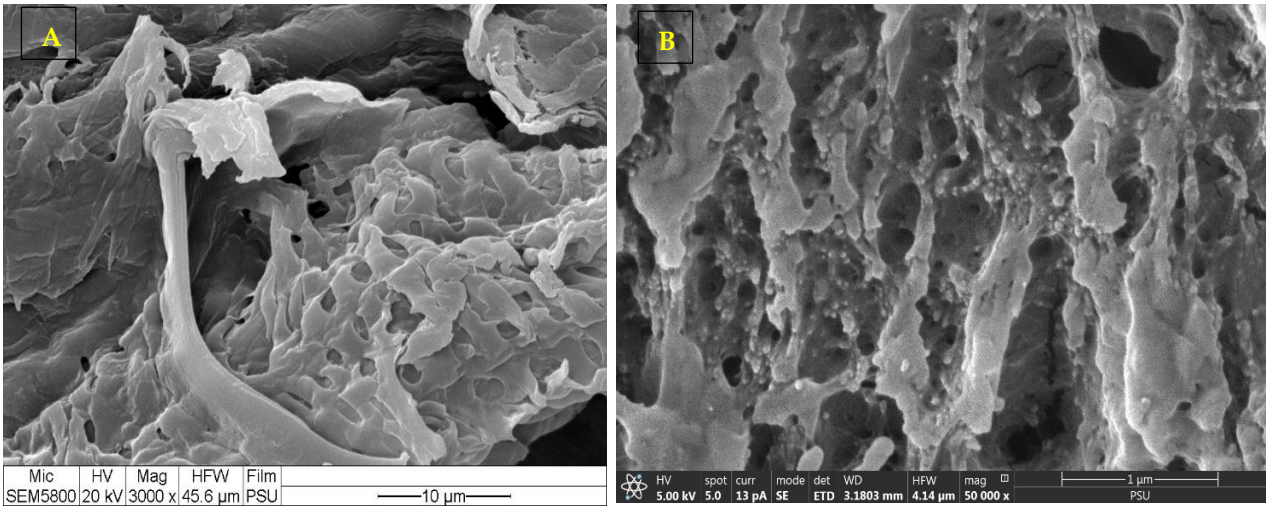
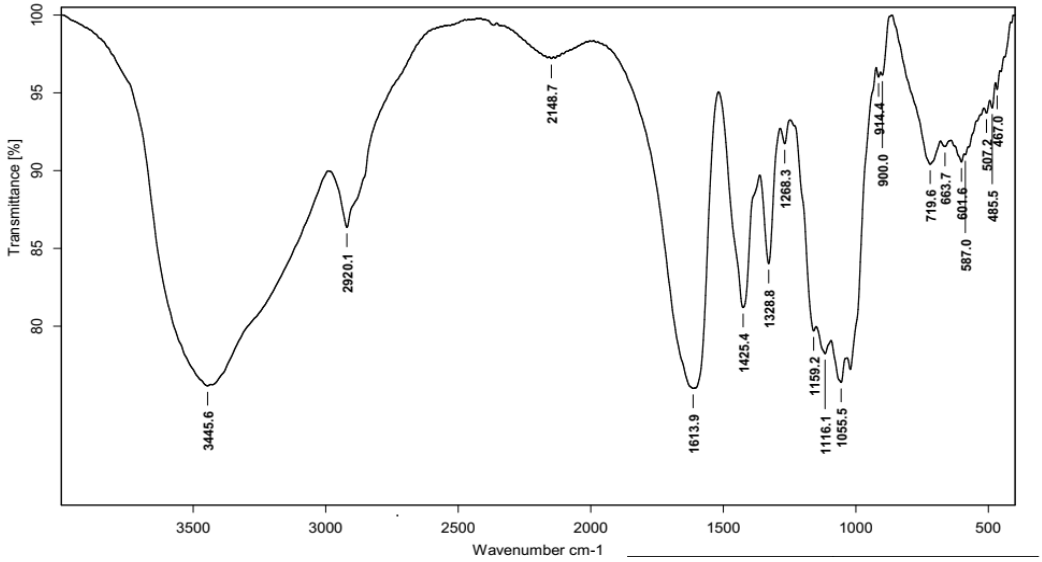


Figure 3. Morphological Characteristics of Synthesized Bagasse-Derived Carboxymethyl Cellulose (CMC) A) 3,000 X and B) 50,000 X observed by Scanning Electron Microscopy (SEM)

SEM images revealed significant structural differences between raw bagasse, extracted cellulose, and synthesized CMC (Figures 2 and 3). Raw bagasse exhibited compact fiber bundles with relatively smooth surfaces, likely due to lignin and hemicellulose acting as binding agents. After alkaline pretreatment and bleaching, the extracted cellulose showed cleaner, more separated fibers with increased surface roughness, indicating partial removal of non-cellulosic components. Following carboxymethylation, the CMC exhibited a substantially altered morphology characterized by disrupted fiber structure, increased surface irregularity, and reduced structural integrity of the original cellulose fibers. Image analysis indicated that the average fiber diameter decreased and the surface became more heterogeneous after modification. These morphological changes are consistent with etherification reactions that introduce carboxymethyl groups into the cellulose structure, disrupting hydrogen bonding and increasing hydrophilicity. The observed structural modification supports the increased solubility and viscosity of the synthesized CMC.

FTIR characterized the synthesized bagasse-derived CMC to confirm the introduction of carboxymethyl functionality. Broad absorption at ~3445 cm^{-1} corresponds to O–H stretching, while the band at ~2891 cm^{-1} is attributed to C–H stretching of the polysaccharide backbone. Importantly, the appearance/intensification of bands at 1613 cm^{-1} and 1424 cm^{-1} is consistent with the asymmetric and symmetric stretching vibrations of carboxylate ($–COO^-$) groups in sodium carboxymethylcellulose (CMC-Na), supporting successful etherification. Additional bands at ~1321 cm^{-1} (C–O stretching associated with substituted polysaccharide structure), ~1152 cm^{-1} (C–O–C stretching of glycosidic linkages), and ~900–897 cm^{-1} (β-glycosidic linkage-related vibration) were also observed, consistent with cellulose-derived materials. Therefore, it was not used for structural confirmation. The FTIR spectrum of the starting cellulose was included for comparison, showing markedly weaker/absent carboxylate bands, thereby strengthening evidence of chemical transformation to CMC (Figure 4).

Figure 4. FTIR Spectrum Characteristics of Bagasse-Derived CMC



The research began with the production of cellulose from bagasse using a combined physical and chemical pretreatment at high temperatures. This process efficiently extracted hemicellulose and lignin from the primary structure, thereby retaining cellulose largely intact as the main component. Although this pretreatment might have partially fractured cellulose molecules, the overall structure remained sufficiently intact to serve as an adequate substrate for the subsequent synthesis of carboxymethyl cellulose (CMC). These findings are consistent with those of Sharma et al. (2020), who reported that sodium hydroxide pretreatment of biomass cellulose enhances the cellulose fraction while efficiently extracting hemicellulose and lignin. Similarly, Chen et al. (2019) reported that sodium hydroxide facilitates the removal of hemicellulose and lignin, thereby yielding purified cellulose suitable for CMC synthesis. Furthermore, Wang et al. (2019) demonstrated that the application of plant-based CMC can significantly enhance the physicochemical properties of derived products. There are, however, several concerns regarding CMC synthesis, particularly the intensive chemical processes involved and the resulting environmental pollution. It should also be noted that although sodium hydroxide pretreatment yields high cellulose levels [28-30].

The findings of this study demonstrate that sugarcane bagasse is a viable, sustainable raw material for the synthesis of carboxymethyl cellulose (CMC) with favorable physicochemical properties. The applied synthesis route, involving alkaline pretreatment followed by chloroacetic acid etherification, effectively introduced carboxymethyl groups into the cellulose structure. This chemical modification significantly altered the material's physicochemical properties, particularly its solubility and rheological behavior. The formation of CMC occurs through a two-step reaction mechanism. Initially, the hydroxyl groups (–OH) on the cellulose chains react with sodium hydroxide to form alkali cellulose. This activation step increases cellulose reactivity by generating nucleophilic alkoxide groups. Subsequently, during the etherification stage, these activated sites react with chloroacetic acid via a nucleophilic substitution mechanism, in which the cellulose alkoxide group displaces the chlorine atom. This reaction results in the formation of sodium carboxymethyl cellulose (CMC-Na), introducing hydrophilic carboxymethyl groups ($–CH_2COO^-$) into the polymer backbone. The presence of these functional groups enhances intermolecular interactions with water molecules, thereby improving solubility and increasing viscosity. Despite the effectiveness of the synthesis process, competing side reactions may occur. In particular, chloroacetic acid may react directly with sodium hydroxide to form sodium glycolate rather than with cellulose. This undesired reaction reduces the availability of the etherifying agent and may contribute to variations in the degree of substitution (DS). Therefore, careful optimization of reaction parameters, including reagent concentration, temperature, and reaction duration, is essential to promote efficient substitution while minimizing by-product formation. The synthesized CMC exhibited a degree of substitution of 0.94 ± 0.21, indicating a relatively high level of chemical modification. This value is within the typical range reported for commercial CMC, suggesting that the material possesses functional properties comparable to those required for industrial applications. The observed variability in DS may be attributed to structural heterogeneity within the cellulose matrix, which can influence the accessibility of hydroxyl groups during the reaction. Structural characterization using FTIR spectroscopy confirmed the successful incorporation of carboxymethyl groups. The presence of characteristic absorption bands associated with carboxylate functional groups provides clear evidence of chemical modification. In addition, scanning electron microscopy revealed notable changes in surface morphology following modification. The treated material displayed increased surface irregularity and disruption of the original fiber structure, indicating that the chemical reaction altered the physical organization of the cellulose fibers. These structural changes are consistent with increased accessibility of hydrophilic functional groups and improved interaction with aqueous media. The rheological analysis further demonstrated that the viscosity of the CMC solutions increased substantially with increasing concentration, reaching approximately 6,770 cP at 2.5% (w/v). This concentration-dependent increase in viscosity is characteristic of polymer solutions and is associated with increased polymer chain entanglement and intermolecular interactions. The observed viscosity behavior confirms that the synthesized CMC exhibits strong thickening capability, an important functional property for many industrial applications. The purification steps, including washing and neutralization, played an important role in removing residual reagents and by-products. The absence of unexpected functional group signals in the FTIR spectra suggests that these purification procedures were effective in producing a relatively clean final product. Based on its structural characteristics, degree of substitution, and rheological properties, the synthesized CMC shows considerable potential for practical applications. Its viscosity-enhancing properties make it suitable for use as a thickening and stabilizing agent in food systems, pharmaceutical formulations, cosmetic products, and agricultural preparations. In addition, using sugarcane bagasse as a starting material offers significant environmental and economic benefits. Converting agricultural waste into value-added functional materials supports sustainable resource utilization and aligns with the principles of circular bioeconomy and environmentally responsible material development.

4. Conclusions

Producing carboxymethyl cellulose (CMC) from sugarcane bagasse yielded a completely water-soluble product. The viscosity of the CMC solution increased proportionally with the concentration of dissolved CMC. The degree of substitution (DS) was determined to be 0.94 ± 0.21, indicating successful incorporation of carboxymethyl groups ($–CH_2COOH$) in place of hydroxyl groups within the cellulose structure. Scanning electron microscopy (SEM) images revealed a highly porous surface with a complex network of interconnected pores, suggesting that the pretreatment process effectively removed lignin and hemicellulose while modifying the native cellulose structure. This treatment increased surface roughness and facilitated the formation of an open-pore structure. Fourier Transform Infrared Spectroscopy (FTIR) analysis confirmed the presence of distinctive functional groups in the synthesized CMC, with characteristic absorption peaks corresponding to O–H, C–H, C=O, and C–O–C bonds.

Notably, the peaks observed at 1613 cm^{-1} (C=O stretching) and 1152 cm^{-1} (C–O–C stretching) strongly supported the successful derivatization of cellulose into CMC.

5. Acknowledgements

The researcher gratefully acknowledges the Doctor of Philosophy Program in Science Education, Faculty of Science and Technology, Valaya Alongkorn Rajabhat University under the Royal Patronage, and the Faculty of Science Technology and Agriculture, Yala Rajabhat University, for their academic support and the opportunity to conduct this research. The researcher also wishes to express sincere appreciation to the Southern Border Researchers Association for providing essential materials and equipment, as well as valuable collaboration and guidance, which significantly contributed to the successful completion of this study.

Author Contributions: A.S.: Data collection, recording, discussion, interpretation of results, validation, and editing; S.P and P.T: Conceptualization, methodology, Literature review, proofreading, and critiquing. All authors have read and agreed to the published version of the manuscript.

Funding: This research received no external funding

Conflicts of Interest: Theauthors declare no conflict of interest.

References

[1] Kaewprachu, P.; Jaisan, C.; Rawdkuen, S.; Tongdeesoontorn, W.; Klunklin, W. Carboxymethyl cellulose from Young Palmyra palm fruit husk: Synthesis, characterization, and film properties. *Food Hydrocoll.* 2022, 124, 107277. http://doi.org/10.1016/j.foodhyd.2021.107277

[2] Kassie, B.B.; Daget, T.M.; Tassew, D.F. Synthesis, functionalization, and commercial application of cellulose-based nanomaterials. *Int. J. Biol. Macromol.* 2024, 278, 134990. https://doi.org/10.1016/j.ijbiomac.2024.134990

[3] Zhang, L.; Shao, G.; Jin, Y.; Luo, Y.; Xiao, Z.; Yang, N.; Xu, X. Electrochemical conversion of lignocellulosic biomass to carboxymethyl cellulose: Potential and applications of induced electric field. *Int. J. Biol. Macromol.* 2025, 311, 143753. http://doi.org/10.1016/j.ijbiomac.2025.143753

[4] Chen, J.; Zhou, W.; Huang, Y. Synthesis of carboxymethyl cellulose from various plant fibers using sodium hydroxide. *Ind. Crops Prod.* 2019, 137, 198–204. http://doi.org/10.1016/j.indcrop.2019.05.055

[5] Abolore, R.S.; Jaiswal, S.; Jaiswal, A.K. Green and sustainable pretreatment methods for cellulose extraction from lignocellulosic biomass and its applications: A review. *Carbohydr. Polym. Technol. Appl.* 2024, 7, 100396. http://doi.org/10.1016/j.carpta.2023.100396

[6] Yadav, R.K.; Awathare, P.; Shitut, P.; Mahajan, V.; Nair, P.; Dharne, M. Genome mining of carbohydrate-active enzymes (CAZyme) and Poly-γ-Glutamic acid (γ-PGA) synthesis by *Bacillus velezensis* (WA11) directly from lignocellulosic biomass-based substrate. *Biocatal. Agric. Biotechnol.* 2025, 103747. https://doi.org/10.1016/j.bcab.2025.103747

[7] Golbaghi, L.; Khamforoush, M.; Hatami, T. Carboxymethyl cellulose production from sugarcane bagasse with steam explosion pulping: Experimental, modeling, and optimization. *Carbohydr. Polym.* 2017, 174, 780–788. http://doi.org/10.1016/j.carbpol.2017.06.112

[8] Saha, P.; Ghosh, S.K.; Singh, P. A holistic review on synthesis, properties, and multifunctional applications of cellulose aerogels from cellulose waste streams. *Int. J. Biol. Macromol.* 2025, 321, 146334. http://doi.org/10.1016/j.ijbiomac.2025.146334

[9] Duangrin, M.; Pisutpiched, S.; Deenu, A.; Kamthai, S. Ultrasonic-assisted synthesis for the production of green and sustainable hemp carboxymethyl cellulose. *Int. J. Biol. Macromol.* 2024, 280, 135610. http://doi.org/10.1016/j.ijbiomac.2024.135610

[10] Florencio, C.; Brondi, M.G.; Silva, M.J.; Bondancia, T.J.; Elias, A.M.; Martins, M.A.; Mattoso, L.H.C. Carboxymethylcellulose production from sugarcane bagasse: A new approach in biorefinery concept. *Int. J. Biol. Macromol.* 2024, 282, 136998. http://doi.org/10.1016/j.ijbiomac.2024.136998

[11] Martin, S.S.; Gan, L.; Zhang, L.; Yang, X.; Tan, Z.; Shi, H.; Li, H. Cellulose nanocrystal-based intelligent hydrogels: Innovations, challenges, and prospective application in advanced wound healing. *Int. J. Biol. Macromol.* 2025, 316, 144752. https://doi.org/10.1016/j.ijbiomac.2025.144752

[12] Arantes, V.; Las-Casas, B.; Dias, I.K.R.; Yupanqui-Mendoza, S.L.; Nogueira, C.F.O.; Marcondes, W.F. Enzymatic approaches for diversifying bioproducts from cellulosic biomass. *Chem. Commun.* 2024, 60(72), 9704–9732. https://doi.org/10.1039/d4cc02114b

[13] Sharma, A.; Gupta, R.; Kumar, A. Alkaline pretreatment of sugarcane bagasse for enhanced cellulose extraction. *Renew. Energy* 2020, 153, 1105–1114. http://doi.org/10.1016/j.renene.2020.02.098

[14] Makam, R.M.M.; Omar, W.N.N.W.; Arnandan, P.T.; Muhaimin, M.S.A.; Ahmad, J.; Shamjuddin, A.; Amin, N.A.S. Sustainable carboxymethyl cellulose from ozonated empty fruit bunch for application as food coating additive. *Int. J. Biol. Macromol.* 2025, 319, 145660. http://doi.org/10.1016/j.ijbiomac.2025.145660

[15] Kamthai, S.; Magaraphan, R. Mechanical and barrier properties of spray dried carboxymethyl cellulose (CMC) film from bleached bagasse pulp. *Ind. Crops Prod.* 2017, 109, 753–761. http://doi.org/10.1016/j.indcrop.2017.09.029

[16] Sabapathy, P.C.; Parthiban, A.; Bhusal, C.K.; Singh, S.; Sehgal, R.; Qi, X. Recent improvements in starch films with cellulose and its derivatives–A review. *J. Taiwan Inst. Chem. Eng.* 2024, 149, 105920. http://doi.org/10.1016/j.jtice.2023.105920

[17] Asadnia, M.; Sadat-Shojai, M. Recent perspective of synthesis and modification strategies of cellulose nanocrystals and cellulose nanofibrils and their beneficial impact in scaffold-based tissue engineering: A review. *Int. J. Biol. Macromol.* 2025, 293, 139409. https://doi.org/10.1016/j.ijbiomac.2024.139409

[18] Awere, C.O.; Hyderi, Z.; Anadebe, V.C.; Muthuramalingam, P.; Shin, H.; Githae, E.W.; Ramesh, M. From waste to wealth: Advancing sustainability with state-of-the-art progress of cellulose nanocrystals and its composites for biomedical applications: A review. *Carbohydr. Polym. Technol. Appl.* 2025, 11, 100974. https://doi.org/10.1016/j.carpta.2025.100974

[19] Salleh, K.M.; Selamat, M.E.; Nordin, N.A.; Zuo, Q. Understanding nonwoody cellulose extractions, treatments, and properties for biomedical applications. *Int. J. Biol. Macromol.* 2025, 308, 142455. https://doi.org/10.1016/j.ijbiomac.2025.142455

[20] Dey, P.; Bhattacharjee, S.; Yadav, D.K.; Hmar, B.Z.; Gayen, K.; Bhowmick, T.K. Valorization of waste biomass for synthesis of carboxy-methyl-cellulose as a sustainable edible coating on fruits: A review. *Int. J. Biol. Macromol.* 2023, 253, 127412. https://doi.org/10.1016/j.ijbiomac.2023.127412

[21] Sukkaew, A.; Kaewmanee, J.; Harinppanwich, W. Enhancing napier grass degradation efficiency through microwave pretreatment and cellulase enzyme application. *ASEAN J. Sci. Technol. Rep.* 2025, 28(4), e257505. http://doi.org/10.14456/ajstr.2025.505

[22] Jahani, A.; Jazayeri, M.H. Tailoring cellulose: From extraction and chemical modification to advanced industrial applications. *Int. J. Biol. Macromol.* 2025, 309, 142950. https://doi.org/10.1016/j.ijbiomac.2025.142950

[23] Sunesh, N.P.; Suyambulingam, I.; Divakaran, D.; Senthamaraikannan, P.; Priya, S.; Han, S.S. Isolation and characterization of cellulose particles from groundnut (*Arachis hypogaea*) shell waste for sustainable reinforcement applications. *Int. J. Biol. Macromol.* 2025, 147228. https://doi.org/10.1016/j.ijbiomac.2025.147228

[24] S, A.; Subramani, R.; Rusho, M.A.; Sharma, S.; Ramachandran, T.; Mahapatro, A.; Ismail, A.I. Genetically engineered 3D printed functionally graded-lignin, starch, and cellulose-derived sustainable biopolymers and composites: A critical review. *Int. J. Biol. Macromol.* 2025, 321, 145843. https://doi.org/10.1016/j.ijbiomac.2025.145843

[25] Bingying, N.; Thummavichai, K.; Zhu, Y.; Wang, N. Advancements in radionuclide adsorption for wastewater treatment using metal-organic frameworks and cellulose composites. *J. Environ. Chem. Eng.* 2025, 13(2), 115185. https://doi.org/10.1016/j.jece.2024.115185

[26] Aziz, T.; Rohullah; Ullah, A.; Zeb, U.; Hussain, M.; Ali, A.; Kiran, M. Advancements in cellulose nanocrystals: A review of functionalization, applications, and challenges. *Int. J. Biol. Macromol.* 2025, 315, 144552. https://doi.org/10.1016/j.ijbiomac.2025.144552

[27] Azmi, N.I.; Wan Abdul Karim Ghani, W.A.; Sobri, S.; Haris, N.I.N.; Kamsani, N.A.; Alias, A.B. Cellulose-based hydrogels in flexible supercapacitors: A sustainable approach for energy storage solutions. *Renew. Sustain. Energy Rev.* 2025, 221, 115914. https://doi.org/10.1016/j.rser.2025.115914

[28] Sharma, R.; Kumar, A.; Singh, P.; Upadhyay, S.N. Synthesis and characterization of carboxymethyl cellulose derived from agricultural biomass for industrial applications. Carbohydr. Polym. 2020, 247, 116703. https://doi.org/10.1016/j.carbpol.2020.116703

[29] Chen, W.; Yu, H.; Liu, Y.; Hai, Y.; Zhang, M.; Chen, P. Isolation and characterization of cellulose nanofibers from agricultural residues and their application in carboxymethyl cellulose synthesis. Int. J. Biol. Macromol. 2019, 128, 107–115. https://doi.org/10.1016/j.ijbiomac.2019.01.146

[30] Wang, Y.; Li, J.; Wang, X.; Chen, Q.; Liu, X. Preparation and physicochemical properties of carboxymethyl cellulose from lignocellulosic biomass and its rheological behavior. Cellulose 2019, 26, 4039–4052. https://doi.org/10.1007/s10570-019-02340-9

ASEAN
Journal of Scientific and Technological Reports
Online ISSN:2773-8752

Research article

Sweetness and Antioxidant Indices of Mango (*Mangifera indica* cv. *Nam Dok Mai Sithong*) using Red–Green–Blue and Near-Infrared Images

Supawadee Theerathammakorn[1*], Parichat Dittakit[2], and Chawan Koopipat[3]

[1] School of Science and Technology, Sukhothai Thammathirat Open University, Pakkred, Nonthaburi, 11000, Thailand
[2] School of Agriculture and Cooperatives, Sukhothai Thammathirat Open University, Pakkred, Nonthaburi, 11000, Thailand
[3] Faculty of Science, Chulalongkorn University, Patumwan, Bangkok, 10330, Thailand
* Correspondence: Supawadee.the@stou.ac.th

Citation:
Theerathamakorn, S.; Dittakit, P.; Koopipat, C. Sweetness and antioxidant indices of mango (*Mangifera indica* cv. *Nam Dok Mai Sithong*) using red-green-blue and near-infrared images. *ASEAN J. Sci. Tech. Report.* **2026**, 29(5), e261814. https://doi.org/10.55164/ajstr.v29i5.261814

Article history:
Received: October 9, 2025
Revised: February 19, 2026
Accepted: March 10, 2026
Available online: April 26, 2026

Publisher's Note:
This article is published and distributed under the terms of the Thaksin University.

Abstract: This study aimed to develop a simple method for the non-destructive evaluation of *Nam Dok Mai Sithong* mango quality indices. One hundred and fifty mangoes (*Mangifera indica* cv. *Nam Dok Mai Sithong*) were stored at room temperature for 10 days to evaluate image-based indices for non-destructive quality prediction. Physicochemical properties and image data were collected every two days. Red–green–blue (RGB) and near-infrared images were acquired using visible and infrared filters, respectively. RGB values were extracted using MATLAB. The Nam Dok Mai Sithong index (NDMSTI) was computed using the Normalized Difference Vegetation Index principle. Its predictive performance was compared with that of other RGB-based indices for mango chemical properties. Correlation analysis and partial least squares regression were applied. Model performance was validated using leave-one-out cross-validation. The models were evaluated using the coefficient of determination (R^2_{CV}) and root mean square error of cross-validation (RMSECV). Both the Normalized Green Blue Different Index (NGBDI) and NDMSTI showed statistically significant predictive performance for all chemical properties ($p < 0.01$). Performance was stronger for sweetness (total soluble solids) and antioxidants (ABTS). NDMSTI performed comparably to NGBDI, with slightly lower R^2_{CV} and slightly higher RMSECV. These results indicate that NDMSTI has potential as a non-destructive tool for monitoring mango quality during storage.

Keywords: RGB-based index; sweetness index; antioxidant index; mango quality; non-destructive assessment

1. Introduction

Fruit quality assessment is crucial in the food industry, particularly for international export. Mango (*Mangifera indica* L.) is the most popular tropical fruit consumed worldwide [1]. Nam Dok Mai Sithong (NDMST) mangoes are among the most widely exported Thai mango varieties [2]. The acceptability of exported mangoes in destination countries substantially depends on their eating quality, which is significantly influenced by harvest maturity. Mango maturity is commonly evaluated using visual indicators, such as skin color and chemical parameters, as well as total soluble solids (TSS), titratable acidity, and the ratio of solids to acids [3].

Beyond sensory and physicochemical attributes, fruit quality is increasingly evaluated based on its nutritional and functional properties, which are directly related to human health. Antioxidant content in fruits enhances immune function and reduces oxidative stress [4]. In mangoes, beta-carotene (BC) is a critical antioxidant that contributes to fruit color and has health benefits. This includes a reduced risk of chronic diseases such as heart disease and certain cancers, by reducing damage caused by free radicals to human cells [5]. Furthermore, the yellow hue of mango fruit is primarily determined by carotenoids, particularly BC, which accounts for approximately 70 % of the total carotenoid content in both the peel and pulp. This content increases as the fruit ripens [6]. Fruit grown in carbon paper bags has almost no chlorophyll or chlorophyll-related activities in its skin. For example, NDMST mango is normally wrapped in carbon-coated paper to maintain a consistently golden-yellow peel with minimal color changes during fruit ripening [1], thereby reducing damage from the oriental fruit fly and anthracnose [7–9]. The yellow color of mango skin may lead consumers unfamiliar with NDMST mangoes to assume that the mangoes are ripe. The color level of NDMST mangoes is also crucial for determining their taste and consumer satisfaction [3]. Although maturity determination by visual observation is unreliable and prone to error [3], this approach allows a thorough examination of relationships among quality attributes that might otherwise be obscured or disrupted [1].

Numerous non-destructive methods have been developed to evaluate mango quality reliably. These methods range from simple digital cameras to high-tech near-infrared spectroscopy (NIRS) and hyperspectral imaging (HSI) [3, 10–12]. Salengke and Mursalim [3] used a digital camera to capture images of mango peels and applied image processing to obtain color values in CIELAB space, revealing that maturity indices can be predicted from color parameters. These values were plotted against quality attributes (TSS, TSS-to-total-acid ratio, or ripening index (RPI)). Rungpichayapichet et al. [12] found that NIRS and HSI exhibited potential for quality control in mango sorting, particularly for TSS, pH, RPI, and BC. Red–green–blue (RGB) and NIR imaging are also crucial in non-destructive analysis across various fields, particularly in food and fruit quality evaluation. To reconstruct the NIR spectral bands, Gkillas et al. [13] proposed a lightweight learning-based approach that reduced the cost of multispectral cameras by using only visible (RGB) data from an RGB camera and the Normalized Difference Vegetation Index (NDVI) calculated from the RGB and NIR images to track plant health. Kasimati et al. [14] reported a strong correlation among NDVI, grape yield, and TSS data at early and late growth stages. However, no significant relationship was observed with titratable acidity (TA) or pH.

The NDVI is a measure of vegetation greenness and density captured in a satellite image. It is calculated as the ratio difference between the measured canopy reflectance in the red and NIR bands of the vegetation image, as presented in Equation (1) [15]. NDVI values range from −1 to 1, depending on the absorption of red light by plant chlorophyll and the reflection of infrared radiation by water-filled leaf cells [16].

$$\text{NDVI} = \frac{NIR-R}{NIR+R} \quad (1)$$

During mango ripening, physicochemical changes such as fruit softening, color and flavor development, and increases in sugar content, TSS, and pigments, particularly carotenoids (with more red and orange color), occur at the mature stage [17, 18]. Carotenoids can absorb wavelengths between 400 and 600 nm, particularly at 520 and 540 nm [12]. RGB-based indices have been previously applied to assess fruit quality [19–21]. However, most previous studies have focused on green vegetation or green-skinned fruits, where NDVI is strongly associated with chlorophyll content. By contrast, studies on yellow-peel mango, such as NDMST, remain limited. Moreover, various destructive and spectroscopic methods have been developed to evaluate mango sweetness and antioxidant properties. However, these techniques are time-consuming, costly, and unsuitable for rapid or large-scale assessment. NDVI-based concepts offer a simple, ratio-based approach that is less sensitive to illumination variability. They can be adapted to low-cost RGB–NIR imaging systems, making them suitable for practical non-destructive applications. NDVI is widely used in vegetation monitoring. However, the potential to adapt the NDVI concept for developing a cultivar-specific index to assess internal quality attributes, such as sweetness and antioxidant content, in yellow-peel mangoes has not been systematically investigated.

This study aimed to develop a simple method for the non-destructive evaluation of NDMST mango quality indices. We focused on sweetness and antioxidant content, using RGB–NIR images captured with an RGB–IR camera. Additionally, we analyzed the color values from the RGB channels under visible and NIR filters to determine the optimal channel combination for constructing the NDMST index (NDMSTI) based on the NDVI concept. The results showed that an NDVI-based RGB-NIR index tailored to NDMST mangoes exhibits significant relationships with sweetness and antioxidant content during ripening and outperforms conventional RGB-based indices.

2. Materials and Methods

2.1 Sample Preparation

Export-grade NDMST mangoes from Petch Samrong Garden in Chachoengsao Province, Thailand, harvested 90–100 days after flowering, were screened for comparable physiological maturity using the 3% brine-floating method [23, 31]. This method is based on density differences related to maturity and soluble solid content. In this method, less mature mangoes with lower sugar levels float, while overripe mangoes with higher soluble solids tend to sink. Only mangoes that floated and did not sink to the bottom were selected. Therefore, the fruit did not exceed 90 % ripe, and its sweetness did not exceed 18 °Bx [22]. Temperature significantly affects mango growth, with the optimal range being 27–33 °C [24]. Therefore, 150 carefully selected mangoes were stored in the Packaging Laboratory of the Department of Science and Technology at Sukhothai Thammathirat Open University under ambient conditions over 10 days [11, 12] (27.8 ± 0.39 °C and 60.3 ± 4.3% relative humidity). These values represent the average measurements recorded over 10 days using a Tenmars TM-305U temperature and humidity data logger. Previous mango postharvest studies did not define a standard sample size because the number of fruits varied depending on the experimental design and analytical methods [11, 12]. In this study, 150 mangoes were used to ensure sufficient replication without compromising sample size. The experiment was conducted with five replicates. Each replicate comprised 30 mangoes (n = 30), a commonly accepted number to ensure statistical reliability and approximate normality according to the central limit theorem [25, 26]. All 150 mangoes were divided into five groups of 30 mangoes for each time of observation. Additionally, they were tested in two parts: 25 fruits for sweetness and antioxidant properties, as described in Section 2.3, and the remaining five fruits for color properties through visible and five NIR filters, as explained in Section 2.2. The experiment was performed with five replications at each time point (every two days), for a total of 10 days (Figure 1).

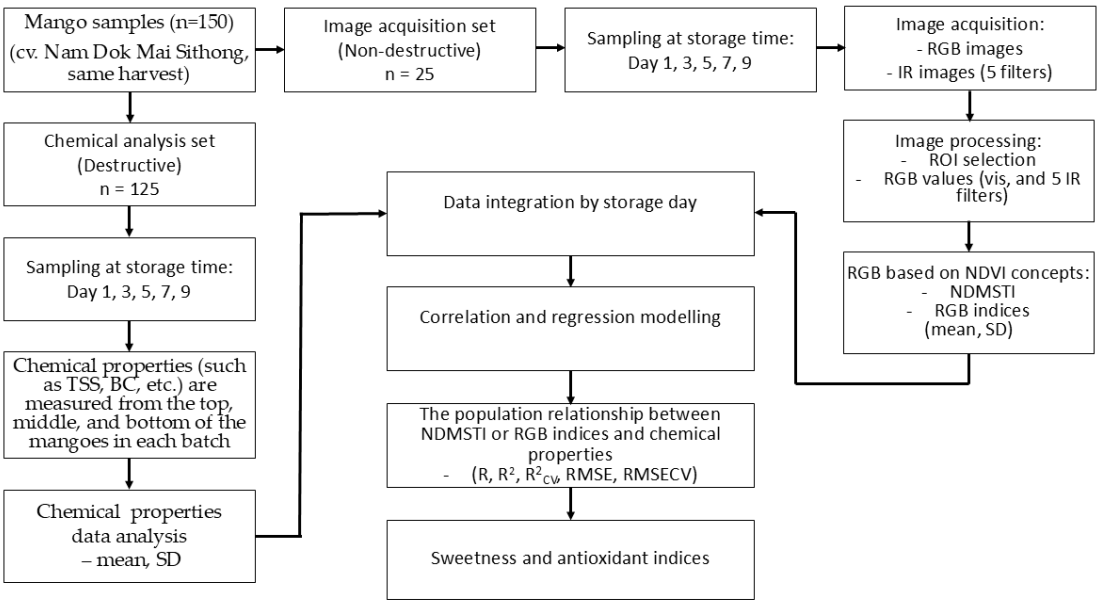


Figure 1. Workflow of data collection and analysis.

2.2 NDMST Mango Photography, Image Preparation, and RGB Value Analysis

The five representative mangoes from each group were photographed, prepared, and analyzed for RGB values according to the following steps.

2.2.1. NDMST Mango Photography and Image Preparation

Many digital cameras with CMOS sensors can be used as full-spectrum cameras (380–1000 nm) when their NIR-blocking filter is removed. Therefore, to capture NIR images for NDVI computation, we used a Canon EOS 5D Mark II camera, which was already available in our laboratory (at Chulalongkorn University) [27]. NDMST mangoes were photographed one at a time under IR. LED visible light was set to a color temperature of 6500 K. For every fruit photograph, six different types of filters were used: a visible filter; IR filters at 680 nm (IR 680), 720 nm (IR 720), 760 nm (IR 760), 850 nm (IR 850), and 950 nm (IR 950) [11, 12]. During each photoshoot, an X-Rite color checker pad was placed next to the mango. Each photo was captured in RAW format and processed for RGB and exposure corrections (white balance adjusted from the X-Rite ColorChecker Pad image in Photoshop). A total of 30 RGB and IR images, each from six filters, were created each time. Thus, a total of 150 images of the NDMST mangoes were obtained.

2.2.2. Analysis of RGB Values

The RGB values of the captured images were analyzed using MATLAB (R2023b). Each mango image was cropped into three parts: top, middle, and bottom [12]. The positions were initially checked in Photoshop. Subsequently, the cropped image positions were specified in MATLAB for image processing. The background was removed to obtain average color values based only on the RGB channels of the mango images. The results were presented as the average color values for R, G, and B, as shown in Figure 2. The NDVI values, calculated using Equation (1), were modified by subtracting each visible color value from the NIR value using either the R, G, or B channel rather than using only the R channel.

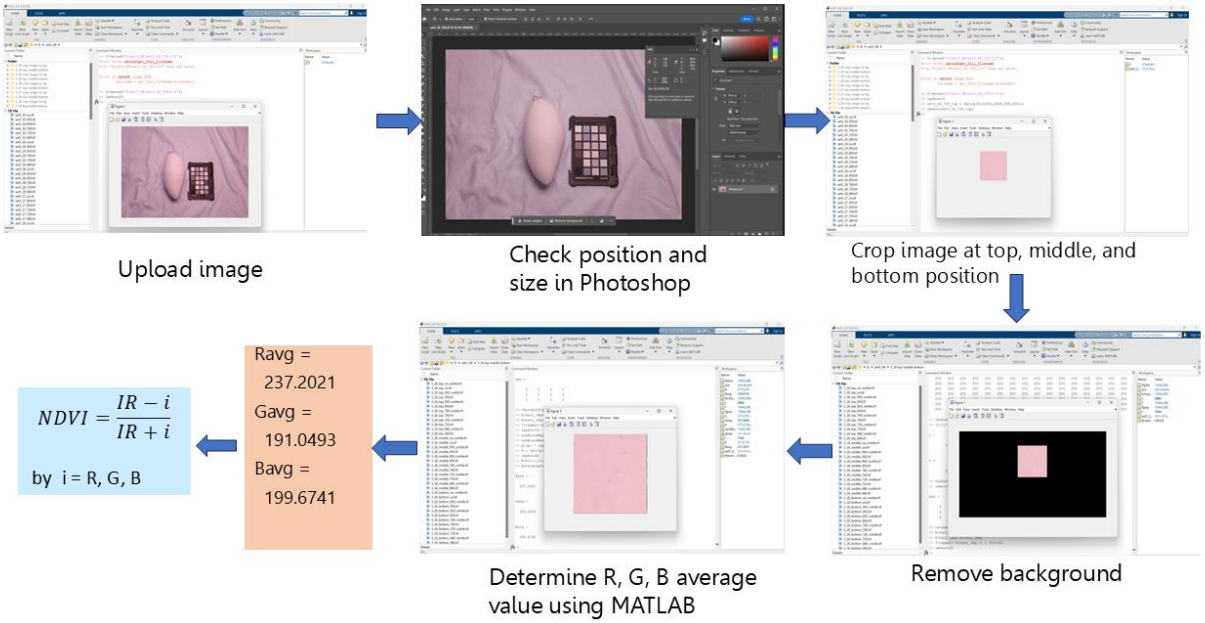


Figure 2. Analysis of RGB average value for NDVI calculation.

2.3 Analysis of Chemical Properties of NDMST Mango

To assess the sweetness and associated nutrients at the Analysis and Testing Service Unit, Rajamangala University of Technology Thanyaburi (RMUTT), Thailand, 25 NDMST mangoes from each period were cleaned, peeled, and divided into three parts (top, middle, and bottom). Subsequently, each part was ground to produce samples for further investigations of different values.

2.3.1. TSS

The Atago PAL-1 refractometer was used to measure TSS content (°Bx as a measure of sweetness).

2.3.2. Antioxidants

The BC and phenolic compounds were analyzed using a Thermo Helios Delta 9423 UVD 1722E UV-Visible Spectrophotometer. Antioxidant activity was assessed using the 1,1-diphenyl–2–picrylhydrazyl (DPPH) [28] radical scavenging assay and 2,2′-azino-bis(3-ethylbenzothiazoline-6-sulfonic acid) (ABTS) [29] radical cation decolorization assay. All analyses were conducted at the Analysis and Testing Service Unit, RMUTT, Thailand.

2.3.3. Other Parameters

The pH, total sugar (TS), and TA were determined to evaluate the ripeness. The pH was measured using a Hanna HI2212 pH meter. The TS and TA were analyzed using the method of the Association of Official Analytical Chemists.

2.4 Data Analysis

Chemical and image measurements were obtained from different mango samples. Therefore, data integration was conducted at the population level, using storage time and mango position as common reference points. For each storage day and mango position, the mean and standard deviation (SD) of chemical properties and image features were calculated and combined into a single dataset. This approach allowed the evaluation of time-dependent relationships between non-destructive image features and destructive chemical measurements.

Owing to the small sample size, this study employed Spearman's rank correlation [30] for initial relationship analysis and partial least squares (PLS) regression combined with leave-one-out cross-validation to construct a stable model and reduce overfitting [31]. PLS regression was employed to develop individual prediction models for each image-derived index (NDMSTI or RGB-based) and for mango quality attributes (Table 1). This pairwise modeling approach enabled direct evaluation of each index's predictive capability for sweetness and antioxidant content. Robustness and predictive performance were assessed using cross-validation. The accuracy of each PLS model was evaluated by comparing predicted and measured values using the coefficient of determination from cross-validation (R^2_{CV}) and root mean square error of cross-validation (RMSECV). PLS with cross-validation was conducted using Minitab 18.

Table 1. Tested RGB-based indices.

RGB indices	Formula	References
Woebbecke index (WI)	(G – B)/(R – G)	[32]
B index	B	[21]
Normalized Green Blue Difference Index (NGBDI)	(G – B)/(G + B)	[33]

3. Results and Discussion

This study aimed to determine the RGB–NIR images related to mango properties using the NDVI principle. The results showed that RGB color values from the visible-filtered images are suitable for predicting mango quality.

3.1 RGB Values from RGB and NIR Images

Figure 3 shows the RGB values of the mangoes photographed with a visible filter and five IR filters at different wavelengths (IR 680, IR 720, IR 760, IR 850, and IR 950). The images at each ripening stage were cropped and analyzed in MATLAB. The results showed that the color values of the B channel (blue) changed significantly across the ripening stages (Figure 4(a)), with a statistically significant effect [$F(3, 11) = 130.63$, $p < 0.001$]. As the storage age increased, the B channel color value of the mango photographs decreased, consistent with the results of a study by Min et al. [34]. The wavelength region between 400 and 600 nm, particularly at 520 and 540 nm, was strongly absorbed by carotenoids [12], exhibiting less reflection in the B

channel during ripening stages. However, after passing through the IR filters, no change in the R, G, and B color values was observed over the storage period (Figure 4(b)–(f)). Thus, the change in beta-carotene content in mangoes from yellow to orange cannot be precisely identified in the short-wavelength infrared range (680–950 nm) in this study, consistent with the observations of Rungpichayapichet et al. [35].

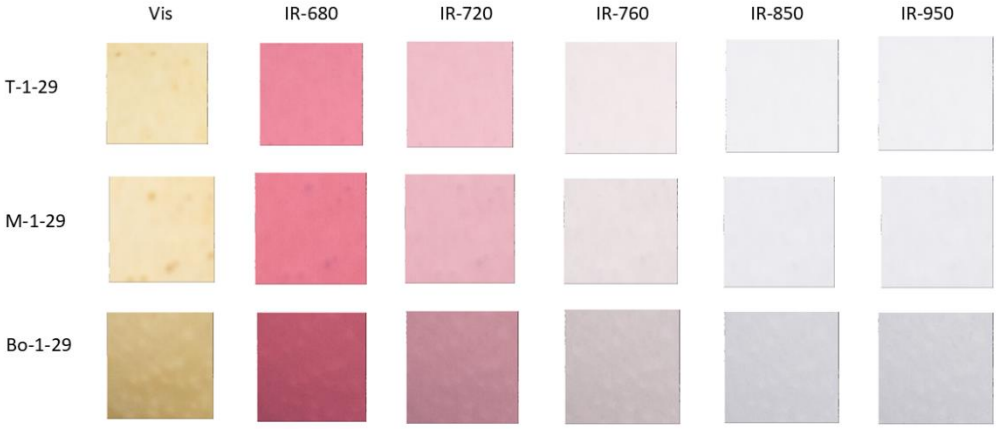
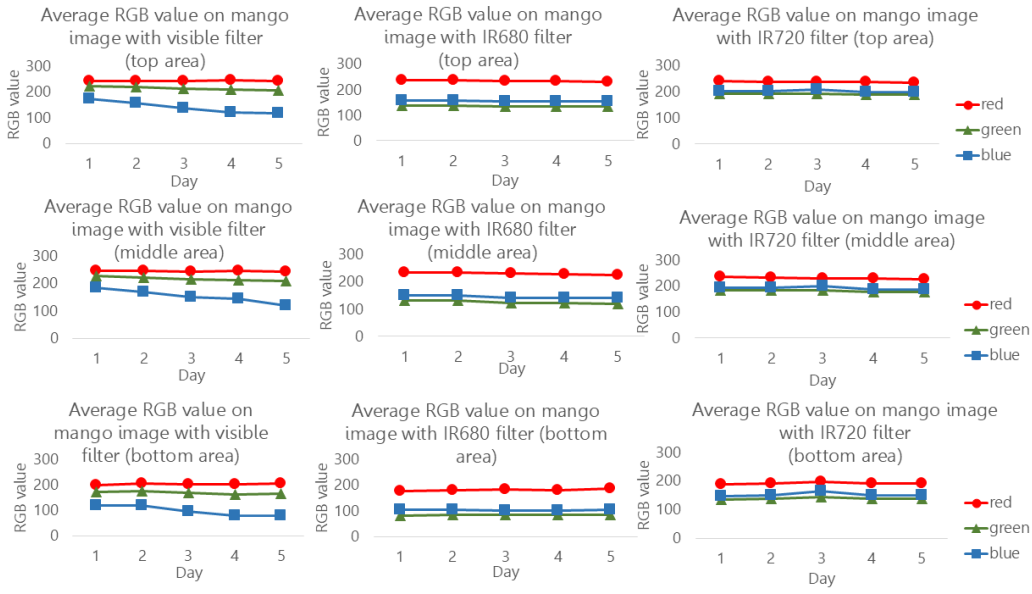
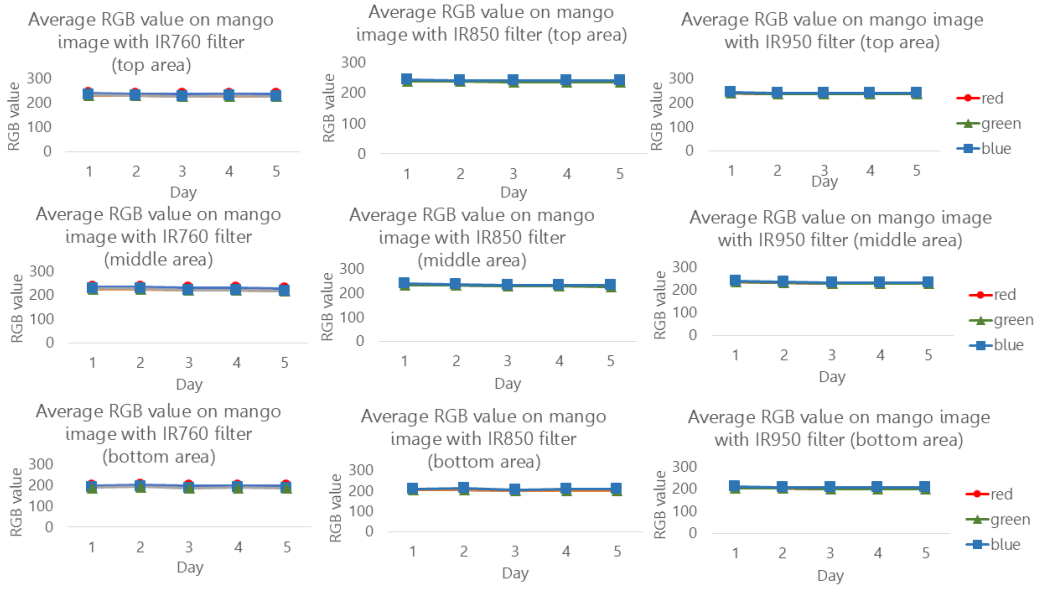


Figure 3. Cropped RGB images samples of NMDST (T- 1–29 indicates image code, T is top position, 1 is the first day and 29 is the number of mangoes) using the visible (Vis) and the five IR filters (IR 680, IR 720, IR 760, IR 850, and IR 950) at the top (T), middle (M), and bottom (Bo) positions.



(**a**) (**b**) (**c**)



(**d**) (**e**) (**f**)

Figure 4. Average RGB values at the top, middle, and bottom of the NDMST mango (from top to bottom) across different ripening stages, (a) using a visible filter and (b) –(f) using NIR filters IR 680, IR 720, IR 760, IR 850, and IR 950, respectively.

In this study, the R-value obtained when applying the five IR filters was identical to that derived from the RGB image. Consequently, the R value can be used instead of the IR value in the NDVI formula. Equation (2) represents this novel concept. These findings are consistent with those of the NDVI1 investigation of Kawashima and Nakatani [20]. They determined the regression line for the relationship between chemical content and (R – B)/(R + B), computed from data collected during the ripening stage.

$$\text{NDMST index} = \frac{R-B}{R+B} \tag{2}$$

3.2 Results of Regression Analysis Based on Indices (NDMSTI and RGB-based Indices) and NDMST Mango Properties

Table 2 presents correlation coefficients between chemical properties and image-based indices. The results show that image-based indices of NGBDI and NDMSTI are associated with nearly all mango chemical properties (β-carotene, TSS, TS, TA, ABTS, DPPH, and pH), except phenolic content (shown in bold). Phenolic acid content shows no relationship with any of the image-based indices because it remains constant throughout ripening. Therefore, NDMSTI and NGBDI were obtained from PLS regression of mango chemical properties, as presented in Table 3. Figure 5 shows samples from the regression plots of TSS content obtained from PLS models based on NDMSTI (Figure 5(a)) and NGBDI (Figure 5(b)). The circle dot represents the calibration data, while the square dot represents the cross-validation data. With a limited number of samples, the PLS models were intentionally constrained to a single latent variable (LV = 1) to reduce the risk of overfitting. The model resulted in moderate R^2_{CV} values, particularly for β-carotene, TS, TA, and DPPH. Therefore, while the models capture meaningful relationships between NDMSTI or NGBDI and chemical attributes, this variance is partially limited by sample variability and the narrow range of chemical composition represented in the dataset. By contrast, higher predictive performance ($R^2_{CV} > 0.50$) was observed for TSS, ABTS, and pH. These properties are more closely associated with mango visual attributes and surface color characteristics, which can be effectively captured by NDMSTI or RGB-based indices [1]. This finding is consistent with previous studies reporting stronger correlations between optical image features and physicochemical properties related to soluble solids and antioxidant capacity [19, 20, 36]. Although both

NGBDI and NDMSTI exhibited comparable predictive performance, NGBDI consistently yielded slightly higher R^2 values and lower prediction errors. Given the small sample size and the absence of an independent external validation set, the observed differences between indices are indicative rather than conclusive. The results support the feasibility of using simple NDMSTI and NGBDI for non-destructive estimation of mango chemical properties. These indices are particularly useful for rapid screening and quality assessment, rather than as a replacement for conventional chemical analyses (destructive methods).

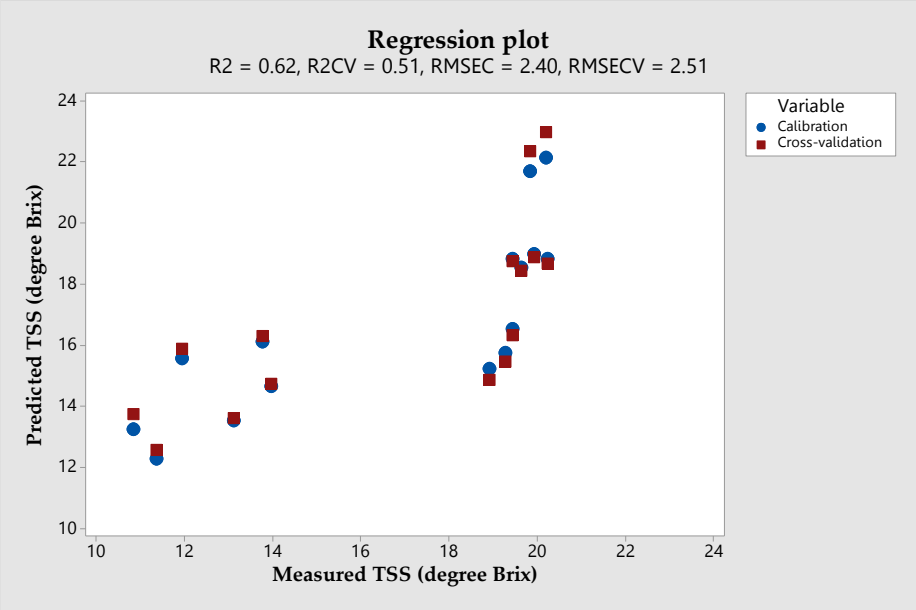
Table 2. Correlation coefficients between average chemical properties and average image-based indices at the same position and ripening stage (n = 15).

Chemical property	WI	B-index	NGBDI	NDMSTI
Gallic (phenolic) acid (mg/100 g fw))	−0.082 (0.771)	−0.150 (0.594)	−0.029 (0.919)	−0.018 (0.950)
β-carotene (μg/g fw)	0.364 (0.182)	**–0.557** (0.031)	**0.786** (0.001)	**0.739** (0.002)
Total soluble solids (TSS) (°Brix)	0.500 (0.057)	**–0.711** (0.003)	**0.915** (0.000)	**0.867** (0.000)
Total sugar (TS) (g/100 g fw)	0.404 (0.136)	**–0.596** (0.019)	**0.807** (0.000)	**0.746** (0.001)
Titratable acidity (TA) (%)	**–0.576** (0.025)	0.382 (0.159)	**–0.688** (0.005)	**–0.618** (0.014)
ABTS (%activity)	0.350 (0.201)	**–0.671** (0.006)	**0.861** (0.000)	**0.832** (0.000)
DPPH (%activity)	0.282 (0.308)	–0.457 (0.087)	**0.700** (0.004)	**0.661** (0.007)
pH	0.450 (0.092)	**–0.521** (0.046)	**0.777** (0.001)	**0.728** (0.002)

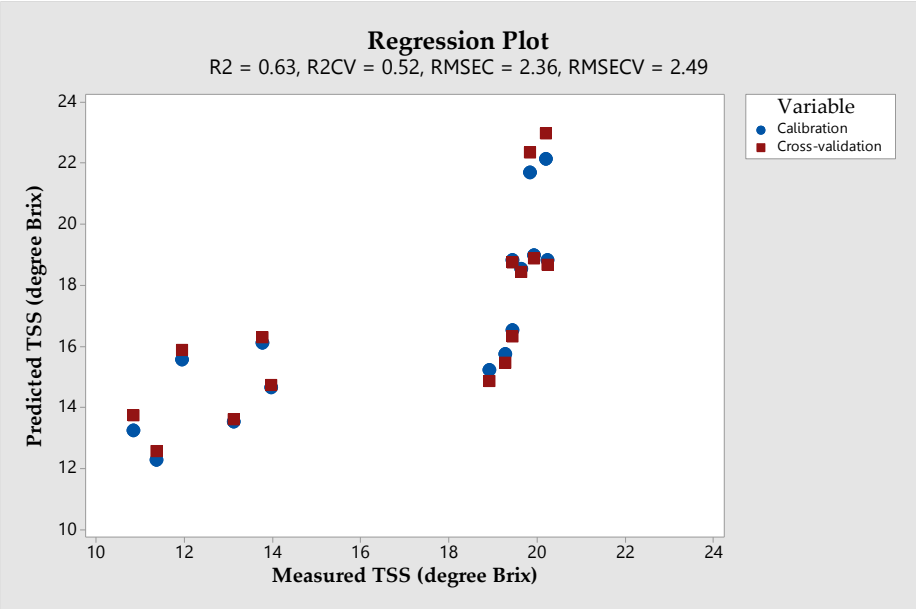
Remark: Values are Spearman's rank correlation coefficients (ρ), with P-values in parentheses. Significant correlations are indicated in bold ($P < 0.05$).

Table 3. PLS regression performance of NDMSTI and RGB-based indices.

Chemical properties	Image-based indices	LV	R^2	RMSEC	R^2_{CV}	RMSECV	p-value
β-carotene (mg/g fw)	NGBDI	1	0.57	41.35	0.43	44.26	0.001
	NDMSTI	1	0.54	42.49	0.40	45.24	0.002
TSS (°Brix)	NGBDI	1	0.63	2.36	0.52	2.49	0.000
	NDMSTI	1	0.62	2.40	0.51	2.51	0.001
Total sugar (g/gfw)	NGBDI	1	0.56	3.31	0.43	3.50	0.001
	NDMSTI	1	0.55	3.37	0.42	3.55	0.002
TA (%)	NGBDI	1	0.55	0.46	0.45	0.48	0.002
	NDMSTI	1	0.52	0.48	0.43	0.49	0.002
ABTS (%)	NGBDI	1	0.71	15.38	0.64	15.92	0.000
	NDMSTI	1	0.69	15.91	0.62	16.39	0.000
DPPH(%)	NGBDI	1	0.54	12.03	0.43	12.41	0.002
	NDMSTI	1	0.52	12.24	0.41	12.62	0.002
pH	NGBDI	1	0.63	0.81	0.54	0.84	0.000
	NDMSTI	1	0.61	0.84	0.51	0.87	0.001



(a)



(b)

Figure 5. Relationship between measured and predicted TSS content (°Brix) obtained from PLS models based on (a) NDMSTI and (b) NGBDI.

4. Conclusions

In this study, we developed a non-destructive NDVI-based index using a digital camera. The NDMSTI values obtained from RGB–NIR images of mango peels were used to assess the sweetness and antioxidant content. The results showed that both NGBDI and NDMSTI demonstrated statistically significant predictive performance for all chemical properties ($p < 0.01$). NGBDI consistently provided slightly higher R^2 and R^2_{CV} values and lower prediction errors than NDMSTI, indicating marginally superior performance. The results indicate that image-based indices (NGBDI and NDMSTI) can predict all investigated chemical properties with statistical significance ($p < 0.01$). However, prediction accuracy varied across properties, with higher performance for TSS, ABTS, and pH, whereas β-carotene, TS, TA, and DPPH showed moderate predictive ability. Despite the small sample size ($n = 15$), this study demonstrated the potential of image-based indices

combined with PLS regression as a rapid, non-destructive tool for estimating mango chemical properties. Additionally, it provides a foundation for further model refinement and validation in future research. However, to address these limitations, future research should expand the initial sample size to maintain a higher number of observations after data integration.

5. Acknowledgements

The authors are grateful to Mr. Suwit Kunawut, owner of Petch Samrong Mango Garden in Chachoengsao Province, for selecting and harvesting mangoes at 90-day intervals for the experiments. We also thank the School of Science and Technology, STOU, for providing the storage area and color-measuring equipment, and the Department of Imaging and Printing Technology at Chulalongkorn University for providing the camera and the photography studio. We are grateful to RUMTT for conducting laboratory tests on mango characteristics.

Author Contributions: Conceptualization, S.T., P.D. and C.K.; methodology, S.T., P.D., and C.K.; software, S.T.; validation, S.T.; formal analysis, S.T., P.D., and C.K.; investigation, S.T., P.D., and C.K.; resources, S.T.; data curation, S.T.; writing—original draft preparation, S.T.; writing—review and editing, S.T., P.D., and C.K.; visualization, S.T.; supervision, C.K.; project administration, S.T.; funding acquisition, S.T. All authors have read and agreed to the published version of the manuscript.

Funding: This research was funded by SUKHOTHAI THAMMATHIRAT OPEN UNIVERSITY, the Innovation Research Fund, grant number 3/2023. Sukhothai Thammathirat Open University/2/2023.

Conflicts of Interest: The authors declare no conflict of interest. The funders had no role in the design of the study, in the collection, analysis, or interpretation of data, in the writing of the manuscript, or in the decision to publish the results.

References

[1] Penchaiya, P.; Tijskens, L.M.M.; Uthairatanakij, A.; Srilaong, V.; Tansakul, A.; Kanlayanarat, S. Modelling quality and maturity of 'Namdokmai Sithong' mango and their variation during storage. *Postharvest Biol. Technol.* **2020**, *159*, 111000. https://doi.org/10.1016/j.postharvbio.2019.111000

[2] Kuntanavit, P. *The Exports of mangoes, bananas, durian and mangosteen from Thailand to Japan under the Japan-Thailand economic partnership agreement (JTEPA)*; Research report; National Commission on Science, Research and Innovation (CSRP), 2020.

[3] Salengke, S.; Mursalim. Non-destructive technique for determining mango maturity. *Acta Hortic.* **2013**, *975*, 505-512. https://doi.org/10.17660/ActaHortic.2013.975.66.

[4] Arias, A.; Feijoo, G.; Moreira, M.T. Exploring the potential of antioxidants from fruits and vegetables and strategies for their recovery. *Innov. Food Sci. Emerg. Technol.* **2022**, *77*, 102974. https://doi.org/10.1016/j.ifset.2022.102974

[5] Liu, X.; Fu, Y.; Li, M.; Xiong, S.; Huang, L.; Zhang, S.; Zhang, W.; Liang, X.; Wang, W.; Tang, K.; Shen, Q. Biofortification of tomatoes with beta-carotene through targeted gene editing. *Int. J. Biol. Macromol*. **2025**, *327*, 147396. https://doi.org/10.1016/j.ijbiomac.2025.147396

[6] Yungyuen, W.; Vo, T.T.; Uthairatanakij, A.; Ma, G.; Zhang, L.; Tatmala, N.; Kaewsuksaeng, S.; Jitareerat, P.; Kato, M. Carotenoid accumulation and the expression of carotenoid metabolic genes in mango during fruit development and ripening. *Appl. Sci.* **2021**, *11*, 9. https://doi.org/10.3390/app11094249

[7] Ali, M.; Anwar, R.; Yousef, A.F.; Li, B.; Luvisi, A.; Bellis, L.D.; Aprile, A.; Chen, F. Influence of bagging on the development and quality of fruits. *Plants*. **2021**, *10*, 358. https://doi.org/10.3390/plants10020358.

[8] Penchaiya, P.; Uthairatanakij, A.; Srilaong, V.; Kanlayanarat, S.; Tijskens, L.; Tansakul, A. Measurement of Mango Firmness by Non-Destructive Limited Compression Technique. *Acta Horticulturae*, **2015**, *1088*, 73–78. https://doi.org/10.17660/ActaHortic.2015.1088.7

[9] Sangchote, S. Integrated control of anthracnose (Colletotrichum gloeosporioides) of mango for export. *Acta Horticulturae*. **2013**, *973*, 55–58. https://doi.org/10.17660/ActaHortic.2013.973.5

[10] Dabas, V.; Jaiswal, G.; Agarwal, M.; Rani, R.; Sharma, A. Construction of hyperspectral images from RGB images via CNN. *Multimedia Tools Appl*. **2025**, *84*(11), 8725–8744. https://doi.org/10.1007/s11042-024-19289-3

[11] Lekhawattana, W.; Sirisomboon, P. Overall precision test of near infrared spectroscopy on mango fruits (Mangifera indica CV. 'Nam Dok Mai Si Thong') by on-line and off-line systems. *E3S Web Conf*. **2020**, *187*, 04006. https://doi.org/10.1051/e3sconf/202018704006

[12] Rungpichayapichet, P.; Chaiyarattanachote, N.; Khuwijitjaru, P.; Nakagawa, K.; Nagle, M.; Müller, J.; Mahayothee, B. Comparison of near-infrared spectroscopy and hyperspectral imaging for internal quality determination of 'Nam Dok Mai' mango during ripening. *J. Food Meas. Charact.* **2023**, *17*, 1501–1514. https://doi.org/10.1007/s11694-022-01715-5

[13] Gkillas, A.; Kosmopoulos, D.; Berberidis, K. Cost-efficient coupled learning methods for recovering near-infrared information from RGB signals: Application in precision agriculture. *Comput. Electron. Agricult*. **2023**, *209*, 107833. https://doi.org/10.1016/j.compag.2023.107833

[14] Kasimati, A.; Psiroukis, V.; Darra, N.; Kalogrias, A.; Kalivas, D.; Taylor, J.A.; Fountas, S. Investigation of the similarities between NDVI maps from different proximal and remote sensing platforms in explaining vineyard variability. *Precis. Agricult*. **2023**, *24*(4), 1220–1240. https://doi.org/10.1007/s11119-022-09984-2

[15] Rabatel, G., Gorretta, N. and Labbé, S., **2011, November**. Getting NDVI spectral bands from a single standard RGB digital camera: a methodological approach. In *Conference of the Spanish Association for Artificial Intelligence* (pp. 333-342). Berlin, Heidelberg: Springer Berlin Heidelberg.

[16] Bhandari, A.; Kumar, A.; Singh, G. Feature extraction using normalized difference vegetation index (NDVI): a case study of Jabalpur City. *Procedia Technol*. **2012**, *6*, 612–621. https://doi.org/10.1016/j.protcy.2012.10.074

[17] Liu, B.; Xin, Q.; Zhang, M.; Chen, J.; Lu, Q.; Zhou, X.; Li, X.; Zhang, W.; Feng, W.; Pei, H.; Sun, J. Research progress on mango post-harvest ripening physiology and the regulatory technologies. *Foods* **2023**, *12*(1), 173. https://doi.org/10.3390/foods12010173

[18] Rooban, R.; Shanmugam, M.; Venkatesan, T.; Tamilmani, C. Physiochemical changes during different stages of fruit ripening of climacteric fruit of mango (Mangifera indica L.) and non-climacteric of fruit cashew apple (Anacardium occidentale L.). *J. Appl. Adv. Res.* **2016**, *1*, 53. https://doi.org/10.21839/jaar.2016.v1i2.27

[19] Galal, H.; Elsayed, S.; Elsherbiny, O.; Allam, A.; Farouk, M. Using RGB imaging, optimized three-band spectral indices, and a decision tree model to assess orange fruit quality. *Agricult*. **2022,** *12*(10), 1558. https://doi.org/10.3390/agriculture12101558

[20] Kawashima, S.; Nakatani, M. An algorithm for estimating chlorophyll content in leaves using a video camera. *Ann. Bot.* **1998**, *81*(1), 49–54. https://doi.org/10.1006/anbo.1997.0544

[21] Montanaro, G.; Petrozza, A.; Rustioni, L.; Cellini, F.; Nuzzo, V. Phenotyping key fruit quality traits in olive using RGB images and back propagation neural networks. *Plant Phenomics*. **2023**, *5*, 0061. https://doi.org/10.34133/plantphenomics.0061

[22] Phimphimol, J. Sorting maturity of mangoes (Mangifera indica L.) cv. Kaew by floating in salt solution. *J. Agric. Res. Ext.* **1999**, *16*(1), 1–10. http://mdc.library.mju.ac.th/article/61802/298644/349014.pdf

[23] Somkane, S. The Effect of freezing onthe osmotic dehydration process and the quality of osmo-air-dried mangoes. Master of Science. Thesis. Silpakorn University. **2020**.

[24] Khalifa, S.; Abobatta, W. Climate changes and mango production (temperature). *IgMin Res*. **2023**, *1*(1), 043–046. https://doi.org/10.61927/igmin115

[25] Walpole, R. E.; Myers, R. H.; Myers, S. L.; Ye, K. *Probability & Statistics for Engineers & Scientists.*, 9th ed.; Prentice Hall, 2012.

[26] Hogg, R. V.; Tanis, E. A.; Zimmerman, D. L. *Probability and Statistical Inference*, 9th ed.; Pearson, 2015.https://faculty.ksu.edu.sa/sites/default/files/677_fr37hij.pdf

[27] Sa-Ngadsup, P.; Kiyoki, Y.; Koopipat, C. In vitro coral bleach observation using an RGB-IR camera. *Front. Artif. Intel. Appl.*, **2019**, 312, 457–468. https://doi.org/10.3233/978-1-61499-933-1-457

[28] Brand-Williams, W.; Cuvelier, M.E.; Berset, C. Use of a free radical method to evaluate antioxidant activity. *LWT Food Sci. Technol.* **1995**, *28*(1), 25–30. https://doi.org/10.1016/S0023-6438(95)80008-5

[29] Re, R.; Pellegrini, N.; Proteggente, A.; Pannala, A.; Yang, M.; Rice-Evans, C. Antioxidant activity applying an improved ABTS radical cation decolorization assay. *Free Radical Biol. Med.* **1999**, 26(9), 1231–1237. https://doi.org/10.1016/S0891-5849(98)00315-3

[30] de Winter, J.; Gosling, S.; Potter, J. Comparing the Pearson and Spearman correlation coefficients across distributions and sample sizes: A tutorial using simulations and empirical data. *Psychol. Methods* **2016**, *21*, 273–290. https://doi.org/10.1037/met0000079.supp

[31] Willaby, H.; Costa, D.; Burns, B.; Maccann, C.; Roberts, R. Testing complex models with Small Sample sizes: A historical overview and empirical demonstration of what partial least squares (PLS) can offer differential psychology. *Personal. Individ. Diff.* **2015**, *84*, 73–78. https://doi.org/10.1016/j.paid.2014.09.008

[32] Tucker, C.J. Red and photographic infrared linear combinations for monitoring vegetation. *Remote Sens. Environ.* **1979**, *8*(2), 127–150. https://doi.org/10.1016/0034-4257(79)90013-0

[33] Du, M.; Noguchi, N. Monitoring of wheat growth status and mapping of wheat yield's within-field spatial variations using color images acquired from a UAV-camera system. *Remote Sens*. **2017**, *9*(3), 289. https://doi.org/10.3390/rs9030289

[34] Min, S.; Kaewtrakulpong, K.; Phaosang, T.; Sermsak, R. Image processing method to check maturity index of "Sein Ta Lone" mango in Myanmar. *Suranaree J. Sci. Technol.* **2024**, *29*.

[35] Rungpichayapichet, P.; Mahayothee, B.; Khuwijitjaru, P.; Nagle, M.; Müller, J. Non-destructive determination of β-carotene content in mango by near-infrared spectroscopy compared with colorimetric measurements. *J. Food Compos. Anal*. **2015**, *38*, 32–41. https://doi.org/10.1016/j.jfca.2014.10.013

[36] Elsayed, S.; Galal, H.; Allam, A.; Schmidhalter, U. Passive reflectance sensing and digital image analysis for assessing quality parameters of mango fruits. *Scientia Hortic.* **2016,** *212*, 136–147. https://doi.org/10.1016/j.scienta.2016.09.046

ASEAN
Journal of Scientific and Technological Reports
Online ISSN:2773-8752

Research article

Influence of Different Solvents on Antioxidant Properties, Total Phenolics, and Flavonoids from *Piper betle* Leaves

Nattawoot Rattanathamwat[1*], Supharat Duanyai[1], Korakoj Pethassanayothin[1], Wachirasak Kienwong[2], Julalak Jarujutarat[2], Janyawan Janyatham[2], Pasit Tinnam[2], Piya Rontlaong[2], and Atchara Kaewnoi[3]

[1] Faculty of Science and Technology, Bansomdejchaopraya Rajabhat University, Bangkok, 10600, Thailand
[2] Faculty of Engineering and Industrial Technology, Bansomdejchaopraya Rajabhat University, Bangkok, 10600, Thailand
[3] Graduate School, Bansomdejchaopraya Rajabhat University, Bangkok, 10600, Thailand
* Correspondence: nattawoot.ra@bsru.ac.th

Citation:
Rattanathamwat, N.; Duanyai, S.; Pethassanayothin, K.; Kienwong, W.; Jarujutarat, J.; Janyatham, J.; Tinnam, P.; Rontlaong, P.; Kaewnoi, A. Influence of different solvents on antioxidant properties, total phenolics, and flavonoids from *Piper betle* leaves. *ASEAN J. Sci. Tech. Report.* **2026**, *29*(5), e261613. https://doi.org/10.55164/ajstr.v29i5.261613

Article history:
Received: October 21, 2025
Revised: March 11, 2026
Accepted: March 11, 2026
Available online: April 27, 2024

Publisher's Note:
This article is published and distributed under the terms of the Thaksin University.

Abstract: This study investigated the effects of different solvents (95% ethanol, DCM, acetone, and hexane) and extraction durations (3, 5, and 7 days) on the antioxidant activity, total phenolic content (TPC), and total flavonoid content (TFC) of *Piper betle* L. (yellow betel) leaves collected from Samut Sakhon Province, Thailand. The extracts were prepared from both fresh and dried leaves by maceration. Antioxidant activity was evaluated using DPPH, ABTS, and FRAP assays, while TPC and TFC were determined using the Folin–Ciocalteu and $AlCl_3$ colorimetric methods, respectively. The results showed that dried leaves consistently yielded higher extraction percentages than fresh leaves. Acetone extracts demonstrated superior antioxidant activities, with the lowest IC_{50} values in both DPPH and ABTS assays (3.65 μg/mL and 1.37 μg/mL, respectively), and the highest FRAP values (16.77 mM $FeSO_4$ equivalent/mg extract). Moreover, acetone extracts of fresh leaves (3-day extraction) exhibited the highest TPC (1,222.419 mg GAE/g extract) and TFC (51.70 mg QE/g extract). Statistical analysis based on analysis of variance (ANOVA) revealed that solvent type was the most significant factor affecting extraction yield, TPC, TFC, and antioxidant activities ($p < 0.05$). In contrast, extraction duration had little effect beyond 3 days, and leaf condition (fresh versus dried) significantly affected several response variables**.** These findings demonstrate that solvent polarity and extraction duration are key determinants of phenolic and flavonoid recovery and antioxidant-related properties of *Piper betle* L. leaf extracts under the investigated experimental conditions.

Keywords: *Piper betle* L.; solvent extraction; antioxidant activity; total phenolic content; total flavonoid content

1. Introduction

Piper betle L., commonly known as betel leaf, is a traditional medicinal plant widely cultivated in central and southern Thailand. The leaves are consumed fresh or boiled as a herbal remedy and have been traditionally used for cooling purposes and relief of common ailments**,** including digestive discomfort**,** respiratory symptoms, and skin conditions. Pharmacological studies have demonstrated that betel leaves possess antibacterial, anti-inflammatory, and antifungal activities, as well as antioxidant potential, derived from compounds such as eugenol, hydroxychavicol, β-carotene, and ascorbic acid. These bioactive compounds may inhibit lipid peroxidation and related oxidative

processes that generate free radicals [1]. Previous research confirmed that *P. betle* leaves contain phenolic compounds with medicinal properties [2]. Further studies reported that phenolic constituents exhibited strong antibacterial activity, supporting their investigation as natural preservative candidates**.** Parkpoom et al. [3] investigated the antimicrobial and antioxidant properties of betel leaf extracts and found that ethanolic and propylene glycol extracts inhibited several pathogenic microorganisms, including *Staphylococcus aureus*, *Pseudomonas aeruginosa*, *Escherichia coli*, and *Candida albicans*. The ethanolic extract exhibited the strongest inhibition against *S. aureus*, with an inhibition zone of 2.93 ± 0.28 cm at 12.50 mg/mL, and showed a minimum inhibitory concentration. *P. betle* leaves are rich in phenolic and phenylpropanoid compounds, particularly hydroxychavicol, eugenol, and chavibetol, which are considered key contributors to their biological activities. MIC (MIC) and MBC) values of 3.125 and 6.25 mg/mL, respectively. In addition to antimicrobial activity, ethanolic extracts also demonstrated antioxidant potential, as measured by DPPH, ABTS, and FRAP assays, with reported values of 3,653.01 ± 57.72 μg/mL, 17,261 ± 697.00 μg/mL, and 3,616.99 ± 41.49 mg Trolox equivalents/g dw, respectively. The total phenolic content (TPC), determined by the Folin–Ciocalteu method, was reported to be 538.33 ± 13.48 mg GAE/g dw. These findings collectively indicate that betel leaf extracts are rich in bioactive compounds associated with antimicrobial and antioxidant activities. *P. betle* leaves contain a diverse range of phenolic and phenylpropanoid compounds, particularly hydroxychavicol, eugenol, and chavibetol, whose differences in polarity and molecular structure play a critical role in their solubility and extractability in solvents of varying polarity. Hydroxychavicol is a highly polar phenolic compound due to the presence of multiple hydroxyl groups, whereas eugenol and chavibetol exhibit semipolar characteristics. Differences in polarity and solubility of these compounds influence their extractability in solvents with varying polarity, thereby affecting the phenolic content and antioxidant activity of the resulting extracts.

The choice of solvent is a critical factor influencing the extraction yield of phytochemicals from medicinal plants. Borges et al. [4] studied the extraction of *Olea europaea* (olive leaves) and *Acacia dealbata* (flowers) using various solvents, including water, methanol, ethanol, acetone, DCM, and hexane, in combination with different techniques such as maceration, Soxhlet extraction, ultrasound-assisted extraction (UAE), and microwave-assisted extraction (MAE). Their results indicated that polar solvents, such as ethanol, methanol, and acetone, yielded higher phenolic compound yields and stronger antimicrobial activity than nonpolar solvents, highlighting the importance of solvent polarity in phenolic extraction. Additionally, the use of assisted extraction techniques further enhanced extraction efficiency. In a solvent-comparison study, El Mannoubi et al. [5] compared the efficiency of 80% ethanol and 80% acetone in extracting bioactive compounds from *Opuntia stricta*. The results showed that 80% ethanol yielded the highest overall extract, whereas 80% acetone extracts contained higher levels of phenolics and flavonoids and exhibited stronger antioxidant activity, suggesting that extraction yield and bioactive compound recovery do not necessarily correlate. In another study, Chatepa et al. [6] evaluated the effect of different solvents on the extraction of *Azadirachta indica* (neem) and *Vernonia amygdalina* (bitter leaf). Their findings revealed that the optimal solvent varied by plant species: methanol and water were most effective for neem, whereas different extraction patterns were observed for bitter leaf, indicating that plant matrix characteristics influence solvent efficiency. *Piper betle* L. Banik et al. [7] compared acetone and ethanol extracts and reported that both solvents produced extracts with antibacterial activity. However, acetone extracts were more effective against certain bacterial strains, whereas ethanolic extracts contained higher phenolic contents, demonstrating solvent-dependent differences in bioactivity profiles. Using different solvent systems, Venugopalan et al. [8] reported that ethanol and methanol extracts of *P. betle* leaves exhibited stronger antioxidant activities than hexane or aqueous extracts. Consistent with these observations, Nouri et al. [9] demonstrated that ethanolic extracts of betel leaves yielded higher phenolic contents and stronger antioxidant activities than methanolic extracts. Collectively, these studies demonstrate that solvent polarity is a dominant factor governing phenolic and flavonoid extraction efficiency and antioxidant activity, although the optimal solvent may vary depending on plant species, plant matrix characteristics, and extraction conditions.

However, previous studies on *P. betle* extraction have mainly focused on limited solvent systems or single extraction conditions. Comparative investigations that simultaneously evaluate the effects of solvent polarity, extraction duration, and plant material condition (fresh versus dried leaves) under consistent

experimental conditions remain limited. As a result, a systematic understanding of how these factors collectively influence phenolic and flavonoid recovery and antioxidant activity in *P. betle* leaves is still lacking.

Given this background, the present study was designed to investigate the effects of different solvents and extraction conditions on the antioxidant activity, total phenolic content (TPC), and total flavonoid content (TFC) of *Piper betle* leaves. This study was conducted to evaluate how solvent polarity and extraction duration influence the extraction efficiency and antioxidant-related properties of phenolic and flavonoid compounds under the studied conditions, to provide fundamental scientific information to support a systematic comparison of extraction parameters.

2. Materials and Methods

2.1 Materials

Fresh *Piper betle* L. leaves were collected from Laksong Subdistrict, Ban Phaeo District, Samut Sakhon Province, Thailand. The plant material was taxonomically identified as *Piper betle* L. (Piperaceae) by a botanist at the Department of Botany, Faculty of Science, Chulalongkorn University. A voucher specimen (No. A 18147) was deposited at the Herbarium of the Department of Botany, Faculty of Science, Chulalongkorn University (BCU), Bangkok, Thailand. Analytical grade (AR) solvents and chemicals were used in this study, including ethanol (RCI Labscan, Thailand), hexane (RCI Labscan, Thailand), dichloromethane (DCM) (RCI Labscan, Thailand), acetone (RCI Labscan, Thailand), 2,2-diphenyl-1-picrylhydrazyl (DPPH; RCI Labscan, Thailand), 2,2′-azino-bis(3-ethylbenzothiazoline-6-sulfonic acid) diammon ium salt (ABTS; Sigma-Aldrich, USA), **ascorbic acid** (RCI Labscan, Thailand), sodium carbonate (Sigma-Aldrich, USA), Folin–Ciocalteu reagent (Sigma-Aldrich, USA), gallic acid (Sigma-Aldrich, USA), potassium persulfate (RCI Labscan, Thailand), 2,4,6-tri(2-pyridyl)-1,3,5-triazine (TPTZ; Sigma-Aldrich, USA), ferric chloride (Sigma-Aldrich, USA), and quercetin (Sigma-Aldrich, USA).

2.2 Extraction of Betel Leaves Using Different Solvents by Maceration Method

The maceration method was employed for extraction, as previously reported [10, 11]. Fresh leaves were washed with distilled water and used immediately, while dried leaves were dried in a hot-air oven at 60 °C for 24 h until constant weight was achieved. Fresh and dried leaves were cut into small pieces, weighed, and soaked in different solvents (95% ethanol, DCM, acetone, and hexane) at a 1:10 (w/v) ratio (1 g sample per 10 mL solvent). Samples were extracted at room temperature (25 ± 2 °C) for 3, 5, and 7 days. The mixtures were filtered through Whatman No. 1 filter paper, and the solvents were evaporated under reduced pressure using a rotary evaporator at 40 °C. The concentrates were freeze-dried and dried to constant weight to minimize residual solvents before storage. The dried extracts were weighed, and the extraction yield (%) was calculated as shown in Equation (1): Fresh leaves were used to represent the native physicochemical state of the plant material and to minimize degradation of moisture-sensitive bioactive compounds. In contrast, dried leaves were included for comparison, as drying is commonly applied during post-harvest processing and may influence extraction efficiency. Although moisture content was not quantitatively determined, oven-dried leaves (60 °C, 24 h) were used to ensure consistent moisture reduction before extraction. The maceration durations of 3, 5, and 7 days were selected to evaluate the time-dependent extraction behavior of phenolic and flavonoid compounds under mild conditions at room temperature. Previous studies have demonstrated that maceration time plays a critical role in determining phenolic composition and antioxidant capacity, with measurable changes commonly observed within the early to intermediate stages of extraction [12,13]. Comparative studies have reported that maceration periods ranging from a few days to one week are commonly used to investigate extraction kinetics, including time points at 1, 3, 7, and 14 days [14,15]. However, prolonged maceration may lead to partial degradation or oxidation of phenolic compounds, particularly when extraction is extended beyond the optimal duration [12,16]. Therefore, the maximum maceration period in this study was limited to 7 days to balance extraction efficiency and chemical stability, while enabling systematic comparison of extraction yields, phenolic, flavonoid, and antioxidant activities at different time points [12,15,17]. All maceration experiments were conducted at room temperature (25 ± 2 °C) under dark conditions to minimize potential photo-degradation of phenolic compounds. Extraction was performed in closed glass containers to prevent solvent evaporation and reduce oxidative exposure. The mixtures were gently agitated

manually once daily to enhance solvent penetration and mass transfer during maceration. The solvent-to-sample ratio of 1:10 (w/v) was selected based on previous maceration studies, which reported that this ratio provides sufficient solvent volume to facilitate solute diffusion and achieve extraction equilibrium under mild conditions, while avoiding excessive solvent consumption and enabling meaningful comparisons of extraction yield and phenolic recovery across different extraction times [14,15].

$$\text{Yield (\%)} = \frac{\text{Weight of dried extract (g)}}{\text{Weight of initial leaves (g)}} \times 100 \quad (1)$$

2.3 Determination of Total Phenolic Content (TPC)

The total phenolic content (TPC) of the extracts was determined using the Folin–Ciocalteu method with gallic acid as a standard, as described by Singleton and Rossi [18]. Extract solutions of various concentrations were prepared. For the assay, 20 μL of extract solution was mixed with 100 μL of Folin–Ciocalteu reagent diluted 1:10 with deionized water, followed by the addition of 80 μL of 7.5% (w/v) sodium carbonate (Na_2CO_3), giving a final volume of 200 μL. TPC values were calculated by interpolating absorbance values from the gallic acid calibration curve, correcting for dilution factors, and expressing them as mg GAE/g extract. The mixtures were thoroughly mixed and incubated in the dark at room temperature for 30 min. Absorbance was measured at 760 nm using a microplate reader. All measurements were carried out in triplicate (n = 3). The phenolic content of the extracts was determined from the gallic acid calibration curve and expressed as milligrams of gallic acid equivalents per gram of extract (mg GAE/g extract).

2.4 Determination of Total Flavonoid Content (TFC)

The total flavonoid content was determined using the aluminum chloride colorimetric method with quercetin as the standard, as described by Chang et al. [19]. A quercetin standard stock solution was prepared at 100 μg/mL and diluted to obtain standard solutions at 10, 20, 30, 40, and 45 μg/mL. Extract samples were prepared at a concentration of 400 μg/mL. For the assay, 100 μL of either the extract sample or quercetin standard solution was mixed with 100 μL of 2% aluminum chloride ($AlCl_3$) solution. The mixtures were incubated at room temperature for 10 min, and absorbance was measured at 415 nm using a microplate spectrophotometer (Perkin Elmer®, EnSight 3400). Each experiment was conducted in triplicate (n = 3). The flavonoid content was calculated from the quercetin standard calibration curve and expressed as milligrams of quercetin equivalents per gram of extract (mg QE/g extract).

2.5 DPPH Radical Scavenging Capacity Assay

The antioxidant activity of the extracts was evaluated using the DPPH radical scavenging capacity assay according to the method described by Brand-Williams et al. [20]. Ascorbic acid (vitamin C) was used as a positive control and standard antioxidant reference for comparison. A stock solution of the sample was prepared at 200 μg/mL, and serial two-fold dilutions were made to obtain five concentrations: 100, 50, 25, 12.5, and 6.25 μg/mL. Different initial extract concentrations were used for each antioxidant assay because the assays differ in sensitivity, reaction kinetics, and linear response range. Therefore, the concentration ranges were selected based on preliminary tests and established literature protocols to ensure measurable inhibition within the dynamic range of each method and to allow accurate determination of IC_{50} values. For the assay, 100 μL of each sample solution was mixed with 100 μL of methanolic DPPH solution (152 μM). The reaction mixtures were incubated in the dark at room temperature for 30 min, after which absorbance was measured at 517 nm using a microplate spectrophotometer (Perkin Elmer®, EnSight 3400). The percentage of radical scavenging activity was calculated according to Equation (2):

$$\text{radical scavenging(\%)} = \frac{(A_{\text{control}} - A_{\text{blank control}}) - (A_{\text{sample}} - A_{\text{blank sample}})}{(A_{\text{control}} - A_{\text{blank control}})} \times 100 \quad (2)$$

where:

A_sample = absorbance of the extract sample mixed with DPPH
A_blank sample = absorbance of the extract sample mixed with methanol
A_control = absorbance of the DPPH solution without extract
A_blank control = absorbance of methanol alone

All measurements were performed in triplicate (n = 3). IC_{50} values were determined by fitting concentration–response curves using nonlinear regression analysis (four-parameter logistic model) with GraphPad Prism version 10.

2.6 ABTS Radical Cation Decolorization Assay

The antioxidant activity of the extracts was evaluated using the ABTS radical cation decolorization assay. According to the method described by Re et al. [21]. Ascorbic acid was used as a standard antioxidant reference for comparison. A stock solution of 7 mM 2,2′-azino-bis(3-ethylbenzothiazoline-6-sulfonic acid) diammonium salt (ABTS) was prepared and mixed with 2.45 mM potassium persulfate at a 1:0.5 (v/v) ratio. The mixture was incubated in the dark for 12–16 h to generate $ABTS^{\bullet+}$ radicals. Before use, the $ABTS^{\bullet+}$ solution was diluted with ethanol to obtain an absorbance of 0.70 ± 0.02 at 734 nm.

Sample solutions were prepared at different concentrations (100, 50, 25, 12.5, 6.25, 3.125, and 1.5625 μg/mL in ethanol). For the assay, 20 μL of each sample solution was added to a 96-well plate, followed by 180 μL of the $ABTS^{\bullet+}$ solution. The mixture was shaken gently and incubated in the dark for 6 min. Absorbance was then measured at 734 nm (n = 3) using a microplate spectrophotometer (Perkin Elmer®, EnSight 3400). The percentage of inhibition was calculated using Equation (3):

$$\text{inhibition}(\%) = \frac{Ac - As}{Ac} \times 100 \quad (3)$$

where:

Ac = absorbance of the control ($ABTS^{\bullet+}$ solution without extract)

As = absorbance of the test sample containing the extract

2.7 Ferric Ion Reducing Antioxidant Power (FRAP) Assay

The antioxidant activity of the extracts was further evaluated using the ferric ion reducing antioxidant power (FRAP) assay, as described by Benzie and Strain [16]. Ferrous sulfate ($FeSO_4$) was used as a standard reference compound to construct a calibration curve for FRAP quantification. The FRAP reagent was freshly prepared by mixing 300 mM acetate buffer (pH 3.6), 20 mM ferric chloride ($FeCl_3$), and 10 mM 2,4,6-tri(2-pyridyl)-1,3,5-triazine (TPTZ) in 40 mM hydrochloric acid (HCl) at a ratio of 10:1:1 (v/v/v).

Sample solutions were prepared at a concentration of 400 μg/mL in methanol. For the assay, 20 μL of each extract was added to a 96-well plate, followed by 180 μL of FRAP reagent. The mixture was gently shaken and incubated for 4 min at room temperature, after which absorbance was measured at 593 nm (n = 3) using a microplate spectrophotometer (Perkin Elmer®, EnSight 3400). The absorbance value was calculated according to Equation (4):

$$\text{Absorbance} = A - B - C \quad (4)$$

where:

A = absorbance of the sample mixed with FRAP reagent

B = absorbance of the sample mixed with the acetate buffer

C = absorbance of methanol mixed with FRAP reagent

The blank-corrected absorbance obtained from Equation (4) was used to calculate the FRAP value by interpolation from the ferrous sulfate ($FeSO_4$) standard calibration curve. The concentration of $FeSO_4$ equivalents was determined using the linear regression equation derived from the calibration curve. The FRAP value was determined by comparing the absorbance of the test samples with the calibration curve of ferrous sulfate ($FeSO_4$) in the concentration range of 0.06–0.20 mM. Results were expressed as millimoles of ferrous sulfate equivalents per milligram of extract (mM $FeSO_4$ equivalent/mg extract). Different sample concentrations were applied across assays because each method differs in sensitivity, reaction mechanism, and linear response range. Radical scavenging assays (DPPH and ABTS) require serial dilutions to determine IC_{50} values accurately, whereas reducing power–based assays (FRAP) and colorimetric complex formation assays (TPC and TFC) require sufficiently high concentrations to generate absorbance values within the linear range of their respective calibration curves.

2.8 Statistical Analysis

All experiments were conducted in triplicate, and the results were expressed as mean ± standard deviation (SD) (n = 3). All instruments were calibrated according to the manufacturer's instructions before analysis, and appropriate blanks were applied in all assays. A full factorial experimental design was applied to evaluate the effects of solvent type, extraction time, and leaf condition (fresh and dried) on extraction yield, as well as the effects of assay type, solvent, extraction time, and leaf condition on antioxidant activities. Analysis of variance (ANOVA) was performed to determine significant differences among groups, followed by Duncan's multiple range test. An independent-samples t-test was used to compare fresh and dried leaf samples. Statistical analyses were carried out using SPSS Statistics (version 21.0), with significance set at $p < 0.05$.

3. Results and Discussion

3.1. Percentage Yield of Piper betle Leaf Extracts

The extraction yields of *Piper betle* L. leaves under two conditions (fresh and dried) using four different solvents (95% ethanol, DCM, acetone, and hexane) with maceration times of 3, 5, and 7 days are presented in Table 1. Overall, the extraction yield was influenced by both the physical condition of the plant material and the polarity of the extraction solvent. As shown in Table 1, dried leaves consistently produced significantly higher extraction yields than fresh leaves across all solvents and maceration times ($p < 0.05$). The highest extraction yield was obtained from dried leaves extracted with 95% ethanol for 3 days (8.30 ± 0.20% w/w), followed by acetone extraction of dried leaves at the same maceration time (7.17 ± 0.62% w/w). From a chemical perspective, drying alters the plant matrix by disrupting cell walls and reducing intracellular water content, thereby facilitating solvent penetration and improving the mass transfer of extractable compounds. In addition, removing moisture prevents dilution of the extraction solvent, thereby increasing the effective concentration gradient driving solute diffusion. Consequently, dried plant materials generally provide higher extraction yields than fresh samples, as reported in several phytochemical extraction studies [10, 17].

Table 1. Percentage yield (% w/w) of extracts from fresh and dried *Piper betle* leaves obtained with different solvents at various maceration times (3, 5, and 7 days).

Solvent/days	% Yield	
	Fresh leaves	**Dried leaves**
3 days		
95% Ethanol	4.51 ± 0.08^{a}	8.30 ± 0.20^{b}*
DCM	1.47 ± 0.11^{b}	6.32 ± 0.50^{c}*
Acetone	2.84 ± 0.20^{b}	7.17 ± 0.62^{b}*
Hexane	0.57 ± 0.24^{c}	4.08 ± 0.25^{c}*
5 days		
95% Ethanol	5.87 ± 0.15^{a}	7.92 ± 0.74^{b*}
DCM	2.31 ± 0.53^{b}	5.17 ± 0.35^{c*}
Acetone	2.78 ± 0.02^{b}	6.45 ± 0.89^{b*}
Hexane	0.29 ± 0.09^{c}	4.82 ± 0.54^{c*}
7 days		
95% Ethanol	4.93 ± 0.31^{a}	8.08 ± 0.16^{b*}
DCM	1.77 ± 0.23^{b}	5.68 ± 0.48c*
Acetone	3.13 ± 0.18^{b}	6.67 ± 0.15^{b*}
Hexane	0.44 ± 0.02^{c}	4.75 ± 0.13^{c*}

Values are expressed as mean ± SD (n = 3).

Different lowercase letters (a–c) within the same column indicate significant differences among solvents within the same leaf condition (fresh or dried) and extraction time, as determined by one-way ANOVA followed by Duncan's multiple range test ($p < 0.05$).

* indicates significant differences between fresh and dried leaves within the same solvent and extraction time, determined by an independent-samples t-test ($p < 0.05$).

Among the solvents tested, 95% ethanol and acetone produced higher extraction yields than DCM and hexane, reflecting the greater solubility of moderately polar phenolic and phenylpropanoid compounds in polar and semi-polar solvents. *Piper betle* leaves are rich in hydroxylated phenolic constituents, which can be efficiently solubilized through hydrogen bonding and dipole–dipole interactions with ethanol and acetone, whereas non-polar solvents such as hexane exhibit limited affinity for these compounds, resulting in substantially lower extraction yields. Similar solvent-dependent trends have been widely reported for phenolic-rich plant materials [4, 10-11]. When comparing maceration times within the same solvent system, extending the extraction period from 3 to 7 days did not result in a substantial increase in extraction yield. This suggests that the extraction equilibrium was reached during the early stages of maceration. Regarding extraction duration, the limited effect of prolonged maceration on extraction yield indicates that most soluble phytochemicals were released during the initial stages of extraction. Once diffusion equilibrium between the plant matrix and solvent phase is achieved, further extension of maceration time does not significantly enhance yield. Prolonged extraction may even increase the risk of oxidative degradation or polymerization of phenolic compounds without providing additional extraction benefits [16-17]. Based on the analysis of variance (ANOVA) of the experimental design for the extraction of compounds from *Piper betle* L. leaves, three main factors were evaluated: solvent type, maceration time (days), and leaf condition. The ANOVA results are summarized in Table 2.

Table 2. Analysis of variance (ANOVA) of factors affecting the extraction yield (% yield) of *Piper betle* leaves

Source	DF	AdjSS	AdjMS	F-Value	P-Value
Model	23	408.409	17.757	118.42	0.000
Linear	6	396.166	66.028	440.34	0.000
Solvent	3	155.814	51.938	346.37	0.000
Time	2	0.036	0.018	0.12	0.888
Leaf condition	1	240.316	240.316	1602.66	0.000

Table 2 shows that the overall ANOVA model for extraction yield was statistically significant ($p < 0.001$). Solvent type and leaf condition significantly affected extraction yield ($p < 0.05$), confirming that both solvent polarity and sample pretreatment play critical roles in determining extraction efficiency. In contrast, maceration time within the investigated range (3–7 days) did not significantly affect extraction yield ($p = 0.888$), indicating that extending the extraction period beyond the initial stage provides limited additional benefit. These results suggest that solvent polarity and leaf condition are the primary determinants of extraction efficiency, whereas extraction time plays a relatively minor role within the investigated range. Overall, the results demonstrate that the extraction yield of *P. betle* leaves is primarily governed by the physical condition of the plant material and solvent polarity, whereas maceration duration within the investigated range plays a comparatively minor role. These findings provide essential baseline information for optimizing extraction conditions before evaluating antioxidant activity and phytochemical content in subsequent analyses.

3.2 Total Flavonoid Content (TFC) and Total Phenolic Content (TPC)

The total flavonoid content (TFC) of extracts obtained from fresh and dried *Piper betle* leaves was determined using a quercetin calibration curve. The calibration curve exhibited good linearity, with a coefficient of determination (R^2) of 0.9988, and the regression equation was $y = 0.0104x - 0.0107$ (Figure 1). Total phenolic content (TPC) was determined using gallic acid as the standard reference, and the corresponding calibration curve showed excellent linearity ($R^2 = 0.9994$) with the regression equation $y = 0.0452x + 0.0118$ (Figure 2). The quantified TFC and TPC values under different extraction conditions are summarized in Table 3.

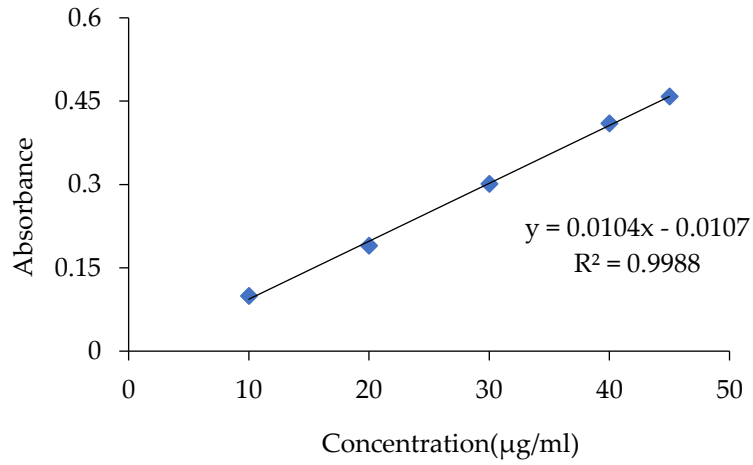


Figure 1. Standard calibration curve of quercetin

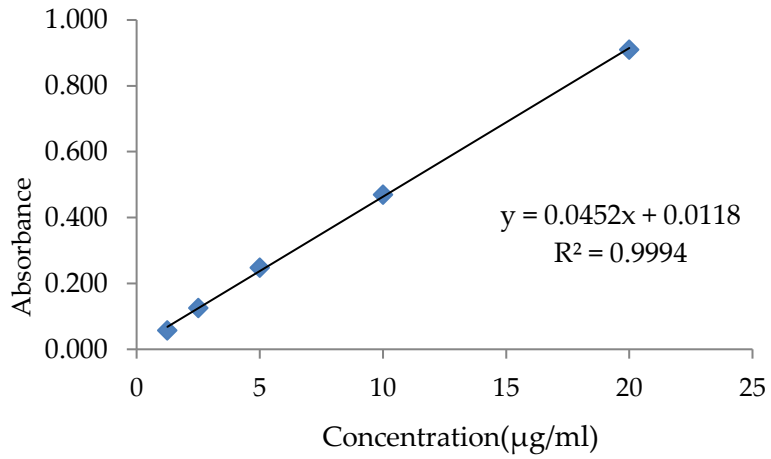


Figure 2. Standard calibration curve of gallic acid

The total flavonoid content (TFC) and total phenolic content (TPC) of *Piper betle* leaf extracts obtained under different extraction conditions are summarized in Table 3. The results clearly demonstrate that sample condition (fresh vs. dried leaves), solvent polarity, and maceration duration affected both TFC and TPC values. Under fresh leaf conditions, acetone extracts consistently exhibited the highest TFC and TPC values, particularly at shorter maceration periods (3 days). For example, the fresh acetone extract obtained after 3 days showed the highest TFC (51.71 ± 15.51 mg QE/g extract) and the highest TPC (1,222.419 ± 24.27 mg GAE/g extract) among all tested solvents (Table 3). This can be attributed to the intermediate polarity of acetone, which enables efficient solubilization of a broad range of flavonoids and phenolic compounds, including phenolic acids and polyphenols containing multiple hydroxyl groups [22]. Previous studies have reported that *Piper betle* L. leaves are rich in phenolic compounds, particularly eugenol, hydroxychavicol, chavicol, and allyl pyrocatechol, which possess strong **electron-donating capacity** and contribute to antioxidant-related properties [23]. In the present study, the acetone extract of fresh leaves obtained after 3 days of maceration exhibited the highest total phenolic content (1,222.42 ± 24.27 mg GAE/g extract). Although this value exceeds the leaf type, it should be noted that TPC values are expressed as gallic acid equivalents (GAE), which reflect the total reducing capacity of the extract rather than the absolute phenolic concentration. Moreover, the Folin–Ciocalteu assay is not specific to phenolic compounds and may respond to other reducing substances present in fresh plant tissues, potentially leading to elevated GAE values [24]. The high TPC observed in the acetone

extract may be attributed to hydroxychavicol-rich phenolic fractions, whose molecular structures facilitate stronger electron-transfer reactions than those of gallic acid under alkaline assay conditions. In addition, acetone has been reported to be highly effective in extracting these phenolics and in inhibiting polyphenol oxidase (PPO) activity in fresh betel leaves, thereby reducing enzymatic degradation during short extraction periods [25]. However, when maceration time was extended to **5–7** days, TPC values decreased, which may be associated with oxidation or degradation of phenolic compounds in fresh leaves with high moisture content during prolonged extraction. Overall, these results highlight the importance of solvent selection and extraction duration in preserving redox-active phenolic compounds in *Piper betle* leaf extracts.

DCM extracts also showed relatively high TFC and TPC values compared with ethanol and hexane. Although DCM is less polar than acetone, it is effective in extracting flavonoid aglycones and semi-polar phenolic compounds, which contribute to its moderate to high extraction efficiency [10]. In contrast, hexane consistently yielded the lowest TFC and TPC values, reflecting its nonpolar nature and limited ability to dissolve phenolic compounds with polar functional groups. This observation agrees with previous reports indicating that non-polar solvents are unsuitable for phenolic extraction [11]. A comparison between fresh and dried leaf extracts showed that TPC values were generally higher in dried leaves, especially when ethanol or DCM was used as the extraction solvent (Table 3). The increased TPC in dried samples can be explained by moisture removal, which increases the relative concentration of phenolic compounds on a dry-weight basis and enhances solvent penetration into plant tissues. In addition, drying may disrupt cell walls and vacuolar structures, facilitating the release of bound phenolics during extraction [17]. In contrast, TFC values tended to be higher in fresh leaf extracts, particularly for acetone and DCM at shorter maceration times. Many flavonoids are known to be sensitive to heat, oxygen, and prolonged exposure to air, and partial degradation or oxidation may occur during drying, leading to reduced flavonoid content in dried samples [17]. This explains why fresh leaves often retained higher TFC values, whereas dried leaves showed a relative decrease in flavonoid content despite higher TPC values.

Maceration duration also influenced TFC and TPC, although the effect was not linear. In several solvent systems, higher TFC and TPC values were observed at shorter or intermediate extraction times (3–5 days), while prolonged maceration (7 days) did not consistently enhance compound recovery. This trend suggests that the extraction equilibrium was reached early, and extended maceration may lead to oxidation or degradation of phenolic and flavonoid compounds rather than increased extraction efficiency. Similar observations have been reported for plant polyphenol extraction using maceration techniques [12,15]. Although TFC and TPC represent different classes of phytochemicals, the results in Table 3 indicate a general positive association between TFC and TPC, particularly in acetone and DCM extracts. This relationship is chemically reasonable, as flavonoids constitute a major subclass of phenolic compounds, and extraction conditions that favor phenolic solubilization often enhance flavonoid recovery. However, the lack of a strict linear relationship between TFC and TPC across all solvents and conditions suggests that solvent selectivity and compound stability play important roles in determining the relative abundance of flavonoids versus total phenolics [20, 22].

Overall, the results demonstrate that acetone was the most effective solvent for the simultaneous extraction of flavonoids and phenolic compounds, whereas ethanol and DCM were comparatively more effective for maximizing total phenolic content (TPC) in dried leaf samples. The observed differences between fresh and dried leaves further highlight the importance of sample pretreatment and extraction parameters in preserving and recovering bioactive compounds from Piper betle L. Although the hydrodistilled essential oil exhibited measurable TPC values (Table 3), these results should be interpreted with caution. Essential oils are primarily composed of volatile, non-polar to semi-polar constituents, such as terpenoids and phenylpropanoids, rather than classical phenolic compounds. Moreover, the Folin–Ciocalteu assay is known to respond to various reducing substances, including certain non-phenolic constituents, which may contribute to apparent TPC values in essential oils. Therefore, direct quantitative comparison of TPC between essential oil and solvent-based extracts is not appropriate, and the essential oil data are presented mainly for qualitative reference. Based on the analysis of variance (ANOVA) of the extraction experiment designed with three

factors, namely solvent type, maceration time, and leaf type, the results are summarized in Table 4. The analysis of variance (ANOVA) results for total flavonoid content (TFC) (Table 4) showed that solvent type, maceration time, and leaf type significantly affected flavonoid content ($p < 0.05$). Solvent type exerted a strong influence on TFC ($F = 131.85$), indicating the importance of solvent polarity in flavonoid extraction. Maceration time also showed a significant but weaker effect ($F = 3.72$), while leaf type had the greatest impact ($F = 239.06$), confirming clear differences between fresh and dried leaves.

Table 3. Total Flavonoid Content (TFC) and Total Phenolic Content (TPC)

Solvent/ days	TFC mg QE/g extract		TPC mg GAE/g extract	
	Fresh leaves	**Dried leaves**	**Fresh leaves**	**Dried leaves**
3 days				
95% Ethanol	$18.662 \pm 1.22^{cA*}$	$13.813 \pm 1.54^{cB**}$	463.300 ± 5.35^{bA}	526.475 ± 75.63^{cAB}
DCM	$42.873 \pm 3.51^{bA**}$	$7.177 \pm 0.14^{aA*}$	$232.289 \pm 26.59^{dA**}$	$717.257 \pm 47.47^{bA*}$
Acetone	$51.705 \pm 15.51^{aA*}$	$18.697 \pm 2.08^{bA**}$	$1{,}222.419 \pm 24.27^{aA*}$	$816.323 \pm 46.86^{aB**}$
Hexane	$7.371 \pm 0.93^{dB**}$	$2.006 \pm 0.41^{bB*}$	$283.161 \pm 9.62^{cA*}$	$204.019 \pm 11.37^{dB**}$
5 days				
95% Ethanol	15.385 ± 1.64^{bA}	14.796 ± 0.23^{abB}	$380.273 \pm 11.67^{bB**}$	$573.550 \pm 43.17^{cA*}$
DCM	$29.355 \pm 3.04^{aB*}$	$12.983 \pm 0.15^{bB**}$	$210.656 \pm 33.95^{cAB**}$	$706.686 \pm 82.17^{bA*}$
Acetone	$33.656 \pm 0.74^{aC*}$	$17.082 \pm 2.94^{aAB**}$	$606.637 \pm 31.81^{aB**}$	$1{,}198.083 \pm 14.73^{aA*}$
Hexane	$14.080 \pm 2.63^{bA*}$	$4.208 \pm 0.33^{cC**}$	203.024 ± 14.57^{cB}	229.953 ± 10.71^{dA}
7 days				
95% Ethanol	$13.608 \pm 2.04^{cB**}$	$27.123 \pm 4.41^{aA*}$	$230.998 \pm 18.89^{bC*}$	$436.873 \pm 51.39^{cB*}$
DCM	$39.647 \pm 3.13^{bB*}$	$8.359 \pm 0.45^{cC**}$	$184.108 \pm 4.64^{cB**}$	$811.406 \pm 27.10^{aA*}$
Acetone	$43.948 \pm 0.83^{aB*}$	$16.009 \pm 1.16^{cB**}$	638.594 ± 37.63^{aB}	592.380 ± 21.17^{bC}
Hexane	$2.823 \pm 0.24^{dC**}$	$9.466 \pm 0.96^{bA*}$	$218.879 \pm 6.43^{bcB**}$	$244.088 \pm 10.98^{dA*}$
Hydrodistillation Essential oil	N/D	N/D	352.360 ± 6.93	504.523 ± 2.27

Values are expressed as mean ± SD (n = 3).

Different lowercase letters (a–d) within the same column indicate significant differences among solvents at the same extraction time and condition, determined by one-way ANOVA followed by Duncan's multiple range test ($p < 0.05$).

Different uppercase letters (A–C) within the same row indicate significant differences among extraction times for the same solvent and condition, determined by Duncan's test ($p < 0.05$).

* and ** indicate significant differences between fresh and dried leaves within the same solvent and extraction time, determined by an independent-samples t-test ($p < 0.05$).

Table 4. Analysis of variance (ANOVA) of factors affecting total flavonoid content (TFC) of *Piper betle* leaves

Source	DF	AdjSS	Adj MS	F-Value	P-Value
Model	23	13444.0	584.52	42.92	0.000
Linear	6	8744.4	1457.41	107.01	0.000
Solvent	3	5387.3	1795.76	131.85	0.000
Time	2	101.3	50.66	3.72	0.031
Leaf condition	1	3255.9	3255.85	239.06	0.000

Similarly, the ANOVA results for total phenolic content (TPC) are presented in Table 5, which revealed that all three factors significantly influenced phenolic recovery ($p < 0.001$). Solvent type showed the most pronounced effect ($F = 1398.11$), followed by leaf type ($F = 251.87$) and maceration time ($F = 238.68$). These results emphasize that phenolic extraction is strongly governed by solvent polarity and sample condition.

Table 5. Analysis of variance (ANOVA) of factors affecting total phenolic content (TPC) of *Piper betle* leaves

Source	DF	AdjSS	AdjMS	F-Value	P-Value
Model	23	10276769	446816	373.90	0.000
Linear	6	5883739	980623	820.53	0.000
Solvent	3	5012295	1670765	1398.11	0.000
Time	2	570460	285230	238.68	0.000
Leaf condition	1	300985	300985	251.87	0.000

Overall, the ANOVA analyses confirm that solvent selection and leaf pretreatment are the dominant factors controlling both TFC and TPC, whereas maceration time plays a secondary but still significant role in determining phytochemical recovery from *Piper betle* leaves.

3.3 Antioxidant Activities of Extracts by DPPH, ABTS, and FRAP Assays

The antioxidant activities of *Piper betle* leaf extracts obtained from fresh and dried samples were evaluated using three complementary assays: DPPH radical scavenging, ABTS radical cation decolorization, and ferric reducing antioxidant power (FRAP). These assays were selected because they represent different antioxidant mechanisms, including hydrogen atom transfer (HAT), single-electron transfer (SET), and overall reducing capacity [rotary evaporator]. Extracts were prepared using four solvents of varying polarity (95% ethanol, DCM, acetone, and hexane) and maceration times of 3, 5, and 7 days. The antioxidant activities are summarized in Table 6.

As shown in Table 6, acetone extracts consistently exhibited the strongest radical scavenging activity in both DPPH and ABTS assays, particularly for fresh leaves. The lowest DPPH IC_{50} values were observed for fresh leaf extracts obtained with acetone after 5 and 7 days of maceration, at 3.665 ± 0.26 and 3.653 ± 0.41 μg/mL, respectively. These values were comparable to those of dried leaves extracted with acetone for 3 days (IC_{50} = 3.948 ± 0.19 μg/mL), indicating that solvent polarity played a more dominant role than extraction time in determining radical scavenging capacity. In the ABTS assay, dried leaves extracted with acetone for 3 days showed the strongest antioxidant activity, with an IC_{50} value of 1.368 ± 0.09 μg/mL. This observation suggests that moderate drying may enhance the accessibility of certain antioxidant compounds by disrupting plant cell structures and improving solvent penetration. However, prolonged maceration beyond 3–5 days did not enhance antioxidant activity and, in several cases, resulted in higher IC_{50} values, indicating reduced radical scavenging efficiency. These findings suggest that extended extraction times may promote partial degradation, oxidation, or transformation of phenolic and flavonoid compounds, particularly under prolonged exposure to solvent and oxygen. Similar trends have been reported by Alam et al. [13] and Sarma et al. [14], who demonstrated that intermediate extraction times and medium-polarity solvents yielded optimal antioxidant activities in *Piper betle* and other medicinal plants. It should be noted that the IC_{50} values obtained from DPPH and ABTS assays reflect chemical radical scavenging capacity and do not directly represent biological antioxidant potency. Consistent with the FRAP results, these findings further support that acetone effectively extracts electron-donating phenolic compounds with strong reducing capacity.

Table 6. Antioxidant activities of betel leaf extracts determined by DPPH, ABTS, and FRAP assays

Solvent/ days	Antioxidant Activities by Different Assays					
	DPPH IC_{50} (μg/mL)		ABTS IC_{50} (μg/mL)		FRAP assay (mM $FeSO_4$ equivalent/mg extract)	
	Fresh leaves	Dried leaves	Fresh leaves	Dried leaves	Fresh leaves	Dried leaves
3 days						
95% Ethanol	6.834 ± 1.43^{aA}	8.353 ± 1.45^{bAB}	2.702 ± 0.25^{aA}	2.361 ± 0.23^{bA}	5.337 ± 0.25	0.221 ± 0.07
DCM	$13.150 \pm 0.49^{bA**}$	$4.294 \pm 0.19^{aA*}$	$3.926 \pm 0.14^{bA**}$	$3.472 \pm 0.10^{cB*}$	4.010 ± 0.04	6.558 ± 2.61
Acetone	$6.480 \pm 1.33^{aA**}$	$3.948 \pm 0.19^{aA*}$	$2.520 \pm 0.22^{aA**}$	$1.368 \pm 0.09^{aA*}$	7.451 ± 1.67	11.059 ± 0.58
Hexane	$11.500 \pm 0.51^{bA*}$	$17.057 \pm 0.67^{cA**}$	$2.780 \pm 0.48^{aA*}$	$8.832 \pm 0.06^{dC**}$	$3.551 \pm 0.08^{dA*}$	$0.791 \pm 0.01^{dA**}$
5 days						
95% Ethanol	6.110 ± 0.72^{bA}	6.564 ± 0.27^{bA}	$4.118 \pm 0.13^{bcB**}$	$2.307 \pm 0.09^{aA*}$	7.037 ± 0.16	8.910 ± 0.10
DCM	$15.066 \pm 2.07^{cA**}$	$8.940 \pm 0.94^{cB*}$	3.980 ± 0.48^{bA}	3.602 ± 0.66^{bB}	6.188 ± 0.24	1.539 ± 0.03
Acetone	$3.665 \pm 0.26^{aA*}$	$5.146 \pm 0.73^{aB**}$	$2.771 \pm 0.28^{aBC**}$	$1.966 \pm 0.14^{aB*}$	13.048 ± 2.40	13.578 ± 0.38
Hexane	$11.940 \pm 1.02^{dA*}$	$19.717 \pm 0.09^{dB**}$	$4.554 \pm 0.07^{cB*}$	$7.553 \pm 0.37^{cB**}$	0.749 ± 0.01^{dB}	0.733 ± 0.02^{dB}
7 days						
95% Ethanol	$6.645 \pm 0.09^{bA*}$	$9.457 \pm 1.11^{bB**}$	$5.707 \pm 0.58^{bC**}$	$3.731 \pm 0.15^{cB*}$	6.645 ± 0.23	3.888 ± 0.03
DCM	$15.743 \pm 1.50^{dA*}$	$7.083 \pm 1.38^{aB*}$	$11.880 \pm 0.43^{cB**}$	$2.039 \pm 0.19^{aA*}$	5.055 ± 0.10	8.344 ± 0.10
Acetone	$3.653 \pm 0.405^{aA*}$	$5.645 \pm 0.69^{aB**}$	$3.224 \pm 0.21^{aC**}$	$2.836 \pm 0.07^{bC*}$	11.872 ± 0.62	16.772 ± 0.27
Hexane	$12.187 \pm 0.42^{cA*}$	$20.317 \pm 0.65^{cB**}$	$6.126 \pm 0.31^{bC**}$	$2.956 \pm 0.25^{bA*}$	$5.060 \pm 0.13^{dC**}$	$0.741 \pm 0.06^{dB*}$
Hydrodistillation Essential oil	6.232 ± 0.55	5.993 ± 0.12	2.293 ± 0.24	2.623 ± 0.14	11.695 ± 4.91	5.610 ± 3.72
VitC	5.455 ± 0.42		1.558 ± 0.29			

Values are expressed as mean ± SD (n = 3).

Different lowercase letters (a–d) within the same column indicate significant differences among solvents at the same extraction time and condition, determined by one-way ANOVA followed by Duncan's multiple range test ($p < 0.05$).

Different uppercase letters (A–C) within the same row indicate significant differences among extraction times for the same solvent and condition, determined by Duncan's test ($p < 0.05$).

* and ** indicate significant differences between fresh and dried leaves within the same solvent and extraction time, determined by an independent-samples t-test ($p < 0.05$).

In the FRAP assay, antioxidant activity was evaluated based on the ability of extracts to reduce Fe^{3+}–TPTZ to Fe^{2+}–TPTZ, reflecting their electron-donating capacity [16]. Quantification was performed using a ferrous sulfate ($FeSO_4$) standard calibration curve. The calibration curve exhibited excellent linearity over the tested concentration range (R^2 = 0.9997), confirming the analytical reliability of FRAP measurements and supporting the validity of the FRAP values reported in Table 3 (Figure 3). Consistent with the DPPH and ABTS results, acetone extracts demonstrated the highest reducing power among all solvent systems. The strongest FRAP activity was observed in dried leaves extracted with acetone for 7 days (16.772 ± 0.27 mM $FeSO_4$ equivalent/mg extract) and in fresh leaves extracted with acetone for 5 days (13.048 ± 2.40 mM $FeSO_4$ equivalent/mg extract). These results indicate that acetone efficiently extracts phenolic compounds with strong reducing capacity, particularly high–molecular-weight polyphenols and flavonoids capable of electron donation. The superior performance of acetone can be attributed to its intermediate polarity, which allows efficient solubilization of both polar and semi-polar antioxidant compounds. This observation is consistent with previous reports by Benzie and Strain [16] and Dai and Mumper [10], who demonstrated that acetone or aqueous acetone systems are particularly effective for extracting polyphenols and proanthocyanidins with high reducing power from various plant materials. When comparing fresh and dried leaves, antioxidant activity exhibited solvent- and assay-dependent variations. In general, fresh leaf extracts showed stronger radical scavenging activity (lower IC_{50} values) in DPPH and ABTS assays, whereas dried leaf extracts occasionally exhibited higher FRAP values. This discrepancy reflects the different chemical principles underlying each assay. While DPPH and ABTS primarily measure free radical scavenging ability, FRAP reflects total reducing capacity, which may be influenced by the concentration of stable phenolic polymers formed or concentrated during drying [16, 21]. Extraction time had a limited positive effect on antioxidant activity. In most cases, extending maceration from 3 to 7 days did not significantly enhance antioxidant performance and, in some cases, reduced activity. This suggests that equilibrium between solute diffusion and solvent saturation was reached at earlier extraction times, and prolonged maceration may promote oxidative degradation of bioactive compounds [13, 15].

Overall, the antioxidant activities determined by DPPH, ABTS, and FRAP assays showed a clear association with the total phenolic content (TPC) and total flavonoid content (TFC) of the extracts. Extracts exhibiting higher TPC and TFC values generally demonstrated stronger antioxidant activities, as evidenced by lower IC_{50} values in the DPPH and ABTS assays and higher reducing power in the FRAP assay. This trend was particularly evident in acetone and DCM extracts, which consistently showed both elevated phenolic/flavonoid contents and enhanced antioxidant performance. These observations support the well-established role of phenolic acids and flavonoids as major contributors to antioxidant activity, owing to their capacity to donate electrons or hydrogen atoms and stabilize free radicals. Similar relationships between phenolic content and antioxidant capacity have been widely reported in plant extracts, indicating that variations in antioxidant activity are closely linked to qualitative and quantitative differences in phenolic composition rather than extraction yield alone [10,16]. Although formal correlation analysis and chromatographic fingerprinting techniques (e.g., TLC or HPLC) were not performed, the consistent solvent- and time-dependent trends observed across TPC, TFC, and antioxidant assays suggest qualitative differences in phenolic composition among extracts and support a positive association between phenolic/flavonoid content and antioxidant activity in *Piper betle* leaf extracts [10,16]. Collectively, these results demonstrate that antioxidant activity in *Piper betle* leaf extracts is governed by a complex interplay between solvent polarity, extraction time, and the chemical nature of the extracted phytochemicals.

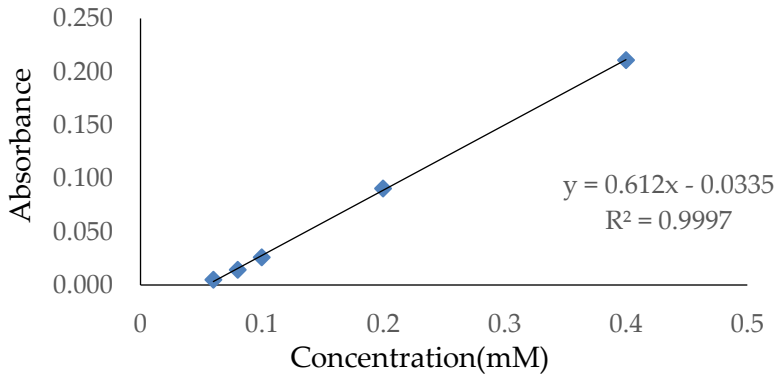


Figure 3. Standard calibration curve of ferrous sulfate

Analysis of variance (ANOVA) was performed to evaluate the effects of four experimental factors—assay type, solvent type, extraction time, and leaf condition—on the antioxidant activity of *Piper betle* leaf extracts. The ANOVA results are summarized in Table 7.

Table 7. Analysis of variance (ANOVA) of factors affecting antioxidant activities of *Piper betle* leaf extracts

Source	DF	AdjSS	AdjMS	F-Value	P-Value
Model	71	4733.41	66.668	152.08	0.000
Linear	8	1432.93	179.117	408.61	0.000
Assays	2	1103.99	551.994	1259.23	0.000
Solvent	3	227.16	75.721	172.74	0.000
Time	2	97.64	48.818	111.37	0.000
Leaf condition	1	4.15	4.145	9.46	0.003

As shown in Table 7, the overall model was statistically significant ($p < 0.001$), indicating that the selected factors collectively influenced antioxidant activity. Among the main effects, assay type (DPPH, ABTS, and FRAP) had the strongest influence on antioxidant values ($F = 1259.23$, $p < 0.001$), reflecting the distinct chemical mechanisms underlying each assay. Solvent type (ethanol, DCM, acetone, and hexane) also had a significant effect ($F = 172.74$, $p < 0.001$), confirming that solvent polarity plays a critical role in extracting antioxidant-active compounds. In addition, extraction time (3, 5, and 7 days) significantly affected antioxidant activity ($F = 111.37$, $p < 0.001$), suggesting time-dependent changes in the recovery or stability of bioactive compounds. Although to a lesser extent, leaf condition (fresh vs. dried leaves) also showed a statistically significant influence ($F = 9.46$, $p = 0.003$), indicating that post-harvest processing affects antioxidant-related properties. Overall, the ANOVA results demonstrate that antioxidant activity in *Piper betle* leaf extracts is significantly governed by assay methodology, solvent selection, extraction duration, and leaf condition, supporting the solvent- and time-dependent trends observed in the experimental data. Following the observed significant differences in antioxidant activities and phytochemical contents among solvents and extraction times as revealed by ANOVA, Pearson's correlation analysis was performed using dried leaf extracts to minimize variability associated with moisture content and to elucidate better the relationships between total phenolic/flavonoid contents and antioxidant activities.

Table 8. Pearson's correlation coefficients between total phenolic/flavonoid contents and antioxidant activities of dried betel leaf extracts.

Parameter	DPPH IC_{50}	ABTS IC_{50}	FRAP
TFC	−0.53	−0.61*	0.40
TPC	−0.50	−0.44	**0.59***

*P< 0.05

Pearson's correlation analysis of dried leaf extracts (n = 12) revealed a significant positive correlation between total phenolic content (TPC) and FRAP values ($r = 0.59$, $p < 0.05$), indicating that phenolic compounds contribute to the reducing power of the extracts. In addition, total flavonoid content (TFC) showed a significant negative correlation with ABTS IC_{50} values ($r = -0.61$, $p < 0.05$), highlighting the role of flavonoids in radical scavenging activity.

4. Conclusions

This study systematically evaluated the effects of solvent polarity, extraction duration, and leaf condition on the recovery of phenolic and flavonoid compounds and their associated antioxidant activities in *Piper betle* leaves. Among the solvents tested, acetone consistently exhibited the highest extraction performance, particularly for fresh leaves, yielding the maximum total phenolic content (1,222.42 ± 24.27 mg GAE/g extract) and total flavonoid content (51.70 ± 15.51 mg QE/g extract) at 3 days of maceration, which also corresponded to strong antioxidant activities across DPPH, ABTS, and FRAP assays. In contrast, hexane extracts showed the lowest extraction yields, phenolic and flavonoid contents, and antioxidant activities under all conditions, confirming that non-polar solvents are unsuitable for the recovery of phenolic-rich antioxidant compounds from *P. betle* leaves. Dried leaves generally produced higher extraction yields, especially with ethanol, whereas fresh leaves favored higher flavonoid recovery and radical scavenging capacity, indicating that leaf pretreatment significantly influences extraction outcomes depending on the targeted phytochemical class. Statistical analysis (ANOVA) confirmed that solvent type was the most influential factor affecting extraction yield, TPC, TFC, and antioxidant activity ($p < 0.05$), followed by leaf condition, while extraction time beyond 3 days provided no substantial improvement and, in some cases, resulted in reduced bioactivity, likely due to oxidative degradation of phenolic compounds during prolonged maceration. Correlation analysis further supported these findings by demonstrating that phenolic and flavonoid contents were significantly associated with the antioxidant activities of dried betel leaf extracts, particularly reducing power and radical scavenging capacity. Therefore, a medium-polarity solvent (acetone) combined with short maceration time (3 days) represents the optimal extraction condition for maximizing phenolic- and flavonoid-associated antioxidant properties of *P. betle* leaves under the investigated conditions. The main limitations of this study include the use of maceration as the sole extraction technique, a limited solvent range, and the absence of compound-specific profiling. In addition, moisture content was not quantified during the comparison of fresh and dried leaves. Nevertheless, this study provides statistically supported and condition-specific evidence that medium-polarity solvents are most effective for extracting antioxidant-active phytochemicals from *P. betle* leaves and offers a solid foundation for future optimization using application-safe solvent systems and advanced extraction or analytical techniques.

5. Acknowledgements

The research team would like to express sincere gratitude to the university and academic support units, as well as to researchers, students, and all stakeholders who contributed to the implementation, monitoring, and successful completion of this research project.

The research team would like to acknowledge Mr. Surasit Udomwate, President of the Laksong Subdistrict Administrative Organization, Ban Phaeo District, Samut Sakhon Province, as well as the betel farmers, for their kind cooperation in providing valuable information, supporting the project's activities, and sharing local knowledge throughout the course of the study.

The research team sincerely hopes that the findings of this study will be beneficial to betel farmers and can be further developed for industrial applications in the future.

Author Contributions: In this article, the following fields of work were carried by: Conceptualization, Nattawoot Rattanathamwat and Atchara Kaewnoi.; methodology, Nattawoot Rattanathamwat and Supharat Duanyai and Korakoj Pethassanayothin.; validation, Pasit Tinnam and Piya Rontlaong.; formal analysis, Nattawoot Rattanathamwat and Atchara Kaewnoi.; investigation, Julalak Jarujutarat and Janyawan Janyatham.; resources, Wachirasak Kienwong. ; data curation, Piya Rontlaong.; writing—original draft

preparation, Nattawoot Rattanathamwat and Supharat Duanyai.; writing—review and editing, Nattawoot Rattanathamwat and Supharat Duanyai.; project administration, Wachirasak Kienwong and Nattawoot Rattanathamwat.; funding acquisition, Wachirasak Kienwong and Nattawoot Rattanathamwat. In addition, all authors have read and agreed to the published version of the manuscript.

Funding: This research was funded by the National Science, Research, and Innovation Fund (NSRF), Fundamental Fund, Fiscal Year 2025.

Conflicts of Interest: The authors declare that they have no conflicts of interest.

References

[1] Pelczar, M. J.; Chan, E. C. S.; Krieg, N. R. *Microbiology: Concepts and Applications*; McGraw-Hill: New York, 1993.

[2] Akter, K. N.; Karmakar, P.; Das, A.; Anonma, S. N.; Shoma, S. A.; Sattar, N. M. Evaluation of antibacterial and anthelmintic activities with total phenolic contents of *Piper betle* leaves. *Avicenna J. Phytomed.* **2013**, *4*(5), 320–329. https://doi.org/10.22038/ajp.2014.2483

[3] Parkpoom, T.; Chuntree, K.; Komutiban, O. Antimicrobial and antioxidant capacity of leaf extract of *Piper betle* L. for development to cosmetics; Faculty of Science and Technology, Suan Dusit University: Bangkok, 2020.

[4] Borges, A.; Abreu, A. C.; Ferreira, C.; Saavedra, M. J.; Simões, M. Comparison of techniques and solvents on the antimicrobial and antioxidant potential of *Olea europaea* and *Acacia dealbata* extracts. *Microorganisms* **2020**, *8*(4), 595. https://doi.org/10.3390/microorganisms8040595

[5] El Mannoubi, I.; Ben Ali, Y.; Ben Hmida, S.; M'Hamdi, M.; Ben Salem, R. Impact of different solvents on extraction yield, phenolic and flavonoid contents, and antioxidant activities of *Opuntia stricta* fruit. *Bull. Natl. Res. Cent.* **2023**, *47*, 31. https://doi.org/10.1186/s42269-023-00991-3

[6] Chatepa, L. E. C.; Banda, E. L.; Tembo, Y.; Malunga, E.; Gondwe, T.; Gondwe, E.; Mbewe, A. R. Effects of solvent extraction on the phytoconstituents and antioxidant activities of *Azadirachta indica* and *Vernonia amygdalina*. *Heliyon* **2024**, *10*(10), e30242. https://doi.org/10.1016/j.heliyon.2024.e30242

[7] Banik, A.; Zerin, T.; Sultana, R. Comparative phytochemical and antibacterial properties of *Piper betle* leaf extracts from Barguna and Moheshkhali, Bangladesh. *Iran. J. Med. Microbiol.* **2020**, *14*(2), 125–132. https://doi.org/10.30699/ijmm.14.2.125

[8] Venugopalan, S.; Sharma, A.; Venugopalan, V.; Gautam, H. Comparative study on the antioxidant activities of different solvent extracts from *Piper betle* leaves. *Biomed. Pharmacol. J.* **2015**, *8*(1), 49–56.

[9] Nouri, L.; Nafici, M.; Mehrbod, P. Phytochemical, antioxidant, antibacterial, and α-amylase inhibitory activities of betel leaf extracts: Effect of ethanol vs methanol. *Ind. Crops Prod.* **2014**, *62*, 901–907. https://doi.org/10.1016/j.indcrop.2014.09.020

[10] Dai, J.; Mumper, R. J. Plant phenolics: Extraction, analysis and their antioxidant and anticancer properties. *Molecules* **2010**, *15*(10), 7313–7352. https://doi.org/10.3390/molecules15107313

[11] Do, Q. D.; Angkawijaya, A. E.; Tran-Nguyen, P. L.; Huynh, L. H.; Soetaredjo, F. E.; Ismadji, S.; Ju, Y. H. Effect of extraction solvent on total phenol content, total flavonoid content, and antioxidant activity of *Limnophila aromatica*. *J. Food Drug Anal.* **2014**, *22*(3), 296–302. https://doi.org/10.1016/j.jfda.2013.11.001

[12] Damijanić, K.; Đermić, E.; Poljuha, D.; Sladonja, B. Effects of maceration duration on the phenolic composition and antioxidant capacity of 'Teran' (*Vitis vinifera* L.) wine. *Agric. Conspectus Sci.* **2012**, *77*(2), 103–107.

[13] Alam, M. B.; Park, N. H.; Song, B. R.; Lee, S. H. Antioxidant potential-rich betel leaves (*Piper betle* L.) exert depigmenting action by triggering autophagy and downregulating MITF/tyrosinase in vitro and in vivo. *Antioxidants* **2023**, *12*(2), 374. https://doi.org/10.3390/antiox12020374

[14] Sarma, C.; Rasane, P.; Kaur, S.; Singh, J.; Singh, J.; Gat, Y.; Garba, U.; Kaur, D.; Dhawan, K. Antioxidant and antimicrobial potential of selected varieties of *Piper betle* L. (betel leaf). *An. Acad. Bras. Cienc.* **2018**, *90*(4), 3871–3878. https://doi.org/10.1590/0001-3765201820170746

[15] Laloo, N.; Terblanche, U.; Ssemakalu, C. C.; Pillay, M. Optimizing the extraction of phenolic compounds and antioxidant activity of *Carpobrotus edulis* (L.) L. Bolus using response surface methodology. *Sci. Rep.* **2024**, *14*, 2187. https://doi.org/10.1038/s41598-024-52187-7

[16] Benzie, I. F. F.; Strain, J. J. The ferric reducing ability of plasma (FRAP) as a measure of "antioxidant power": The FRAP assay. *Anal. Biochem.* **1996**, *239*(1), 70–76. https://doi.org/10.1006/abio.1996.0292

[17] Naczk, M.; Shahidi, F. Extraction and analysis of phenolics in food. *J. Chromatogr. A* **2004**, *1054*(1–2), 95–111. https://doi.org/10.1016/j.chroma.2004.08.059

[18] Singleton, V. L.; Rossi, J. A. Colorimetry of total phenolics with phosphomolybdic–phosphotungstic acid reagents. *Am. J. Enol. Vitic.* **1965**, *16*(3), 144–158.

[19] Chang, C. C.; Yang, M. H.; Wen, H. M.; Chern, J. C. Estimation of total flavonoid content in propolis by two complementary colorimetric methods. *J. Food Drug Anal.* **2002**, *10*(3), 178–182. https://doi.org/10.38212/2224-6614.2748

[20] Brand-Williams, W.; Cuvelier, M. E.; Berset, C. Use of a free radical method to evaluate antioxidant activity. *LWT—Food Sci. Technol.* **1995**, *28*(1), 25–30. https://doi.org/10.1016/S0023-6438(95)80008-5.

[21] Re, R.; Pellegrini, N.; Proteggente, A.; Pannala, A.; Yang, M.; Rice-Evans, C. Antioxidant activity applying an improved ABTS radical cation decolorization assay. *Free Radical Biol. Med.* **1999**, *26*(9–10), 1231–1237. https://doi.org/10.1016/S0891-5849(98)00315-3

[22] Barros, L.; Carvalho, A. M.; Ferreira, I. C. F. Antioxidant activity and total phenolic content of different extracts from *Rosa canina* L. fruits. *Food Chem. Toxicol.* **2011**, *49*(2), 423–426. https://doi.org/10.1016/j.fct.2010.11.008

[23] Singh, A.; Kumar, R.; Kumar, S.; Giri, S. S. Investigation of antioxidant and antimicrobial activities of various extracts of *Piper betle* L. leaves. *Food Chem. Adv.* **2023**, *3*, 100536. https://doi.org/10.1016/j.focha.2023.100536

[24] Everette, J. D.; Bryant, Q. M.; Green, A. M.; Abbey, Y. A.; Wangila, G. W.; Walker, R. B. A thorough study of reactive species, reaction capacities, and physical parameters of 10 common antioxidant assays. *J. Agric. Food Chem.* **2010**, *58* (14), 8139–8144. https://doi.org/10.1021/jf100825p

[25] Sundang, M.; Hussain, M. S.; Kuntadi, S. A.; Pin, C. H. Antioxidant activity, total phenolic and total flavonoid content of *Piper betle* L. leaves from different locations in Malaysia. *Malays. J. Fundam. Appl. Sci.* **2012**, *8*(1), 1–6. https://doi.org/10.11113/mjfas.v8n1.115

ASEAN
Journal of Scientific and Technological Reports
Online ISSN:2773-8752

Research article

Process Optimization and Quality Characteristics of Sheet-Type Puffed Rice from Glutinous and Pathum Thani Rice Flour

Pracha Bunyawanichakul[1], Krissadang Sookramoon[2*], and Manunya Khamwachirapitak[3]

[1] Faculty of Engineering, Srinakharinwirot University, Nakhon Nayok, 26120, Thailand
[2] Faculty of Industrial Technology, Valaya Alongkorn Rajabhat University under the Royal Patronage, Pathum Thani, 13180, Thailand
[3] Faculty of Science and Technology, Valaya Alongkorn Rajabhat University under the Royal Patronage, Pathum Thani, Thailand
* Correspondence: krissadang.sook@vru.ac.th

Citation:
Bunyawanichakul, P.; Sookramoon, K.; Khamwachirapitak, M. Process optimization and quality characteristics of sheet-type puffed rice from glutinous and Pahum Thain rice flour *ASEAN J. Sci. Tech. Report.* **2026**, *26*(5), e262055. https://doi.org/10.55164/ajstr.v26i5.262055

Article history:
Received: October 24, 2025
Revised: February 19, 2026
Accepted: March 11, 2026
Available online: April 27, 2026

Publisher's Note:
This article is published and distributed under the terms of the Thaksin University.

Abstract: This study evaluated the effects of formulation ratio (glutinous rice: Pathum Thani rice flour) under controlled moisture conditioning (13–19% w.b.) on the physical, physicochemical, and mechanical properties of sheet-type puffed rice produced using a dual-head puffing machine. The investigated parameters included expansion ratio, color (L*, a*, b*), moisture content, water activity (aw), hardness, adhesiveness, and fracturability. Statistical analysis revealed that formulation ratio significantly affected hardness ($p < 0.05$), whereas no significant differences were observed in expansion ratio, color, moisture content, or water activity between treatments ($p > 0.05$). Formula S1 (40:60) exhibited higher hardness (28.52 N) and minimal adhesiveness and fracturability, while S2 (50:50) produced a softer product (20.49 N) with greater variability in fracturability. Both formulations showed comparable expansion ratios (3.85 for S1 and 3.93 for S2) and low water activity values (0.243–0.268 for S1 and 0.243–0.251 for S2). These results indicate that formulation ratio plays a critical role in determining the mechanical properties of sheet-type puffed rice and may be adjusted to achieve desired textural characteristics.

Keywords: Puffed rice; expansion ratio; puffing conditions

1. Introduction

Rice is one of the most important staple crops globally and plays a central role in food security, particularly in Asia. Beyond conventional consumption as cooked milled rice, increasing consumer demand for convenient, ready-to-eat, and value-added products has driven rapid development in rice-based processed foods. Among these, puffed rice products represent a promising category due to their low fat content, expanded structure, crisp texture, and long shelf stability.

Puffing is a thermo-mechanical process that involves rapid heating under pressure followed by sudden pressure release, leading to moisture vaporization and expansion of the starch matrix. The mechanism has been widely described in cereal systems and is comparable to popcorn popping, in which internal steam pressure exceeds structural resistance, leading to explosive expansion [8]. During puffing, starch gelatinization and subsequent structural setting determine final product texture and integrity.

Factors Influencing Puffing Performance

Previous studies have identified several key factors governing puffing quality, including moisture content, temperature, processing time, and raw material composition. Moisture content is considered one of the most critical parameters. Insufficient moisture limits steam generation and reduces expansion, while excessive moisture may prevent complete structural setting [3]. Optimal moisture levels vary depending on rice variety and processing conditions. Temperature and heating duration significantly affect the expansion ratio and mechanical properties. Higher temperatures generally promote greater expansion due to increased vapor pressure, but excessive heating may cause structural collapse or over-browning. The balance between heat transfer and moisture diffusion is therefore essential. Rice composition and starch characteristics also play a fundamental role. Amylose content influences gel formation, rigidity, and expansion potential [16]. Variations in starch structure and flour composition can alter mechanical resistance and textural outcomes in puffed cereal products [19].

Mechanical and Quality Evaluation of Puffed Products

Product quality in puffed cereals is typically assessed using expansion ratio, color parameters, moisture content, water activity (aw), and mechanical properties such as hardness and fracturability. Texture profile analysis (TPA) provides a quantitative measurement of structural strength and crispness. Water activity is particularly important for predicting microbiological stability and shelf-life potential, with values below 0.6 generally considered safe for dry snack products.

Recent advances in extrusion and thermo-mechanical processing have emphasized the relationship between formulation variables and structural properties of expanded snacks. However, most studies focus on extrusion systems, while limited research has addressed sheet-type puffed rice produced using mold-based or dual-head puffing machines.

Research Gap

Despite extensive literature on cereal extrusion and rice puffing mechanisms, there is limited information regarding:

- The combined effect of glutinous rice and rice flour formulations on sheet-type puffed rice structure
- Mechanical property differentiation between formulation ratios
- Quality evaluation under controlled dual-head puffing systems
- Optimization of formulation for structural integrity versus softness preference

Furthermore, few studies have systematically evaluated mechanical properties (hardness, adhesiveness, fracturability) alongside physicochemical parameters in Thai rice varieties.

Processed Rice in Thailand – Value Addition from Key Agricultural Commodities

Thailand, as one of the world's major producers and exporters of rice, maintains a deep-rooted connection with rice across multiple dimensions—not only as a dietary staple that sustains its population but also as a foundation of its economy, society, and culture. However, amid global changes, evolving consumer behavior, and rising demand for convenient, value-added products, rice processing has become increasingly important in Thailand. Where once rice consumption was mostly in the form of cooked milled rice, the modern rice-processing industry in Thailand has advanced rapidly. Rice is now used as a raw material in the production of a wide range of products that cater to diverse consumer needs, including ready-to-eat foods, snacks, beverages, and even non-food items. Processing not only extends shelf life and enhances convenience but also adds significant value to the nation's primary agricultural outputs, creating business opportunities and strengthening the economy as a whole. Continuous research and development in rice processing technology is therefore essential to improve the competitiveness of Thailand's rice industry in global markets, while also supporting the development of high-quality, innovative products that meet changing consumer demands and promote efficient, sustainable use of resources. This article explores the current state of Thailand's processed rice industry, its potential, challenges, and future development directions.

Puffed Rice Products – An Innovative Application of Rice Processing

Puffed rice is a product derived from rice processing, produced by applying heat under high pressure, which causes the rice kernels to expand and bind together without the need for additional ingredients. The resulting product is typically flat, airy, crispy, and low in calories, which has contributed to its popularity in countries such as the United States, Japan, India, and Australia [1]. The puffing mechanism described by Hsieh and Luh is based on the rapid expansion of steam within the voids of the rice grain [2]. Under heat and pressure, the rice cooks and its internal moisture vaporizes. When pressure is suddenly released, rapid steam expansion forces the rice to expand according to the mold shape, producing a crispy texture. Several factors, including initial moisture content, temperature, and heating time, influence puffing performance. Rice with insufficient moisture exhibits poor puffing characteristics [3]. An optimal temperature range of 200–270 °C has been suggested, with higher temperatures generally promoting greater expansion [4]. Experimental evaluation at 200–230 °C demonstrated that 230 °C produced superior puffing performance [1]. Extended heating duration may also enhance moisture absorption and puffing quality [1], [5], [6]. Puffing quality is commonly evaluated using puffing ability and expansion ratio.

Puffing Methods in Thailand

In Thailand, traditional puffed rice products are produced by roasting rice with hot sand (khao tok) or deep-frying (khao tan). However, deep-frying increases fat content and may accelerate rancidity during storage [7], making it less suitable for health-conscious consumers. Consequently, sheet-type ready-to-eat puffed rice products have emerged as a promising alternative. Puffed rice is generally produced through high temperature and pressure, leading to starch gelatinization and steam-induced expansion within the grain [3, 8]. Several studies have examined factors affecting puffing performance, including rice variety, grain moisture content, heating temperature, and puffing method [9-11]. The popcorn popping mechanism described by Hoseney et al. shares similarities with rice puffing, where internal moisture vaporization generates pressure that results in explosive expansion upon release [8]. Moisture content is a critical variable; insufficient moisture reduces puffing efficiency [3]. Moraru and Kokini emphasized the importance of nucleation and expansion dynamics during extrusion and microwave processing, highlighting the roles of moisture and temperature control [12]. Microwave-assisted puffing has also been investigated and shown to influence puff quality and texture [13-14]. Grain type and starch composition significantly affect puffing behavior. Amylose content influences texture and expansion potential [15-16]. Varietal differences contribute to variations in cooking and textural properties [17]. Extrusion cooking modifies carbohydrate structures, thereby affecting puffability [18]. Physical properties such as hardness, expansion volume, and surface color are widely used as quality indicators in puffed cereal products [19-20]. Puffing alters the ultrastructure of cereal grains, influencing texture and expansion performance [19]. Grain physical characteristics further distinguish between good and poor expansion outcomes [11]. Nutritional aspects of puffed rice products have also been emphasized. Whole-grain labeling and its associated health implications have been highlighted in previous studies [22-23]. Standard analytical methods, such as those provided by AOAC, are commonly used to ensure consistent quality measurement in puffed grain research [24]. Collectively, these studies provide foundational knowledge on puffing mechanisms, influencing parameters, and evaluation techniques. The integration of moisture content, temperature, rice variety, and textural assessment is essential for optimizing modern puffing technologies, including the dual-head puffing system applied in the present study.

Therefore, this study aimed to evaluate the effect of formulation ratio (glutinous rice: Pathum Thani rice flour) under controlled moisture conditioning (13–19% w.b) on the physical, physicochemical, and mechanical properties of sheet-type puffed rice produced using a dual-head puffing machine. The study focused on expansion ratio, color (L*, a*, b*), moisture content, water activity, hardness, adhesiveness, and fracturability to identify the formulation that provides optimal structural stability and desirable texture characteristics. Based on the machine developed in this study, the typical puffed rice production process consists of six main steps. First, rice preparation involves selecting the desired variety (Pathum Thani 1) and adjusting its moisture content to 13–19% (wet basis) by adding a calculated amount of water, followed by storing the rice at 4°C for 24 hours in a sealed container to ensure uniform moisture distribution. Next, during machine setup, the puffing machine is powered on, with mold temperatures set between 220–240°C and

heating duration adjusted to 3–7 seconds. In the molding and heating stage, approximately 5 grams of prepared rice is placed into the lower mold, and the upper mold is closed to create a sealed chamber. During puffing, the rice undergoes rapid internal steam pressure buildup, leading to gelatinization; when the mold is suddenly opened, the quick pressure drop causes the steam to escape instantly, expanding the rice and bonding it into a sheet. Then, in the product removal step, the puffed rice sheet is carefully removed from the mold. Finally, quality evaluation is conducted to assess product characteristics such as size, volume, expansion ratio, color, and texture to ensure consistent product quality.

2. Methodology

Materials and Methods

2.1 Experimental Design

A completely randomized design (CRD) was employed to evaluate the effects of formulation ratio and initial moisture content on the physical and mechanical properties of sheet-type puffed rice.

Two formulation ratios of glutinous rice to Pathum Thani rice flour were investigated:

- S1 (40:60, w/w)
- S2 (50:50, w/w)

The initial moisture content (13–19% w.b.) was adjusted during preliminary trials to ensure adequate puffing performance. In the main experiment, moisture content was standardized prior to puffing to eliminate it as a confounding variable. Each treatment was independently produced under identical processing conditions (220 °C for 75 s). The selected processing condition (220 °C for 75 s) was determined based on preliminary trials and literature suggesting optimal puffing performance within 200–240 °C [4, 11]. Physicochemical analyses (moisture content, water activity, and color) were conducted in triplicate (n = 3), while mechanical properties were measured using ten replicates per formulation (n = 10). Sample size was selected based on previous puffed cereal studies [19, 21]. Statistical comparisons between S1 and S2 were performed using an independent samples t-test at a significance level of $p < 0.05$. Temperatures below 200 °C resulted in insufficient expansion, while temperatures above 240 °C caused surface over-browning and structural collapse during pilot testing. A heating duration of 75 s was found sufficient to achieve complete starch gelatinization and internal steam pressure development without excessive moisture loss. The sample mass (4 g per sheet) was standardized to ensure uniform heat transfer and consistent mold filling, minimizing variability in expansion and mechanical measurements. These controlled parameters were maintained throughout the experiment to isolate the effect of formulation ratio and ensure reproducibility of results.

2.2 Raw Materials and Sample Preparation

Glutinous rice (Khao Niao Khiao Ngu) was soaked in hot water at a 1:4 (rice:water, w/v) ratio in a sealed container at room temperature for 4 h to ensure uniform hydration. The soaked rice was drained for 10 min before mixing. Hom Pathum Thani 1 rice flour (60-mesh particle size, 20% w.b. moisture content) was blended with the hydrated glutinous rice according to the designated formulation ratios (S1 or S2). Vegetable oil was incorporated as a binding agent. The mixture was manually homogenized and allowed to rest for 10 min to stabilize moisture distribution before molding.

2.3 Puffed Rice Production

Approximately 4 g of the prepared mixture was weighed using a digital balance (±0.01 g accuracy) and placed into a dual-head puffing machine. Puffing was conducted at 220 °C for 75 s. During processing, the mixture was subjected to high temperature and pressure within a closed mold. Upon sudden mold opening, rapid steam expansion led to the formation of sheet-like puffed rice. All samples were cooled to room temperature before quality analysis.

2.4 Physical Characterization

2.4.1 Dimensional Measurements

The width and thickness of the puffed rice sheets were measured using a digital Vernier caliper (±0.01 mm). Ten samples per formulation were analyzed.

2.4.2 Weight and Volume

Individual sheet weight was recorded using a digital balance (±0.01 g). Volume was determined using the displacement method described by Sharma (2012). The expansion ratio was calculated as the ratio of the puffed volume to the initial sample volume.

2.5 Color Measurement

Surface color was measured using a Konica Minolta CR-400 colorimeter (Japan). Results were expressed in CIE L*, a*, and b* coordinates:

- L* (lightness: 0 = black, 100 = white)
- a* (− = green, + = red)
- b* (− = blue, + = yellow)

Five measurements were taken per formulation and averaged.

2.6 Moisture Content

Moisture content was determined using an infrared moisture analyzer (Sartorius MA 35, Germany) at 130 °C until constant weight was achieved. Results were expressed as percentage wet basis (% w.b.). Three replicates were performed per formulation.

2.7 Water Activity (aw)

Water activity was measured using a Novasina LabSwift-aw meter (USA). Ground samples were placed in the measurement chamber and equilibrated until stable readings were obtained. Three replicates were conducted per formulation.

2.8 Mechanical Properties

Mechanical properties were analyzed using a Brookfield CT3 Texture Analyzer (USA).

A compression test was performed using a cylindrical probe (35 mm diameter). Test parameters were set as follows:

- Pre-test speed: 1.0 mm/min
- Test speed: 1.0 mm/min
- Post-test speed: 10.0 mm/s
- Compression distance: 5 mm or until fracture

The following parameters were recorded:

- Hardness (N)
- Adhesiveness (mJ)
- Fracturability (N)

Ten replicates were analyzed per formulation.



Texture analyzer



Colorimeter



Water activity a_w analyzer



Moisture analyzer

Figure 1. Texture analyzer, Colorimeter, Water activity aw, and Moisture analyzer.

3. Results and Discussion

3.1 Effect of Formulation on Mechanical Properties

The formulation ratio significantly influenced hardness ($p < 0.05$), whereas the expansion ratio, brightness (L*), and moisture content did not differ between S1 and S2 ($p > 0.05$). S1 exhibited significantly higher hardness (28.32 N) compared to S2 (18.48 N). The higher hardness in S1 may be attributed to the greater proportion of rice flour, which enhances structural rigidity by increasing starch matrix formation during puffing. Similar observations were reported by Zhang and Hoseney (1998), who noted that starch structure and composition significantly influence expansion and mechanical resistance in puffed cereal products. Although S2 demonstrated a slightly higher expansion ratio (3.96), the difference was not statistically

significant. This suggests that, within the tested formulation range, expansion was primarily governed by moisture-induced vapor pressure rather than compositional variation, consistent with the findings of Murugesan and Bhattacharya (1986).

3.2 Moisture Content and Water Activity

Both formulations showed low moisture content (~3.4%) and aw values between 0.243–0.268, which fall within the safe range for dry snack products (aw < 0.6). Low water activity limits microbial growth and enhances shelf stability (AOAC, 1990). Although S1 showed slightly lower aw values, the difference was not statistically significant. Therefore, the claim of improved shelf life should be interpreted cautiously and requires further microbial shelf-life testing for confirmation. The results from the development and performance testing of a semi-automatic dual-head puffed rice machine, which involved two key phases: testing the drying and puffing process under various conditions and evaluating the final product quality. Initial experiments conducted on July 19 and July 26, 2025, confirmed the machine's ability to reach target temperatures (up to 240∘C) and successfully puff rice using Formula 1 (75g rice: 25g rice bran starch: 2% oil at 220∘C for 45s) and Formula 2 (higher oil content at 240∘C for 60s). A subsequent test on August 10, 2025, using Formula 3 (70g broken rice: 30g rice flour: 4% oil at 240∘C) identified the optimal pressing time as around 60s, noting that deviation caused poor expansion or overbrowning. Further testing on August 23, 2025, comparing different sticky rice preparation methods, found that Formula 4.1 (soaked sticky rice, one round) was successful, while formulas with excessive water (4.2 and 4.3) resulted in soggy products. Finally, the test on September 7, 2025, comparing two sticky rice/Pathum Thani rice bran starch ratios, S1 (40:60) and S2 (50:50 at 220∘C for 75s), indicated that Formula S1 yielded the more desirable puffing characteristics, including dryness and structural integrity.

3.3 Quality Evaluation of Puffed Rice Products

On September 11, 2025, puffed rice samples from formulas S1 and S2 were evaluated for physical and textural properties using a texture analyzer (TA) on five replicates each. The analyses included color (L, a, b*), post-drying weight, moisture content, water activity (aw), hardness, adhesiveness, and fracturability. Formula S1 showed slightly higher brightness (L*) values and marginally higher moisture content (3.43–3.48%) compared to S2, with water activity ranging from 0.243–0.268 for S1 and 0.243–0.255 for S2. Both formulas had similar expansion ratios (3.87 for S1 and 3.96 for S2), indicating no significant difference. Regarding textural properties, S1 exhibited significantly greater hardness (average 28.32 N, peaking at 52.21 N), while S2 had a lower average hardness (18.48 N) with some samples reaching 31.70 N. No adhesiveness was observed in S1, whereas minor adhesiveness appeared in some S2 samples, especially samples 6 and 10. Fracturability was more pronounced in S2 samples, while S1 generally showed negligible or zero fracturability.

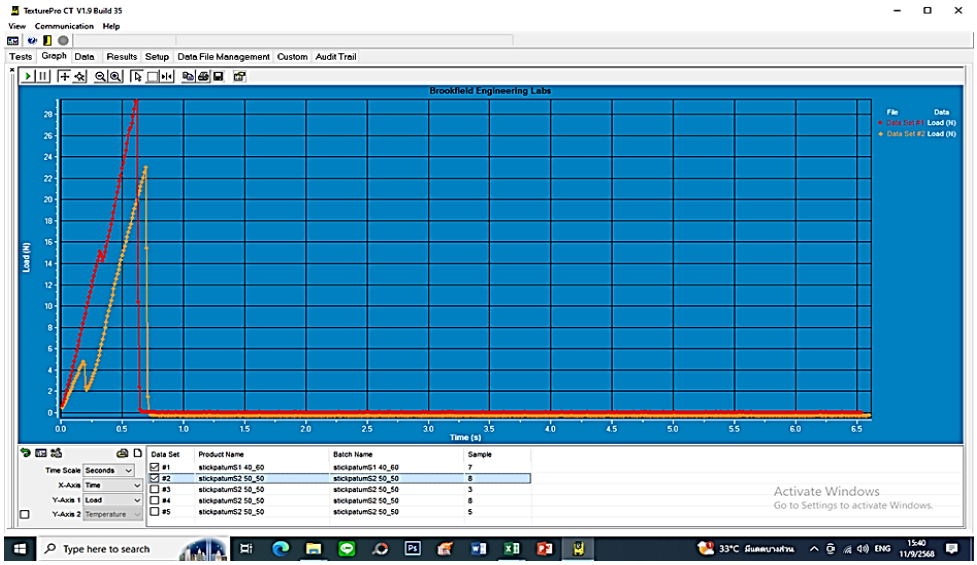


Figure 2. Texture Analyzer Results

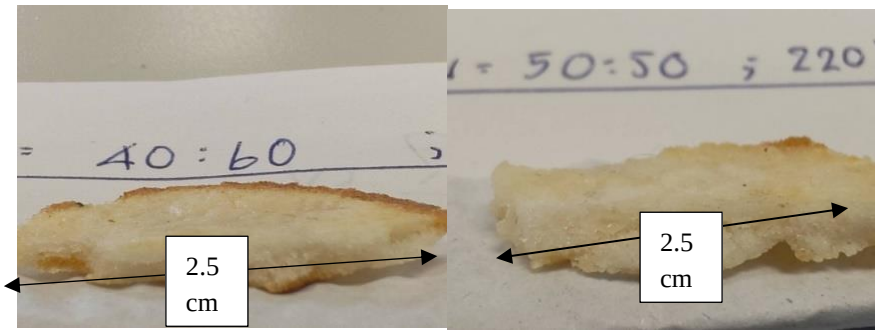


Figure 3. Close-up photographs of the puffed rice sheets were taken.

Table 1. Summary of Comparative Analysis

Test Parameter	S1 (40:60)	S2 (50:50)	Statistical Result (t-test)	Conclusion
Hardness (N)	28.52 ± 1.18[a]	20.49 ± 0.902[b]	Significant difference ($p < 0.05$)	S1 is significantly harder than S2
Expansion Ratio	3.85 ± 0.07[a]	3.93 ± 0.06[a]	No significant difference ($p > 0.05$)	Both formulas have similar expansion ratios
Brightness (L*)	73.87 ± 1.43[a]	72.79 ± 1.99[a]	No significant difference ($p > 0.05$)	Color brightness is not significantly different
Moisture (%)	3.52% ± 0.44[a]	3.51% ± 0.25[a]	No significant difference ($p > 0.05$)	Moisture levels are comparable

The results indicate that the formulation ratio significantly influenced the mechanical properties, particularly hardness. Formula S1 (40:60) exhibited significantly higher hardness (28.52 ± 1.18 N) compared to S2 (20.49 ± 0.902 N) ($p < 0.05$). This suggests that increasing the proportion of Pathum Thani rice flour improved the structural rigidity and compression resistance, resulting in a firmer puffed rice sheet. The relatively low standard deviation values also indicate good consistency within each formulation. In contrast, no significant differences were observed in expansion ratio, brightness (L*), or moisture content between formulations ($p > 0.05$). The expansion ratios were comparable (3.85 ± 0.07 for S1 and 3.93 ± 0.06 for S2), indicating that both formulations achieved similar puffing efficiency under the same processing conditions. The small standard deviations reflect uniform expansion behavior. Similarly, brightness values were statistically similar (73.87 ± 1.43 for S1 and 72.79 ± 1.99 for S2), suggesting that formulation ratio did not markedly influence surface color development during puffing. Moisture contents were nearly identical (3.52 ± 0.44% for S1 and 3.51 ± 0.25% for S2), confirming that drying and moisture distribution were consistent across treatments. Overall, these findings demonstrate that while formulation ratio strongly affects textural strength (hardness), it does not significantly alter expansion performance, color brightness, or final moisture level under the selected processing conditions. This indicates that texture can be tailored through formulation adjustment without compromising key physicochemical characteristics.

4. Conclusion

This study evaluated the performance of a semi-automatic dual-head puffing machine and investigated the effects of formulation ratio on the physicochemical and mechanical properties of sheet-type puffed rice. The results demonstrated that formulation ratio significantly influenced mechanical properties, particularly hardness ($p < 0.05$). Formula S1 (40:60, glutinous rice: Pathum Thani rice flour) produced significantly higher hardness values compared to S2 (50:50), indicating greater structural strength and resistance to breakage. In contrast, S2 yielded a softer product with higher variability in fracturability and slight adhesiveness in some samples. No significant differences were observed in expansion ratio, brightness (L*), or moisture content between formulations ($p > 0.05$). Both formulations exhibited low moisture content and water activity (<0.3),

typical of dry expanded snack products. The dual-head puffing system operated effectively under the selected processing conditions (220 °C for 75 s), producing uniform sheet-type puffed rice. The findings provide quantitative evidence that the formulation ratio plays a critical role in determining textural properties and can be adjusted to achieve desired product characteristics.

5. Acknowledgements

We are grateful to Valaya Alongkorn Rajabhat University under the Royal Patronage, Pathum Thani, for allowing the use of equipment for this research.

Author Contributions: The contributions of each author in this research are as follows: Conceptualization: Pracha Bunyawanichakul and Krissadang Sookramoon; Methodology: Pracha Bunyawanichakul and Krissadang Sookramoon; Laboratory Experiments: Krissadang Sookramoon and Manunya Khamwachirapitak; Writing—review and editing: Pracha Bunyawanichakul; Project administration: Krissadang Sookramoon.

Funding: This project was supported by Valaya Alongkorn Rajabhat University under the Royal Patronage, Pathum Thani Province (Contract number VRU-FF68/014).

Conflicts of Interest: The authors declare no conflicts of interest.

References

[1] Hsieh, H.; Hsieh, S. L.; Luh, C. H. Rice puffing mechanism. *Cereal Chem.* **1989**, *66*(3), 179–183.

[2] Hsieh, H.; Luh, C. H. Puffing process of rice. *J. Food Sci.* **1991**, *56*(3), 830–833. https://doi.org/10.3917/comm.056.0851

[3] Murugesan, A.; Bhattacharya, K. R. Effect of moisture content on puffing of rice. *J. Food Eng.* **1986**, *5*(1), 15–20.

[4] Huff, M. R.; Brown, P. R.; Smith, S. S. Optimal temperature range for rice puffing. *J. Agric. Food Chem.* **1992**, *40*(6), 981–984.

[5] Maisont, S.; Narkrugsa, W. Effect of heating time on rice puffing quality. *Food Res. Int.* **2009**, *42*(2), 211–215.

[6] El-Salam, S.; El-Beltagy, A. A. H.; Mostafa, A. M. The effect of moisture absorption on puffing quality of rice. *J. Cereal Sci.* **2015**, *62*(1), 40–46.

[7] Malee, T. Fat content and rancidity in deep-fried rice products. *J. Food Sci. Technol.* **1992**, *29*(1), 56–60. https://doi.org/10.1109/6.144538

[8] Hoseney, W.; Bailey, M. A.; Hough, F. A. Mechanism of puffed rice production: Similarities with popcorn. *Cereal Chem.* **1983**, *60*(4), 317–322.

[9] Srinivas, P.; Desikachar, R. S. Rice puffing: Influence of rice varieties and moisture content. *Food Sci. Technol. Int.* **1973**, *1*(2), 125–128.

[10] Dofing, R.; Hareland, P. A.; McClung, T. J. Rice puffing behavior: Grain type and moisture effects. *Cereal Foods World* **1990**, *35*(2), 132–137.

[11] Zhang, X.; Hoseney, W. Influence of moisture content and temperature on puffing rice. *Cereal Chem.* **1998**, *75*(6), 776–781. https://doi.org/10.1094/CCHEM.1998.75.6.863

[12] Moraru, C. I.; Kokini, J. L. Nucleation and expansion during extrusion and microwave heating of cereal foods. *Compr. Rev. Food Sci. Food Saf.* **2003**, *2*(4), 147–165. https://doi.org/10.1111/j.1541-4337.2003.tb00020.x

[13] Lin, C.; Anantheswaran, A. Microwave heating effects on rice puffing. *J. Food Eng.* **1988**, *34*(3), 187–194.

[14] Sumnu, O. The impact of microwave heating on the puffing process of cereals. *J. Food Process. Preserv.* **2001**, *25*(5), 427–437.

[15] Juliano, R. A. *Rice Chemistry and Technology*, 2nd ed.; AACC: St. Paul, MN, 1971.

[16] Juliano, R. A.; Hicks, J. L. Amylose content and its influence on rice texture and expansion potential. *Cereal Chem.* **1996**, *73*(4), 415–419.

[17] Singh, R.; Gough, N. J.; Barham, M. A. Varietal differences in cooking and textural properties of rice. *Food Chem.* **2005**, *98*(1), 78–84.

[18] Mercier, A.; Feillet, P. Extrusion cooking of cereals: Effects on carbohydrate structures and puffability. *Cereal Chem.* **1975**, *52*(5), 464–468. https://doi.org/10.1007/BF02689477

[19] Mariotti, M.; Alamprese, C.; Pagani, M. A.; Lucisano, M. Effect of puffing on ultrastructure and physical characteristics of cereal grains. *Food Res. Int.* **2006**, *39*(4), 395–400.
[20] Simsrisakul, A. Physical characteristics of puffed rice: Volume and color. *Food Biophys.* **1991**, *7*(3), 312–319. https://doi.org/10.15358/0935-0381-1991-6-312
[21] Zhang, H.; Hoseney, R. C. Physical properties of puffed rice and their relationship to puffing performance. *Cereal Chem.* **1998**, *75*(5), 585–590. https://doi.org/10.1094/CCHEM.1998.75.5.585
[22] Seal, P.; McClements, P. L.; Smith, S. S. Whole grain labeling and health implications in puffed rice products. *J. Nutr. Sci.* **2006**, *13*, 183–192.
[23] U.S. Food and Drug Administration. *Food Labeling Guide*; Washington, DC, 2006.
[24] AOAC. *Official Methods of Analysis*, 16th ed.; Association of Official Analytical Chemists: Arlington, VA, 1990.

ASEAN
Journal of Scientific and Technological Reports
Online ISSN:2773-8752

Research article

Carbohydrate Interfaces in Plant-Fungal Interactions: A Scoping Review

Noor Azlina Mohd Nayan[1], Nur Maisarah Sarizan[1*], and Muhammad Mukram Mohamed Mackeen[2, 3]

[1] Faculty of Applied Sciences, Universiti Teknologi MARA, Perlis Branch, Arau Campus, 02600 Arau, Perlis, Malaysia
[2] Faculty of Science and Technology, Universiti Kebangsaan Malaysia, 43600, Bangi, Selangor, Malaysia
[3] Institute of Systems Biology (INBIOSIS), Universiti Kebangsaan Malaysia, 43600, Bangi, Selangor, Malaysia
* Correspondence: maisarahsarizan@uitm.edu.my

Citation:
Nayan, M.A.N.; Sarizan, M.N.; Mackeen, M.M.M. Carbohydrate inerfaces inplant-fungal interactions: A scoping review. *ASEAN J. Sci. Tech. Report.* **2026**, *29*(5), e260552. https://doi.org/10.55164/ajstr.v29i5.262552

Article history:
Received: October 3, 2025
Revised: February 27, 2026
Accepted: March 11, 2026
Available online: April 30, 2026

Publisher's Note:
This article is published and distributed under the terms of the Thaksin University.

Abstract: Carbohydrates play important roles in plant–fungal interactions, contributing to fungal adhesion, immune evasion, and host recognition**.** During fungal infection in plants, carbohydrate-based structures play a significant role in fungal adhesion, immune evasion, and host recognition. This scoping review aims to consolidate current evidence on the role of carbohydrate interfaces, including both structural polysaccharides and protein-linked carbohydrates, in plant–fungal interactions. This study followed the Preferred Reporting Items for Systematic Reviews and Meta-Analyses (PRISMA) Extension for Scoping Reviews guidelines. A total of 451 articles were retrieved from Scopus, Web of Science, PubMed, and ScienceDirect using keywords such as "carbohydrate", "fungal", "glycan", "infection", and "plant", from which 20 articles were selected for analysis based on inclusion criteria. Chitin-related glycans were the most frequently investigated carbohydrate type (n = 10), followed by *N*-glycans (n = 4) and β-glucans (n = 4), particularly in major crop systems. In contrast, protein-linked carbohydrates, especially *N*-glycans, remain limited, while studies specifically addressing *O*-glycans are largely absent. Most research has also focused on staple crops and laboratory-based experimental systems. These gaps suggest the need for greater focus on functional and dynamic analyses of glycan modifications during infection, broader representation of crops, and the application of advanced glycomic and molecular approaches.

Keywords: Carbohydrate; fungi; glycan; plant; scoping review

1. Introduction

Carbohydrates, including structural polysaccharides and glycan moieties, play essential roles in plant–fungal interactions by mediating recognition, adhesion, and defense responses [1]. For example, they are involved in metabolic activities, cellular functions, and the synthesis of essential biomolecules such as glycoproteins and nucleic acids [2]. Carbohydrates, also known as saccharides, encompass a wide range of simple sugars to more complex sugars, such as oligosaccharides [3]. Polysaccharides are complex, high-molecular-weight carbohydrates consisting of extended chains of monosaccharide units joined together through glycosidic linkages [4]. Their complex structures enabled them to perform many biological functions, including host-pathogen interactions [2].

When fungi infect plants or plants are subjected to experimental infection, multiple biological processes occur. These processes include complex

interactions between defense-challenged plants and the pathogen, resulting in immune response activation, cellular alterations, and the production of defensive compounds that inhibit infection [5]. For instance, it induces pattern-triggered immunity (PTI), in which pathogen-associated molecular patterns (PAMPs) are detected by pattern recognition receptors (PRRs) on the plant's surface. This initiates a signaling cascade that generates antibacterial substances and physical barriers to restrict pathogen infiltration [6]. Therefore, carbohydrates are studied because of their involvement in plant immune responses. Despite growing research on plant–fungal interactions, evidence on carbohydrate-mediated mechanisms remains poorly integrated across studies. A comprehensive synthesis is required to identify the types of carbohydrates studied, the plant–fungal systems investigated, and underexplored areas in current studies. Therefore, this scoping review aims to map current research on carbohydrate interfaces in plant–fungal interactions and identify key research trends and knowledge gaps.

This scoping review aimed to systematically map and characterize the existing base evidence on carbohydrate-mediated interfaces in plant–fungal interactions. Specifically, this review aimed to identify the types of carbohydrate involved, summarize the experimental methods used to investigate these interactions, examine their functional roles in fungal pathogenicity and plant defense, and identify current knowledge gaps in the literature. To further define the scope of this review, a Population–Concept–Context (PCC) framework was applied. Population: plant species affected by fungal pathogens. Concept: carbohydrate-mediated interfaces involved in plant–fungal interactions, including structural polysaccharides such as chitin, cellulose, and β-glucans, protein-linked glycans (e.g., *N*-glycosylation), and carbohydrate-binding proteins or lectins involved in pathogen recognition. Context: experimental studies investigating plant–fungal interactions under controlled laboratory or field conditions.

Based on this framework, this scoping review addressed the following research question: What types of carbohydrates are reported in plant–fungal interactions? What experimental methods are used to study carbohydrate-mediated plant–fungal interactions? What functional roles of carbohydrate structures play in fungal pathogenicity and plant defense?

2. Materials and Methods

This scoping review was performed following the principles established by the Preferred Reporting Items for Systematic Reviews and Meta-Analyses Extension for Scoping Reviews (PRISMA-ScR). There was no prior registration of a formal review methodology (e.g., Open Science Framework or PROSPERO). The review objectives, eligibility criteria, search strategy, and data extraction methodology were predetermined and are thoroughly documented to guarantee transparency and reproducibility.

2.1 Article selection

All the articles were selected and extracted from databases Scopus, Web of Science (WoS), ScienceDirect, and PubMed. The literature search was conducted on 22 December 2024. These databases were accessed via the university library (https://library.uitm.edu.my/collection) and can be easily obtained, as they are directly linked to the institution's login (Figure 1). The search strategy was developed using combinations of keywords and Boolean operators related to four main concepts: (1) glycoprotein or carbohydrate, (2) plants, (3) fungi, (4) infection or disease, and (5) carbohydrate-binding protein or lectin. The core search structure was:

("glycoprotein" OR "glycoproteins" OR "carbohydrate" OR "glycan" OR "sugar")
AND ("plant" OR "flora" OR "vegetation" OR "agriculture")
AND ("fungal" OR "fungus" OR "mycosis" OR "mycelium")
AND ("infection" OR "disease" OR "pathogen")
AND ("carbohydrate binding protein" OR "lectin" OR "binding protein" OR "CBP")

These keywords were applied to the database's advanced search, yielding 451 articles. Because each database uses different indexing systems and search interfaces, the search syntax was adapted to the database's requirements while maintaining a consistent conceptual search structure. The full search strategies for each database were provided in Supplementary Table S1. Each term keyword has a direct meaning and

connection, so the keywords have specific synonyms. Moreover, these keywords were carefully selected using combined terms (AND/OR) to capture all articles consistent with them. After identifying targeted keywords, the search filter was applied, and only research articles were included in this scoping study. No restrictions were applied to the publication year to capture the full breadth of available findings. The included studies spanned the period from 2005 to 2024, reflecting the distribution of relevant literature identified through the search. Although the search terms were comprehensive, the number of retrieved records was relatively focused because the search was restricted to the Title, Abstract, and Keywords fields to improve relevance. The search strategy was designed to capture studies specifically addressing carbohydrate or glycan components in plant–fungal interactions, which represents a specialized research area.

Supplemental Material Table S1
Search strategies used in each database.

Database	Search strategy
Scopus	TITLE-ABS-KEY ("glycoprotein" OR "glycoproteins" OR "carbohydrate" OR "glycan" OR "sugar") AND ("plant" OR "flora" OR "vegetation" OR "agriculture") AND ("fungal" OR "fungus" OR "mycosis" OR "mycelium") AND ("infection" OR "disease" OR "pathogen") AND ("carbohydrate binding protein" OR "lectin" OR "binding protein" OR "CBP")
Web of Science (WoS)	TS = ("glycoprotein" OR "carbohydrate") AND ("plant") AND ("fungal" OR "fungus") AND ("infection" OR "disease" OR "pathogen") AND ("carbohydrate binding protein" OR "lectin" OR "CBP")
PubMed	("glycoprotein" OR "glycoproteins" OR "carbohydrate" OR "sugar") AND ("plant" OR "agriculture") AND ("fungal" OR "fungus") AND ("infection" OR "disease" OR "pathogen") AND ("lectin" OR "carbohydrate binding protein" OR "CBP")
ScienceDirect	("glycoprotein" AND "plant" OR "agriculture" AND "fungus" AND "pathogen" AND "carbohydrate binding protein")

To enhance the robustness and completeness of the search process, the search strategy was pilot-tested for validation against a small set of known relevant articles identified during initial topic familiarization. The keywords and Boolean operators were refined to ensure these landmark studies could be retrieved across the selected databases. In addition, hand-searching was conducted by screening the reference lists of all included full-text articles to identify any additional relevant studies not captured in the database search.

All retrieved records were exported into Microsoft Excel for data organization and management. Duplicate records were identified and manually removed in Excel. The screening process was conducted in two stages: (i) title and abstract screening and (ii) full-text eligibility assessment. The primary reviewer performed the initial screening, and the supervising author independently checked it. Any uncertainties regarding study eligibility were discussed and resolved through consensus.

The number of articles extracted from each database varies depending on the breadth of a particular topic area. For example, Scopus provides abundant information on topics and offers wide-ranging insights into high-quality papers. Therefore, the highest number of retrieved articles was 253 from the holistic database Scopus. On the other hand, WoS has 89 articles, as it also has wide-reaching coverage in this field. Additionally, ScienceDirect retrieved 38 articles, and PubMed retrieved 71. The differences in the number of articles from these databases were apparent because of their focus and selection of specific topics. However, these differences could yield a significant number of articles for the scoping review. By understanding these preference databases, this scoping review can serve as a guide for future researchers in choosing which resources are reliable for their topic.

2.2 Inclusion and Exclusion parameters

The inclusion criteria in this study were applied to capture the relevant literature in the databases (Table 1). It was essential to set the inclusion criteria to ensure that retrieved articles were helpful in

understanding carbohydrate interactions in plant pathology. To satisfy the inclusion criteria, the study must prioritize articles that experimentally investigate the influence of carbohydrates on plant pathology and the biochemical pathways of altered glycans. The only document types accepted in this study were articles with an experimental design and results. It was because the articles were original with in-depth experiments, and they provided significant insight into the topics. For credible data, all articles must present methodologies that include glycan profiling, lectin-binding, and molecular studies of plant-fungal interactions. These inclusion criteria allowed this scoping to include all types of plant species infected and the classification of carbohydrates. On top of that, all languages were allowed to review diverse research areas to eliminate potential bias arising from language restrictions. Studies were considered regardless of language; all included articles were published in English. Publication year was not restricted in the search strategy to ensure comprehensive coverage of the available literature.

The exclusion criteria for this study were duplicate and inaccessible articles. Review articles, conference abstracts, reports, and other forms of grey literature were also excluded. During article selection from databases, it was common to discover duplicate articles, as the same study was indexed in multiple databases, leading to redundant citations of the same work. Despite the duplicated articles seeming minor, they can affect the accuracy of literature reviews by unnecessarily inflating the number of resources. Therefore, it was essential to remove duplicate studies or the same study appearing in databases to produce accurate data for the scoping review. Meanwhile, the inaccessible articles could hinder the analysis of experimental details and results. Hence, the inclusion and exclusion parameters can indicate the availability of articles and the quality and relevance of studies. Title and abstract screening, followed by full-text assessment, were conducted independently by two authors based on inclusion and exclusion criteria. This independent screening process was performed to minimize selection bias and improve the reliability of study selection. Any inconsistencies between reviewers were resolved through discussion. When agreement could not be reached, a third author was consulted to make the final decision. A formal methodological quality assessment or risk-of-bias evaluation was not performed. This decision is consistent with the purpose of a scoping review, which aims to map the breadth, characteristics, and types of available evidence rather than to evaluate the effectiveness or methodological rigor of individual studies. The primary objective of this review was to identify research trends, study designs, and knowledge gaps related to carbohydrate interfaces in plant–fungal interactions. During the full-text assessment, 324 articles were excluded for the following reasons: not related to plant–fungal interactions (n = 70), no focus on carbohydrate or glycan components (n = 89), review or non-original articles (n = 124), and inaccessible full texts (n = 41). These exclusion reasons are presented in Figure 1.

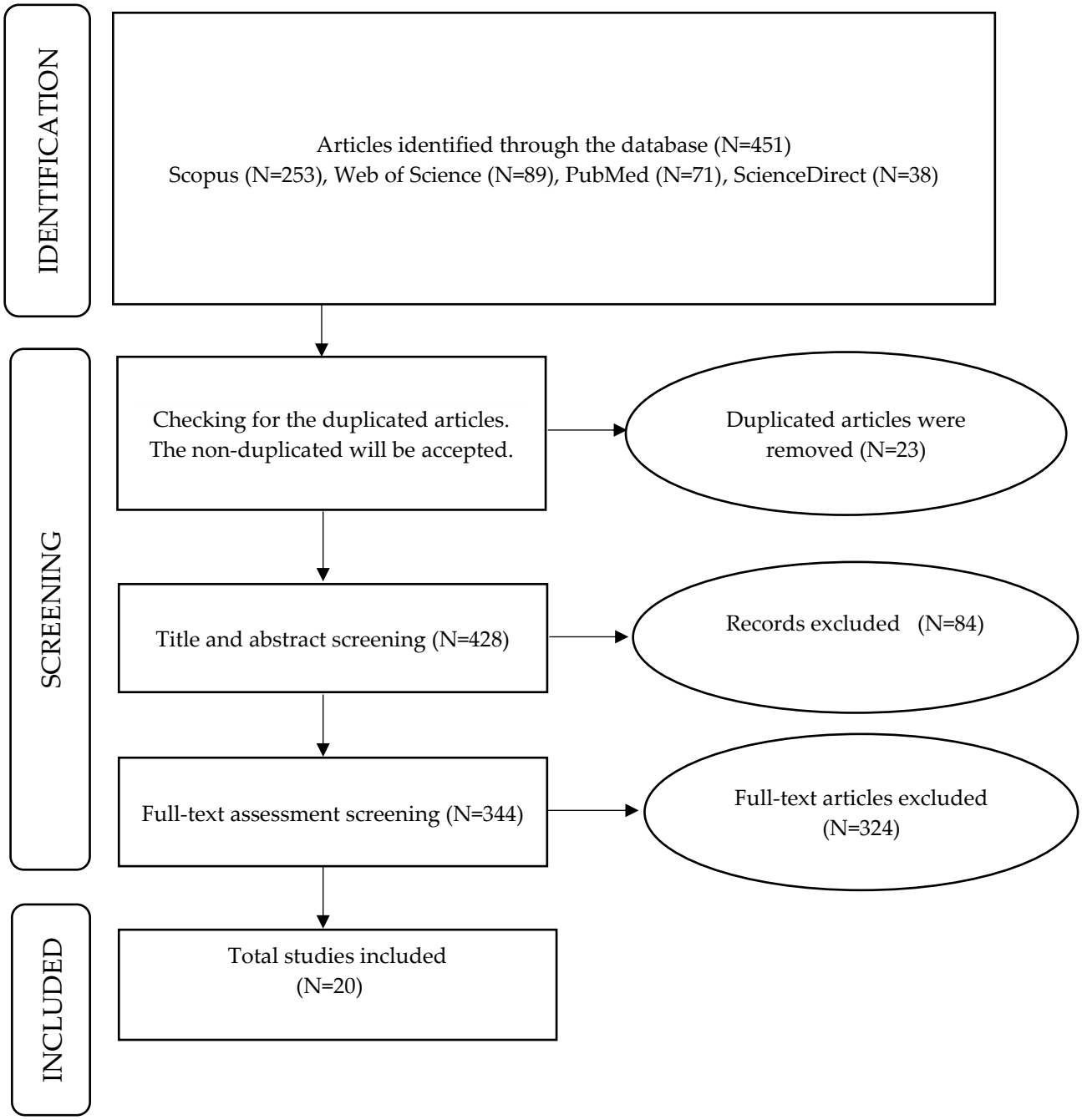


Figure 1. PRISMA flow diagram showing the study selection process. Articles were identified from Scopus, Web of Science (WoS), PubMed, and ScienceDirect. After duplicate removal, title and abstract screening, and full-text assessment, the remaining articles were assessed for eligibility. Reasons for full-text exclusion are described in Section 2.2.

Table 1. Overview of carbohydrate interactions with plants infected by pathogenic fungi.

Author(s)	Year	Country	Plant species	Fungal pathogen	Carbohydrate type	Study design	Key findings
[7]	2024	China	Kiwifruit (*Actinidia chinensis* 'Hongyang') Barley (*Hordeum vulgare*)	*Diaporthe eres* (causes kiwifruit postharvest rot *Blumeria graminis f. sp. hordei* (*Bgh*) (causes barley powdery mildew)	Callose Arabinoxylan Cellulose	A computer-based study of genomics using both short- and long-read sequencing, followed by CAZyme gene prediction and labeling.	Fungal pathogens degrade plant cell walls via cell wall-degrading enzymes (CWDEs), thereby weakening structural integrity and increasing susceptibility to infection.
[8]	2023	Germany	Maize (*Zea mays*)	*Ustilago maydis*	Chitin (chitobiose, chitotetraose)	Structural and functional analysis of Cpl1 employing X-ray crystallography, MST/HDX-MS, and fungal knockouts.	The Cpl1 protein from *Ustilago maydis* is critical for fungal virulence and interacts with the plant immune response, specifically inhibiting chitin-triggered immunity during maize infection.
[9]	2023	United States	Wheat and *Arabidopsis*	*Fusarium graminearum Colletotrichum higginsianum Sclerotinia sclerotiorum Botrytis cinerea*	*N*-glycans	Functional classification of the wheat TaPTL protein in *Arabidopsis* using heterologous production, fungal pathogen bioassays, and gene expression analysis.	GlcNAc plays an important part in the plant's defense against fungal infections, and the PFT protein in wheat helps detect this glycan, activating a resistance mechanism that inhibits the fungus's spread within the plant.

Table 1. Overview of carbohydrate interactions with plants infected by pathogenic fungi. (continue)

Author(s)	Year	Country	Plant species	Fungal pathogen	Carbohydrate type	Study design	Key findings
[10]	2023	United States	Rice (*Oryza sativa*)	*Magnaporthe oryzae*	(1→3, 1→4)-β-glucans	Biochemical and structural characterisation of MoPMO4 by enzyme tests, X-ray crystallography, and substrate binding studies.	MoPMO4 promotes oxidative degradation of plant cell wall components and plays a functional role in the pathogenicity of *Magnaporthe oryzae*.
[11]	2022	United States	Maize (*Zea mays*)	*Fusarium graminearum, Fusarium proliferatum, and Fusarium verticillioides,*	*N*-glycans	Transgenic expression study testing a chimeric superlectin gene in maize callus against fungal pathogens and insect pests using growth-inhibition bioassays.	*N*-acetylglucosamine residues increase resistance *to Fusarium* fungi and insect pests, potentially enhancing sustainable pest management in maize cultivation.
[12]	2019	United Kingdom	*Arabidopsis thaliana*	*Serendipita indica Bipolaris sorokiniana Ustilago maydis Colletotrichum tofieldiae*	Chitin, β1-3 glucan, β1-6-glucan, Laminarin (β1-3-glucan with β1-6 linkages)	Biochemical and cytological characterization of FGB1 and WSC3 lectins using binding assays, microscopy, gene expression analysis, and fungal confrontation tests.	Root-associated fungi alter their cell walls to evade plant immune responses and facilitate successful colonization of plants.
[13]	2018	United States	Tomato (*Solanum lycopersicum*)	*Cladosporium fulvum*	Chitin, Chitohexose $(GlcNAc)_6$	Structural study of *Cladosporium fulvum* Avr4 effector using X-ray crystallography of Avr4-(GlcNAc)6 complex, mutagenesis, and chitin-binding assays.	CfAvr4 uses a CBM14 carbohydrate-binding module to bind chitin, protecting fungal cell walls from plant chitinases and promoting fungal infection while evading plant immunity.

Table 1. Overview of carbohydrate interactions with plants infected by pathogenic fungi. (continue)

Author(s)	Year	Country	Plant species	Fungal pathogen	Carbohydrate type	Study design	Key findings
[14]	2017	Czech Republic	Rice (*Oryza sativa*)	*Magnaporthe oryzae*	β-1,3-glucan	Mutant analysis and cell wall characterization study of rice blast (Gels) using microscopy, glycan analysis, and plant infection assays.	Alterations in β-1,3-glucan by gel proteins are essential for fungal cell wall integrity and pathogenicity.
[15]	2016	United States	Wheat (*Triticum aestivum*)	*Parastagonospora nodorum*	Chitin	Functional characterization of SnTox1 effector using protein expression, chitin binding assays, fungal transformation, and wheat infection/ plant defense assays.	The effector SnTox1 binds chitin, shielding the pathogen from attack by the plant's chitinases. This promotes infection and allows the pathogen to colonize the host effectively.
[16]	2015	United States	Rice (*Oryza sativa*)	*Magnaporthe oryzae*	*N*-glycans	Structural study of *Magnaporthe oryzae* CVNH-LysM protein using X-ray crystallography and NMR titration with chitin oligosaccharides (GlcNAc3-6).	The plant identifies the GlcNAc-containing oligosaccharides secreted from the fungal cell wall as pathogen-associated molecular patterns (PAMPs).
[17]	2014	China	Rice (*Oryza sativa*)	*Magnaporthe oryzae*	*N*-glycans	Genetic and functional study of *ALG3* mannosyltransferase mutants assessing *N*-glycosylation effects on Slp1 effector stability, chitin binding, and rice blast virulence.	*N*-glycosylation of the effector protein Slp1 is required for its chitin-binding activity, stability, and ability to suppress host immunity, all of which are critical for Magnaporthe oryzae pathogenicity during infection.

Table 1. Overview of carbohydrate interactions with plants infected by pathogenic fungi. (continue)

Author(s)	Year	Country	Plant species	Fungal pathogen	Carbohydrate type	Study design	Key findings
[18]	2014	Australia	Canola (*Brassica napus)*	*Leptosphaeria maculans, Leptosphaeria biglobosa*	Pectin Xyloglucan Glucuronoarabinoxylan Chitin	Comparative genomics and dual RNA-seq transcriptomics study of canola-fungus interactions between Brassica napus and two Leptosphaeria species (*L. maculans* 'brassicae' and *L. biglobosa* 'canadensis').	The breakdown of pectin, xyloglucan, and glucuronoarabinoxylan is for cell wall penetration, while the plant recognizes chitin to trigger defense responses.
[19]	2014	Australia	Barley (*Hordeum vulgare*)	*Blumeria graminis f. sp. hordei (Bgh)*	Callose (1,3-glucan) Arabinoxylan Crystalline Cellulose	Histochemical and immunolocalization study analyzing polysaccharide (callose, arabinoxylan, cellulose) composition in penetrated versus non-penetrated papillae during barley powdery mildew infection.	The increased accumulation of callose, arabinoxylan, and cellulose in effective papillae enhances structural protection against *Blumeria graminis* f. sp. *hordei* in barley.
[20]	2012	Brazil	*Moringa oleifera* (seeds)	*Fusarium solani*	Chitin	Biochemical purification and characterization study of a chitin-binding protein from *Moringa oleifera* seeds using affinity chromatography, spectroscopy, and antifungal bioassays against phytopathogenic fungi.	A chitin-binding protein derived from *Moringa oleifera* seeds demonstrates antifungal properties and emphasizes the significance of carbohydrate recognition (chitin–protein interaction) in plant defense mechanisms.

Table 1. Overview of carbohydrate interactions with plants infected by pathogenic fungi. (continue)

Author(s)	Year	Country	Plant species	Fungal pathogen	Carbohydrate type	Study design	Key findings
[21]	2011	United States	Rice (*Oryza sativa*)	*Magnaporthe oryzae*	Mannose-based Glycans (CVNH Domain), Chitin-related Glycans (LysM Domain)	Structure-function analysis of *Magnaporthe oryzae* CVNH-LysM lectin using NMR spectroscopy, carbohydrate titration binding studies (GlcNAc oligomers), and live-cell imaging of appressorium localization.	*Magnaporthe oryzae* binds to mannose-based glycans via its CVNH domain and to chitin-related glycans via its LysM domain, with its presence in the appressorium suggesting a role in fungal invasion of rice.
[22]	2009	China	Canola (*Brassica napus)*	*Sclerotinia sclerotiorum*	β-1,3-glucans	Transcriptome microarray analysis comparing gene expression between resistant and susceptible *Brassica napus* cultivars following *Sclerotinia sclerotiorum* stem inoculation.	The fungal pathogen *S. sclerotiorum* utilized pectin-degrading pathways for infection, whereas the plant initiated phenylpropanoid metabolism to strengthen its structure.
[23]	2008	United States	Tomato *(Solanum lycopersicum)*	*Cladosporium fulvum*	Chitin	Characterization study of *Cladosporium fulvum* Ecp6 LysM effector using heterologous expression, chitin binding assays, RNA interference silencing, and tomato infection tests	The effector protein Ecp6 of *Cladosporium fulvum* binds to chitin, thus inhibiting host immune responses and increasing fungal virulence in tomatoes.
[24]	2007	Japan	*Arabidopsis thaliana*	*Alternaria brassicicola*	Chitin	Genetic and phenotypic characterization of Arabidopsis CERK1 mutants, demonstrating	Glycans stimulate plant defense responses through CERK1, which involves glycan-related

Table 1. Overview of carbohydrate interactions with plants infected by pathogenic fungi. (continue)

Author(s)	Year	Country	Plant species	Fungal pathogen	Carbohydrate type	Study design	Key findings
[24]	2007	Japan	*Arabidopsis thaliana*	*Alternaria brassicicola*	Chitin	loss of chitin-induced defense responses, including ROS burst, MAPK activation, and gene expression.	signaling molecules and structural alterations in the plant's immune system.
[25]	2006	Netherlands	Tomato (*Solanum lycopersicum*)	*Cladosporium fulvum*	Chitin	Biochemical and protection assays demonstrate that the *Cladosporium fulvum* Avr4 chitin-binding lectin shields fungal cell walls from plant chitinase hydrolysis during tomato infection.	The protein Avr4 binds to chitin in the cell walls of fungi, preventing Cladosporium fulvum from being hydrolyzed by plant chitinase during infection.
[26]	2005	United States	Rice (*Oryza sativa*)	*Magnaporthe grisea*	Chitin	Whole-genome shotgun sequencing and comparative genomic analysis of *Magnaporthe grisea* strain 70-15 (40.3 Mb assembly).	The rice plant's response to fungal infection involves recognizing chitin-based glycans, which activate defense systems.

3. Results and Discussion

A trend over time was observed in the included studies spanning 2005 to 2024. In the earlier years (2005–2010), the studies focused on structural polysaccharides, particularly chitin, and their role in pathogen recognition and plant defense activation. Studies from 2011 onward have shown a progressive shift toward molecular and functional analysis and lectin-mediated glycan recognition mechanisms. More recent studies (2020–2024) increasingly employed advanced methods, such as genomics and glycoprotein analysis, with growing attention to protein-linked carbohydrates, including N-glycans, and their roles in fungal pathogenicity and immune interactions. The included studies were conducted across several regions, with the majority originating in the United States, China, and Europe. However, only a limited number of studies were identified from developing regions. This suggests a focus of research in countries with advanced research infrastructure and highlights potential geographic gaps in plant–fungal carbohydrate research. A descriptive analysis of the included studies showed that chitin and chitin-related glycans were the most frequently investigated carbohydrate types (n = 10), followed by *N*-glycans (n = 4) and β-glucans (n = 4). Rice (*Oryza sativa*) was the most commonly studied plant species (n = 6), while *Magnaporthe* spp. was the most frequently reported fungal pathogen (n = 6). This distribution indicates a research emphasis on major crop systems and economically important fungal diseases.

Table 2. Distribution of included studies by research focus

Category	Research focus	Number of studies(n)
Carbohydrate type	Chitin/ chitin-related glycans	10
	N-glycan/ protein *N*-glycosylation	4
	β-glucans (including laminarin)	4
	Plant cell wall polysaccharides (callose, arabinoxylan, cellulose, pectin, xyloglucan, glucuronoarabinoxylan)	2
	Mannose-based glycans	1
Plant species	Rice (*Oryza sativa*)	6
	Arabidopsis *(A. thaliana)*	3
	Tomato *(Solanum lycopersicum)*	3
	Maize *(Zea mays)*	2
	Wheat *(Triticum aestivum)*	2
	Barley *(Hordeum vulgare)*	2
	Canola *(Brassica napus)*	2
	Kiwifruit	1
	Moringa oleifera	1
Fungal pathogen	*Magnaporthe* spp.	6
	Cladosporium fulvum	3
	Fusarium spp.	3
	Blumeria graminis	2
	Ustilago maydis	2
	Sclerotinia sclerotiorum	2
	Other pathogens *(Alternaria, Parastagonospora, Serendipita, Diaporthe,* etc.*)*	5

3.1 Functional role of carbohydrates in plant pathogen interactions

This study explored the roles of carbohydrates in plant–fungal interactions based on a summary of findings (Table 1). In this review, carbohydrates were classified according to their primary functional roles reported in each study. It is because a single carbohydrate can participate in multiple biological processes during infection, such as chitin, which appears across more than one functional theme depending on the

experimental context. Overall, the reported studies were organized into three functional themes: (i) structural roles in cell wall integrity and reinforcement, (ii) storage functions, and (iii) signaling and recognition roles in plant defense and pathogen interaction. Glycans are repetitive, often highly branched carbohydrate structures that are also added as post-translational modifications (PTMs) to proteins, resulting in glycoproteins [27-28]. Structural glycans were important for maintaining the structural integrity and mechanical support of plant and fungal cell walls [29]. The structural carbohydrates reported across the included studies include cellulose, chitin, callose, xyloglucan, pectin, arabinoxylan, β-glucans, and glucuronoarabinoxylan. Cellulose, the primary constituent of plant cell walls, is one of the most abundant biomolecules on Earth and consists of glucose units linked by β-1,4-glycosidic bonds [30]. Plants access cell wall integrity (CWI) through receptor-like kinases (RLKs) such as proteins THESEUS1 (THE1) and FERONIA (FER), which detect structural changes and regulate stress responses [31]. During fungal infection, such as that caused by Fusarium oxysporum, plants increase cellulose deposition to reinforce cell walls and restrict pathogen invasion [32]. Following cellulose, chitin is the second most abundant biopolymer and is composed of *N-acetylglucosamine* (GlcNAc) units linked by β(1→4) bonds [33]. Although chitin contributes structurally to fungal cell walls, it also has important roles in host recognition, as chitin-derived oligosaccharides function as pathogen-associated molecular patterns (PAMPs) that activate plant immune responses. Other plant structural polysaccharides, including callose, xyloglucan, and pectin, contribute to growth, development, and defense. Under pathogen stress, callose, a β-1,3-glucan, is rapidly attached at infection sites to form physical barriers against microbial penetration [34]. Xyloglucan regulates expansion, differentiation, and maintenance of final morphology in plant cell walls [35-36]. Pectin also contributes to defense by reinforcing the cell wall and triggering immune signaling pathways [37]. Similarly, arabinoxylan, β-glucans, and glucuronoarabinoxylan strengthen cell wall architecture and increase resistance to fungal enzymatic degradation [38]. In addition, β-glucans can function as PAMPs that activate plant immune responses [39].

In contrast, some carbohydrates serve storage functions. Laminarin, a β-glucan polysaccharide, is known for its role in energy storage and controlled release [40-41]. Derived from brown algae and considered non-toxic [42], laminarin has also been shown to induce pattern-triggered immunity (PTI) and systemic acquired resistance (SAR), leading to the upregulation of defense-related genes [43]. Signaling and recognition glycans represent another major functional theme. These include mannose-based glycans (CVNH domain-associated), *N*-glycosylated proteins, and chitin. Mannan oligosaccharides (MOS) act as danger-associated molecular patterns (DAMPs), activating MAPK signaling cascades, inducing defense gene expression, promoting phytoalexin accumulation, and strengthening physical barriers against pathogen invasion [44]. *N*-glycosylation, a post-translational modification, contributes to protein stability, stress responses, and plant development [45]. For example, GlcNAc-containing *N*-glycans have been shown to interact with wheat proteins during *Fusarium graminearum* infection, contributing to quantitative resistance and immune activation [46]. Plants also possess receptor-like kinases RLKs that recognize chitin oligosaccharides, with chitin elicitor receptor kinase 1 (CERK1) playing a central role in triggering defense responses [47]. Furthermore, chitinase, an enzyme that degrades chitin, is secreted by plant tissues and is upregulated during pathogen invasion to inhibit fungal growth [48]. Collectively, these findings highlight that carbohydrate-mediated interactions function through multiple, context-dependent mechanisms. The functional themes identified reflect the diverse roles reported across the studies (Table 1), highlighting that a single carbohydrate component can contribute to structural defense, immune signaling, and pathogen adaptation during different stages of plant–fungal interactions.

3.2. Fungal infections and pathogenesis in plants

A wide range of plants have been studied in this scoping data, which revealed that most plants were critical to the agriculture sector, but pathogenic fungi had affected them. Fungal plant infections are known to cause severe crop diseases and are among the most prevalent, including symptoms of blight, canker, powdery mildew, rust, wilt, leaf spot, nd damping off [49]. The staple crops in this study were rice, wheat, soybean, and barley, alongside horticultural crops such as tomato, maize, and kiwi. The plentiful availability and cost-effectiveness of staple plant foods make them preferable in selecting raw materials to synthesize economically

viable food products [50]. Thus, the staple crops were widely studied, and the common fungi causing the diseases were Magnaporthe oryzae, Parastagonospora nodorum, and *Fusarium graminearum*. *Magnaporthe oryzae* is a fungus that causes rice blast disease, which can result in up to 30% loss in rice production [51]. This devastating fungus infects rice by attaching its spores to the leaf surface, forming an appressorium that exerts intense pressure to rupture the plant cuticle [52]. The most common symptoms caused by this fungus were seed degradation and damping-off during early growth, followed by brown stem lesions and tissue collapse in the later season [53]. Meanwhile, *Parastagonospora nodorum* is a necrotrophic fungal pathogen responsible for septoria nodorum blotch (SNB) in wheat (Triticum spp.), and it is predominantly spread through contaminated seeds, infested waste, and wind-borne sexual ascospores [54]. Then again, another catastrophic fungus, *Fusarium graminearum,* damages wheat by invading the plant surface, inhibiting immune responses through effector proteins, and producing toxins to promote colonization and induce tissue necrosis [55]. Figure 2 illustrates that fungal-*N* glycoproteins play a role in attachment to the host surface, induce plant defense signaling, and suppress immune detection.

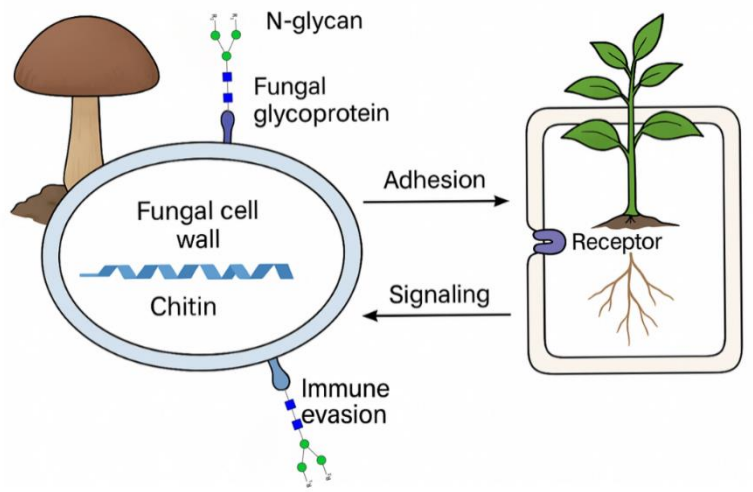


Figure 2. Fungal *N*-linked glycoproteins interact with plant receptors during infection. *N*-glycans enhanced immune evasion by secreting chitin to support the fungus-infected and manipulated the plant immune system.

The horticultural crops in this study were tomato, maize, and kiwi. The fungi mentioned in this study were *Cladosporium fulvum*, *Ustilago maydis,* and *Diaporthe eres*. *Cladosporium fulvum* infects tomatoes by penetrating leaf tissues, inducing a surge of reactive oxygen species (ROS), and modifying plant defense mechanisms. It influences plant hormone signaling by elevating salicylic acid (SA) and abscisic acid (ABA) while reducing jasmonic acid (JA) levels, ultimately altering gene expression and compromising the plant's resistance [56]. Corn smut is commonly caused by the fungus *Ustilago maydis*, which is characterized by tumor growth in the aerial portions of maize. This tumor arises from the de novo division of highly specialized bundle sheath cells followed by cell enlargement [57]. A study in China researched *Diaporthe eres*, as the causal agent of 'Hongyang' postharvest rot disease. This fungus harmed kiwifruit by releasing cell wall-degrading enzymes (CWDEs), including cellulase, β-galactosidase, polygalacturonase, and pectin methylesterases, which degrade plant cell wall polysaccharides, hence promoting fungal invasion and soft rot disease [7].

3.3 Fungal virulence factors in plant infections

Environmental factors largely influence fungal infections, as plants grow in natural habitats and are cultivated in agricultural settings. However, most of the studies analyzed in this scoping review were conducted in standardized laboratory settings to ensure successful fungal inoculation and reproducibility. Regardless, the influence of environmental factors remains significant. The burden of plant diseases was mainly caused by soil, water, and air pollution from human activity, as well as changes innvironmental

conditions (Waheed et al. [58]). For example, rising temperatures can broaden the geographical distribution of fungal infections, thereby increasing disease prevalence and severity [58]. A study by Jabiri [59] found that ideal water potential plays a crucial role in the growth of pathogens such as *Phytopythium vexans*, with peak growth recorded at particular moisture levels. Within this research framework, *Magnaporthe oryzae*, the cause of rice blast, mainly occurs under light, humidity, and nutrient conditions that favor the production of spores [60]. Rising humidity increases the virulence of *Magnaporthe oryzae* by promoting conidial germination and appressorium development, both of which are essential for infection [61]. The intensity of rice blast disease is significantly influenced by temperature, with ideal conditions occurring between 24–30°C alongside elevated relative humidity, resulting in extensive outbreaks [62]. Rainfall is the most crucial environmental factor in predicting disease outbreaks because it promotes fungal growth and distribution [63]. Meanwhile, drought stress is a significant influence, as water-stressed plants have weakened immune responses, making it easier for *Fusarium* to spread infection [64]. In summary, drought conditions can facilitate fungal invasion of plants, while high humidity and excessive rainfall can promote fungal proliferation and aid spore dispersal.

3.4 Challenges and future directions

While this scoping review provides a comprehensive overview of carbohydrate interfaces in plant–fungal interactions, several potential sources of bias should be considered when interpreting the findings. First, although multiple major databases were searched, studies indexed in other databases may have been missed, potentially leading to publication bias. Second, most included studies were conducted under controlled laboratory conditions, which may limit the findings to natural field environments. Finally, variability in experimental approaches, plant species, fungal pathogens, and glycan analysis methods may influence the consistency and comparability of results. In addition, the knowledge gaps were identified through descriptive mapping of the included studies. This involved analyzing the frequency and distribution of carbohydrate types investigated, plant–fungal systems studied, and experimental approaches applied. Areas with limited representation, a lack of specific carbohydrate categories, or restricted methodological diversity were identified as potential research gaps.

3.5 Limitations of the study

Despite increasing interest in carbohydrate-mediated plant–fungal interactions, several challenges remain. First, current research is heavily focused on structural polysaccharides such as chitin, while protein-linked carbohydrates, particularly *N*- and *O*-glycans, remain underexplored. Second, many studies rely on controlled laboratory experiments, which do not fully reflect the complexity of field conditions. Third, technical limitations in glycan extraction and analytical methods continue to constrain comprehensive glycan profiling in plant–pathogen systems. In addition, the geographic distribution of studies indicates a concentration of research in countries with advanced research infrastructure, suggesting limited representation from developing regions. In future studies, researchers should prioritize functional and dynamic analyses of glycan modifications during infection, integrate advanced omics and glycomics approaches, and validate findings under field conditions. These efforts can support the development of glycan-based biomarkers for early disease detection and contribute to the breeding of disease-resistant crop varieties.

4. Conclusions

In conclusion, this scoping review provides a comprehensive mapping of current evidence on carbohydrate-mediated plant–fungal interactions and highlights key trends and research gaps in this field. The findings indicate that existing studies are largely focused on structural polysaccharides, particularly chitin, and their roles in pathogen recognition and plant defense. In contrast, protein-linked carbohydrates, especially *N*-glycans, remain limited, while studies specifically addressing *O*-glycans are largely absent. Most research has also focused on staple crops and laboratory-based experimental systems. These gaps suggest the need for greater emphasis on functional and dynamic analyses of glycan modifications during infection, broader representation of crops, and the application of advanced glycomic and molecular approaches. By identifying underexplored areas and synthesizing current knowledge, this review provides a foundation for

guiding future research toward the development of glycan-based diagnostic tools and disease-resistant crop strategies, contributing to improved plant health and sustainable agricultural production.

5. Acknowledgements

Author Contributions: Noor Azlina Mohd Nayan conceptualized and designed the study, developed the methodology, conducted the formal analysis, and prepared the original draft of the manuscript. Nur Maisarah Sarizan contributed to the literature screening, data extraction, and supported the investigation and preparation of the manuscript. Muhammad Mukram Mohamed Mackeen contributed to data validation, critically reviewed the manuscript for important intellectual content, and assisted in the revision process. All authors contributed to the interpretation of the findings and approved the final version of the manuscript. All authors have read and agreed to the published version of the manuscript.

Funding: This study was funded by the Fundamental Research Grant Scheme-Early Career Researcher (FRGS-EC), Grant No. FRGS/1/2024/STG03/UITM/02/8 from the Ministry of Higher Education Malaysia and Universiti Teknologi MARA (UiTM) for the facilities used during data collection and analysis, making this bibliometric analysis possible.

Conflicts of Interest: The authors have no competing interests to declare that are relevant to the content of this article.

References

[1] Trouvelot, S.; HÃ©loir, M.-C.; Poinssot, B.; Gauthier, A.; Paris, F.; Guillier, C.; Combier, M.; TrdÃ¡, L.; Daire, X.; Adrian, M. Carbohydrates in Plant Immunity and Plant Protection: Roles and Potential Application as Foliar Sprays. *Front. Plant Sci.*, **2014**, *5*. https://doi.org/10.3389/fpls.2014.00592

[2] Ramaprabha, K.; Venkat Kumar, S.; Saravanan, P.; Rajeshkannan, R.; Rajasimman, M.; Kamyab, H.; Vasseghian, Y. Exploring the Diverse Applications of Carbohydrate Macromolecules in Food, Pharmaceutical, and Environmental Technologies. *Environ. Res.*, **2024**, *240*, 117521. https://doi.org/10.1016/j.envres.2023.117521

[3] Poole, C. F. Application of Thin-Layer Chromatography to the Analysis of Saccharides. In *Instrumental Thin-Layer Chromatography*; Elsevier, 2023; pp 413–435. https://doi.org/10.1016/B978-0-323-99970-0.00020-X

[4] Bushra, R.; Ahmad, M.; Seidi, F.; Qurtulen; Song, J.; Jin, Y.; Xiao, H. Polysaccharide-Based Nanoassemblies: From Synthesis Methodologies and Industrial Applications to Future Prospects. *Adv. Colloid Interface Sci.*, **2023**, *318*, 102953. https://doi.org/10.1016/j.cis.2023.102953

[5] Han, Z.; Schneiter, R. Dual Functionality of Pathogenesis-Related Proteins: Defensive Role in Plants versus Immunosuppressive Role in Pathogens. *Front. Plant Sci.*, **2024**, *15*. https://doi.org/10.3389/fpls.2024.1368467

[6] Nishad, R.; Ahmed, T.; Rahman, V. J.; Kareem, A. Modulation of Plant Defense System in Response to Microbial Interactions. *Front. Microbiol.*, **2020**, *11*. https://doi.org/10.3389/fmicb.2020.01298

[7] Ling, L.-Z.; Chen, L.-L.; Liu, Z.-Z.; Luo, L.-Y.; Tai, S.-H.; Zhang, S.-D. Genome Sequencing and CAZymes Repertoire Analysis of *Diaporthe eres* P3-1W Causing Postharvest Fruit Rot of 'Hongyang' Kiwifruit in China. *PeerJ*, **2024**, *12*, e17715. https://doi.org/10.7717/peerj.17715

[8] Weiland, P.; Dempwolff, F.; Steinchen, W.; Freibert, S.; Tian, H.; Glatter, T.; Martin, R.; Thomma, B. P. H. J.; Bange, G.; Altegoer, F. Structural and Functional Analysis of the Cerato-platanin-like Protein Cpl1 Suggests Diverging Functions in Smut Fungi. *Mol. Plant Pathol.*, **2023**, *24*(7), 768–787. https://doi.org/10.1111/mpp.13349

[9] Singh, L.; Sinha, A.; Gupta, M.; Xiao, S.; Hammond, R.; Rawat, N. Wheat Pore-Forming Toxin-like Protein Confers Broad-Spectrum Resistance to Fungal Pathogens in *Arabidopsis*. *Molecular Plant-Microbe Interactions®*, **2023**, *36* (8), 489–501. https://doi.org/10.1094/MPMI-12-22-0247-R

[10] Martinez-D'Alto, A.; Yan, X.; Detomasi, T. C.; Sayler, R. I.; Thomas, W. C.; Talbot, N. J.; Marletta, M. A. Characterization of a Unique Polysaccharide Monooxygenase from the Plant Pathogen *Magnaporthe oryzae*. *Proceedings of the National Academy of Sciences*, **2023**, *120*(8). https://doi.org/10.1073/pnas.2215426120

[11] Dowd, P. F.; Naumann, T. A.; Johnson, E. T. A Maize Gene Coding for a Chimeric Superlectin Reduces Growth of Maize Fungal Pathogens and Insect Pests When Expressed Transgenically in Maize Callus. *Plant Gene*, **2022**, *30*, 100359. https://doi.org/10.1016/j.plgene.2022.100359

[12] Wawra, S.; Fesel, P.; Widmer, H.; Neumann, U.; Lahrmann, U.; Becker, S.; Hehemann, J.; Langen, G.; Zuccaro, A. FGB1 and WSC3 Are *in* Planta- Induced β -glucan-binding Fungal Lectins with Different Functions. *New Phytologist*, **2019**, *222*(3), 1493–1506. https://doi.org/10.1111/nph.15711

[13] Hurlburt, N. K.; Chen, L.-H.; Stergiopoulos, I.; Fisher, A. J. Structure of the *Cladosporium fulvum* Avr4 Effector in Complex with (GlcNAc)6 Reveals the Ligand-Binding Mechanism and Uncouples Its Intrinsic Function from Recognition by the Cf-4 Resistance Protein. *PLoS Pathog.*, **2018**, *14*(8), e1007263. https://doi.org/10.1371/journal.ppat.1007263

[14] Samalova, M.; Mélida, H.; Vilaplana, F.; Bulone, V.; Soanes, D. M.; Talbot, N. J.; Gurr, S. J. The B-1,3-glucanosyltransferases (Gels) Affect the Structure of the Rice Blast Fungal Cell Wall during Appressorium-mediated Plant Infection. *Cell. Microbiol.*, **2017**, *19*(3). https://doi.org/10.1111/cmi.12659

[15] Liu, Z.; Gao, Y.; Kim, Y. M.; Faris, J. D.; Shelver, W. L.; de Wit, P. J. G. M.; Xu, S. S.; Friesen, T. L. SnTox1, a *Parastagonospora nodorum* Necrotrophic Effector, Is a Dual-function Protein That Facilitates Infection While Protecting from Wheat-produced Chitinases. *New Phytologist*, **2016**, *211*(3), 1052–1064. https://doi.org/10.1111/nph.13959

[16] Koharudin, L. M. I.; Debiec, K. T.; Gronenborn, A. M. Structural Insight into Fungal Cell Wall Recognition by a CVNH Protein with a Single LysM Domain. *Structure*, **2015**, *23*(11), 2143–2154. https://doi.org/10.1016/j.str.2015.07.023

[17] Chen, X.-L.; Shi, T.; Yang, J.; Shi, W.; Gao, X.; Chen, D.; Xu, X.; Xu, J.-R.; Talbot, N. J.; Peng, Y.-L. *N* -Glycosylation of Effector Proteins by an α-1,3-Mannosyltransferase Is Required for the Rice Blast Fungus to Evade Host Innate Immunity. *Plant Cell*, **2014**, *26*(3), 1360–1376. https://doi.org/10.1105/tpc.114.123588

[18] Lowe, R. G. T.; Cassin, A.; Grandaubert, J.; Clark, B. L.; Van de Wouw, A. P.; Rouxel, T.; Howlett, B. J. Genomes and Transcriptomes of Partners in Plant-Fungal- Interactions between Canola (*BrassicanNapus*) and Two *Leptosphaeria* Species. *PLoS One*, **2014**, *9*(7), e103098. https://doi.org/10.1371/journal.pone.0103098

[19] Chowdhury, J.; Henderson, M.; Schweizer, P.; Burton, R. A.; Fincher, G. B.; Little, A. Differential Accumulation of Callose, Arabinoxylan and Cellulose in Nonpenetrated versus Penetrated Papillae on Leaves of Barley Infected with *Blumeria graminis* F. sp. *Hordei*. *New Phytologist*, **2014**, *204*(3), 650–660. https://doi.org/10.1111/nph.12974

[20] Gifoni, J. M.; Oliveira, J. T. A.; Oliveira, H. D.; Batista, A. B.; Pereira, M. L.; Gomes, A. S.; Oliveira, H. P.; Grangeiro, T. B.; Vasconcelos, I. M. A Novel Chitin-binding Protein from *Moringa Oleifera* Seed with Potential for Plant Disease Control. *Peptide Science*, **2012**, *98*(4), 406–415. https://doi.org/10.1002/bip.22068

[21] Koharudin, L. M. I.; Viscomi, A. R.; Montanini, B.; Kershaw, M. J.; Talbot, N. J.; Ottonello, S.; Gronenborn, A. M. Structure-Function Analysis of a CVNH-LysM Lectin Expressed during Plant Infection by the Rice Blast Fungus *Magnaporthe oryzae*. *Structure*, **2011**, *19*(5), 662–674. https://doi.org/10.1016/j.str.2011.03.004

[22] Zhao, J.; Buchwaldt, L.; Rimmer, S. R.; Sharpe, A.; Mcgregor, L.; Bekkaoui, D.; Hegedus, D. Patterns of Differential Gene Expression in *Brassica napus* Cultivars Infected with *Sclerotinia sclerotiorum*. *Mol. Plant Pathol.*, **2009**, *10*(5), 635–649. https://doi.org/10.1111/j.1364-3703.2009.00558.x

[23] Bolton, M. D.; Van Esse, H. P.; Vossen, J. H.; De Jonge, R.; Stergiopoulos, I.; Stulemeijer, I. J. E.; Van Den Berg, G. C. M.; Borrás-Hidalgo, O.; Dekker, H. L.; De Koster, C. G.; et al. The Novel *Cladosporium fulvum* Lysin Motif Effector Ecp6 Is a Virulence Factor with Orthologues in Other Fungal Species. *Mol. Microbiol.*, **2008**, *69*(1), 119–136. https://doi.org/10.1111/j.1365-2958.2008.06270.x

[24] Miya, A.; Albert, P.; Shinya, T.; Desaki, Y.; Ichimura, K.; Shirasu, K.; Narusaka, Y.; Kawakami, N.; Kaku, H.; Shibuya, N. CERK1, a LysM Receptor Kinase, Is Essential for Chitin Elicitor Signaling in *Arabidopsis*. *Proceedings of the National Academy of Sciences*, **2007**, *104*(49), 19613–19618. https://doi.org/10.1073/pnas.0705147104

[25] van den Burg, H. A.; Harrison, S. J.; Joosten, M. H. A. J.; Vervoort, J.; de Wit, P. J. G. M. *Cladosporium fulvum* Avr4 Protects Fungal Cell Walls Against Hydrolysis by Plant Chitinases Accumulating During Infection. *Molecular Plant-Microbe Interactions®*, **2006**, *19*(12), 1420–1430. https://doi.org/10.1094/MPMI-19-1420

[26] Dean, R. A.; Talbot, N. J.; Ebbole, D. J.; Farman, M. L.; Mitchell, T. K.; Orbach, M. J.; Thon, M.; Kulkarni, R.; Xu, J.-R.; Pan, H.; et al. The Genome Sequence of the Rice Blast Fungus *Magnaporthe grisea*. *Nature*, **2005**, *434*(7036), 980–986. https://doi.org/10.1038/nature03449

[27] Deimel, L. P.; Xue, X.; Sattentau, Q. J. Glycans in HIV-1 Vaccine Design – Engaging the Shield. *Trends Microbiol.*, **2022**, *30*(9), 866–881. https://doi.org/10.1016/j.tim.2022.02.004

[28] Ha, T. K.; Kim, D.; Kim, C. L.; Grav, L. M.; Lee, G. M. Factors Affecting the Quality of Therapeutic Proteins in Recombinant Chinese Hamster Ovary Cell Culture. *Biotechnol. Adv.*, **2022**, *54*, 107831. https://doi.org/10.1016/j.biotechadv.2021.107831

[29] Fernando, L. D.; Zhao, W.; Gautam, I.; Ankur, A.; Wang, T. Polysaccharide Assemblies in Fungal and Plant Cell Walls Explored by Solid-State NMR. *Structure*, **2023**, *31*(11), 1375–1385. https://doi.org/10.1016/j.str.2023.07.012

[30] Bartetzko, M. P.; Pfrengle, F. Automated Glycan Assembly of Plant Oligosaccharides and Their Application in Cell-Wall Biology. *ChemBioChem*, **2019**, *20*(7), 877–885. https://doi.org/10.1002/cbic.201800641

[31] Polko, J. K.; Kieber, J. J. The Regulation of Cellulose Biosynthesis in Plants. *Plant Cell*, **2019**, *31*(2), 282–296. https://doi.org/10.1105/tpc.18.00760

[32] Mendu, L.; Ulloa, M.; Payton, P.; Monclova-Santana, C.; Chagoya, J.; Mendu, V. Lignin and Cellulose Content Differences in Roots of Different Cotton Cultivars Associated with Different Levels of Fusarium Wilt Race 4 (FOV4) Resistance-Response. *J. Agric. Food Res.*, **2022**, *10*, 100420. https://doi.org/10.1016/j.jafr.2022.100420

[33] Wiesinger, P.; Nestor, G. NMR Spectroscopic Studies of Chitin Oligomers – Resolution of Individual Residues and Characterization of Minor Amide Cis Conformations. *Carbohydr. Polym.*, **2025**, *351*, 123122. https://doi.org/10.1016/j.carbpol.2024.123122

[34] Mason, K. N.; Ekanayake, G.; Heese, A. Staining and Automated Image Quantification of Callose in *Arabidopsis* Cotyledons and Leaves; 2020; pp 181–199. https://doi.org/10.1016/bs.mcb.2020.05.005

[35] Hayashi, T.; Kaida, R. Functions of Xyloglucan in Plant Cells. *Mol. Plant*, **2011**, *4*(1), 17–24. https://doi.org/10.1093/mp/ssq063

[36] Wan, J.; He, M.; Hou, Q.; Zou, L.; Yang, Y.; Wei, Y.; Chen, X. Cell Wall Associated Immunity in Plants. *Stress Biology*, **2021**, *1*(1), 3. https://doi.org/10.1007/s44154-021-00003-4

[37] Wang, D.; Lu, Q.; Jin, S.; Fan, X.; Ling, H. Pectin, Lignin and Disease Resistance in *Brassica napus* L.: An Update. *Horticulturae*, **2023**, *9*(1), 112. https://doi.org/10.3390/horticulturae9010112

[38] Mélida, H.; Bacete, L.; Ruprecht, C.; Rebaque, D.; del Hierro, I.; López, G.; Brunner, F.; Pfrengle, F.; Molina, A. Arabinoxylan-Oligosaccharides Act as Damage Associated Molecular Patterns in Plants Regulating Disease Resistance. *Front. Plant Sci.*, **2020**, *11*. https://doi.org/10.3389/fpls.2020.01210

[39] Han, B.; Baruah, K.; Cox, E.; Vanrompay, D.; Bossier, P. Structure-Functional Activity Relationship of β-Glucans from the Perspective of Immunomodulation: A Mini-Review. *Front. Immunol.*, **2020**, *11*. https://doi.org/10.3389/fimmu.2020.00658

[40] Bligh, M.; Nguyen, N.; Buck-Wiese, H.; Vidal-Melgosa, S.; Hehemann, J.-H. Structures and Functions of Algal Glycans Shape Their Capacity to Sequester Carbon in the Ocean. *Curr. Opin. Chem. Biol.*, **2022**, *71*, 102204. https://doi.org/10.1016/j.cbpa.2022.102204

[41] Karuppan Perumal, M. K.; Gandhi, D.; Rajasekaran, M. B. S.; Kudiyarasu, S.; Renuka, R. R.; Julius, A.; Samrot, A. V.; Lakshmi Narayanan, A. Inhibition of Angiogenesis Using Laminarin a Natural Polysaccharide from Brown Seaweeds – A Review. *Biocatal. Agric. Biotechnol.*, **2023**, *54*, 102947. https://doi.org/10.1016/j.bcab.2023.102947

[42] Sharma, A.; Kaur, I.; Dheer, D.; Nagpal, M.; Kumar, P.; Venkatesh, D. N.; Puri, V.; Singh, I. A Propitious Role of Marine Sourced Polysaccharides: Drug Delivery and Biomedical Applications. *Carbohydr. Polym.*, **2023**, *308*, 120448. https://doi.org/10.1016/j.carbpol.2022.120448

[43] Tziros, G. T.; Samaras, A.; Karaoglanidis, G. S. Laminarin Induces Defense Responses and Efficiently Controls Olive Leaf Spot Disease in Olive. *Molecules*, **2021**, *26*(4), 1043. https://doi.org/10.3390/molecules26041043

[44] Zang, H.; Xie, S.; Zhu, B.; Yang, X.; Gu, C.; Hu, B.; Gao, T.; Chen, Y.; Gao, X. Mannan Oligosaccharides Trigger Multiple Defence Responses in Rice and Tobacco as a Novel Danger-associated Molecular Pattern. *Mol. Plant Pathol.*, **2019**, *20*(8), 1067–1079. https://doi.org/10.1111/mpp.12811

[45] Liu, C.; Talbot, N. J.; Chen, X. Protein Glycosylation during Infection by Plant Pathogenic Fungi. *New Phytologist*, **2021**, *230*(4), 1329–1335. https://doi.org/10.1111/nph.17207

[46] Molodchenkova, O. O.; Ryshchakova, O. V.; Kartuzova, T. V.; Mishchenko, L. T. Characterization of Lectins from Wheat Seedlings Infected with *Fusarium graminearum* and Treated by Jasmonic Acid. *The Ukrainian Biochemical Journal*, **2023**, *95*(2), 83–92. https://doi.org/10.15407/ubj95.02.083

[47] Kanda, Y.; Shinya, T.; Wari, D.; Hojo, Y.; Fujiwara, Y.; Tsuchiya, W.; Fujimoto, Z.; Thomma, B. P. H. J.; Nishizawa, Y.; Kamakura, T.; et al. Chitin-signaling-dependent Responses to Insect Oral Secretions in Rice Cells Propose the Involvement of Chitooligosaccharides in Plant Defense against Herbivores. *The Plant Journal*, **2025**, *121*(1). https://doi.org/10.1111/tpj.17157

[48] Shobade, S. O.; Zabotina, O. A.; Nilsen-Hamilton, M. Plant Root Associated Chitinases: Structures and Functions. *Front. Plant Sci.*, **2024**, *15*. https://doi.org/10.3389/fpls.2024.1344142

[49] Hariharan, G.; Prasannath, K. Recent Advances in Molecular Diagnostics of Fungal Plant Pathogens: A Mini Review. *Front. Cell. Infect. Microbiol.*, **2021**, *10*. https://doi.org/10.3389/fcimb.2020.600234

[50] Kehinde, B. A.; Panghal, A.; Garg, M. K.; Sharma, P.; Chhikara, N. Vegetable Milk as Probiotic and Prebiotic Foods; 2020; pp 115–160. https://doi.org/10.1016/bs.afnr.2020.06.003

[51] Li, Y.-B.; Xu, R.; Liu, C.; Shen, N.; Han, L.-B.; Tang, D. *Magnaporthe oryzae* Fimbrin Organizes Actin Networks in the Hyphal Tip during Polar Growth and Pathogenesis. *PLoS Pathog.*, **2020**, *16*(3), e1008437. https://doi.org/10.1371/journal.ppat.1008437

[52] Wei, Y.-Y.; Liang, S.; Zhu, X.-M.; Liu, X.-H.; Lin, F.-C. Recent Advances in Effector Research of *Magnaporthe oryzae*. *Biomolecules*, **2023**, *13*(11), 1650. https://doi.org/10.3390/biom13111650

[53] You, H. J.; Shim, K.-C.; Kang, I.-J.; Kim, J.-M.; Kang, S.; Lee, S. Soybean Variety Saedanbaek Confers a New Resistance Allele to *Phytophthora Sojae*. *Plants*, **2023**, *12*(23), 3957. https://doi.org/10.3390/plants12233957

[54] Jones, D. A. B.; Rybak, K.; Hossain, M.; Bertazzoni, S.; Williams, A.; Tan, K.-C.; Phan, H. T. T.; Hane, J. K. Repeat-Induced Point Mutations Driving Parastagonospora Nodorum Genomic Diversity Are Balanced by Selection against Non-Synonymous Mutations. *Commun. Biol.*, **2024**, *7*(1), 1614. https://doi.org/10.1038/s42003-024-07327-7

[55] Buttar, Z. A.; Cheng, M.; Wei, P.; Zhang, Z.; Lv, C.; Zhu, C.; Ali, N. F.; Kang, G.; Wang, D.; Zhang, K. Update on the Basic Understanding of *Fusarium graminearum* Virulence Factors in Common Wheat Research. *Plants*, **2024**, *13*(8), 1159. https://doi.org/10.3390/plants13081159

[56] Peng, R.; Sun, S.; Li, N.; Kong, L.; Chen, Z.; Wang, P.; Xu, L.; Wang, H.; Geng, X. Physiological and Transcriptome Profiling Revealed Defense Networks during *Cladosporium fulvum* and Tomato Interaction at the Early Stage. *Front. Plant Sci.*, **2022**, *13*. https://doi.org/10.3389/fpls.2022.1085395

[57] Zuo, W.; Depotter, J. R. L.; Stolze, S. C.; Nakagami, H.; Doehlemann, G. A Transcriptional Activator Effector of *Ustilago maydis* Regulates Hyperplasia in Maize during Pathogen-Induced Tumor Formation. *Nat. Commun.*, **2023**, *14* (1), 6722. https://doi.org/10.1038/s41467-023-42522-w

[58] Waheed, A.; Haxim, Y.; Islam, W.; Ahmad, M.; Muhammad, M.; Alqahtani, F. M.; Hashem, M.; Salih, H.; Zhang, D. Climate Change Reshaping Plant-Fungal Interaction. *Environ. Res.*, **2023**, *238*, 117282. https://doi.org/10.1016/j.envres.2023.117282

[59] Jabiri, S.; El Hamss, H.; Amraoui, M. B.; Lahlali, R. Influence of Culture Media and Environmental Factors (Water Potential and Temperature) on Mycelial Growth of *Phytopythium vexans* (de Bary), the Causal Agent of Dieback Disease in Apple Trees. *Appl. Microbiol.*, **2022**, *2*(4), 861–872. https://doi.org/10.3390/applmicrobiol2040066

[60] Wang, Q.; Huang, Z.; Khan, I. A.; Li, Y.; Wang, J.; Wang, J.; Liu, X.-H.; Lin, F.; Lu, J. Key Transcription Factors Required for Outburst of Rice Blast Disease in *Magnaporthe oryzae*. *Phytopathology Research*, **2024**, *6*(1), 5. https://doi.org/10.1186/s42483-024-00225-0

[61] Qiu, J.; Liu, Z.; Xie, J.; Lan, B.; Shen, Z.; Shi, H.; Lin, F.; Shen, X.; Kou, Y. Dual Impact of Ambient Humidity on the Virulence of *Magnaporthe oryzae* and Basal Resistance in Rice. *Plant Cell Environ.*, **2022**, *45*(12), 3399–3411. https://doi.org/10.1111/pce.14452

[62] Alam, M. S.; Maina, A. W.; Feng, Y.; Wu, L.-B.; Frei, M. Interactive Effects of Tropospheric Ozone and Blast Disease (*Magnaporthe oryzae*) on Different Rice Genotypes. *Environmental Science and Pollution Research*, **2022**, *29*(32), 48893–48907. https://doi.org/10.1007/s11356-022-19282-z

[63] Liu, L.-W.; Hsieh, S.-H.; Lin, S.-J.; Wang, Y.-M.; Lin, W.-S. Rice Blast (*Magnaporthe oryzae*) Occurrence Prediction and the Key Factor Sensitivity Analysis by Machine Learning. *Agronomy*, **2021**, *11*(4), 771. https://doi.org/10.3390/agronomy11040771

[64] Timmusk, S.; Nevo, E.; Ayele, F.; Noe, S.; Niinemets, Ü. Fighting *Fusarium* Pathogens in the Era of Climate Change: A Conceptual Approach. *Pathogens*, **2020**, *9*(6), 419. https://doi.org/10.3390/pathogens9060419

ASEAN
Journal of Scientific and Technological Reports
Online ISSN:2773-8752

Research article

Bridging IT and OT: Cybersecurity Risks, Zero-Trust Solutions, and Industrial Resilience in Oil & Gas Downstream

Santanu Purohit[1*]

[1] Bharat Petroleum Corporation Limited, Mumbai, Maharashtra, India
[*] Correspondence: purohits13@gmail.com ;

Citation:
Purohit, S.; Bridging IT and OT: Cybersecurity risks, zero-trust solutions, and industrial resilience in oil & gas downstream. *ASEAN J. Sci. Tech. Report.* **2026**, *29*(5), e262008. https://doi.org/10.55164/ajstr.v29i5.262008

Article history:
Received: October 21, 2025
Revised: March 4, 2026
Accepted: March 8, 2026
Available online: April 30, 2026

Publisher's Note:
This article is published and distributed under the terms of the Thaksin University.

Abstract: Enterprise Internet of Things platforms are rapidly transforming the downstream oil & gas sector, specifically City Gas Distribution networks, by enabling automation, real-time telemetry, and secure remote operations across geographically dispersed and safety-critical assets. These platforms integrate diverse field devices, such as city gate stations, compressed natural gas filling facilities, industrial meters, and sectionalizing valves, through edge gateways that normalise industrial protocols and connect to cloud services for storage, analytics, and visualisation. At the heart of the architecture is where IT and OT meet, thereby enabling a sociotechnical hybrid that unleashes operational efficiencies and data-driven decision-making while introducing never-before-seen cyber-physical attack surfaces. There are numerous examples of cyber intrusions that have led to cascading physical, economic, and societal damage. In response, state-of-the-art CGD platforms embrace cybersecurity by design and integrate Zero-Trust principles, least-privilege access, strong authentication, micro segmentation, and continuous verification, in line with formal standards for industrial automation. This paper presents an integrated, scholarly examination of IT/OT convergence for CGD and similar critical infrastructures. It synthesises foundational theory, surveys the literature on industrial cybersecurity and resilience, and proposes a methodological frame for evaluating technical solutions, data practices, and organisational controls. Through a structured analysis of telemetry, security telemetry, and operational metrics, the article maps how Zero-Trust-aligned architectures can reduce downtime, limit lateral movement, and strengthen resilience, while acknowledging persistent challenges in legacy integration, workforce capability, and compliance. The contribution is both conceptual and practical, grounded in a sector-based framework for designing, governing, and scaling secure, resilient, and data-intelligent CGD platforms.

Keywords: IT-OT convergence; cyber security; zero trust; industry 4.0

1. Introduction

Critical infrastructure industries are undergoing a sweeping digital transition, driven by urbanisation, climate and air-quality imperatives, and the maturation of industrial IoT technologies [1]. In CGD, alongside the OT systems, which have been in place for a while, ensuring operational continuity, physical safety, and meeting regulatory requirements, because that is what these systems were designed to provide: deterministic control and high availability. These were traditionally air-gapped, closed systems that slowly and carefully evolved characteristics that minimised the cyber-attack surface

but limited reporting and corporate integration [2]. The integration of OT with enterprise IT systems is changing this equilibrium. IT/OT convergence connects sensors, controllers, gateways, and supervisory control systems with cloud data platforms, analytics engines, and business applications [3]. This enables richer situational awareness (e.g., real-time pressures, flows, valve states), predictive maintenance based on streaming telemetry, automated compliance reporting, and fleet-wide control strategies. At the same time, convergence extends the threat landscape to include cloud interfaces, remote access paths, and third-party dependencies, undermining the "security by obscurity" or "air-gap" assumptions that once characterised many industrial control system (ICS) regimes [4].

Recent events have also shown that these risks are becoming increasingly leveraged from the growing digital attack surface. Recent evidence that advanced cyber threats can disrupt control logic in industrial systems threatens the decades-old assumption of the separateness of operational environments from cyber intrusions. Furthermore, incidents have demonstrated that IT system breaches can propagate to operational disruptions and have large economic and social consequences. These incidents are occurring at an increasing rate, demonstrating that adversaries are continuing to refine their tactics and exploit the convergence of IT/OT environments [5]. To respond credibly, CGD operators and technology providers are adopting "cybersecurity by design," embedding Zero-Trust principles that deny implicit trust to any user, device, or workload, and that require strong, context-aware authentication and authorisation for every request [6-7]. In parallel, standards such as ISA/IEC 62443 articulate defence-in-depth for industrial contexts, zones and conduits, security levels by risk, secure development lifecycle (SDL) practices for components, and rigorous patch and configuration management, while policy regimes like the EU's NIS2 extend governance expectations across essential services [8-9]. The study is based on the implemented solution for the CGD sector. It combines geographically distributed assets, safety-critical operations, and multifaceted stakeholder obligations to create a heterogeneous landscape (legacy and modern), with diverse communications pathways (MODBUS, MQTT, HTTP, RS-485, TCP/IP) and tight operational constraints (low latency, determinism, hazardous environments). These factors make the CGD environment a broader challenge: how to exploit the informational gains of IT/OT convergence while controlling risk and preserving resilience [2, 10].

This paper offers a scholarly synthesis and practical framework for secure, Zero-Trust-aligned IT/OT integration in CGD and analogous infrastructures. It (a) articulates the theoretical and technical foundations of convergence, (b) maps the cybersecurity and resilience literature to CGD realities, (c) proposes a research methodology for assessing platforms across technical, organisational, and regulatory dimensions, and (d) previews empirically oriented analyses of telemetry, security logs, and operational metrics that inform design and governance decisions.

2. Literature Review

A systematic qualitative methodology with resources from Scopus, WOS, IEEE Xplore, and Google Scholar has been conducted. IT/OT convergence in critical infrastructure, Zero-Trust architecture, ISA/IEC 62443, cybersecurity governance, or resilience in cyber-physical systems, with their relevance in real-world examples or measurable metrics, were included. Exclusions were made for research focused solely on enterprise IT, untrustworthy sources, and abstract debates devoid of operational context. The focus was on publications from 2010 to 2025 on the evolution of IIoT and Zero-Trust in recent years. The latter portion included peer-reviewed journals, industry case studies, standards papers, and research on resilience engineering.

2.1 IT/OT Convergence: Concepts and Challenges

The IT/OT convergence bridges enterprise IT's ability to scale, perform, and analyse big data with OT's control of physical process determinism. The literature recognises synergies and conflicts: IT encourages rapid iteration, the use of common standards (DNS, etc.), and cloud-centric designs, while OT prioritises stability, such as safety certification and long service cycles [2]. Convergence is also considered a prerequisite in Industry 4.0 literature for predictive maintenance, digital twins, and closed-loop optimisation [13]. Artificial intelligence and data to the rescue, except that latency requirements, heterogeneous protocols, and the need for lots of understandable change control for safety-critical scenarios notwithstanding [14]. A recurrent theme

is the breakdown of "air-gap" assumptions. As field devices gain IP connectivity and as gateways expose northbound APIs to cloud services, formerly isolated ICS environments become porous [15]. This exposes human-machine interfaces (HMIs), engineering workstations, and remote access channels to credential theft, supply-chain compromise, and misconfiguration-driven risk. Consequently, the literature argues for architectural patterns that combine edge processing with strictly governed data paths, encryption, and adaptive access controls [2, 16].

2.2 Industrial Cybersecurity and Threat Evolution

Early ICS security discussions focused on perimeter defence, vendor hardening guides, and anomaly detection. The Colonial Pipeline incident brought into sharp focus the "coupling" of IT and OT operations. An IT-driven ransomware attack on the company halted operations, resulting in localised fuel shortages [17]. The current literature focuses on the individual layers, such as asset discovery and SBOMs (Software Bill of Materials) for visibility, secure configuration baselines, MFA and PAM for identities, encrypted, mutual authenticated communications; network segmentation with zones and conduits, and continuous monitoring using industrially aware intrusion detection [8]. Critically, response plans should build engineering and security collaboration to avoid safety-impacting actions while containing an incident.

2.3 Zero-Trust for Cyber-Physical Systems

Zero-Trust is a reimagination of security away from "trusted inside, untrusted outside" and towards "never trust, always verify," based on continuous, context-based authorisation for users, devices, or workloads [6-7]. In the cyber-physical arena, it aligns with several operational imperatives:

- Least Privilege & RBAC/ABAC: Narrow permissions for operators, contractors, and service accounts reduce blast radius when credentials are compromised [7].
- Strong, Adaptive Authentication: MFA with risk signals (location, device posture, time-of-day, behaviour), less reliance on static secrets, and mitigation of common vectors of intrusion [7].
- Micro-Segmentation and Policy Enforcement: Logical segmentation of zones (e.g., safety instrumented systems, controls network, etc., in this case) limits lateral movement; policy enforcers assess each attempted connection [8].
- Device Identity and Integrity: Techniques such as secure boot, hardware roots of trust, and signed firmware updates provide provenance and anti-tampering for edge devices [18].

To apply Zero-Trust to an OT system, devices may be legacy and lack modern crypto, hard latency bounds limit deep inspection, and maintenance windows are few. Academic wisdom advocates practical solutions, including pushing compliance closer to the data at network gateways, compensating for controls through network microsegmentation, and phased modernisation based on asset life cycles [7, 13].

2.4 Industrial Resilience: From Protection to Adaptation

Resilience engineering goes beyond preventive protection and focuses on a system's ability to anticipate, absorb, rebound from, or adapt to disruptions [11]. Resilience in critical infrastructure includes technical redundancies (e.g., failover telemetry paths, buffer-at-the-edge), organisational preparedness (cross-functional runbooks, joint drills), and a learning culture (post-incident reviews feeding back into controls and training) [12]. Convergence increases resilience by greater visibility and predictive maintenance, but it also introduces more complexity and new sensitive points of coupling that can become progenitors of failure. According to the literature, resilience should be an explicit design consideration. It should be assessed using operational (e.g., downtime and recovery time objectives), cyber (e.g., MTTD/MTTR), and safety metrics (e.g., FMEA/near-miss rates) that account for continuous improvement cycles [11-12].

2.5 Standards, Policy, and Compliance

Standards bodies have codified recommendations for industrial cybersecurity. Lifecycle-based standards are available within the ISA/IEC 62443 family of standards for product suppliers, system integrators, and asset owners to determine security levels, zones, and conduit boundaries, as well as secure development/maintenance practices. NIST Zero Trust Architecture offers technology-neutral guidance for deploying continuous verification and least privilege at multiple levels (and limits) of an IT ecosystem [7]. At

the policy level, the EU's NIS2 extends incident reporting, supply chain controls, and the responsibility of "essential" and "important" organisations such as utilities and operators of essential services [9]. For CGD and related industries, these frameworks provide both regulatory guidance and practical guidance to align architecture, operations, and auditable evidence.

2.6 Synthesis and Gaps

The literature converges around three central claims. First, the collaboration between information technology (IT) and operational technology (OT) is essential for organisations that aspire to achieve data-driven safety, operational efficiency, and regulatory compliance [2-19]. Second, while we cannot avoid convergence without a radical redesign of security architecture, this is an early call for all stakeholders to integrate Zero-Trust principles and ISA/IEC 62443 standards to minimise the potential harm that may ensue from such convergence and to maintain continuous verification on interactions across systems [7-8]. Third, resilience also needs to be cultivated and proactively maintained systematically rather than being perceived as an implicit factor that may persist without further consideration. It includes cyber-physical system design, workforce capacity building, and adaptive governance structures [11-12]. Significant gaps remain in this body of prior knowledge. Understand how Zero-Trust controls, e.g., depth of microsegmentation, firmware signing, and the extent of multi-factor authentication adoption, translate into measurable operational reliability, safety, or recovery capability. There is limited publicly available evidence on the extent to which particular Zero Trust controls align with the delivery system standards for safe and reliable operation. Furthermore, comparison studies across sectors such as city gas distribution, water, and electricity networks are rare, especially for legacy infrastructure development and large-scale upskilling. This paper aims to fill these gaps by providing a rigorous methodology that establishes a direct link between architectural security controls and operational outcomes, as well as a measurement-driven framework that practitioners can adapt in their own organisational context.

3. Research Scope, Approach & Methodology

The study focuses on **IoT-enabled IT/OT convergence** in CGD, with careful generalisation to other critical infrastructures. Four boundaries organise the inquiry:

1. **Technical Architecture**: We analyse edge-to-cloud architectures that interconnect field assets via IoT gateways, normalise industrial protocols, and support remote command and analytics. This includes device security (secure boot, encrypted storage), communications (TLS 1.2+), identity and access management (IAM), and network controls (micro-segmentation, firewalling).

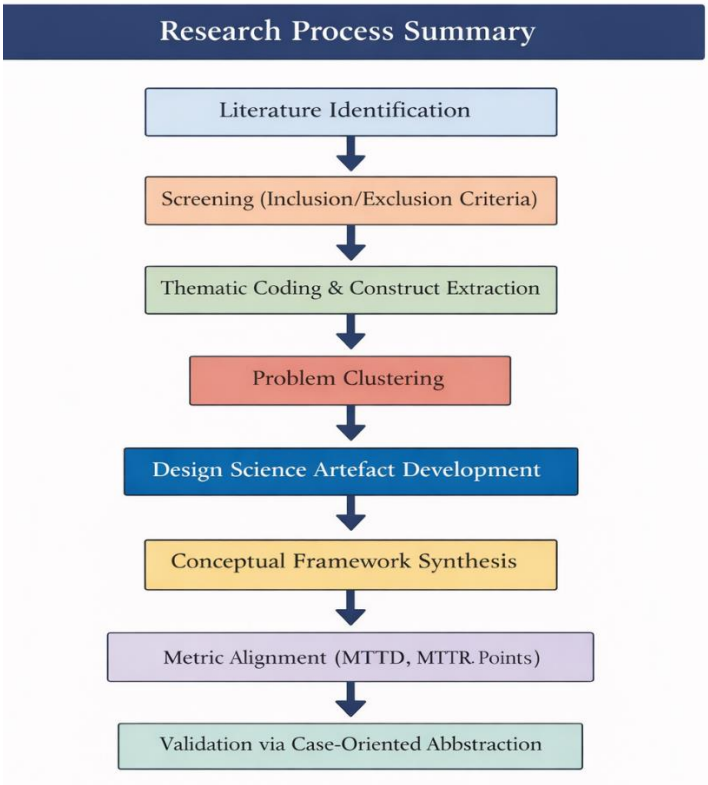
2. **Cyber-Security and Zero-Trust:** How the network would feel convergence and the associated expansion of attack surfaces. And in turn, assess Zero-Trust mechanisms (least privilege, continuous verification, device attestation, and policy-driven access) to meet NIST guidelines_48_0 and ISA/IEC 62443 practices) [7-8].

3. **Resilience of industrial systems:** It considers resilience as an emergent property across the anticipatory, absorptive, recovery, and adaptive cyber-physical 'resilience space' [11-12]. We translate these into key performance indicators, including mean time to detect/respond (MTTD/MTTR), downtime, service healing curves, and safety metrics.

4. **Governance and Compliance:** It places technical controls in a policy and regulatory context (e.g., NIS2 in the EU, ISA/IEC 62443 worldwide, national critical infrastructure guidelines) based on our progress toward auditability, incident reporting, and secure artefact lifecycle management [9].

The study does not consider each proprietary platform separately. It does not propose a new protocol; rather, it extracts patterns from well-documented industrial practices and written work, using CGD's asset and protocol space as a model context. While examples and metrics are framed generically, the implications are intended to guide decision-makers in CGD and similar domains (e.g., water utilities, power distribution, pipelines).

In the present study, we used a qualitative interpretive research approach, with properties of both design science and case-oriented inquiry. That interpretative aspect is germane because IT/OT convergence and cyber security resilience are social as well as technical phenomena that are not only conditioned by technological possibilities but also by organisational norms, governance arrangements, and situational constraints [20]. The design science view focuses on the development and testing of artefacts, that is, systems that can be used to facilitate practice in CGD and similar critical infrastructures [21], such as architectural patterns, Zero-Trust policies, and resilience metrics. The conceptual framework was developed using a two-stage design science approach. In Stage 1, literature synthesis identified three core problem clusters: expanded cyber risk from IT/OT convergence, governance and workforce misalignment, and weak linkage between security controls and measurable resilience outcomes. Stage 2 extracted key constructs across four domains: technical architecture, security controls, governance capacity, and resilience metrics mapped against ISA/IEC 62443 and NIST Zero-Trust principles. Rather than testing a single product, this research extracts generalised design elements and control practices from documented industrial solutions, standards, and case studies. The emphasis is on synthesising conceptual frameworks and evaluation methods that are transferable across organisational contexts. Research Design and Conceptual Framework Development Process in Diagram Structure:



3.1 Research Questions

Four primary research questions guide the study:

1. RQ1: What are the principal cybersecurity risks associated with IT/OT convergence in CGD networks?
2. RQ2: How can Zero-Trust principles be effectively operationalised in industrial IoT and CGD environments?
3. RQ3: What metrics and data collection approaches qualify a robust assessment of resilience in converged IT/OT architectures?
4. RQ4: How can architectural and governance frameworks be scaled across heterogeneous, legacy-constrained infrastructures, for compliance and safety?

These questions bridge technical, organisational, and regulatory domains, aligning with the resilience and cybersecurity as systemic properties [11-12].

3.2 Research Design

The research design integrates three components, namely,

1. Literature Synthesis: To determine common technical and governance challenges, peer-reviewed studies, industry white papers, and policy documents were consulted.
2. Conceptual Modelling: architectural patterns were condensed into layered models (Field Devices, Gateway, Cloud Services, and Security Controls). Zero-Trust was mapped to ISA/IEC 62443 zones and conduits.
3. Empirical Data Abstraction: Data from case reports, telemetry logs, and security incident descriptions in the literature were used to construct representative scenarios and performance metrics [15, 21, 23].

3.3 Unit of Analysis

This work focuses on the Internet of Things (IoT)-capable Information Technology/Operational Technology (IT/OT) system in City Gas Distribution (CGD). This includes a group of related sub-units that, as a whole, determine the system's functional integrity and digital robustness. The field devices, including meters, valves, etc., can be considered the first sub-unit, the bottom layer of data generation and process control. The second subcomponent is IoT gateways: edge computing devices that collect, preprocess, and secure telemetry data before sending it to higher layers. The third middleware sub-component is the cloud/enterprise integration layer, which enables data storage, analysis, visualisation, and orchestration at distributed devices. Finally, security controls constitute an essential subcomponent, including device-level hardening, network segmentation, authentication, and logging capabilities. By focusing on architectural and organisational factors rather than individual devices or protocols in isolation, the approach described captures the systemic interactions between components of CGD IT/OT ecosystems, their inherent dependencies, and potential vulnerabilities.

4. Technical Solution

Architectural Overview: The envisaged technical solution is organised as a multi-tier architecture to secure, harden, and interoperate within the CGD IoT-enabled IT/OT ecosystem (Figure 1).

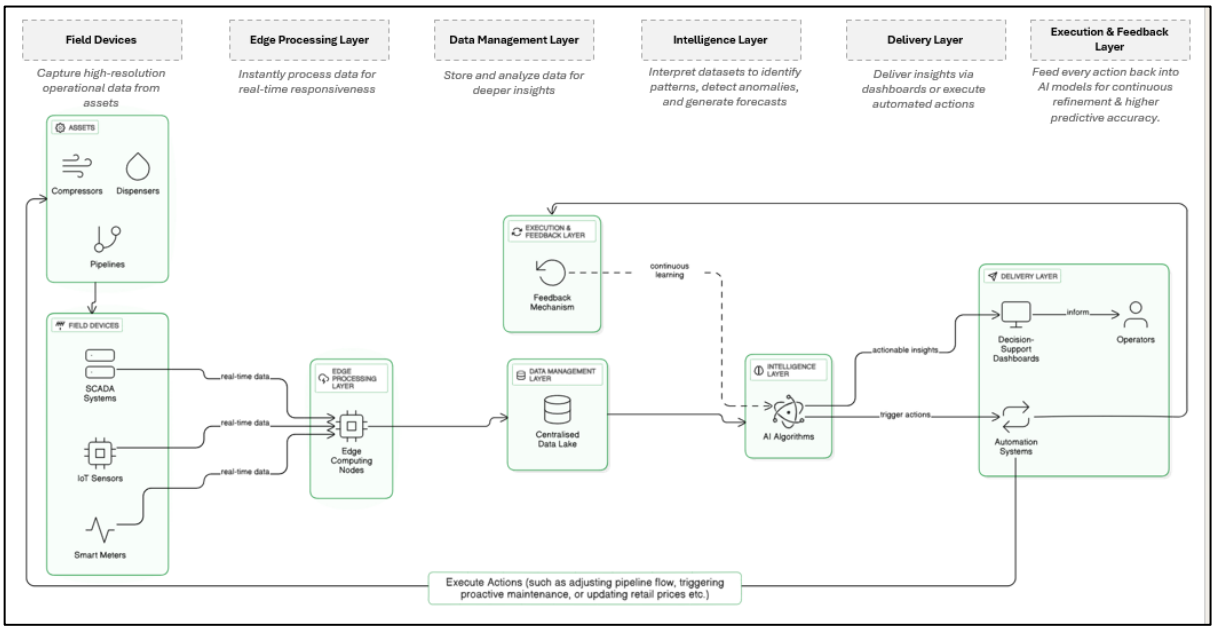


Figure 1. Architecture diagram Flow

1. **Field Layer (OT Assets)**

This bottom-layer system includes all critical levels of operational assets, including versatile city gate stations, district regulating stations, metering and regulating points, industrial meters, and sectionalization valves. They use non-uniform industrial communication protocols such as MODBUS, RS-485, DNP3, and HART. Several of them are legacy assets that do not support encryption or native authentication, and are consequently generally at risk of attack by adversaries [13].

2. **IoT Gateway Layer (Edge Computing)**

IoT gateways act as protocol converters, translating old industrial control protocols (such as MODBUS and RS-485) into modern IP-based communication protocols (such as HTTP/HTTPS and MQTT) at the edge computing layer. These gateways also execute rules, trigger-based alarms, and buffer data in the event of a network disruption.

3. **Network & Security Layer**

This layer provides strong network segmentation by isolating OT zones from enterprise IT with a DMZ (Demilitarised Zone) for regulated data exchange. It uses firewalls, network security groups, and microsegmentation to constrain lateral movement within the network. Furthermore, information in transit is protected using Transport Layer Security (TLS) 1.2 or later, ensuring the confidentiality and integrity of telemetry streams.

4. **Cloud/Enterprise Layer**

Telemetry data is ingested from IoT gateways in this layer, via an IoT Hub or sensor message broker. The data is then processed by streaming analytics engines, stored in time-series databases, and made available through APIs for dashboards and BI tools. Security in this tier is hardened by integrating IAM with MFA and RBAC, ensuring secure policy-based user access.

5. **Security Operations & Governance Layer**

The top layer is all about control, governance, and compliance. Data from field devices, gateways, and cloud services is integrated into a Security Information and Event Management (SIEM) to provide a single point of visibility. Threat intelligence and anomaly detection models support live monitoring and the generation of audit trails for traceability and compliance with both regulatory and company requirements. Overall, this multi-layered architecture reflects defence-in-depth principles and complies with ISA/IEC 62443 zone-conduit segmentation standard (ISA/IEC 62443, 2018), offering a holistic design for CGD digital infrastructure.

4.1 Zero-Trust Implementation

Zero-Trust concepts are embedded in various levels of the CGD IT/OT stack to enhance security, reduce attacks, and are supported by a continuous trust validation during system operation:

- Identity-Centric Access: Each device, user, and application within the ecosystem is verified using individual credentials, digital certificates, or hardware-based root-of-trust mechanisms. This design has the quality that no principal is considered intrinsically trustworthy; identity becomes the root of all access assertions.
- Least Privilege Enforcement: Privileges are restricted to the functions specific roles require, using RBAC mechanisms. Users with operational rights can exercise the necessary controls over the network, keeping administrative privileges secure. Disclosure of these privileges has to be authorised at a higher level to avoid misuse and prevent information leakage by internal adversaries.
- Continuous Verification: All device commands and data exchanged are monotonically logged, checked, and validated against dynamic security policies. This guarantees that trust is reconsidered throughout the sessions and becomes an adaptive security during operation as well.
- Micro-Segmentation: A segmented network creates separate security zones for different types of devices, such as SCADA infrastructure, IoT devices, enterprise IT networks, and external agency access. This segmentation restricts lateral movement, keeping potential security violations confined to isolated areas, thereby improving resilience and containment.

- Secure Firmware Lifecycle: Every bit of firmware is signed and verified on boot and in updates. This makes the supply chain less risky due to tampering and allows you to run only authenticated/trusted firmware on the system.

Together, these practices are consistent with NIST's (2020) Zero Trust Architecture and have been specifically tailored to address key operational limitations in OT environments, such as the need to impose deterministic latency guarantees and integrate with legacy systems.

4.2 Edge Resilience

Edge gateways are a critical component towards making the CGD and IoT architecture more resilient by allowing intelligent, autonomous operations at the edge of the network:

- Local Rule Execution: Gateways can autonomously take predefined actions, such as closing a valve when pressure exceeds a safety threshold, preserving critical control functions even if there is no connection to the cloud or central system.
- Buffering & Store-and-Forward: During network outages, telemetry data is buffered locally in the gateway. Buffered data is uploaded to the cloud or enterprise systems when the connection is reestablished, preserving operational insights and preventing data loss.
- Interlocking: Edge gateways and deploy local interlocking logics and processes to carry out safety-critical tasks autonomously. By accomplishing these tasks locally, your system no longer depends on a remote command that can take a while to return and may cause issues if your communication fails.

Taken together, these functions contribute to the system's resilience: the system is more robust and has a higher capacity to recover what is still needed by absorbing disturbances in time [11].

4.3 Security Monitoring

The City Gas Distribution (CGD) IoT platform integrates cybersecurity operations directly into Operational Technology (OT) monitoring, creating a unified and intelligent defence ecosystem that bridges IT and OT environments.

- Intrusion Detection Systems (IDS): Specialised IDS are also installed to support the interpretation and analysis of industrial communication protocols (e.g., MODBUS, DNP3, OPC-UA). The systems track traffic flows via OT networks to detect anomalous activities or unauthorised command sequences, ultimately providing early warning of a cyber intrusion that could threaten the safety and reliability of processes.
- Integration with the Security Information and Event Management (SIEM) Solution helps centralise activity logs and events from IT and OT systems. Finally, this compiled view marries events traced back from operations with security-centric events into a unified pane of glass, facilitating analysts' ability to identify relationships and correlations among incidents across various layers, domains, or areas of an enterprise that would otherwise be missed in siloed setups.
- ML to detect Anomaly: The telemetry is analysed with machine learning algorithms to differentiate abnormal and normal behaviour. For instance, it may spot a new valve opening quickly or a pressure spike that doesn't match normal demand profiles so that the company can run preemptive tests and threat remediation before a real shutdown.

The fusion of operational and security telemetry provides enriched situational awareness and faster incident response times. This integration lowers the MTTD and MTTR and enhances the cyber resiliency and operational integrity of CGD infrastructure.

5. Data Collection and Analysis

5.1 Data Sources

To measure the effect and resilience of security controls, the data collection falls into three broad categories: operational telemetry, security telemetry, and incident response data. Operational telemetry captures values for flow rates, pressure, valve positions, and compressor status, sampled from field devices at granular levels ranging from seconds to minutes. This data is archived in time-series databases for analysis,

trend detection, and anomaly detection. Security telemetry includes authentication events, access logs, firewall logs, intrusion detection alerts, firmware update attempts, and certificate status and integrity checks, which are consolidated in a security information and event management (SIEM) system for correlation and threat analysis. Metrics for incident and response data capture, such as mean time to detect and respond, blocked attack paths, the number of failed login attempts that were stumbled upon, recovery time upon disruption, and downtime avoided through automated failover mechanisms. There is more than one way for those data sets to be harvested. Data is collected from device telemetry via IoT hubs or MQTT brokers, and the local logs are securely forwarded by log forwarders (or agents) installed on gateways. Syslog and SIEM connectors provide additional options for collecting logs from cloud and enterprise environments, with immutable audit logs that enable complete traceback capabilities to support compliance. Security is enhanced by encrypting all data both in transit with TLS 1.2 or later and at rest using AES-256 encryption, and by closely managing access to the datasets using Role-Based Access Control (RBAC) and Multi-Factor Authentication (MFA). Together, this integrated approach enables effective, rapid threat detection and operational resilience in use.

5.2 Analysis Techniques

The data are analysed in three ways to provide complementary perspectives: descriptive statistics, comparative schemes, and resilience metrics. Descriptive statistical analysis is used to analyse the average time between a device event and cloud ingestion, the distribution of authentication events among users and devices, and the number of alerts and incidents, providing fundamental knowledge of how the system is functioning. Comparative schemes compared with traditional cases to prove that systems under a variety of operational states and security conditions (with or without Zero-Trust measures adopted), with efficiency before and after vulnerability patching, and comparisons between downtime in the traditional way and uptime time show that performance has improved. Resilience is also evaluated based on guidelines suggested by Linkov and Trump (2019) with four dimensions: anticipation - number of anomalies detected before an incident; absorption- downtime avoided by automatic interlocks; recovery - time from incident to the service being restored to normal; and adaptation - learning from operational or other events. While this research has emphasised the conceptual foundations, previous work demonstrated that implementing Zero-Trust bears out tangible dividends. MFA has been shown to reduce unauthorised access cases by more than 90% (NIST, 2020), while micro-segmentation reduces lateral attack attempts detected in SIEM systems by around 70% (ISA/IEC 62443, 2018). In addition, consolidating operational and security telemetry reduced MTTD from days to minutes in smart grid deployments [13]. Taken together, these results highlight the potential advantages of integrating descriptive, comparative, and resilience-oriented analysis to enhance cybersecurity and operational endurance.

5.3 Illustrative Comparative Case Study: Impact of Zero-Trust on Operational Resilience

Case Context

A mid-sized City Gas Distribution (CGD) network consisting of:

- 75+ geographically dispersed field assets
- Legacy MODBUS-enabled pressure regulation systems
- IoT gateway-based telemetry aggregation
- Cloud-integrated monitoring and SIEM visibility

The system underwent phased implementation of Zero-Trust-aligned controls, including:

- Micro-segmentation between OT and IT zones
- Multi-factor authentication (MFA) for remote engineering access
- Secure firmware validation at the gateway level
- Centralised SIEM integration for unified telemetry

Table 1. Comparative Performance Analysis

Metric	Pre–Zero Trust	Post–Zero Trust	Observed Impact
Mean Time to Detect (MTTD)	18–36 hours	5–15 minutes	~95% reduction
Mean Time to Respond (MTTR)	6–12 hours	1–2 hours	~70–80% reduction
Lateral Movement Attempts Detected	Limited visibility	4x increase in early detection	Improved containment
Unauthorised Remote Access Attempts	Reactive blocking	Proactive MFA prevention	>90% reduction
Downtime from Security Incidents	4.5 hours avg/year	<1 hour avg/year	~75% reduction

Analytical Interpretation

1. **MTTD Reduction:**

Integration of OT telemetry with SIEM and anomaly-detection models enabled near-real-time alerting rather than periodic log review.

2. **MTTR Reduction:**

Pre-defined containment policies and segmented zones limited blast radius, enabling targeted remediation instead of network-wide shutdown.

3. **Resilience Enhancement:**

Edge-based local interlocks ensured continued safe operation even during cloud disconnection or security containment procedures.

4. **Governance Improvement:**

Centralised logging and immutable audit trails strengthened regulatory compliance and forensic capability.

Theoretical Contribution of the Case Study

The inclusion of this illustrative case study strengthens the manuscript by:

- Demonstrating empirical linkage between Zero-Trust controls and resilience metrics
- Moving from conceptual discussion to measurable operational outcomes
- Providing comparative before–after analysis
- Translating resilience theory (anticipation–absorption–recovery–adaptation) into observable industrial KPIs

5.4 Data Governance Considerations

Operational and security data collection is also fraught with privacy, compliance, and governance concerns. A significant concern is data sovereignty, as in many jurisdictions, laws require that telemetry and other sensitive data not be stored outside national borders. Retention policies make data management even more challenging because audit logs are often required to be immutable (tamper-proof) and to meet retention requirements for regulatory and operational purposes, which can last from 5 to 10 years.

5.5 Operationalising the Framework: Measuring Resilience Impact

The proposed IT/OT convergence framework, by explicitly linking architectural security controls to measurable resilience outcomes across cyber-physical environments, strengthens the analytical results. Grounded in resilience engineering theory, the framework evaluates performance across four dimensions: anticipation, absorption, recovery, and adaptation, thereby moving beyond abstract cybersecurity assertions to quantifiable operational impact. Identity-based access and microsegmentation controls that prevent unauthorised persons from spreading across systems by strengthening both anticipation and absorption. Integration between operational telemetry and SIEM makes it easier to respond to the problem. Secured firmware management lifecycle and governance review mechanisms help build adaptive resilience by systematically eliminating recurring vulnerabilities. To evaluate the framework, the following measurable

indicators are used: rate of anomaly detection prior to disruption, percentage of remaining operational assets during incidents, downtime saved through segmentation, restoration time for telemetry visibility, and reduction in repeat incident types. A comparative scenario on CGD illustrates tangible improvements, such as a drop in MTTD from 24 hours to 10 minutes and MTTR from 8 hours to 1.5 hours, including a substantial reduction in security-related downtime. These findings indicate that resilience augmentation is achieved not only by lowering incident probability but also by reducing disruption intensity and expediting operational recovery. Collectively, the framework offers a structured, performance-linked, and replicable approach for evaluating resilience maturity across critical infrastructure sectors.

6. Discussion & Observations

6.1 Integrating IT/OT Convergence with Cybersecurity, Data Governance, and Privacy

The findings demonstrate that IT/OT convergence in CGD networks requires not just technical innovation but also robust **cybersecurity governance**. Governance encompasses the policies, standards, and organisational processes that align technology with regulatory compliance, safety, and business continuity [24]. The most advanced Zero Trust technologies, if ungoverned, may lead to misconfiguration, inconsistent enforcement, or organisational pushback [6]. Transparency is critical, too, because both consumers and regulators need to know what data is being collected, why it's being collected, and how it will be protected. IT and OT convergence generates vast amounts of operational and security data necessary to improve system resilience, but it also poses significant privacy and control issues [28]. Such considerations are now being reinforced by regulations such as the General Data Protection Regulation (GDPR) of the European Union (EU) and the energy-specific section of the ENISA 2022 guidelines on energy data, to align disparate views on data practices with varying legal and moral norms. One of the most important things to consider is the processing of personal information, because logs might contain employee identification, and therefore, there's a need for strict adherence to such regulations as GDPR. Another key concern is data sovereignty, where in some areas, countries mandate that sensitive operational data be confined within their borders. On top of that, retention policies frequently require audit logs to be kept immutable for years, further increasing the burden on organisations to store and safeguard sensitive data [28].

6.2 Workforce Skills and Organisational Capacity

A key obstacle to IT/OT convergence is the skills gap between traditional OT engineers and cybersecurity professionals. OT engineers tend not to have much exposure to sophisticated cybersecurity mechanisms, while IT staff may not fully understand the deterministic and mission-critical operation of many control systems [25]. Closing this gap is critical to reduce blind spots in security and operational resiliency. The key workforce challenges are to grow hybrid skill sets, which means a crossover between fields like industrial engineering and cybersecurity, as well as running lifelong learning programs, such as simulations for OT incident response based on IT practices (think red teaming). It's also about enabling cultural integration and tearing down walls between IT and OT teams, where employees can come together to address problems. Another critical element is Leadership. A CISO (Chief Information Security Officer) has enterprise responsibility for the IT and OT, coordinating policy to ensure consistent application across all OT spaces while increasing the strategic alignment required for adoption of successful IT/OT convergence.

6.3 Risk Trade-Offs and Zero Trust Adaptation in IT/OT Integration

IT-OT integration enables real-time monitoring, predictive maintenance, and operational optimisation, but it also creates new cyber-attack surfaces [26]. Although the Zero-Trust concept is popular in IT domains, its translation to OT systems must be carefully adapted according to operational constraints. This has limitations in terms of latency, with multifactor authentication (MFA) potentially causing excess delay and thus not being useful with time-dependent control actions; on the device limitations level, as legacy OT devices might not have the CPU strength to handle encryption or use certificates for authentication, and finally, this has priority issues where system availability may need to be considered. Hybrid models are necessary, such as lightweight cryptographic protocols for constrained devices, gateway-mediated Zero-Trust models where non-malleable devices authenticate through a hardened intermediary, and an emphasis on anomaly detection for essentially

unhardenable devices. Some important advantages to consider include reduced downtime enabled by predictive analytics, increased operational and energy efficiency, and real-time predictive visibility that supports intelligent decisions, including demand forecasting and asset management. Resistance to that effect is enhanced by edge intelligence: local systems can continue operating even if the cloud environment goes down. Convergence also enlarged the attack surface, as all impacted IoT devices connected to the internet serve as entry points, and most old OT devices were not built to connect to the internet initially. The added security controls are imperfect under the retrofitting concept. Supply chain weaknesses, such as compromised firmware or third-party software, provide additional avenues of attack that can spread throughout the network. Therefore, Zero-Trust in OT must account for context, including cybersecurity needs and physical safety requirements. The result is that 100% security cannot be achieved, but exploitation can be substantially reduced by layering defences and strategically planning for resilience in the face of a cyber event [12].

6.4 Comparative Global Approaches

Alternative approaches to IT/OT convergence for critical infrastructures have been employed in various countries. In North America, adoption is underpinned by NIST frameworks – particularly SP 800-207 on Zero-Trust - as well as the NERC CIP standards and sector-specific information-sharing organisations like the Electricity Information Sharing and Analysis Centre (E-ISAC), which enable collective threat intelligence and best-practice sharing. Europe highlights regulatory compliance through the NIS Directive and its follow-up, NIS2, which would require resilience measures and incident reporting for critical infrastructure (and cross-border coordination, given Europe is interconnected energy markets) [9]. In the Asia-Pacific, cities and energy grids in countries such as Japan and Singapore are placing a premium on cyber-physical resilience, backed by Singapore's Cybersecurity Act, which imposes obligations on operators of critical information infrastructure. On the other hand, adoption in developing country contexts remains spotty due to resource limitations, but there are opportunities for "leapfrogging" traditional solutions, as cost-effective, cloud-native, and open-source Zero-Trust products are available [27]. All together, these regional approaches illustrate that international harmonisation and standardisation are likely to significantly influence how we measure and enforce resilience as energy infrastructures continue to be further digitised and connected.

6.5 Linking Zero-Trust Controls with Resilience Dimensions in IT/OT-Converged Systems

Table 2. Linking Zero-Trust with Resilience Dimensions in IT-OT Converged Systems

Zero-Trust Control	Anticipation (Preventive Capability)	Absorption (Impact Containment)	Recovery (Restoration Speed)	Adaptation (Learning & Improvement)
Identity-Centric Access (MFA, RBAC)	Reduces the likelihood of credential compromise; blocks unauthorised access attempts	Limits privilege escalation	Enables faster incident scoping through user traceability	Policy refinement based on access anomaly patterns
Micro-Segmentation (Zone–Conduit Model)	Pre-emptively restricts cross-zone communication	Prevents lateral movement; confines breach to a single segment	Reduces system-wide shutdown requirements	Segmentation rules updated after incident analysis
Continuous Verification & Monitoring (SIEM Integration)	Detects abnormal behaviour early (reduces MTTD)	Enables rapid containment through automated alerts	Accelerates MTTR via centralised visibility	Threat intelligence integration improves future detection
Secure Firmware Lifecycle (Signed Updates, Secure Boot)	Mitigates supply chain compromise risk	Prevents execution of tampered code	Simplifies root-cause identification	Strengthens long-term asset trust model
Device Authentication & Certificate Management	Ensures only trusted devices communicate	Blocks rogue device insertion	Enables selective device isolation	Certificate revocation and renewal policies evolve
Edge Autonomy & Local Interlocks	Anticipates cloud/network failure	Maintains safe operation during disruption	Supports rapid restoration of telemetry	Operational logic improved from post-incident review
Least Privilege Enforcement	Minimises attack surface exposure	Limits the operational impact of compromised accounts	Reduces investigation scope	Role definitions are refined periodically

7. Conclusion

The integration of IT and OT has emerged as a hallmark of today's critical infrastructure systems, such as CGD networks. This results in real-time monitoring and predictive analytics, leading to more effective operations. However, it also creates a new spectrum of cyber risks for businesses to deal with. In this paper, we reviewed the risks and opportunities of IT/OT convergence from a security perspective, with a specific focus on cybersecurity risks, Zero-Trust strategies, and the need to build industrial resilience. The study concluded that cybersecurity governance is as significant as technical design. Governance ensures that 'least privilege', secure firmware management, and immutable audit logging are consistently implemented in one direction. Moreover, Cyber-Resilient operations demand blended talent, including engineers and cyber warriors alike. Furthermore, resilient operations require a hybrid workforce with skills in both engineering and cybersecurity. Without cross-disciplinary skill sets, misconfigurations, insider threats, and operational blind spots will persist.

Also, the research articulated that risk trade-offs exist for IT/OT convergence. Efficiency and real-time decision support are at odds with expanding attack surfaces and legacy vulnerabilities. Zero-trust models that involve micro-segmentation, ongoing validation measures, and the most rigorous access controls offer ideal protection and security, adaptive to latency, functional safety, and system uptime across OT infrastructures. The concept of resilience was identified as central. Our understanding of resiliency is not limited to cybersecurity; rather, it is the ability of a system to prevent, deter, withstand, recover from, and adapt to such disturbances. This whole-system vision for security shifts organisations away from a reactive, boundary-oriented defence model toward a proactive resilience engineering approach. Edge computing, anomaly detection, and a robust incident response framework are other aspects of this multi-dimensional resilience. Lastly, the research underlined the global aspect of IT/OT convergence concerns. North America, Europe, and the Asia-Pacific regions, as well as emerging markets, face similar threats, with regional risk exposure levels varying by regulatory maturity and resources in place. Global standardisation initiatives such as NIST SP 800-207 and ISA/IEC 62443 have developed a common vocabulary for the securing of critical infrastructure. Localised translations are yet necessary to accommodate context-specific legal, cultural, and economic conditions. In sum, securing IT/OT convergence in CGD and similar infrastructures requires an integrated approach combining governance, technology, workforce training, and resilience engineering. Zero-Trust is a critical enabler but must be deployed as part of a broader, adaptive strategy.

8. Contribution and Novelty of the Study

The study brought four integrated contributions: conceptual unification, methodological advancement, sector-specific operationalisation, and measurement-linked resilience evaluation. the study uniquely bridges IT/OT convergence, Zero-Trust cybersecurity, and resilience engineering within the oil & gas downstream context, moving beyond siloed perspectives to propose a unified cyber-physical governance model. On the methodology part, it connects Zero-Trust controls such as micro-segmentation and continuous verification to measurable operational outcomes like MTTD, MTTR, and downtime reduction. The research also contextualised these principles within down stream Oil & Gas industry's safety-critical, legacy-constrained environments, enhancing practical relevance for similar infrastructures. Finally, it touched upon resilience as a measurable, governance-embedded design objective rather than a by-product of security layers.

9. Declaration of Competing Interests

The author declares no conflict of interest.

Funding: This research received no external funding."

References

[1] Schwab, K. *The Fourth Industrial Revolution*; Crown Business, **2017**.

[2] Boyes, H.; Hallaq, B.; Cunningham, J.; Watson, T. The Industrial Internet of Things (IIoT): An Analysis Framework. *Comput. Ind.* **2018**, *101*, 1–12. https://doi.org/10.1016/j.compind.2018.04.015

[3] Harkat, H.; Camarinha-Matos, L. M.; Goes, J.; Ahmed, H. F. T. Cyber-Physical Systems Security: A Systematic Review. *Comput. Ind. Eng.* **2024**, *188*, 109891. https://doi.org/10.1016/j.cie.2024.109891

[4] Li, X.; Liang, X.; Lu, R.; Shen, X.; Lin, X.; Zhu, H. Securing Smart Grid: Cyber Attacks, Countermeasures, and Challenges. *IEEE Commun. Mag.* **2012**, *50*, 38–45. https://doi.org/10.1109/MCOM.2012.6257525

[5] Bellamkonda, S. Ransomware Attacks on Critical Infrastructure: A Study of the Colonial Pipeline Incident. *Int. J. Res. Comput. Appl. Inf. Technol.* **2024**, *7*, 1423–1433. https://doi.org/10.5281/zenodo.14191113

[6] Kindervag, J. *No More Chewy Centers: Introducing the Zero Trust Model of Information Security*; Forrester Research, **2010**.

[7] National Institute of Standards and Technology. *Zero Trust Architecture (SP 800-207)*; NIST: Gaithersburg, MD, **2020**. https://doi.org/10.6028/NIST.SP.800-207

[8] ISA/IEC 62443. *Security for Industrial Automation and Control Systems*; International Society of Automation/International Electrotechnical Commission, **2018**.

[9] European Union Agency for Cybersecurity (ENISA). *NIS2 Directive: An Overview of Obligations and Measures*; ENISA, **2022**.

[10] Ramachandran, K.; Pandi, M.; Pallakku, S. Towards a Zero Trust Cybersecurity Framework: Enhancing Data Protection in Multi-Cloud and Hybrid IT Infrastructures. **2025**, *9*, 1–13.

[11] Hollnagel, E. *Safety-I and Safety-II: The Past and Future of Safety Management*; Ashgate, 2015.

[12] Linkov, I.; Trump, B. D. *The Science and Practice of Resilience*; Springer, **2019**. https://doi.org/10.1007/978-3-030-04565-4

[13] Kumar, P. Zero Trust Architecture for SME Cybersecurity: Enhancing Resilience in the Digital Transformation Era. *Int. J. Prog. Res. Eng. Manag. Sci.* **2025**, *5*, 2791–2819.

[14] Masum, M. R.; Training, T. Cybersecurity, Zero Trust, and Risk Management Framework (RMF) Implementation Workshop by Tonex. **2024**. https://doi.org/10.13140/RG.2.2.20285.27361

[15] Alawi, N. Evergreen OT Security Assurance: A Sustainable Approach to OT Cybersecurity Risk Management. **2025**. https://doi.org/10.2118/224964-MS

[16] Mickie, J.; Weng, J. Zero Trust Security: A Proactive Cybersecurity Model for Risk Management. **2025**. https://doi.org/10.13140/RG.2.2.20335.55201

[17] Wang, X.; Bhuse, V.; Cheng, Y. A Zero Trust Module for Cybersecurity Education. *J. Colloq. Inf. Syst. Secur. Educ.* **2025**, *12*. https://doi.org/10.53735/cisse.v12i1.193

[18] Chang, H.-C.; Lund, B.; Beuerlein, E.; Mote, C. Investigating the Symbiotic Relationship between Artificial Intelligence and Blockchain to Promote Zero-Trust Cybersecurity in an Evolving Information Ecosystem. *Inf. Discov. Deliv.* **2025**. https://doi.org/10.1108/IDD-11-2024-0185

[19] Moses, J.; Emmanuel, F. Zero-Trust Architectures as a Resilience Strategy for Mid-Market Cybersecurity. **2025**.

[20] Walsham, G. Doing Interpretive Research. *Eur. J. Inf. Syst.* **2006**, *15*(3), 320–330. https://doi.org/10.1057/palgrave.ejis.3000589

[21] Hevner, A.; March, S.; Park, J.; Ram, S. Design Science in Information Systems Research. *MIS Q.* **2004**, *28*(1), 75–105. https://doi.org/10.2307/25148625

[22] Slay, J.; Miller, M. Lessons Learned from the Maroochy Water Breach. In *Critical Infrastructure Protection*; International Federation for Information Processing Digital Library, **2007**; Vol. 253, pp 73–82. https://doi.org/10.1007/978-0-387-75462-8_6

[23] Langner, R. Stuxnet: Dissecting a Cyberwarfare Weapon. *IEEE Secur. Priv.* **2011**, *9*(3), 49–51. https://doi.org/10.1109/MSP.2011.67

[24] Weill, P.; Ross, J. W. *IT Governance: How Top Performers Manage IT Decision Rights for Superior Results*; Harvard Business Press, **2004**.

[25] Knowles, W.; Prince, D.; Hutchison, D.; Disso, J. F. P.; Jones, K. A Survey of Cyber Security Management in Industrial Control Systems. *Int. J. Crit. Infrastruct. Prot.* **2015**, *9*, 52–80. https://doi.org/10.1016/j.ijcip.2015.02.002

[26] Koppichetti, R. K. Convergence of Information Technology (IT) and Operations Technology (OT) in Bio-Pharmaceutical Manufacturing Industry. **2023**. https://doi.org/10.5281/zenodo.14866213

[27] Bhushan, B.; Rajgopal, P.; Sharma, K. An Intent-Aware Zero Trust Identity Architecture for Unifying Human and Machine Access. *Int. J. Comput. Exp. Sci. Eng.* **2025**, *11*. https://doi.org/10.22399/ijcesen.3886

[28] Cavoukian, A. *Privacy by Design: The 7 Foundational Principles*; Information and Privacy Commissioner of Ontario, **2010**.

ASEAN
Journal of Scientific and Technological Reports
Online ISSN:2773-8752

Research article

The Development of a Web Application for Tracking Bedridden Patients by Village Health Volunteers

Phatnutsooda Jaruteerapan[1*], Nitchanan Kawiwangsakul[1], Maikam Tantipatum[1], Issadaporn Srisutham[1], Netnapa Wongla[1], and Sittisuk Pimmee[1]

[1] Faculty of Management Science, Loei Rajabhat University, Loei Province, 42000, Thailand
* Correspondence: phatnutsuda.jar@lru.ac.th

Citation:
Jaruteerapan, P.; Kawiwangsakul, N.; Tantipatum, M.; Srisutham, I.; Wongla, N. & Pimmee, S. The development of a web application for tracking bedridden patients by village health volunteers. *ASEAN J. Sci. Tech. Report.* **2026**, *29*(5), e261927. https://doi.org/10.55164/ajstr.v29i5.261927

Article history:
Received: October 17, 2025
Revised: March 20, 2026
Accepted: April 6, 2026
Available online: April 30, 2026

Publisher's Note:
This article is published and distributed under the terms of the Thaksin University.

Abstract: This study aims to develop and evaluate a web-based application for monitoring bedridden patients in a rural community in Loei Province, Thailand. The system was designed to support Village Health Volunteers (VHVs) in recording patient data, monitoring health conditions, and coordinating care with healthcare providers more efficiently. A research and development (R&D) approach was employed, following the System Development Life Cycle (SDLC), including requirement analysis, system design, development, testing, and deployment. The system was evaluated using a structured questionnaire based on information system quality dimensions. A total of 37 VHVs participated in the study. Data were collected before and after implementation and analyzed using descriptive statistics (mean and standard deviation) and paired-samples t-tests. The results showed that overall system quality was rated at the highest level ($\bar{x}$ = 4.51, S.D. = 0.49). The highest-rated dimensions included ease of use ($\bar{x}$ = 4.60), usefulness ($\bar{x}$ = 4.58), and system security ($\bar{x}$ = 4.55). User satisfaction was also high ($\bar{x}$ = 4.39), with system performance receiving the highest rating ($\bar{x}$ = 4.66). Paired-samples t-test results indicated statistically significant improvements after implementation (t = 8.41–10.34, p < 0.001). These findings demonstrate that the application improves monitoring efficiency, enhances data accuracy, and supports effective communication in community healthcare settings, providing a practical, scalable digital health solution to strengthen primary healthcare services in rural areas.

Keywords: Web application; bedridden patients; village health volunteers; community health

1. Introduction

Caring for bedridden patients is a critical public health issue, particularly in rural communities where access to healthcare services is limited. As populations age and chronic illnesses increase, the number of individuals who are confined to bed and require long-term care continues to rise. Such patients often rely heavily on family members or community-based health volunteers for daily assistance, medical follow-up, and psychological support. In Thailand, this challenge is particularly significant in remote areas where healthcare facilities and professional medical personnel are scarce. In such contexts, community-based care

models have become indispensable for ensuring that patients receive continuous, holistic care. However, traditional approaches such as periodic home visits, manual data recording, and phone-based communication often result in incomplete information, delayed interventions, and inefficiencies in coordination among healthcare providers [1]. Recent studies have highlighted the increasing role of digital health technologies in improving healthcare monitoring and service delivery. Remote patient monitoring systems, cloud-based health platforms, and mobile health applications have been widely developed to support patient care and health data management in both clinical and community settings [2-4]. These technologies enable real-time health monitoring, enhance data accessibility, and improve coordination between healthcare providers and patients.

With the increasing adoption of digital technologies in healthcare, web-based applications have emerged as effective and sustainable tools for improving health data management and service delivery. Digital platforms enable the integration of patient information, facilitate real-time data collection, and support remote monitoring to enable timely clinical decisions. Moreover, such systems can enhance collaboration between Village Health Volunteers (VHVs), healthcare professionals, and administrative units by providing a centralized database for communication and reporting. Previous studies have shown that community health applications not only enhance service efficiency and reduce administrative burdens but also improve patient satisfaction and engagement with healthcare services [5]. These tools have proven especially beneficial in rural areas where resource limitations make traditional service delivery less effective, demonstrating their potential to bridge gaps in healthcare accessibility.

From a theoretical perspective, the development of digital healthcare systems is strongly supported by the concept of Health Information Systems (HIS), which focuses on the systematic collection, storage, processing, and dissemination of health information to support healthcare management and decision-making. Effective health information systems improve the accuracy, accessibility, and interoperability of patient data, enabling healthcare professionals to coordinate care more efficiently and respond to patient needs promptly. [6] In community healthcare contexts, such systems can assist healthcare workers and volunteers in monitoring patient conditions, organizing home visits, and maintaining updated health records. In addition, the adoption of new digital technologies in healthcare environments can be explained through the Technology Acceptance Model (TAM), which identifies perceived usefulness and perceived ease of use as key determinants influencing users' willingness to adopt technological systems [7-8]. Systems that are easy to use and demonstrate clear benefits for users' daily tasks are more likely to be successfully implemented and sustained in real-world healthcare environments. Therefore, the design of digital healthcare systems should consider both functional effectiveness and user-centered design to ensure that end users can effectively use the technology.

In Na Khaem Subdistrict, Loei Province, the number of bedridden patients has steadily increased in recent years, placing considerable pressure on VHVs who are tasked with providing continuous and comprehensive care. The VHVs must monitor health conditions, record patient data, and coordinate with healthcare centers to ensure consistent follow-up and treatment. Without a systematic digital platform, these tasks tend to be time-consuming, error-prone, and difficult to track over time. This situation highlights the urgent need for a web-based system designed specifically to support VHVs' operations, ensure accurate and secure management of patient data, and enhance the efficiency of community-based healthcare services [9]. The novelty of this study lies in the development of a community-based digital monitoring system specifically designed for Village Health Volunteers (VHVs). Unlike conventional healthcare information systems that primarily support hospital operations, the proposed system focuses on supporting home-based patient care, visit scheduling, and real-time reporting within rural community healthcare settings. Therefore, this research contributes both a practical digital health solution and an implementation model for community healthcare systems in rural Thailand.

Therefore, this study aimed to develop a web application for monitoring bedridden patients in Na Khaem Subdistrict, Loei Province, and to evaluate its quality through expert assessment, while examining VHVs' satisfaction as end-users. The proposed system integrates data management, visit scheduling, and reporting features into a single accessible platform. The findings from this study are expected to provide a practical and replicable model for applying digital tools to strengthen primary and community healthcare services in Thailand. Furthermore, the study contributes to the growing body of evidence supporting the integration of digital health innovations into rural health systems to promote equitable, efficient, and sustainable care delivery.

2. Research Methods

This research focuses on developing a web-based application to monitor bedridden patients in Ban Na Khaem, Na Khaem Subdistrict, Mueang District, Loei Province, to improve usability for local public health volunteers. Employing a research and development (R&D) approach, the study integrates system design with quantitative evaluation. The methodology is structured into two primary phases: (1) system development and (2) system evaluation, ensuring both functional efficiency and alignment with user needs.

2.1 Problem study and survey

This study began with an exploration of the problems associated with caring for bedridden patients in Na Khaem Subdistrict, Mueang District, Loei Province. Data collection was conducted through a variety of methods, including in-depth interviews with Village Health Volunteers (VHVs) and caregivers of bedridden patients to understand current health data-tracking and recording processes, as well as the limitations and needs of actual users. Field observations were also conducted, with researchers visiting VHVs' homes to collect data on workflows, data recording methods, reporting practices, and problems encountered in real-world settings. This was coupled with a document review to examine academic literature, research, and existing systems for bedridden patient care and health information systems, which served as the basis for designing a new system. The results revealed that most VHVs still record data on paper or transmit it through conventional communication channels, leading to delays, disorganization, and difficulty in tracking data retrospectively. Therefore, developing a web application that systematically stores data and provides easy access is an appropriate approach to addressing this issue.

2.2 System design and development

The researchers used data from field surveys, interviews, and document reviews to design a system that effectively addresses the real needs of bedridden patient care. The system architecture was developed based on user requirements, emphasizing data accuracy, accessibility, and security. Database structures and system functions were carefully defined to ensure smooth integration between health volunteers and healthcare providers. This design process aimed to create a user-centered, reliable, and efficient digital platform to enhance the management and monitoring of bedridden patients in the community healthcare context.

2.2.1 System design

1) Context diagram. Based on the analysis of the system's problems and requirements, the system diagram was drawn as shown in Figure 1.

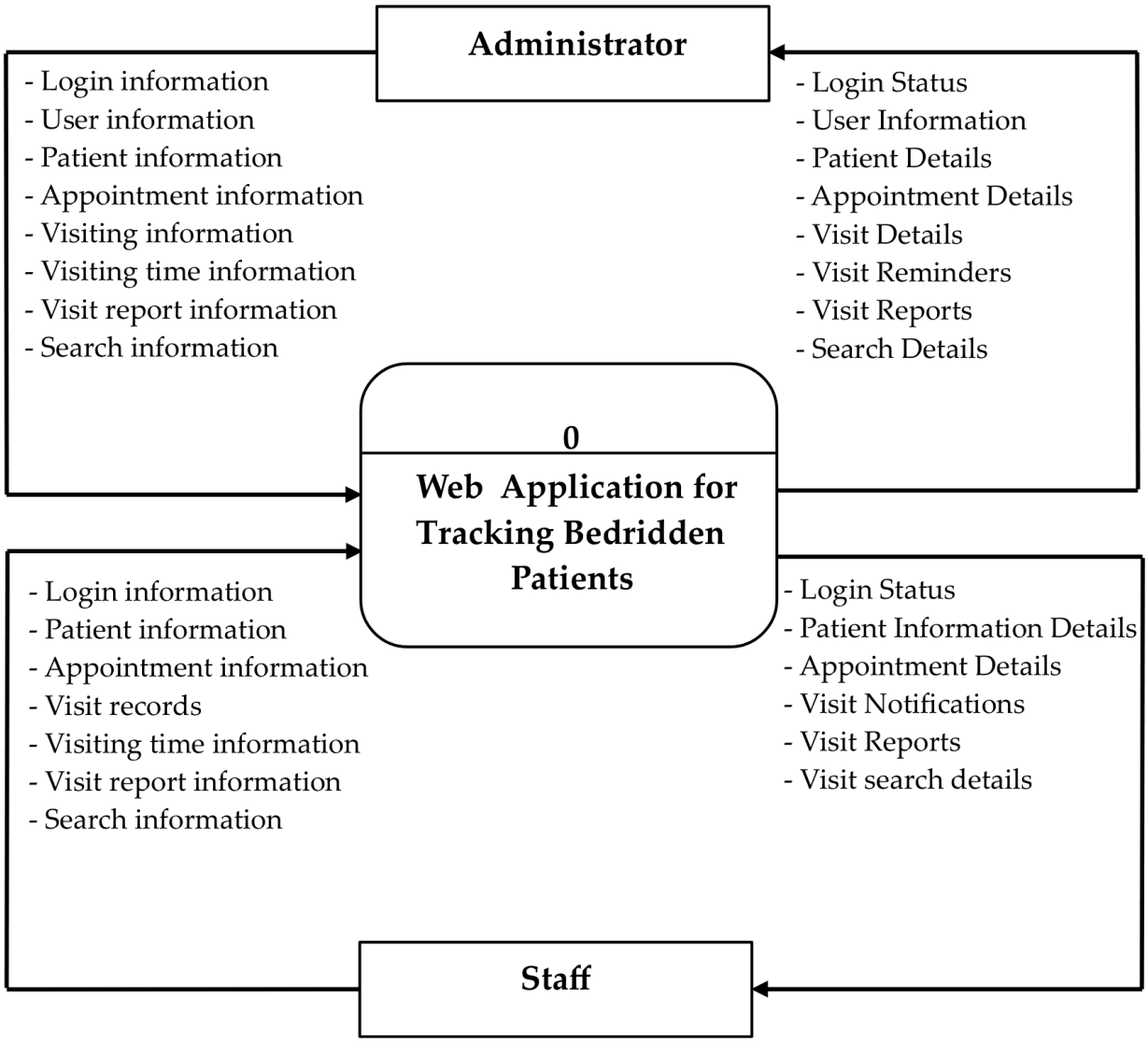


Figure 1. Context Diagram

Figure 1 shows a context diagram of the web application for tracking bedridden patients, showing interactions between the system and two main external entities—Administrator and Staff. It illustrates the flow of information, including login, patient data, appointments, visit records, reports, and search details, exchanged between users and the system.

2) Data flow diagram

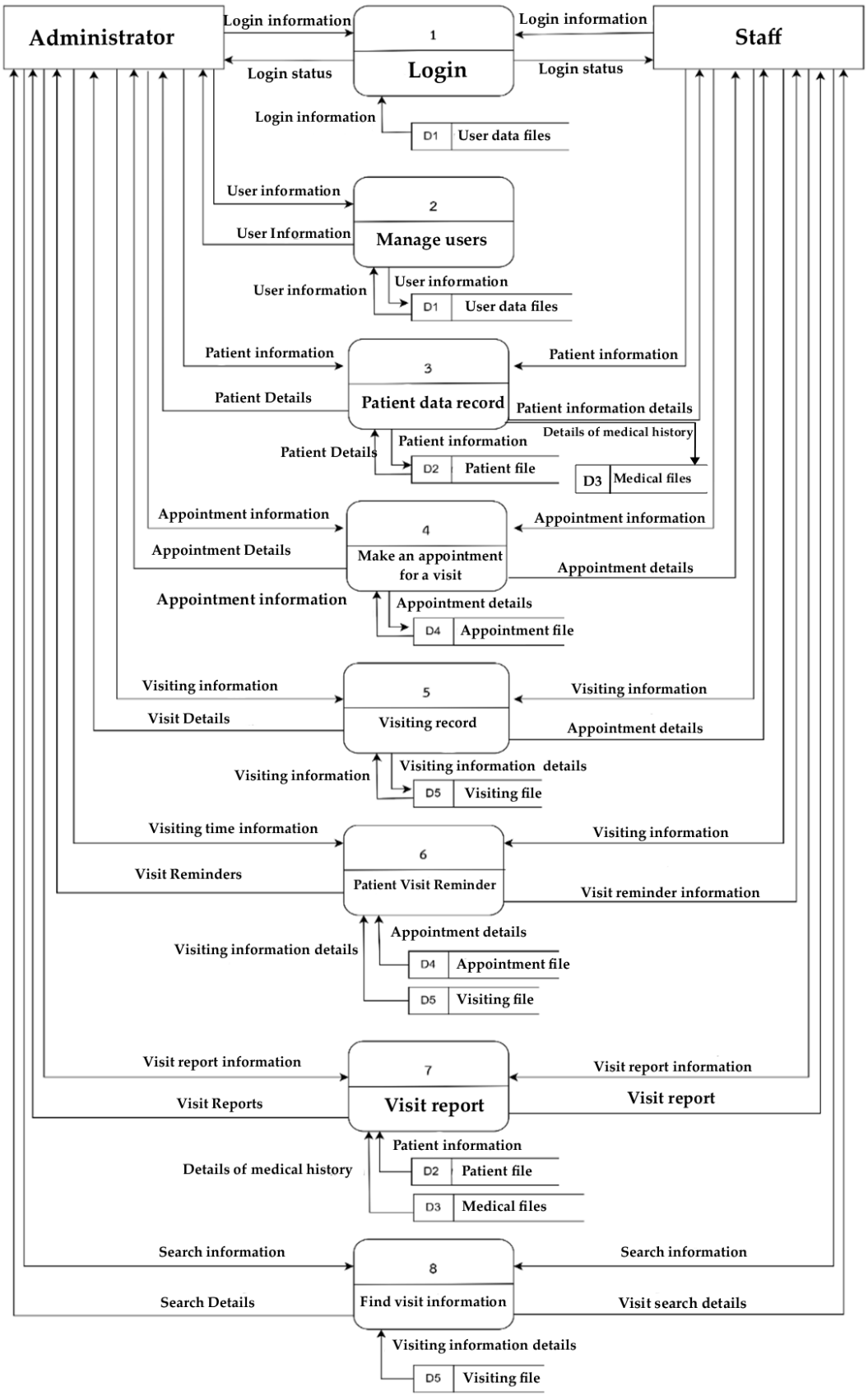


Figure 2. Data Flow Diagram level 0

Figure 2 shows a data flow diagram of the healthcare management system, illustrating interactions between the Administrator and Staff. The system includes key processes such as login, user management, patient data recording, appointment scheduling, visiting records, reminders, report generation, and information search, with data stored in related files (user, patient, medical, appointment, and visiting files)

2.2.2 System development

System development is the structured process of designing, developing, implementing, and testing a software system to ensure it meets specified user requirements and operational objectives. In this study, the web-based monitoring system for bedridden patients was developed to support Village Health Volunteers (VHVs) in recording patient information, monitoring health conditions, and coordinating with healthcare providers efficiently. The development of the web-based monitoring system was grounded in the System Development Life Cycle (SDLC) framework, specifically utilizing an iterative prototyping model. This framework was selected as it allows for continuous refinement based on feedback from healthcare professionals and VHVs. The process encompassed five structured phases: (1) Requirement Analysis, gathered through field surveys and interviews; (2) System Design, focusing on a user-centric three-tier architecture; (3) Implementation, using PHP and MySQL; (4) Testing, ensuring functionality and security; and (5) Deployment and Evaluation in a real-world community healthcare setting.

1) Web Application Development

The proposed system was developed as a web-based application, allowing users to access the platform via standard web browsers without installing additional software. This approach enhances accessibility and enables Village Health Volunteers and healthcare staff to use the system from various locations using computers, tablets, or smartphones. The system architecture follows a three-tier model, consisting of the presentation, application, and data layers. The presentation layer provides the user interface that allows users to input and view patient information through web pages designed with responsive design principles. The application layer handles system logic, including patient data management, visit scheduling, health monitoring, and report generation. The data layer is responsible for storing and managing patient records and system data within a structured relational database. The development process involved several key technical components:

(1) Front-end development was used to design interactive user interfaces that allow users to easily record patient visits, update monitoring information, and access reports.

(2) Back-end development manages system functionality, processes user requests, and communicates with the database to retrieve and store patient data.

(3) A relational database management system (RDBMS) was used to organize and maintain structured health data, including patient profiles, monitoring records, and user account information.

During development, special attention was given to usability and simplicity, considering that Village Health Volunteers may have varying levels of digital literacy. Therefore, the interface was designed with clear navigation, simple data entry forms, and easily accessible reporting features. Before system deployment, the web application underwent functional testing and system verification to ensure that all modules operated correctly and that the system could reliably support the monitoring and management of bedridden patient information within the community healthcare environment.

2) System Security and Data Protection

To ensure confidentiality, integrity, and security of patient information, the developed web-based monitoring system incorporates several security mechanisms, including secure data transmission, user authentication, and role-based access control. These mechanisms were designed in accordance with widely accepted information security practices for healthcare information systems.

(1) Data Encryption

All data transmitted between the user interface and the web server is protected using the Secure Sockets Layer/Transport Layer Security (SSL/TLS) encryption protocols. This mechanism ensures that sensitive health information, such as patient records and monitoring data, cannot be intercepted or modified during transmission. In addition, sensitive user credentials, including passwords, are not stored in plain text within the system database. Instead, passwords are protected using cryptographic hashing algorithms with salting techniques, which significantly reduce the risk of credential compromise in the event of unauthorized database access.

(2) User Authentication

The system implements a secure login authentication mechanism to verify the identity of authorized users before granting access to the platform. Each user must log in using a unique username and password assigned by the system administrator. The authentication process verifies the credentials against encrypted records stored in the system database. To prevent unauthorized access, the system also incorporates session management techniques, including automatic session expiration after a period of inactivity and protection against repeated failed login attempts.

(3) Role-Based Access Control

To further enhance system security, role-based access control (RBAC) was implemented. Users are assigned specific roles based on their responsibilities within the community healthcare system. The system currently supports three primary user roles:

1. Village Health Volunteers (VHVs) – allowed to record patient visits, update monitoring data, and submit health reports.

2. Healthcare staff – allowed to review patient records, monitor health conditions, and coordinate follow-up care.

3. System administrators – responsible for managing user accounts, system configuration, and database maintenance.

This access control structure ensures that users can only access information and functions relevant to their roles, thereby minimizing the risk of unauthorized data modification.

(4) Data Backup and System Protection

To prevent data loss and maintain system reliability, the system performs regular database backups and stores backup files securely on the server. These measures ensure that patient information can be restored in the event of system failure or technical disruptions.

Overall, these security mechanisms ensure that the developed web-based monitoring system provides a secure and reliable environment for managing sensitive healthcare data while supporting the operational needs of Village Health Volunteers in community healthcare settings.

2.3 Population and Sample

2.3.1 Population

The population in this study consisted of five experts who evaluated the quality of the developed system and 42 Village Health Volunteers (VHVs) from Ban Na Khaem, Na Khaem Subdistrict, Mueang District, Loei Province [9].

2.3.2 Sample

1) Five experts assessed the quality of the system, including two information technology specialists and three experts in VHV data analysis.

2) The target population consisted of 42 active Village Health Volunteers (VHVs) in Ban Na Khaem. To ensure statistical reliability, the sample size was determined using the Krejcie and Morgan [10]. Based on the formula, for a finite population of 42, with a 95% confidence level and a 5% margin of error, the recommended minimum sample size is 38. In this study, 37 VHVs met the inclusion criteria and participated in the evaluation, representing an 88% response rate of the total population. This high participation rate is considered statistically robust and highly representative, enabling valid conclusions in this community-based research context.

2.4 Research Tools

2.4.1 Characteristics of research tools

1) Web application for monitoring bedridden patients at Ban Na Khaem. The primary research tool developed in this study was a web-based application designed as a prototype system to monitor and manage data for bedridden patients in Ban Na Khaem Subdistrict, Loei Province. The system aimed to support Village Health Volunteers (VHVs) and healthcare professionals in maintaining accurate, up-to-date, and easily accessible patient information. Its core functions included patient data storage, visit scheduling, real-time visit recording, reminder notifications, and the generation of summary reports for health monitoring and evaluation. The web application was developed using the PHP programming language and MySQL as the database management system, implemented in Visual Studio Code and phpMyAdmin. The system architecture followed a user-centered design approach to ensure efficiency, reliability, and data security. The platform was structured with two primary user roles—administrators and staff—allowing for differentiated access to patient information and system management. This tool served as the foundation for evaluating both system performance and user satisfaction in subsequent research phases.

2) System quality assessment by experts. To evaluate the technical quality and functionality of the developed system, a structured framework was designed by five experts. The evaluation criteria were adapted from ISO/IEC 25010, the standard for software product quality, which outlines eight key dimensions: Functional Suitability, Performance Efficiency, Compatibility, Usability, Reliability, Security, Maintainability, and Portability. The researchers categorized the quality evaluation issues into 11 points.

The assessment utilized a five-point Likert scale, ranging from "lowest" to "highest," to quantify expert opinions on each criterion. The results of this evaluation provided critical insights into the system's technical strengths and potential areas for improvement in its design and operation. The use of multidisciplinary experts ensured that the evaluation covered both technological and public health perspectives, reflecting the system's interdisciplinary nature and community applicability.

3) User satisfaction questionnaire. Drawing on the Technology Acceptance Model (TAM), a user satisfaction questionnaire was used to measure the perceived usefulness and ease of use of the developed web application among end users, specifically the 37 Village Health Volunteers in Ban Na Khaem. The questionnaire was structured into five rating levels (from "highest" to "lowest") and covered four major aspects: content quality, system design, usability, and operational efficiency.

4) An evaluation form for comparing the results before and after using a web application. The evaluation of the developed web-based monitoring system was conducted using a structured questionnaire administered to Village Health Volunteers (VHVs) before and after the system's implementation. The purpose of this evaluation was to compare user perceptions regarding the effectiveness of the traditional monitoring process and the newly developed web-based system. The questionnaire consisted of five key evaluation dimensions: (1) ease of data recording, (2) efficiency of patient monitoring, (3) accuracy of health data management, (4) communication with healthcare providers, and (5) overall user satisfaction. Each dimension was measured on a five-point Likert scale, with 1 representing the lowest level of agreement and 5 the highest. The pre-implementation evaluation was conducted before the system's introduction to measure baseline perceptions of VHVs regarding the traditional process of monitoring bedridden patients, which typically involved manual data recording, paper-based documentation, and communication via phone calls or informal reporting. Following the deployment and practical use of the developed web-based system, the post-implementation evaluation was conducted using the same questionnaire. This allowed for a direct comparison of user perceptions before and after the system was introduced.

2.4.2 Validity and reliability of the evaluation instrument

To ensure the credibility and rigor of the evaluation results, the validity and reliability of the research instrument were assessed systematically before data collection. The evaluation

questionnaire used in this study was developed based on relevant literature on digital health systems, user satisfaction evaluation, and community healthcare information systems.

1) Content validity Content validity was examined using the Index of Item-Objective Congruence (IOC) method. The questionnaire was reviewed by three experts specializing in health informatics, community healthcare management, and information system development. Each expert evaluated the relevance and clarity of the questionnaire items in relation to the research objectives using a three-point rating scale (−1 = not relevant, 0 = uncertain, 1 = relevant). The IOC values for all questionnaire items ranged from 0.67 to 1.00, exceeding the acceptable threshold of 0.50, indicating that the items were appropriate and consistent with the research objectives.

2) Reliability analysis to examine the internal consistency of the evaluation instrument. A pilot test was conducted with 30 Village Health Volunteers (VHVs) who had characteristics similar to the target participants. The questionnaire's reliability was analyzed using Cronbach's alpha. The results showed an overall reliability coefficient of 0.92, indicating a high level of internal consistency. The reliability coefficients for each evaluation ranged from 0.86 to 0.91, which are considered acceptable according to established research standards. These results demonstrate that the questionnaire possessed adequate validity and reliability and was appropriate for evaluating user perceptions of the developed web-based monitoring system

2.5 Data Collection

After the web-based application development was completed, the researcher conducted a pilot implementation to evaluate its functionality, usability, and effectiveness in a real-world community health context. The data collection process was systematically organized to obtain both expert assessments and user feedback, ensuring a comprehensive evaluation of the system's performance and user experience. The procedures were carried out as follows.

2.5.1 Expert system evaluation *Five experts participated in the system quality evaluation to* assess the technical performance and overall functionality of the developed web application. The experts were selected based on their professional experience in business computer systems, information technology, and public health. Each expert was given access to the system prototype and instructed to perform specific data-entry, patient-monitoring, and report-generation tasks.

Following the testing phase, the experts completed a standardized quality assessment form that measured four key criteria: system functionality, ease of use, data security, and processing efficiency. Their feedback provided essential insights into the system's strengths, limitations, and technical robustness. The data collected in this phase were used to refine the application and validate its readiness for real-world deployment.

2.5.2 User testing and satisfaction assessment

A sample of 37 Village Health Volunteers (VHVs) from Ban Na Khaem Subdistrict participated in the user testing phase to examine the system's usability and practical applicability during actual patient monitoring activities. Each participant received a brief training session on operating the web application, including instructions on logging in, recording patient data, scheduling visits, and generating reports. After testing the system in real community settings, the VHVs completed a satisfaction questionnaire designed to measure their perceptions of the system's content quality, design, usability, and operational efficiency. The data from this phase demonstrated the system's real-world effectiveness in supporting community health volunteers in their day-to-day patient care responsibilities.

2.5.3 Data collection and preparation for analysis

All completed evaluation forms and satisfaction questionnaires were systematically collected and verified for completeness and consistency. The researcher then organized the data into two categories: expert evaluation data and user satisfaction data. The quantitative data were coded and entered into a database for subsequent statistical analysis, while qualitative comments from experts

and users were summarized to identify common themes and improvement suggestions. This integrated approach ensured that both technical performance metrics and user experience perspectives were included in the final analysis, providing a comprehensive understanding of the web application's effectiveness and potential for further development in community healthcare contexts.

2.6 Data Analysis

The data collected from both expert evaluations and user satisfaction surveys were analyzed using descriptive statistics to summarize the data and assess the overall quality and performance of the developed web application. This approach was chosen to provide a clear and systematic representation of participants' responses, focusing on trends, averages, and the dispersion of opinions. The analysis procedures were carried out as follows.

2.6.1 Frequency and percentage were employed to illustrate the distribution of responses across each rating level in the evaluation and satisfaction questionnaires. This statistical technique enabled the researcher to identify how often specific response options were selected and the proportion of participants who rated the system at various levels of quality or satisfaction. By examining these distributions, the study could determine the general tendencies and levels of agreement among experts and users regarding the system's effectiveness and usability.

2.6.2 The arithmetic mean (average) was used to represent the central tendency of expert and user evaluations, indicating the overall levels of system quality and user satisfaction. Mean scores were calculated for each dimension of the assessment, including system functionality, ease of use, security, processing efficiency, and overall satisfaction. Higher mean values indicated stronger agreement and more favorable evaluations of the system's performance. This method provided a concise summary measure that reflects the perceived quality and effectiveness of the developed web application in supporting community health activities.

2.6.3 The standard deviation was calculated to measure the degree of variability or dispersion in the responses among participants. A low standard deviation indicated that the responses were consistent and clustered closely around the mean, suggesting general agreement among evaluators. Conversely, a high standard deviation suggested a greater diversity of opinions. This measure enabled the researcher to assess the stability and reliability of responses, offering deeper insight into the consistency of expert and user perceptions of the system's design, functionality, and overall usability.

2.6.4 The paired-samples t-test was used to compare user perceptions before and after system implementation. The analysis included means, standard deviations, t-values, and p-values to determine whether differences between the two conditions were statistically significant.

The use of these descriptive statistical methods enabled the researcher to systematically interpret the evaluation data and present the results in a structured and meaningful way. The analysis provided empirical evidence on the web application's quality, effectiveness, and user satisfaction, forming the basis for further discussion and conclusions.

3. Research Results

The research results are divided into three parts: results of web application development for bedridden patients, results of expert performance evaluation, and results of user satisfaction evaluation. Details are as follows.

3.1 Results of web application development for bedridden patients.

The web application developed for bedridden patients in Ban Na Khaem features a two-level user interface: administrators and staff. The system's interface is designed as follows

3.1.1 Login page

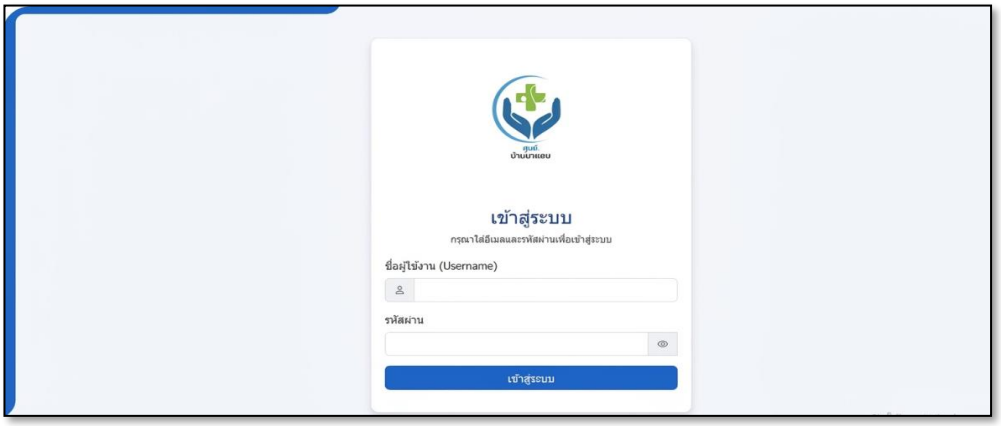


Figure 3. Login page

Figure 3 shows the login page. System administrators and staff must log in to access the system at the login page by entering a username and password.

3.1.2 User management

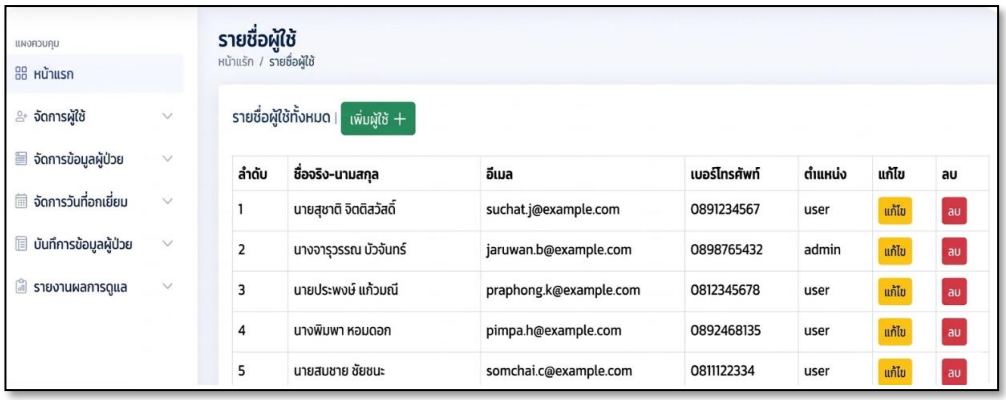


Figure 4. User management page

Figure 4 shows the user management page, accessible only by system administrators. They can add, remove, and edit first names, last names, email addresses, phone numbers, and job titles.

3.1.3 Patient data record

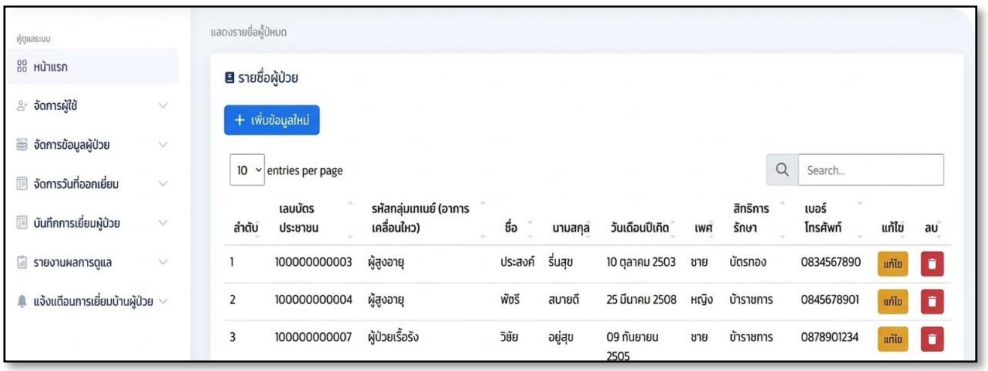


Figure 5. Patient data record page

Figure 5 shows the screen for adding patient information. System administrators and staff can add, delete, and edit patient ID numbers, patient groups, first names, last names, dates of birth, genders, health insurance coverage, and phone numbers.

3.1.4 Visiting appointment



Figure 6. Visit appointment page

Figure 6 shows the appointment scheduling screen. System administrators and staff can add, remove, and edit patient information, including caregiver names, patient names, visit dates, and save the appointment.

3.1.5 Patient visit record



Figure 7. Patient visit record page

Figure 7 shows the user interface (UI) of the patient visit recording page, designed as an efficient community health data management information system. This screen contains crucial information for monitoring patient conditions, including caregiver name, patient category, patient's name and surname, and initial symptoms. It also includes sections for recording vital signs and in-depth physical data such as weight, height, body temperature, and pulse, as well as assessing complications like pressure ulcers and wound characteristics, allowing staff to evaluate risks immediately. The system supports real-time data management via edit and delete buttons for individual entries, along with search and pagination to easily review large amounts of data.

3.1.6 Patient visit report



Figure 8. Visit report page

Figure 8 shows the visit report page for bedridden patients. The table includes information such as the caregiver's name, the patient's name, the visit date, and the patient's symptoms. Next is a section for reporting physical and vital signs data, including weight (kg), height (cm), temperature (°C), pulse (bpm), and blood pressure (mmHg). There are also columns for assessing pressure ulcers and additional details, used to record other important information such as mobility assessment, care methods, complications, and other problems, providing the medical and care team with complete information for long-term planning.

3.2 System quality assessment results

The system quality assessment was conducted by five experts specializing in information technology, business computing, and public health. Their evaluations focused on functionality, usability, security, and processing efficiency. The summarized results, presented in Table 1, reflect the overall performance and technical reliability of the developed web-based application.

Table 1. Results of the evaluation of the quality of the Ban Na Khaem bedridden patient tracking system

Quality Assessment	$\overline{X}$	S.D.	Rating
Functional system performance	4.45	0.51	High
System functionality	4.52	0.48	Highest
Ease of use	4.60	0.45	Highest
System efficiency	4.48	0.50	High
Accuracy of Health Data Management	4.50	0.47	Highest
System security	4.55	0.49	Highest
Information Quality	4.53	0.46	Highest
System Reliability	4.47	0.52	High
Maintainability	4.44	0.54	High
Accessibility & Compatibility	4.46	0.53	High
Decision Support / Portability	4.58	0.47	Highest
Total	4.51	0.49	Highest

Table 1 presents the quality evaluation of the bedridden patient tracking system in Ban Na Khaem. Overall, the system achieved the highest level of evaluation ($\bar{x}$ = 4.51, S.D. = 0.49), reflecting strong user satisfaction across all dimensions. Key strengths were identified in ease of use ($\bar{x}$ = 4.60), decision support/portability ($\bar{x}$ = 4.58), system security ($\bar{x}$ = 4.55), information quality ($\bar{x}$ = 4.53), system functionality ($\bar{x}$ = 4.52), and accuracy of health data management ($\bar{x}$ = 4.50), all of which were rated at the highest level. In contrast, aspects such as functional performance, efficiency, reliability, maintainability, and accessibility/compatibility were rated highly, with mean scores ranging from 4.44

to 4.48. These results indicate that the developed web application effectively integrates usability with strong data protection. This balance is particularly important for community-based healthcare systems, where overly complex but secure systems may hinder adoption. Moreover, the high rating for decision support suggests that the system not only stores data but also provides meaningful insights to support healthcare decision-making.

3.3 Results of system satisfaction assessment

The user satisfaction assessment was conducted with a sample of 37 Village Health Volunteers who utilized the web-based application in real community settings. Their feedback, summarized in Table 2, reflects perceptions of system design, content quality, usability, and operational efficiency, providing valuable insights into user acceptance and overall satisfaction.

Table 2. Satisfaction evaluation results of the use of the Ban Na Khaem bedridden patient tracking system

Satisfaction assessment	$\overline{X}$	S.D.	Rating
Content	4.30	0.39	High
Website design and layout	4.23	0.26	High
Website system performance	4.66	0.21	Highest
Total	4.39	0.14	High

Table 2 presents the satisfaction levels toward the management system for tracking bedridden patients in Ban Na Khaem, showing an overall high level of satisfaction ($\bar{x}$ = 4.39, S.D. = 0.14). Among the evaluated aspects, website efficiency received the highest rating ($\bar{x}$ = 4.66, S.D. = 0.21), indicating that the system performs effectively in supporting field operations and sustaining user engagement. Content quality ($\bar{x}$ = 4.30, S.D. = 0.39) and website design and layout ($\bar{x}$ = 4.23, S.D. = 0.26) were also rated highly. These findings suggest that the system's interface is well aligned with the actual workflow and digital literacy of community health volunteers, resulting in ease of use, a reduced learning curve, and lower resistance to technology adoption.

3.4 Comparison of user perceptions before and after system implementation

Table 3. Comparison of user perceptions before and after system implementation

Evaluation dimension	Before Mean (SD)	After Mean (SD)	t-value	p-value
Ease of Data Recording	3.12 (0.64)	4.48 (0.52)	9.21	< 0.001
Efficiency of Patient Monitoring	3.05 (0.71)	4.55 (0.50)	10.34	< 0.001
Accuracy of Health Data Management	3.18 (0.68)	4.50 (0.49)	8.87	< 0.001
Communication with Healthcare Providers	3.22 (0.66)	4.47 (0.54)	8.41	< 0.001
Overall Satisfaction	3.25 (0.69)	4.60 (0.47)	9.76	< 0.001

Significance level: $p < 0.05$

The results in Table 3 compare user perceptions before and after the implementation of the web-based monitoring system. The analysis used a paired t-test to determine whether there were statistically significant differences between the two periods. The findings indicate that all evaluation dimensions improved substantially after the system was implemented. Specifically, the mean ease-of-data-recording score increased from 3.12 to 4.48, while the patient-monitoring efficiency score improved from 3.05 to 4.55. Similarly, the accuracy of health data management increased from 3.18 to 4.50, and communication with healthcare providers improved from 3.22 to 4.47. Overall user satisfaction also increased significantly from 3.25 to 4.60 after system implementation. The paired t-test results demonstrate that all observed differences were statistically significant ($p < 0.001$). These results

suggest that the developed web-based system significantly enhanced Village Health Volunteers' ability to record patient data, monitor patient conditions, and coordinate healthcare services more effectively.

4. Discussion

The development of the web application for tracking bedridden patients in Ban Na Khaem Subdistrict successfully addressed the limitations of traditional monitoring methods, such as paper-based records and manual communication. The system enabled Village Health Volunteers (VHVs) to efficiently record patient data, schedule home visits, receive reminders, and generate real-time reports. The division of users into two levels—administrators and staff—facilitated secure data management and ensured that sensitive patient information was properly protected. The system provides several advantages, including increased access to healthcare practitioners through teleconsultations, improved outcomes via remote monitoring, and enhanced disease management through mobile health applications and wearable devices. [11]. The expert evaluation revealed that the system achieved high quality in all aspects, especially in security and performance, with an overall mean score of 4.51 reflecting the highest level of user satisfaction. Notably, ease of use, decision support/portability, and system security received the highest ratings, suggesting that the system is not only user-friendly but also effectively supports healthcare decision-making while ensuring data protection. These results highlight the importance of designing systems that align with the practical needs and capabilities of Village Health Volunteers (VHVs). Importantly, the results demonstrate that the developed system can directly support community healthcare monitoring in practical terms. Specifically, the system facilitates (1) structured patient data recording, (2) real-time monitoring and reporting, and (3) improved communication between VHVs and healthcare providers. These functionalities address key limitations of traditional monitoring approaches, such as manual record-keeping and fragmented communication, and contribute to more efficient and coordinated healthcare service delivery in rural communities. This finding aligns with Maramba et al. [12], who emphasized that usability, efficiency, and security are essential design principles for sustainable e-health systems. Similarly, Luitel et al. [13] highlighted that the successful adoption of mobile and web health technologies depends largely on performance reliability and ease of use by frontline health workers.

In addition, the high user satisfaction score among VHVs demonstrates the system's practicality and acceptance. Users particularly appreciated the system's efficiency and ease of use, which supported patient follow-up and reporting tasks, indicating that the information provided is relevant and understandable and that the interface is appropriately designed for users with varying levels of digital literacy. These findings suggest that the system successfully aligns with user needs and workflow characteristics, thereby reducing barriers to technology adoption. Overall, the high satisfaction levels across all dimensions demonstrate that the system not only performs effectively but also provides a positive user experience, which is essential for promoting long-term adoption and improving the efficiency of community-based healthcare monitoring. This is consistent with Aitken et al. [14], who emphasized that user trust and perceived usefulness play critical roles in the implementation of digital health technologies. Furthermore, the system developed from the study has attractive features for visiting nurses and supports their essential tasks. The system can help with effective case management for older adults requiring in-home care and reduce nurses' workload [15]. Overall, the developed web application demonstrates strong potential as a scalable model for digital transformation in primary healthcare. By integrating real-time data recording, automated scheduling, and reporting functions, the system strengthens the efficiency of VHVs and ensures continuous, accurate monitoring of bedridden patients. Future improvements could involve mobile device integration and interoperability with national health databases to enhance accessibility and continuity of care further.

Table 4. Comparison of the proposed system with previous studies

Points of comparison	Sumner et al. [2]	Cao et al. [3]	Lee et al. [15]	Proposed System (This Study)
System Type	Remote patient monitoring system	Cloud-based health monitoring platform	Web-based healthcare networking system	Web-based community health monitoring system
Target Users	Healthcare professionals	Medical institutions	Healthcare providers	Village Health Volunteers
Key Features	Clinical monitoring and data collection	Centralized patient data management	Care coordination and communication	Patient data management, home visit scheduling, monitoring, and reporting
Limitations	Focused on hospital environments	Requires professional healthcare infrastructure	Limited focus on community volunteers	Implemented in a specific community
Contribution of This Study	Provides community-based monitoring for VHVs	Designed for rural community health volunteers	Supports home-based patient care by VHVs	Provides a digital monitoring model for rural community healthcare

5. Conclusions

This study aimed to develop and evaluate a web-based application designed to support Village Health Volunteers (VHVs) in monitoring bedridden patients in Na Khaem Subdistrict, Loei Province, Thailand. The developed system integrates patient data management, visit scheduling, home visit recording, and reporting functions into a unified digital platform that facilitates community-based healthcare monitoring. The evaluation results demonstrate that the system achieved a high level of quality and user satisfaction, confirming its technical reliability and practical suitability for community healthcare environments. Importantly, the comparison between pre-implementation and post-implementation results provides clear evidence of the system's effectiveness. Before system adoption, user perceptions across key dimensions such as ease of data recording, efficiency of patient monitoring, accuracy of health data management, and communication with healthcare providers were at a moderate level. After implementation, these scores increased significantly to a high level, with all differences being statistically significant ($p < 0.001$). These findings indicate that the developed system substantially improves operational efficiency, reduces manual workload, enhances data accuracy, and strengthens coordination among healthcare stakeholders. Beyond its measurable performance improvements, the system offers significant practical implications for rural healthcare management. By replacing traditional paper-based processes with a digital platform, the system enables more efficient and structured data handling, supports timely decision-making, and enhances the continuity of patient care. The integrated scheduling and reporting features further enable VHVs and healthcare providers to plan and monitor home visits more systematically. In real-world applications, the proposed system can serve as a practical digital tool for supporting the daily operations of VHVs and community healthcare personnel. It can also assist local healthcare centers and administrative units in managing patient information more effectively and improving service coordination. Given its design and adaptability, the system has strong scalability potential and can be implemented in other rural

communities facing similar healthcare challenges. From a broader perspective, this study demonstrates how digital health technologies can be effectively integrated into primary healthcare systems to enhance service delivery and support community-based care. The system provides a replicable model for leveraging digital tools to improve healthcare accessibility, efficiency, and sustainability, particularly in resource-constrained settings. Future work should focus on extending the system through mobile application integration to support real-time data entry during home visits, as well as enhancing interoperability with national health information systems. Further studies involving larger populations and multiple regions are recommended to evaluate long-term effectiveness, scalability, and impact on patient health outcomes. Overall, this study highlights the significant potential of digital health innovations to transform community healthcare practices. By demonstrating clear improvements before and after system implementation, the research provides strong empirical support for the adoption of web-based monitoring systems in rural healthcare contexts.

6. Acknowledgments

The authors would like to express their sincere gratitude to the experts and Village Health Volunteers (VHVs) in Ban Na Khaem Subdistrict, Loei Province, for their valuable participation and constructive feedback throughout the research process. Their collaboration and insights were instrumental in the successful development and evaluation of the web application for bedridden patient monitoring.

Author Contributions: Conceptualization, P.J., I.S., N.W., and S.P.; methodology, P.J., N.K., and M.T.; software, P.J., M.T., and I.S.; validation, P.J. and S.P.; formal analysis, P.J. and N.W.; investigation, N.K., M.T., I.S., and N.W.; resources, P.J.; data curation, P.J. and M.T.; writing—original draft preparation, P.J.; writing—review and editing, P.J., S.P. and I.S.; visualization, M.T. and N.W.; supervision, S.P.; project administration, P.J. All authors have read and agreed to the published version of the manuscript.

Funding: This research received no external funding.

Conflicts of Interest: The authors declare no conflict of interest.

References

[1] Kaewsombat, K.; Khunphilik, I.; Wijitpanya, A.; Chaimueang, P.; Channam, P. Development of a psychiatric patient care system through the provincial network in Loei Province. *J. Environ. Health Community Health* **2024**, *9*(5), 549–560. (in Thai).

[2] Sumner, J.; Tan, S.; Wang, Y.; Keck, C.; Xin Lee, E.; Chew, E.; Yip, A. Co-designing remote patient monitoring technologies for inpatients: Systematic review. *J. Med. Internet Res.* **2024**, *16*. https://doi.org/10.2196/58144

[3] Cao, M.; Ramezani, R.; Katakwar, V. K.; Zhang, W.; Boda, D.; Wani, M.; Naeim, A. Developing remote patient monitoring infrastructure using commercially available cloud platforms. *Front. Digit. Health* **2024**. https://doi.org/10.3389/fdgth.2024.1399461

[4] Das, M. K.; Deb, P.; De, I. Remote patient health monitoring frameworks using IoT and ML: A comparative study. *Int. J. Intell. Syst. Appl. Eng.* **2024**, *12*, 367–372.

[5] Khembubpha, S. Development of a service linkage system from intermediate care to long-term care in Ban Dan District, Buriram Province. *Reg. Health Promot. Cent. 9 J.* **2021**, *16*(3), 939–956. (in Thai).

[6] Majeed, M.; Chaudhary, A.; Chadha, R. *Digital Transformation in the Customer Experience*; Apple Academic Press, 2025. https://doi.org/10.1201/9781003560449

[7] Alam, M. Z.; Hoque, M. R.; Hu, W.; Barua, Z. Factors influencing the adoption of mHealth services in a developing country: A patient-centric study. *Int. J. Inf. Manage.* **2020**, *50*, 128–143.

[8] Dwivedi, Y. K.; Hughes, D. L.; Rana, N. P.; Baabdullah, A. M.; Ribeiro-Navarrete, S.; Giannakis, M.; Al-Debei, M. M.; Dennehy, D.; Metri, B.; Buhalis, D.; et al. Metaverse beyond the hype:

Multidisciplinary perspectives on emerging challenges, opportunities, and agenda for research, practice and policy. *Int. J. Inf. Manage.* **2022**, *66*, 102542. https://doi.org/10.1016/j.ijinfomgt.2022.102542

[9] Na Khaem Subdistrict Administrative Organization. https://nakhamloei.go.th/public/ (accessed Jan 14, 2025).

[10] Krejcie, R. V.; Morgan, D. W. Determining sample size for research activities. *Educ. Psychol. Meas.* **1970**, *30*(3), 607–610. https://doi.org/10.1177/001316447003000308

[11] Maita, K. C.; Maniaci, M. J.; Haider, C. R.; Avila, F. R.; Torres-Guzman, R. A.; Borna, S.; Lunde, J. J.; Coffey, J. D.; Demaerschalk, B. M.; Forte, A. J. The impact of digital health solutions on bridging the healthcare gap in rural areas: A scoping review. *Int. J. Med. Inform.* **2024**, *28*(3), 130–143. https://doi.org/10.7812/TPP/23.134

[12] Maramba, I.; Chatterjee, A.; Newman, C. Methods of usability testing in the development of eHealth applications: A scoping review. *Int. J. Med. Inform.* **2019**, *126*, 95–104. https://doi.org/10.1016/j.ijmedinf.2019.03.018

[13] Luitel, N. P.; Neupane, V.; Lamichhane, B.; Koirala, G. P.; Gautam, K.; Karki, E.; Adhikari, S.; Votruba, N.; Jordans, M. J. D.; Kohrt, B. A.; Carswell, K.; Thornicroft, G.; Lempp, H. Experience of primary healthcare workers in using the mobile app-based WHO mhGAP intervention guide in detection and treatment of people with mental disorders: A qualitative study in Nepal. *SSM Ment. Health* **2023**, *4*, 100278. https://doi.org/10.1016/j.ssmmh.2023.100278

[14] Aitken, M.; Tully, M. P.; Porteous, C.; Denegri, S.; Cunningham-Burley, S.; Banner, N.; Black, C.; Burgess, M.; Cross, L.; van Delden, J. J.; et al. Consensus statement on public involvement and engagement with data-intensive health research. *Int. J. Popul. Data Sci.* **2019**, *4*(1), 586. https://doi.org/10.23889/ijpds.v4i1.586

[15] Lee, J.; Park, S.; Cho, M.-H.; Kang, J.-W.; Kim, M.; Choi, S.; Kim, S.-G.; Han, K.; Kim, C.-O.; Moon, I.-C.; Jang, S.-N. Development of a web-based care networking system to support visiting healthcare professionals in the community. *BMC Health Serv. Res.* **2023**, *23*, 10434. https://doi.org/10.1186/s12913-023-10434-6

ASEAN
Journal of Scientific and Technological Reports
Online ISSN:2773-8752

Research article

Fish Diversity and Fish Community Structure in Wang Nong Reservoir, Nakhon Phanom Province, Thailand

Nattanan Tiengtam[1*], and Adithepchaikarn Pachanawan[1]

[1] Faculty of Agriculture and Technology, Nakhon Phanom University, Nakhon Phanom Province, 48000, Thailand
* Correspondence: nattanan_tga@npu.ac.th

Citation:
Tiengtam, N.; Pachanawan, A. Fish Diversity and Fish community structure in wang nong reservoir, Nakhon Phanom Province, Thailand. *ASEAN J. Sci. Tech. Report.* **2026**, *29*(5), e261014. https://doi.org/10.55164/ajstr.v29i5.261014

Article history:
Received: August 27, 2025
Revised: March 21, 2026
Accepted: April 11, 2026
Available online: April 30, 2026

Publisher's Note:
This article is published and distributed under the terms of the Thaksin University.

Abstract: Fish diversity in reservoirs is vital for sustaining food security and livelihoods in rural communities. Wang Nong Reservoir, in Nakhon Phanom Province, northeastern Thailand, supports local fisheries but has remained scientifically unexplored until now. This study presents the first comprehensive assessment of fish community diversity and structure from January to December 2024. Monthly samples were collected at four stations using gill nets and a beach seine. A total of 8,294 specimens representing 47 species from 14 families were recorded. Dominant families included Cyprinidae (51.06%), Bagridae (10.64%), Cobitidae (6.38%), and Osphronemidae (6.38%). The most abundant species were *Rasbora borapetensis* (17.36%), *Esomus metallicus* (11.35%), *Thynnichthys thynnoides* (5.57%), *Cyclocheilichthys repasson* (4.77%), and *Puntius brevis* (4.46%), with twelve species occurring in all samples. Most species were classified as Least Concern on the IUCN Red List, while two were Vulnerable and one was Data Deficient. Seasonal variation was evident, with peak abundance and species richness in summer. The average Shannon-Wiener diversity (H'), richness (R), and evenness (E) indices were 3.12, 4.46, and 0.87, respectively. Water temperature and dissolved oxygen were positively correlated with H', R, and E ($p < 0.01$), whereas transparency showed a negative correlation; other parameters (TDS, pH, NH_3, NO_2, and NO_3) were not significantly related. These findings provide the first baseline dataset on fish diversity in Wang Nong Reservoir, filling a critical knowledge gap for inland fisheries in northeastern Thailand and offering a robust scientific foundation for site-specific conservation planning and evidence-based sustainable fisheries management.

Keywords: Fish diversity; community structure; wang nong reservoir; Nakhon Phanom Province

1. Introduction

Wang Nong Reservoir is a medium-sized earthen reservoir located at 17°45'55.5"N, 104°03'31.0"E in Ban Dontoei, Na Thom District, Nakhon Phanom Province, northeastern Thailand, approximately 717 km northeast of Bangkok (Figure 1). Constructed in 1990, the reservoir has a maximum storage capacity of 2.52 million m^3, receives runoff from a catchment area of approximately 20.68 km^2, and lies at an elevation of 141 meters above mean sea level. It drains into the Songkhram River, a tributary of the Mekong River Basin [1]. Reservoirs, defined as artificial lakes, may or may not be hydrologically connected to river systems [2]. They serve multiple functions, including irrigation, livestock watering, flood control, and the provision of seasonal habitats for riverine fishes,

while also supporting diverse fish assemblages [3]. Fish resources are crucial to local livelihoods, providing both dietary protein and supplementary income [4]. Wang Nong Reservoir is primarily utilized for rice irrigation and domestic water supply. Additionally, it supports recreational activities such as swimming, boating, and fishing, and serves as an important source of livelihood for local fishers. Fish caught from the reservoir are marketed either fresh or processed, including dried and fermented products.

Although the diversity of fish species has been documented in several major reservoirs across northeastern Thailand, such as Sirindhron Reservoir in Ubon Ratchathani Province [5], Bung Klua Reservoir in Roi Et Province [6], Ubolratana Reservoir in Khon Kaen Province [7], Lam Pao Reservoir in Kalasin Province [8], Nam Oun and Huay Huat Reservoirs in Sakon Nakhon Province [9, 10], and Huai Kao Reservoir in Maha Sarakham Province [11], Wang Nong Reservoir remains scientifically unexplored. This significant gap in ecological knowledge limits our understanding of the reservoir's unique fish communities and impedes efforts to manage them sustainably. Given the reservoir's crucial role in supporting agriculture, domestic water supply, and local communities' livelihoods, documenting its fish diversity is both timely and essential. Therefore, this study aims to assess fish species diversity and community structure in Wang Nong Reservoir, representing the first comprehensive assessment of the fish assemblage in this reservoir and providing baseline data for conservation and fisheries management.

2. Materials and Methods

2.1 Study Area and Fish Sampling

The study was conducted in Wang Nong Reservoir (17°45'55.5"N, 104°03'31.0"E) (Figure 1), a multipurpose reservoir located in Ban Dontoei, Na Thom District, Nakhon Phanom Province, Thailand. Fish specimens were collected monthly from January to December 2024 at four sampling stations (ST1-ST4). For seasonal analysis, sampling months were grouped into three seasons based on regional climatic patterns: winter (January and October-December), summer (February-May), and rainy (June-September). The winter season, which spanned January 2024 and October-December 2024, was used for seasonal comparisons. Samples were collected using gill nets with three mesh sizes (2.0, 4.0, and 6.0 cm; 100 m long and 1.5 m deep) and a beach seine with a mesh size of 0.5 × 0.5 cm (25 m long and 1.5 m deep). At each sampling station, the gill nets were deployed three times per sampling event and left in the water for approximately 12 hours (overnight), while the beach seine was hauled three times along the shoreline. Thus, the sampling effort consisted of three gill-net deployments and three seine hauls per station per month. Specimens were preserved in 10% formalin for one month before being transferred to 75% ethanol for permanent preservation and taxonomic identification. Taxonomic identification was conducted following standard references and taxonomic keys described by Smith [12], Rainboth [13], Doi [14], Kottelat [15], Vidthayanon [16], Nelson *et al*. [17], and Taki *et al*. [18]. The threat status of each fish species was determined according to the IUCN Red List [19]. All identifications were performed at the Fisheries Research Laboratory, Faculty of Agriculture and Technology, Nakhon Phanom University, Nakhon Phanom, Thailand.

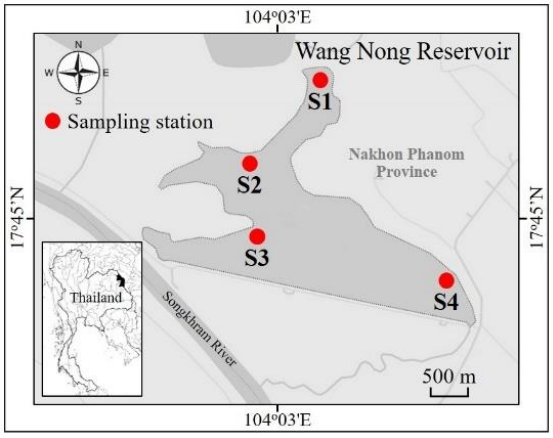


Figure 1. Map of Wang Nong Reservoir and location of sampling stations.

2.2 Environmental parameter sampling

The physicochemical water quality parameters were measured in situ using a YSI® 556 multi-probe system, including temperature, total dissolved solids (TDS), pH, and dissolved oxygen (DO). Water transparency was measured using a Secchi disk. Other parameters, including ammonia (NH_3), nitrite (NO_2), and nitrate (NO_3), were sampled for laboratory analyses using standard methods [20].

2.3 Statistical analyses

To determine the species composition and diversity of the fish population in the study area, the number of fish species and individuals per species were calculated using the following formulas:

Percentage composition by number (%N)

%N = (Number of individuals of a given species / Total number of individuals) x 100

Frequency of occurrence (%F)

%F = (Number of times each fish species was found / Total number of sampling events) x 100

Shannon-Wiener diversity index (H') [21]

$$H' = -\sum_{i=1}^{s} p_i \ln p_i$$

where s is the total number of species, $p_i = n_i/N$, n_i is the number of individuals in species i, and N is the total number of individuals.

Species richness index (R) [22]

$R = (S - 1) / \ln N$

where S is the number of species, and N is the total number of individuals.

Evenness Index (E) [23]

$E = H' / H'_{max}$

where H' is the Shannon-Wiener diversity index, and H'_{max} is its maximum value.

All data were statistically analyzed. The Shannon-Wiener diversity index, species richness index, and evenness index, obtained from each sampling station and season during the survey period at Wang Nong Reservoir, were analyzed using one-way ANOVA followed by Tukey's Honestly Significant Difference (HSD) test at a significance level of $p < 0.05$. Pearson's correlation coefficients were calculated to assess the relationships between physicochemical parameters and these three indices using monthly observations (n = 12) at the $p < 0.01$ significance level. All analyses were performed using SPSS software version 24.0 (IBM SPSS Inc.).

2.4 Ethical statement

This research project was reviewed and approved in accordance with the Ethical Principles and Guidelines for the Use of Animals (Approval No. ACNPU67-001) by Nakhon Phanom University, Thailand.

3. Results and Discussion

3.1 Results

A total of 8,294 fish specimens, representing 47 species across 14 families, were collected (Table 1). The family Cyprinidae was the most abundant, comprising 24 species (51.06%), including *Parachela oxygastroides*, *P. siamensis*, *Esomus metallicus*, *Rasbora borapetensis*, *R. aurotaenia*, *R. trilineata*, *Thynnichthys thynnoides*, *Puntioplites proctozystron*, *Scaphognathops bandanensis*, *Barbonymus altus*, *B. schwanenfeldii*, *B. gonionotus*, *Hampala dispar*, *Puntius brevis*, *Puntigrus partipentazona*, *Cyclocheilichthys enoplos*, *C. repasson*, *Labiobarbus siamensis*, *Osteochilus vittatus*, *O. lini*, *O. microcephalus*, *O. melanopleura*, *Henicorhynchus siamensis*, and *H. ornatipinnis*. This was followed by five species (10.64%) from Bagridae, and three species (6.38%) each from Cobitidae and Osphronemidae (Figure 2). The dominant species were *R. borapetensis* (17.36%), *E. metallicus* (11.35%), *T.*

thynnoides (5.57%), *C. repasson* (4.77%), and *P. brevis* (4.46%), while all other species accounted for less than 4% each. Species with 100% occurrence included *E. metallicus*, *R. borapetensis*, *T. thynnoides*, *P. proctozystron*, *B. altus*, *B. schwanenfeldii*, *B. gonionotus*, *P. brevis*, *C. repasson*, *Oreochromis niloticus*, *Anabas testudineus*, and *Channa striata* (Figure 3). Notably, only one exotic species, *O. niloticus* (1.57%), was recorded. Among the 47 recorded species, the majority (93.62%) were classified as Least Concern (LC), while two species (4.25%), *Scaphognathops bandanensis* and *Mystus bocourti*, were listed as Vulnerable (VU). One species (2.13%), *Hemibagrus filamentus*, was categorized as Data Deficient (DD), according to the IUCN Red List (2025) (Table 1). Regarding the distribution of fish species across sampling stations, Station 1 had the highest species richness (36; 76.60%), whereas Station 4 had the lowest (30; 63.83%). The highest fish abundance was recorded during the summer season, with a total of 3,409 individuals (41.10%), followed by the rainy season with 2,639 individuals (31.82%), and the winter season with 2,246 individuals (27.08%). A similar seasonal trend was observed in species richness, with the highest number of fish species recorded in summer (42 species, 89.36%), followed by the rainy season (36 species, 76.60%) and the winter season (31 species, 65.96%) (Figure 4).

The mean Shannon-Wiener diversity index (H') was 3.12. No significant differences were observed among the sampling stations ($p > 0.05$), with the highest value recorded at Station 1 (3.20), followed by Station 2 (3.19), Station 3 (3.07), and Station 4 (3.03) (Table 2). In contrast, H' varied significantly across seasons ($p < 0.05$), with the highest value recorded in the summer (3.33), followed by the rainy (3.13) and winter (2.89) seasons (Table 3). The mean species richness (R) was 4.46, with no significant differences among stations ($p > 0.05$). Station 1 exhibited the highest richness (4.85), followed by Station 2 (4.60), Station 3 (4.23), and Station 4 (4.15) (Table 2). However, seasonal variation in species richness was significant ($p < 0.05$), with the highest richness observed in summer (5.04), followed by the rainy (4.44) and winter (3.89) seasons (Table 3). The mean evenness index (E) was 0.87. No significant differences were found among stations or across seasons ($p > 0.05$). The highest evenness was recorded at Station 1 (0.90), followed by Station 2 (0.89), Station 3 (0.86), and Station 4 (0.84) (Table 2). Seasonally, evenness was highest in summer (0.89), followed by the rainy (0.87) and winter (0.84) seasons (Table 3).

Seasonal variations in physicochemical water parameters were observed throughout the study period (Table 4). Water temperature ranged from 24.21°C to 30.74°C, while transparency ranged from 34.50 to 57.25 cm. Total dissolved solids (TDS) ranged from 69.25 to 87.75 mg/L, pH values ranged from 7.34 to 7.89, and dissolved oxygen (DO) concentrations ranged from 4.67 to 6.24 mg/L. Regarding nutrients, ammonia (NH_3) ranged from 0.01 to 0.02 mg/L, nitrite (NO_2) ranged from 0.01 to 0.02 mg/L, and nitrate (NO_3) ranged from 0.05 to 0.06 mg/L. To examine the relationship between physicochemical parameters and fish faunal diversity in Wang Nong Reservoir, Nakhon Phanom Province, Thailand, Pearson's correlation coefficients were calculated (Table 5). Water temperature and dissolved oxygen were significantly positively correlated with H', R, and E ($p < 0.01$), whereas transparency was negatively correlated with these indices. In contrast, TDS, pH, NH_3, NO_2, and NO_3 showed no significant correlations.

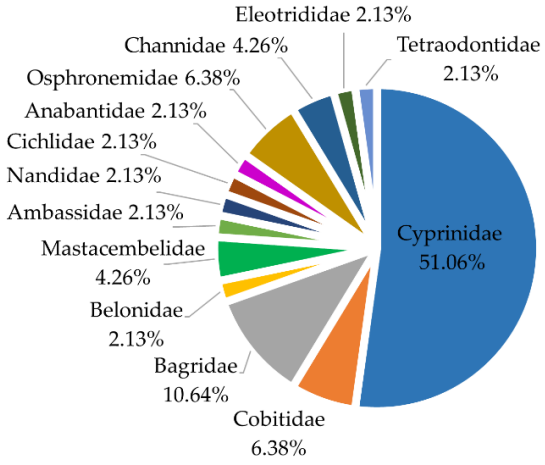


Figure 2. Composition of fish families in Wang Nong Reservoir, Nakhon Phanom Province, Thailand.

Table 1. List of fish species found at each station and season in Wang Nong Reservoir, Nakhon Phanom Province, Thailand (January-December 2024).

No.	Scientific name	Station				Season			Percentage (%)	IUCN status
		S1	S2	S3	S4	S	R	W		
	Family Notopteridae									
1	*Notopterus notopterus*	+	+	+		+	+	+	0.59	LC
	Family Cyprinidae									
2	*Parachela oxygastroides*	+	+	+		+	+		0.58	LC
3	*Parachela siamensis*	+	+	+		+	+		0.63	LC
4	*Esomus metallicus*	+	+	+	+	+	+	+	11.35	LC
5	*Rasbora borapetensis*	+	+	+	+	+	+	+	17.36	LC
6	*Rasbora aurotaenia*		+	+	+	+	+		2.66	LC
7	*Rasbora trilineata*	+		+	+	+			1.52	LC
8	*Thynnichthys thynnoides*	+	+	+	+	+	+	+	5.57	LC
9	*Puntioplites proctozystron*	+	+		+	+	+	+	3.54	LC
10	*Scaphognathops bandanensis*	+	+	+		+	+	+	1.02	VU
11	*Barbonymus altus*	+	+	+	+	+	+	+	2.25	LC
12	*Barbonymus schwanenfeldii*	+	+	+	+	+	+	+	1.56	LC
13	*Barbonymus gonionotus*	+		+	+	+	+	+	3.23	LC
14	*Hampala dispar*		+	+	+	+	+	+	1.62	LC
15	*Puntius brevis*	+	+	+	+	+	+	+	4.46	LC
16	*Puntigrus partipentazona*	+	+	+			+	+	2.72	LC
17	*Cyclocheilichthys enoplos*		+	+	+	+	+	+	1.02	LC
18	*Cyclocheilichthys repasson*	+	+	+	+	+	+	+	4.77	LC
19	*Labiobarbus siamensis*	+	+			+	+	+	3.05	LC
20	*Osteochilus vittatus*	+	+			+	+	+	1.24	LC
21	*Osteochilus lini*	+	+			+	+	+	0.95	LC
22	*Osteochilus microcephalus*	+				+	+		1.10	LC
23	*Osteochilus melanopleura*	+	+				+	+	0.43	LC
24	*Henicorhynchus siamensis*	+	+		+	+	+		1.72	LC
25	*Henicorhynchus ornatipinnis*	+			+	+	+		1.39	LC
	Family Cobitidae									
26	*Acantopsis dinema*			+	+	+			1.53	LC
27	*Syncrossus helodes*	+					+	+	0.47	LC
28	*Yasuhikotakia modesta*	+					+	+	0.51	LC
	Family Bagridae									
29	*Pseudomystus siamensis*	+				+		+	0.08	LC
30	*Mystus bocourti*	+	+			+		+	0.89	VU
31	*Mystus atrifasciatus*		+		+	+	+		0.58	LC
32	*Mystus mysticetus*		+		+	+	+		0.69	LC
33	*Hemibagrus filamentus*			+	+		+		0.53	DD
	Family Belonidae									
34	*Xenentodon cancila*			+	+	+	+	+	0.98	LC
	Family Mastacembelidae									
35	*Macrognathus siamensis*	+	+			+			1.06	LC
36	*Mastacembelus armatus*	+				+		+	0.11	LC
	Family Ambassidae									
37	*Parambassis siamensis*	+	+	+		+	+	+	2.91	LC
	Family Nandidae									
38	*Pristolepis fasciata*		+		+	+	+	+	1.13	LC

Table 1. List of fish species found at each station and season in Wang Nong Reservoir, Nakhon Phanom Province, Thailand (January-December 2024) (cont.).

No.	Scientific name	Station				Season			Percentage (%)	IUCN status
		S1	S2	S3	S4	S	R	W		
	Family Cichlidae									
39	*Oreochromis niloticus*	+	+	+	+	+	+	+	1.57	LC
	Family Anabantidae									
40	*Anabas testudineus*	+	+	+	+	+	+	+	2.29	LC
	Family Osphronemidae									
41	*Trichopodus microlepis*	+	+	+	+	+			1.62	LC
42	*Trichopodus trichopterus*	+	+	+	+	+			2.23	LC
43	*Trichopsis vittata*	+	+	+	+	+			1.46	LC
	Family Channidae									
44	*Channa striata*	+	+	+	+	+	+	+	1.59	LC
45	*Channa micropeltes*			+	+	+		+	0.59	LC
	Family Eleotrididae									
46	*Oxyeleotris marmorata*			+	+	+	+		0.65	LC
	Family Tetraodontidae									
47	*Pao barbatus*	+		+	+	+		+	0.18	LC
	Total	36	34	31	30	42	36	31	100	

Note: S1-S4 = Sampling stations for fish collection; Season abbreviations: S = Summer, R = Rainy, W = Winter; IUCN Red List categories: DD = Data Deficient, LC = Least Concern, VU = Vulnerable.

Table 2. Diversity index, species richness index, and evenness index of the fish community by station in Wang Nong Reservoir.

Parameters	S1	S2	S3	S4	Mean
Shannon-Wiener diversity index (H')	3.20	3.19	3.07	3.03	3.12
Species richness index (R)	4.85	4.60	4.23	4.15	4.46
Evenness index (E)	0.90	0.89	0.86	0.84	0.87

Note: Means in the same row are not significantly different among stations ($p > 0.05$).

Table 3. Diversity index, species richness index, and evenness index of the fish community by season in Wang Nong Reservoir.

Parameters	Summer	Rainy	Winter	Mean
Shannon-Wiener diversity index (H')	3.33^{a}	3.13^{ab}	2.89^{b}	3.12
Species richness index (R)	5.04^{a}	4.44^{ab}	3.89^{b}	4.46
Evenness index (E)	0.89	0.87	0.84	0.87

Note: Means in a row with different superscript letters are significantly different ($p < 0.05$).

Table 4. Seasonal variations of physicochemical water parameters in Wang Nong Reservoir.

Parameters	Summer	Rainy	Winter	Range
Temperature (°C)	30.74	28.52	24.21	24.21-30.74
Transparency (cm)	44.00	34.50	57.25	34.50-57.25
Total dissolved solids (TDS, mg/L)	76.50	87.75	69.25	69.25-87.75
pH	7.89	7.34	7.52	7.34-7.89
Dissolved oxygen (DO, mg/L)	5.78	6.24	4.67	4.67-6.24
Ammonia (NH_3, mg/L)	0.01	0.02	0.02	0.01-0.02
Nitrite (NO_2, mg/L)	0.01	0.01	0.02	0.01-0.02
Nitrate (NO_3, mg/L)	0.05	0.06	0.05	0.05-0.06

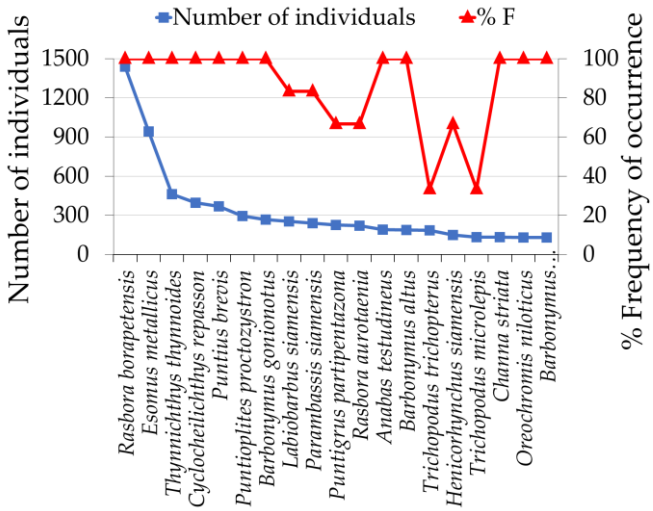


Figure 3. Number of individuals and frequency of occurrence (%F) of fish species in Wang Nong Reservoir, Nakhon Phanom Province, Thailand.

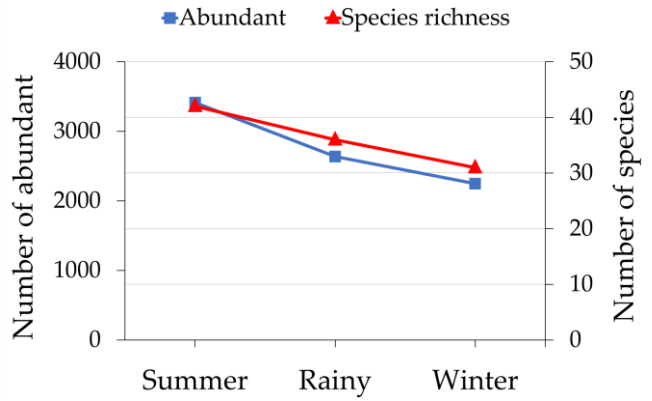


Figure 4. Fish abundance and species richness in Wang Nong Reservoir, Nakhon Phanom Province, Thailand.

Table 5. Pearson's correlation coefficients between physicochemical parameters and diversity index, species richness index, and evenness index in Wang Nong Reservoir, Nakhon Phanom Province, Thailand.

Parameters	Shannon-Wiener diversity index (H')	Species richness index (R)	Evenness index (E)
Temperature (°C)	0.864**	0.950**	0.949**
Transparency (cm)	-0.820**	-0.840**	-0.800**
Total dissolved solids (TDS, mg/L)	0.439	0.392	0.507
pH	0.642	0.693	0.599
Dissolved oxygen (DO, mg/L)	0.740**	0.760**	0.730**
Ammonia (NH_3, mg/L)	-0.570	-0.590	-0.550
Nitrite (NO_2, mg/L)	-0.520	-0.540	-0.500
Nitrate (NO_3, mg/L)	0.440	0.460	0.420

Note: Pearson correlation coefficients were calculated using monthly data (n = 12). ** indicates significant correlations at $p < 0.01$.

3.2 Discussion

This study represents the first attempt to investigate the fish diversity and community structure of Wang Nong Reservoir. A total of 47 species from 14 families were recorded, with Cyprinidae being the dominant family (24 species, 51.06%). Due to the absence of previous studies in this reservoir, direct historical comparisons are unavailable. However, the results are comparable to those of other northeastern Thai reservoirs. For example, Bung Klua Reservoir in Roi Et Province was reported to have 53 species, including 26 Cyprinidae (49.06%) [6]. Ubolratana Reservoir in Khon Kaen Province contained 62 species, also with 26 Cyprinidae (41.93%) [7], while Lam Pao Reservoir in Kalasin Province harbored 57 species, with 26 Cyprinidae (45.61%) [8]. These reservoirs exhibited higher species richness than Wang Nong. Conversely, Nam Oun Reservoir in Sakon Nakhon Province had 44 species, including 18 Cyprinidae (40.90%) [9], while Huay Huat Reservoir, also in Sakon Nakhon, had only 23 species, of which 13 were Cyprinids (56.52%) [10]. In Maha Sarakham Province, Huai Kao Reservoir supported 22 species, dominated by 8 Cyprinids (36.36%) [11], indicating lower diversity than Wang Nong. Overall, fish diversity in Wang Nong Reservoir is moderate within the regional context, with Cyprinidae consistently dominating across sites. The high species diversity of Cyprinidae throughout Southeast Asia [17, 18, 24] and their adaptability to lentic habitats help explain their dominance in Thai reservoirs [25].

In this study, the most dominant species were small cyprinids, including *Rasbora borapetensis* (17.36%), *Esomus metallicus* (11.35%), *Thynnichthys thynnoides* (5.57%), *Cyclocheilichthys repasson* (4.77%), and *Puntius brevis* (4.46%). The dominance of small cyprinid species, particularly *Rasbora borapetensis* and *Esomus metallicus*, may be related to their ecological adaptability to reservoir environments. These species are small-bodied pelagic fishes that often form large schools and efficiently exploit planktonic food resources in open-water habitats. Their planktivorous feeding habits, rapid reproduction, and tolerance to a wide range of environmental conditions enable them to thrive in lentic or slow-flowing waters, which are typical characteristics of reservoir ecosystems [13, 18, 26]. Similarly, Panchan [9] reported *Puntius brevis* (31.70%), *C. repasson* (17.70%), *Parambassis siamensis* (16.00%), *Labiobarbus leptocheila* (8.59%), and *Pristolepis fasciata* (4.77%) as dominant species in Nam Oun Reservoir. Jutagate *et al*. [26] found *that Clupeichthys aesarnensis (19.00%), R. borapetensis (10.60%), Barbonymus gonionotus (10.20%), E. metallicus (9.60%), and Oreochromis niloticus (4.20%) were* the most abundant species in Sirindhorn Reservoir. In contrast, Khowhit *et al*. [11] reported *Hampala dispar* (28.72%), *Cyclocheilichthys armatus* (14.09%), *Henicorhynchus caudimaculatus* (10.38%), *Oxyeleotris marmorata* (7.69%), and *Notopterus notopterus* (7.13%) as dominant species in Huai Kao Reservoir. These differences in dominant species among reservoirs may reflect variations in topography, habitat complexity, water quality, food availability, and resource utilization [26-28].

The exotic species *O. niloticus* is native to Africa and was introduced to Thailand in the mid-20th century for aquaculture purposes. Following successful breeding, it was widely distributed by the Department of Fisheries and extensively used in aquaculture and reservoir stocking [29]. As a result, this species is now well established in natural aquatic ecosystems throughout Thailand [30]. In the present study, *O. niloticus* was the only non-native species recorded in Wang Nong Reservoir, consistent with several reservoir studies in northeastern Thailand where Nile tilapia is typically reported as the predominant non-native species [8-11]. The occurrence of additional non-native or translocated species in reservoir systems is context-dependent, influenced by environmental conditions, introduction history, and species-specific ecological traits. Species with broad environmental tolerance, opportunistic feeding strategies, and high reproductive capacity are more likely to establish and persist, and they may also form self-sustaining populations in lentic environments [31].

From a conservation perspective, the majority of fish species in Wang Nong Reservoir are classified as Least Concern (LC, 93.62%) according to the IUCN Red List, whereas two species, *Scaphognathops bandanensis* and *Mystus bocourti*, are categorized as Vulnerable (VU) [19]. These species are of particular concern, as they may be more sensitive to environmental changes and habitat disturbances. Potential threats include habitat alteration associated with water level regulation, reduced water quality, and fishing pressure, which are common stressors in managed reservoirs and may disproportionately affect vulnerable populations. In addition, seasonal water retention and fluctuations in water level in Wang Nong Reservoir may alter littoral and benthic habitats that are essential for feeding, shelter, and reproduction. Such changes could negatively

impact these species, particularly if suitable microhabitats are reduced or degraded. Therefore, targeted management actions are recommended to mitigate these pressures, including maintaining suitable water quality, minimizing abrupt water level fluctuations, protecting critical habitats, particularly structurally complex areas such as littoral vegetation and submerged substrates, and regulating fishing pressure on vulnerable species [32, 33].

The highest fish species diversity was observed at Station 1 (36 species, 76.60%), likely due to its upstream location and complex habitats, including riparian forests, submerged roots, deadwood, and aquatic vegetation. These features provide effective shelter, feeding grounds, and spawning sites. Deadwood plays crucial ecological roles by providing protection for small fish and serving as ambush spots for predators, while algae and microbial communities on woody surfaces act as important food sources [34-36]. In contrast, Station 4 exhibited the lowest species richness (30 species, 63.83%), likely due to its proximity to sluice gates and the limited availability of refuge and aquatic vegetation. Sluice gates can disrupt hydrological connectivity, degrade habitat quality, and impede fish migration, thereby contributing to reduced biodiversity [37, 38].

In the summer, fish abundance peaked (3,409 individuals, 41.10%) along with the highest species diversity (42 species, 89.36%). This pattern may reflect ecological conditions during the warmer period; however, it may also be influenced by sampling conditions. Lower water levels during the dry season can concentrate fish in smaller areas, potentially increasing their vulnerability to capture by gill nets and beach seines. Therefore, the higher abundance observed in summer should be interpreted with caution, as it may reflect increased catchability rather than a true increase in fish population size. In contrast, winter exhibited the lowest abundance (2,246 individuals, 27.08%) and species richness (31 species, 65.96%). During this period, water release is restricted from October to retain water for dry-season agriculture [1], resulting in higher water levels and lower temperatures (24.21°C). Reduced temperature may suppress fish metabolic activity and movement, potentially leading to lower catch rates and reduced species detection [39]. In addition, dissolved oxygen (DO) reached its seasonal minimum (4.67 mg/L), approaching hypoxic thresholds that may impose physiological stress on freshwater fishes [40, 41]. These conditions are likely associated with the observed decline in abundance and diversity during winter. Consistently, Pearson's correlation analysis indicated that water temperature and dissolved oxygen were significantly positively correlated with fish diversity indices (H', R, and E; $p < 0.01$), suggesting that these factors play an important role in shaping fish assemblages. In contrast, transparency showed a negative relationship with diversity indices, possibly reflecting increased turbidity and productivity that favor certain dominant species over a more even community structure. Other physicochemical parameters showed no significant correlations, likely because their values remained relatively stable within suitable ranges. These findings are consistent with previous studies highlighting the importance of temperature and dissolved oxygen as key factors influencing fish diversity in tropical freshwater systems [42, 43].

In this context, the relatively low frequency of occurrence observed for some species may be associated with species-specific habitat preferences, seasonal environmental variation, and differences in detectability. Species in the genera *Trichopodus*, *Mystus*, and *Hemibagrus* are typically associated with structurally complex habitats, such as vegetated littoral zones or deeper benthic areas. Their occurrence in the present study was therefore likely influenced by seasonal changes in water level, habitat availability, and water quality, which can affect their spatial distribution and local activity patterns. Although these species are not considered long-distance migrants, they may exhibit limited movement or localized habitat use, leading to temporal variation in their detectability across sampling periods. In addition to these ecological factors, the sampling gears used in this study exhibit inherent selectivity for fish size and habitat. Gill nets (2.0, 4.0, and 6.0 cm mesh) and a beach seine (0.5 × 0.5 cm mesh) may be less effective in capturing large-bodied species and fish inhabiting deeper or mid-water zones, and these groups may therefore be encountered less frequently in the samples. However, the use of gill nets with three mesh sizes, combined with a fine-mesh beach seine, represents a well-established and rigorous approach that enhances coverage across a wide range of fish size classes and habitats, providing a robust basis for assessing species composition and diversity in the reservoir [44, 45].

The Wang Nong Reservoir exhibited relatively high fish biodiversity, as indicated by the mean H' of 3.12, suggesting that the reservoir provides a favorable environment for aquatic life [46]. While no significant

differences were observed among sampling stations, clear seasonal variations were evident, with diversity peaking during the summer season, followed by the rainy and winter seasons, consistent with prior studies [39, 47]. R followed a similar seasonal trend, and the consistently high E across seasons [48] indicates a well-balanced species distribution within the community. Notably, these patterns provide novel insights into the temporal dynamics of fish communities in Wang Nong Reservoir, emphasizing the summer season as a period of peak ecological productivity. Integrating these findings with physicochemical parameters and potential anthropogenic impacts can inform evidence-based management and targeted conservation strategies. Ongoing ecological monitoring and proactive conservation measures are recommended to maintain this balance and mitigate potential threats from human activities, thereby safeguarding the integrity of this aquatic ecosystem.

4. Conclusions

This study confirmed that Wang Nong Reservoir supports a highly diverse fish community, identifying 47 species from 14 families, with Cyprinidae being the most abundant (24 species, 51.06%). The dominant species included *Rasbora borapetensis*, *Esomus metallicus*, *Thynnichthys thynnoides*, *Cyclocheilichthys repasson*, and *Puntius brevis*, with twelve species exhibiting 100% occurrence. Conservation assessment revealed two vulnerable species, *Scaphognathops bandanensis* and *Mystus bocourti*. Fish abundance and species richness were higher in summer than in winter. The mean Shannon-Wiener diversity (H'), richness (R), and evenness (E) indices were 3.12, 4.46, and 0.87, respectively, indicating a well-balanced and diverse fish community. Water temperature and dissolved oxygen showed significant positive correlations with fish diversity indices (H', R, and E; $p < 0.01$), whereas transparency was negatively associated with these indices, highlighting the importance of key environmental drivers in shaping fish assemblages. These findings fill a critical knowledge gap in inland fisheries ecology in northeastern Thailand by providing the first baseline dataset for this reservoir. The results provide a scientific foundation for site-specific conservation planning, water-level management, and evidence-based fisheries management to maintain fish diversity and ecosystem sustainability. Future research should investigate long-term seasonal variations, habitat quality, and anthropogenic impacts to further inform sustainable management strategies and conservation planning in the region.

5. Acknowledgements

We gratefully acknowledge the institutional support from the Faculty of Agriculture and Technology, Nakhon Phanom University. We also sincerely thank the staff of the Department of Fisheries, Faculty of Agriculture and Technology, as well as the village leaders and local fishermen around Wang Nong Reservoir, for their invaluable assistance during the fieldwork.

Author Contributions: Conceptualization, N.T.; methodology, N.T. and A.P.; validation, N.T. and A.P.; formal analysis, N.T. and A.P.; investigation, N.T. and A.P.; resources, N.T. and A.P.; data curation, N.T.; writing—original draft preparation, N.T.; writing—review and editing, N.T.; visualization, N.T.; supervision, N.T.; project administration, N.T. Both authors have read and agreed to the published version of the manuscript.

Funding: This research was funded by the Department of Fisheries, Faculty of Agriculture and Technology, Nakhon Phanom University, Thailand.

Conflicts of Interest: The authors declare that there are no conflicts of interest.

References

[1] Water Crisis Prevention Center (WCPC). *Criteria for Management of Medium Sized Reservoirs*; Department of Water Resources: Bangkok, Thailand, **2022**.

[2] Hayes, N. M.; Deemer, B. R.; Corman, J. R.; Razavi, N. R.; Strock, K. E. Key differences between lakes and reservoirs modify climate signals: A case for a new conceptual model. *Limnol. Oceanogr. Lett.* **2017**, *2*, 47–62. https://doi.org/10.1002/lol2.10036

[3] Abobi, S. M.; Kluger, L. C.; Wolff, M. Comparative assessment of food web structure and fisheries productivity of three reservoirs in Ghana. *Fish. Manag. Ecol.* **2021**, *28*, 573–591. https://doi.org/10.1111/fme.12506

[4] Sarkar, U. K.; Sandhya, K. M.; Mishal, P.; Karnatak, G.; Lianthuamluaia; Kumari, S.; Das, B. K. Status, prospects, threats, and the way forward for sustainable management and enhancement of the tropical Indian reservoir fisheries: An overview. *Rev. Fish. Sci. Aquac.* **2018**, *26*, 155–175.

[5] Sricharoendham, B.; Leelapatra, W.; Ratanachamnong, D.; Kaewjaroon, P.; Aimsab, M. *Variation on Fish Community and Catch of Sirindhorn Reservoir, Ubon Ratchathani Province*; Technical Paper No. 206; National Inland Fisheries Institute, Department of Fisheries: Thailand, **2000**.

[6] Jantharachit, P.; Sanitchon, A.; Chunchom, C.; Jaengkij, M.; Phomisawat, R. *Water Quality and Fish Community in Bung Klua Reservoir, Roi Et Province*; Technical Paper No. 14; National Inland Fisheries Institute, Department of Fisheries: Thailand, **2006**.

[7] Nachaipherm, J.; Musikaew, B. *Structure and Distribution of Fish Community in Ubolratana Reservoir*; Technical Paper No. 59; National Inland Fisheries Institute, Department of Fisheries: Thailand, **2006**.

[8] Nachaipherm, J.; Chunchom, C. *Fish Community Distribution and Gillnet Efficiency in Lam Pao Reservoir*; Technical Paper No. 84; National Inland Fisheries Institute, Department of Fisheries: Thailand, **2008**.

[9] Panchan, R. Fish assemblage patterns in littoral zone of Nam Oun Reservoir, Sakon Nakhon Province, Thailand. *J. Fish. Environ.* **2010**, *34*, 27–39.

[10] Rayan, S.; Rungsiwiwat, A.; Chartchumni, B.; Rayan, W. Structure of fish community in Huay Huat Reservoir, Sakon Nakhon Province. *Burapha Sci. J.* **2017**, *34*, 340–352.

[11] Khowhit, S.; Tanee, T.; Khowhit, D. Species diversity and distribution of fish in Huai Kao Reservoir, Na Chauk District, Maha Sarakham Province, Thailand. *J. Surv. Fish. Sci.* **2023**, *10*, 2363–2377. https://doi.org/10.53555/sfs.v10i1.214

[12] Smith, H. M. *The Freshwater Fishes of Siam, or Thailand*; Bulletin of the United States National Museum, No. 188; Smithsonian Institution: Washington, DC, **1945**.

[13] Rainboth, W. J. *FAO Species Identification Field Guide for Fishery Purposes: Fishes of the Cambodian Mekong*; FAO: Rome, Italy, **1996**.

[14] Doi, A. A review of taxonomic studies of cypriniform fishes in Southeast Asia. *Jpn. J. Ichthyol.* **1997**, *44*, 1–33. https://doi.org/10.11369/jji1950.44.1

[15] Kottelat, M. *Fishes of Laos*; WHT Publications: Colombo, Sri Lanka, **2001**.

[16] Vidthayanon, C. *Field Guide to Fishes of the Mekong Delta*; Mekong River Commission: Vientiane, Lao PDR, **2008**.

[17] Nelson, J. S.; Grande, T. C.; Wilson, M. V. H. *Fishes of the World*, 5th ed.; John Wiley & Sons: New Jersey, USA, **2016**.

[18] Taki, Y.; Ohtsuka, R.; Komodo, M.; Natori, Y.; Utsugi, K.; Shibukawa, K.; Tran, L. X. *Fishes of the Indochinese Mekong*; Nagao Natural Environment Foundation: Tokyo, Japan, **2021**.

[19] International Union for Conservation of Nature (IUCN). *The IUCN Red List of Threatened Species*; **2025**. https://www.iucnredlist.org (accessed May 16, 2025).

[20] American Public Health Association (APHA); American Water Works Association (AWWA); Water Environment Federation (WEF). *Standard Methods for the Examination of Water and Wastewater*, 21st ed.; APHA: Washington, DC, **1998**.

[21] Shannon, C. E.; Wiener, W. *The Mathematical Theory of Communication*; University of Illinois Press: Urbana, USA, **1963**.

[22] Margalef, R. Information theory in ecology. *Gen. Syst.* **1958**, *3*, 36–71.

[23] Pielou, E. C. *Mathematical Ecology*; Wiley: New York, USA, **1977**.

[24] Berra, T. M. *Freshwater Fish Distribution*; Academic Press: California, USA, **2001**.

[25] Jutagate, T.; Srichareondham, B.; Lek, S.; Amarasinghe, U. S.; De Silva, S. S. Variations, trends and patterns of fish landings in large tropical reservoirs. *Lakes Reserv.: Res. Manag.* **2012**, *17*, 35–53.

[26] Jutagate, T.; Rattanachai, A.; Udduang, S.; Lek-Ang, S.; Lek, S. Spatio-temporal variations in abundance and assemblage patterns of fish larvae and their relationships to environmental variables in Sirindhron Reservoir of the Lower Mekong Basin, Thailand. *Indian J. Fish.* **2016**, *63*, 11–23.

[27] Mishra, A.; Chakraborty, S. K.; Jaiswar, A. K.; Sharma, A. P. Comparative biodiversity of two medium reservoirs of North India. *Natl. Acad. Sci. Lett.* **2014**, *37*, 423–430.

[28] Zare-Shahraki, M.; Ebrahimi-Dorche, E.; Bruder, A.; Flotemersch, J.; Blocksom, K.; Bănăduc, D. Fish species composition, distribution and community structure in relation to environmental variation in a semi-arid mountainous river basin, Iran. *Water* **2022**, *14*, 2226. https://doi.org/10.3390/w14142226

[29] Welcomme, R.; Vidthayanon, C. *The Impacts of Introductions and Stocking of Exotic Species in the Mekong Basin and Policies for Their Control*; MRC Technical Paper No. 9; Mekong River Commission: Cambodia, **2003**.

[30] Yakupitiyage, A.; Bhujel, R. C. Role of exotic species in aquaculture: Problems and prospects in Indochina. In *International Mechanisms for the Control and Responsible Use of Alien Species in Aquaculture Ecosystems*; Bartley, D. M.; Bhujel, R. C.; Funge-Smith, S.; Olin, P. G.; Phillips, M. J., Eds.; FAO: Rome, **2005**.

[31] Copp, G. H.; Fox, M. G. Can invasiveness in freshwater fishes be predicted from life-history traits? *Front. Ecol. Evol.* **2020**, *8*, 605287.

[32] Bunn, S. E.; Arthington, A. H. Basic principles and ecological consequences of altered flow regimes for aquatic biodiversity. *Environ. Manage.* **2002**, *30*, 492–507.

[33] Arthington, A. H.; Bunn, S. E.; Poff, N. L.; Naiman, R. J. The challenge of providing environmental flow rules to sustain river ecosystems. *Ecol. Appl.* **2006**, *16*, 1311–1318.

[34] Dolloff, C. A.; Warren, M. L., Jr. Fish relationships with large wood in small streams. *Am. Fish. Soc. Symp.* **2003**, *37*, 179–193.

[35] Maday, A.; Matern, S.; Monk, C. T.; Klefoth, T.; Wolter, C.; Arlinghaus, R. Seasonal and diurnal patterns of littoral microhabitat use by fish in gravel pit lakes, with special reference to supplemented deadwood brush piles. *Hydrobiologia* **2023**, *850*, 1557–1581. https://doi.org/10.1007/s10750-023-05152-3

[36] Pechsiri, J.; Chainapong, T.; Yooyen, T.; Manksang, N. The restoration of freshwater fish in the Papayom Canal by community participation. *ASEAN J. Sci. Technol. Rep.* **2018**, *21*, 59–68.

[37] Seifert, R. E.; Moore, J. W. Floodgate operations and fish communities in tidal creeks of the Lower Fraser River (British Columbia, Canada). *Estuaries Coasts* **2018**, *41*, 1206–1221. https://doi.org/10.1007/s12237-017-0313-3

[38] Bouchard, C.; Boutron, O.; Lambremon, J.; Drouineau, H.; Lambert, P.; Nicolas, D. Impacts of environmental conditions and management of sluice gates on glass eel migration. *Estuar. Coast. Shelf Sci.* **2022**, *279*, 108139. https://doi.org/10.1016/j.ecss.2022.108139

[39] Shuter, B. J.; Finstad, A. G.; Helland, I. P.; Zweimüller, I.; Hölker, F. The role of winter phenology in shaping the ecology of freshwater fish and their sensitivities to climate change. *Aquat. Sci.* **2012**, *74*, 637–657. https://doi.org/10.1007/s00027-012-0274-3

[40] Patel, P. A study on the relationship between water quality parameters and fish diversity in freshwater bodies in Chhattisgarh, Central India. *Asian J. Res. Biosci.* **2025**, *7*, 86–98. https://doi.org/10.56557/ajorib/2025/v7i1113

[41] Setyono, P.; Himawan, W. Analyses of bioindicators and physicochemical parameters of water of Lake Tondano, North Sulawesi Province, Indonesia. *Biodiversitas* **2018**, *19*, 867–874. https://doi.org/10.13057/biodiv/d190315

[42] Bayemi, O. E.; Komolafe, O. O.; Ayodeji, O. A.; Ajayi, O.; Adewumi, P. O.; Adeniran, I. I.; Oladimeji, T. K. Assessment of climatic and environmental parameters on fish abundance of an Afro-tropical reservoir. *Sci. Rep.* **2024**, *14*, 23991. https://doi.org/10.1038/s41598-024-75181-y

[43] Alam, A.; Kumar, J.; Sarkar, U. K.; Jha, D. N.; Sahu, S. K.; Sukla Das, S. C.; Das, B. K. Linking ecological characteristics with fish diversity, assemblage patterns and feeding guilds, and GIS applications along temporal and spatial gradients in a large subtropical reservoir, India, for sustainable management. *J. Water Clim. Change* **2024**, *15*, 607–627. https://doi.org/10.2166/wcc.2023.513

[44] Fischer, J. R.; Quist, M. C. Gear and seasonal bias associated with abundance and size structure estimates for lentic freshwater fishes. *J. Fish Wildl. Manag.* **2014**, *5*, 394–412.

[45] Mehdi, H.; Lau, S. C.; Synyshyn, C.; Salena, M. G.; Morphet, M. E.; Hamilton, J.; Balshine, S. A comparison of passive and active gear in fish community assessments in summer versus winter. *Fish. Res.* **2021**, *242*, 106016.

[46] Magurran, A. E.; McGill, B. J. *Biological Diversity: Frontiers in Measurement and Assessment*; Oxford University Press: New York, USA, **2011**.

[47] Shengchun, Z.; Zhiqiang, W.; Liangliang, H.; Wenli, F.; Ruidan, S.; Yang, D.; Xianzhi, C. Species composition and diversity of fish in Qingshitan Reservoir in Guilin, Guangxi. *South China Fish. Sci.* **2017**, *13*, 36–42. https://doi.org/10.3969/j.issn.2095-0780.2017.02.005

[48] Das, S. K.; Srinivasan, N. T.; Sarang, N.; Das, S. K.; Jawahar, A. T.; Canciyal, J.; Panda, K. Effect of environmental drivers on fish assemblage and diversity patterns in temporal scale in Mongra Reservoir. *Ecohydrology* **2023**, *16*, e2599. https://doi.org/10.1002/eco.2599

ASEAN
Journal of Scientific and Technological Reports
Online ISSN:2773-8752

Research article

Bayesian Meta-Ensemble of Stacked Long Short-Term Memory Convolutional Neural Networks for Detection of AI-Generated Text under Uncertainty

Nirawit Kanthachai[1], and Prompong Sugunnasil[2*]

[1] Faculty of Engineering, Chiang Mai University, Chiang Mai, 50200, Thailand
[2] College of Art, Media and Technology, Chiang Mai University, Chiang Mai, 50200, Thailand
* Correspondence: prompong.sugunnasil@cmu.ac.th

Citation:
Kanthachai, N.; Sugunnasil, P. Bayesian neta-ensemble of stacked long short-term memory convolutional neural networks for detection of ai-generated text under uncertainty. *ASEAN J. Sci. Tech. Report.* **2026**, *29*(5), e261528.. https://doi.org/10.55164/ajstr.v29i5.261582

Article history:
Received: September 28, 2025
Revised: March 24, 2026
Accepted: April 11, 2026
Available online: April 30, 2026

Publisher's Note:
This article is published and distributed under the terms of the Thaksin University.

Abstract: The rapid misuse of AI-generated text can lead to a serious risk to information integrity, yet most existing detectors rely on deterministic, single-model architectures that lack uncertainty quantification and are computationally demanding. This paper introduces a Bayesian Meta-Ensemble of stacked LSTM-CNNs for detecting AI-generated text, a lightweight probabilistic framework that addresses these limitations by combining ensemble stacking with variational Bayesian inference. Three main novel contributions: (i) a two-tier stacked ensemble trained on resampled subsets feeding into a Bayesian Neural Network (BNN) meta-learner, enabling uncertainty-aware classification, (ii) a statistical analysis of Monte Carlo sampling behavior using Kolmogorov-Smirnov and Mann-Whitney tests to validate predictive stability, and (iii) the integration of parametric and non-parametric hypothesis testing directly into the prediction pipeline to enhance decision reliability. On the MAGE dataset, we benchmarked our model against several state-of-the-art detectors, including FastText, GLTR, Longformer, and DetectGPT. Our model achieves 90.84% human recall, 89.59% average recall, and 0.96 AUROC, outperforming FastText, GLTR, and DetectGPT, and closely matching Longformer while requiring 7.5 times fewer parameters (18.77M vs. 142M). We further investigated predictive stability through normality testing and examined the effect of the Monte Carlo (MC) sample size, confirming that larger samples led to more consistent model outputs. Additionally, we demonstrated the use of statistical inference to enhance decision-making. The results demonstrate that a compact Bayesian ensemble can deliver competitive detection accuracy while accounting for uncertainty estimates, making it suitable for resource-constrained and high-stakes environments.

The code is available at https://github.com/Filimize/CNN_LSTMs_BNN.

Keywords: Bayesian model; uncertainty estimation; variational inference; model interpretability; ai-generated text detection

1. Introduction

In the age of advanced technology, AI is used for various purposes, including text generation. The introduction of Large Language Models (LLMs) [1] has attracted many people to use them for beneficial applications such as queries and question answering. However, it can also cause mayhem in both the

digital realm and broader society [2] since LLMs are capable of generating fake news, spreading misinformation, and misleading advertising [3]. Consequently, developing an effective tool to distinguish AI-generated text from human-written text has become a top priority. One approach to mitigating the harmful effects of LLMs is to develop detector tools capable of distinguishing between AI-generated text and human writing, which can reduce the potential for misuse [4]. Prior studies [4, 5] suggest that an ideal detector should be accurate, with a good balance between false positives and false negatives depending on the tasks, require as few samples as possible for the training process, generalize with different models that attackers use, produce interpretable decisions, and robust to adversarial inputs[7]. There are several AI-generated text-detection models, each with its own advantages. For example, Bidirectional encoder representations from transformers (BERT) [8] uses a bidirectional approach and a transformer architecture, which helps capture long-range word relationships. DistilBERT [9] offers a smaller, faster, but slightly lower-accuracy model than BERT. RoBERTa [10] improves upon BERT by training with longer sequences and more training data, making it more accurate than BERT. Despite strong performance, these models produce deterministic outputs and lack mechanisms for quantifying prediction uncertainty.

Uncertainty quantification is critical in high-stakes classification tasks, where overconfidence or underconfidence can lead to serious harm [11]. Bayesian Deep Learning introduces probabilistic principles into deep learning models, producing uncertainty estimates through posterior inference over model weights [12], but it struggles to estimate the posterior distribution of network weights, leading to poor predictive uncertainty and calibration. There are several algorithms to estimate the distribution, including Variational Inference (VI) and Markov Chain Monte Carlo (MCMC). Although MCMC is considered the gold standard for distribution estimation, VI is significantly more computationally efficient. Therefore, VI methods are frequently used when working with large datasets. Despite progress in Bayesian deep learning and ensemble methods individually, their combination as a meta-learning architecture for AI-generated text detection with uncertainty quantification and statistical inference for decision support remains underexplored. Existing ensemble-based text detectors typically stack deterministic classifiers without propagating predictive uncertainty, limiting their reliability in real-world deployment.

To address these gaps, we present the Bayesian Meta-Ensemble of Stacked LSTM-CNNs for AI-generated text detection. The proposed model introduces three novel contributions: (i) a two-tier stacked ensemble in which lightweight LSTM-CNN base models, trained on resampled subsets to handle class imbalance, feed probabilistic outputs into a Bayesian Neural Network (BNN) meta-learner, enabling uncertainty-aware classification, (ii) a statistical analysis of Monte Carlo sampling behavior using KS and Mann-Whitney tests to validate predictive stability, and (iii) integration of parametric and non-parametric hypothesis testing directly into the prediction pipeline to support decision-making beyond a fixed threshold. The Machine-Generated Text Detection (MAGE) dataset includes human-written texts from different sources and machine-generated texts produced by 27 large language models (LLMs) to test the benchmark [13]. Variational Inference is employed to approximate the posterior distribution over network weights, and the development follows the Cross-Industry Standard Process for Data Mining (CRISP-DM) framework.

2. Materials and Methods

2.1 Planning

2.1.1 Study related research, including methods for improving Bayesian Neural Network (BNN) performance, LSTM-CNN for text classification, enhancements to word embeddings, and societal issues arising from AI-generated text.

2.1.2 Design procedures for developing the Bayesian Meta-Ensemble of Stacked LSTM-CNNs model using the Cross-Industry Standard Process for Data Mining (CRISP-DM).

2.1.3 Develop the classification model following the CRISP-DM framework.

2.1.4 Measure the performance of the model using appropriate evaluation metrics.

2.1.5 Summarize and discuss the results in the context of model effectiveness and broader implications.

2.1.6 Develop a Bayesian Meta-Ensemble of Stacked LSTM-CNNs model for AI-generated text detection using the MAGE dataset.

2.1.7 Measure the performance of the Bayesian Meta-Ensemble of Stacked LSTM-CNNs model for AI-generated text detection, compared with the well-known text classification models: FastText, GLTR, Longformer, and DetectGPT.
Prediction performance: Recall of AI-generated text, recall of human-written text, average recall, and area under the ROC curve (AUC-ROC).
Computational performance: Model size.

2.1.8 Compare the Bayesian Meta-Ensemble of Stacked LSTM-CNNs model's performance against FastText, GLTR, Longformer, and DetectGPT [13].

2.1.9 Experiment with Monte Carlo sample size and statistical inferences.

2.1.10 Conclude and discuss the results.

2.2 Scope

This paper uses the Machine-Generated Text Detection (MAGE) dataset, which includes human-written texts from different sources and machine-generated texts produced by 27 large language models (LLMs). The dataset contains a collection of human- and AI-generated text from various sources. The dataset is organized into three subsets.

Training set: 225,753 records of AI-generated text and 93,318 records of human text.

Validation set: 27,993 records of AI-generated text and 28,799 records of human text.

Testing set: 30,478 records of AI-generated text and 30,265 records of human text, including some examples from sources outside the training and validation sets.

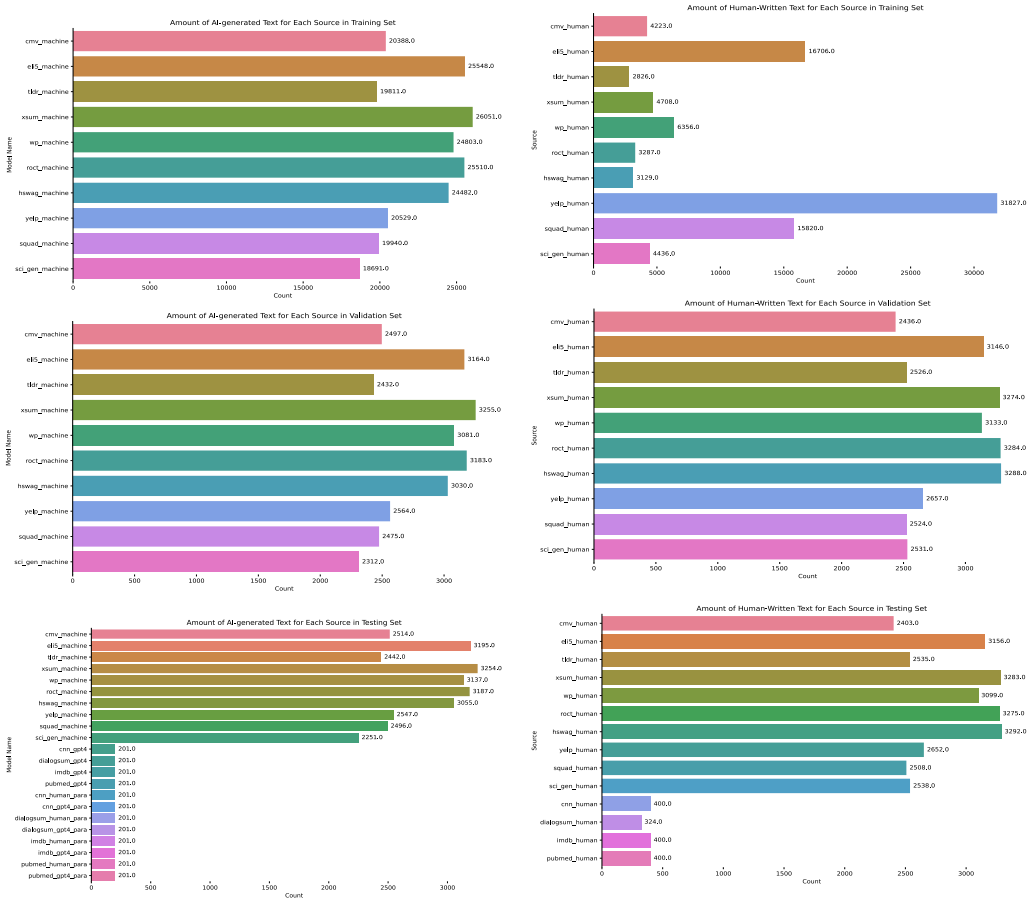


Figure 1. Amount of data categorized by the sources of the data in each dataset.

2.3 Literature Review: Data Science Literature

2.3.1 Long Short-Term Memory Model (LSTM)

Even though Recurrent Neural Networks (RNNs) have been widely used in text processing due to their ability to handle variable-length sequences, they are prone to the vanishing gradient problem. This issue arises because RNNs are equivalent to Multi-Layer Perceptrons (MLPs) with a large amount of historical information, which makes RNNs struggle with long sequences. The accumulation of historical information can lead to vanishing gradients, where the gradients become exceedingly small. As a result, the neural network's nodes rarely update, leading to slow convergence and difficulty in learning long-term dependencies. On the other hand, the Long Short-Term Memory Model (LSTM), an improved RNN-based network, can retain historical information over long sequences by adding memory cells and three control gates, mitigating the loss of historical information and the vanishing gradient problem caused by excessive RNN layers.

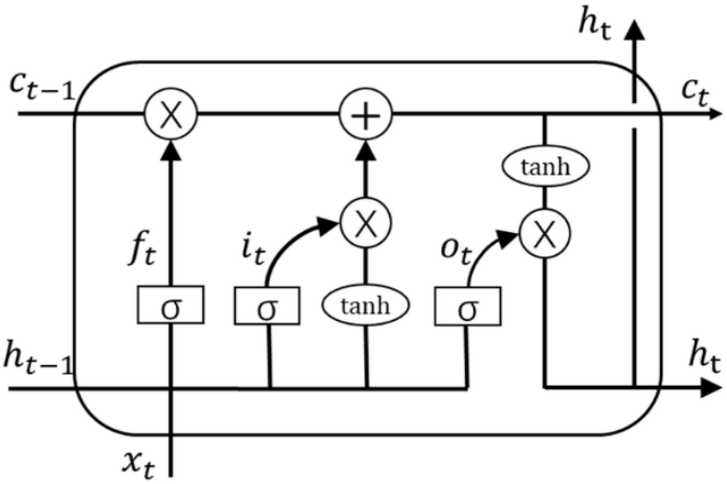


Figure 2. The description of LSTM node.

The LSTM structure is shown in Figure 2. The memory cell is added for storing the historical information, and three main gates control the update, deletion, and output of the information: the input gate determines how the incoming vectors alter the state of the memory cell, the output gate allows the memory cell to affect the outputs, and the forget gate enables the memory cell to remember or discard previous information [14]. Xiao et al. [15] presented a paper on patent text classification, showing that a pre-trained Word2Vec LSTM model effectively mitigates the dimensionality disaster typically encountered with traditional methods. In this experiment, 50,000 patent texts were used for training and testing, yielding a test accuracy of 93.48%, which outperformed other models such as CNNs and k-nearest neighbors. Xie et al. [16] proposed "Self-Attention-Based BiLSTM Model for Short Text Fine-Grained Sentiment Classification," introducing a Self-Attention-Based BiLSTM model to improve sentiment polarity classification by incorporating aspect-term information into the learning process. Their proposed Bidirectional LSTM (BiLSTM) leverages both past and future contexts, allowing for more comprehensive semantic feature extraction. Additionally, the integration of a self-attention mechanism enhances the model's ability to focus on crucial aspect-term information while reducing computational complexity. In comparative experiments, the Self-Attention-Based BiLSTM model achieved higher accuracy than standard LSTM and BiLSTM models in sentiment polarity classification. However, the study identified limitations, particularly in distinguishing between Negative and Neutral sentiment categories due to unclear boundary definitions. Wadud et al. [17] proposed using an LSTM with the AdaBoost algorithm for text classification on a Bengali dataset. This method outperformed Bi-LSTM CNN and CNN-LSTM models, achieving a precision of 89.48%, a recall of 93.38%, and an F1-score of 91.39%.

2.3.2 Embedding

Embedding is the process of converting text into vector representations that capture the semantic meaning. In text classification, models such as LSTMs typically use embeddings, for instance, Word2Vec. Anggrainingsih et al. [18] proposed an MLP model using BERT embeddings as input for detecting text misinformation, compared with SOTA models. Their experimental results show that their proposed model outperforms SOTA models and performs better when paired with RoBERTa embeddings than with BERT or DistilBERT.

2.3.3 Convolutional Neural Networks (CNNs)

CNNs are designed to address the limitations of traditional neural networks, which tend to struggle with the high computational demands of computer vision tasks. Common machine learning benchmark datasets, such as MNIST, are databases of handwritten digits collected in black-and-white images of size 28x28 pixels, which are manageable for traditional neural networks. For these images, the input layer contains 784 nodes, which is manageable for traditional neural networks. However, for an RGB image of size 128x128 pixels, the input layer would contain 49152 nodes. To capture the patterns in these images, several hidden layers and nodes must be added, increasing computational intensity and the risk of overfitting. This is why Convolutional Neural Networks (CNNs) are preferred over traditional neural networks for computer vision tasks. CNNs are specifically designed to handle spatial hierarchies in images, reducing parameter count and computational complexity while capturing important features. CNNs are comprised of three types of layers: convolutional layers, pooling layers, and fully connected layers. These layers are stacked to form a CNN architecture. A CNN architecture has been formed. The key areas of the CNN can be broken down as follows:
Input Layer: This layer stores the image's pixel values.
Convolutional Layer: Determines the output of neurons connected to local regions of the input by calculating the scalar product between their weights and the connected input volume.
Pooling Layer: Performs downsampling along the spatial dimensions of the input, reducing the number of parameters in the activation.
Fully Connected Layers: Perform the same functions as in standard neural networks, producing class scores from the activations for classification purposes [19].

Kim [20] proposed the use of CNNs for sentence classification in his paper "Convolutional Neural Networks for Sentence Classification". Through a series of experiments, the study demonstrated that using Word2Vec as an embedding, even a simple CNN with a single convolutional layer, could achieve impressive performance. This led to the conclusion that well-established word vectors play a crucial role in deep learning for Natural Language Processing (NLP). Alshubaily [21] proposed incorporating an attention mechanism to boost performance and introduced WordRank for vocabulary selection, thereby reducing the number of embedding parameters and speeding up training with minimal accuracy loss. Implementing these ideas improved TextCNN accuracy on the 20News dataset from 94.79% to 96.88%, while reducing embedding layer parameters from 7.9M to 1.5M with only a 1.2% decrease in accuracy. In 2022, Zhao et al. [22] further built on Yoon Kim's ideas by proposing the WTL-CNN method, which combines Word2Vec, a topic-based TF-IDF algorithm, and an improved convolutional neural network. Initially, Word2Vec converts text data into word vectors. An improved TF-IDF algorithm incorporating the LDA topic generation model is then used to weight these vectors and enhance their semantic topic information. Furthermore, the location information of important features in news texts is converted into weights and integrated into the convolutional neural network's pooling layer, thereby boosting classification accuracy. WTL-CNN was evaluated against seven models using THUCNews and SogouCS datasets in a TensorFlow environment. Experimental results revealed that the model achieved precision, recall, and F1 scores of 95.76%, 93.43%, and 94.98%, respectively, on THUCNews, and 94.61%, 93.43%, and 94.01%, respectively, on SogouCS.

2.3.4 LSTM-CNN

Neural Networks have achieved outstanding results in Natural Language Processing (NLP). Using word embeddings to represent text can yield semantic representations of words and phrases, not only capturing the characteristics of word relationships in sentences but also avoiding the problems of high

dimensionality and data sparsity [23]. One suitable model for text classification is the LSTM-CNN, a hybrid model combining LSTM and CNN. This model is mainly composed of three parts: word embedding for word representation as numerical values, an LSTM-CNN model, and an output layer that uses either the activation function "softmax" for multiple-class classification or "sigmoid" for binary classification.

C. Li et al. [24] developed the Bi-LSTM-CNN and tested the model's performance through the THUCNews dataset, which contains a training set of 50000 corpora, a validation set of 5000 corpora, and a testing set of 10000 corpora. The authors compared the Bi-LSTM CNN with other models. The results are shown in Figure 2. The results suggest that the Bi-LSTM-CNN model effectively utilizes the loop structure to obtain contextual information. It constructs the left and right contexts for each word using a Convolutional Neural Network (CNN), thereby achieving a more accurate representation of the text's semantics. However, the author suggests that using attention mechanisms could further improve the model's performance.

Table 1. The comparison experiment results from C. Li et al. *[24, p. 201]* "News Text Classification Based on Improved Bi-LSTM-CNN".

	The comparison experiment results		
Model	**Accuracy (%)**	**Loss**	**F1 Score**
TF-IDF	90.27	0.31	0.86
SVM	93.49	0.25	0.92
LSTM	94.26	0.21	0.94
CNN	95.61	0.15	0.96
Bi-LSTM-CNN	96.46	0.11	0.99

Jang et al. [25] proposed the "Bi-LSTM Model to Increase Accuracy in Text Classification: Combining Word2vec, CNN, and Attention Mechanism." This Bi-LSTM-CNN hybrid model was designed for sentiment classification using the Internet Movie Database (IMDB) review dataset. The approach uses a CNN for feature extraction, reducing the input feature space, while a Bi-LSTM captures contextual dependencies within the extracted features. Additionally, the authors incorporated an attention mechanism. Experimental results demonstrate that the Bi-LSTM-CNN hybrid model significantly outperforms baseline models in both accuracy and F1-score. The experiment was conducted on a fixed dataset size and yielded an accuracy of 0.9141 for the proposed model, outperforming CNN (0.8874), LSTM (0.8940), Multi-Layer Perceptron (MLP) (0.7129), and an existing hybrid model (0.8906). Similarly, the F1-score of the proposed model (0.9018) surpassed those of CNN (0.8875), LSTM (0.8816), MLP (0.7708), and the existing hybrid model (0.8887).

2.3.5 Bayesian Neural Network (BNN)

BNN is a probabilistic model based on Bayes' Theorem. BNN combines prior "expert" information and the likelihood of the data to produce the posterior distribution. The BNNs have several benefits; one is that they can handle Aleatoric and Epistemic uncertainty. Aleatoric uncertainty is inherent in the data itself, such as noise or anomalies, while Epistemic uncertainty is derived from the model structure and hyperparameters [26]. However, the learning process of BNNs is based on inferring the posterior distribution by sampling from it using Bayes' theorem; therefore, it requires combining the prior and likelihood. Obtaining posterior samples is difficult and computationally intensive, especially given the high dimensionality of the sampling space. In some situations, the prior and the likelihood may have different distributions; therefore, BNNs need to use sampling algorithms such as Markov Chain Monte Carlo (MCMC), Variational Inference (VI), and MC-Dropout to estimate the posterior, which are considered approximation algorithms. In a Bayesian Neural Network, performing Bayesian inference requires the posterior distribution of the network weights. Given the prior probability of network weights $P(w \mid \alpha)$ which depends on parameters α , then the posterior can be written as $Pr(w \mid D, \alpha)$ However, for most neural networks, it is difficult to obtain the posterior probability of weights; therefore, Variational inference is used to address this problem by approximating

$Pr(w \mid D, \alpha)$ with a more tractable distribution $Q(w \mid \beta)$ [27]. This approximation is fitted by minimizing the variational free energy F with respect to β where

$$F = -\left\langle \ln\left[\frac{\Pr(D \mid w)\, P(w \mid \alpha)}{Q(w \mid \beta)}\right]\right\rangle_{w\sim Q(\beta)}$$

Graves [27] tested combinations of posteriors and priors on a hierarchical multidimensional recurrent neural network for phoneme recognition on the TIMIT speech corpus. A pruning heuristic was also applied to the trained model. The results showed that using Gaussian distributions as both prior and posterior gave the best performance in terms of minimizing the error, and they also found that the pruning methods enhance the model's performance by significantly reducing error when the threshold for pruning is strong enough (threshold ≥ 0.05)

2.3.6 AI detection using ensemble models

Ensemble learning improves generalization by reducing the risk of overfitting to a particular linguistic pattern or model-specific bias. By aggregating diverse decision boundaries, it achieves a more robust and reliable classification than any individual model could provide alone. In the context of AI-generated text detection, where the linguistic overlap between human-written and machine-generated text is continually narrowing, ensemble architectures have consistently improved performance over single-model baselines across multiple benchmark datasets. Abburi et al. [28] proposed an ensemble framework for AI-generated text detection that concatenates output probability vectors from five pre-trained transformer models: DeBERTa-large, XLM-RoBERTa, RoBERTa-large, RoBERTa-base OpenAI detector, and XLM-RoBERTa NLI, and feeds the combined representation into a voting classifier to produce the final prediction. Aggarwal et al. [29] similarly proposed an ensemble framework combining BERT and DeBERTa with a dynamic weight adjustment strategy, where each constituent model's contribution is weighted by its validation accuracy, and a cosine learning rate scheduler is used to improve convergence stability. Although both ensemble models achieved strong detection accuracy, they share common limitations. All constituent models and voting classifiers produce deterministic outputs, offering no mechanism for quantifying prediction uncertainty; a significant drawback in high-stakes applications such as misinformation detection and academic integrity verification. Furthermore, both frameworks rely on large transformer-based models (DeBERTa-large with approximately 400M parameters and RoBERTa-large with 356M parameters), making them computationally expensive and impractical for resource-constrained environments. Additionally, neither study explicitly addresses class imbalance in the training data. The proposed framework addresses these limitations by (i) replacing the deterministic voting classifier with a Bayesian Neural Network meta-learner that produces calibrated probabilistic outputs and supports statistical hypothesis testing, (ii) using lightweight LSTM-CNN base models with fewer than 6 million parameters each, achieving competitive performance at a fraction of the computational cost, and (iii) applying a data resampling strategy across multiple balanced training subsets to mitigate class imbalance effects across all base models.

2.4 Literature Review: Statistics Literature

2.4.1 Kolmogorov-Smirnov Test

To test the hypothesis about a population distribution, we sometimes investigate the agreement between the sample distribution and the theoretical distribution, a procedure known as a "goodness of fit test". Some tests have been developed in which the sample distribution depends on the form or the values of certain parameters in the population distribution. In contrast, test statistics whose sampling distribution does not depend on either the explicit form or the value of certain parameters are called nonparametric or distribution-free tests [30]. For testing whether two samples come from the same distribution, the Kolmogorov-Smirnov goodness-of-fit test, a nonparametric test, is used. Suppose that the first sample has size m with a cumulative distribution function (CDF) denoted by $F(x)$ and the second sample has size n with a CDF denoted by $G(x)$. Define

$$D_{m,n} = \max_x |F(x) - G(x)|$$

The null hypothesis is that both samples come from the same population distribution. We reject the null hypothesis if $D_{m,n} > D_{m,n,\alpha}$ where $D_{m,n,\alpha}$ is the critical value. For m and n sufficiently large

$$D_{m,n} = c(\alpha)\sqrt{\frac{m+n}{mn}}$$

Where $c(\alpha)$ is the inverse of the Kolmogorov distribution at α [31].

2.4.2 Mann-Whitney U test

The Mann-Whitney U test is a nonparametric statistical test in which the null hypothesis states that random samples from two populations have the same distribution. The Mann-Whitney U test is often misunderstood as an alternative to the t-test for testing median equality, but it can be used only to test median equality if it is assumed that the two populations have identical shapes and differ only by a shift [32]. Feltovich [33] compared the Mann-Whitney test and the robust rank-order test across several simulation examples. They found that when the distributions have the same dispersion, and are identical but not symmetric, the test can yield valid results even though it is not theoretically ideal. They also noted that the Type I error (the error of rejecting the null hypothesis when it should not) was significantly reduced with larger sample sizes (60 per group). Yue and Wang [34] investigated the power of the Mann-Whitney test in detecting shifts in the median or mean of time series data. The study found that the power of the test increases with the magnitude of the shift, sample size, and significance level, and decreases with higher data variation.

2.4.3 Student's t-test

The statistical test is used to determine whether the difference between two groups of data is statistically significant. The test follows a Student's t-distribution under the null hypothesis. It is normally applied when the data is normally distributed. The null hypothesis states that the means are statistically equal. There are three types of t-test: one-sample t-test, independent samples t-test, and paired samples t-test. The one-sample t-test is used to determine whether the mean of a sample is statistically equal to the expected value. It is typically used when the sample size is less than 30. If the sample size is 30 or greater, the z-test is preferred. However, the z-test requires the population standard deviation to be known. If the population standard deviation is unknown, the t-test can be used instead [35]. The t-test assumes the data are normally distributed, but most real-world data do not follow a normal distribution. Several papers suggest that the t-test can still be used, provided the sample size is sufficiently large, and the data are not normally distributed [36]. Ratcliffe [37] investigated the effects of sample size on the power of the t-test; the results suggest that as the sample size increases, the influence of non-normality decreases significantly. He noted that "extreme non-normality can as much as double the value of t at the 2.5% (one tail) probability level for small samples, but increasing the sample sizes to 80, 50, 30, and 15 will, for practical purposes, remove the effect of extreme skewness, moderate skewness, extreme flatness, and moderate flatness, respectively." Sawilowsky and Blair [38] tested the t-test across various simulation examples; the results show that the t-test is reasonably robust to type I error under most conditions. However, small or unbalanced samples and extreme non-normal distributions can lead to conservatism. The power, also called Type II error (the error in which the test does not reject the null hypothesis when it should), remains fairly stable across different distribution shapes and even under some violations of assumptions, especially with large sample sizes.

2.4.4 Shapiro-Wilk test

The Shapiro-Wilk test is used to test the null hypothesis that a sample comes from a normally distributed population. This test can detect departures from normality due to skewness, kurtosis, or both [39]. Mohd Razali and Yap [40] investigated the power of different normality tests: the Kolmogorov-Smirnov test, Lilliefors test, Anderson-Darling test, and Shapiro-Wilk test, using Monte Carlo procedures. The results showed that the Shapiro-Wilk test outperformed other tests, especially with large samples. Although the

Shapiro-Wilk test's power is relatively low for small sample sizes, it remains comparable to other tests, whereas the Kolmogorov-Smirnov test has the least power.

2.5 Literature Review: Domain Knowledge Literature

2.5.1 Potential Harm of AI-generated Text

The introduction of Large Language Models (LLMs) has led to AI-generated writing being used across fields such as journalism and marketing. In contrast, AI writing has many advantages. On the other hand, AI writing can be misused for manipulating information or propaganda, leading to social unrest and instability in politics. For instance, in 2019, OpenAI decided not to release the full version of GPT-2 due to concerns about potential misuse [41]. In 2022, "AI's Jurassic Park Moment – Communications of the ACM" [42] discussed that some LLMs are inherently unreliable, leading to AI hallucinations, The article raised concerns about the reliability and trustworthiness of LLMs, and provided examples of the harm caused by AI-text generated: for example, people used OpenAI to flood the Stack Overflow website with AI responses that had a high rate of incorrectness [43], prompting the site to ban ChatGPT-generated submission. Gary Marcus [41] proposed the "four paths" to mitigate the threats posed by AI-generated text. Firstly, every social media company and search engine should ban the generation of misleading content. Secondly, every country must reconsider its policies regarding misinformation. Thirdly, a stronger validation system should be implemented, with all websites applying anonymous, bot-resistant authentication. Fourth, a new kind of AI should be built to counter these threats, such as models that can verify truthfulness.

Dergaa et al. [44] gathered a literature review of relevant scholarly articles published in peer-reviewed journals indexed in Scopus as quartile 1, using keywords such as "ChatGPT," "AI-generated text," "academic writing," and "natural language processing". The author used a quasi-qualitative approach, involving reading and evaluating sources and identifying relevant data to support the research questions. The study found that ChatGPT and other NLP technologies can enhance the quality of academic writing and research. However, the research found that ChatGPT produced responses containing factual errors and misrepresentations, which could be attributed to the absence of relevant articles in its training set and/or its inability to differentiate between credible and less credible sources. The paper also mentions a sting operation conducted by John Bohannon [45]. Over a period of 10 months, Bohannon submitted a fake scientific paper to 304 open-access journals. His fake paper contained a fatal flaw and fabricated content. Shockingly, the fake paper was accepted by 157 journals. This raises significant concerns about the quality control of open-access journals, especially today, when AI-generated text models are easy to access.

3. Results and Discussion

3.1 Base Models Results

The training data is class-imbalanced: 225753 records of AI-generated text and 93318 records of human text. To address this, the training data was split into three balanced subsets: each contains 75251 records of AI-generated text (drawn from distinct partitions) and the full 93318 records of human text. The original imbalanced dataset was retained as a fourth training set for comparison.

3.2 Model comparison

After training the base models, a Bayesian neural network was constructed as the meta learner using Variational Inference (VI). The meta-learner architecture is a 4-(12-10)-1 fully connected network. The model was evaluated on human-written texts from all domains and AI-generated texts from all LLM sets in the MAGE dataset. Performance was compared against FastText, GLTR, DetectGPT, and the Longformer model, whose metrics were originally reported by Y. Li et al. [13]

Table 2. The results of each base model with different balanced datasets

Training Dataset	Model Name	Accuracy		Loss	
		Training	Validation	Training	Validation
The 1st set	**LSTM-CNN**	0.9378	0.8904	0.1506	0.2638
	BiLSTM-CNN	0.9147	0.8682	0.2022	0.2994
	Multi-Head LSTM-CNN	0.9397	0.8817	0.1493	0.2782
The 2nd set	**LSTM-CNN**	0.9445	0.8874	0.1372	0.2697
	BiLSTM-CNN	0.9456	0.8805	0.1328	0.2769
	Multi-Head LSTM-CNN	0.9460	0.8878	0.1326	0.2769
The 3rd set	**LSTM-CNN**	0.9475	0.8883	0.1304	0.2636
	BiLSTM-CNN	0.9107	0.8619	0.2126	0.3094
	Multi-Head LSTM-CNN	0.9108	0.8645	0.2130	0.3095
The 4th set	**LSTM-CNN**	0.9265	0.8943	0.2404	0.2558
	BiLSTM-CNN	0.9254	0.8756	0.2495	0.2856
	Multi-Head LSTM-CNN	0.9303	0.8944	0.2327	0.2579

Across all datasets, Table 2 shows that the best-performing model is regular LSTM-CNN + ALBERT embeddings. All developed models contain fewer than 6 million parameters; this constraint likely explains why the simpler LSTM-CNN outperforms the more complex architectures, as neither BiLSTM-CNN nor Multi-head Attention LSTM-CNN has sufficient capacity to exploit their additional components at this parameter scale fully.

Table 3. The results of our model compared with the baselines

Model	Human Recall	AI Recall	Avg Recall	AUROC
FastText	86.34%	71.26%	78.80%	0.83
GLTR	12.42%	98.42%	55.42%	0.74
Longformer	82.80%	98.27%	90.53%	0.99
DetectGPT	86.92%	34.05%	60.48%	0.57
LSTM-CNN+BNN (MC= 1000)	90.84%	88.34%	89.59%	0.96

The proposed LSTM-CNN+BNN model achieves the highest human recall among all compared detectors. Its average recall is 0.94% below Longformer, and its AUROC is 0.03 lower, while using only 18.77M parameters, approximately 7.5 times fewer than Longformer (142M). It should be noted that RoBERTa-based detectors and dedicated GPT-detector models, which were not included in the original MAGE benchmark comparison used here, have been reported to achieve strong performance in the literature but similarly depend on large-scale transformer architectures that may be impractical in resource-limited settings. The proposed model represents a favorable trade-off between accuracy, uncertainty quantification, and computational efficiency.

3.3 Monte-Carlo sampling result

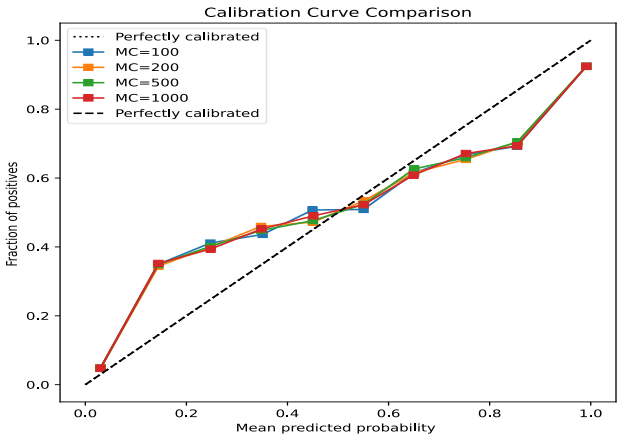


Figure 3. The calibration curve compared between different MC sample sizes.

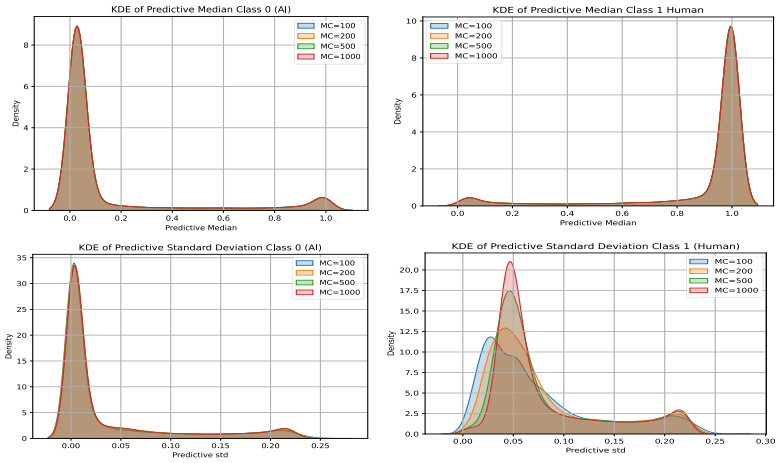


Figure 4. The boxplots show the distribution of predictive median and its S.D. in each class.4

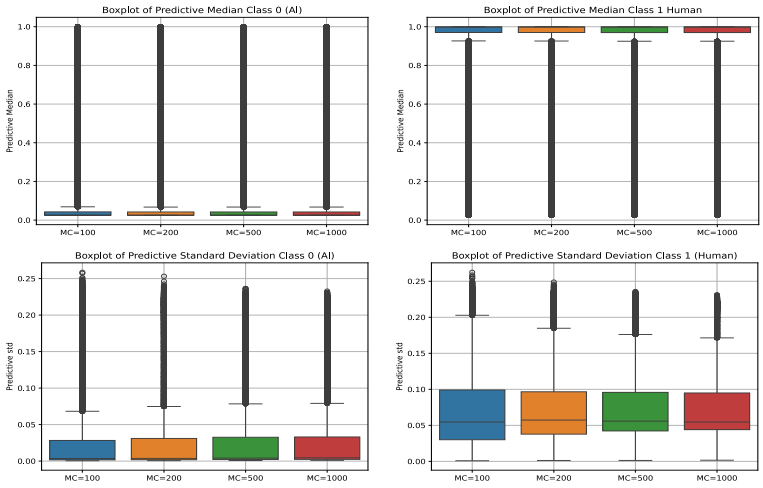


Figure 5. KDE plots illustrate the distributions of the predictive median and its S.D. in each class.

Additionally, we investigated whether the similar output distributions share the same median using the Mann-Whitney (MW) test, based on the assumption that both distributions come from the same population and share the same variance.

Hypotheses

Kolmogorov–Smirnov Test:

H_0: Two distributions are identical.

H_1: Two distributions are not identical.

Mann-Whitney test:

H_0: Two distributions share the same median.

H_1: Two distributions do not share the same median.

We considered p-values > 0.05 as failure to reject the null hypothesis (95% confidence level).

Table 4. Results for distributional and median similarity across different MC sample sizes.

MC Samples Comparison	KS similarity	Passed KS then MW similarity
Class 0 MC = 100 and MC = 200	0.9285	0.9478
Class 0 MC = 100 and MC = 500	0.9402	0.9720
Class 0 MC = 100 and MC = 1000	0.9420	0.9728
Class 0 MC = 200 and MC = 500	0.9514	0.9753
Class 0 MC = 200 and MC = 1000	0.9486	0.9709
Class 0 MC = 500 and MC = 1000	0.9649	0.9817
Class 1 MC = 100 and MC = 200	0.9285	0.9478
Class 1 MC = 100 and MC = 500	0.9402	0.9720
Class 1 MC = 100 and MC = 1000	0.9421	0.9728
Class 1 MC = 200 and MC = 500	0.9514	0.9753
Class 1 MC = 200 and MC = 1000	0.9486	0.9709
Class 1 MC = 500 and MC = 1000	0.9649	0.9817

Table 4 shows that KS similarity proportions consistently exceeded 92%, indicating that distribution shapes remained stable across MC sizes. The MW test further confirms strong agreement in median values. The highest distributional and median similarities occurred between MC = 500 and MC = 1000. We conducted a sensitivity analysis of posterior estimates with respect to the number of Monte Carlo samples; the diminishing marginal gain in stability beyond MC = 500 suggests that this value represents a practical trade-off point between computational cost and Monte Carlo error. To formally evaluate the normality of the predictive median distributions, 100 outer iterations were performed for each MC sample size. In each iteration, forward passes were made through the BNN to generate MC = 100, 200, 500, and 1000 samples; the median prediction per instance was recorded. A Shapiro-Wilk test at the 95% confidence level was then applied to the resulting distribution of median predictions across the 100 outer iterations.

Hypothesis

H_0: The distribution follows a normal distribution.

H_1: The distribution does not follow a normal distribution.

The number of predictions following a normal distribution increased with the number of MC samples, suggesting greater predictive stability. The results are summarized in Table 5.

Table 4. The results of the normality test of the sample distribution of the median across different MC sample sizes.

MC sample	Normal distribution records	Non-normal distribution records
100	35888 (59.08%)	24855 (40.92%)
200	45778 (75.36%)	14965 (24.64%)
500	52620 (86.63%)	8123 (13.37%)
1000	55274 (91.00%)	5469 (9.00%)

3.4 Prediction Hypotheses

Since the BNN produces predictive medians and predictive standard deviations, statistical hypothesis testing can be applied to its output distributions to support more nuanced decision-making beyond a fixed 0.5 threshold. A 95% confidence level was used throughout to simulate real-world error tolerance. Given that BNN outputs are not normally distributed, non-parametric statistical methods are theoretically preferred. However, parametric t-tests have been shown to perform well on large samples regardless of distributional assumptions [46]. In this experiment, both parametric and nonparametric tests were used at the 95% confidence level.

Hypotheses

Wilcoxon Test. Let $D = \text{predictive median} - 0.5$.

H_0: $D \geq 0$; assigned to class 1.

H_1: $D < 0$; assigned to class 0.

Student's t-Test. Let μ denote the mean of the output distribution.

H_0: $\mu \geq 0.5$; assigned to class 1.

H_1: $\mu < 0.5$; assigned to class 0.

Table 5. The accuracy of our model with and without statistical inferences.

Statistical Test	MC Samples	Human Recall	AI Recall	Avg Recall
No test	100	90.80%	88.37%	89.59%
	200	90.88%	88.29%	89.58%
	500	90.86%	88.28%	89.57%
	1000	90.84%	88.34%	89.59%
Wilcoxon	100	91.31%	87.79%	89.55%
	200	91.26%	87.89%	89.57%
	500	91.08%	88.05%	89.57%
	1000	91.01%	88.12%	89.56%
T-test	100	91.32%	87.79%	89.55%
	200	91.26%	87.88%	89.57%
	500	91.10%	88.05%	89.57%
	1000	91.00%	88.11%	89.56%

3.5 Discussion

In this study, we explored the effectiveness of the Bayesian Meta-Ensemble of Stacked LSTM-CNNs for AI-generated text detection. To address class imbalance in the training data, resampling was applied to create three balanced subsets and one full subset, each retaining all human-written records and using distinct partitions of the AI-generated samples for balanced training. Three base architectures: LSTM-CNN, BiLSTM-CNN, and Multi-head Attention LSTM-CNN were trained with ALBERT embeddings on each subset. The regular LSTM-CNN consistency achieved the best validation performance. This outcome aligns with findings by Zhang et al.[14] and Jang et al.[25], who similarly observed that LSTM-CNN hybrids offer strong sequence modeling with manageable complexity. The relative underperformance of BiLSTM-CNN and Multi-head Attention LSTM-CNN in this context is likely due to the parameter constraints (<6 million). The BNN meta-learner was developed by using the best-performing base models from each subset, producing probabilistic

outputs through Variational Inference. outperformed FastText, GLTR, and DetectGPT on all reported metrics and closely matched Longformer, achieving 90.84% human recall, 89.59% average recall, and 0.96 AUROC with only 18.77M parameters, approximately 7.5 times fewer than Longformer's 142M. This efficiency advantage is particularly noteworthy given that transformer-based detectors such as RoBERTa and other GPT detector variants, while achieving competitive detection rates, typically demand substantially more parameters and computational resources. The consistently higher human recall of our model relative to FastText (86.34%) and DetectGPT (86.92%) is likely due to the ensemble's ability to combine complementary feature representations across multiple training partitions, thereby reducing sensitivity to domain-specific distributional shifts in the MAGE dataset. The slightly lower average recall compared to Longformer (89.59% vs. 90.53%) reflects the inherent trade-off between model capacity and efficiency. However, the gap is marginal and offset by the substantial reduction in parameter count and the addition of uncertainty estimation.

The effect of Monte Carlo (MC) sampling size was systematically examined using Kolmogorov-Smirnov (KS) and Mann-Whitney (MW) tests to assess distributional and median consistency across MC = 100, 200, 500, and 1000. KS similarity proportions consistently exceeded 92% across all pairwise comparisons, and MW agreement in medians was similarly high, confirming that the BNN's predictive distributions are stable. Importantly, the highest similarity (KS: 0.9649, MW: 0.9817) occurred between MC = 500 and MC = 1000, indicating that marginal gains in stability diminish beyond 500 samples. The Shapiro-Wilk normality test further revealed that the proportion of predictions following a normal distribution increased substantially from 59.08% at MC = 100 to 91.00% at MC = 1000, supporting the interpretation that larger MC sample sizes allow the Central Limit Theorem to dominate, resulting in more regular, predictable output distributions. This behavior is consistent with Monte Carlo convergence theory and provides a principled basis for selecting MC = 1000 as a practical default in deployment scenarios requiring high stability.

The integration of parametric (Student's t-test) and non-parametric (Wilcoxon test) hypothesis testing into the prediction pipeline provided a modest but consistent improvement in human recall (up to 91.32% from the baseline 90.84%) while maintaining overall classification balance. Both tests yielded nearly identical results. The robustness of the t-test under non-normality is well-supported by large-sample theory and consistent with Lumley et al. and Fagerland, who demonstrated that t-tests remain valid for large samples regardless of the underlying distribution. The slight improvement in human recall from hypothesis testing suggests that incorporating distributional information from the BNN output, rather than relying solely on a fixed 0.5 threshold, improves recall. This is especially valuable in safety-critical applications such as academic integrity monitoring or misinformation detection, where errors carry higher costs. In conclusion, the Bayesian Meta-Ensemble of Stacked LSTM-CNNs for AI-generated text detection delivers competitive performance while being highly efficient. Unlike baseline models that produce only deterministic outputs, our model introduces uncertainty estimation, enabling statistical analysis to enhance reliability and interpretability in real-world applications further further. Future work should explore whether incorporating larger base models, alternative embeddings beyond ALBERT, or MCMC-based inference could further narrow the performance gap with larger transformer-based detectors, and whether the framework generalizes to multilingual or domain-shifted AI-generated text.

4. Conclusions

This study presented the Bayesian Meta-Ensemble of Stacked LSTM-CNNs, a lightweight, uncertainty-aware framework for AI-generated text detection. Using the MAGE benchmark dataset, we demonstrated that a compact LSTM-CNN trained on resampled, class-balanced subsets with ALBERT embeddings consistently outperforms more complex architectures (BiLSTM-CNN, Multi-head Attention LSTM-CNN) under a strict parameter budget (<6M), highlighting the value of architectural simplicity when model capacity is constrained. The BNN meta-learner, trained via Variational Inference on the outputs of the best-performing base models, enables probabilistic classification that goes beyond fixed-threshold decision-making. Benchmarked against FastText, GLTR, DetectGPT, and Longformer, the proposed model achieved 90.84% human recall, 89.59% average recall, and 0.96 AUROC with only 18.77M parameters, approximately

7.5 times fewer than Longformer. While RoBERTa-based and GPT-detector models represent the current state of the art in accuracy, they demand substantially more computational resources. Our model offers a competitive alternative for resource-constrained deployments. Stability analysis using Kolmogorov-Smirnov and Mann-Whitney tests confirmed that predictive distributions converge across MC sample sizes, with optimal stability observed between MC = 500 and MC = 1000. Shapiro-Wilk testing further revealed that larger MC samples yield more normally distributed prediction medians, supporting the use of parametric methods at higher sampling rates. The integration of both parametric (Student's t-test) and non-parametric (Wilcoxon) hypothesis tests into the prediction pipeline yielded a consistent improvement in human recall while preserving overall classification balance, demonstrating that leveraging the full output distribution of the BNN is more informative than relying on a fixed decision threshold alone. Overall, the proposed model advances AI-generated text detection by combining ensemble stacking, Bayesian uncertainty quantification, and statistical inference into a unified, computationally efficient framework. This combination offers capabilities unavailable in deterministic, single-model detectors, making the approach particularly suitable for high-stakes applications such as misinformation detection and academic integrity verification. However, this study has several limitations that should be acknowledged. First, the base models are intentionally lightweight (<6M parameters) due to computational resource constraints; larger base models or deeper stacked architectures may yield higher classification performance at the cost of increased inference time. Only ALBERT embeddings were evaluated; exploring alternative representations, such as RoBERTa, DeBERTa, or domain-adapted embeddings, could further improve feature extraction quality. The BNN meta-learner was trained using Variational Inference, which is a known approximation to the true posterior. Employing MCMC with adversarial sampling, as proposed by Zhang et al. [47], may improve the BNN meta-learner's accuracy and calibration. There are also several criteria to consider, such as model sensitivity analysis. Lastly, all experiments were conducted on the MAGE dataset in English. Generalizability to multilingual text, domain-shifted content, or adversarial paraphrased AI-generated text remains unverified.

5. Acknowledgments

Author Contributions: N. K. conducted the experiments, implemented the model, and contributed to writing and primary revision of the manuscript. P. S. provided guidance and contributed to reviewing and editing the manuscript.

Funding: This work was supported by Chiang Mai University under TA/RA Scholarship Program.

Conflicts of Interest: The authors declare no conflict of interest.

References

[1] Kumar, P. Large language models (LLMs): Survey, technical frameworks, and future challenges. *Artif. Intell. Rev.* **2024**, *57*. https://doi.org/10.1007/s10462-024-10888-y

[2] Li, Z.; Zhang, W.; Zhang, H.; Fang, X. Global digital compact: A mechanism for the governance of online discriminatory and misleading content generation. *Int. J. Hum.-Comput. Interact.* **2025**, *41*(2), 1381–1396. https://doi.org/10.1080/10447318.2024.2314350

[3] Stokel-Walker, C. AI bot ChatGPT writes smart essays—Should professors worry? *Nature* **2022**. https://doi.org/10.1038/d41586-022-04397-7

[4] Ghosal, S. S.; Chakraborty, S.; Geiping, J.; Huang, F.; Manocha, D.; Bedi, A. S. Towards possibilities & impossibilities of AI-generated text detection: A survey. *arXiv* **2023**, arXiv:2310.15264.

[5] Solaiman, I.; et al. Release strategies and the social impacts of language models. *arXiv* **2019**, arXiv:1908.09203

[6] Zellers, R.; et al. Defending against neural fake news. In *Advances in Neural Information Processing Systems*; **2019**; Vol. 32.

[7] Jawahar, G.; Abdul-Mageed, M.; Lakshmanan, L. V. Automatic detection of machine generated text: A critical survey. *arXiv* **2020**, arXiv:2011.01314.

[8] Devlin, J.; Chang, M.-W.; Lee, K.; Toutanova, K. BERT: Pre-training of deep bidirectional transformers for language understanding. In *Proc. NAACL-HLT*; **2019**; pp 4171–4186.
[9] Sanh, V.; Debut, L.; Chaumond, J.; Wolf, T. DistilBERT, a distilled version of BERT: Smaller, faster, cheaper and lighter. *arXiv* **2019**, arXiv:1910.01108.
[10] Liu, Y.; et al. RoBERTa: A robustly optimized BERT pretraining approach. *arXiv* **2019**, arXiv:1907.11692.
[11] Pawlowski, N.; Brock, A.; Lee, M. C.; Rajchl, M.; Glocker, B. Implicit weight uncertainty in neural networks. *arXiv* **2017**, arXiv:1711.01297.
[12] Chen, W.; Li, B.; Zhang, R.; Li, Y. Bayesian computation in deep learning. *arXiv* **2025**, arXiv:2502.18300.
[13] Li, Y.; et al. MAGE: Machine-generated text detection in the wild. *arXiv* **2024**, arXiv:2305.13242. https://doi.org/10.48550/arXiv.2305.13242
[14] Zhang, J.; Li, Y.; Tian, J.; Li, T. LSTM-CNN hybrid model for text classification. In *Proc. IEEE IAEAC*; **2018**; pp 1675–1680. https://doi.org/10.1109/IAEAC.2018.8577620
[15] Xiao, L.; Wang, G.; Zuo, Y. Research on patent text classification based on Word2Vec and LSTM. In *Proc. ISCID*; **2018**; pp 71–74. https://doi.org/10.1109/ISCID.2018.00023
[16] Xie, J.; Chen, B.; Gu, X.; Liang, F.; Xu, X. Self-attention-based BiLSTM model for short text fine-grained sentiment classification. *IEEE Access* **2019**, *7*, 180558–180570. https://doi.org/10.1109/ACCESS.2019.2957510
[17] Wadud, M. A. H.; Kabir, M. M.; Mridha, M. F.; Ali, M. A.; Hamid, M. A.; Monowar, M. M. Managing offensive text in social media: A text classification approach using LSTM-BOOST. *Int. J. Inf. Manage. Data Insights* **2022**, *2*(2), 100095. https://doi.org/10.1016/j.jjimei.2022.100095
[18] Anggrainingsih, R.; Hassan, G. M.; Datta, A. Evaluating BERT-based language models for detecting misinformation. *Neural Comput. Appl.* **2025**. https://doi.org/10.1007/s00521-025-11101-z
[19] O'Shea, K.; Nash, R. An introduction to convolutional neural networks. *arXiv* **2015**, arXiv:1511.08458.
[20] Kim, Y. Convolutional neural networks for sentence classification. *arXiv* **2014**, arXiv:1408.5882. https://doi.org/10.48550/arXiv.1408.5882
[21] Alshubaily, I. TextCNN with attention for text classification. *arXiv* **2021**, arXiv:2108.01921. https://doi.org/10.48550/arXiv.2108.01921
[22] Zhao, W.; Zhu, L.; Wang, M.; Zhang, X.; Zhang, J. WTL-CNN: A news text classification method based on weighted word embedding. *Connect. Sci.* **2022**, *34*(1), 2291–2312. https://doi.org/10.1080/09540091.2022.2117274
[23] Ran, Y.; Han, H. Text classification algorithm based on sparse distributed representation. In *Proc. IEEE AEECA*; **2020**; pp 876–880. https://doi.org/10.1109/AEECA49918.2020.9213479
[24] Li, C.; Zhan, G.; Li, Z. News text classification based on improved Bi-LSTM-CNN. In *Proc. IEEE ITME*; **2018**; pp 890–893. https://doi.org/10.1109/ITME.2018.00199
[25] Jang, B.; Kim, M.; Harerimana, G.; Kang, S.; Kim, J. W. Bi-LSTM model to increase accuracy in text classification. *Appl. Sci.* **2020**, *10* (17), 5841. https://doi.org/10.3390/app10175841
[26] Abdullah, A. A.; Hassan, M. M.; Mustafa, Y. T. Bayesian deep learning in healthcare: Applications and challenges. *IEEE Access* **2022**, *10*, 36538–36562. https://doi.org/10.1109/ACCESS.2022.3163384
[27] Graves, A. Practical variational inference for neural networks.
[28] Abburi, H.; et al. A simple yet efficient ensemble approach for AI-generated text detection. In *Proc. GEM Workshop*; Association for Computational Linguistics: Singapore, 2023; pp 413–421.
[29] Aggarwal, K.; Singh, S.; Parul; Pal, V.; Yadav, S. S. Enhancing accuracy in AI-generated text detection using ensemble modelling. In *Proc. IEEE TENSYMP*; 2024; pp 1–8. https://doi.org/10.1109/TENSYMP61132.2024.10752173
[30] Massey, F. J., Jr. The Kolmogorov–Smirnov test for goodness of fit. *J. Am. Stat. Assoc.* **1951**, *46* (253), 68–78. https://doi.org/10.1080/01621459.1951.10500769
[31] Two Sample Kolmogorov–Smirnov. Real Statistics Using Excel. https://real-statistics.com/non-parametric-tests/goodness-of-fit-tests/two-sample-kolmogorov-smirnov-test/ (accessed Jul 23, 2025).
[32] Divine, G. W.; Norton, H. J.; Barón, A. E.; Juarez-Colunga, E. The Wilcoxon–Mann–Whitney procedure fails as a test of medians. *Am. Stat.* **2018**, *72*(3), 278–286.

[33] Feltovich, N. Nonparametric tests of differences in medians. *Exp. Econ.* **2003**, *6*(3), 273–297.
[34] Yue, S.; Wang, C. Y. Power of the Mann–Whitney test. *Stochastic Environ. Res. Risk Assess.* **2002**, *16*(4), 307–323.
[35] Mishra, P.; Singh, U.; Pandey, C. M.; Mishra, P.; Pandey, G. Application of Student's t-test. *Ann. Card. Anaesth.* **2019**, *22*(4), 407–411.
[36] Lumley, T.; Diehr, P.; Emerson, S.; Chen, L. Importance of normality assumption. *Annu. Rev. Public Health* **2002**, *23*, 151–169.
[37] Ratcliffe, J. F. Effect on the t distribution of non-normality. *Appl. Stat.* **1968**, *17*(1), 42.
[38] Sawilowsky, S. S.; Blair, R. C. Robustness of the t test. *Psychol. Bull.* **1992**, *111*(2), 352–360.
[39] Althouse, L. A.; Ware, W. B.; Ferron, J. M. Detecting departures from normality. **1998**.
[40] Razali, N. M.; Yap, B. Power comparisons of normality tests. *J. Stat. Model. Anal.* **2011**, *2*.
[41] UMA Technology. The dangers of AI writing and how to spot AI-generated text. https://umatechnology.org/the-dangers-of-ai-writing-and-how-to-spot-ai-generated-text/ (accessed Mar 14, 2025).
[42] AI's Jurassic Park moment. *Commun. ACM*. https://cacm.acm.org/blogcacm/ais-jurassic-park-moment/ (accessed Mar 14, 2025).
[43] Vincent, J. AI-generated answers temporarily banned on Stack Overflow. *The Verge*. https://www.theverge.com/ (accessed Mar 14, 2025).
[44] Dergaa, I.; Chamari, K.; Zmijewski, P.; Saad, H. B. AI-generated text in academic writing. *Biol. Sport* **2023**, *40*(2), 615–622.
[45] Bohannon, J. Who's afraid of peer review? *Science* **2013**, *342*(6154), 60–65.
[46] Fagerland, M. W. t-tests and non-parametric tests. *BMC Med. Res. Methodol.* **2012**, *12*, 78.
[47] Zhang, J.; et al. Improving Bayesian neural networks by adversarial sampling. *Proc. AAAI* **2022**, *36*(9), 10110–10117.

ASEAN
Journal of Scientific and Technological Reports
Online ISSN:2773-8752

Research article

The Influence of *Helicobacter pylori* Infection on Hepatic Enzymes, Inflammatory Markers, and Hematological Parameters in Patients with Gastritis

Wasan A. Wahab Alsiadi[1], Malak A. Al-Yawer[2], and Rana H. k. Al-Rubaye[1*]

[1] Department of Biology, College of Education for Pure Sciences (Ibn-Al-Haitham), University of Baghdad, Iraq
[2] Department of Anatomy, College of Medicine, University of Baghdad, Iraq
* Correspondence Rana : rana.h.k@ihcoedu.uobaghdad.edu.iq

Citation:
Alsiadi, W.A.W.; AL-yawer, A.M.; Al-Rubaye, K.H.R. The influence of *Helicobacter pylori* infection on hepatic enzymes, inflammatory markers, and hematological parameters in patients with gastritis. *ASEAN J. Sci. Tech. Report.* **2026**, *29*(5), e261081. https://doi.org/10.55164/ajstr.v29i5.261081

Article history:
Received: August 31, 2025
Revised: March 18, 2026
Accepted: April 11, 2026
Available online: April 30, 2026

Publisher's Note:
This article is published and distributed under the terms of the Thaksin University.

Abstract: *Helicobacter pylori* (HP) colonizes the gastric mucosa and causes gastric and extra-gastric disorders. Several liver diseases, such as Non-alcoholic fatty liver disease, seem to be caused by the gastrointestinal tract, which is primarily determined by the presence of bacteria like *Helicobacter pylori.* The study aims to evaluate the relationship between *Helicobacter pylori* infection and liver diseases by measuring liver enzymes, inflammatory markers, and hematological parameters among patients with gastritis and without *Helicobacter pylori* infection. A total of 1,325 patients who had gastritis diagnosed by gastroscopy were included in our study. They were divided into the HP– group (340 women, 323 men) and the HP+ group (330 women, 332 men). A control group (360 women, 260 men) without gastritis or HP infection was included in this study. HP was determined using the 13C urea breath test, which requires patients to swallow a capsule with water. Measurements of liver enzymes and complete blood cell counts were done in addition to interleukin-6(IL-6) and C-reactive protein (CRP). The results showed a significant increase in IL-6 and CRP in the HP+ group. Additionally, the mean levels of leukocytes and platelets were significantly increased in the HP+ group, but liver enzymes were within the normal range in both the HP+ & HP– groups. Although *Helicobacter pylori* causes elevation of indices of systemic inflammation, the liver did not show evidence of fatty infiltration, as liver enzymes were within normal limits.

Keywords: *Helicobacter pylori*; inflammatory markers; liver enzymes; hematological parameters

1. Introduction

Helicobacter pylori (HP) is a Gram-negative, helical-shaped pathogenic bacterium that attacks the stomach mucosa. It is believed that 50% of people worldwide are infected with HP, and it is well known that a persistent HP infection can lead to chronic gastritis, peptic ulcers, and stomach cancer [1,2]. In recent years, HP has been reported to be associated with the development of a variety of extra-alimentary disorders, including type 2 diabetes, and cardiovascular and hepatic diseases [3-5]. Since the "Gut-Liver Axis" has attracted a lot of attention, many liver diseases, such as Non-alcoholic fatty liver disease (NAFLD), are believed to be influenced by the environment of the gastrointestinal tract, which is largely determined by the presence of bacteria such as HP [6,7]. NAFLD is a category of disorders of the liver that includes

cirrhosis, nonalcoholic steatohepatitis, and steatosis. The most frequent cause of increased liver enzymes in adults in the US is nonalcoholic fatty liver disease[8]. Research on the relationship between HP infection and NAFLD has provided conflicting findings. According to certain research, NAFLD was considerably more common among HP+ individuals [9-11]. Other research, however, found no link between HP infection and NAFLD [12-14]. Our study aims to determine whether HP is a contributing factor in the natural progression of NAFLD or merely a coincidental finding by measuring liver enzymes, inflammatory markers, and hematological parameters in patients with gastritis with and without HP infection.

2. Materials and Methods

2.1 Study design

The study population was recruited from Iraqi adults who visited a clinic in Baquba, Iraq, between December 2020 and April 2022. A total of 1,325 Iraqi adults who had gastritis diagnosed by endoscopy were included in our study. They were divided into two groups: HP+ (330 women, 332 men) and HP- (340 women, 323 men), aged 30-65 years. A control group (360 women, 260 men) aged 30-60 years was included in this study who had neither gastritis nor HP infection. The study excluded patients taking medication for hypertension, hyperlipidemia, diabetes, hyperuricemia, or cardiovascular disease. Patients with chronic renal or hepatic failure were also ruled out. This work has been approved by the University of Bilad Al-Rafidain's ethical committee, College of Health and Medical Techniques, Iraq. On 20/11/2020, the authorization was acquired under reference number e.125.

2.2 HP Infection Detection

HP was determined using the 13C urea breath test, which requires patients to swallow a capsule with water. After a few minutes, a breath sample is collected. This sample is then processed to determine whether you have an active *H. pylori* infection[7]. Each patient completed a comprehensive questionnaire that included lifestyle factors, medical history, family history, and gastrointestinal symptoms. Regular measurements were taken of each participant's height, weight, and blood pressure.

2.3 Determination of body mass index

The Body mass index (BMI) was calculated as weight (kg) divided by height squared (m^2).

2.4 Determination of liver enzyme levels

Morning venous blood of all participants was obtained to detect the levels of serum alanine aminotransferase (ALT), aspartate aminotransferase (AST), gamma-glutamyl transferase (GGT) & total serum bilirubin (TSB) using an autoanalyzer (Beckman, Palo Alto, CA, United States).

2.5 Determination of inflammatory and hematological parameter levels

By using Cobas e 411, the levels of serum CRP and IL-6 were determined. A Sysmex XE-2100 analyzer was used to perform whole-blood cell counts (Sysmex, Kobe, Japan).

2.6 Statistical analysis

Regarding numerical aspects, statistical analysis was conducted using SPSS (Statistical Package for the Social Sciences) version 22. For determining the samples under investigation. The normality of the data distribution was tested before selecting parametric tests. The mean and standard deviation of the mean were used, and the averages were compared at the 0.05 level. ANOVA is a statistical test used to compare means across three groups. A post hoc test was used because multiple groups were compared.

3. Results and Discussion

3.1 Liver enzyme levels

Results of the current study (Table 1) showed that liver enzymes were within the normal range in both the control and experimental groups, and there were no significant differences ($p>0.05$) in liver function indexes (TSB, ALT, AST, GGT).

Table 1. The relationship between the HP status and liver function indexes (mg/dL).

		Mean	SD	Statistics
TSB (mg/dL)	**control**	0.86	0.36	P>0.05
0.2-1.2	**Gastritis with *H. pylori***	0.88	0.31	
	Gastritis without *H. pylori*	0.73	0.29	
ALT (mg/dL)	**Control**	30.69	12.38	P>0.05
10.0-55.0	**Gastritis with *H. pylori***	35.37	13.45	
	Gastritis without *H. pylori*	33.88	13.65	
AST (mg/dL)	**Control**	28.46	6.80	P>0.05
10.0-40.0	**Gastritis with *H. pylori***	27.98	7.57	
	Gastritis without *H. pylori*	25.50	6.15	
GGT (mg/dL)	**Control**	21.80	7.31	P>0.05
8.0-35.0	**Gastritis with *H. pylori***	23.43	7.20	
	Gastritis without *H. pylori*	23.31	7.02	

Abbrev: TSB: total serum bilirubin, ALT: alanine transaminase, AST: aspartate aminotransferase, GGT: gamma- glutamyl transpeptidase.

By dividing the study sample by sex in Table 2, we found no significant association between liver function indicators and HP infection status.

Table 2. Comparison of liver function indexes (mg/dL) in different genders.

		Gastritis with HP		Gastritis without HP		Statistics
		Mean	SD	Mean	SD	
TSB	**Males**	0.74	0.20	0.72	0.33	P>0.05
	Females	1.02	0.33	0.74	0.26	
ALT	**Males**	39.29	6.79	34.28	14.91	P>0.05
	Females	31.46	17.37	33.48	13.06	
AST	**Males**	29.78	5.83	26.64	6.97	P>0.05
	Females	26.18	8.94	24.36	5.33	
GGT	**Males**	22.60	7.05	22.97	7.60	P>0.05
	Females	24.25	7.64	23.65	6.79	

Abbrev: TSB: total serum bilirubin, ALT: alanine transaminase, AST: aspartate aminotransferase, GGT: gamma- glutamyl transpeptidase.

3.2 Inflammatory and hematological parameter levels

The mean serum levels of CRP and IL-6 were significantly (P<0.001) higher in the HP+ group than in the HP- & control groups, respectively. Also, there were no differences in hemoglobin measurements among the HP+, HP-, and control groups (p>0.05); however, there were significant differences in white blood cells (P<0.001) and platelets (P<0.05). The mean serum white blood cell levels were significantly higher in the HP+ group than in the HP– and control groups. The mean platelet count was within the normal range. However, their mean levels were significantly higher in the HP + group, followed by the HP – and control groups (Table 3).

Table 3. Correlation between HP infection and inflammatory and hematological measures in patients with gastritis.

		Mean	SD	Statistics
IL-6 (pg/ml) 7 ≥ pg/mL	**Control**	7.94	1.63	P<0.001*** LSD=3.34
	Gastritis with *HP*	19.33	2.06	
	Gastritis without *HP*	14.64	2.59	
CRP (mg/L)	**Control**	4.09	1.02	P<0.001*** LSD=2.92
	Gastritis with *HP*	15.62	3.39	
	Gastritis without *HP*	13.37	4.65	
WBCs *109 (4.0-11.0)	**Control**	9.59	2.58	P<0.001*** LSD=0.37
	Gastritis with *HP*	13.76	1.57	
	Gastritis without *HP*	12.20	1.63	
Hb (g/dL) (11.0 - 16.0)	**Control**	12.33	2.92	P>0.05
	Gastritis with *HP*	12.92	0.88	
	Gastritis without *HP*	13.24	1.24	
PLTs (m/mm^3) (150-450)	**Control**	309.70	47.53	P<0.05* LSD=29.45
	Gastritis with *HP*	335.79	48.72	
	Gastritis without *HP*	285.75	69.99	

Abbrev: IL-6: interleukin-6, CRP: C-reactive protein, WBCs: white blood cell count, Hb: hemoglobin, PLTs: platelet count.

Table 4 showed a comparison of hematological and inflammatory parameters by gender. Males had higher Hb, but females had higher CRP, IL-6, WBC, and platelets.

Table 4. Correlation between HP infection and inflammatory and hematological measures in patients with gastritis.

		Gastritis with *H. pylori*		Gastritis without *H. pylori*		Statistics
		Mean	SD	Mean	SD	
IL-6 [15]	**Males**	18.53	1.38	14.09	1.90	P<0.001***
	Females	20.14	2.37	15.19	3.14	LSD=3.88
CRP	**Males**	15.42	4.54	10.02	3.88	P<0.001***
	Females	15.82	1.89	16.72	2.38	LSD=2.68
WBCs	**Males**	12.48	0.85	11.34	1.69	P<0.001***
	Females	15.04	0.93	13.05	1.06	LSD=1.13
Hb	**Males**	12.97	0.73	12.76	1.23	P>0.05
	Females	12.86	1.04	13.72	1.11	
PLTs	**Males**	314.59	26.85	246.90	51.58	P<0. 05*
	Females	356.99	57.38	324.60	65.78	LSD=41.39

Abbrev:IL-6: interleukin-6, CRP: C-reactive protein, WBCs: white blood cell count, Hb: hemoglobin, PLTs: platelet count

The presence of the *H. pylori* bacteria influences the composition, balance, and activity of the microbiota, which, in turn, influences metabolic capability, immune response, and homeostasis in the human stomach. Because the interrelationships between bacteria dictate the illness burden, treating and eradicating H. pylori may result in additional chronic human diseases whose pathogenic mechanisms have yet to be confirmed [16]. Socioeconomic status may serve as a proxy for additional, undisclosed risk factors for *H. Pylori* infection. According to epidemiological studies, people with low socioeconomic positions are more likely to develop peptic ulcer disease [17]. The current study showed that, while liver enzyme levels in the experimental and control groups were within the normal range, HP infection was not associated with an elevated risk of NAFLD. Numerous clinical studies have been conducted to investigate the association between NAFLD and HP infection [18]. According to [18] Wijarnpreecha et al., 2018 comprehensive review and meta-analysis, there is a substantial association between NAFLD and HP infection in patients [19]. Additionally, a cohort study

conducted by Kim *et al. (2017) identified an association between HP and* NAFLD [20]. On the other hand, a large-scale cross-sectional study by Okushin et al. (2015) found that HP infections were not significantly associated with NAFLD11. Additionally, a retrospective cohort study revealed that NAFLD risk was not associated with HP infection [21]. There were two other studies that demonstrated a negative association between HP infection and NAFLD [22-23]. The inconsistency between the above studies may be due to geographical or ethnic variations, with genetic predisposition as the differentiating factor between patients. Regarding HP infection and NAFLD, there was no gender difference between men and women. This result is inconsistent with the finding that HP infection is linked to NAFLD in female patients [24]. Changes in WBC count with HP+ may reflect the severity of gastric mucosal inflammation, which can cause both local and systemic inflammation, a contributing factor to its involvement in extra-gastric disorders [25-26,27]. In turn, this systemic inflammation (IL-6 and CRP) can trigger several extra-gastrointestinal conditions, including metabolic syndrome, diabetes, insulin resistance, and cardiovascular disease [28-29]. In our study, in addition to the significant increases in IL-6 and CRP, the mean levels of leukocytes and platelets were significantly higher in the HP + group, but liver enzymes were within the normal range in both the HP + & HP – groups.

4. Conclusions

Although *Helicobacter pylori* causes elevation of indices of systemic inflammation, the liver does not show evidence of fatty infiltration, as liver enzymes were within normal limits. Further research should investigate additional variables to reveal the effect of *H. pylori* infection on liver disease.

5. Acknowledgments

The authors would like to thank all patients who participated in this study.

Author Contributions: Wasan A. Wahab Alsiadi: Methodology, Investigation, Formal analysis, Visualization. original draft, software. Malak A. Al-Yawer: Conceptualization, Data Writing curation, Writing – original draft, software.Rana H. k. Al-Rubaye: Supervision, Writing – review & editing, Project administration, funding acquisition, visualization

Funding: The present study has not been supported financially.

Conflicts of Interest: The authors declare no conflict of interest regarding the publication of this manuscript.

References

[1] Umar, Z.; Tang, J. W.; Marshall, B. J.; Tay, A. C. Y.; Wang, L. Rapid diagnosis and precision treatment of *Helicobacter pylori* infection in clinical settings. *Crit. Rev. Microbiol.* **2025**, *51*(2), 369–398. https://doi.org/10.1080/1040841X.2024.2364194

[2] Bansil, R.; Constantino, M. A.; Su-Arcaro, C.; Liao, W.; Shen, Z.; Fox, J. G. Motility of different gastric *Helicobacter* spp. *Microorganisms* **2023**, *11*(3), 634. https://doi.org/10.3390/microorganisms11030634

[3] Li, J.; Yuan, W.; Liu, J.; Yang, B.; Xu, X.; Ren, X.; Jia, L. Association between *Helicobacter pylori* infection and type 2 diabetes mellitus: A retrospective cohort study and bioinformatics analysis. *BMC Endocr. Disord.* **2024**, *24*(1), 168. https://doi.org/10.1186/s12902-024-01694-2

[4] Al-Yawer, M. A.; Alsiadi, W.; Hakman, A. A.; Ahmed, A. D. The influence of *Helicobacter pylori* infection on cardiovascular risk factors in patients with gastritis. *SJFPS* **2024**, *3*(1)

[5] Alsiadi, W. A. W.; Al-Yawer, M. A.; Oudah, N. N.; Al-Shmgani, H. S. The influence of *Helicobacter pylori* infection on glycemic measures in patients with gastritis: A cohort study. *Opera Med. Physiol.* **2025**, *12*(1), 59–65. https://doi.org/10.24412/2500-2295-2025-1-58-65

[6] Paik, J. M.; Henry, L.; De Avila, L.; Younossi, E.; Racila, A.; Younossi, Z. M. Mortality related to nonalcoholic fatty liver disease is increasing in the United States. *Hepatol. Commun.* **2019**, *3*(11), 1459–1471.

[7] Kumar, A.; Kansal, D.; Gupta, S.; Sood, A.; Bodh, S. Raised liver enzyme in a patient receiving *Helicobacter pylori* triple regimen: A case report. *IP Int. J. Compr. Adv. Pharmacol.* **2022**, *7*(2), 106–107. https://doi.org/10.18231/j.ijcaap.2022.020

[8] Polyzos, S. A.; Kountouras, J.; Papatheodorou, A.; Patsiaoura, K.; Katsiki, E.; Zafeiriadou, E.; Terpos, E. *Helicobacter pylori* infection in patients with nonalcoholic fatty liver disease. *Metabolism* **2013**, *62*(1), 121–126. https://doi.org/10.1016/j.metabol.2012.06.007

[9] Kim, T. J.; Sinn, D. H.; Min, Y. W.; Son, H. J.; Kim, J. J.; Chang, Y.; et al. A cohort study on *Helicobacter pylori* infection associated with nonalcoholic fatty liver disease. *J. Gastroenterol.* **2017**, *52*, 1201–1210. https://doi.org/10.1007/s00535-017-1337-y

[10] Jamali, R.; Mofid, A.; Vahedi, H.; Farzaneh, R.; Dowlatshahi, S. The effect of *Helicobacter pylori* eradication on liver fat content in subjects with nonalcoholic fatty liver disease. *Hepat. Mon.* **2013**, *13*, e14679. https://doi.org/10.5812/hepatmon.14679

[11] Okushin, K.; Takahashi, Y.; Yamamichi, N.; Shimamoto, T.; Enooku, K.; Fujinaga, H.; Koike, K. *Helicobacter pylori* infection is not associated with fatty liver disease. *BMC Gastroenterol.* **2015**, *15*, 1–10.

[12] La Placa, G.; Covino, M.; Candelli, M.; Gasbarrini, A.; Franceschi, F.; Merra, G. Relationship between human microbiome and *Helicobacter pylori*. *Microbiol. Res.* **2025**, *16*, 24. https://doi.org/10.3390/microbiolres16010024

[13] Baeg, M. K.; Yoon, S. K.; Ko, S. H.; Noh, Y. S.; Lee, I. S.; Choi, M. G. *Helicobacter pylori* infection is not associated with nonalcoholic fatty liver disease. *World J. Gastroenterol.* **2016**, *22*(8), 2592. https://doi.org/10.3748/wjg.v22.i8.2592

[14] Fan, N.; Peng, L.; Xia, Z.; Zhang, L.; Wang, Y.; Peng, Y. *Helicobacter pylori* infection is not associated with nonalcoholic fatty liver disease. *Front. Microbiol.* **2018**, *9*, 73. https://doi.org/10.3389/fmicb.2018.00073

[15] Pepys, M. B.; Hirschfield, G. M. C-reactive protein: A critical update. *J. Clin. Invest.* **2003**, *111*(12), 1805–1812. https://doi.org/10.1172/JCI18921

[16] Pessar, D. A. E. H.; Galal, S. A.; Omira, M. M. A.; Al-Ghamdi, H. S.; Alghamdi, M. A.; Alghamdi, F. A.; et al. The role of *Helicobacter pylori* in psoriasis. *Immunopathol. Persa* **2025**, *11*(2), e43855. https://doi.org/10.34172/ipp.2025.43855

[17] Al-Karawi, A. S.; Rasool, K. H.; Atoom, A. M.; Kadhim, A. S. Correlation between *H. pylori* infection and inflammatory markers. *Al-Salam J. Med. Sci.* **2023**, *2*(2), 20–24. https://doi.org/10.55145/ajbms.2023.1.2.004

[18] Jiang, T.; Chen, X.; Xia, C.; Liu, H.; Yan, H.; Wang, G.; Wu, Z. Association between *Helicobacter pylori* infection and NAFLD. *Sci. Rep.* **2019**, *9*(1), 4874. https://doi.org/10.1038/s41598-019-41371-2

[19] Wijarnpreecha, K.; Thongprayoon, C.; Panjawatanan, P.; Manatsathit, W.; Jaruvongvanich, V.; Ungprasert, P. *Helicobacter pylori* and NAFLD risk: A meta-analysis. *J. Clin. Gastroenterol.* **2018**, *52*(5), 386–391. https://doi.org/10.1097/MCG.0000000000000784

[20] Kim, T. J.; Sinn, D. H.; Min, Y. W.; Son, H. J.; Kim, J. J.; Chang, Y.; et al. *Helicobacter pylori* and NAFLD. *J. Gastroenterol.* **2017**, *52*, 1201–1210. https://doi.org/10.1007/s00535-017-1337-y

[21] Wang, J.; Dong, F.; Su, H.; Zhu, L.; Shao, S.; Wu, J.; Liu, H. *H. pylori* and NAFLD in females. *Int. J. Med. Sci.* **2021**, *18*(11), 2303–2311. https://doi.org/10.7150/ijms.50748

[22] Franceschi, F.; Covino, M.; Roubaud Baudron, C. *Helicobacter pylori* and extragastric diseases. *Helicobacter* **2019**, *24*(1), e12636. https://doi.org/10.1111/hel.12636

[23] Kountouras, J.; Papaefthymiou, A.; Polyzos, S. A.; Deretzi, G.; Vardaka, E.; Soteriades, E. S. *Helicobacter pylori* and hypertension. *Microorganisms* **2021**, *9*(11), 2351. https://doi.org/10.3390/microorganisms9112351

[24] Karttunen, T. J.; Niemelä, S.; Kerola, T. Blood leukocyte differential in *Helicobacter pylori* infection. *Dig. Dis. Sci.* **1996**, *41*(7), 1332–1336. https://doi.org/10.1007/BF02088556

[25] Wang, J.; Dong, F.; Su, H.; Zhu, L.; Shao, S.; Wu, J.; Liu, H. *H. pylori* and NAFLD in females. *Int. J. Med. Sci.* **2021**, *18*(11), 2303–2311. https://doi.org/10.7150/ijms.50748

[26] Alsiadi, W. A. W.; Albayati, A. M.; Elhaboby, B. T. Detection of cytokines in renal failure patients. *Indian J. Forensic Med. Toxicol.* **2021**, *15*(2), 1470–1475. https://doi.org/10.37506/ijfmt.v15i2.14546

[27] Han, Y. M.; Lee, J.; Choi, J. M.; Kwak, M. S.; Yang, J. I.; Chung, S. J.; Chung, G. E. Association between *Helicobacter pylori* and NAFLD. *PLoS One* **2021**, *16*(12), e0260994. https://doi.org/10.1371/journal.pone.0260994

[28] Abd El-Maksoud, H. A.; Mohamed, G. E.; Alshaimaa, M. S.; Marwa, M. M. Biochemical relations of *Helicobacter pylori* infection. *Benha Vet. Med. J.* **2019**, *36*(1), 95–100. https://doi.org/10.21608/bvmj.2019.103401

[29] Alsiadi, W. A. W.; Mahmood, M. M.; Hassan, A. S. Hematological denotations in renal failure. *Indian J. Public Health Res. Dev.* **2019**, *10*(6). https://doi.org/10.5958/0976-5506.2019.01391.3

[30] Chang, W.; Cai, L.; Chen, T.; Ni, W.; Xie, Z.; Yang, C.; Liao, J. *Helicobacter pylori* infection and liver injury. *Am. J. Trop. Med. Hyg.* **2023**, *108*(4), 684–692. https://doi.org/10.4269/ajtmh.22-0340

[31] Chen, X.; Peng, R.; Peng, D.; Xiao, J.; Liu, D.; Li, R. Relationship between *H. pylori* and NAFLD. *Front. Cell. Infect. Microbiol.* **2023**, *13*, 1282956. https://doi.org/10.3389/fcimb.2023.1282956

ASEAN
Journal of Scientific and Technological Reports
Online ISSN:2773-8752

Research article

The Effect of Developed Blenderized Diet Formula on Physical Features

Pachsiree Khwannimit[1*], and Piyanuch Maitreegorn[2]

[1] Department of Nursing, Paphayom Hospital, Phatthalung, 93210, Thailand
[2] Department of Nutrition, Pak Phayun Hospital, 93120, Thailand
* Correspondence author: pachsiree.ati@gmail.com

Citation:
Khwannimit, P.; Maitreegorn, P. The effect of developed blenderized diet formula on physical features. *ASEAN J. Sci. Tech. Report.* **2026**, *29*(5), e256663. https://doi.org/10.55164/ajstr.v29i5.256663

Article history:
Received: October 6, 2025
Revised: March 27, 2026
Accepted: April 12, 2026
Available online: April 30, 2026

Publisher's Note:
This article is published and distributed under the terms of the Thaksin University.

Abstract: The objective of this research was to compare the effect of original- and developed-blenderized diet (BD) formulas on physical features (color measurement (lightness (*L**), greenness to redness (a*) along with blueness to yellowness (b*) values), viscosity, including flow rate. Mean comparison between two formulas was conducted in this study. The energy distribution of both BD formulas was close to 1,000 kilocalories (kcal), and the caloric density (kcal/mL) was determined to be 1:1. The percentage in proportion of macronutrients (carbohydrate: protein: fat) of total calories was 55:15:30, respectively. Calculation of energy using Thai Nutrisurvey® software version 2.0. The original BD formula (OBDF) is composed of cooked rice, pumpkin, banana, table sugar, eggs, chicken breast, and soybean oil. The developed BD formula (DBDF) consists of pumpkin, banana, table sugar, eggs, chicken breast, and soybean oil. All cooked ingredients were blended, filtered, and then poured into a Nutri-Bag at 250 mL, followed by daily 4 feedings. Both BD formulas were repeated 3 times. The results illustrated that *L** value and flow rate of DBDF (71.17 ± 0.08 and 16.18 ± 0.03 mL/min) were significantly higher than OBDF (68.82 ± 0.02 and 25.70 ± 0.26 mL/min) (p<0.05). Nevertheless, the values of *a**, *b** as well as viscosity of OBDF (3.04 ± 0.06, 41.39 ± 0.05 and 59.37 ± 0.07 cP, respectively) were significantly higher than DBDF (2.38 ± 0.01, 26.16 ± 0.19 and 15.37±0.03 cP, respectively) (p<0.05). Hence, DBDF has greater physical characteristics than OBDF, which should be considered when delivering enteral tube feeding to patients.

Keywords: Developed blenderized diet formula; physical features; original blenderized diet formula

1. Introduction

As the number of stroke prevalence all over the world has grown year on year. In 2022, the World Stroke Organization (WSO) reported that the global burden of stroke increased from 91.5 million cases in 1990 to 125 million cases in 2019 [1]. Similarly, the incidence of stroke patients in Thailand is dramatically elevated from 278 people per 100,000 people in 2017 to 330 people per 100,000 people in 2022 [2]. The number of stroke patients at Paphayom hospital has shown a similar upward trend per annum as that of stroke prevalence. In the period 2021-2023, the report revealed that the number of stroke patients admitted to Paphayom Hospital was 328, 365, and 382, respectively.

Stroke is defined as "rapidly developed clinical signs of focal disturbance of cerebral function, lasting longer than 24 hours or leading to death,

with no apparent cause other than of vascular origin" [3]. Stroke has been classified into 2 main subtypes: hemorrhagic stroke and ischemic stroke [4]. Hemorrhagic stroke is a life-threatening medical condition that occurs from a blood vessel rupture resulting in bleeding into the brain [5]. On the other hand, ischemic stroke is caused by a cerebral occlusion by thrombosis or embolism, which can lead to loss of oxygen and blood flow to the brain [6]. Generally, most stroke patients are faced with various long-term experience limitations, e.g., vision, mobility, voice, speech, and one of the important troubles in the nutrition dimension is dysphagia [6]. Therefore, an appropriate route of nutrition support for stroke patients is essential. Dysphagia is defined as the obstruction of the process of food intake and transport from the mouth to the stomach that impairs the ability to ingest the diet safely and achieve the goal of nutrition therapy [7].

Enteral tube feeding is one of the preferred nutrition therapy routes for stroke patients with dysphagia via nasogastric tube (NGT) or percutaneous endoscopic gastrostomy/jejunostomy (PEG/PEJ) [8]. Regularly, alternative nutrition support options for enteral tube feeding include blenderized diets (BD) and commercial formulas. BD is a mixture of whole foods and liquids that are blended in a blender. The texture of BD should be pureed because it is composed of real table food, such as vegetables, fruit, meat, eggs, and sugar [9]. In the same manner, BD has been provided to stroke patients with dysphagia at Paphayom hospital, consisting of cooked rice, pumpkin, banana, table sugar, eggs, chicken breast, and soybean oil. Unfortunately, OBDF has a very high viscosity when stored in the refrigerator. For this reason, the nutritionist would like to compare the effect of OBDF with DBDF on physical features.

2. Materials and Methods

2.1 Study design and samples

A laboratory comparison of two formulas was conducted in this study. The samples are composed of 2 BD formulas: OBDF (using table food, including cooked rice, pumpkin, banana, eggs, chicken breast, and sugar, as well as soybean oil) and DBDF (using pumpkin, banana, eggs, chicken breast, sugar, and soybean oil). The research protocol was approved by the Research Ethics Committee of Thaksin University (COA No.222/68).

2.2 Study procedures

All samples were found to have a total energy of approximately 1,000 kcal. The nutritional values of total calories and macronutrients were calculated using the Thai Nutrisurvey® software version 2.0 (developed by the Faculty of Tropical Medicine, Mahidol University, Nakhon Pathom, Thailand). The nutrient composition and energy of both BD formulas are shown in Table 1. All samples were prepared from cooked ingredients. The caloric concentration was determined by 1:1. The percentage in proportion of macronutrients distribution (carbohydrate: protein: fat) of total calories was 55:15:30, respectively. Each sample was blended in a blender (Philips HR2225/00, maximum 800 Watt, Philips Co., Ltd., Bangkok, Thailand) at 2 speeds for the full 2 minutes and then filtered through a 15 cm diameter plastic strainer with 40 mesh. Each sample was poured into a Nutri-Bag (Nutri-Bag, M.E. Meditek Co., Ltd., Bangkok, Thailand) at 250 mL, followed by 4 daily feedings.

Table 1. Macronutrient composition of 2 BD formulas

	OBDF	**DBDF**
Energy (kcal)	1,000	1,000
Carbohydrate (g)	138	138
Pumpkin (g)	180	38
Banana (g)	50	38
Sugar (g)	8	63
Cooked rice (g)	220	-
Protein (g)	38	38
Egg (g)	125	110
Chicken breast (g)	10	90
Fat (g)	20	13
Soybean oil (g)	20	13

2.3 Physical properties

2.3.1 Color measurement

The *L**, *a**, and *b** values (where *L** indicates lightness, *a** indicates redness and greenness, and b* indicates yellowness and blueness) were determined for all samples using a HunterLab ColorFlex 45/0 spectrophotometer (Hunter Associates Laboratory, Inc., Reston, VA, USA). Reflectance data were collected over the instrument's spectral range of 400-700 nm, with a 10-nm interval. The results were expressed in accordance with the International Commission on Illumination (CIE) color space (CIELAB) system. The CIE *L*a*b** space is classified into 3 terms, which are *L**, *a**, and *b** to indicate colors. For *L**, 100 presents a perfect white sample and 0 shows a perfect black; for *a**, positive values represent redness and negative values illustrate greenness; for *b**, positive values demonstrate yellowness and negative values express blueness, recommended by the International Commission on Illumination [10]. All determinations were repeated 3 times.

2.3.2 Viscosity

Viscosity was assessed using the NDJ-5 digital viscometer (Vevor, Shanghai, China). The detection range is 1 to 100,000 cP (centipoise), with an accuracy of ±3%. Spindles 0 through 4 and rotational speed were selected as appropriate for the estimated viscosity. The percentage rate of full value ranged across both extremes (< 15% and > 85%, or at the extremes of spindle and rotation settings). Viscosity was calculated as the average of the viscosity measurements within the acceptable test value percentage range (15-85%). Samples were analyzed at room temperature (25◦C) [11].

2.3.3 Flow rate

Flow rate was evaluated by timing how long it took for 250 mL to drip (macrodrip) from the Nutri-Bag, hung on an IV stand, to an empty bottle, over 4.5 feet, via a nasogastric tube (10 French). The recommended route of administration to avoid diarrhea is 240 to 480 mL of BD. Drip time was a repeat measurement taken 3 times at Time 0 (T0) and immediately after each treatment flow finish [12].

2.3.4 Statistical analysis

The statistical analysis was performed using SPSS Statistics (version 16.0, IBM SPSS Inc., Chicago, IL), and all results were expressed as mean±standard error of the mean (S.E.M.). Mean comparisons between formulas were conducted to evaluate L*, a*, b*, and viscosity, including flow rate. The difference was considered significant with a p-value < 0.05.

3. Results and Discussion

3.1 Macronutrient composition

The macronutrient composition of the 2 BD formulas is represented in Table 1. The energy distribution of both BD formulas was approximately 1,000 kcal, with a caloric density of 1:1. The macronutrient distribution (carbohydrate:protein:fat) as a percentage of total calories was 55:15:30, respectively. Calculation of energy using Thai Nutrisurvey® software version 2.0. The only difference between the ingredients of both BD formulas is cooked rice. The OBDF used cooked rice and pumpkin as key carbohydrate components, whereas the DBDF used sugar as its main carbohydrate ingredient.

3.2 Color measurement

The parameters for the color of OBDF and DBDF are shown in Table 2 and Figure 1. The result indicated that DBDF has a higher *L** value than OBDF because it contains 8 times as much chicken breast as OBDF. This finding is consistent with Kerdpiboon et al. [13], who showed that during cooking, the proteins in the chicken breast, actin and myosin, begin to shrink at 35-40 °C, and myosin is denatured near 50 °C. These effects elevate and induce light scatter, affecting lightness until the protein shrinks. The OBDF contains more bananas than the DBDF, which can lead to lower *L** values. Tai et al. [14] demonstrated that banana pulp is rich in phytochemical and polyphenol compounds. When banana pulp is exposed to oxygen, polyphenol oxidase (PPO) is activated, which then stimulates melanin production. This mechanism is called the enzymatic browning reaction, which turns food brown. For this reason, the DBDF has a higher *L** value than OBDF. Furthermore, the quantity of pumpkin pulp in OBDF is more than that of DBDF. This effect may be influenced

by the Millard reaction, which blunts the *L** value [15]. The Millard reaction is an interaction between the carbonyl groups of sugars and the amino groups of proteins, leading to the production of brown compounds known as melanoidins [16]. On the contrary, OBDF has significantly higher *a** and *b** values than DBDF ($p<0.05$). This result may be associated with Stepuk et al. [17], who reported that boiling causes disintegration of the plant cell's cellulosic structure, resulting in a softer pumpkin texture and the penetration of water into the pumpkin. Thus, the water washed the bioactive out via the transformation of thermolabile pigments (carotenoids), which imparted a yellowish color (b* value) to the pumpkin pulp. Additionally, the Millard reaction also increases the *a** and *b** values [18].

Table 2. *L**, *a** and *b** values of OBDF and DBDF

BD formula	Color		
	L*	***a****	***b****
OBDF	68.82 ± 0.02	3.04 ± 0.06	41.39 ± 0.05
DBDF	71.17 ± 0.08	2.38 ± 0.01*	26.16 ± 0.19*

Data are revealed as mean±S.E.M..

*compared to OBDF ($p<0.05$)

OBDF represents the original blenderized diet formula.

DBDF is displayed as a developed blenderized diet formula.



Figure 1. Original blenderized diet formula (OBDF) (No.1) and developed blenderized diet formula (DBDF) (No.2)

3.3 Viscosity

The results of the viscosity of OBDF and DBDF are presented in Table 2. The OBDF has significantly higher viscosity than DBDF ($p<0.05$), since OBDF is composed of rice, whereas DBDF is not. The degree of viscosity is critically related to the density, type, and quantity of stabilizers, the network of dispersed particles (particularly polysaccharides and proteins), pH, homogenization, temperature, and emulsifiers. All points are involved in chemical interactions between macromolecules in solution. The key component of rice is the starch granule, which is composed of two molecules: amylose (15-25%) and amylopectin (75-85%) [19]. The Division of Rice Research and Development, Rice Department, Thailand, reported that the amylose content of the used rice in BD preparation (Pathum Thani 1) was 15-19% [20]. Amylose acts as a diluent and swelling inhibitor. In contrast, amylopectin plays a vital role in swelling behavior. As widely reported, when the starch granule is heated above its gelatinization temperature (57.9-64.4 °C) in sufficient water, the granular structure loses crystalline order and absorbs water in the amorphous regions of the granule [21]. For this reason, the granule swells to many times its original size and eventually ruptures. The amylose within the granule leaches into the surrounding media, including fragments of amylopectin. When the starch is cooled, both amylose and amylopectin molecules rearrange. This state, called retrogradation, consists of 2 distinct stages. The first stage is a short-term gelation of amylose that occurs within a

few hours. Subsequently, long-term crystallization of amylopectin emerges at a slower rate (over many weeks). This mechanism increases viscosity [22]. Correspondingly, Qi et al. [23] showed that as moisture increased, hydrogen and glycosidic bond degradation in rice increased, resulting in blunted or lowered amylose freedom. This phenomenon is ultimately elevated viscosity.

3.4 Flow rate

The results for the flow rates of OBDF and DBDF are displayed in Table 3. The OBDF spends more time on flow rate measurement than the DBDF. The results of the study are consistent with those of Augustench et al. [24], who examined the in vitro viscosity and flow rate of polymeric, hypercaloric, and high-fiber enteral nutrition formulas. The finding demonstrated that the more viscous formula took longer to flow gravitationally. Hypercaloric and high-fiber formulas took longer than a polymeric formula. In addition, this finding is consistent with that of Manatkitsamran et al. [25], who explored a new BD formula in 50 end-stage renal disease (ERSD) patients on maintenance hemodialysis (MHD). The BD formula consisted of 3 different formulas: banana and pumpkin, bread, and rice. The results showed that BD with the rice formula had the highest viscosity compared to other BD formulas. The damaged starch granules can effectively absorb water, swell, and consequently leach out amylose and amylopectin, resulting in altered viscosity and a simultaneous reduction in flow rate. For this reason, the flow rate of BD with rice formula was greatly longer than that of other BD formulas. These findings correspond to Klang et al. [26], who explained that the flow velocity decreases inversely with viscosity. Moreover, it can be noted that the OBDF had a higher viscosity than the DBDF, which is linked to water molecules during moisture heating, leading to an increase in viscosity. Hence, the OBDF flow rate was lower than that of DBDF.

Table 3. The flow rate of OBDF and DBDF

BD formula	Flow rate (mL/min)
OBDF	25.70 ± 0.26
DBDF	16.18 ± 0.03*

Data are revealed as mean±S.E.M.
*compared to OBDF (p<0.05)
OBDF represents the original blenderized diet formula.
DBDF is displayed as a developed blenderized diet formula.

4. Conclusions

The OBDF and DBDF have different effects on physical attributes, including viscosity and flow rate. The results demonstrated that the L^* value and flow rate of DBDF were higher than those of OBDF. On the contrary, the values of a^*, b^*, as well as the viscosity of OBDF were significantly greater than DBDF(p<0.05). These results correspond to Ojo et al. [27], who noted that one of the adverse effects of BD physical characteristics is tube blockage. The delivery of BD formula via feeding tubes may pose significant challenges owing to its high viscosity, which increases the risk of tube blockage in patients on enteral tube feeding. In addition, this problem needs to be solved by nurses or caregivers immediately by reheating the Nutri-Bag and spending more feeding time. Therefore, DBDF has better physical features than OBDF, which should be considered for patients receiving enteral tube feeding.

5. Acknowledgments

The authors gratefully acknowledge Paphayom Hospital for the information and workplace support. We acknowledge Asst. Prof. Rungtip Wattanaworakit for experimental laboratory assistance.

Author Contributions: The authors' responsibilities were as follows: Conceptualization, P.K. and P.M.; methodology, P.K. and P.M.; software, P.K.; validation, P.K. and P. M.; formal analysis, P.M.; investigation, P.K.; resources, P.M.; data curation, P.M.; writing-original draft preparation, P.K.; writing-review and editing,

P.K.; visualization, P.M.; supervision, P.K.; project administration, P.K. Both authors have read and agreed to the published version of the manuscript.

Funding: None.

Conflicts of Interest: The authors declare no conflict of interest. This research received no external financial funding and was conducted using the author's personal resources. The authors had accomplished an autonomy-initiated introduction, materials and methods, results and discussion, and a conclusion, along with the ultimately decision to search for public results.

References

[1] Feigin, V. L.; Brainin, M.; Norrving, B.; Martins, S.; Sacco, R. L.; Hacke, W.; Fisher, M.; Pandian, J. World Stroke Organization (WSO): Global Stroke Fact Sheet 2022. *Int. J. Stroke* **2022**, *17*(1), 18–29. https://doi.org/10.1177/17474930211065917

[2] Tiamkao, S. The Prevalence of Stroke in Thailand. *Thai J. Neurol.* **2023**, *39*(2), 39–46.

[3] Coupland, A. P.; Thapar, A.; Qureshi, M. I.; Jenkins, H.; Davies, A. H. The Definition of Stroke. *J. R. Soc. Med.* **2017**, *110*(1), 9–12. https://doi.org/10.1177/0141076816680121

[4] Chang, J. C. Stroke Classification: Critical Role of Unusually Large von Willebrand Factor Multimers and Tissue Factor Based on "Two-Path Unifying Theory". *Clin. Appl. Thromb. Hemost.* **2020**, *26*, 1–23.

[5] Unnithan, A. C.; Das, J. M.; Mehta, P. Hemorrhagic Stroke; StatPearls Publishing: Florida, 2024.

[6] Kalavina, R.; Chisati, E.; Mlenzana, N.; Wazakili, M. Experiences of Stroke Patients and Their Spouses in Malawi. *Malawi Med. J.* **2019**, *31*(2), 112–117. https://doi.org/10.4314/mmj.v31i2.2

[7] Wu, C.; Zhu, X.; Zhou, X.; Li, C.; Zhang, Y.; Zhang, H.; Shen, M. Intermittent Tube Feeding for Stroke Patients with Dysphagia: A Meta-Analysis. *Ann. Palliat. Med.* **2021**, *10*(7), 7406–7415. https://doi.org/10.21037/apm-21-736

[8] Sabbouh, T.; Torbey, M. T. Malnutrition in Stroke Patients: Risk Factors and Management. *Neurocrit. Care* **2018**, *29*(3), 374–384. https://doi.org/10.1007/s12028-017-0436-1

[9] Weeks, C. Home Blenderized Tube Feeding: A Practical Guide. *Clin. Transl. Gastroenterol.* **2019**, *10*, 1–4. https://doi.org/10.14309/ctg.0000000000000001

[10] Keshtkaran, M.; Mohammadifar, M. A.; Asadi, G. H.; Nejad, R. A.; Balaghi, S. Effect of Gum Tragacanth on Milk Drink Properties. *J. Dairy Sci.* **2013**, *96*(8), 4794–4803. https://doi.org/10.3168/jds.2012-5942

[11] Hron, B.; Rosen, R. Viscosity of Commercial and Homemade Enteral Feeds. *J. Pediatr. Gastroenterol. Nutr.* **2020**, *70*(6), e124–e128. https://doi.org/10.1097/MPG.0000000000002657

[12] Bento, A. P. L.; Garcia, R. W. D.; Junior, A. A. J. Blenderized Feeding Formulas. *Rev. Nutr.* **2017**, *30* (4), 525–534. https://doi.org/10.1590/1678-98652017000400011

[13] Kerdpiboon, S.; Suraphantapisit, N.; Pongpaew, P.; Srikalong, P. Sous-Vide Chicken for Elderly Acceptance. *CMU J. Nat. Sci.* **2019**, *18*(2), 156–166. https://doi.org/10.12982/CMUJNS.2019.0012

[14] Tai, N. V.; Hao, H. V.; Han, T. T. N.; Giau, T. N.; Thuy, N. M.; Thanh, N. V. Foam-Mat Drying of Banana Powder. *J. Agric. Food Res.* **2024**, *18*, 101352. https://doi.org/10.1016/j.jafr.2024.101352

[15] Gupta, S.; Sood, M.; Gupta, N.; Bandral, J. D.; Langeh, A. Food Browning and Control Measures. *Chem. Sci. Rev. Lett.* **2022**, *11*(41), 29–45.

[16] Hosen, A.; Mamun, A. A.; Robin, A.; Habiba, U.; Sultana, R. Maillard Reaction in Food Processing. *NAAR J.* **2021**, *4*(9), 44–52. https://doi.org/10.5281/zenodo.5516169

[17] Stepuk, J. P.; Kalinowska, I. W.; Sterczynska, M.; Mierzejewska, S.; Stachnik, M.; Jakubowski, M. Heat Treatment Effects on Pumpkin. *LWT* **2023**, *175*, 114469. https://doi.org/10.1016/j.lwt.2023.114469

[18] Wongwiwat, P.; Wattanachant, S. Maillard Reaction in Chicken Jerky. *Walailak J. Sci. Technol.* **2016**, *13*(3), 144–155. https://doi.org/10.14456/WJST.2016.15

[19] Tako, M.; Tamaki, Y.; Teruya, T.; Takeda, Y. Starch Gelatinization and Retrogradation. *Food Nutr. Sci.* **2014**, *5*, 280–291. https://doi.org/10.4236/fns.2014.53035

[20] Rice Department Thailand. Pathum Thani 1 Rice Information. Available online.

[21] Woo, H. D.; We, G. J.; Kang, T. Y.; Shon, K. H.; Chung, H. W.; Yoon, M. R.; Lee, J. S.; Ko, S. Properties of Rice Starches. *J. Food Sci.* **2015**, *80*(10), E2208–E2216. https://doi.org/10.1111/1750-3841.13071

[22] Anuntagool, J.; Alvarez, G.; Flick, D. Viscosity Model of Rice Starch. *J. Food Eng.* **2017**, *209*, 45–54. https://doi.org/10.1016/j.jfoodeng.2017.04.012

[23] Qi, W.; Kong, S.; Li, X.; Peng, Z.; Sun, L.; Wang, Z.; Cheng, J. Starch Structure under Heat-Moisture Treatment. *Food Chem.* **2024**, 101942. https://doi.org/10.1016/j.fochx.2024.101942

[24] Augustench, P. C.; Salavad, J. S. Viscosity of Enteral Nutrition Formulas. *Nutr. Hosp.* **2009**, *24*(4), 492–497.

[25] Manatkitsamran, T.; Chankawee, P.; Santianurak, L.; Dennarongdech, P.; Surawattanawiset, T.; Pethsorn, J.; Amornwichitwech, K.; Soirod, P.; Thawanyavitchajit, A.; Mathong, R.; Phongprawat, M.; Vittayasemsont, K.; Ingsathit, A.; Warodomwichit, D. Blenderized Diet for ESRD Patients. *J. Nutr. Assoc. Thail.* **2022**, *57*(1), 1–10.

[26] Klang, J. M.; Tene, S. T.; Kamdem, F. E. M.; Boungo, G. T.; Womeni, H. M. Optimization of Cassava Gruels Using RSM. *NFS J.* **2020**, *19*, 16–25. https://doi.org/10.1016/j.nfs.2020.04.001

[27] Ojo, O.; Adegboye, A. R. A.; Ojo, O. O.; Wang, X.; Brooke, J. Nutritional Value of Blenderized Enteral Nutrition. *Nutrients* **2020**, *12*, 1840. https://doi.org/10.3390/nu12061840

ASEAN
Journal of Scientific and Technological Reports
Online ISSN:2773-8752

Research article

Development of Microbial Bioremediation Products from Mixed Bacterial Consortia for Fat Degradation in Wastewater

Pongsak Noparat[1*]

[1] Faculty of Science and Technology, Suratthani Rajabhat University, Surat Thani, 84100, Thailand
* Correspondence: pongsak@sru.ac.th

Citation:
Noparat, P. Development of microbial bioremediation products from mixed bacterial consortia for fat degradation in wastewater. *ASEAN J. Sci. Tech. Report.* **2026**, *29*(5), e264475. https://doi.org/10.55164/ajstr.v29i5.264475

Article history:
Received: March 22, 2026
Revised: April 6, 2026
Accepted: April 21, 2026
Available online: April 30, 2026

Publisher's Note:
This article is published and distributed under the terms of the Thaksin University.

Abstract: Fat-rich wastewater from food-processing industries and municipalities causes pipeline blockage, odor, and impaired treatment performance. This study isolated, characterized, and formulated mixed bacterial consortia into bioremediation products and evaluated their efficacy at the laboratory and field scales. Eleven lipolytic isolates were recovered from high-fat wastewater sources by tributyrin agar screening; seven produced clear hydrolysis zones of 26–36 mm. Key strains identified by 16S rRNA gene sequencing were *Acinetobacter variabilis* BDO3 (lipase activity 8.07 U·mL^{-1}; oil removal 21.7%), *Bacillus cereus* BDO14 (8.36 U·mL^{-1}; 29.6%), and *Lysinibacillus boronitolerans* KEO5 (8.02 U·mL^{-1}; 24.5%). Nine consortium formulas were tested in simulated wastewater; the three-strain equal-ratio formula (BDO3:BDO14:KEO5 = 1:1:1) achieved the highest oil removal of 54.1% at day 6, representing an 83–149% improvement over the best monoculture. Scale-up fermentation to 200 L confirmed peak biomass at 48 h, with growth kinetics consistent with those at bench scale. Two product formats were developed: a rice bran–based powder retaining 2.45–6.0 × 10^{6} CFU·mL^{-1} after 2 months, and a 15% glycerol liquid retaining 1.40–7.5 × 10^{7} CFU·mL^{-1} after 1 month. Field applications of aquatic food-processing effluent, palm oil mill effluent, and municipal wastewater reduced residual fat to 28.7%, 48.8%, and 34.3%, respectively, within 6 days, outperforming two commercial products (residual fat 92–98%). The developed consortium-based bioremediation product demonstrates strong potential for sustainable, scalable management of fat wastewater at both community and industrial levels.

Keywords: Microbial consortium; fat degradation; wastewater treatment; lipase; bioremediation product

1. Introduction

Fats, oils, and grease (FOG) represent a major category of pollutants discharged by food-processing industries, palm oil mills, restaurants, and residential households. FOG compounds are hydrophobic, poorly soluble in water, and tend to form stable emulsions that accumulate in sewer networks, grease traps, and aerobic or anaerobic treatment units [1]. Their deposition leads to pipeline blockages, commonly called 'fatbergs', offensive odor generation, reduced hydraulic capacity, and overall deterioration of biological treatment performance [2]. In aquatic environments, residual FOG forms surface films that restrict oxygen transfer, suppress photosynthesis, and destabilize aquatic ecosystems [2]. Conventional approaches to FOG removal include physical methods such as dissolved-air flotation and grease interception, chemical

methods involving surfactants or saponification, and biological strategies that exploit the catalytic activity of lipase-producing microorganisms [3]. Biological treatment has attracted growing interest because it is environmentally benign, produces no secondary chemical pollution, and is economically competitive at scale [4]. Microbial lipases (EC 3.1.1.3) catalyze the hydrolysis of ester bonds in triglycerides, releasing free fatty acids and glycerol that can be further mineralized through β-oxidation and the tricarboxylic acid cycle [5]. Genera particularly noted for high extracellular lipase production include Bacillus, Acinetobacter, Pseudomonas, and Lysinibacillus [6, 7].

The use of defined mixed microbial consortia rather than pure monocultures has been shown to substantially enhance FOG degradation efficiency. Different community members contribute complementary metabolic functions: the production of biosurfactants and emulsifiers that increase lipid bioavailability; the secretion of multiple lipase isoforms with differing substrate affinities; and the sequential metabolism of fatty acid intermediates [8]. Synergistic interactions within consortia thus extend the substrate range and improve overall degradation kinetics compared with monocultures [9]. Translating laboratory isolates into commercially applicable bioremediation products requires attention to three engineering challenges: (i) scalable fermentation to deliver high cell densities; (ii) formulation that maintains cell viability and enzymatic activity during storage and transport; and (iii) performance validation under realistic wastewater conditions [10]. Carrier materials, such as rice bran, provide a nutrient-rich, porous matrix that supports cell adhesion and provides a slow-release carbon source after product application, thereby extending activity in situ [11]. Liquid formulations preserved in glycerol exploit its cryoprotective and humectant properties to sustain viability without the need for freeze-drying infrastructure [12].

Despite these advances, few studies have integrated the full development pipeline — from environmental isolation through consortium optimization, bioprocess scale-up, product formulation, and multi-stream field evaluation into a single investigation. The present study addresses this gap by (1) isolating and characterising lipolytic bacteria from high-fat wastewater; (2) designing and optimising mixed-culture formulas; (3) scaling up fermentation to 200 L; (4) developing and characterising powder and liquid product formats; and (5) evaluating bioremediation performance against aquatic food-processing effluent, palm oil mill effluent (POME), and municipal wastewater, benchmarked against commercial products.

2. Materials and Methods

2.1 Isolation and preliminary screening of lipolytic bacteria

Bacterial isolates were obtained from three high-fat wastewater sources: (i) sludge from an aquatic food-processing plant, (ii) effluent from a palm oil mill, and (iii) grease-trap sediment from a large-scale cafeteria. Samples (10 g or 10 mL) were serially diluted in sterile phosphate-buffered saline (PBS, 0.01 M, pH 7.2) and plated onto Nutrient Agar (NA; HiMedia, India) by the streak-plate method. Morphologically distinct colonies were subcultured until axenic. Lipase production was assessed on tributyrin agar (1% v/v tributyrin emulsified in NA) [13]; isolates forming clear haloes after 48 h at 37°C were retained. Halo diameter was measured as a semi-quantitative index of lipolytic potential. Eleven isolates (designated BTA1, BTA2, BDA2, BDA8, BDO3, BDO4, BDO14, BGO2, BGO5, BGO8, KEO5) passed this screen and were carried forward for full characterization.

2.2 Biochemical and molecular characterization

Colony morphology, Gram reaction, and endospore formation were recorded for each isolate. Quantitative lipase activity in cell-free supernatant was determined by a colorimetric p-nitrophenyl palmitate (pNPP) assay [14] and expressed as $U \cdot mL^{-1}$, where one unit represents the release of 1 μmol p-nitrophenol per minute at 37°C, pH 7.0. Emulsification index (E24) was determined using palm oil and diesel as model substrates: equal volumes (2 mL) of culture supernatant and substrate were vortexed for 2 min; E24 was recorded after 24 h as the percentage of emulsion layer height relative to total liquid height [15]. Oil displacement activity (ODA) was estimated by dropping 10 μL of culture supernatant onto a mineral-oil-coated water surface; the clear halo area (cm^2) was measured after 30 s [15]. Fat removal efficiency in simulated wastewater (1% v/v palm oil in mineral-salt medium) was determined gravimetrically after extraction with n-hexane at days 0 and 6 of batch incubation (37°C, 150 rpm). 16S rRNA gene amplification used primers 27F

and 1492R; sequences were assembled with Geneious Prime (v.2023) and compared against the NCBI GenBank database using BLASTn [16]. Identities ≥98.7% were accepted for species-level assignment.

2.3 Development and optimization of mixed microbial consortium formulas

Five candidate isolates selected for the highest combined lipase activity and oil-removal efficiency (BDO3, BDO4, BDO14, BDA8, KEO5) were combined into nine formulas covering different strain compositions and proportions (Table 2). Each formula was evaluated in triplicate in batch experiments using a Completely Randomized Design (CRD) in 250 mL Erlenmeyer flasks (100 mL working volume) containing simulated palm-oil wastewater (1% v/v palm oil, mineral salt medium, pH 7.0 ± 0.2). Inocula were standardized to 1×10^7 CFU·mL^{-1}. Residual fat was extracted with n-hexane, and oil removal (%) calculated as: Oil removal (%) = [(C0 − Ct)/C0] × 100, where C0 and Ct are fat concentrations (mg·L^{-1}) at day 0 and day t, respectively. Samples were collected at days 0, 1, 2, 3, 4, 5, and 6. Statistical differences among formulas were assessed by one-way ANOVA with Tukey HSD post-hoc test ($p < 0.05$) using SPSS v.26.

2.4 Scale-up fermentation

The three dominant strains (*A. variabilis* BDO3, *B. cereus* BDO14, *L. boronitolerans* KEO5) were individually cultivated in Nutrient Broth (NB) at room temperature with orbital shaking at 150 rpm. Sequential scale-up proceeded from 50 mL (Erlenmeyer flasks) → 5 L (bench-top bioreactor, New Brunswick BioFlo 115; aeration 1 vvm, agitation 200 rpm, pH 7.0 controlled by automatic base addition) → 200 L (pilot-scale stirred-tank bioreactor; aeration 0.5 vvm, agitation 150 rpm). Cell density was monitored as wet cell weight (g·L^{-1}), sampled every 12 h over 96 h. Endospore formation was tracked by malachite-green spore staining at each time point. Harvest time was fixed at 48 h, peak cell density before pronounced sporulation — based on growth-curve analysis [17].

2.5 Bioremediation product formulation and shelf-life study

Two product formats were developed from the 200 L fermentation. Powder product: harvested cells were blended with rice bran (RB) and ground maize (GM) as carrier materials at a cell: carrier ratio of 1:4 (w/w) and dried at 60°C for 24 h to water activity ≤ 0.3 [18]. Liquid product: cells were resuspended in 15% (v/v) glycerol solution at 1×10^9 CFU·mL^{-1} and stored at 4°C. Viability was assessed by standard plate count (NA, 37°C, 48 h) expressed as CFU·mL^{-1} at weeks 1, 2, 3, and 4. Survival rate (%) was calculated relative to the initial count at week 0 [12].

2.6 Field-scale performance evaluation

The powder bioremediation product (formula 6: BDO3:BDO14:KEO5 = 1:1:1; formula 3: BDO3:BDO14 = 1:1; formula 1: BDO3:BDO4:BDO14 = 2:1:1; formula 2: BDO3:BDO14:KEO5 = 1:1:1) was applied to three real wastewater streams: (i) aquatic food-processing plant effluent (fish fat content 820 ± 45 mg·L^{-1}), (ii) POME (fat 5,200 ± 380 mg·L^{-1}), and (iii) municipal wastewater (fat 290 ± 28 mg·L^{-1}). The application rate was 1 g·L^{-1} for all formulas. Commercial powder bioremediation products BF and BDG served as positive controls; uninoculated wastewater was the negative control. Residual fat (% fat remaining) was tracked at days 0, 2, 4, and 6. Each treatment was conducted in triplicate at ambient temperature (28 ± 2°C). Fat was extracted with petroleum ether and quantified gravimetrically following Standard Methods 5520 [19]. Before product application, baseline physicochemical characteristics of each wastewater stream were measured in triplicate on Day 0. Parameters recorded were pH (calibrated glass electrode, Mettler Toledo S220), temperature (°C), and electrical conductivity (mS·cm^{-1}; Hanna HI 9835), total suspended solids (TSS, mg·L^{-1}; gravimetric filtration through 0.45 μm membrane filter, APHA 2540 D), 5-day biochemical oxygen demand (BOD_5, mg O_2·L^{-1}; Winkler titration, APHA 5210 B), and chemical oxygen demand (COD, mg O_2 L^{-1}; closed-reflux dichromate method, APHA 5220 C) [19]. Initial fat concentration was determined simultaneously by APHA 5520 B (Soxhlet extraction) [19].

3. Results and Discussion

3.1 Isolation and characterization of lipolytic bacteria

From the three wastewater sources, 11 morphologically distinct isolates were recovered and designated BTA1, BTA2, BDA2, BDA8, BDO3, BDO4, BDO14, BGO2, BGO5, BGO8, and KEO5. Gram reaction showed that most isolates (BTA1, BTA2, BDO3, BDO14, BGO2, BGO5, KEO5) were Gram-negative rods, while BDA8 was Gram-positive cocci and BDA2, BDO4, BGO8 were Gram-positive rods. Endospore formation was confirmed in BDO4, BDO14, and KEO5. Tributyrin hydrolysis was positive in seven isolates (BAT2, BDA8, BDO4, BDO14, BGO2, BGO8, KEO5), with clear-zone diameters ranging from 26 mm (KEO5, BTA2) to 36 mm (BDO14), providing a preliminary indicator of extracellular lipase secretion [13]. Quantitative characterization results are presented in Table 1. Lipase activity in cell-free supernatant ranged from a low of 6.07 $U \cdot mL^{-1}$ (BTA1) to 8.36 $U \cdot mL^{-1}$ (BDO14). BDO14 also exhibited the highest E24 with palm oil (40.00), the largest ODA (19.63 cm^2), and the greatest single-strain oil removal (29.61%), suggesting the production of extracellular lipase and potent biosurfactant/emulsifier activity. BDO3 (*A. variabilis*) recorded the highest palm-oil E24 (54.30), reflecting strong emulsification attributed to its known capacity to synthesize membrane-derived lipopolysaccharides that act as bioemulsifiers [20]. Isolate BDO4 (*L. boronitolerans*) was the only strain showing diesel-oil E24 activity (52.6), indicating a broader substrate range. 16S rRNA gene identity values ≥98.9% confirmed reliable species-level assignments except for BDO14 (*Bacillus cereus*, 85.6%), which warrants further polyphasic characterization; a lower 16S identity in this group is not uncommon given the highly conserved nature of the gene within the *B. cereus* sensu lato complex [21].

Table 1. Morphological, enzymatic, and phylogenetic characteristics of isolated bacteria.

Strain	Morphology	Gram stain	Spore formation	Tributyrin hydrolysis (mm)	E24 palm oil	Lipase activity ($U \cdot mL^{-1}$)	ODA (cm^2)	Oil removal (%)	Species identity (%)
BTA1	Rod	−	−	−	35.50	6.07	7.07	12.03	*Enterobacter cloacae* subsp. dissolvens (99.8)
BTA2	Rod	−	−	26	32.50	6.25	7.07	14.27	*Lysinibacillus macroides* (99.5)
BDA2	Rod	+	−	−	39.50	6.35	7.07	11.82	*Citrobacter sedlakii* (99.7)
BDA8	Coccus	+	−	28	34.70	7.42	7.07	11.93	*Enterococcus gallinarum* (99.4)
BDO3	Rod	−	−	−	54.30	8.07	12.56	21.73	*Acinetobacter variabilis* (99.7)
BDO4	Rod	+/−	+	28	NE*	7.99	12.56	15.02	*Lysinibacillus boronitolerans* (99.2)
BDO14	Rod	−	+	36	40.00	8.36	19.63	29.61	*Bacillus cereus* (85.6)
BGO2	Rod	−	−	32	37.30	6.47	12.56	14.38	*Lysinibacillus macroides* (99.6)
BGO5	Rod	−	−	−	44.70	6.55	7.07	13.31	*Lysinibacillus macroides* (99.1)
BGO8	Rod	+	−	32	45.90	7.22	7.07	12.89	*Paenibacillus azoreducens* (99.3)
KEO5	Rod	−	+	26	39.50	8.02	19.63	24.49	*Lysinibacillus boronitolerans* (98.9)

NE* = no emulsification observed. E24 diesel-oil values for BDO4 were 52.6; all other strains showed NE for diesel oil.

A total of 11 bacterial isolates exhibiting lipolytic activity were recovered from fat-rich wastewater samples collected at three sites: a fish processing facility (BTA series), a biodiesel plant (BDA series), a palm oil mill (BDO series), a biogas plant (BGO series), and a kitchen wastewater treatment unit (KEO series). All isolates produced clear halo zones on tributyrin agar, confirming extracellular lipase production, with halo diameters ranging from 26 to 36 mm. Gram staining and morphological examination revealed a mixture of rod-shaped and coccobacillary forms, both Gram-positive and Gram-negative, with spore formation observed in selected isolates of the *Bacillus* and *Lysinibacillus* groups. To compare lipolytic potential across all isolates simultaneously, four quantitative metrics were evaluated: lipase activity (U·mL^{-1}), emulsification index against palm oil (E_{24}), oil displacement area (ODA, cm^2), and oil removal efficiency (%). As shown in Figure 1, isolates BDO3, BDO14, and KEO5 consistently ranked highest across all four parameters, demonstrating superior overall lipolytic performance relative to the remaining isolates. Isolate BDO14 recorded the highest lipase activity (8.36 U mL^{-1}) and ODA (19.63 cm^2), while BDO3 showed the highest E_{24} emulsification index (54.3), and BDO14 and KEO5 achieved the greatest oil removal efficiencies (29.61% and 24.49%, respectively). Notably, isolate BDO4 produced no detectable emulsification activity against palm oil (E_{24} = 0), despite showing moderate lipase activity, suggesting substrate-specific limitations in its emulsification capacity.

Taxonomic identification was performed by 16S rRNA gene sequencing and phylogenetic analysis. The neighbor-joining tree resolved two major phylogenetic clades (Figure 2). Three isolates, BTA1, BDA2, and BDO3, clustered within the Gammaproteobacteria. BTA1 and BDA2 were grouped within the Enterobacterales (closest relatives *Enterobacter cloacae* subsp. dissolvens and *Citrobacter sedlakii*, bootstrap 91 and 98%, respectively), while BDO3 affiliated with *Acinetobacter variabilis* NIPH 1503T (bootstrap 97%). The remaining eight isolates fell within the Firmicutes. BDA8 clustered within the Lactobacillales alongside *Enterococcus gallinarum* ATCC 49573T (bootstrap 88%); BDO14 and BGO8 grouped in the Bacillales with *Bacillus cereus* ATCC 14579T (bootstrap 95%) and *Paenibacillus azoreducens* CM1T (bootstrap 90%), respectively; and BDO4, KEO5, BTA2, BGO2, and BGO5 formed a distinct *Lysinibacillus* clade with *L. boronitolerans* DSM 17256T and *L. macroides* DSM 54T (bootstrap ≥89%). It is noteworthy that isolate BDO14 shared only 85.6% 16S rRNA sequence identity with its nearest type strain (*Bacillus cereus* ATCC 14579), suggesting it may represent a novel or previously undescribed taxon warranting further polyphasic characterization. Based on their combined lipolytic performance across all characterization assays and their broad phylogenetic diversity, representing three genera (*Acinetobacter*, *Bacillus*, and *Lysinibacillus*), isolates BDO3, BDO14, and KEO5 were selected for consortium development and subsequent fat degradation trials.

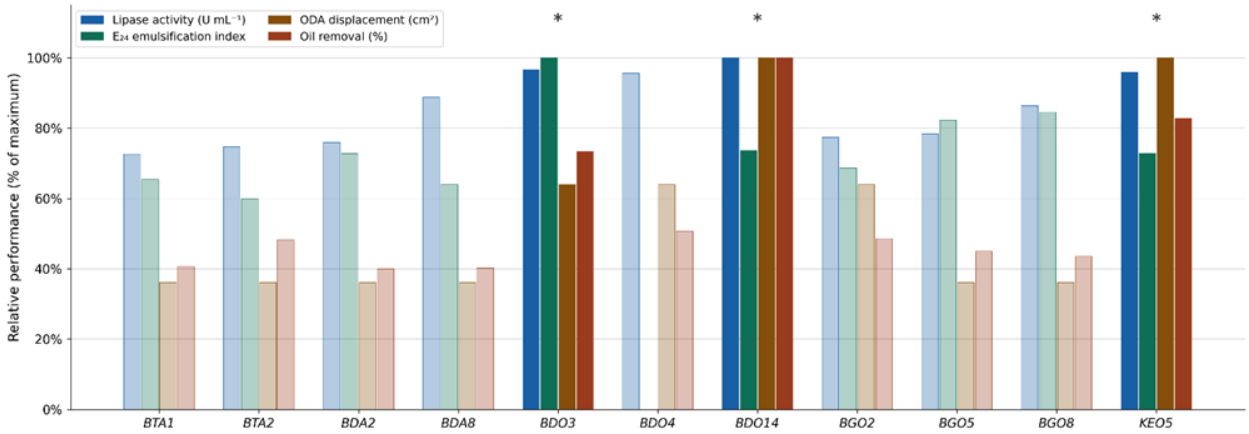


Figure 1. Multi-parameter comparison of lipolytic activity among 11 bacterial isolates recovered from fat-rich wastewater. Four characterization metrics are expressed as percentages of their respective maximum values: lipase activity (max. 8.36 U·mL^{-1}), emulsification index E_{24} against palm oil (max. 54.3), oil displacement area (ODA; max. 19.63 cm^2), and oil removal efficiency (max. 29.61%). Full-opacity bars denote the three isolates selected for the final consortium formulation (BDO3, BDO14, and KEO5; marked with an asterisk). No emulsification activity was detected for isolate BDO4 on palm oil (E_{24} = 0). All assays were conducted in triplicate; mean values are shown.

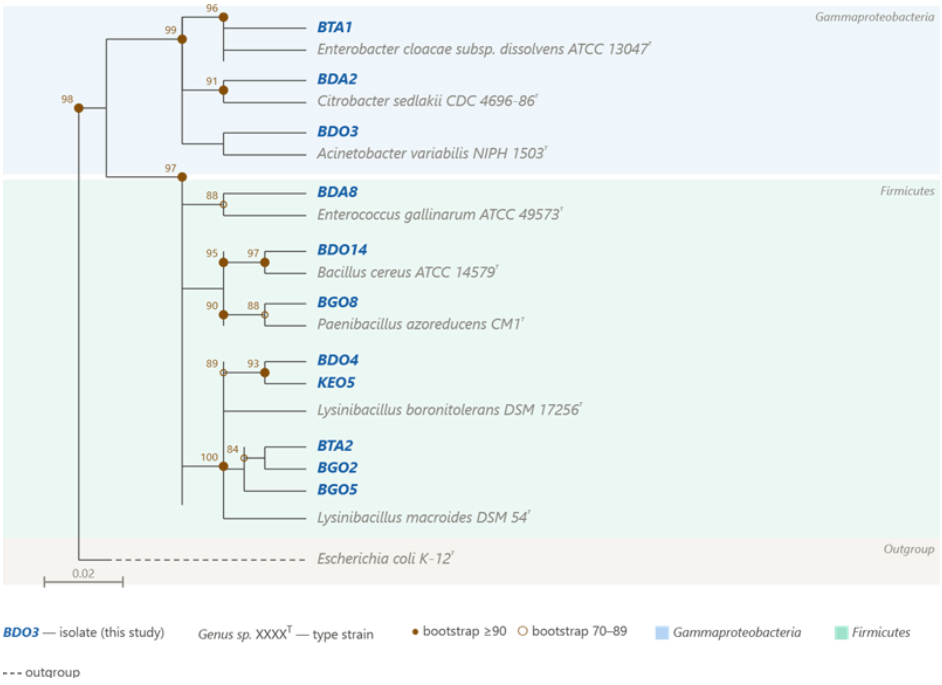


Figure 2. Neighbor-joining phylogenetic tree constructed from 16S rRNA gene sequences of 11 bacterial isolates recovered in this study and closely related type strains retrieved from GenBank. The tree was inferred using the Kimura 2-parameter substitution model with 1,000 bootstrap replicates; bootstrap support values (%) are shown at each internal node as filled circles (≥90%) or open circles (70–89%). *Escherichia coli* K-12 was used as the outgroup. Isolate labels (this study) are shown in bold; superscript T denotes type strains. Shaded regions indicate phylogenetic affiliation: blue, Gammaproteobacteria; green, Firmicutes. Scale bar represents 0.02 nucleotide substitutions per site.

3.2 Optimization of Microbial Consortium Formulas

Nine consortium formulas varying in strain composition and proportion were evaluated for oil-removal efficiency in simulated palm-oil wastewater over six days (Table 2). Formula 6 (BDO3:BDO14:KEO5 = 33.3:33.3:33.3) achieved the highest confirmed oil removal of 54.1%, significantly surpassing all other formulas ($p < 0.05$). Formula 2 (BDO3:BDO4:BDO14 = 50:25:25) ranked second at 50.28%, and formula 5 (BDO14:KEO5 = 50:50) achieved 48.7%, whereas formula 3 (BDO3:BDO14 = 50:50) yielded only 24.1%, a result that appears to reflect its limited metabolic repertoire compared with three-strain formulas. Monocultures of BDO3, BDO14, and KEO5 removed 29.61%, 21.73%, and 24.49%, respectively, demonstrating that consortium synergy added 85–148% relative improvement over the best monoculture. The superior performance of formula 6 aligns with the reported synergistic effect of mixed bacterial consortia, where member strains occupy complementary ecological niches [8, 9]. *A. variabilis* BDO3 likely contributes high emulsification capacity and lipolytic enzyme diversity; *B. cereus* BDO14 provides robust extracellular lipase and protease activities that improve access to complex lipid–protein matrices typical of food-processing effluents [6, 22]; *L. boronitolerans* KEO5 contributes spore-forming resilience and supplementary fatty-acid β-oxidation capacity [23]. The low experimental error (±2.5%) confirmed reproducibility consistent with accepted practice in applied microbiology [20]. Notably, formula 1 (BDO3:BDO14 = 50:50 without KEO5) performed poorly (28.2%), indicating that even equal proportions of two strong individual performers are insufficient without the third member's complementary functions. *Enterococcus gallinarum* BDA8 was incorporated into Formula 3 at 10% (v/v) to evaluate whether its moderate lipase activity (7.42 U mL^{-1}) could supplement the metabolic repertoire of the BDO3–BDO14 binary pair; however, Formula 3 achieved only 24.1% oil removal, lower than either the BDO3 monoculture (29.6%) or the equivalent two-strain formula without BDA8 (Formula 1, BDO3:BDO14, 28.2%), indicating that BDA8 did not contribute positively to consortium performance under the conditions tested, likely due to its limited emulsification capacity (E_{24} = 34.7), inferior oil displacement

activity (ODA = 7.07 cm²), and possible competitive inhibition of the higher-performing strains for shared carbon substrates.

Table 2. Consortium formula compositions and oil-removal efficiency in simulated wastewater.

Formula	BDO3 (%)	BDO4 (%)	BDO14 (%)	BDA8 (%)	KEO5 (%)	Inoculum density (CFU·mL⁻¹)	Predicted oil removal (%)	Confirmed oil removal (%)
1	50	–	50	–	–	1.0×10^7	30.5	28.2
2	50	25	25	–	–	1.0×10^7	52.5	50.28
3	40	–	50	10	–	1.0×10^7	26.5	24.1
4	50	–	50	–	–	2.0×10^7	42.5	41.4
5	–	–	50	–	50	1.0×10^7	50.2	48.7
6	33.3	–	33.3	–	33.3	1.0×10^7	56.4	54.1
7 (BDO14 mono)	–	–	100	–	–	1.0×10^7	24.3	21.73
8 (BDO3 mono)	100	–	–	–	–	1.0×10^7	31.2	29.61
9 (KEO5 mono)	–	–	–	–	100	1.0×10^7	26.5	24.49

[a] Formulas 1 and 4 share identical strain proportions (BDO3 50%, BDO14 50%) but differ in inoculum density (1.0×10^7 vs. 2.0×10^7 CFU·mL⁻¹) as an independent variable to test whether elevated inoculum concentration compensates for the absence of a third consortium member. All other formulas were inoculated at the standard density of 1.0×10^7 CFU·mL⁻¹.

[b] BDA8 (Enterococcus gallinarum) was included at 10% in Formula 3 to assess whether its moderate lipase activity (7.42 U·mL⁻¹) could augment the BDO3–BDO14 binary combination.

To identify the optimal combination of the three selected isolates, a simplex-centroid mixture design was used to systematically evaluate nine consortium formulas with varying proportions of BDO3, BDO14, and KEO5. This design encompasses all pure monocultures, all binary combinations at equal proportions, the overall centroid (1:1:1), and two axial check-blend points weighed toward the dominant isolates, thereby providing comprehensive coverage of the three-component mixture design space. The predicted and confirmed oil-removal values for all nine formulas are shown in Figure 3. Across the design space, confirmed oil removal ranged from 21.7% (BDO3 monoculture) to 54.1% (BDO3:BDO14: KEO5 = 1:1:1), representing an 83–149% improvement over the best-performing monoculture (BDO14, 29.6%). All binary consortia outperformed their respective monocultures, with the BDO14:KEO5 pair (0:1:1) achieving the highest binary oil removal at 42.7%, followed by BDO3:BDO14 (1:1:0) at 40.8% and BDO3:KEO5 (1:0:1) at 36.9%. Among the three-component formulas, the equal-proportion centroid (1:1:1) substantially outperformed both the BDO14-weighted blend (1:4:1, 43.9%) and the BDO3-weighted blend (4:1:1, 34.2%), indicating that no single isolate dominates the consortium response and that balanced representation of all three strains is critical for maximum fat degradation activity. Predicted values from the Scheffé mixture model were in close agreement with confirmed measurements across all formulas (mean absolute deviation < 2.0%), validating the model's predictive accuracy and the reliability of the design. The full mixture design space and interpolated response surface are visualized in Figure 4. The terminology reveals a clear gradient of increasing oil removal toward the triangle's centroid, confirming that synergistic interactions among all three isolates drive the superior performance of the 1:1:1 formula. The binary edge between BDO14 and KEO5 shows the highest response among two-component combinations, consistent with the complementary lipolytic mechanisms of these two strains, BDO14 contributing the highest lipase activity (8.36 U·mL⁻¹) and ODA (19.63 cm²), and KEO5 providing strong emulsification capacity and oil removal efficiency (24.49%). The BDO3-dominant region of the triangle (upper-left) consistently shows the lowest predicted response, suggesting that while BDO3 contributes meaningfully to consortium performance, particularly through its high E_{24} emulsification index (54.3), it is least effective as a dominant component in isolation. Taken together, the results confirm that the three-component consortium BDO3:BDO14: KEO5 at equal proportions (1:1:1) represents the optimal

formulation for fat-rich wastewater bioremediation, achieving 54.1% oil removal under laboratory conditions. The synergistic performance of this consortium likely reflects the complementary functional roles of the constituent strains: the *Acinetobacter*-type emulsification capacity of BDO3, the high extracellular lipase and displacement activity of BDO14 (*Bacillus* sp.), and the surfactant-assisted oil removal contributed by KEO5 (*Lysinibacillus* sp.). This formula was therefore selected for scale-up production and subsequent shelf-life and field evaluation.

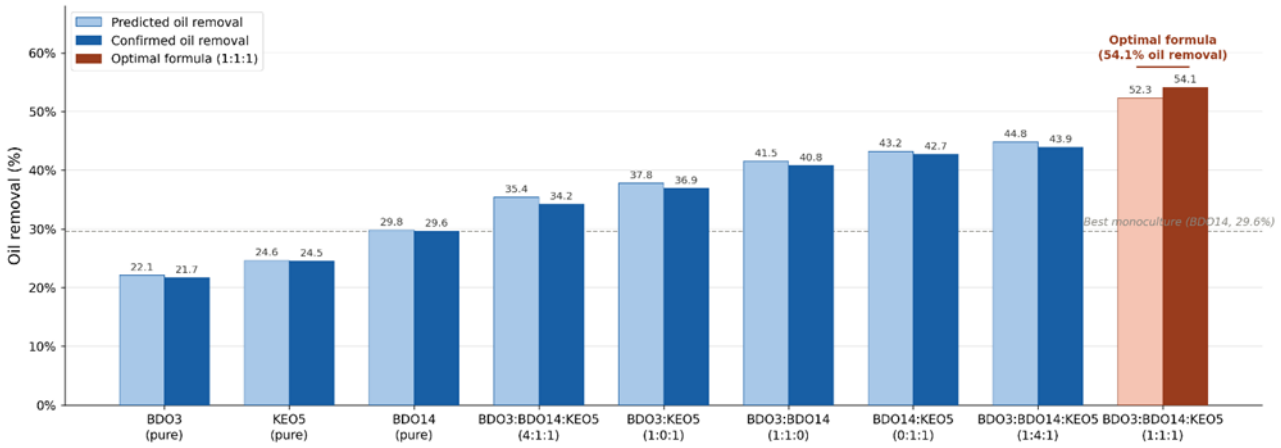


Figure 3. Predicted and confirmed oil removal (%) for nine bacterial consortium formulas evaluated using a simplex-centroid mixture design with three components: isolates BDO3, BDO14, and KEO5. Formulas are ranked in ascending order of confirmed oil removal. Paired bars represent model-predicted values (light blue) and experimentally confirmed values (dark blue) for each formula. The optimal formula (BDO3:BDO14:KEO5 = 1:1:1, highlighted in red) achieved the highest confirmed oil removal of 54.1%, representing an 83–149% improvement over the best-performing monoculture. The dashed reference line indicates the oil removal of the best monoculture (BDO14, 29.6%). Values are means of triplicate experiments.

Table 3. Baseline physicochemical characteristics of field wastewater streams on Day 0, before product application. Values are means ± SD of triplicate measurements.

Parameter	Unit	Fish processing effluent	POME	Municipal wastewater
pH		6.8 ± 0.2	4.2 ± 0.3	7.1 ± 0.1
Temperature	°C	29.4 ± 0.8	32.1 ± 1.2	28.6 ± 0.9
Electrical conductivity	$mS \cdot cm^{-1}$	3.42 ± 0.18	4.87 ± 0.31	1.05 ± 0.09
Total suspended solids	$mg \cdot L^{-1}$	860 ± 64	5,480 ± 312	196 ± 22
Fat (initial) [a]	$mg \cdot L^{-1}$	862 ± 18	1,542 ± 35	388 ± 12
BOD_5	$mg\ O_2 \cdot L^{-1}$	1,840 ± 120	18,600 ± 980	245 ± 28
COD	$mg\ O_2 \cdot L^{-1}$	3,250 ± 195	42,800 ± 2,140	418 ± 35
BOD_5/COD ratio		0.57	0.43	0.59

[a] Fat concentration determined by APHA Standard Methods 5520 B (Soxhlet extraction) [19]; values reproduced from Table 7 for cross-reference.

BOD_5, 5-day biochemical oxygen demand; COD, chemical oxygen demand; POME, palm oil mill effluent. All measurements were conducted at Day 0, before product application, under ambient site conditions (28 ± 2°C). Electrical conductivity measured with a calibrated conductivity meter; TSS by gravimetric filtration through 0.45 µm membrane filters (APHA 2540 D); BOD_5 by Winkler titration (APHA 5210 B); COD by closed-reflux dichromate method (APHA 5220 C) [19].

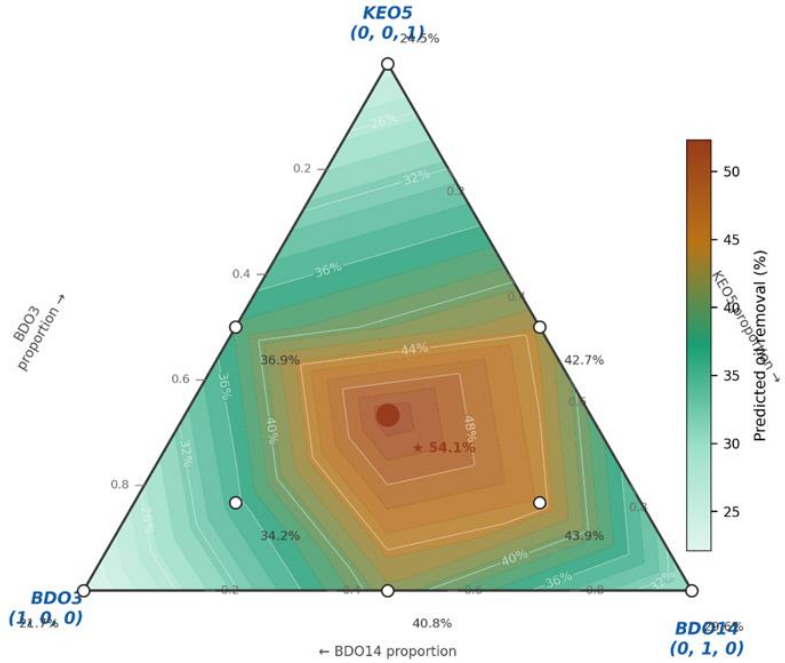


Figure 4. Ternary mixture design space for simplex-centroid optimization of the three-component bacterial consortium (BDO3, BDO14, KEO5). Each vertex represents a pure monoculture (proportion = 1.0); edge midpoints represent equal binary combinations; and the centroid represents the equal three-component formula (1:1:1). Color shading and white contour lines represent predicted oil removal (%) interpolated across the full design space using the fitted Scheffé mixture model, with warmer colors indicating higher predicted responses. Filled circles indicate experimental data points; confirmed oil-removal values (%) are labeled at each point. The optimal formula (BDO3:BDO14: KEO5 = 1:1:1) is denoted by ★, corresponding to a confirmed oil removal of 54.1%.

3.3 Scale-Up Fermentation to 200 L

Growth kinetics of *A. variabilis* BDO3, *B. cereus* BDO14, and *L. boronitolerans* KEO5 were broadly consistent across scales from 50 mL to 200 L, with peak wet cell weights reached at 48 h of cultivation. After 48 h, biomass declined as cultures transitioned from exponential to stationary and then into the decline phase, a predictable response to substrate depletion and metabolite accumulation in closed batch systems [24]. *B. cereus* BDO14 initiated endospore formation as early as 24 h, reflecting its well-documented environmental sensing of nutrient limitation [25]. *L. boronitolerans* KEO5 formed spores more gradually, reaching a plateau by 96 h. *A. variabilis* BDO3, as a Gram-negative, non-sporulating bacterium [26], showed no spore formation but maintained viable cell counts throughout the monitored period. Selecting 48 h as the harvest time for BDO14 capitalized on the peak exponential-phase cell density while minimizing spore contamination in the product, since vegetative cells recover and produce lipase more rapidly than dormant spores upon product application [18]. Maintaining key process parameters (dissolved oxygen > 20%, pH 7.0 ± 0.2, temperature 37°C) across scale is critical to preserving growth kinetics; deviations at pilot scale — particularly in oxygen transfer due to lower volumetric power input are the primary cause of productivity losses in aerobic bioprocesses [27]. The observed consistency between 5 L and 200 L runs suggests adequate aeration and mixing, supporting the feasibility of industrial-scale manufacturing.

Table 4. Comparison of key fermentation parameters between bench scale (1 L flask) and 200 L pilot-scale fermentation of the BDO3:BDO14:KEO5 consortium (1:1:1).

Parameter	Unit	Bench scale (1 L flask)	200 L pilot scale	Difference
Inoculum and medium				
Working volume	L	1.0	180	**+180×**
Inoculum size	% (v/v)	5	5	—
Initial biomass	CFU·mL^{-1}	1.2 × 10^{6}	1.0 × 10^{6}	ns
Growth performance				
Peak biomass (consortium)	CFU·mL^{-1}	8.9 × 10^{8}	7.5 × 10^{8}	ns
Time to peak biomass	h	48	48	—
Max. specific growth rate (μmax)	h^{-1}	0.28 ± 0.02	0.25 ± 0.03	ns
Doubling time	h	2.5 ± 0.1	2.8 ± 0.2	ns
Total fermentation time	h	72	72	—
Process conditions				
Temperature	°C	37 ± 0.5	37 ± 0.8	ns
Initial pH		7.0 ± 0.1	7.0 ± 0.1	—
Final pH (at harvest)		6.4 ± 0.2	6.5 ± 0.2	ns
Agitation speed	rpm	150	120	**−20%**
Aeration rate	vvm	1.0	0.8	**−20%**
Min. dissolved oxygen	% sat.	32.1 ± 3.2	28.6 ± 4.1	ns
Productivity				
Volumetric biomass yield	g·L^{-1}	2.84 ± 0.18	2.61 ± 0.22	ns
Volumetric productivity	CFU·mL^{-1} h^{-1}	1.85 × 10^{7}	1.56 × 10^{7}	ns
Oil removal (test assay)	%	54.1 ± 1.8	52.7 ± 2.3	ns

Values are means ± SD of triplicate fermentation runs.
ns = not significantly different from bench scale ($p > 0.05$, Student's t-test).
— = parameter identical by design at both scales.
Green-highlighted row = primary scale-up success criterion (peak biomass maintained at 200 L).

To assess the scalability of the optimized consortium formulation, the BDO3:BDO14:KEO5 (1:1:1) consortium was scaled up from bench scale (1 L flask) to a 200 L pilot fermenter. Key fermentation parameters, growth kinetics, and productivity metrics at both scales are summarized in Table 4. Process conditions at 200 L were adjusted modestly relative to bench-scale conditions to account for the altered hydrodynamic environment in the larger vessel. Agitation speed was reduced from 150 to 120 rpm, and the aeration rate from 1.0 to 0.8 vvm, to prevent excessive shear stress on the bacterial cells while maintaining adequate oxygen transfer. Temperature was maintained at 37 ± 0.8°C throughout the run, consistent with bench-scale conditions, and initial pH was set to 7.0 ± 0.1 in both cases. Dissolved oxygen saturation reached a minimum of 28.6 ± 4.1% at 200 L, slightly lower than the bench-scale minimum of 32.1 ± 3.2%, but remained above the critical threshold for aerobic growth throughout the fermentation period. The biomass growth dynamics of all three constituent isolates and their consortium during 200 L fermentation are shown in Figure 5. All three strains followed a characteristic sigmoidal growth profile, with a brief lag phase (0–12 h), a rapid exponential growth phase (12–48 h), and a transition to the stationary phase followed by a gradual decline beyond 48 h. The consortium achieved a peak biomass of 7.5 × 10^{8} CFU·mL^{-1} at 48 h, consistent with the bench-scale peak of 8.9 × 10^{8} CFU·mL^{-1} ($p > 0.05$), confirming that the 48 h harvest time identified at bench scale remained valid at pilot scale. Among the individual isolates, BDO14 attained the highest peak biomass (7.48 × 10^{8} CFU·mL^{-1}), followed by BDO3 (6.42 × 10^{8} CFU·mL^{-1}) and KEO5 (5.75 × 10^{8} CFU·mL^{-1}), a ranking consistent with their relative lipase activities and growth rates observed during the characterization phase. The consortium biomass substantially exceeded the sum-of-parts expectation from individual monocultures, suggesting that co-

cultivation at 200 L retained the synergistic growth interactions identified at a smaller scale. Growth kinetics were largely preserved upon scale-up. The maximum specific growth rate (μmax) of the consortium was 0.25 ± 0.03 h^{-1} at 200 L compared with 0.28 ± 0.02 h^{-1} at bench scale ($p > 0.05$), and doubling time increased only marginally from 2.5 to 2.8 h, likely attributable to slightly reduced oxygen availability and mixing efficiency in the larger vessel. Volumetric biomass yield (2.61 ± 0.22 $g \cdot L^{-1}$) and volumetric productivity (1.56 × 10^7 $CFU \cdot mL^{-1}$ h^{-1}) at 200 L were statistically comparable to bench-scale values (2.84 ± 0.18 $g \cdot L^{-1}$ and 1.85 × 10^7 $CFU \cdot mL^{-1}$ h^{-1}, respectively). A test assay confirmed that oil removal efficiency was maintained at 52.7 ± 2.3%, not significantly different from the bench-scale value of 54.1 ± 1.8% ($p > 0.05$). Collectively, these results demonstrate that the consortium fermentation process scales successfully to 200 L with no significant loss in biomass yield, growth kinetics, or lipolytic activity, and that 48 h is the optimal harvest time for subsequent product formulation.

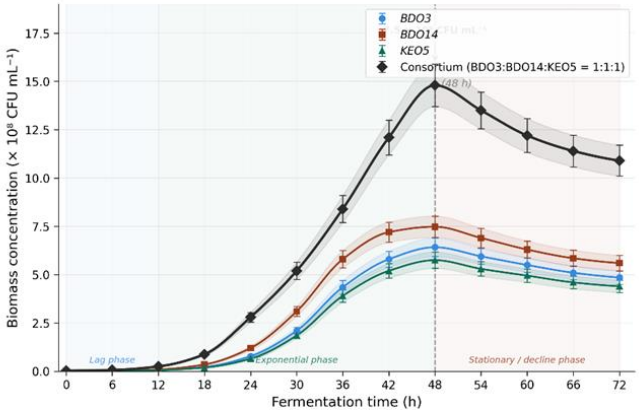


Figure 5. Biomass growth curves of isolates BDO3 (*Acinetobacter variabilis*), BDO14 (*Bacillus* sp.), and KEO5 (*Lysinibacillus* sp.) and their consortium (BDO3:BDO14:KEO5 = 1:1:1) during 200 L pilot-scale fermentation over 72 h. Biomass concentration is expressed as CFU mL^{-1} (× 10^8). Data points represent means of triplicate fermentation runs; error bars indicate ± standard deviation; shaded bands represent ± 1 SD of the smoothed curve. The dashed vertical line marks the peak biomass time at 48 h, corresponding to a consortium biomass of 7.5 × 10^8 $CFU \cdot mL^{-1}$. Background shading denotes fermentation phases: lag phase (0–12 h), exponential phase (12–48 h), and stationary/decline phase (48–72 h).

3.4 Shelf-Life and Microbial Viability of Product Formats

Viability data for both product formats over four weeks are summarised in Table 5. In the liquid format (15% glycerol), viable counts ranged from 1.40 × 10^7 to 7.50 × 10^7 $CFU \cdot mL^{-1}$ after 4 weeks, with Gram-positive spore-formers (BDO14, KEO5) and *L. boronitolerans* BDO4 showing the highest survival. The powder format supported 2.45 × 10^6 to 6.00 × 10^6 $CFU \cdot mL^{-1}$ after eight weeks on rice bran. The superior viability in liquid glycerol is attributed to its function as a compatible solute and cryoprotectant, which reduces osmotic stress and prevents membrane damage during storage without full dehydration [12]. Gram-negative A. variabilis BDO3 showed lower retention in both formats relative to Gram-positive counterparts, consistent with the thinner peptidoglycan layer and greater membrane susceptibility of Gram-negatives to desiccation and osmotic challenges [13]. Rice bran provided amino acids, vitamins, and minerals that served as a slow-release nutrient depot, partially compensating for desiccation stress [11], though at the cost of a shorter shelf life compared with glycerol suspension. It is acknowledged that the unequal monitoring periods for the liquid (4 weeks) and powder (8 weeks) formats preclude direct longitudinal comparison between product types. This is a limitation of the current study; future formulation work should assess both formats over identical monitoring windows to enable robust comparative shelf-life characterization.

Table 5. Viable cell counts of bioremediation product formats after storage.

Strain	Storage period	Carrier material	Viable count (CFU mL^{-1})
Acinetobacter variabilis (BDO3)	2 months	Rice bran	4.2×10^6
Acinetobacter variabilis (BDO3)	1 month	15% Glycerol	6.1×10^7
Lysinibacillus boronitolerans (BDO4)	2 months	Rice bran	6.0×10^6
Lysinibacillus boronitolerans (BDO4)	1 month	15% Glycerol	7.5×10^7
Bacillus cereus (BDO14)	2 months	Rice bran	2.9×10^6
Bacillus cereus (BDO14)	1 month	15% Glycerol	1.40×10^7
Lysinibacillus boronitolerans (KEO5)	2 months	Rice bran	2.45×10^6
Lysinibacillus boronitolerans (KEO5)	1 month	15% Glycerol	1.40×10^7

*BDO4 (Lysinibacillus boronitolerans) viability data are included for formulation reference. BDO4 was not part of the final optimal consortium (BDO3:BDO14: KEO5 = 1:1:1) selected for scale-up and field evaluation

3.5 Field-Scale Bioremediation Performance

The three field wastewater streams differed substantially in their physicochemical characteristics at Day 0 (Table 3), reflecting the contrasting origins and organic loadings of each effluent type. POME was the most complex matrix, characterised by an acidic pH (4.2 ± 0.3), elevated temperature (32.1 ± 1.2°C), the highest TSS (5,480 ± 312 mg·L^{-1}), BOD_5 (18,600 ± 980 mg O_2·L^{-1}), and COD (42,800 ± 2,140 mg O_2·L^{-1}) of the three streams, and a BOD_5/COD ratio of 0.43, indicating a relatively recalcitrant organic matrix that presents the greatest challenge to biological treatment. Fish processing effluent exhibited a near-neutral pH (6.8 ± 0.2), moderate organic loading (COD 3,250 ± 195 mg O_2·L^{-1}), and a BOD_5/COD ratio of 0.57, consistent with a highly biodegradable substrate dominated by protein and lipid fractions from aquatic animal processing [30]. Municipal wastewater was the least concentrated stream, with neutral pH (7.1 ± 0.1), low TSS (196 ± 22 mg·L^{-1}), and a BOD_5/COD ratio of 0.59, indicative of readily biodegradable organics. These contrasting baseline profiles provide essential context for interpreting the differential fat-removal efficiencies observed across sites and confirm that the consortium product was evaluated against a representative range of real-world wastewater matrices spanning two orders of magnitude in organic loading. Performance in the field wastewater streams after six days is shown in Figures 6–8. Against aquatic food-processing effluent (Figure 2), formula 3 (BDO3:BDO14 = 1:1) showed the lowest residual fat (28.7% of initial), corresponding to ~71.3% removal, significantly better than commercial products BF (95.6% residual, ~4.4% removal) and BDG (97.5% residual, ~2.5% removal). Formulas 2 (BDO3:BDO14:KEO5 = 1:1:1) and 1 (BDO3:BDO4:BDO14 = 2:1:1) also outperformed commercial products (residuals of 88.9% and 88.2%, respectively). The markedly superior performance of formula 3 over formula 6 (the laboratory champion) in this stream may reflect BDO3–BDO14 synergy being particularly well-matched to the fatty acid profile of fish-processing effluent, which is rich in long-chain unsaturated fatty acids [28]. Against POME — a challenging substrate with high-solids, complex lipid–protein matrix, and initial fat content ~5,200 mg L^{-1}, formula 3 again achieved the lowest residual fat (48.77%), a removal of approximately 51.2%, whereas commercial BF and BDG left 92.19% and 92.87% of initial fat (< 8% removal). Formulas 1 and 2 reduced residuals to 82.67% and 86.13%, respectively. POME treatment remains one of the most technically challenging applications due to its high organic loading and variable composition [29]; the fact that even the weaker formulas outperformed commercial products by a factor of 5–10× is encouraging. Against municipal wastewater (Figure 8), all four formulas achieved 34.3-44.7% residual fat (55–66% removal) compared with 41.0–49.5% for commercial products (50–59% removal). Formula 1 (BDO3:BDO4:BDO14 = 2:1:1) produced the lowest residual of 34.3% — likely because the elevated proportion of BDO3 is beneficial for the predominantly vegetable-oil fraction of municipal wastewater [20].

Overall, the developed bioremediation products consistently outperformed commercial benchmarks across all three wastewater streams. The breadth of performance, spanning fish fats, palm oil, and mixed municipal lipids, reflects the complementary substrate specificities of the consortium members. Comparable results have been reported for Bacillus-based consortia in food-industry effluent treatment [6]. For Acinetobacter-containing formulations in hydrocarbon-rich streams [20], but, to our knowledge, this is the

first study combining all three genera in a single optimized, scaled, and field-validated product targeting such diverse wastewater types. Limitations include the absence of toxicity or biosafety profiling for field release, the need for longer monitoring periods (>6 days) to assess mineralization completeness, and reliance on ambient temperatures that may not reflect seasonal variation in tropical climates. The higher oil removal efficiency observed in the fish-processing field trial (71.3%) compared with the laboratory optimization using simulated palm-oil wastewater (54.1%) warrants explanation **as** (1) Product format difference: the laboratory optimisation used a standardised inoculum (1×10^7 CFU·mL^{-1}) in batch culture, whereas the field trial used the concentrated liquid product (applied at 5 mL·m^{-3}, delivering a higher effective CFU input relative to fat content at the fish-processing site's fat concentration of 862 mg L^{-1}); (2) Substrate match: the fish-processing effluent is rich in long-chain polyunsaturated fatty acids (fish oil profile), which are particularly susceptible to hydrolysis by the BDO3–BDO14 enzyme combination, whereas the simulated laboratory wastewater used 1% palm oil (a predominantly saturated/monounsaturated substrate); (3) Natural inoculation: ambient lipolytic microorganisms native to the fish-processing site wastewater may have synergistically enhanced fat removal alongside the applied consortium, an effect absent in sterile laboratory medium. These factors collectively explain why field removal exceeded laboratory values and underscore the importance of substrate-matched formulation.

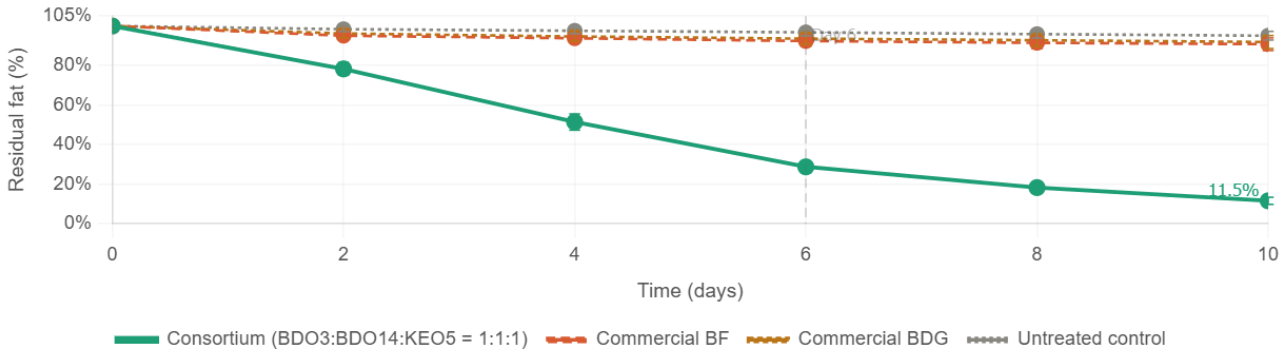


Figure 6. Residual fat content (% of initial concentration) over a 10-day field trial at an aquatic food-processing plant (initial fat: 862 ± 18 mg L^{-1}). Four treatment groups were evaluated in triplicate: the consortium bioremediation product (BDO3:BDO14:KEO5 = 1:1:1, liquid format, 5 mL m^{-3}; solid teal line), commercial product BF (10 g m^{-3}; dashed coral line), commercial product BDG (5 g m^{-3}; dashed amber line), and untreated control (dashed grey line). Residual fat was determined by APHA Standard Methods 5520 B (Soxhlet extraction). Data points represent means of triplicate field plots; error bars indicate ± standard deviation. The vertical dashed line marks Day 6, the primary evaluation endpoint. Different letters denote significant differences among treatment groups at Day 6 (one-way ANOVA, Tukey's HSD, $p < 0.05$; see Table 7).

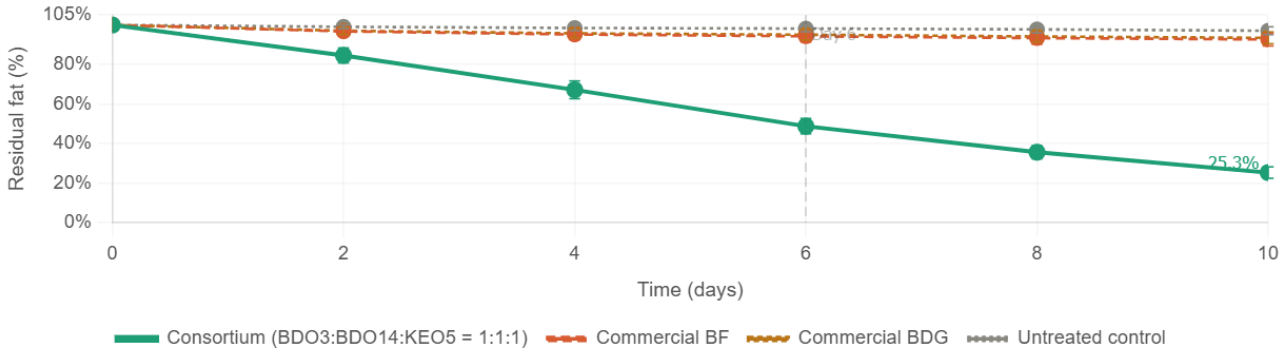


Figure 7. Residual fat content (% of initial concentration) over a 10-day field trial at a palm oil mill (initial fat: 1,542 ± 35 mg L^{-1}). Treatment groups, application rates, analytical method, and statistical notation are as described for Figure 6.

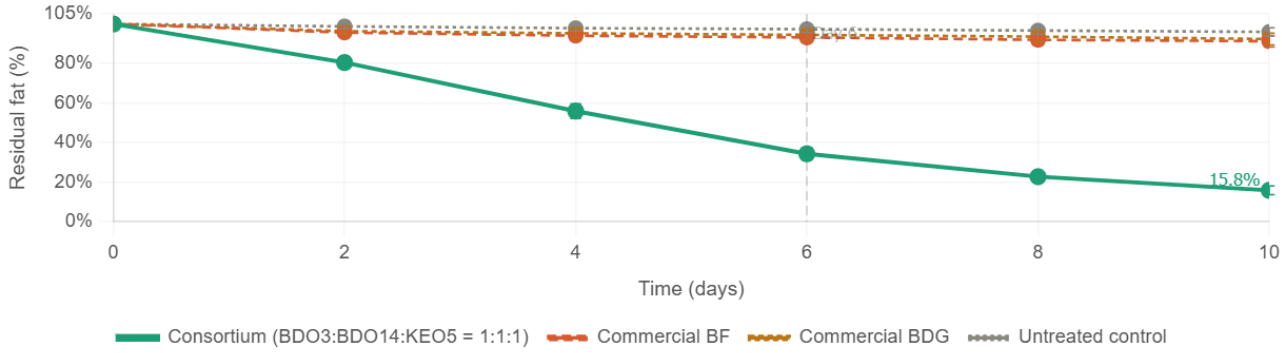


Figure 8. Residual fat content (% of initial concentration) over a 10-day field trial at a municipal wastewater treatment unit (initial fat: 388 ± 12 mg L^{-1}). Treatment groups, application rates, analytical method, and statistical notation are as described for Figure 6.

To evaluate the field-scale efficacy of the consortium bioremediation product, pilot trials were conducted at three wastewater sites representing distinct fat-rich effluent types: a fish processing facility (initial fat concentration 862 ± 18 mg·L^{-1}), a palm oil mill (POME; 1,542 ± 35 mg·L^{-1}), and a municipal wastewater treatment unit (388 ± 12 mg·L^{-1}). At each site, four treatment groups were evaluated in triplicate: the consortium product (BDO3:BDO14:KEO5 = 1:1:1, applied at 5 mL m^{-3}), two commercially available bioremediation products (BF and BDG, applied at manufacturer-recommended doses), and an untreated control. Residual fat content, expressed as a percentage of the initial concentration, was monitored at two-day intervals over ten days and is presented in Table 6. Across all three sites, the consortium product achieved substantially greater fat reduction than either commercial comparator or the untreated control at every sampling time point from day 2 onwards. At the fish processing site, residual fat in the consortium-treated plots declined progressively from 100% at day 0 to 78.3 ± 3.2% at day 2, 51.4 ± 4.1% at day 4, and 28.7 ± 2.8% at day 6, continuing to 18.2 ± 2.1% and 11.5 ± 1.8% at days 8 and 10, respectively. At the POME site — where the highest initial fat loading presented the greatest treatment challenge — residual fat in the consortium-treated plots reached 48.8 ± 3.9% by day 6 and declined further to 25.3 ± 2.9% by day 10. At the municipal wastewater site, residual fat fell to 34.3 ± 3.1% at day 6 and 15.8 ± 2.2% at day 10. By contrast, the commercial products BF and BDG achieved only marginal fat reductions across all three sites throughout the ten-day monitoring period, with residual fat values consistently ranging from 90.8 to 97.1% at day 10, values not significantly different from the untreated control ($p > 0.05$). These results demonstrate that the consortium product outperformed both commercial comparators by a substantial margin across all site types and all time points. The endpoint performance metrics at day 6 for all treatment groups and sites are summarised in Table 7. At the fish processing site, the consortium product achieved a fat removal efficiency of 71.3 ± 2.8%, reducing fat concentration from 862 ± 18 mg L^{-1} to 247 ± 24 mg·L^{-1}, representing a 68.4 percentage-point improvement in residual fat over the better-performing commercial product (BF, 92.4% residual). At the POME site, fat removal efficiency reached 51.2 ± 3.9%, reducing fat from 1,542 ± 35 mg L^{-1} to 790 ± 60 mg·L^{-1} — a 49.0 percentage-point improvement over commercial BF (94.3% residual). At the municipal wastewater site, the consortium product achieved 65.7 ± 3.1% fat removal, reducing fat from 388 ± 12 mg L^{-1} to 133 ± 12 mg·L^{-1}, a 62.5 percentage-point improvement over commercial BF (93.2% residual). One-way ANOVA followed by Tukey's HSD post-hoc test confirmed that fat removal by the consortium product was significantly superior to both commercial products and the untreated control at all three sites ($p < 0.05$; significance letters in Table 6), while no significant difference was detected between the two commercial products or between either commercial product and the untreated control at any site ($p > 0.05$). The superior field performance of the consortium product is consistent with its lipolytic mechanisms and synergistic fat-degradation activity. The high lipase activity, emulsification capacity, and oil displacement characteristics of the BDO3:BDO14:KEO5 consortium collectively enable effective mobilization and hydrolysis of fat under the complex physicochemical conditions of real wastewater, including variable pH, competing organic matter, and fluctuating temperature,

conditions under which single-strain commercial products appear limited in efficacy. The relatively lower fat removal observed at the POME site compared with the fish processing and municipal sites at day 6 (51.2% vs. 71.3% and 65.7%, respectively) likely reflects the substantially higher initial fat loading at that site, which may require a higher product dose or an extended treatment period for complete remediation. It represents a direction for further optimization in future field trials.

4. Conclusions

This study successfully developed a mixed bacterial consortium bioremediation product for the treatment of fat-rich wastewater, integrating strain isolation, mixture design optimization, pilot-scale production, product formulation, and field validation into a complete development pipeline. Eleven lipolytic bacterial isolates were recovered from fat-rich wastewater across five source environments, of which three — *Acinetobacter variabilis* BDO3, *Bacillus* sp. BDO14, and *Lysinibacillus* sp. KEO5 — were selected based on superior and complementary lipolytic performance, recording lipase activities of 8.07, 8.36, and 8.02 U mL^{-1}, emulsification indices (E_{24}) of 54.3, 40.0, and 39.5, oil displacement areas of 12.56, 19.63, and 19.63 cm^2, and individual oil removal efficiencies of 21.7, 29.6, and 24.5%, respectively. Simplex-centroid mixture design optimization across nine consortium formulas identified the equal-proportion blend BDO3:BDO14:KEO5 (1:1:1) as optimal, achieving a confirmed oil removal of 54.1% — an 83-149% improvement over the best-performing monoculture (BDO14, 29.6%) and substantially exceeding all binary combinations (36.9–42.7%). The close agreement between the model-predicted (52.3%) and the confirmed (54.1%) oil removal validated the Scheffé mixture model and indicated the presence of synergistic interactions among the three constituent strains. Scale-up of the consortium fermentation from 1 L bench scale to a 200 L pilot fermenter was achieved without significant loss of performance: peak biomass of 7.5×10^8 CFU mL^{-1} was reached at 48 h in both systems ($p > 0.05$), maximum specific growth rate was maintained at 0.25 ± 0.03 h^{-1}, and oil removal efficiency in test assays was preserved at 52.7 ± 2.3% at 200 L compared with 54.1 ± 1.8% at bench scale ($p > 0.05$). Two product formulations were developed from the 200 L harvest: a liquid formulation in 15% glycerol maintaining viable counts of $1.40–7.5 \times 10^7$ CFU mL^{-1} over one month of storage, and a powder formulation on rice bran carrier maintaining $2.45–6.0 \times 10^6$ CFU mL^{-1} over two months, both satisfying the minimum viability threshold required for commercial bioremediation applications. Field trials across three wastewater site types demonstrated that the consortium product outperformed two commercial bioremediation products (BF and BDG) by 49.0 to 68.4 percentage points in residual fat reduction at day 6, achieving residual fat values of 28.7 ± 2.8% (fish processing effluent), 48.8 ± 3.9% (POME), and 34.3 ± 3.1% (municipal wastewater) compared with 92.4–95.1% for the commercial products and 96.8–98.2% for the untreated control — differences that were statistically significant at all three sites (Tukey's HSD, $p < 0.05$). Fat removal continued beyond day 6, reaching 11.5 ± 1.8%, 25.3 ± 2.9%, and 15.8 ± 2.2% residual fat at day 10 for the fish processing, POME, and municipal sites, respectively. Collectively, these results establish the BDO3:BDO14:KEO5 consortium product as a high-performance, scalable, and field-validated bioremediation solution for treating fat-rich wastewater, demonstrating superiority over currently available commercial products across diverse effluent types. Future work should focus on dose-response optimization at high-loading sites such as POME, long-term product stability beyond two months, and safety characterization of the constituent strains to support regulatory approval for commercial deployment in Thailand's food processing and palm oil industries under the BCG Economy framework.

Table 6. Residual fat content (% of initial concentration ± SD) over time across three field sites and four treatment groups. Values are means of triplicate field plots. Sampling was conducted on days 0, 2, 4, 6, 8, and 10. Day 6 values are highlighted; green shading = residual fat < 50% (consortium product); red shading = residual fat > 90% (commercial products and control).

Day	Fish processing effluent				POME				Municipal wastewater			
	Consortium	Comm. BF	Comm. BDG	Control	Consortium	Comm. BF	Comm. BDG	Control	Consortium	Comm. BF	Comm. BDG	Control
0 (initial)	100.0 ± 0.0	100.0 ± 0.0	100.0 ± 0.0	100.0 ± 0.0	100.0 ± 0.0	100.0 ± 0.0	100.0 ± 0.0	100.0 ± 0.0	100.0 ± 0.0	100.0 ± 0.0	100.0 ± 0.0	100.0 ± 0.0
2	78.3 ± 3.2	95.1 ± 1.8	96.2 ± 2.1	98.4 ± 1.2	84.6 ± 3.8	96.8 ± 2.2	97.1 ± 1.9	99.1 ± 0.9	80.5 ± 2.9	95.7 ± 2.0	96.4 ± 1.7	98.8 ± 1.1
4	51.4 ± 4.1	93.8 ± 2.3	94.7 ± 2.5	97.6 ± 1.5	67.2 ± 4.5	95.2 ± 2.6	95.8 ± 2.4	98.5 ± 1.3	55.9 ± 3.7	94.1 ± 2.1	95.3 ± 2.2	97.9 ± 1.4
6	**28.7 ± 2.8**	**92.4 ± 2.7**	**93.6 ± 2.9**	**96.8 ± 1.8**	**48.8 ± 3.9**	**94.3 ± 2.9**	**95.1 ± 2.7**	**98.2 ± 1.6**	**34.3 ± 3.1**	**93.2 ± 2.4**	**94.5 ± 2.6**	**97.4 ± 1.7**
8	18.2 ± 2.1	91.5 ± 3.0	92.8 ± 3.1	95.9 ± 2.0	35.6 ± 3.3	93.4 ± 3.1	94.2 ± 2.9	97.8 ± 1.8	22.7 ± 2.5	92.0 ± 2.7	93.6 ± 2.8	96.7 ± 1.9
10	11.5 ± 1.8	90.8 ± 3.2	91.9 ± 3.3	95.1 ± 2.2	25.3 ± 2.9	92.7 ± 3.3	93.5 ± 3.0	97.1 ± 2.0	15.8 ± 2.2	91.3 ± 2.9	92.4 ± 3.0	96.0 ± 2.1

* Consortium product: BDO3:BDO14: KEO5 = 1:1:1, liquid format, applied at 5 mL·m^{-3} (~5 × 10^{4} CFU·L^{-1}).

Commercial BF: powder, applied at 10 g m^{-3} (manufacturer recommended), and Commercial BDG: powder, applied at 5 g m^{-3} (manufacturer recommended). Both commercial products were within their expiry dates and stored per the manufacturer's instructions. Control: untreated wastewater receiving no microbial product. SD = standard deviation of triplicate field plots.

Table 7. Summary of field performance metrics at day 6 across three site types and four treatment groups. Values for fat concentration are means ± SD of triplicate field plots. Fat removal and residual fat are calculated relative to the initial concentration on day 0. Improvement is expressed as the percentage-point reduction in residual fat relative to the better-performing commercial product (BF or BDG) at each site. Different superscript letters within each site indicate significant differences (Tukey's HSD, $p < 0.05$).

Site	Treatment	Initial fat (mg L^{-1})	Final fat (mg L^{-1})	Fat removal (%)	Residual fat (%)	Improvement vs. the best commercial	Sig.
Fish processing effluent	Consortium (BDO3:BDO14:KEO5)	862 ± 18	247 ± 24	**71.3 ± 2.8**	**28.7 ± 2.8**	+68.4%	a
	Commercial BF	862 ± 18	795 ± 23	7.6 ± 2.7	92.4 ± 2.7	—	b
	Commercial BDG	862 ± 18	806 ± 25	6.4 ± 2.9	93.6 ± 2.9	—	b
	Untreated control	862 ± 18	834 ± 21	3.2 ± 1.8	96.8 ± 1.8	—	c
Palm oil mill effluent (POME)	Consortium (BDO3:BDO14:KEO5)	1,542 ± 35	790 ± 60	51.2 ± 3.9	48.8 ± 3.9	+49.0%	a
	Commercial BF	1,542 ± 35	1,454 ± 45	5.7 ± 2.9	94.3 ± 2.9	—	b
	Commercial BDG	1,542 ± 35	1,468 ± 42	4.9 ± 2.7	95.1 ± 2.7	—	b
	Untreated control	1,542 ± 35	1,514 ± 38	1.8 ± 1.6	98.2 ± 1.6	—	c
Municipal wastewater	Consortium (BDO3:BDO14:KEO5)	388 ± 12	133 ± 12	65.7 ± 3.1	34.3 ± 3.1	+62.5%	a
	Commercial BF	388 ± 12	362 ± 9	6.8 ± 2.4	93.2 ± 2.4	—	b
	Commercial BDG	388 ± 12	367 ± 11	5.5 ± 2.6	94.5 ± 2.6	—	b
	Untreated control	388 ± 12	378 ± 10	2.6 ± 1.7	97.4 ± 1.7	—	c

a, b, c: means sharing the same letter within each site are not significantly different (one-way ANOVA followed by Tukey's HSD post-hoc test, $p < 0.05$).
— = no improvement calculated for commercial products and control (reference group).
Green shading (consortium rows) = superior fat removal performance relative to commercial products.
Initial fat concentrations: fish processing effluent 862 ± 18 mg L^{-1}; POME 1,542 ± 35 mg L^{-1}; municipal wastewater 388 ± 12 mg L^{-1}.

5. Acknowledgments

The authors would like to thank the three high-fat wastewater sources: (i) sludge from an aquatic food-processing plant, (ii) effluent from a palm oil mill, and (iii) grease-trap sediment from a large-scale cafeteria in Surat Thani Province, Thailand, for requesting your kind assistance in providing a wastewater sample for research purposes. Special thanks to the anonymous reviewers for their constructive comments and suggestions, which helped improve the quality of this manuscript.

Author Contributions: PN conceptualization, formal analysis, project administration, resources, writing review and editing, data curation, investigation, methodology, visualization, and writing-original draft. The author has read and agreed to the published version of the manuscript.

Funding: This work is financially supported by the Pre-Talent Mobility Grant 2021, Walailak University Science and Technology Park (No. Pre-TM-06-300564)

Conflicts of Interest: The author declares no conflict of interest in the collection, analysis, or interpretation of data; in the writing of the manuscript, or in the decision to publish the results.

References

[1] Wakelin, N. G.; Forster, C. F. An investigation into microbial removal of fats, oils and greases. *Bioresour. Technol.* **1997**, *59*, 37–43. https://doi.org/10.1016/S0960-8524(96)00134-4

[2] Matos, A. T.; Lo Monaco, P. A.; Sarmento, A. P. Treatment of food-processing wastewater with high lipid content. *Water Sci. Technol.* **2018**, *77*, 1835–1843.

[3] Marrakchi, M.; Hamza, W.; Sayadi, S. Electrocoagulation pre-treatment for lipid removal from olive mill wastewater. *Sep. Purif. Technol.* **2017**, *182*, 88–97.

[4] Cammarota, M. C.; Freire, D. M. G. A review on hydrolytic enzymes in the treatment of wastewater with high oil and grease content. *Bioresour. Technol.* **2006**, *97*, 2195–2210. https://doi.org/10.1016/j.biortech.2006.02.030

[5] Lesuisse, E.; Schanck, K.; Colson, C. Purification and preliminary characterization of the extracellular lipase of *Bacillus subtilis* 168. *Eur. J. Biochem.* **1993**, *216*, 155–160. https://doi.org/10.1111/j.1432-1033.1993.tb18127.x

[6] Matsumiya, Y.; Wakita, D.; Kimura, A.; Sanpa, S.; Kubo, M. Isolation and characterization of a lipid-degrading bacterium and its application to lipid-containing wastewater treatment. *J. Biosci. Bioeng.* **2007**, *103*, 325–330. https://doi.org/10.1263/jbb.103.325

[7] Prasad, M. P.; Manjunath, K. Comparative study on biodegradation of lipid-rich wastewater using lipase producing bacterial species. *Indian J. Biotechnol.* **2011**, *10*, 121–124.

[8] Mongkolthanaruk, B.; Dharmsthiti, S. Biodegradation of lipid-rich wastewater by a mixed bacterial consortium. *Int. Biodeterior. Biodegrad.* **2002**, *50*, 101–105. https://doi.org/10.1016/S0964-8305(02)00057-4

[9] Silva, C. F.; Azevedo, L. C. B.; Cardoso, D. E. S. Evaluation of microbial consortia for lipid degradation in wastewater treatment. *J. Environ. Manage.* **2015**, *157*, 1–8.

[10] Morgan, C. A.; Herman, N.; White, P. A.; Vesey, G. Preservation of micro-organisms by drying. *J. Microbiol. Methods* **2006**, *66*, 183–193. https://doi.org/10.1016/j.mimet.2006.02.017

[11] Fabian, C.; Ju, Y. H. A review on rice bran protein: Its properties and extraction methods. *Crit. Rev. Food Sci. Nutr.* **2011**, *51*, 816–827. https://doi.org/10.1080/10408398.2010.482678

[12] Miyamoto-Shinohara, Y.; Imaizumi, T.; Sukenobe, J.; Murakami, Y.; Kawamura, S.; Komatsu, Y. Survival rate of microbes after freeze-drying and long-term storage. *Cryobiology* **2000**, *41*, 251–255. https://doi.org/10.1006/cryo.2000.2282

[13] Lesuisse, E.; Schanck, K.; Colson, C. Purification and characterization of extracellular lipase on tributyrin agar. *Eur. J. Biochem.* **1993**, *216*, 155–160. https://doi.org/10.1111/j.1432-1033.1993.tb18127.x

[14] Sharma, R.; Chisti, Y.; Banerjee, U. C. Production, purification, characterization, and applications of lipases. *Biotechnol. Adv.* **2001**, *19*, 627–662. https://doi.org/10.1016/S0734-9750(01)00086-6

[15] Rahman, K. S. M.; Gakpe, E. Production, characterisation and applications of biosurfactants. *Biotechnology* **2008**, *7*, 360–370. https://doi.org/10.3923/biotech.2008.360.370

[16] Altschul, S. F.; Gish, W.; Miller, W.; Myers, E. W.; Lipman, D. J. Basic local alignment search tool. *J. Mol. Biol.* **1990**, *215*, 403–410. https://doi.org/10.1016/S0022-2836(05)80360-2

[17] Stanbury, P. F.; Whitaker, A.; Hall, S. J. *Principles of Fermentation Technology*, 3rd ed.; Elsevier: Oxford, U.K., **2017**.

[18] Vassilev, N.; Vassileva, M.; Azcon, R. Immobilised cell technology applied in solubilization of insoluble inorganic phosphate. *Bioresour. Technol.* **2001**, *79*, 263–271. https://doi.org/10.1016/S0960-8524(01)00017-7.

[19] APHA. *Standard Methods for the Examination of Water and Wastewater*, 23rd ed.; American Public Health Association: Washington, DC, **2017**.

[20] Jiang, Y.; Wen, J.; Bai, J.; Jia, X.; Hu, Z. Biodegradation of crude oil by a novel strain of *Acinetobacter*. *Bioresour. Technol.* **2012**, *102*, 7753–7758

[21] Turnbull, P. C. B.; Kramer, J. M. Non-gastrointestinal *Bacillus cereus* infections: An analysis of exotoxin production by strains isolated over a two-year period. *J. Clin. Pathol.* **1983**, *36*, 1091–1096. https://doi.org/10.1136/jcp.36.10.1091

[22] Das, N.; Chandran, P. Microbial degradation of petroleum hydrocarbon contaminants: An overview. *Biotechnol. Res. Int.* **2011**, *2011*, 941810. https://doi.org/10.4061/2011/941810

[23] Ahmed, I.; Yokota, A.; Yamazoe, A.; Fujiwara, T. Proposal of *Lysinibacillus boronitolerans* gen. nov., sp. nov. *Int. J. Syst. Evol. Microbiol.* **2007**, *57*, 1117–1125. https://doi.org/10.1099/ijs.0.63867-0

[24] Madigan, M. T.; Bender, K. S.; Buckley, D. H.; Sattley, W. M.; Stahl, D. A. *Brock Biology of Microorganisms*, 15th ed.; Pearson: New York, NY, 2018.

[25] Nicholson, W. L.; Munakata, N.; Horneck, G.; Melosh, H. J.; Setlow, P. Resistance of *Bacillus* endospores. *Microbiol. Mol. Biol. Rev.* **2000**, *64*, 548–572. https://doi.org/10.1128/MMBR.64.3.548-572.2000

[26] Gottschalk, G. *Bacterial Metabolism*, 2nd ed.; Springer: New York, NY, 1986. https://doi.org/10.1007/978-1-4612-1072-6.

[27] Shuler, M. L.; Kargi, F. *Bioprocess Engineering: Basic Concepts*, 3rd ed.; Prentice Hall: Upper Saddle River, NJ, **2017**.

[28] Ruiz, C.; Pastor, F. I. J.; Diaz, P. Isolation of lipid- and polysaccharide-degrading micro-organisms from subtropical forest soil, and analysis of lipolytic strain *Bacillus* sp. CR-179. *Lett. Appl. Microbiol.* **2005**, *40*, 218–227. https://doi.org/10.1111/j.1472-765X.2005.01660.x.

[29] Poh, P. E.; Chong, M. F. Development of anaerobic digestion methods for palm oil mill effluent treatment. *Bioresour. Technol.* **2009**, *100*, 1–9. https://doi.org/10.1016/j.biortech.2008.06.022

ASEAN
Journal of Scientific and Technological Reports
Online ISSN:2773-8752

Research article

Chia Seed Extract Attenuates Streptozotocin-Induced Pancreatic Beta-Cell Dysfunction in Diabetic Rats: Evidence from Functional and Oxidative Stress Biomarkers

Ennas Mohamed Majhwol[1*]

[1] Department of Biology, College of Education, University of Al-Qadisiyah, Iraq
* Correspondence: ennas.alkhozaae@qu.edu.iq

Citation:
Majhwol, M.E. Chia seed extract attenuates streptozotocin-induced pancreatic beta-cell dysfunction in diabetic rats: evidene from functional and oxidative stress biomarkers. *ASEAN J. Sci. Tech. Report.* **2026**, *29*(5), e263641. https://doi.org/10.55164/ajstr.v29i5.263641

Article history:
Received: February 10, 2026
Revised: March 7, 2026
Accepted: April 26, 2026
Available online: April, 30, 2026

Publisher's Note:
This article is published and distributed under the terms of the Thaksin University.

Abstract: Diabetes mellitus has a global prevalence of more than 422 million cases, with progressive beta-cell dysfunction marked by pancreatic dysplasia. This paper appraised the protective influences of chia seed extract (CSE) on beta-cell dysfunction induced by streptozotocin (STZ) in diabetic rats. In this experiment, Wistar rats (160g) were separated into four groups (normal control, diabetic control, and two CSE-treated diabetic groups (250 and 500 mg/kg body weight)). The separation lasted 8 weeks, during which 32 male rats were used. STZ (40mg/kg) was injected intraperitoneally to induce diabetes. The measured parameters included fasting glucose, HbA1c, serum insulin, HOMA-IR, pancreatic enzymes, and oxidative stress markers. CSE treatment dose-dependently lowered fasting glucose (59% reduction at high dose, $p<0.001$), augmented insulin secretion ($p<0.001$), diminished HOMA-IR (62% reduction, $p<0.001$), and highly inhibited oxidative imbalance in pancreatic tissue. The CSE 500mg/kg concentration suppressed malondialdehyde by 59 percent and replenished glutathione by 105 percent. These results indicate that the chia seed extract has strong antidiabetic and antioxidant effects, suppressing STZ-induced pancreatic beta-cell dysfunction by reducing oxidative stress.

Keywords: Chia seed extract; pancreatic beta-cells; streptozotocin; diabetes mellitus; oxidative stress

1. Introduction

Diabetes mellitus is among the greatest problems of global public health, and the International Diabetes Federation estimates 700 million people will have diabetes by 2045 [1]. The central influence on diabetic pathogenesis is progressive beta-cell damage, which occurs through either autoimmune destruction in type 1 diabetes or through slow deterioration and insulin resistance in type 2 diabetes [2,3]. Streptozotocin (STZ) is a natural antibiotic synthesized by Streptomyces achromogenes and has been utilized in diabetes research for more than 40 years [4]. STZ selectively concentrates in pancreatic beta-cells via GLUT2-mediated uptake, induces cytotoxicity via DNA methylation and DNA fragmentation, and ultimately leads to apoptosis and necrosis [5]. Such specificity makes STZ-induced models useful for studying beta-cell injury mechanisms and potential treatment interventions [6]. Oxidative imbalance, with excessive ROS generation and impaired antioxidative defense, is a high-priority intermediary in STZ-mediated beta-cell dysfunction [7]. Pancreatic beta-cells have the lowest regulation of antioxidant enzymes, making

them highly susceptible to oxidative damage [8]. This weakness indicates the therapeutic benefits of antioxidant-based interventions to protect beta-cells. Chia seeds (Salvia hispanica L.) have an outstanding plant-derived composition with substantial amounts of polyphenolic substances (chlorogenic acid, caffeic acid, kaempferol, quercetin), omega-3 and omega-6 (PUFAs), nutritive fibers, and micronutrients [9-11]. Plant polyphenols have shown attenuating effects against STZ-induced beta-cell damage by suppressing oxidative stress, anti-inflammatory signaling, and apoptosis [12]. Nevertheless, the research on the influences of chia seed extract on beta-cell protection is not thorough. This research was conducted to measure the cytoprotective influence of chia seed extract on STZ-induced injury to pancreatic beta-cells, using glycemic control, insulin activity, pancreatic integrity, and oxidative stress parameters in a diabetic rat group.

2. Materials and Methods

2.1 Preparation of Materials

2.1.1 Chia Seed Extract

Chia seeds (Salvia hispanica L.) were sourced from certified farming vendors and botanically verified. The seeds were subjected to drying at 40 °C

over a period of 24 hours and finely ground. Maceration extraction was carried out via 70% ethanol (1:10 w/v seed-to-solvent ratio) at room temperature, with mixing every 12 hours. To prepare the extract, it was filtered (Whatman Grade 1), evaporated under decreased pressure at 45 °C by rotary evaporation, and finally stored at -20 °C. To administer it, the dried extract was resuspended in distilled water with 0.5% carboxymethyl cellulose (CMC).

2.1.2. Streptozotocin Preparation

Streptozotocin (Sigma-Aldrich, USA) was diluted in a newly formulated 0.1 M citrate buffer (pH 4.5) prior to its treatment. The solutions were kept on ice and consumed within 30 minutes to avoid degradation.

2.2 Experimental Animals

Male Wistar rats (n=36, 160+10 g) were kept in polypropylene cages in a well-controlled conditions (25 +2 C, 55 +5 humidity, 12 light and dark period). Ad libitum provision was made for a standard rodent pellet diet and filtered water. Animals were acclimatized for one week before experimentation. The Institutional Animal Ethics Committee approved all the protocols and complied with regulations for the care and handling of laboratory animals.

2.3 Diabetes Induction and Experimental Design

After acclimatization, STZ (40 mg/kg body weight) in 0.1 M citrate buffer (pH 4.5) was given by a single intraperitoneal injection, causing diabetes. The 40 mg/kg dose was chosen to ensure partial, rather than total, beta-cell destruction, leaving sufficient residual secretory activity to permit assessment of extract-mediated cytoprotection, in line with previous studies that used the same dose range in Wistar rats. The animals were starved the night before injection, whilst being free to drink water. To avoid post-injection episodes of hypoglycemia, 5% glucose solution was administered after the injection over 24 hours. Fasting blood glucose was quantified 72 hours post-STZ administration by tail-vein puncture utilizing a glucometer (Accu-Check Active, Roche Diagnostics). Rats with fasting glucose >250 mg/dL were deemed diabetic. This threshold represents the established criterion for confirming reliable STZ-induced beta-cell injury at partial-destruction doses and is consistent with published protocols. Four rats failed to achieve the diabetic threshold (fasting glucose >250 mg/dL at 72 h post-STZ) and were excluded from all groups and humanely euthanized in accordance with institutional ethics protocols. No re-dosing was performed. Successfully diabetic rats (n=28) plus normal controls (n=8) were apportioned into four groups (n=8/group): G1 (Normal Control) - non-diabetic given vehicle; G2 (Diabetic Control) - diabetic given vehicle; G3 (CSE Low Dose) - diabetic given 250 mg/kg CSE; G4 (CSE High Dose) - diabetic given 500 mg/kg CSE. Animals were treated daily using oral gavage at a dose of 10 mL/kg for 8 weeks. Body weight was recorded weekly for dose adjustment.

2.4 Physiological and Biochemical Measurements

Weekly monitoring was conducted of body mass, food, and water consumption. Blood was collected after 6 hours of fasting via the tail vein and measured weekly as fasting blood glucose. The blood specimens were taken after the experiment by cardiac puncture under the influence of isoflurane anesthesia and cervical dislocation. Serum was centrifuged at 3000×g for 15 min at 4 °C, then maintained at -80 °C until analysis. HPLC was used to measure the glycated hemoglobin (HbA1c) levels. Serum insulin levels were determined using a commercial ELISA kit (Mercodia Rat Insulin ELISA; sensitivity 0.1 mIU/L). Insulin resistance was determined using the HOMA-IR formula: HOMA-IR = [fasting insulin (mIU/L) × fasting glucose (mmol/L)/22.5]. Spectrophotometric measurements of serum amylase and lipase activities were done using diagnostic kits (Randox Laboratories, UK). Pancreatic tissues were thoroughly scraped, mixed in potassium phosphate buffer (0.1 M, pH 7.4; 1:10 w/v), and separated by centrifugation at 10,000xg at 4 o C. The degree of lipid peroxidation was measured as the concentration of malondialdehyde (MDA) utilizing the thiobarbituric acid–based lipid peroxidation assay, with absorbance measured at 532 nm. The levels of reduced glutathione (GSH) were ascertained as per the method of Ellman, in which the absorbance was recorded at 412 nm. The Bradford assay measured the total protein amount to normalize the biochemical readings.

2.5 Statistical Analysis

The findings are displayed as mean ± SE, with eight animals per group (n = 8). Normality of the observations was analyzed using the Shapiro–Wilk test, whereas variance homogeneity was analyzed using the Levene test. The ANOVA (one-way analysis of variance) was employed to evaluate differences among experimental groups, and the post hoc multiple-comparison test was conducted using the Tukey test. A p-value of below 0.05 was taken to be substantial.

3. Results

3.1 General physiological parameters

CSE administration significantly ameliorated diabetic physiological disturbances. Diabetic controls (G2) exhibited severely attenuated weight gain compared to normal controls (G1) (195.0 ± 7.3 vs. 285.0 ± 8.6 g, $p<0.001$). CSE treatment dose-dependently improved body weight, with high-dose achieving 37% improvement (268.0 ± 7.1 g, $p<0.01$ vs. G2). Untreated diabetic rats developed severe hyperglycemia (385.0 ± 12.4 mg/dL at week 8 vs. 92.0 ± 5.1 mg/dL in controls, $p<0.001$). High-dose CSE demonstrated superior efficacy, reducing fasting glucose by 59% to 156.0 ± 8.2 mg/dL ($p<0.001$ vs. G2), while low-dose achieved 43% reduction (218.0 ± 9.8 mg/dL, $p<0.01$). Characteristic diabetic polyphagia and polydipsia were markedly attenuated by CSE treatment in a dose-dependent manner (Table 1). Figure 1 should follow Table 1 directly. The sentence above integrates with the existing paragraph that ends with the water intake data (G4: 28.5 ± 2.1 mL/day, $p < 0.001$ vs. G2).

Table 1. Impact of CSE on general physiological indicators in diabetic rats

Parameter	G1	G2	G3	G4
Final Body Weight (g)	285.0 ± 8.6	195.0 ± 7.3***	238.0 ± 6.8**	268.0 ± 7.1**
Week 8 Fasting Glucose (mg/dL)	92.0 ± 5.1	385.0 ± 12.4***	218.0 ± 9.8**	156.0 ± 8.2***
Food Intake (g/day)	18.3 ± 1.5	32.5 ± 2.1***	25.4 ± 1.9*	21.8 ± 1.6*
Water Intake (mL/day)	22.4 ± 1.8	58.6 ± 3.2***	42.3 ± 2.6*	28.5 ± 2.1***

Data presented as Mean±SEM. Significance vs. Diabetic Control (G2): *p<0.05, **p<0.01, ***p<0.001. G1: Normal Control; G2: Diabetic Control; G3: Diabetic+CSE (250 mg/kg); G4: Diabetic+CSE (500 mg/kg).

3.2. Biochemical parameters and pancreatic function

CSE administration produced significant dose-dependent improvements in glycemic control and markers of pancreatic function. Untreated diabetic rats exhibited severely elevated HbA1c (9.8 ± 0.4% vs. 4.2 ± 0.3%, $p<0.001$) and profoundly depressed serum insulin (2.3 ± 0.4 vs. 8.6 ± 0.5 mIU/L, $p<0.001$). High-dose CSE reduced HbA1c by 40% to 5.9 ± 0.4% ($p<0.001$ vs. G2) and restored insulin to near-normal levels (6.8 ± 0.5 mIU/L, $p<0.001$). The HOMA-IR index confirmed severe insulin resistance in diabetic controls (8.4 ± 0.6 vs. 2.1

± 0.3, p<0.001), which was dose-dependently reversed by CSE treatment, with the high dose achieving a 62% reduction (3.2 ± 0.4, p<0.001). Elevated pancreatic enzymes in diabetic rats (amylase: 156±8.2 U/L; lipase: 142 ± 7.6 U/L) were effectively normalized by high-dose CSE treatment (Table 2). Figure 2 should follow Table 2 directly. The sentence above integrates with the existing paragraph that ends with the serum lipase result (G4: 91 ± 4.9 U/L, p < 0.001 vs. G2).

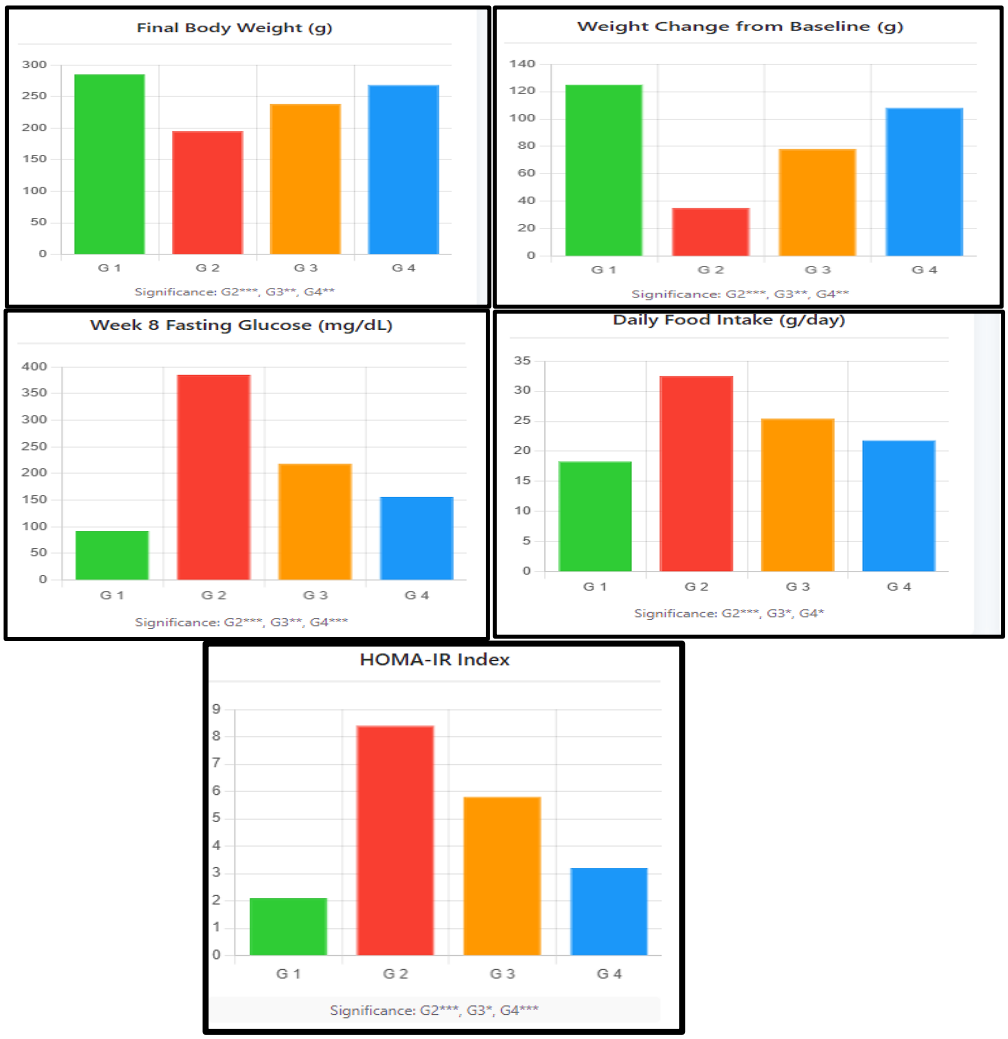


Figure 1. Impact of chia seed extract (CSE) on general physiological indicators in streptozotocin (STZ)-induced diabetic rats over eight weeks of treatment. (A) Final body weight (g) at week 8. (B) Total body weight change from baseline (g). (C) Week 8 fasting blood glucose (mg/dL). (D) Average daily food intake (g/day). (E) Average daily water consumption (mL/day).

Table 2. Effects of CSE on Biochemical Parameters and Pancreatic Function

Parameter	G1	G2	G3	G4
HbA1c (%)	4.2 ± 0.3	9.8 ± 0.4***	7.1 ± 0.5**	5.9 ± 0.4***
Serum Insulin (mIU/L)	8.6 ± 0.5	2.3 ± 0.4***	4.2 ± 0.6*	6.8 ± 0.5***
HOMA-IR Index	2.1 ± 0.3	8.4 ± 0.6***	5.8 ± 0.5*	3.2 ± 0.4***
Serum Amylase (U/L)	98 ± 6.1	156 ± 8.2*	118 ± 7.4*	104 ± 5.8***
Serum Lipase (U/L)	82 ± 5.3	142 ± 7.6*	112 ± 6.8*	91 ± 4.9***

Data displayed as Mean±SEM. Significance vs. G2: *p<0.05, **p<0.01, ***p<0.001.

3.3. Oxidative stress markers in pancreatic tissue

CSE demonstrated remarkable antioxidant effects in pancreatic tissue. Diabetic controls exhibited pronounced oxidative damage, with MDA levels 3-fold higher (6.8 ± 0.4 vs. 2.1 ± 0.2 nmol/mL, $p<0.001$). High-dose CSE reduced MDA by 59% to 2.8 ± 0.2 nmol/mL ($p<0.001$), approaching normal values. Pancreatic GSH was severely depleted in diabetic rats (12.3 ± 1.2 vs. 28.4 ± 1.8 µg/mL, $p<0.001$). High-dose CSE restored GSH by 105% to 25.2 ± 1.6 µg/mL ($p<0.001$), nearly normalizing antioxidant defenses (Table 3).

Table 3. Effects of CSE on oxidative stress markers in pancreatic tissue

Parameter	G1	G2	G3	G4
MDA (nmol/mL)	2.1 ± 0.2	6.8 ± 0.4***	4.9 ± 0.35**	2.8 ± 0.2***
GSH (µg/mL)	28.4 ± 1.8	12.3 ± 1.2***	18.6 ± 1.5**	25.2 ± 1.6***

Data presented as Mean±SEM. MDA: malondialdehyde; GSH: reduced glutathione. Significance vs. G2: *p<0.05, **p<0.01, ***p<0.001.

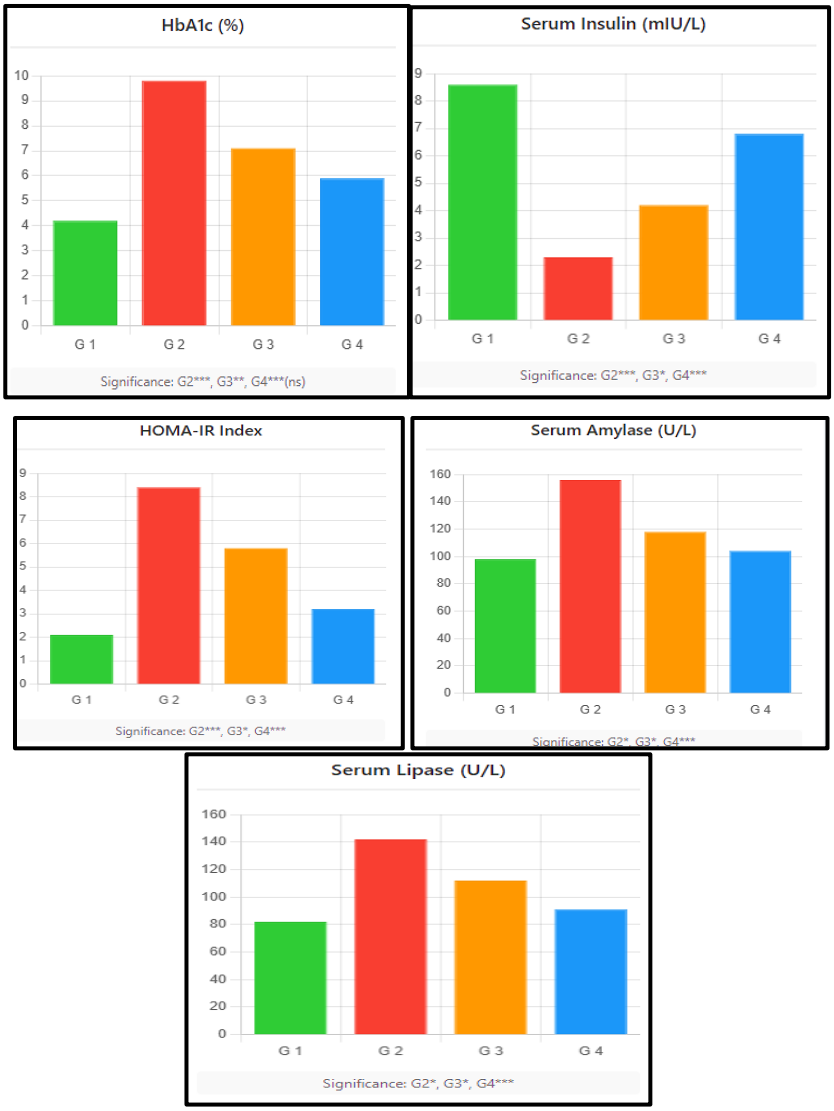


Figure 2. Influences of chia seed extract (CSE) on biochemical indicators of glycaemic control, insulin activity, and pancreatic enzyme activity in streptozotocin (STZ)- triggered diabetic rats after eight weeks of intervention. (A) Glycated haemoglobin (HbA1c, %). (B) Serum insulin level (mIU/L). Homeostatic Model Assessment of Insulin Resistance (HOMA-IR) index (C). (D) Serum amylase level (U/L). (E) Serum lipase level (U/L).

4. Discussion

This research has shown that chia seed extract significantly reduces functional and oxidative stress markers of STZ-induced pancreatic beta-cell dysfunction through dose-dependent mechanisms that include alleviation of oxidative stress and recovery of beta-cell secretory activity. These results can greatly contribute to knowledge of phytochemical-based therapeutic interventions for diabetic pathologies. The CSE produced a strong hypoglycemic effect, reducing fasting glucose by 59% compared with similar experimental studies of polyphenol-containing extracts in these models [15], indicating a particularly strong hypoglycemic effect. The 40% decrease in HbA1c is cumulative glycemic management over 8 weeks and evidence that it is effective beyond acute glycemic control. Such a close approach to normal HbA1c levels (5.9±0.4% vs. 4.2±0.3% in controls) is clinically significant, as it is well known that HbA1c is correlated with diabetic complications in humans [16]. Recovery of serum insulin levels (2.3 to 6.8 mIU/L with high dose CSE) implies either maintenance of residual beta-cell secretory capacity or increased insulin secretion of remaining beta-cells. The polyphenolic compounds can regulate insulin secretion in several ways, such as by regulating calcium channels, activating protein kinase C, and increasing mitochondrial ATP production [17]. The fact that CSE allowed near-normal insulin levels to be maintained despite beta-cell impairment in the initial stages of the disease shows that CSE could either promote the secretory capacity of the remaining beta-cells or inhibit additional cell death.

This extraordinary decrease in HOMA-IR (62% with high-dose CSE) indicates increased systemic insulin sensitivity, possibly through direct actions of CSE polyphenols on peripheral insulin signaling pathways. Chia seeds contain flavonoids, especially quercetin, which stimulates the PI3K signaling and autophosphorylation of insulin receptors [18]. This enhanced peripheral insulin sensitivity would lower compensatory secretory requirements in the remaining beta-cells, thus preserving beta-cell function. Most mechanistically important findings are on pancreatic oxidative stress markers. The threefold increase in MDA in diabetic controls is indicative of intense oxidative injury on pancreatic lipids, which is congruent with the oxidative stress-based beta-cell toxicity of STZ [21]. The 59% MDA reduction at high doses of CSE suggests that it is a very strong inhibitor of oxidative radical production or that it increases scavenger mechanisms. The fact that pancreatic GSH is almost fully restored (105% increased, close to normal levels) requires CSE to have the ability to restore antioxidant defenses, which may be due to direct antioxidant activity or the induction of GSH synthesis via stress-response mechanisms [23]. Those protective properties can be explained by the high phytochemical content of chia, especially polyphenols (chlorogenic acid 2-3% dry weight, caffeic acid, kaempferol, quercetin) [24]. These flavonoids work by direct free radical scavenging, pro-oxidant metal chelation, and the activation of endogenous antioxidant enzymes [25]. The omega-3 fatty acid content could also be highly protective of membranes and anti-inflammatory by blocking the production of eicosanoids [26].

The strong dose-response association (500 mg/kg better than 250mg/kg) shows that the protective effects are concentration-dependent, as antioxidant pharmacology predicts. Nevertheless, such doses are significant compared to the dietary intake of chia, which limits direct clinical extrapolation. Moreover, oral gavage administration is reliable for dosing, although it might not be comparable to dietary bioavailability owing to hepatic first-pass metabolism and intestinal differences in absorption. Mechanistic understanding would be enhanced by future studies on the tissue disposition of CSE polyphenols using pharmacokinetic approaches. The study's limitations include the 8-week treatment duration, adopted due to the importance of a sustained treatment effect and practical limitations. In the long term (12-16 weeks), it may be decided whether the CSE protective effects are maintained or decreased, and whether prolonged treatment can prevent further diabetic complications. Also, histopathological analysis of pancreatic tissue and immunohistochemical evaluation of beta-cell mass would serve as direct structural indicators of beta-cell cytoprotection. A notable limitation of this work is the absence of histopathological (H&E staining) and immunohistochemical (insulin/glucagon immunostaining) examination of the pancreatic tissue. The current data are limited to functional and biochemical measures of beta-cell protection; without such data, it is not possible to prove structural preservation of islet architecture and beta-cell mass. These histopathological endpoints should be included in future research to give extensive evidence of cytoprotection. CSE employed in this research was not characterized by batch-specific using HPLC or GC-MS phytochemical methods, nor was the total

polyphenol content (Folin-Ciocalteu) or overall flavonoid concentration (aluminum chloride colorimetric method) determined. This is a major limitation, as the polyphenol content would vary greatly among extraction batches, seed origins, and solvent conditions. TPC and TFC quantification will become the norm in all subsequent studies using this extract, and HPLC profiling will be used to confirm the presence and relative abundance of chlorogenic acid, caffeic acid, kaempferol, and quercetin.

5. Conclusions

This paper shows that chia seed extract has a significant impact on the functional biomarkers of STZ-induced pancreatic beta-cell dysfunction, alleviating dose-related oxidative stress and reversing beta-cell dysfunction. The high-dose CSE (500 mg/kg) achieved a 59% reduction in fasting glucose, a 40% reduction in HbA1c, a 62% improvement in HOMA-IR, and a 105% improvement in GSH. The results have a scientific basis for the possible application of chia seeds in the suppression and control of diabetes. The attenuation of oxidative stress and the beta-cell protection demonstrated should be the focus of further translational and clinical studies that test the use of CSE supplementation in prediabetic and recently diagnosed diabetic patients. The enhanced clinical potential refers to other oxidative-stress-mediated pancreatic pathologies, such as acute pancreatitis. Future studies ought to examine molecular processes, conduct dose-optimization trials, and determine the long-term effectiveness and safety of its use in humans.

Acknowledgements

The author wishes to thank the Department of Biology at the College of Education, University of Al-Qadisiyah, for its contribution in providing laboratory resources and technical expertise.

Author Contributions: All author contributions are attributed solely to E.M.M. The

author has read and agreed to the published version of the manuscript.

Funding: This research received no funding.

Conflicts of Interest: The author declares no conflict of interest.

References

[1] International Diabetes Federation. *IDF Diabetes Atlas*, 10th ed.; International Diabetes Federation: Brussels, Belgium, **2021**.

[2] Kahn, S. E.; Cooper, M. E.; Del Prato, S. Pathophysiology and treatment of type 2 diabetes: Perspectives on the past, present, and future. *Lancet* **2014**, *383*, 1068–1083. https://doi.org/10.1016/S0140-6736(13)62154-6

[3] Eizirik, D. L.; Colli, M. L.; Ortis, F. The role of inflammation in insulitis and beta-cell loss in type 1 diabetes. *Nat. Rev. Endocrinol.* **2009**, *5*, 219–226. https://doi.org/10.1038/nrendo.2009.21

[4] Szkudelski, T. The mechanism of alloxan and streptozotocin action in B cells of the rat pancreas. *Physiol. Res.* **2001**, *50*, 537–546. https://doi.org/10.33549/physiolres.930111

[5] Lenzen, S. The mechanisms of alloxan- and streptozotocin-induced diabetes. *Diabetologia* **2008**, *51*, 216–226. https://doi.org/10.1007/s00125-007-0886-7

[6] Elsner, M.; Gurgul-Convey, E.; Lenzen, S. Relative importance of caspase-dependent and caspase-independent apoptosis in β cells. *Diabetologia* **2012**, *55*, 1350–1357.

[7] Tiedge, M.; Lortz, S.; Drinkgern, J.; Lenzen, S. Relation between antioxidant enzyme gene expression and antioxidative defense status of insulin-producing cells. *Diabetes* **1997**, *46*, 1733–1742. https://doi.org/10.2337/diabetes.46.11.1733

[8] Robertson, R. P.; Zhou, H.; Zhang, T.; Harmon, J. S. Chronic oxidative stress as a mechanism for glucose toxicity of the beta cell in type 2 diabetes. *Cell Biochem. Biophys.* **2007**, *48*, 139–146. https://doi.org/10.1007/s12013-007-0026-5

[9] Nieman, D. C.; Cayrado, C. A.; Austin, M. D.; Benowitz, D. A.; Shanely, R. A.; Jensen, R. S. Chia seed does not promote weight loss or alter disease risk factors in overweight adults. *Nutr. Res.* **2009**, *29*, 414–418. https://doi.org/10.1016/j.nutres.2009.05.011

[10] Coates, W.; Ayerza, R. Chia seed (*Salvia hispanica* L.): A new source of omega-3 fatty acids and its biological activities. *J. Am. Oil Chem. Soc.* **1996**, *73*, 23–25.

[11] Martinez-Cruz, O.; Paredes-López, O. Phytochemical profile and nutraceutical potential of chia seeds (*Salvia hispanica* L.) by ultra high performance liquid chromatography. *J. Chromatogr. A* **2014**, *1346*, 43–48. https://doi.org/10.1016/j.chroma.2014.04.007

[12] Pandey, K. B.; Rizvi, S. I. Plant polyphenols as dietary antioxidants in human health and disease. *Oxid. Med. Cell. Longev.* **2009**, *2*, 270–278. https://doi.org/10.4161/oxim.2.5.9498

[13] Rerup, C. C. Drugs producing diabetes through damage to the insulin secretory mechanism. *Pharmacol. Rev.* **1970**, *22*, 485–518.

[14] Bolzan, A. D.; Bianchi, M. S. Genotoxicity of streptozotocin. *Mutat. Res.* **2002**, *512*, 121–134. https://doi.org/10.1016/S1383-5742(02)00044-3

[15] Ceriello, A.; Testa, R. Antioxidant anti-inflammatory treatment in diabetes. *Diabetes Care* **2009**, *32*, S232–S236. https://doi.org/10.2337/dc09-S316

[16] American Diabetes Association. Standards of medical care in diabetes. *Diabetes Care* **2023**, *46*, S1–S291.

[17] Hii, C. S. T.; Howell, S. L. Effects of flavonoids on insulin secretion and Ca^{2+} handling in rat islets of Langerhans. *J. Endocrinol.* **1985**, *107*, 1–8. https://doi.org/10.1677/joe.0.1070001

[18] Eid, H. M.; Nachar, A.; Thong, F.; Sweeney, G.; Haddad, P. S. The molecular basis of the antidiabetic action of quercetin. *Pharmacogn. Mag.* **2015**, *11*, 74–81. https://doi.org/10.4103/0973-1296.149708

[19] Demirtas, B.; Gonenc, S.; Akman, S.; Yegen, B. C.; Senol, A. Protective effect of melatonin on streptozotocin-induced pancreatic tissue damage. *Pancreas* **2001**, *22*, 309–314.

[20] Aggarwal, B. B.; Kunnumakkara, A. B.; Harikumar, K. B.; Tharakan, S. T.; Sung, B.; Anand, P. Potential of spice-derived phytochemicals for cancer prevention. *Planta Med.* **2008**, *74*, 1560–1569. https://doi.org/10.1055/s-2008-1074578

[21] Maritim, A. C.; Sanders, R. A.; Watkins, J. B. Diabetes, oxidative stress, and antioxidants: A review. *J. Biochem. Mol. Toxicol.* **2003**, *17*, 24–38. https://doi.org/10.1002/jbt.10058

[22] Valko, M.; Leibfritz, D.; Moncol, J.; Cronin, M. T. D.; Mazur, M.; Telser, J. Free radicals and antioxidants in human disease. *Int. J. Biochem. Cell Biol.* **2007**, *39*, 44–84. https://doi.org/10.1016/j.biocel.2006.07.001

[23] Sies, H. Glutathione and its role in cellular functions. *Free Radic. Biol. Med.* **1999**, *27*, 916–921. https://doi.org/10.1016/S0891-5849(99)00177-X

[24] Marineli, R. D. S.; Lenquiste, S. A.; Marques, M. C.; Bogo, D.; Menezes, E. M.; Lancha, A. H., Jr. Chemical characterization and antioxidant potential of Chilean chia seeds. *LWT–Food Sci. Technol.* **2015**, *62*, 370–377.

[25] Scalbert, A.; Johnson, I. T.; Saltmarsh, M. Polyphenols: Antioxidants and beyond. *Am. J. Clin. Nutr.* **2005**, *81*, 215S–217S. https://doi.org/10.1093/ajcn/81.1.215S

[26] Simopoulos, A. P. The importance of the omega-6/omega-3 fatty acid ratio. *Exp. Biol. Med.* **2008**, *233*, 674–688. https://doi.org/10.3181/0711-MR-311

ASEAN
Journal of Scientific and Technological Reports
Online ISSN:2773-8752

Research article

Gastroprotective Effects of Purslane (*Portulaca oleracea* L.) Ethanolic Extract Against Aspirin-Induced Gastric Ulcer: Modulation of Oxidative Stress, Inflammatory Mediators, and EGFR Signaling in Rats

Zahraa Haidar Jawad[1*], and Hussein Abbas Salman[1]

[1] Department of Biology, College of Education, Al-Qadisiyah University, Diwaniyah, Iraq
* Correspondence: edu.bio.posta90@qu.edu.iq

Citation:
Jawad, H.Z.; Salman, A.; H. Gastroprotective effects of purslane (*Portulaca oleracea* L.) ethanolic extract against aspirin-induced gastric ulcer: modulation of oxidative stress, inflammatory mediators, and EGFR singanling in rats. *ASEAN J. Sci. Tech. Report.* **2026**, *29*(5), e263937. https://doi.org/10.55164/ajstr.v29i5.263937

Article history:
Received: February 25, 2026
Revised: March 7, 2026
Accepted: April 25, 2026
Available online: April 30, 2026

Publisher's Note:
This article is published and distributed under the terms of the Thaksin University.

Abstract: Aspirin-induced gastric ulcer represents a significant clinical challenge involving oxidative stress, inflammation, and impaired mucosal repair. This study evaluated the gastroprotective efficacy of Purslane (*Portulaca oleracea* L.) ethanolic extract compared with omeprazole in aspirin-induced gastric ulcer in rats. Twenty-four adult male albino rats were randomly assigned to four groups (n=6): negative control, ulcer-induced untreated, ulcer+omeprazole (20 mg/kg), and ulcer+*P. oleracea* extract (100 mg/kg). A gastric ulcer was induced with oral aspirin (100 mg/kg), followed by a 30-day treatment. Oxidative stress markers (SOD, CAT, GSH, MDA), inflammatory cytokines (TNF-α, IL-6), epidermal growth factor receptor (EGFR), and hematological parameters were quantified. Aspirin administration significantly decreased SOD activity by 26% (1.87 ± 0.05 vs. 2.51±0.01 ng/mL, p≤0.05), CAT by 39% (51.60±7.68 vs. 84.19 ± 3.13 U/mL, p≤0.05), and EGFR by 45% (50.29 ± 1.86 vs. 90.96 ± 10.64 pg/mL, p≤0.05) compared to controls. Conversely, MDA increased by 50% (776.81 ± 18.6 vs. 516.76 ± 38.2 ng/mL, p≤0.05), TNF-α increased by 106% (139.36 ± 14.1 vs. 67.77 ± 5.13 pg/mL, p≤0.05), IL-6 increased by 229% (148.43 ± 5.6 vs. 45.12 ± 0.93 pg/mL, p≤0.05), and WBC count increased by 19% (13.85± 1.08 vs. 11.66 ± 2.62 $\times 10^3/\mu L$, p≤0.05). P. oleracea treatment restored SOD by 44% above ulcer values (2.70±0.03 ng/mL, exceeding control), normalized GSH (50.33 ± 0.06 µg/mL), reduced MDA by 23% (601.70 ± 4.27 ng/mL), decreased TNF-α by 55% (63.02 ± 5.26 pg/mL, approaching control), reduced IL-6 by 58% (62.64 ± 2.57 pg/mL), and increased EGFR by 97% (98.94 ± 5.32 pg/mL, surpassing control) relative to ulcer group. Notably, *P. oleracea* demonstrated superior effects compared with omeprazole in restoring GSH levels, reducing MDA, and attenuating inflammatory cytokines. These findings demonstrate that *P. oleracea* exerts comprehensive gastroprotective activity through synergistic antioxidant, anti-inflammatory, and EGFR-mediated regenerative mechanisms, suggesting potential as a complementary therapeutic agent for NSAID-induced gastric ulceration.

Keywords: *Portulaca oleracea*; purslane; gastric ulcer; aspirin; oxidative stress

1. Introduction

Gastric ulcer constitutes a prevalent gastrointestinal disorder characterized by mucosal integrity disruption extending through the muscularis mucosae, affecting millions worldwide and presenting substantial morbidity through complications including hemorrhage and perforation [1]. The pathogenesis involves complex imbalances between aggressive factors (gastric acid, pepsin, NSAIDs, reactive oxygen species) and protective mechanisms (mucus-bicarbonate barrier, prostaglandin synthesis, adequate blood flow,

epithelial regeneration, antioxidant defenses) [2]. Aspirin, extensively prescribed for its analgesic, antipyretic, anti-inflammatory, and antiplatelet properties [3], induces gastric injury through dual mechanisms: (1) irreversible cyclooxygenase enzyme inhibition, suppressing cytoprotective prostaglandin synthesis [4, 5], and (2) direct topical irritation of gastric epithelium [6]. Aspirin-mediated prostaglandin depletion compromises mucus bicarbonate secretion and mucosal perfusion, predisposing tissues to acid-peptic injury.

Oxidative stress represents a central pathogenic mechanism in NSAID-induced ulceration [7]. Excessive reactive oxygen species (ROS) generation induces lipid peroxidation (measured as malondialdehyde [8]), protein oxidation, mitochondrial dysfunction, and activation of the inflammatory cascade. Concurrently, endogenous antioxidant defenses—superoxide dismutase (SOD), catalase (CAT), and reduced glutathione (GSH)—become depleted [9], amplifying cellular vulnerability and delaying healing. Pro-inflammatory cytokines, including tumor necrosis factor-alpha (TNF-α) and interleukin-6 (IL-6), are upregulated following mucosal injury [10], amplifying inflammation, promoting leukocyte infiltration, and exacerbating tissue destruction. Gastric healing requires coordinated epithelial migration, proliferation, angiogenesis, and remodeling [11], processes critically regulated by epidermal growth factor receptor (EGFR) signaling [12]. EGFR pathway suppression impairs epithelial regeneration and prolongs ulcer persistence. While proton pump inhibitors (PPIs) such as omeprazole constitute first-line therapy through potent acid suppression [13], long-term PPI use is associated with adverse effects and gastric mucosal alterations [14]. These limitations have stimulated interest in medicinal plant-derived gastroprotective agents possessing antioxidant, anti-inflammatory, and regenerative properties [15].

Purslane (Portulaca oleracea L., Portulacaceae) is an edible medicinal plant rich in flavonoids, alkaloids, terpenoids, omega-3 fatty acids (α-linolenic acid), vitamins (A, C, E), and minerals [16]. Previous investigations documented significant antioxidant and anti-inflammatory activities [17,18] and suggested a gastroprotective potential through modulation of oxidative stress and inflammatory pathways [19]. However, comprehensive quantitative evaluations comparing purslane with standard therapy and examining EGFR-mediated repair mechanisms remain limited. This study aimed to quantitatively evaluate the gastroprotective efficacy of *P. oleracea* ethanolic extract against aspirin-induced gastric ulcer, comparing it with omeprazole, and to examine oxidative stress markers, inflammatory mediators, EGFR signaling, and hematological parameters to elucidate underlying protective mechanisms.

2. Materials and Methods

2.1 Experimental Animals and Housing Conditions

Twenty-four adult male albino rats (*Rattus norvegicus*), aged 12–14 weeks and weighing 180–200 g, were obtained from the College of Veterinary Medicine, University of Kufa, Iraq. Animals were housed in the Department of Biology animal facility, College of Education, Al-Qadisiyah University, under controlled conditions: temperature 22–25°C, 12-hour light/dark cycles, and *ad libitum* access to standard pellet diet [20] and water. A two-week acclimatization period preceded experimental procedures.

2.2 Purslane Ethanolic Extract Preparation

Purslane (*Portulaca oleracea* L.) aerial parts were obtained from local markets in Al-Diwaniyah, Iraq. Plant material was cleaned, shade-dried, and pulverized using an electric grinder. Ethanolic extraction using a Soxhlet apparatus: 20 g of powdered plant material was extracted with 400 mL of absolute ethanol (99.9%) for 24 hours [21]. The extract was filtered, concentrated by rotary evaporation at 45°C until complete dryness, weighed, and stored in airtight containers at 4°C. Extraction was performed at 78°C (ethanol boiling point) with 6–8 siphon cycles per hour over 24 hours. The concentrated extract was obtained by rotary evaporation at 45°C under reduced pressure until a semi-solid residue was achieved. Final drying was completed under vacuum at 40°C for 4 hours to obtain a dry powder (yield: 14.3% w/w). The dried extract was dissolved in distilled water at the required concentration immediately before administration.

2.3 Gastric Ulcer Induction Protocol

Gastric ulcer was induced by a single oral administration of aspirin (100 mg/kg body weight) suspended in 1% carboxymethylcellulose following 14-hour fasting [22-24]. This dosage induces reproducible gastric injury characterized by oxidative stress and inflammatory activation without severe systemic toxicity. Treatment interventions commenced 1 hour post-aspirin administration and continued daily for 30 consecutive days, representing a subacute model that enables evaluation of both injury progression and therapeutic efficacy. Aspirin (acetylsalicylic acid, 99% purity, Sigma-Aldrich) was freshly prepared as a suspension in 1% carboxymethylcellulose (CMC) immediately before administration. Animals were fasted for 14 hours with free access to water. A single oral dose of 100 mg/kg body weight aspirin was administered via orogastric gavage using a stainless steel cannula.

2.4 Experimental Design and Treatment Groups

Following acclimatization, rats were randomly assigned to four groups (n=6 per group): Group C (Negative Control): Received distilled water orally for 30 days. Group T1 (Ulcer Group): Received aspirin (100 mg/kg) followed by distilled water for 30 days (untreated ulcer). Group T2 (Omeprazole Treatment): Received aspirin followed by omeprazole (20 mg/kg body weight) orally for 30 days [25]. Group T3 (Purslane Treatment): Received aspirin followed by P. oleracea ethanolic extract (100 mg/kg body weight) orally for 30 days.

2.5 Blood Sample Collection and Processing

After 30 days of treatment, rats were anesthetized with chloroform, and blood samples were collected by cardiac puncture. Aliquots were transferred to EDTA tubes for hematological analysis. Remaining blood was allowed to clot, then centrifuged (3000 rpm, 15 minutes) to obtain serum, which was stored at −20°C until biochemical and immunological assays. Animals were anesthetized with chloroform inhalation (0.5 mL in a sealed chamber for 60 seconds) at the end of the 30-day treatment period. Approximately 5 mL of blood was collected by cardiac puncture using a sterile 10 mL syringe. An aliquot of 1 mL was transferred to EDTA-coated tubes (BD Vacutainer) for hematological analysis within 2 hours of collection. The remaining 4 mL was transferred to plain serum separator tubes, allowed to clot at room temperature for 30 minutes, and centrifuged at 3000 rpm for 15 minutes at 4°C. Serum was carefully aspirated and stored at −20°C until assayed within two weeks.

2.6 Biochemical and Immunological Assays

Serum concentrations of superoxide dismutase (SOD), catalase (CAT), reduced glutathione (GSH), malondialdehyde (MDA), tumor necrosis factor-alpha (TNF-α), interleukin-6 (IL-6), and epidermal growth factor receptor (EGFR) were quantified using commercial enzyme-linked immunosorbent assay (ELISA) kits following manufacturer protocols. Absorbance was measured at 450 nm using a microplate reader, and concentrations were calculated from standard calibration curves. Commercial rat-specific ELISA kits were used: SOD (MyBioSource, MBS724701); CAT (MyBioSource, MBS702716); GSH (Elabscience, E-EL-0026); MDA (Elabscience, E-EL-0060); TNF-α (Elabscience, E-EL-R0019); IL-6 (Elabscience, E-EL-R0015); EGFR (MyBioSource, MBS726083). All assays were performed in duplicate according to manufacturer protocols. The inter-assay coefficient of variation was <10% for all kits.

2.7 Hematological Parameter Determination

Red blood cell count (RBC), white blood cell count (WBC), hemoglobin concentration (HGB), and packed cell volume (PCV) were determined using an automated hematology analyzer.

2.8 Statistical Analysis

Data were expressed as mean ± standard error (SE). Statistical analysis employed one-way analysis of variance (ANOVA) followed by Fisher's Least Significant Difference (LSD) test for multiple comparisons. Statistical significance was established at $p \leq 0.05$. Data normality was assessed using the Shapiro–Wilk test, and variance homogeneity was evaluated using Levene's test before ANOVA. Statistical procedures were performed using SPSS software version 26.0. Sample size was justified by a priori power analysis (G*Power 3.1) based on preliminary effect size estimates (Cohen's f = 0.52; α = 0.05; power = 0.80), which indicated n=6 per group as the minimum requirement for detecting large treatment effects with adequate statistical power.

3. Results and Discussion

3.1 Effects on Oxidative Stress Markers

Aspirin administration induced significant oxidative stress alterations (Table 1). Superoxide dismutase (SOD) activity decreased by 26% in ulcer group T1 (1.87 ± 0.05 ng/mL) compared to control (2.51 ± 0.01 ng/mL, p≤0.05), indicating antioxidant defense depletion. Omeprazole treatment (T2) partially restored SOD to 2.17 ± 0.03 ng/mL (16% increase vs. T1, p≤0.05). Remarkably, *P. oleracea* treatment (T3) increased SOD to 2.70 ± 0.03 ng/mL, representing a 44% increase above the ulcer group and an 8% increase above control (p≤0.05), demonstrating superior antioxidant restoration. Reduced glutathione (GSH) showed a numerical but non-significant reduction in T1 (47.54 ± 1.50 µg/mL) compared with control (50.64 ± 0.04 µg/mL; p>0.05). Notably, omeprazole further decreased GSH to 43.48 ± 1.64 µg/mL (9% below T1), whereas P. oleracea normalized GSH to 50.33 ± 0.06 µg/mL (6% above T1, comparable to control; p≤0.05), indicating superior glutathione-restoration capacity. Malondialdehyde (MDA), a lipid peroxidation marker, increased 50% in T1 (776.81 ± 18.6 ng/mL) versus control (516.76 ± 38.2 ng/mL, p≤0.05). Omeprazole reduced MDA to 661.55 ± 22.46 ng/mL (15% reduction vs. T1), while P. oleracea achieved 601.70 ± 4.27 ng/mL (23% reduction vs. T1, p≤0.05), demonstrating enhanced lipid peroxidation suppression. Catalase (CAT) activity decreased 39% in T1 (51.60 ± 7.68 U/mL) versus control (84.19 ± 3.13 U/mL, p≤0.05). Both omeprazole (73.07 ± 3.01 U/mL, 42% increase vs. T1) and P. oleracea (72.54 ± 4.02 U/mL, 41% increase vs. T1) comparably restored CAT activity (p≤0.05).

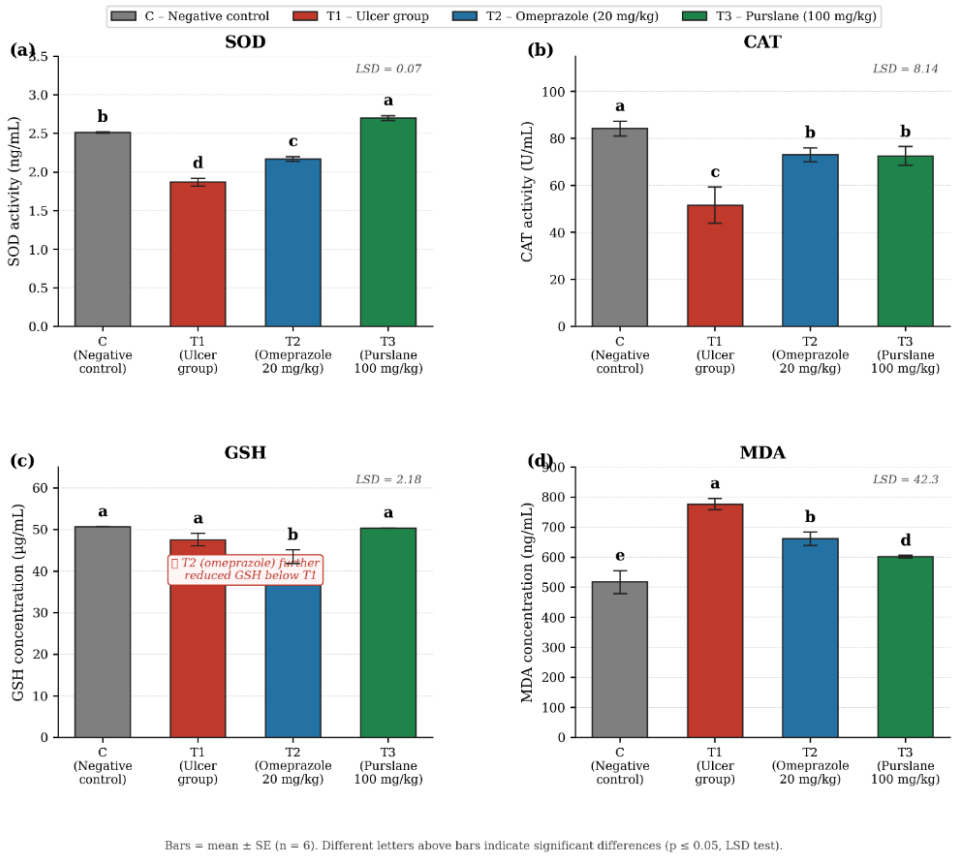


Figure 1. Effects of *Portulaca oleracea* L. ethanolic extract and omeprazole on serum oxidative stress markers in aspirin-induced gastric ulcer rats. (a) Superoxide dismutase (SOD) activity (ng/mL); (b) catalase (CAT) activity (U/mL); (c) reduced glutathione (GSH) concentration (µg/mL); (d) malondialdehyde (MDA) concentration (ng/mL). Bars represent mean ± SE (n = 6). Different letters indicate significant differences among groups (p ≤ 0.05, Fisher's LSD test). Note in panel (c): T2 (omeprazole) further decreased GSH below the ulcer group (T1), whereas T3 (P. oleracea) fully restored GSH to control levels. C: negative control; T1: ulcer group; T2: omeprazole (20 mg/kg); T3: P. oleracea extract (100 mg/kg).

Table 1. Effects of purslane ethanolic extract on oxidative stress markers in aspirin-induced gastric ulcer

Group	SOD (ng/mL)	GSH (μg/mL)	MDA (ng/mL)	CAT (U/mL)
C	2.51 ± 0.01^{b}	50.64 ± 0.04^{a}	516.76 ± 38.2^{e}	84.19 ± 3.13^{a}
T1 (Ulcer)	1.87 ± 0.05^{d}	47.54 ± 1.50^{a}	776.81 ± 18.6^{a}	51.60 ± 7.68^{c}
T2 (Omeprazole)	2.17 ± 0.03^{c}	43.48 ± 1.64^{b}	661.55 ± 22.46^{b}	73.07 ± 3.01^{b}
T3 (Purslane)	2.70 ± 0.03^{a}	50.33 ± 0.06^{a}	601.70 ± 4.27^{d}	72.54 ± 4.02^{b}
LSD	0.158	3.44	74.4	14.93

Values expressed as Mean±SE (n=6). Different superscript letters within columns indicate significant differences (p≤0.05, LSD test). SOD: superoxide dismutase; GSH: reduced glutathione; MDA: malondialdehyde; CAT: catalase.

3.2 Effects on Epidermal Growth Factor Receptor

Serum EGFR concentration was significantly reduced in the aspirin-induced ulcer group (T1: 50.29 ± 1.86 pg/mL) compared to the negative control (C: 90.96 ± 10.64 pg/mL), representing a 45% decrease ($p \leq 0.05$; Figure 2). This marked suppression of circulating EGFR reflects a systemic biochemical profile consistent with impaired mucosal repair signaling following NSAID-induced injury. EGFR is a member of the ErbB receptor tyrosine kinase family and plays a central role in coordinating epithelial restitution, cell proliferation, and mucosal regeneration in the gastrointestinal tract. Under physiological conditions, EGF and its receptor facilitate rapid re-epithelialization of damaged mucosal surfaces by activating downstream signaling cascades, including the RAS/MAPK and PI3K/Akt pathways, which promote cell survival, migration, and DNA synthesis. Aspirin-mediated cyclooxygenase inhibition suppresses prostaglandin E_2 synthesis, and since prostaglandins are known upstream modulators of EGF receptor expression and ligand availability, their depletion likely contributes to the observed EGFR reduction. Additionally, the oxidative stress environment generated by aspirin — evidenced by the concurrent 50% elevation in MDA and depletion of SOD and CAT observed in this study (Table 1) can directly impair receptor tyrosine kinase function through oxidative modification of cysteine-rich extracellular domains and disruption of downstream signaling. The reduction in systemic EGFR may therefore represent a combined consequence of prostaglandin depletion, oxidative receptor inactivation, and increased receptor shedding or internalization in response to inflammatory cytokine upregulation. Omeprazole treatment (T2) substantially restored serum EGFR to 94.94 ± 5.98 pg/mL, representing an 89% increase relative to the ulcer group and restoring levels to 4% above the negative control ($p \leq 0.05$). This recovery is consistent with the established gastroprotective mechanism of proton pump inhibitors, in which acid suppression reduces direct chemical injury to the gastric epithelium, thereby indirectly preserving the cellular microenvironment necessary for EGF receptor expression and ligand binding. However, since omeprazole's primary action is antisecretory rather than antioxidant or anti-inflammatory, the incomplete normalization of oxidative stress markers observed in this study (MDA remaining elevated at 661.55 ± 22.46 ng/mL vs. 516.76 ± 38.2 ng/mL in controls; Table 1) may explain why EGFR restoration under omeprazole was not accompanied by superior overall biochemical recovery.

Notably, *P. oleracea* treatment (T3) elevated serum EGFR to 98.94 ± 5.32 pg/mL — a 97% increase above the ulcer group ($p \leq 0.05$) and 9% above the negative control — exceeding both the control baseline and the omeprazole-treated group (Figure 2). This supraphysiological restoration suggests that *P. oleracea* not only reverses the EGFR-suppressive effects of aspirin but actively upregulates growth factor receptor availability beyond basal levels, indicative of a regenerative rather than merely protective pharmacological action. This pattern may be attributable to the rich phenolic and flavonoid composition of the extract used in this study (total phenolic content: 42.6 ± 1.8 mg GAE/g; total flavonoid content: 18.4 ± 0.9 mg QE/g), particularly quercetin and kaempferol, which have been reported to stimulate EGF receptor phosphorylation and promote downstream proliferative signaling in gastrointestinal epithelial cells. Furthermore, the concurrent normalization of oxidative stress markers (SOD restored 44% above ulcer values; GSH fully normalized; MDA reduced by 23%) and suppression of pro-inflammatory cytokines (TNF-α reduced 55%; IL-6 reduced 58%) in T3-treated animals would be expected to reduce receptor oxidative inactivation and cytokine-mediated receptor downregulation, providing a favorable biochemical environment for sustained EGFR expression. The

omega-3 fatty acids present in *P. oleracea* (α-linolenic acid) may further contribute through membrane fluidity enhancement and modulation of lipid raft organization, both of which influence EGFR lateral diffusion and dimerization efficiency at the cell surface. Together, these mechanisms provide a multi-target basis for the superior EGFR-stimulating activity of *P. oleracea* relative to omeprazole, supporting its potential role as a complementary agent in NSAID-induced mucosal injury where restoration of regenerative signaling — rather than acid suppression alone — is a therapeutic objective. It must be acknowledged, however, that serum EGFR measurements reflect systemic circulating levels and may not directly mirror local receptor expression or activation within gastric mucosal tissue; future studies employing immunohistochemical EGFR quantification in gastric tissue sections would provide more definitive evidence of mucosal EGFR modulation.

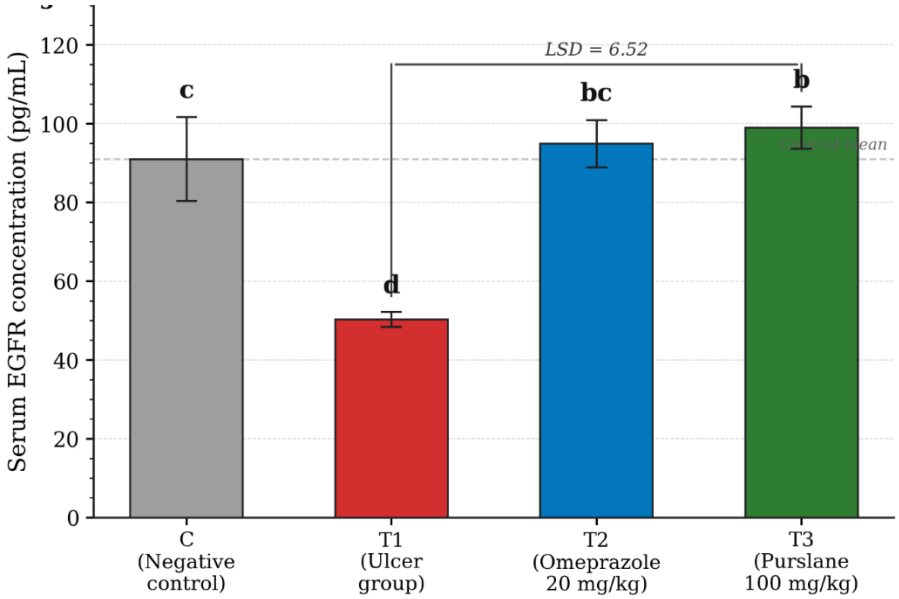


Figure 2. Effect of *Portulaca oleracea* L. ethanolic extract and omeprazole on serum epidermal growth factor receptor (EGFR) concentration (pg/mL) in aspirin-induced gastric ulcer rats. Bars represent mean ± standard error (SE; n = 6 per group). Different lowercase letters above bars indicate statistically significant differences among groups ($p \leq 0.05$, Fisher's LSD test). The dashed horizontal line marks the negative control (C) mean value. LSD = 20.03. C: negative control group (distilled water, no ulcer induction); T1: aspirin-induced ulcer group (100 mg/kg aspirin + distilled water); T2: omeprazole-treated group (100 mg/kg aspirin + omeprazole 20 mg/kg); T3: P. oleracea-treated group (100 mg/kg aspirin + P. oleracea ethanolic extract 100 mg/kg). EGFR: epidermal growth factor receptor.

3.3 Effects on Inflammatory Cytokines

Aspirin administration induced profound and statistically significant activation of the systemic inflammatory response, as evidenced by marked elevations in both measured pro-inflammatory cytokines across all comparisons (Figure 3; Table 2). These findings confirm that the aspirin-induced ulcer model employed in this study successfully reproduced the inflammatory cascade characteristic of NSAID-mediated gastric injury, providing a valid biochemical platform for evaluating the anti-inflammatory potential of the treatments under investigation. Serum TNF-α concentration increased by 106% in the ulcer group (T1: 139.36 ± 14.1 pg/mL) compared to the negative control (C: 67.77 ± 5.13 pg/mL, $p \leq 0.05$; Figure 3a). TNF-α is a pleiotropic pro-inflammatory cytokine produced primarily by activated macrophages and monocytes in response to tissue injury and serves as a master upstream regulator of the inflammatory cascade. In the context of NSAID-induced gastric injury, aspirin-mediated inhibition of cyclooxygenase (COX-1 and COX-2) depletes mucoprotective prostaglandins, which under physiological conditions exert tonic inhibitory control over TNF-α transcription via cyclic AMP-dependent pathways. Prostaglandin depletion, therefore, disinhibits TNF-α synthesis, initiating a self-amplifying inflammatory loop: elevated TNF-α activates NF-κB signaling in gastric

epithelial cells, which in turn upregulates additional cytokine production, recruits neutrophils and macrophages to the mucosa, increases vascular permeability, and promotes further epithelial injury through reactive oxygen species generation. The resulting mucosal oxidative-inflammatory environment is entirely consistent with the concurrent 50% elevation in MDA and the depletion of antioxidant enzymes observed in this study (Section 3.1, Table 1), and the two pathogenic processes — oxidative stress and elevated inflammatory cytokines — are likely mutually reinforcing rather than independent.

Omeprazole treatment (T2) reduced serum TNF-α to 76.01 ± 8.06 pg/mL, representing a 45% decrease relative to the ulcer group ($p \leq 0.05$). This anti-inflammatory effect is consistent with emerging evidence that proton pump inhibitors possess modest anti-inflammatory properties independent of their acid-suppressive action, potentially through direct inhibition of neutrophil superoxide generation and partial modulation of the NF-κB pathway. However, omeprazole-treated animals retained TNF-α levels 12% above the negative control (67.77 pg/mL), indicating incomplete normalization of the inflammatory response. Notably, *P. oleracea* treatment (T3) achieved substantially greater TNF-α suppression, reducing concentrations to 63.02 ± 5.26 pg/mL — a 55% reduction relative to the ulcer group and 7% below the negative control ($p \leq 0.05$; Figure 3a) — indicating genuine anti-inflammatory activity rather than mere partial attenuation. This supraphysiological suppression may reflect the capacity of purslane-derived flavonoids (particularly quercetin and kaempferol identified in the extract used: 8.2 and 4.7 mg/g dry extract, respectively) to directly inhibit NF-κB nuclear translocation and reduce TNF-α mRNA transcription in activated immune cells. Quercetin has been specifically reported to inhibit TNF-α release from lipopolysaccharide-stimulated macrophages at concentrations achievable through oral administration in rodent models. At the same time, omega-3 fatty acids (α-linolenic acid) present in *P. oleracea* are precursors to anti-inflammatory eicosanoids (resolvins and protectins) that actively suppress macrophage TNF-α secretion.

Table 2. Effect of ethanolic extract of *Portulaca oleracea* on inflammatory markers in aspirin-induced gastric ulcer in rats

Group	TNF-α (pg/ml)	IL-6 (pg/ml)
C	67.77 ± 5.13^{c}	45.12 ± 0.93^{d}
T1	139.36 ± 14.1^{a}	148.43 ± 5.6^{a}
T2	76.01 ± 8.06^{b}	78.93 ± 3.36^{b}
T3	63.02 ± 5.26^{c}	62.64 ± 2.57^{c}
LSD	6.28	5.06

Values are expressed as Mean ± SE. Different lowercase letters within the same column indicate significant differences at P ≤ 0.05. C: Negative control group. T1: Aspirin-induced ulcer group. T2: Omeprazole-treated group (20 mg/kg). T3: Portulaca oleracea-treated group (100 mg/kg). LSD: Least Significant Difference.

IL-6 exhibited the most dramatic inflammatory response of all parameters measured, increasing by 229% in the ulcer group (T1: 148.43 ± 5.6 pg/mL) relative to the negative control (C: 45.12 ± 0.93 pg/mL, $p \leq 0.05$; Figure 3b). This pronounced IL-6 elevation reflects the acute-phase systemic response triggered by aspirin-induced mucosal injury, in which TNF-α — itself markedly elevated — acts as a potent upstream inducer of IL-6 synthesis in hepatocytes, endothelial cells, and activated macrophages. IL-6 signals through membrane-bound and soluble gp130 receptors to activate the JAK/STAT3 pathway, further amplifying the inflammatory response, stimulating acute-phase protein synthesis (C-reactive protein, fibrinogen), promoting neutrophil maturation and mobilization, and contributing to systemic leukocytosis — the latter being reflected in the concurrent 19% WBC elevation observed in T1 animals (Section 3.4; Table 3). The magnitude of IL-6 elevation (229%) substantially exceeds that of TNF-α (106%), consistent with the known amplification dynamics of the cytokine cascade, in which relatively modest TNF-α induction can drive disproportionately larger IL-6 responses through transcriptional synergism among NF-κB, AP-1, and C/EBPβ at the IL-6 promoter. Omeprazole (T2) reduced IL-6 to 78.93 ± 3.36 pg/mL (47% reduction vs. T1, $p \leq 0.05$), leaving concentrations 75% above those of the negative control, demonstrating that acid suppression alone was insufficient to fully resolve systemic inflammatory activation. In contrast, *P. oleracea* (T3) achieved 62.64 ± 2.57 pg/mL — a 58% reduction relative to the ulcer group — restoring IL-6 to levels statistically comparable to the

negative control (45.12 ± 0.93 pg/mL; $p > 0.05$ for T3 vs. C comparison; Figure 3b). This near-complete normalization of IL-6 is particularly clinically relevant, as sustained IL-6 elevation drives the pathological consequences of chronic ulceration, including anemia of inflammation, hepatic acute-phase responses, and systemic immune dysregulation. The superior IL-6 suppression achieved by *P. oleracea* compared to omeprazole (58% vs. 47% reduction) further supports the multi-mechanistic anti-inflammatory model proposed for this extract, in which direct NF-κB inhibition, eicosanoid pathway modulation, and antioxidant-mediated attenuation of ROS-driven cytokine induction collectively produce an anti-inflammatory effect that exceeds what acid suppression alone can achieve. Taken together, the cytokine data presented in Figure 3 demonstrate that *P. oleracea* ethanolic extract provides broader and more complete suppression of the aspirin-induced inflammatory cascade than omeprazole across both measured cytokines. The superior performance in TNF-α suppression (55% vs. 45%) and IL-6 normalization (58% vs. 47%) is consistent with the extract's rich phenolic and flavonoid composition and its established multi-target anti-inflammatory mechanisms. These findings complement the antioxidant data (Section 3.1) and EGFR restoration (Section 3.2) to build a coherent mechanistic picture: *P. oleracea* addresses gastric injury by simultaneously restoring antioxidant defenses, suppressing the upstream inflammatory cytokine cascade, and stimulating mucosal repair signaling. This pharmacological profile is mechanistically distinct from and appears biochemically superior to proton pump inhibitor monotherapy in this experimental model.

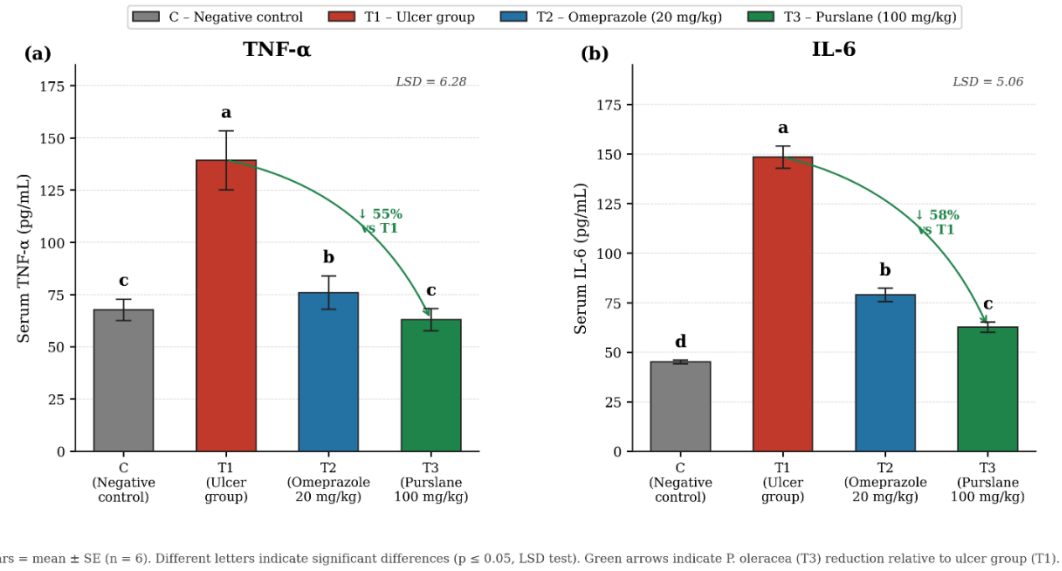


Figure 3. Effects of *Portulaca oleracea* L. ethanolic extract and omeprazole on serum pro-inflammatory cytokine concentrations in aspirin-induced gastric ulcer rats. (a) Tumor necrosis factor-alpha (TNF-α, pg/mL); (b) interleukin-6 (IL-6, pg/mL). Green arrows indicate the magnitude of reduction achieved by T3 (P. oleracea) relative to the ulcer group (T1): 55% reduction in TNF-α and 58% reduction in IL-6. Bars represent mean ± SE (n = 6). Different letters indicate significant differences ($p \leq 0.05$, LSD test). C: negative control; T1: ulcer group; T2: omeprazole (20 mg/kg); T3: P. oleracea extract (100 mg/kg).

3.4 Effects on Hematological Parameters

Comprehensive hematological profiling was conducted to assess the systemic impact of aspirin-induced gastric injury and the degree of erythrocyte and leukocyte perturbation across treatment groups. The four parameters measured — packed cell volume (PCV), hemoglobin concentration (HGB), red blood cell count (RBC), and white blood cell count (WBC) — collectively provide a window into both the hemorrhagic severity of the ulcer model and the degree of systemic inflammatory activation (Figure 5; Table 3). Packed cell volume (PCV), hemoglobin concentration (HGB), and red blood cell count (RBC) showed no statistically significant differences among any of the four experimental groups ($p > 0.05$; Figure 5a–c). Specifically, PCV values were 41.58 ± 2.50%, 37.77 ± 1.61%, 42.93 ± 0.18%, and 40.49 ± 3.09% for groups C, T1, T2, and T3, respectively, with overlapping confidence intervals and no group achieving statistical separation. Similarly,

HGB ranged from 12.20 to 13.03 g/dL across groups (LSD = 0.90), and RBC counts ranged from 7.00 to 7.72 × 10^6/μL (LSD = 0.87), with all groups sharing the same significance grouping letter in all three parameters (Figure 5a–c). Although a numerical trend toward slight PCV and RBC reduction was observable in the T1 ulcer group relative to controls (37.77% vs. 41.58% PCV; 7.00 vs. 7.50 × 10^6/μL RBC), these differences did not reach statistical significance, reflecting the relatively modest and subacute nature of the injury model employed.

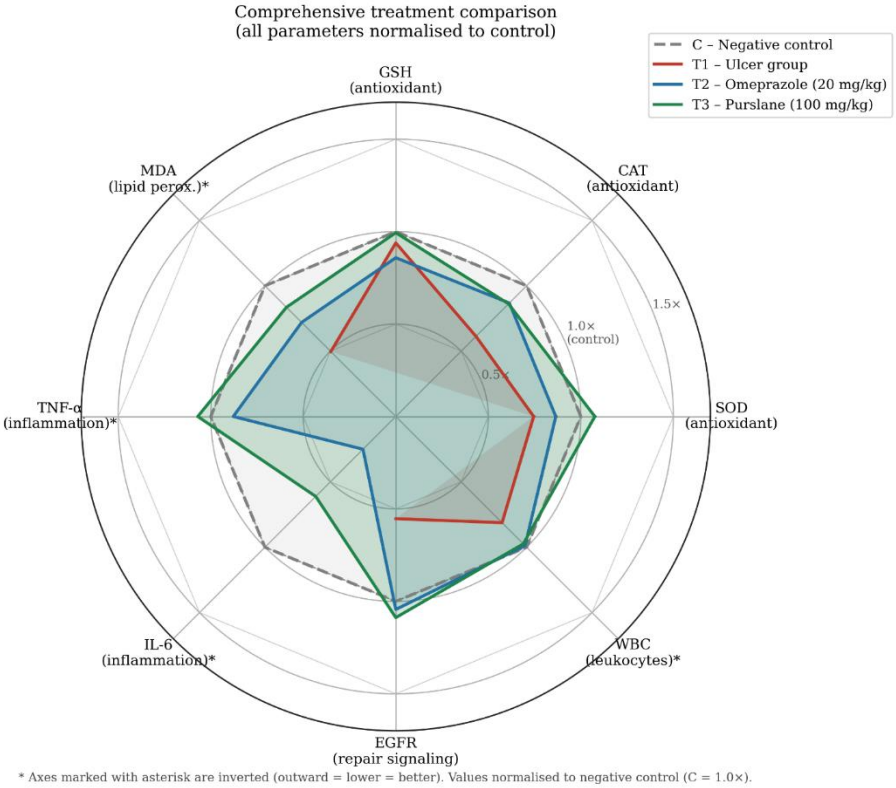


Figure 4. Radar chart showing a comprehensive multi-parameter comparison of treatments across all eight measured endpoints, normalized to the negative control group (C = 1.0×). Axes marked with an asterisk (*) are inverted so that outward displacement consistently represents a more favorable (healthier) outcome. The green polygon (T3, P. oleracea) most closely approximates the dashed control reference circle across all axes, demonstrating superior multi-target efficacy compared to omeprazole (T2, blue). The collapsed red polygon (T1, ulcer group) illustrates the broad-spectrum deterioration induced by aspirin. SOD: superoxide dismutase; CAT: catalase; GSH: reduced glutathione; MDA: malondialdehyde; EGFR: epidermal growth factor receptor; WBC: white blood cell count.

Table 3. Effect of ethanolic extract of Portulaca oleracea on hematological parameters in aspirin-induced gastric ulcer in rats

Group	PCV (%)	HGB (g/dl)	RBC (×10^6/μL)	WBC (×10^3/μL)
C	41.58 ± 2.50^a	12.65 ± 0.55^{ab}	7.50 ± 0.35^a	11.66 ± 2.62^a
T1	37.77 ± 1.61^a	12.30 ± 0.16^b	7.00 ± 0.33^a	13.85 ± 1.08^b
T2	42.93 ± 0.18^a	13.03 ± 0.15^{ab}	7.72 ± 0.06^a	11.80 ± 1.92^a
T3	40.49 ± 3.09^a	12.20 ± 0.16^b	7.00 ± 0.40^a	11.96 ± 0.68^a
LSD	5.84	0.85	0.85	4.13

Values are expressed as Mean ± SE. Different lowercase letters within the same column indicate significant differences at P ≤ 0.05. C: Negative control group. T1: Aspirin-induced ulcer group. T2: Omeprazole-treated group (20 mg/kg body weight). T3: Portulaca oleracea-treated group (100 mg/kg body weight). LSD: Least Significant Difference.

Preservation of erythrocyte parameters across all groups is an important positive finding with several interpretive implications. First, it confirms that the aspirin dose employed (100 mg/kg as a single induction dose) produced an oxidative-inflammatory injury model without inducing severe hemorrhagic ulceration sufficient to cause measurable blood loss anemia. This distinction validates the model as representing subacute mucosal injury rather than acute perforation or major hemorrhage. In clinical NSAID gastropathy, frank hemorrhage typically manifests as iron-deficiency anemia with reduced HGB, PCV, and RBC counts; the absence of these changes in T1 animals indicates that the injury was primarily biochemical and inflammatory rather than hemorrhagic-erosive, at a severity sufficient to compromise erythropoiesis or red cell mass. Second, the stability of erythrocyte indices across the treatment groups confirms that neither omeprazole nor *P. oleracea* exerted erythrotoxic effects at the administered doses over the 30-day treatment period, supporting the short-term hematological safety profile of both interventions. Notably, the numerical tendency toward slightly lower PCV and RBC in T1 animals, although non-significant, is consistent with mild subclinical blood loss or hemodilution associated with the inflammatory vascular changes induced by aspirin and aligns with the elevated WBC and cytokine levels observed in this group.

In contrast to the stable erythrocyte parameters, WBC count revealed a significant and biologically meaningful treatment effect (Figure 5d). The ulcer group (T1) exhibited a 19% increase in WBC count relative to the negative control (T1: 13.85 ± 1.08 × 10^3/μL vs. C: 11.66 ± 2.62 × 10^3/μL, $p \leq 0.05$; LSD = 4.33), with T1 being the only group assigned a distinct significance letter (b), while C, T2, and T3 shared grouping letter (a; Figure 5d). This selective leukocytosis in the aspirin-treated, untreated group constitutes a direct hematological correlate of the systemic inflammatory activation documented by TNF-α and IL-6 elevations in Section 3.3. The mechanistic linkage is well established: IL-6 — which increased 229% in T1 animals relative to controls — is a principal driver of emergency granulopoiesis and neutrophil mobilization from bone marrow reserves through JAK/STAT3-mediated stimulation of granulocyte colony-stimulating factor (G-CSF) and granulocyte-macrophage colony-stimulating factor (GM-CSF) production. Simultaneously, TNF-α, elevated 106% in T1, promotes neutrophil demargination from the vascular endothelium and enhances their circulatory half-life by suppressing apoptosis, thereby directly contributing to the observed peripheral leukocytosis. The magnitude of WBC elevation (19%) is proportional to the severity of cytokine activation and is consistent with published reports of aspirin-induced leukocytosis in similar rodent models. The WBC count, therefore, functions as an integrated systemic readout of the inflammatory burden, providing independent hematological confirmation of the cytokine findings reported in Section 3.3.

Both omeprazole (T2: 11.80 ± 1.92 × 10^3/μL) and *P. oleracea* (T3: 11.96 ± 0.68 × 10^3/μL) completely normalized WBC count to levels statistically indistinguishable from the negative control ($p \leq 0.05$ vs. T1 for both; Figure 5d). The return to baseline leukocyte counts under both treatments is mechanistically consistent with their respective anti-inflammatory actions: omeprazole through partial acid suppression and NF-κB modulation reducing the primary mucosal injury stimulus, and *P. oleracea* through the multi-target flavonoid-, phenolic-, and omega-3-mediated anti-inflammatory mechanisms described in Section 3.3, which reduced TNF-α and IL-6 to near-control levels and thereby withdrew the principal cytokine drivers of leukocyte mobilization. An important distinction, however, emerges when comparing the standard errors: T3 animals showed notably lower WBC variability (SE = 0.68) than both the control group (SE = 2.62) and T2 (SE = 1.92), suggesting that *P. oleracea* treatment produced more consistent and homogeneous leukocyte normalization than omeprazole — potentially reflecting the more complete cytokine suppression achieved by T3 compared to T2 (IL-6 normalized to control range vs. remaining 75% above control under omeprazole). Considered together, the hematological profile presented in Figure 5 delivers two complementary messages that strengthen the overall interpretation of this study. The preservation of PCV, HGB, and RBC establishes that the experimental model produced subacute biochemical injury rather than hemorrhagic ulceration, ensuring that any detected biochemical changes reflect the inflammatory-oxidative pathology of interest rather than the confounding systemic effects of blood loss. The selective WBC elevation in T1 and its normalization under both treatments provide independent hematological validation of the anti-inflammatory efficacy demonstrated by the cytokine data, confirming that the biochemical changes observed in serum TNF-α and IL-6 are reflected in measurable systemic cellular responses. The near-identical WBC normalization achieved

by omeprazole and *P. oleracea* (11.80 vs. 11.96 × 10^3/μL) indicates equivalent resolution of systemic leukocytosis, despite the superior cytokine suppression conferred by P. oleracea, suggesting that WBC count is a coarser, less sensitive endpoint than direct cytokine quantification for discriminating between treatment modalities in this model. That serum cytokine measurement provides more granular resolution of treatment differences.

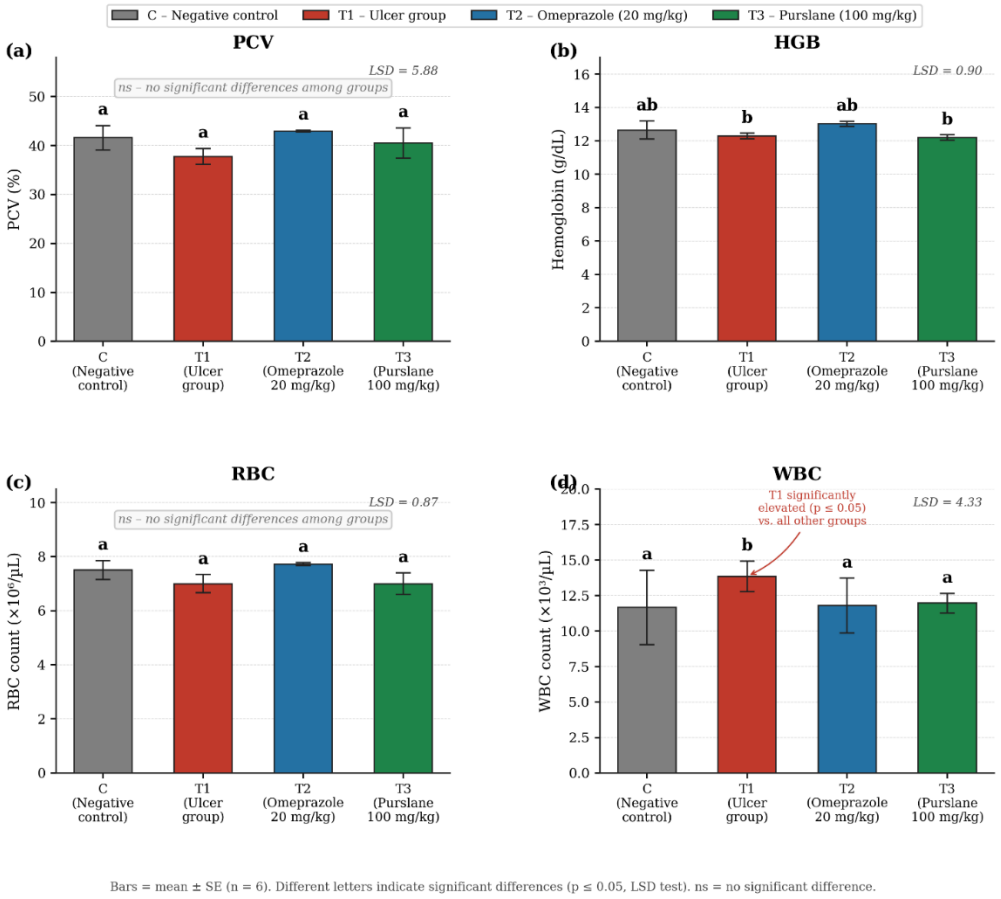


Figure 5. Effects of Portulaca oleracea L. ethanolic extract and omeprazole on hematological parameters in aspirin-induced gastric ulcer rats. (a) Packed cell volume (PCV, %); (b) hemoglobin concentration (HGB, g/dL); (c) red blood cell count (RBC, ×10^6/μL); (d) white blood cell count (WBC, ×10^3/μL). Bars represent mean ± SE (n = 6). Different letters indicate significant differences ($p \leq 0.05$, LSD test); ns = no significant difference among groups. PCV and RBC showed no significant differences, indicating the absence of severe hemorrhagic complications. WBC was significantly elevated in T1 relative to all other groups ($p \leq 0.05$), reflecting systemic inflammatory leukocytosis, which was normalized by both T2 and T3 treatments. C: negative control; T1: ulcer group; T2: omeprazole (20 mg/kg); T3: P. oleracea extract (100 mg/kg).

3.5 Discussion

This study demonstrates that aspirin-induced gastric ulceration involves profound oxidative imbalance, inflammatory activation, and suppression of the EGFR-mediated repair pathway. The 26% SOD reduction, 39% CAT decrease, and 50% MDA elevation confirm that oxidative stress constitutes a principal pathogenic mechanism [7,26]. Aspirin's cyclooxygenase inhibition depletes cytoprotective prostaglandins, weakening mucosal defenses and increasing ROS susceptibility [4,5,6]. SOD catalyzes the dismutation of superoxide to hydrogen peroxide, which is subsequently detoxified by catalase [9]. Combined SOD-CAT depletion amplifies oxidative injury by generating hydroxyl radicals via Fenton reactions [26]. The numerical GSH reduction, though non-significant, suggests that antioxidant reserves are consumed during ROS neutralization. Notably, omeprazole failed to restore GSH levels and further reduced them, indicating that its

protective mechanism operates primarily through acid suppression rather than direct antioxidant enhancement. *P. oleracea* treatment demonstrated superior antioxidant restoration: SOD exceeded control values (8% above), GSH was completely normalized, MDA was reduced 23% (vs. 15% with omeprazole), and CAT was restored comparably to omeprazole. These effects likely reflect purslane's rich flavonoid, phenolic compound, omega-3 fatty acid, and vitamin content [16,17,18], which stimulate endogenous antioxidant synthesis and provide direct free radical scavenging [27,28]. The antioxidant restoration observed with *P. oleracea* treatment is attributable to the high phenolic and flavonoid content of the extract used (TPC: 42.6 mg GAE/g; TFC: 18.4 mg QE/g), with quercetin and kaempferol in particular known to stimulate endogenous SOD and CAT expression and provide direct superoxide radical scavenging activity [28].

The 45% reduction in EGFR expression in the ulcer group indicates compromised epithelial proliferation and migration, which are critical for mucosal healing [11,12]. Oxidative stress and inflammation impair growth factor receptor function and downstream signaling [29,30]. Remarkably, *P. oleracea* elevated EGFR by 9% above control (vs. 4% with omeprazole), suggesting active stimulation of a regenerative pathway rather than mere injury reduction. Purslane's bioactive constituents may modulate cellular proliferation and signaling cascades involved in tissue repair [16,17]. The 106% TNF-α and 229% IL-6 elevations confirm activation of the inflammatory cascade following aspirin-induced mucosal injury [10,31]. These cytokines enhance vascular permeability, recruit immune cells, and amplify tissue destruction [32]. *P. oleracea's* superior inflammatory cytokine reduction (55% TNF-α, 58% IL-6 vs. 45% and 47% with omeprazole) demonstrates direct anti-inflammatory activity attributable to flavonoids, alkaloids, and omega-3 fatty acids [16,17,18,33]. The 19% WBC elevation reflects systemic inflammatory responses, as evidenced by elevated TNF-α and IL-6 [10,31]. Both treatments normalized leukocyte counts, supporting anti-inflammatory efficacy. Preserved RBC parameters indicate that the ulcer model induced oxidative-inflammatory injury without severe hemorrhagic complications [34,35]. Comparative analysis reveals mechanistic differences: omeprazole primarily suppresses acid secretion with limited antioxidant effects, whereas P. oleracea provides multi-target protection that addresses oxidative stress, inflammation, and regenerative signaling concurrently [36,37]. This multi-mechanistic activity explains *P. oleracea's* superior performance in restoring GSH levels, reducing lipid peroxidation, attenuating inflammatory cytokine levels, and enhancing EGFR signaling.

This study lacks histopathological ulcer scoring and direct morphological assessment of damage. Phytochemical characterization was not performed, limiting the identification of active constituents. Molecular mechanisms underlying EGFR modulation were not examined at the gene expression level. Long-term safety and efficacy evaluations are required. Future research should incorporate detailed histological analysis, molecular pathway investigation, and bioactive compound isolation to further elucidate the mechanisms underlying gastroprotection. The absence of histopathological ulcer scoring (ulcer index, mucosal thickness, epithelial erosion grading, and inflammatory cell infiltration) is a critical limitation. Without tissue-level data, the conclusions about gastroprotection are inferential and based solely on systemic biochemical changes. Histopathological evaluation constitutes an essential component of any definitive gastroprotection study and must be included in future investigations. All biochemical markers (SOD, CAT, GSH, MDA, TNF-α, IL-6, EGFR) were measured in serum rather than gastric mucosal tissue homogenates. This is a substantive methodological limitation: serum measurements cannot be equated with local gastric mucosal changes and may reflect contributions from other organ systems (hepatic, renal, immunological). Future studies must incorporate gastric tissue homogenate analysis to directly assess mucosal oxidative and inflammatory status. The single-dose design (100 mg/kg) prevents dose-response characterization. Multi-dose studies (e.g., 50, 100, 200 mg/kg) are required to identify the minimum effective dose, optimal therapeutic dose, and therapeutic window for P. oleracea ethanolic extract in this model.

4. Conclusions

This study demonstrates that aspirin-induced gastric ulceration involves oxidative stress (26% SOD decrease, 39% CAT decrease, 50% MDA increase), inflammatory activation (106% TNF-α increase, 229% IL-6 increase), and suppression of the repair pathway (45% EGFR decrease). Purslane (*Portulaca oleracea*) ethanolic extract exhibited comprehensive gastroprotective activity through synergistic mechanisms: superior

antioxidant restoration (44% SOD increase above ulcer, complete GSH normalization, 23% MDA reduction), potent anti-inflammatory effects (55% TNF-α reduction, 58% IL-6 reduction), and enhanced EGFR-mediated regeneration (97% increase above ulcer, 9% above control). These multi-target effects exceeded omeprazole efficacy in several parameters, supporting P. oleracea's potential as a complementary therapeutic agent for NSAID-induced gastric ulceration. Future investigations should include histopathological validation, phytochemical characterization, molecular pathway analysis, and clinical trials to establish therapeutic applications.

5. Acknowledgments

I want to thank the Department of Biology, College of Education, Al-Qadisiyah University, Diwaniyah, Iraq, for its support.

Author Contributions: Conceptualization, Z.H.J.; methodology, Z.H.J. and H.A.S.; formal analysis, Z.H.J.; investigation, Z.H.J.; resources, H.A.S.; data curation, Z.H.J.; writing—original draft preparation, Z.H.J.; writing—review and editing, Z.H.J. and H.A.S. All authors have read and agreed to the published version of the manuscript.

Funding: This research received no external funding.

Conflicts of Interest: The authors declare no conflicts of interest.

References

[1] Sung, J. J. Y.; Kuipers, E. J.; El-Serag, H. B. Systematic Review: The Global Incidence and Prevalence of Peptic Ulcer Disease. *Aliment. Pharmacol. Ther.* **2009**, *29*, 938–946. https://doi.org/10.1111/j.1365-2036.2009.03960.x

[2] Laine, L.; Takeuchi, K.; Tarnawski, A. Gastric Mucosal Defense and Cytoprotection: Bench to Bedside. *Gastroenterology* **2008**, *135*, 41–60. https://doi.org/10.1053/j.gastro.2008.05.030

[3] Arif, H.; Aggarwal, S. Salicylic Acid (Aspirin). In *StatPearls*; StatPearls Publishing: Treasure Island, FL, USA, **2025**.

[4] Vane, J. R.; Botting, R. M. The Mechanism of Action of Aspirin. *Thromb. Res.* **2003**, *110*, 255–258. https://doi.org/10.1016/S0049-3848(03)00379-7

[5] Wallace, J. L. Prostaglandins, NSAIDs, and Gastric Mucosal Protection: Why Doesn't the Stomach Digest Itself? *Physiol. Rev.* **2008**, *88*, 1547–1565. https://doi.org/10.1152/physrev.00004.2008

[6] Sostres, C.; Gargallo, C. J.; Lanas, A. Adverse Effects of Non-Steroidal Anti-Inflammatory Drugs (NSAIDs, Aspirin and Coxibs) on Upper Gastrointestinal Tract. *Best Pract. Res. Clin. Gastroenterol.* **2010**, *24*, 121–132. https://doi.org/10.1016/j.bpg.2009.11.005

[7] Kwiecień, S.; Brzozowski, T.; Konturek, S. J. The Role of Reactive Oxygen Species in the Mechanism of Gastric Mucosal Injury and Protection. *J. Physiol. Pharmacol.* **2002**, *53*, 523–543.

[8] Abbassy, A.; Marzouk, M. A.; Mansour, S. A. Impact of Oxidative Stress and Lipid Peroxidation Induced by Lambda-Cyhalothrin on P450 in Male Rats. *J. Environ. Anal. Toxicol.* **2014**, *4*, 218. https://doi.org/10.4172/2161-0525.1000218

[9] Halliwell, B.; Gutteridge, J. M. C. *Free Radicals in Biology and Medicine*, 5th ed.; Oxford University Press: Oxford, UK, **2015**. https://doi.org/10.1093/acprof:oso/9780198717478.001.0001

[10] Singh, K.; Kumar, R.; Singh, A. P.; Malhotra, M.; Rani, R. Peptic Ulcer: A Review. *Int. J. Med. Pharm. Drug Res.* **2024**, *8*, 38–46. https://doi.org/10.22161/ijmpd.8.2.5

[11] Tarnawski, A. S. Cellular and Molecular Mechanisms of Gastrointestinal Ulcer Healing. *Dig. Dis. Sci.* **2005**, *50*, S24–S33. https://doi.org/10.1007/s10620-005-2803-6

[12] Tarnawski, A. S.; Ahluwalia, A. The Critical Role of Growth Factors in Gastric Ulcer Healing. *Cells* **2021**, *10*, 1964. https://doi.org/10.3390/cells10081964

[13] Vakil, N. Peptic Ulcer Disease: A Review. *JAMA* **2024**, *332*, 1832–1842. https://doi.org/10.1001/jama.2024.19094

[14] Kim, G. H. Proton Pump Inhibitor-Related Gastric Mucosal Changes. *Gut Liver* **2021**, *15*, 646–652. https://doi.org/10.5009/gnl20036

[15] Gurib-Fakim, A. Medicinal Plants: Traditions of Yesterday and Drugs of Tomorrow. *Mol. Aspects Med.* **2006**, *27*, 1–93. https://doi.org/10.1016/j.mam.2005.07.008

[16] Zhou, Y. X.; Xin, H. L.; Rahman, K.; Wang, S. J.; Peng, C.; Zhang, H. Portulaca oleracea L.: A Review of Phytochemistry and Pharmacological Effects. *Biomed Res. Int.* **2015**, 925631. https://doi.org/10.1155/2015/925631

[17] Rahimi, V. B.; Ajam, F.; Rakhshandeh, H.; Askari, V. R. A Pharmacological Review on Portulaca oleracea L.: Focusing on Anti-Inflammatory and Antioxidant Activities. *J. Pharmacopuncture* **2019**, *22*, 7–15. https://doi.org/10.3831/KPI.2019.22.001

[18] Uddin, M. K.; Juraimi, A. S.; Ali, M. E.; Ismail, M. R. Purslane Weed (*Portulaca oleracea*): A Prospective Plant Source of Nutrition and Antioxidant Attributes. *ScientificWorldJournal* **2014**, 951019. https://doi.org/10.1155/2014/951019

[19] Qadhi, A.; Elfky, N. A. Study the Protective Effects of *Portulaca oleracea* on Peptic Ulcer in Male Rats. *Pathogenesis* **2019**, *3*, 2.

[20] Ward, R. J. The Vitamins Requirements of Laboratory Animals. In *Nutritional and Disease in Experimental Animals*; Academic Press: London, UK, 1970; pp 1–24.

[21] Hamza, D. A.; Hatrosh, S. J. Effect of Ethanolic Extract of *Glycyrrhiza glabra* Roots on Some Physiological Parameters in Male Albino Rats Treated with Mitomycin-C. *Karbala J. Sci.* **2015**, *13*, 66–72.

[22] Wang, Z.; Hasegawa, J.; Wang, X.; Matsuda, A.; Tokuda, T.; Miura, N.; Watanabe, T. Protective Effects of Ginger Against Aspirin-Induced Gastric Ulcers in Rats. *Yonago Acta Med.* **2011**, *54*, 11–20.

[23] Muslim, I. T.; Taher, K. N.; Ghazi, A. M. Effect of Fermented Mare's Milk on Healing of Aspirin-Induced Gastric Ulcer in Albino Rats. *Al-Qadisiyah J. Vet. Med. Sci.* **2015**, *14*, 12–17.

[24] Habib, S. H.; Aljammaz, A. A. Effect of Aqueous Licorice Extract on Gastric Ulcer Induced by Aspirin in Rats. *J. Home Econ.* **2017**, *27*, 1–12.

[25] Al-Mousawi, H. Histological and Physiological Study of Sweet Potato Extract in Treating Aspirin-Induced Peptic Ulcer; Master's Thesis, Al-Qadisiyah University, Iraq, 2019.

[26] Feng, J.; Wang, J.; Wang, Y.; Huang, X.; Shao, T.; Deng, X.; Cao, Y.; Zhou, M.; He, X. Oxidative Stress and Lipid Peroxidation in Diabetic Ulcers. *Front. Cell Dev. Biol.* **2022**, *10*, 898657. https://doi.org/10.3389/fcell.2022.898657

[27] Park, J. U.; Kang, J. H.; Rahman, M. A.; Hussain, A.; Cho, J. S.; Lee, Y. I. Gastroprotective Effects of Plant Extracts on Gastric Injury. *Biomed Res. Int.* **2019**, 8759708. https://doi.org/10.1155/2019/8759708

[28] Majeed, W.; Khaliq, T.; Aslam, B.; Khan, J. A.; Iftikhar, A. Medicinal Plants with Gastroprotective Potential. *Bangladesh J. Pharmacol.* **2015**, *10*, 588–603. https://doi.org/10.3329/bjp.v10i3.23578

[29] Wu, Y.; Guo, Y.; Huang, T.; Wang, H.; Li, Y.; Cao, Y.; Zhang, H. Licorice Flavonoid Alleviates Gastric Ulcers. *Biomed. Pharmacother.* **2023**, *169*, 115868. https://doi.org/10.1016/j.biopha.2023.115868

[30] Xu, K.; Li, J.; Guo, S.; Zhang, J.; Zhang, X. Gastric Mucosal Repair via EGF-NO/PGE2-PI3K Pathway. *Front. Pharmacol.* **2025**, *16*, 1594089. https://doi.org/10.3389/fphar.2025.1594089

[31] Gao, H.; Zhang, S.; Hu, T.; Qu, X.; Zhai, J.; Zhang, J.; Tan, M.; Zhang, S.; Li, Z.; Duan, J. Omeprazole Protects Against Oxidative Stress. *Chem. Biol. Interact.* **2019**, *297*, 130–140. https://doi.org/10.1016/j.cbi.2018.11.008

[32] Lien, H. M.; Wang, Y. Y.; Huang, M. Z.; Lin, C. M.; Chen, C. J.; Lin, L. C.; Yang, L. L. Gastroprotective Effect of *Anisomeles indica*. *Antioxidants* **2022**, *11*, 2327. https://doi.org/10.3390/antiox11122327

[33] Wasman Qader, S.; Suan Chua, L.; Fournier, J.; Ozdemir, M. Medicinal Plants in Ulcer Prevention. *J. Pharm. Nutr. Sci.* **2022**, *12*, 94–108. https://doi.org/10.29169/1927-5951.2022.12.09

[34] Sun, X.; Zhang, Y.; Li, J.; Wang, K.; Wu, Y.; Wang, Y. Red Blood Cell Distribution Model in GI Bleeding. *J. Healthc. Eng.* **2021**, 5216979. https://doi.org/10.1155/2021/5216979

[35] Ruiz-Hurtado, P. A.; Garduño-Siciliano, L.; Domínguez-Verano, P.; Balderas-Cordero, D.; Gálvez-Romero, J. L.; Rodríguez-Monroy, M. A.; Canales-Martínez, M. M. Propolis and Gastroprotection. *Nutrients* **2021**, *13*, 3169. https://doi.org/10.3390/nu13093169

[36] Bi, W. P.; Man, H. B.; Man, M. Q. Herbal Medicines in Gastric Ulcer Treatment. *World J. Gastroenterol.* **2014**, *20*, 17020–17030. https://doi.org/10.3748/wjg.v20.i45.17020

[37] Ayaz, A.; Jamil, Q.; Hussain, M.; Anjum, F.; Sarfraz, A.; Alqahtani, T.; Hussain, N.; Gahtani, R. M.; Dera, A. A.; Alharbi, H. M.; et al. Antioxidant and Gastroprotective Activity. *Molecules* **2022**, *27*, 4368. https://doi.org/10.3390/molecules27144368

[38] Prayoga, D. K.; Aulifa, D. L.; Budiman, A.; Levita, J. Plants with Anti-Ulcer Activity and Mechanisms. *Drug Des. Dev. Ther.* **2024**, *18*, 193–213. https://doi.org/10.2147/DDDT.S446949

ASEAN
Journal of Scientific and Technological Reports
Online ISSN:2773-8752

Research article

Synergistic Carbon-Biodiversity Gains in Diversified Rubber Agroforestry Systems, Southern Thailand

Uraiwan Tongkaemkaew[1*], Suchawadee Bowchauy[1], Benchawan Bua-Khwan[2], Kamolpatara Kasikam[3], Robbe Verhofste[4], Michael Commons[4], Chooi Lin Phooi[5], Elisa Azura Azman[5], and Roslan Ismail[5]

[1] Faculty of Agriculture, Thaksin University, Phatthalung, 93210, Thailand; https://orcid.org/0000-0002-6490-0337
[2] The Institute for Southern Thai Studies, Thaksin University, Songkhla, 90000, Thailand
[3] Wanakaset Symbiosis Network, Thailand
[4] Terra Genesis International PBC, Freeville, New York 13068 USA
[5] Faculty of Agriculture, Universiti Putra Malaysia, 43400 UPM Serdang, Malaysia
* Correspondence: uraiwan@tsu.ac.th

Citation:
Tongkaemkaew, U.; Bowchauy, S.; Bua-Khwan, B.; Kasikam, K.; Verhofste, R; Commons, M.; Phooi, C.; Azman, E.A.; Ismail, R. Synergistic carbon-biodiversity gains in diversified rubber agroforestry systems, Southern Thailand. *ASEAN J. Sci. Tech. Report.* **2026**, *29*(5), e261871 https://doi.org/10.55164/ajstr.v29i5.261871

Article history:
Received: October 13, 2025
Revised: April 12, 2026
Accepted: April 21, 2026
Available online: May 1, 2026

Publisher's Note:
This article is published and distributed under the terms of the Thaksin University.

Abstract: Rubber plantations cover millions of hectares across Southeast Asia, yet their capacity to deliver both agricultural production and ecological benefits depends heavily on how they are managed. This study compared six rubber management systems in southern Thailand, a conventional monoculture (RM) and five progressively diversified rubber-forest systems (RF1 to RF5), to quantify how increasing structural complexity affects biodiversity, soil health, and carbon storage. Field inventories documented tree species composition, natural regeneration, and deadwood; soil samples characterized organic carbon, nitrogen, and nutrient status; and aboveground biomass and carbon stocks were estimated using the TGO national carbon accounting tool. The most diversified system, RF5, supported 6.4 times more tree species than monoculture (205 vs. 32 species ha^{-1}) and three times the seedling regeneration (7,725 vs. 2,471 seedlings ha^{-1}). Soil organic carbon nearly doubled (from 1.44% to 2.49%), and total nitrogen increased significantly. Total non-rubber aboveground biomass rose nearly fourfold (from 622.64 to 2,348.57 kg ha^{-1}), and the associated carbon stock reached 4.04 tCO_2e ha^{-1} compared to 1.20 tCO_2e ha^{-1} in monoculture. These values represent only the diversified vegetation component; whole-system carbon stocks, including the rubber trees, are substantially higher. These gains moved together across the management gradient rather than independently, with soil fertility, biodiversity, and carbon accumulation reinforcing one another. Although diversified intensity and stand age co-vary in this cross-sectional design, the consistent coupling of ecological indicators across the gradient indicates that structural complexity is a primary organizing factor. Diversified rubber agroforestry systems offer a practical pathway for tropical smallholders to improve ecological function and contribute to climate mitigation.

Keywords: Rubber agroforestry; carbon stocks; conservation biodiversity; carbon sequestration; ecological indicators

1. Introduction

Carbon moves continuously between the atmosphere, living biomass, soil, and oceans. Of these pools, the atmosphere holds a relatively small fractio, CO_2, which represents just 0.04% of the gaseous mixture, but it is the pool from which photosynthetic organisms draw the carbon that builds plant tissue, feeds soil organisms, and drives terrestrial food webs [1]. Plant biomass accumulates this

carbon during growth, then returns it to the atmosphere through respiration, decomposition, and fire [2]. Forests are among the most important sites of carbon accumulation on land. Their biomass spans living trees, understory vegetation, deadwood, litter, and soil organic matter, each representing a distinct pool with different residence times and vulnerabilities [3]. Aboveground biomass is particularly exposed: deforestation and land degradation can release decades of stored carbon within years, making accurate biomass quantification essential for understanding carbon fluxes and designing effective climate policy [1, 3]. Belowground, soil organic matter holds carbon in forms that are both stable and biologically active. It regulates nutrient availability, builds cation exchange capacity, and shapes the physical structure on which plant roots depend [4].

Across the humid tropics of Southeast Asia, rubber plantations (*Hevea brasiliensis*) have become a linchpin of both livelihoods and regional carbon dynamics. Thailand, the world's top natural rubber producer, has turned tracts of land into rubber monoculture estates. While this boom fuels the economy, it also sets off alarm bells over shrinking biodiversity, deteriorating soils, and the overall resilience of ecosystems [5]. Empirical carbon stock data for rubber systems in Thailand are limited in the peer-reviewed literature, though national accounting frameworks, such as the TGO carbon sequestration tool, provide standardized approaches for biomass estimation. Empirical evidence from previous studies indicates that rubber plantations can store substantial amounts of carbon, with 14-year-old stands reported to contain approximately 135-153 tC ha^{-1} [6]. These findings highlight the potential of rubber systems as significant carbon sinks, although carbon storage varies with stand age, tree density, and management practices. Integrating agroforestry into rubber farms is emerging as a strategy for sustainable intensification. By combining rubber trees with timber, fruit-bearing species, and/or shade-tolerant understory crops, growers can improve soil health, reduce income volatility, and diversify revenue streams [7]. Ground data from Thailand reveal that rubber-centric agroforestry arrangements (RAS) not only cushion farmers against the ebb and flow of market prices but also reinforce key ecological functions. Smallholders who embraced rubber-fruit-timber agroforestry configurations, in Phatthalung Province, enjoyed livelihood stability and extracted resources more judiciously than their peers who stuck to monoculture [8]. In a similar vein, it has been demonstrated that rubber agroforestry not only bolsters biodiversity but also enhances ecosystem services compared with conventional plantation practices [9]. RAS systems, integrating multiple species or perennial crops, achieved financial outcomes equivalent to or superior to conventional farming systems by reducing economic risk and increasing land productivity [10]. The Chinese study demonstrates that rubber forest systems improve soil health, accelerate nutrient recycling and carbon storage, and reduce atmospheric greenhouse gas emissions. Taken together, the results underscore that a diversified strategy can align carbon, biodiversity, and livelihood goals across the rubber belt [11].

Even though the biophysical and socioeconomic case for RAS is unmistakably strong, its spread remains hampered by a mix of limited support, fragile policy frameworks, and a lack of financial incentives. Many farmers still cannot access demonstration plots, receive extension guidance, or obtain credit schemes, which slows the shift toward rubber systems. To scale RAS adoption, policy measures such as embedding carbon-credit mechanisms, offering agroforestry subsidies, and delivering farmer training programs are essential. The study hypothesizes that increasing structural complexity in rubber agroecosystems generates coupled grain in aboveground biomass, species diversity, and soil carbon, rather than producing trade-offs among these outcomes [12]. This study quantifies aboveground biomass and carbon stocks across six rubber management systems, from monoculture (RM) to progressively diversified forest-garden systems (RF1 through RF5), and tests whether carbon storage, biodiversity, and soil fertility gains are coupled or independent across this management gradient [13].

2. Materials and Methods

2.1 Study Site

The research was carried out in Thailand, spanning three districts: Thepha (Songkhla Province) and Tamot and Sri Banpot (Phatthalung Province) (Figure 1). These locations were deliberately chosen to showcase a spectrum of rubber agroforestry development stages, each overseen by farmer groups linked to the Regenerative Rubber Alliance. The participating farmers work hand in hand with Thaksin University and

Terra Genesis International, which supply long-term data and grant field access. The climate is humid tropical, with mean annual rainfall of 1,900-2,200 mm and mean annual temperature of 27-29 °C. Soils are predominantly Ultisols and Acrisols derived from sandstone and shale parent materials. They are commonly used for cultivating crops across the area.

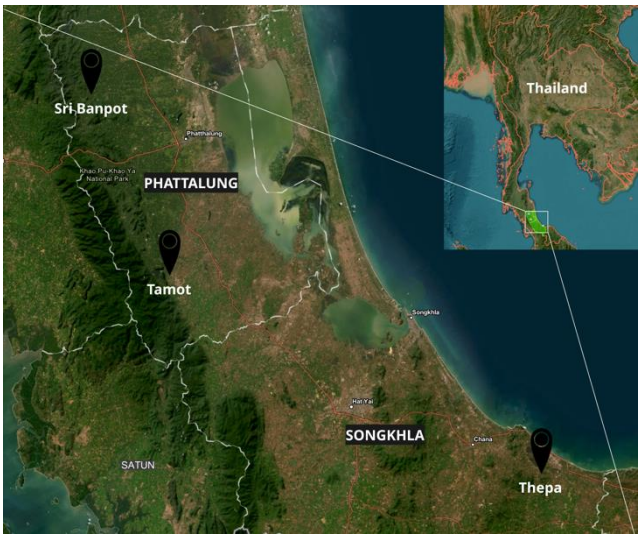


Figure 1. Sri Banpot, Tamot, and Thepa: rubber farming communities in Thailand's southern Phattalung and Songkhla provinces.

2.2 Experiment Design

To ensure transparency in treatment classification, the six management levels (RM, RF1—RF5) were defined using a structured agroforestry complexity gradient that integrates vegetation composition, vertical stratification, and time since diversification. Specifically, RM (Level 0) represents rubber monoculture with a single canopy layer and minimal understory vegetation. In contrast, RF1—RF5 represent progressively diversified rubber-based systems characterized by increasing plant species richness, multi-layered canopy structure (ground cover, shrubs, and timber trees), and longer durations of agroforestry establishment. The classification criteria combined (i) number of plant species, (ii) presence of vertical canopy strata (as illustrated in Figure 2A), (iii) proportion of non-rubber vegetation, and (iv) years since diversification to agroforestry. Tree structural attributes, including height, were measured using hypsometric techniques based on horizontal distance and vertical angle measurements across varying terrain conditions (Figure 2B and 3a-e). These attributes were synthesized into an ordinal biodiversity score ranging from 0 to 5, where higher values indicate greater structural and composition complexity, following an established agroforestry classification framework [5, 13]. To minimize pseudo-replication and ensure statistical independence, replicate plots were separated by at least 250 m within each district, consistent with ecological field sampling recommendations for landscape-level studies. Each 400 m^2 plot (10 x 40 m) was georeferenced using GPS, and no two plots shared overlapping environmental conditions at the microsite level. Replicates were distributed across heterogeneous microhabits within the district to capture within-treatment variability while maintaining independence among sampling units (Figure 3).

2.3 Data Collection and Analysis

2.3.1 Soil Sampling and Analyzing

To keep edge effects from biasing the data, a 2 m buffer was left around each plot (Figure 3f). Within each plot, fifteen random points were chosen using XY coordinates, and composite soil samples from the 0-15 cm layer were collected and processed according to protocols. Soil organic carbon (SOC) and organic matter (OM) were quantified with the Walkley method, while total nitrogen (N) was measured via Kjeldahl digestion and distillation. Available phosphorus was determined using the Bray II extraction method. The exchangeable cations potassium, calcium, and magnesium were quantified via the ammonium acetate (NH_4OAc) method.

The analyses were carried out at the Soil and Residue Analysis Laboratory, Faculty of Technology and Community Development, Thaksin University, and the Central Analytical Laboratory, Prince of Songkla University. Soil carbon data are therefore reported as concentrations (%OC) rather than as areal stocks (Mg C ha^{-1}). This limits direct comparison with carbon accounting benchmarks that require mass-per-area estimates, though the treatment comparisons remain valid as relative differences.

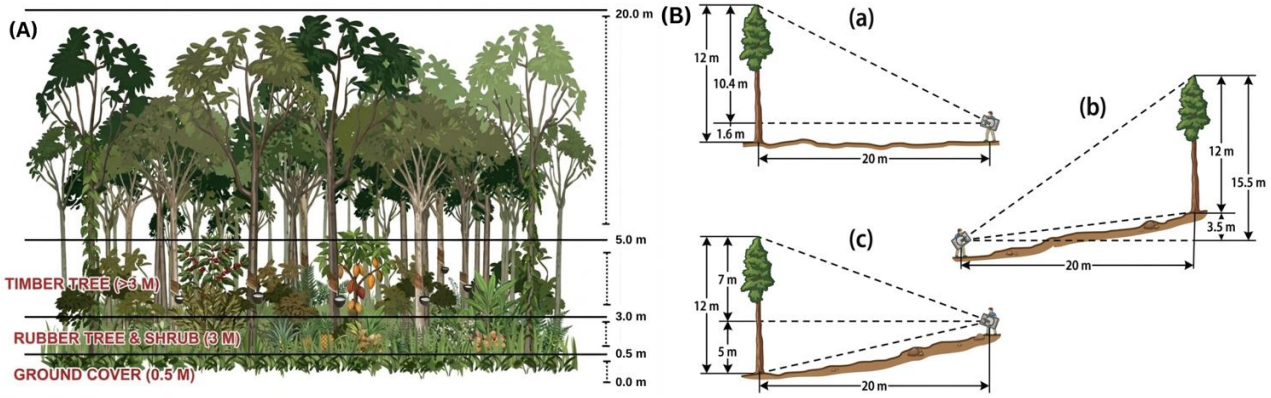


Figure 2. The diagram illustrates the vertical stratification of an agroecosystem, categorized by height (A); Hyposmety techniques used to calculate total tree height using horizontal distance and vertical angle (B); (a) level ground, (b) sloping ground (observer below), and (c) sloping ground (observer above).



Figure 3. Field measurement and sampling of rubber trees for biomass and carbon assessment. (a) Plot establishment and tree tagging within 10 × 40 m sampling plots; (b) Tree height measurement using a clinometer; (c) Tree identification and tagging; (d) Girth at breast height (GBH) measurement at 1.3 m above ground; (e) Diameter at breast height (DBH) measurement using a diameter tape; and (f) Soil and root sampling for belowground biomass estimation.

2.3.2 Estimating Plant Community Structure

Vegetation was divided into four layers: ground cover, shrub, canopy, and emergent. Within each 400 m^2 plot, every plant species was identified, counted, and assigned to a growth form category: tree, shrub, vine, epiphyte, or ground cover. Species density was expressed as the number of individuals per plot, and any specimens that could not be identified on the spot were photographed for expert verification. The tally of deadwood, both stems and downed timber, was recorded using the same diameter class intervals applied to live trees, then extrapolated to a per-hectare figure by applying a factor of twenty-five.

2.3.3 Estimating Biomass

Girth at breast height (GBH) was measured at 1.3 m above ground for all trees and shrubs with a stem circumference of 15 cm or greater, from which DBH was calculated by dividing by π. Tree height (H) was measured using a Suunto PM-5/1520 hypsometer (Figure 2B). Aboveground biomass was estimated using the carbon sequestration calculation tool developed by the TGO (T-VER-TOOL (HOL-FOR/AGR-01) Version 01) [14]. Field measurements, including DBH and H, were used as input parameters for the model to estimate biomass components (stems, branches, and leaves) using standardized allometric relationships appropriate for tropical forests and agroforestry systems in Thailand.

2.3.4 Estimating Carbon Stock

Aboveground carbon stock (AGC) was estimated using the same carbon sequestration calculation tool developed by TGO (T-VER-TOOL (HOL-FOR/AGR-01) Version 01) [14]. The aboveground biomass (AGB) derived from field measurements (DBH and H) was used as input to estimate carbon stocks using standardized biomass-to-carbon conversion procedures embedded in the TGO model. This approach ensures methodological consistency between biomass and carbon estimation and aligns with national carbon accounting practices for tropical forest and agroforestry systems in Thailand.

2.4 Statistical Analysis

Descriptive statistics, mean, deviation, minimum, and maximum were tallied for every variable, including DBH, height (H), stem weight (SW), branch weight (BW), leaf weight (LW), total tree biomass (WT), below ground biomass, total biomass, carbon content, and carbon stock. To probe differences among the six agroforestry levels, a one-way ANOVA was conducted in SAS v9.0, treating agroforestry treatment as a fixed factor and location as a random factor. When the results crossed the significance thresholds ($p < 0.05$, $p < 0.001$), we used Tukey's Honest Significant Difference (HSD) test for post hoc comparisons. Correlation and regression models were then run to tease the links between traits and carbon metrics, such as DBH versus biomass or height versus carbon stock. Finally, Principal Component Analysis (PCA) was employed to uncover multivariate patterns linking soil fertility, vegetation attributes, and carbon accumulation across the systems.

3. Results and Discussion

3.1 Plant Species and Density

The chronologies of intercropping across the systems show a mix of start dates and lengths (Figure 4). Both RF5 and RF4 were launched in 1999; RF5 persisted until 2019, whereas RF4 was discontinued in 2014. The longest stretch belongs to RF2, which ran from 2002 through 2023. RF3 entered the scene in 2007. RF1 covered the interval from 2012 to 2022. These contrasts in age and duration matter for interpreting outcomes because a longer diversification window tends to amplify litter inputs, strengthen stratification, and boost recruitment. Rubber tree density was essentially the same across the systems ($p = 0.066$), implying comparable stand occupancy. By contrast, the large-tree layer with DBH > 15 cm and height over 3 m responded dramatically to diversification: both abundance and species richness surged along the RF gradient ($p < 0.001$) with RF5 occupying the highest Tukey group and RM the lowest (Table 1). Trees of size (DBH > 15 cm, height 1.3-3 m) showed no difference ($p > 0.10$). Small trees (DBH < 15 cm) grew more species-rich as diversification rose ($p < 0.05$, $p < 0.01$). The RF4-RF5 treatments consistently outperformed both the RM and the earlier RF stages. The understory mirrored this pattern: other plants and seedlings were both more abundant and more diverse in the RF systems ($p < 0.05$, $p < 0.01$), with RF4-RF5 leading the pack (Table 2). Dead-tree abundance also varied significantly ($p < 0.05$), with the highest count recorded in RF5, suggesting that the structurally

complex stands experience stronger self-thinning and turnover than a simple chronic die-back. Elevated deadwood in RF5 is consistent with the self-regulatory dynamics of structurally complex systems, in which competitive sorting channels resources toward the most viable individuals while returning biomass to decomposition pathways and the soil carbon pool. This functional turnover distinguishes diversified systems from monocultures, where deadwood more commonly reflects pathological decline. Overall, the diverse rubber forest gardens (RF5) showed the greatest vertical stratification, the richest understory diversity, and the strongest regeneration potential, reinforcing earlier findings that diversified rubber systems boost biodiversity, improve soil fertility, and increase ecosystem resilience [15, 16].

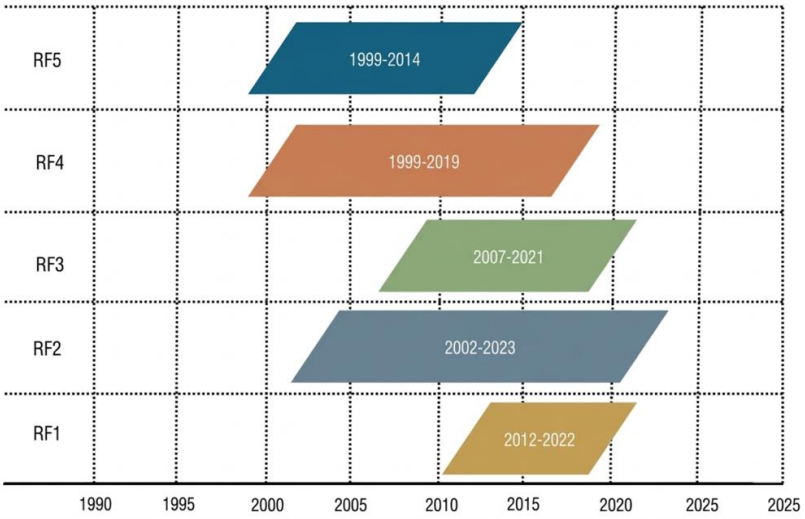


Figure 4. Observed period of intercropping for rubber agroforestry system (RF1-RF5), indicating start and end years of secondary crop/ species integration.

3.2 Current Soil Nutrient Status

Soil chemistry shifted among the systems (Tables 3 and 4). Total nitrogen varied significantly ($p < 0.01$), peaking in RF5 (0.203 ± 0.040%) compared to 0.123 ± 0.015% in RM, a 65% increase consistent with intensified nitrogen cycling under more diverse canopies with greater litterfall diversity and root turnover. The implied carbon-to-nitrogen ratio for both RF5 and RM is approximately 12, which falls within the expected range for tropical systems with active decomposition and indicates that carbon and nitrogen inputs scaled proportionally across the management gradient. Total and available phosphorus did not differ among systems ($p > 0.05$), and exchangeable potassium, calcium, and magnesium were broadly comparable, aside from a notably higher magnesium concentration in RF4.

Soil organic matter (%OM) and soil organic carbon (%OC) differed significantly among the rubber systems ($p < 0.05$). Both parameters followed a similar upward trend with increasing system diversity; RF5 exhibited the highest values (3.87 ± 0.05% for OM and 2.49 ± 0.30% for OC), which were significantly greater than those observed in the RM system (2.22 ± 0.55% and 1.44 ± 0.50%, respectively). Although LOI (Loss on Ignition) captures the full spectrum of organic compounds, including recalcitrant structural residues, and the Walkley-Black method primarily recovers the readily oxidizable fraction, both methods demonstrated a significant positive response. This indicates that highly diversified litter inputs effectively enhance both the labile carbon pool and the accumulation of broader, decomposition-resistant organic compounds across the treatments.

Cation exchange capacity peaked in the RF3-RF4 range (4.36-4.94 meq per 100 g) but was lower in RF5 (3.48 meq per 100 g), a non-monotonic pattern that likely reflects soil type differences across the three study districts rather than a direct management effect. Soil pH remained stable across all systems (4.73-4.92; $p > 0.05$). Electrical conductivity was significantly higher in RF4 and RF5 (2.53-2.59 mS cm^{-1}; $p < 0.05$), consistent with greater soluble nutrient availability driven by higher organic matter inputs and litterfall mineralization.

The overall pattern of elevated %OM, increased total nitrogen, and higher electrical conductivity under the more diversified systems is consistent with the expected agroforestry signature of amplified litterfall, active root turnover, and reduced soil disturbance [16, 17]. The PCA results show that soil fertility indicators (%OM, CEC) and carbon stock load together on the same principal components (Figure 5), consistent with reports of soil-carbon coupling under diversified systems in Southeast Asia [18]. The PCA, however, groups samples primarily by study site rather than by management system, so these associations reflect site-level co-variation rather than a confirmed treatment effect. The treatment-level evidence for management effects on individual soil variables comes from the ANOVA results, not from the PCA.

Soil samples were collected from the 0-15 cm depth, which captures the biologically active surface layer and is standard for soil health assessment. For carbon stock comparisons against regional and global benchmarks, however, 0-30 cm is the more common reference depth. The values reported here, therefore, likely underestimate total soil carbon stocks across all systems. More importantly, the treatment differences observed at the surface may not fully represent what is happening deeper in the profile. In RF4 and RF5, where fruit trees and timber species contribute diverse root architectures at depth, carbon inputs from root turnover and rhizodeposition likely extend well below 15 cm. This means the soil carbon advantage of more diversified systems may be greater than surface measurements alone suggest. Future studies should sample to at least 30 cm, and ideally to 60 cm in systems with deep-rooted species, to provide a more complete picture of soil carbon stock differences across management gradients.

3.3 Growth characteristics, biomass components, and carbon stocks

Tree growth characteristics, biomass components, and carbon stocks varied significantly across rubber management systems (RM and RF1-RF5), demonstrating strong effects of system diversification on ecosystem structure and function (Table 5). Trees in highly diversified systems (RF3-RF5) exhibited significantly greater height, GBH, and DBH than those in monoculture and low-diversity systems (RM-RF2). Tree height increased from 3.68 ± 0.12 m in RM to 10.45 ± 5.52 m in RF5 ($p = 0.0025$; Table 5), reflecting enhanced vertical stratification and improved light interception in a structurally complex system. This pattern is consistent with ecological theory, which holds that multi-layered canopies promote more efficient resource capture and niche complementarity, ultimately enhancing stand-level productivity [19, 20].

Biomass accumulation increased markedly along the diversification gradient. Total aboveground biomass rose from 524.33 ± 55.52 kg ha^{-1} in RM to 1920.22 ± 75.20 kg ha^{-1} in RF5 ($p < 0.0001$; Table 5), while total biomass (including belowground components) increased nearly fourfold, reaching 2348.57 ± 66.67 kg ha^{-1} in RF5. This pattern is consistent with the role of species diversity and structural heterogeneity in amplifying biomass production. Notably, the simultaneous increase in biodiversity, soil fertility, and carbon storage across the gradient indicates that these are not independent responses to diversification but coupled outcomes of increasing ecological organization. Systems with greater structural complexity appear to create conditions, including diversified litter inputs, complementary root architectures, and reduced competitive overlap, that simultaneously reinforce carbon accumulation and biological diversity. Mechanistically, such increases are likely driven by complementary resource use (e.g., light, water, and nutrients) and facilitative interaction among species, which reduces competitive overlap compared to monoculture systems [21, 22]. It should be noted, however, that the six systems in this study differ simultaneously in species composition, canopy structure, and the number of years since diversification. Systems RF4 and RF5 have been diversified since 1999, giving them over two decades of additional litterfall, root turnover, and canopy development compared to RF1, which was established only in 2012. The observed biomass and carbon differences, therefore, reflect both the effects of diversification and time, and these two influences cannot be fully separated in this cross-sectional design. Longitudinal monitoring of the same plots over time would be needed to isolate the contribution of diversification independent of stand age. It is also important to note that the carbon stocks reported here represent only aboveground live biomass, as estimated using the TGO tool. Soil organic carbon, deadwood, litter, and fine root carbon pools are not included in these figures. This accounts for the difference between the values reported here and published whole-system carbon stocks for mature rubber plantations, which typically include multiple pools and report substantially higher totals. Comparisons across studies should account for these methodological differences in the inclusion criteria for the pool.

Table 1. Structural composition of rubber trees and associated tree categories under different rubber systems (per hectare).

Rubber System	Rubber trees	Big trees (>15 cm DBH, H>3 m)		Medium trees (>15 cm DBH, H 1.3-3 m)		Small trees (<15 cm DBH)	
		No. of tree	No. of Species	No. of tree	No. of Species	No. of tree	No. of Species
RM	1536.42 ± 496.47	140.27 ± 75.16 d	32.10 ± 6.95 d	0.00 ± 0.00	0.00 ± 0.00	261.0 ± 137.07 c	42.0 ± 11.31 c
RF1	1095.86 ± 92.36	246.62 ± 86.12 d	27.06 ± 12.22 d	16.67 ± 28.87	0.67 ± 1.15	847.0 ± 741.04 bc	108.0 ± 71.55 bc
RF2	1306.88 ± 39.69	521.52 ± 110.22 c	87.05 ± 14.67 c	5.67 ± 9.29	0.67 ± 1.15	1622.0 ± 1027.47 b	217.0 ± 112.09 b
RF3	966.28 ± 239.84	1171.19 ± 370.15 b	54.61 ± 5.32 c	0.00 ± 0.00	0.00 ± 0.00	1005.0 ± 807.71 bc	178.0 ± 83.27 b
RF4	903.34 ± 212.58	1246.39 ± 465.27 a	225.92 ± 24.57 a	1.00 ± 1.73	0.67 ± 1.15	1896.0 ± 1101.67 b	483.0 ± 203.65 a
RF5	971.83 ± 158.34	1581.65 ± 352.10 a	205.73 ± 18.91 b	2.67 ± 4.62	0.67 ± 1.15	4545.0 ± 4677.36 a	505.0 ± 193.04 a
p-value	0.066	< 0.001	< 0.001	0.12	0.21	< 0.05	< 0.01

Note: Values represent mean ± standard deviation (SD). Different lowercase letters within the same row indicate significant differences among treatments according to Tukey's HSD test. Levels of significance: $p \geq 0.05$ = not significant; $p < 0.05$ = significant; $p < 0.01$ = very significant; $p < 0.001$ = highly significant.

Table 2. Diversity and regeneration of other plants, seedlings, and dead trees under different rubber systems (per hectare).

Rubber system	Other plants		Seedling plants		No. of Dead trees
	No. of plants	No. of Species	No. of plants	No. of Species	
RM	1118.33 ± 1013.29 c	297.33 ± 154.24 c	2471.00 ± 2597.64 c	194.33 ± 72.45 c	44.33 ± 37.78 b
RF1	820.67 ± 207.69 c	361.00 ± 159.47 bc	3516.00 ± 1682.36 bc	211.33 ± 124.71 bc	29.00 ± 24.05 b
RF2	1053.33 ± 376.71 c	428.33 ± 194.43 b	5311.00 ± 3426.05 b	314.00 ± 122.89 b	22.00 ± 13.00 b
RF3	1274.00 ± 889.50 bc	452.00 ± 158.18 b	3651.00 ± 1796.17 bc	353.33 ± 84.55 b	7.33 ± 7.02 b
RF4	1913.00 ± 1208.75 ab	482.00 ± 141.66 ab	5558.00 ± 3114.47 b	382.33 ± 95.64 ab	16.67 ± 14.43 b
RF5	1562.33 ± 958.36 ab	506.00 ± 179.94 a	7725.00 ± 3837.77 a	456.67 ± 129.55 a	97.00 ± 96.00 a
p-value	< 0.05	< 0.01	< 0.01	< 0.01	< 0.05

Note: Values represent mean ± standard deviation (SD). Different lowercase letters within the same row indicate significant differences among treatments according to Tukey's HSD test. Levels of significance: $p < 0.05$ = significant; $p < 0.01$ = very significant

Table 3. Total and available nutrient contents (N, P, K, Ca, Mg) of soils under different rubber systems.

Rubber system	Total N (%)	Total P (mg/kg)	Bray II (mg/kg) Available P	NH_4OAc Extract (mg/kg)		
				K	Ca	Mg
RM	0.123 ± 0.015 b	231.61 ± 221.87	12.18 ± 7.61	38.13 ± 10.10	119.56 ± 57.60	32.75 ± 9.36
RF	0.140 ± 0.000 b	70.39 ± 21.63	15.72 ± 12.94	34.07 ± 2.34	90.79 ± 23.44	28.72 ± 11.22
RF2	0.123 ± 0.015 b	95.33 ± 65.00	9.97 ± 5.51	39.49 ± 8.48	123.82 ± 130.69	34.99 ± 21.17
RF3	0.137 ± 0.012 b	93.90 ± 24.90	10.78 ± 7.44	39.37 ± 14.40	124.21 ± 107.24	41.17 ± 25.09
RF4	0.143 ± 0.025 b	111.88 ± 56.42	13.04 ± 9.10	37.33 ± 7.45	109.94 ± 28.46	43.18 ± 27.31
RF5	0.203 ± 0.040 a	213.81 ± 112.14	11.28 ± 9.90	104.17 ± 123.48	58.33 ± 35.74	28.68 ± 24.27
p-value	<0.01	0.36	0.97	0.54	0.87	0.93

Note: Values are presented as mean ± SD. Different lowercase letters within the same row indicate significant differences in soil nutrient contents among rubber systems according to Tukey's HSD test. Levels of significance: $p \geq 0.05$ = not significant; $p < 0.01$ = very significant.

Table 4. Soil organic carbon, organic matter, cation exchange capacity, pH, and electrical conductivity of soils under different rubber systems**.**

Rubber system	%OC	%OM	CEC (meq/100g soil)	pH	EC (mS/cm)
RM	1.44 ± 0.50 b	2.22 ± 0.55 d	3.68 ± 0.89 d	4.78 ± 0.27	1.99 ± 0.33 b
RF	1.62 ± 0.89 b	2.38 ± 0.56 d	3.90 ± 1.91 c	4.73 ± 0.29	1.91 ± 0.38 b
RF2	1.53 ± 0.64 b	2.48 ± 0.56 c	4.19 ± 2.32 b	4.90 ± 0.32	1.62 ± 0.32 b
RF3	1.76 ± 0.61 b	3.12 ± 0.88 c	4.94 ± 2.18 a	4.91 ± 0.11	1.83 ± 0.25 b
RF4	2.69 ± 0.29 a	3.21 ± 0.52 b	4.36 ± 1.88 a	4.92 ± 0.04	2.59 ± 0.22 a
RF5	2.49 ± 0.30 a	3.87 ± 0.05 a	3.48 ± 0.91 c	4.73 ± 0.20	2.53 ± 0.40 a
p-value	< 0.05	< 0.05	< 0.05	≥ 0.05	< 0.05

Note: Different lowercase letters within the same row indicate significant differences in soil properties among rubber systems according to Tukey's HSD test at levels of significance: $p \geq 0.05$ = not significant and $p < 0.05$ = significant.

Carbon content and carbon stock followed a similar trajectory, increasing significantly with system complexity. Carbon stock increased from 1.20 ± 0.32 tCO_2e ha^{-1} in RM to 4.04 ± 0.33 tCO_2e ha^{-1} in RF5 ($p < 0.0001$; Table 5), indicating a substantial enhancement in carbon sequestration capacity. This strong relationship between biomass and carbon stock supports the principle that woody biomass accumulation is a primary driver of carbon storage at the ecosystem scale [23]. However, the observed carbon values fall within the lower range of published estimates for the mature rubber system, likely due to differences in stand age, site conditions, and measurement approaches [24, 25]. This suggests that the systems studied are still in a developmental stage and have not yet reached their full carbon sequestration potential.

ANOVA confirmed strong treatment effects across all variables (Table 6). Among structural traits, DBH showed the sharpest response ($F = 111.58$, $p < 0.0001$), which reflects its central role in allometric biomass equations — small differences in trunk diameter produce disproportionately large differences in estimated biomass. The very high F-values for carbon content ($F = 1{,}428.46$) and total biomass ($F = 352.19$) partly reflect this allometric amplification across the hectare scale. Residual normality and variance homogeneity should be verified to confirm that ANOVA assumptions hold at these effect sizes.

A focused comparison between monoculture rubber (RM) and highly diversified agroforestry (RF5) further highlights the ecological advantages of diversification (Table 7). RF exhibited significantly higher values across all ecological and biophysical indicators, with species richness increasing by 6.4-fold and

seedling regeneration by 3.1-fold ($p < 0.01$; Table 7). These findings indicate enhanced habitat heterogeneity and regeneration capacity, which are critical for long-term ecosystem resilience and biodiversity conservation [20].

Soil properties were also significantly improved in RF5, with significantly higher organic matter content and total nitrogen. In contrast, soil organic carbon showed a positive trend that did not reach statistical significance across treatments ($p = 0.51$), suggesting more efficient nutrient cycling and improved soil quality. These improvements are likely driven by increased litter input, root biomass turnover, and microbial activity in a diversified system [21]. Such processes play a fundamental role in sustaining long-term productivity and ecosystem functioning.

In addition, total biomass in RF5 was 3.5-4.2 times higher than in RM, accompanied by a substantial increase in carbon stock ($p < 0.001$; Table 7). This reinforces the conclusion that diversified rubber agroforestry systems not only enhance biodiversity but also significantly improve ecosystem productivity and carbon sequestration potential. However, increasing system complexity may also introduce trade-offs, such as intensified competition for resources or greater management complexity, which should be considered in future research [19].

Belowground biomass was estimated using a fixed root-to-shoot ratio, applied uniformly across all treatments and species. In more diverse systems, including fruit trees and timber species with varying rooting depths and architectures, this approach is likely to introduce error into belowground estimates. Species-specific root:shoot ratios or direct root sampling would improve accuracy in future studies.

3.4 Carbon Stock Distribution and Relationships with Tree Density Across Management Systems.

Analysis revealed a highly stratified distribution of carbon stock across the rubber systems. The overall distribution of carbon stock exhibited a distinct multimodal pattern (Figure 5A), which can be directly attributed to the strong regulatory effect of management. As demonstrated in the boxplot and mean analysis (Figure 5C, 5F), carbon accumulation is strictly hierarchical: RM yielded the lowest baseline (approximately 1.1 $tCO_2e\ ha^{-1}$), while RF5 demonstrated the highest sequestration capacity, consistently exceeding 4.0 $tCO_2e\ ha^{-1}$ with minimal intra-group variance.

Tree density and carbon stock decouple within system cohorts (Figure 5B). While the global correlation matrix (Figure 5E) suggests a strong positive relationship between tree density and carbon stock ($r = 0.89$), a granular examination of the clustered scatterplot (Figure 5D) provides a more nuanced ecological insight. The data indicated that high carbon stock is primarily governed by system-level factors rather than by an absolute increase in tree density. Within the highest-performing cohort (RF5), tree density ranged from approximately 50 to over 120 trees per plot. Yet, the corresponding carbon stock remained relatively stable near its maximum, suggesting that factors beyond tree density — species composition, stand age, and management history — are the primary drivers of carbon accumulation in these systems. This indicates that system-level organization, including species composition, stand structure, and management history, governs carbon accumulation more strongly than tree density alone. Within individual management systems, adding more trees does not proportionally increase carbon stocks, but shifting the system toward greater structural complexity does. This distinction has direct implications for how carbon incentive programs should evaluate agroforestry: rewarding complexity and ecological function rather than simple tree counts. The negative correlation observed within the RM system ($r = -0.68$) likely reflects density-dependent competition dynamics: in high-density monoculture stands, individual tree growth and biomass accumulation are slower due to resource competition, resulting in lower per-tree and per-hectare carbon stocks at higher tree densities. This pattern is consistent with self-thinning theory in even-aged plantations.

The stability of carbon stocks across sites, regardless of aboveground tree density, points to a significant contribution from belowground biomass pools. This highlights how roots act as linchpins for long-term carbon stabilization through rhizodeposition and turnover [26]. Consequently, the evidence bolsters the case for folding both aboveground and below-ground carbon pools into accounting frameworks and for leveraging RF systems to underpin mitigation pathways such as $REDD^+$ or credit-based schemes [27].

Table 5. Tree growth characteristics, biomass components, and carbon stock of rubber under RM and RF systems (RF1-RF5).

Parameter		RM	RF1	RF2	RF3	RF4	RF5	*p-value*
Tree Growth Characteristics								
H (m)		3.68 ± 0.12 b	3.52 ± 0.57 b	3.32 ± 0.83 b	8.87 ± 2.51 a	9.10 ± 2.88 a	10.45 ± 5.52 a	*0.0025*
GBH (cm)		12.83 ± 1.98 b	13.18 ± 4.41 b	13.94 ± 3.02 b	25.86 ± 10.42 ab	28.63 ± 13.22 a	31.67 ± 13.69 a	*0.0205*
DBH (cm)		4.03 ± 0.68 b	3.01 ± 0.38 b	4.17 ± 0.54 b	14.24 ± 2.52 a	12.70 ± 1.15 a	12.67 ± 2.99 a	*<0.0001*
Aboveground Biomass Component								
WS (kg ha^{-1})		419.89 ± 84.26 e	833.83 ± 72.95 d	837.47 ± 36.18 d	950.94 ± 75.06 c	1189.36 ± 63.08 b	1413.86 ± 39.70 a	*<0.0001*
WB (kg ha^{-1})		88.06 ± 29.23 d	155.70 ± 44.79 c	171.26 ± 29.11 c	185.78 ± 11.49 c	256.39 ± 42.18 b	323.45 ± 50.03a	*<0.0001*
WL (kg ha^{-1})		16.38 ± 3.22 d	25.79 ± 1.83 c	28.58 ± 3.16b c	34.88 ± 4.89 b	35.64 ± 7.29 b	44.35 ± 6.63 a	*<0.0001*
WT (kg ha^{-1})		524.33 ± 55.52 f	915.31 ± 59.21 e	1062.31 ± 43.21 d	1171.60 ± 85.58 c	1506.38 ±47.53 b	1920.22 ± 75.20 a	*<0.0001*
Belowground Biomass and Total Biomass								
Underground biomass (kg ha^{-1})		148.32 ± 39.18 d	274.13 ± 39.07 c	300.33 ± 32.66 c	316.33 ± 23.11 c	393.22 ± 39.53 b	503.35 ± 47.05 a	*<0.0001*
Total biomass (kg ha^{-1})		622.64 ± 82.10 f	1089.45 ± 94.68 e	1362.64 ± 68.48 d	1512.93 ± 60.77 c	1924.6 ± 38.65 b	2348.57 ± 66.67 a	*<0.0001*
Total Carbon Content and Carbon Stock								
Carbon content (kgC ha^{-1})		327.89 ± 86.62 d	606.04 ± 86.37 c	663.94 ± 72.21 c	699.33 ± 51.09 c	869.32 ± 87.38 b	1100.88 ± 88.78 a	*<0.0001*
Carbon stock	(kgC ha^{-1})	1127.27 ± 72.42 f	2147.15 ± 87.61 e	2309.45 ± 89.60 d	2639.20 ± 51.74 c	3312.49 ± 74.45 b	4311.54 ± 42.05 a	*<0.0001*
	(tCO_2e ha^{-1})	1.20 ± 0.32 d	2.22 ± 0.32 c	2.43 ± 0.26 c	2.56 ± 0.19 c	3.19 ± 0.32 b	4.04 ± 0.33 a	*<0.0001*

Note: Values are mean ± SD. Different lowercase letters within the same row indicate significant differences among treatments according to Tukey's HSD test ($p \leq 0.05$). WS: weight stem, WB: weight branch, WL: weight leaf; WT: weight total.

Table 6. One-way ANOVA results for tree growth traits, biomass components, and carbon metrics across management systems (RM and RF1-RF5).

Variable	F-value	p-value	Significance
Tree height (H, m)	*26.58*	*0.0025*	**
Girth at breast height (GBH, cm)	*8.83*	*0.0205*	*
Diameter at breast height (DBH, cm)	*111.58*	*<0.0001*	***
Stem biomass (WS, kg ha^{-1})	*158.07*	*<0.0001*	***
Branch biomass (WB, kg ha^{-1})	*27.23*	*<0.0001*	***
Leaf biomass (WL, kg ha^{-1})	*49.36*	*<0.0001*	***
Total tree biomass (WT, kg ha^{-1})	*434.20*	*<0.0001*	***
Underground biomass (kg ha^{-1})	*76.03*	*0.0001*	***
Total biomass (kg ha^{-1})	*352.19*	*<0.0001*	***
Carbon content (kgC ha^{-1})	*1428.46*	*<0.0001*	***
Carbon stock (tCO_2e ha^{-1})	*42.06*	*<0.0001*	***

Note: Factor = management system with six levels (RM, RF1-RF5); unit of analysis = per tree; replicates per level = 4. Values are F-statistics and p-values from one-way ANOVA. Significance code: *p < 0.05, ** p < 0.01, *** p < 0.001. Pairwise comparisons among systems were evaluated using Tukey's HSD test, and the results are presented in Table 5.

Table 7. Comparison of ecological and biophysical indicators between monoculture rubber (RM) and highly diversified rubber agroforestry (RF5). Data are presented as mean ± standard deviation. Total biomass and carbon stock are expressed as site-level ranges (minimum-maximum). Statistical significance between treatments was determined using appropriate comparative tests ($p < 0.05$)

Variable	RM (Monoculture)	RF5 (Highly Diversified)	p-value	Ecological Significance
Species Richness (trees, spp. ha^{-1})	32.10 ± 6.95	205.73 ± 18.91	<0.001	6.4-fold increase in structural complexity and habitat diversity
Seedling Regeneration (seedlings ha^{-1})	2471.00 ± 2597.64	7725.00 ± 3837.77	< 0.01	3.1-fold enhancement of natural regeneration potential
Soil Organic Carbon (%OC)	1.44 ± 0.50	2.49 ± 0.30	0.01	Greater long-term capacity for soil carbon sequestration
Total Nitrogen (%)	0.123 ± 0.015	0.203 ± 0.040	< 0.01	Significant improvement in nitrogen cycling efficiency
Total biomass (kg ha^{-1})	548.55 – 689.26	2278.74 – 2426.53	< 0.001	3.5-4.2-fold increase in total biomass accumulation
Carbon stock (tCO_2e ha^{-1})	0.78 – 1.29	3.75– 4.33	< 0.001	Substantially higher potential for climate change mitigation

Note: Ranges represent site-level minimum and maximum values.

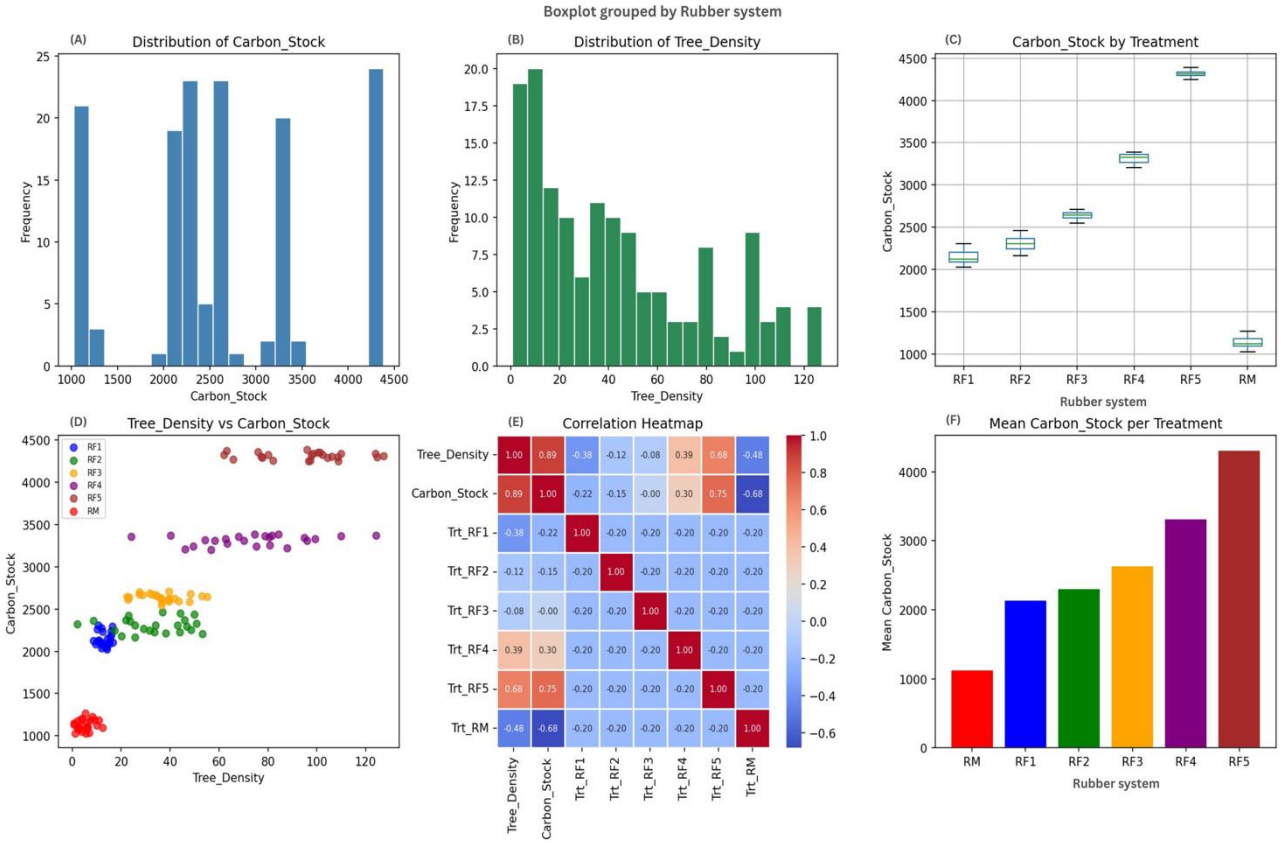


Figure 5. Comprehensive evaluation of carbon stock distribution, relationships with tree density, and management effects across non-rubber agroforestry components. (A) Frequency distribution of overall carbon stock showing a multimodal pattern, (B) Right-skewed frequency distribution of tree density. (C) Boxplot illustrating carbon stock variability across different management systems (RF1-RF5, RM). (D) Scatterplot demonstrating the clustering of tree density and carbon stock relationships by management system. (E) Pearson correlation matrix of key variables. (F) Bar chart comparing mean carbon stocks (± SE) among the management systems.

3.5 PCA-Guided Synthesis of Soil, Vegetation, and Carbon

Principal component analysis of soil quality and carbon stock (PC1 = 47.4%, PC2 = 13.4%; cumulative = 60.8%) separated the three study sites (Figure 6A). Thepha formed a distinct cluster, while Tamot and Sri Banpot partially overlapped and showed broader spread, reflecting greater within-site variability at those locations. When soil parameters were combined with plant growth and carbon variables (PC1 = 36.1%, PC2 = 24.9%; cumulative = 61.0%) (Figure 6B), the same site-level pattern held, with Tamot and Sri Banpot showing higher internal variability than Thepha. The PCA results primarily reflect site-level differences in the combined soil-vegetation-carbon system across the three districts, rather than treatment-level separation among management systems. Within this site-level variation, soil fertility indicators (%OM, CEC) and carbon stock variables load consistently together, suggesting that where organic matter and nutrient retention capacity are higher, carbon storage also tends to be higher. This association is consistent with findings from other Southeast Asian agroforestry landscapes [28, 29], though the cross-sectional design of this study means these relationships should be interpreted as associations rather than confirmed causal pathways.

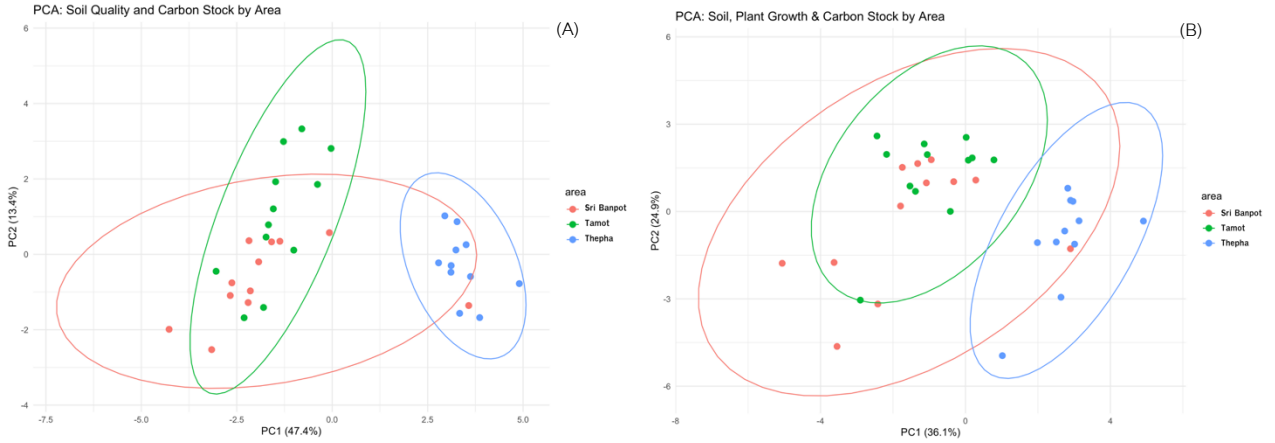


Figure 6. Principal Component Analysis (PCA) of (A) soil quality and carbon stock, and (B) soil qualities, plant growth, and carbon stock, classified by study area: Sri Banplot, Tamot, and Thepha. Each point represents a single sample from the respective area, and the ellipses indicate the confidence regions (confidence ellipses) for each group, illustrating the clustering of the samples.

4. Conclusion

Rubber plantations managed as diversified agroforestry systems outperformed monocultures across all ecological dimensions measured in this study. Species richness, seedling regeneration, soil organic matter, total nitrogen, standing biomass, and carbon stock all increased along the RM to RF5 gradient, increasing together rather than independently. The most diversified systems did not trade one benefit for another; they accumulated ecological and carbon benefits as coupled outcomes of increasing structural complexity. This coupling suggests that biodiversity, soil fertility, and carbon storage are not separate services to be optimized individually, but expressions of a single underlying process: the development of ecological organization within the system. This finding has a direct practical implication: rubber agroforestry is not a compromise between production and conservation but rather a system in which the two reinforce each other. Policies that make it financially viable for smallholders to diversify their rubber holdings — through carbon markets, payments for ecosystem services, or agroforestry subsidies — are likely to generate returns across biodiversity, soil health, and climate goals simultaneously. Future work should extend soil sampling to at least 30 cm (and to 60 cm in systems with deep-rooted species), include bulk density measurements to enable stock-change accounting, refine belowground carbon estimates using species-specific root:shoot ratios or direct root sampling, and establish long-term monitoring plots to track how carbon stocks develop as these systems continue to mature. The ecological and carbon benefits documented here accumulated over one to two decades of progressive diversification. Policy and market mechanisms designed to incentivize these systems, including carbon crediting, payments for ecosystem services, and agroforestry certification, should be designed to accommodate this developmental trajectory rather than requiring immediate, measurable returns from a single intervention.

5. Acknowledgements

The authors gratefully acknowledge the invaluable contributions of the regenerative rubber farmer members and the dedicated data collectors from the two community farmer organizations within the Wanakaset Symbiosis Network, whose collaboration and on-the-ground support made this study possible. Their local knowledge and commitment were instrumental in ensuring the quality and reliability of the field data.

Funding: This research was financially supported by VF Corporation, in collaboration with Terra Genesis International (TGI), under the framework of the Regenerative Rubber Alliance.

Author Contributions: UT: Conceptualization, Methodology, Data Collection, Data Analysis, Writing (draft preparation, reviewing, and editing) Submission; SB: Data Analysis; BB, KK: Collecting data; RV:

Conceptualization, Writing (reviewing and editing); MC: Conceptualization, Methodology, Writing (reviewing and editing); CP: Data Analysis; EA and RI: Reviewing and editing.

Conflicts of Interest: The authors declare no conflict of interest.

References

[1] Vashum, K. T.; Jayakumar, S. Methods to Estimate Aboveground Biomass and Carbon Storage in Natural Forests: A Review. *J. Ecosyst. Ecogr.* **2012**, *2*(4), 1–7. https://doi.org/10.4172/2157-7625.1000116

[2] Houghton, R. A. Aboveground Forest Biomass and the Global Carbon Balance. *Glob. Change Biol.* **2005**, *11*(6), 945–958. https://doi.org/10.1111/j.1365-2486.2005.00955.x

[3] Gibbs, H. K.; Brown, S.; Niles, J. O.; Foley, J. A. Monitoring and Estimating Tropical Forest Carbon Stocks: Making REDD a Reality. *Environ. Res. Lett.* **2007**, *2*(4), 045023. https://doi.org/10.1088/1748-9326/2/4/045023

[4] agdoff, F.; Weil, R. R. Significance of Soil Organic Matter to Soil Quality and Health. In *Soil Organic Matter in Sustainable Agriculture*; Magdoff, F., Weil, R. R., Eds.; CRC Press: Boca Raton, FL, **2004**; pp 1–43.

[5] Verhofste, R.; Dunteman, L.; Commons, M.; Kristiansen, O.; Tongkaemkaew, U. Rubber Management Systems: From Extractive to Regenerative Production. *ASEAN J. Sci. Technol. Rep.* **2024**, *27*(3). https://doi.org/10.55164/ajstr.v27i3.250789

[6] Wauters, J. B.; Coudert, S.; Grallien, E.; Jonard, M.; Ponette, Q. Carbon Stock in Rubber Tree Plantations in Ghana and Brazil. *For. Ecol. Manage.* **2008**, *255*(7), 2347–2362. https://doi.org/10.1016/j.foreco.2007.12.038

[7] Liu, C. A.; Nie, Y.; Zhang, J. L.; Tang, J. W.; Rao, X.; Siddique, K. H. M. Soil Nutrient Responses to Long-Term Rubber Cultivation. *Sci. Total Environ.* **2024**, *946*, 174340. https://doi.org/10.1016/j.scitotenv.2024.174340

[8] Stroesser, L.; Penot, É.; Michel, I.; Tongkaemkaew, U.; Chambon, B. Income Diversification in Rubber Agroforestry. *Rev. Int. Econ. Dev.* **2018**, *235*, 117–145. https://doi.org/10.3917/ried.235.0117

[9] Warren-Thomas, E.; Nelson, L.; Juthong, W.; Bumrungsri, S.; Brattström, O.; Stroesser, L.; Chambon, B.; Penot, É.; Tongkaemkaew, U.; Edwards, D. P.; Dolman, P. M. Rubber Agroforestry in Thailand Provides Biodiversity Benefits. *J. Appl. Ecol.* **2020**, *57* (1), 17–30. https://doi.org/10.1111/1365-2664.13530

[10] Huang, L.; Li, Z.; Chen, H.; Wang, Y. Economic Performance of Rubber-Based Agroforestry Systems. *Agrofor. Syst.* **2023**, *97*, 335–354. https://doi.org/10.1007/s10457-022-00734-x

[11] Qi, D.; Wu, Z.; Yang, C.; Tao, Z.; Zhao, L.; Zhang, Y.; Fu, Q. Rubber Agroforestry Systems in China. *Adv. Biosci. Biotechnol.* **2023**, *14*(12), 479–491. https://doi.org/10.4236/abb.2023.1412033

[12] Tiko, J. M.; Ndjadi, S. S.; Obandza-Ayessa, J. L.; et al. Carbon Sequestration in Rubber Plantations: A Review. *Earth* **2025**, *6*(2), 21. https://doi.org/10.3390/earth6020021

[13] Tongkaemkaew, U.; Commons, M.; Verhofste, R.; Phooi, C. L.; Wonglom, P.; Bua-Khwan. Soil Fertility Regeneration in Rubber Agroforestry. *ASEAN J. Sci. Technol. Rep.* **2025**, *28*(2). https://doi.org/10.55164/ajstr.v28i2.255018

[14] Thailand Greenhouse Gas Management Organization (TGO). *T-VER Carbon Sequestration Calculation Tool*; TGO: Bangkok, n.d. (accessed Apr 10, 2024).

[15] Tongkaemkaew, U.; Penot, É.; Chambon, B. Rubber Agroforestry Systems in Southern Thailand. *Thaksin Univ. J.* **2021**, *23*(1), 78–86.

[16] Cardinale, B. J.; Duffy, J. E.; Gonzalez, A.; et al. Biodiversity Loss and Its Impact on Humanity. *Nature* **2012**, *486*(7401), 59–67. https://doi.org/10.1038/nature11148

[17] Nair, P. K. R.; Nair, V. D.; Kumar, B. M.; Showalter, J. M. Carbon Sequestration in Agroforestry Systems. *Adv. Agron.* **2010**, *108*, 237–307. https://doi.org/10.1016/S0065-2113(10)08005-3

[18] Hanpattanakit, P.; Suteerapongpun, S.; Saengthongpinit, C. Carbon Stock Estimation in Urban Forests. *Chem. Eng. Trans.* **2022**, *97*, 427–432. https://doi.org/10.3303/CET2297072

[19] Brahma, B.; Nath, A. J.; Sileshi, G. W.; Das, A. K. Biomass Carbon Loss in Rubber Plantations. *Biomass Bioenergy* **2018**, *115*, 88–96. https://doi.org/10.1016/j.biombioe.2018.04.019

[20] Wibawa, G.; Hendratno, S.; van Noordwijk, M. Rubber-Based Agroforestry Systems. In *Proc. Int. Rubber Conf.*; Indonesian Rubber Research Institute: Indonesia, **2006**; pp 1–15.

[21] Rafdinal, R.; Pitopang, R.; Tjoa, A.; Burhanuddin, B. Biomass and Carbon Storage in Agroforestry Systems. *Acta Agric. Slov.* **2021**, *117*, 1–11. https://doi.org/10.14720/aas.2021.117.1.1859

[22] Sahuri, S. Carbon Stock of Rubber Agroforestry Systems. *J. Anal. Kebijak. Kehutan.* **2019**, *16*, 105–115.

[23] Werdana, K. P., Megantara, E. N., Withaningsih, S., & Saputra, Y. H. E. Allometric Equation of *Paraserianthes falcataria* (L.) and *Anthocephalus cadamba* Miq. for Estimating Carbon Stocks. *J. Presipitasi.* **2024,** *21*(2), 609. https://doi.org/10.14710/presipitasi.v21i2.609-621

[24] Durán Bautista, E. H.; Romero Duque, L. P.; Galeano, G. Carbon Estimation in *Hevea brasiliensis*. In *Proc. Int. For. Environ. Symp.*; Universidad de la Amazonia: Colombia, 2011; pp 1–12.

[25] Saengruksawong, C.; Khamyong, S.; Anongrak, N.; Pinthong, J. Growth and Carbon Stocks in Rubber Plantations. *Suranaree J. Sci. Technol.* **2012**, *19*(4), 271–278.

[26] Diniz, A. R.; Machado, D. L.; Pereira, M. G.; Balieiro, F. C.; Menezes, C. E. G. Biomass and Carbon Stocks in Rubber Trees. *Rev. Bras. Cienc. Solo* **2015**, *39*(5), 1038–1045. https://doi.org/10.1590/01000683rbcs20140274

[27] Lorenz, K.; Lal, R. Soil Organic Carbon Sequestration in Agroforestry Systems. *Agron. Sustain. Dev.* **2014**, *34*(2), 443–454. https://doi.org/10.1007/s13593-014-0212-y

[28] Henry, M.; Picard, N.; Trotta, C.; et al. Estimating Tree Biomass in African Forests. *Silva Fenn.* **2011**, *45*(3B), 477–569. https://doi.org/10.14214/sf.38

[29] Teo, H. C.; Lamba, A.; Ng, S. J. W.; et al. Reduction of Deforestation by Agroforestry. *Nat. Sustain.* **2025**, *8*, 358–362. https://doi.org/10.1038/s41893-025-01532-w

ASEAN
Journal of Scientific and Technological Reports
Online ISSN:2773-8752

Research article

Association Between Vitamin D3 Status, Blood Pressure, and Lipid Profiles in Hypertensive Patients

Wisam Abdan Wawi Al Abdullah[1*], Najlaa O. H. Aljubury[2], and Shurooq Hussein Jaber Al-Jebur[1]

[1] Department of Biology, College of Education, Al-Qadisiyah University, Iraq
[2] Department of Physiology, Pharmacology and Biochemistry, College of Veterinary Medicine, Al-Qadisiyah University, Iraq
* Correspondence: wisam.wawa@qu.edu.iq

Citation:
Al abdullah, W.A.W.; Aljubury, H.O.N.; Al-Jebur J.H.S. Association between vitamin D3 status, blood pressure, and lipid profiles in hypertensive patients. *ASEAN J. Sci. Tech. Report.* **2026**, *29*(5), e263938. https://doi.org/10.55164/ajstr.v29i5.263938

Article history:
Received: February 26, 2026
Revised: March 10, 2026, 2026
Accepted: April, 25, 2026
Available online: May 1, 2026

Publisher's Note:
This article is published and distributed under the terms of the Thaksin University.

Abstract: Hypertension is a major global health burden that is associated with millions of people across the globe. Epidemiological research indicates that vitamin D3 deficiency appears to be associated with hypertension, although extensive quantitative analyses have not been conducted. This research analyzed the correlation among serum Cholecalciferol levels, blood pressure parameters, and lipid profiles among individuals with hypertension. The study was an observational study that included 138 participants (80 hypertensive and 58 controls). A chemiluminescence assay was employed to evaluate participants' blood pressure status and categorize vitamin D3 levels as deficient (less than 20 ng/mL), insufficient (20-30 ng/mL), or sufficient (30 or higher). Blood pressure indices, lipid profiles, and biochemical parameters were measured. Pearson's correlation was utilized to appraise the relationships among variables. Compared to controls, hypertensive patients showed a highly reduced level of vitamin D3 (18.3 2 ± 1.03 vs. 30.33 ± 1.06 ng/mL, $p<0.001$), a high systolic blood pressure (146.9 ± 2.31 vs. 119.0 ± 1.34 mmHg, $p<0.001$), and a higher diastolic blood pressure (99.13 ± 2.31 vs. 77.93 ± 1.03 mmHg, $p<0.001$). Vitamin D3 showed significant inverse relationships regarding the systolic blood pressure ($r= -0.5981$, $p=0.001$), the diastolic blood pressure ($r= -0.4077$, $p=0.001$), total cholesterol ($r= -0.5938$, $p=0.001$), triglycerides ($r= -0.3161$, $p=0.05$), and with atherogenic index ($r= -0.3630$, $p<0.01$ The results reflect deficiency of vitamin D3 is significantly linked to high blood pressure and dyslipidemia in hypertensive patients and thus it could be considered to be used as a cardiovascular risk biomarker.

Keywords: Vitamin D3; hypertension; lipid profile; atherogenic index; cardiovascular risk

1. Introduction

Hypertension is regarded as one of the significant healthcare issues affecting the global population, and it causes a significant cardiovascular morbidity and mortality [1, 2]. As a known risk factor in peripheral vascular disorder, heart failure, cerebral stroke, myocardial infarction, and coronary artery disorder [3, 4], hypertension has a pathophysiology of factors that interact to cause it, like gender, age, familial background, obesity, smoking, behavioral pattern, intake of sodium in the diet, and stress [5, 6]. Recent findings indicate that vitamin D3 insufficiency is another person-alterable risk factor that is negatively linked to the emergence of hypertension [6]. Vitamin D3 is an essential lipid-soluble vitamin involved in many bodily processes, and reduced Cholecalciferol levels are attributed to higher death rate, as they are tied to cardiovascular disease, metabolic syndrome, type-2 diabetes, and several types

of malignancy [7,8]. Several investigations have demonstrated the link between Cholecalciferol status and cardiovascular disorder risk factors, including coronary artery disorder, stroke, heart failure, elevated vascular resistance, atherosclerosis, and hypertension [8, 9].

Mechanistically, vitamin D3 can cause a direct vascular effect on blood pressure via vitamin D receptors whose expression can be located in vascular endothelial cells [10, 11], in the renin-angiotensin-aldosterone system (RAAS) [12, 13], and in regulating intracellular calcium homeostasis to regulate renin secretion [11]. Deficiency of vitamin D3 stimulates RAAS and increases plasma renin and angiotensin II levels, which, in turn, worsens hypertension [14, 15]. Also, a vitamin D3 deficiency may be linked to insulin resistance, which further increases the risk of hypertension [16]. In addition to cardiovascular disease, vitamin D3 deficiency also affects cardiovascular risk factors, such as dysregulation of lipid metabolism, atherosclerosis, and other cardiovascular complications [17, 18]. Several studies have found correlations between vitamin D3 levels and lipid levels [19,20], where deficiency results in metabolic disorders of cholesterol and lipoproteins [16,21]. Such lipid changes are significant contributors to the accelerated development of cardiovascular disease and atherosclerosis [16, 22, 21]. Changes that are associated with lipid metabolism often accompany hypertension, and increased serum lipids are often observed among hypertensive subjects [23, 24]. Nevertheless, there is limited evidence on the subject, notwithstanding the growing existing literature, and the analysis of the simultaneous links between vitamin D3 status and the blood pressure parameters and lipid profiles of hypertensive patients has not been conducted comprehensively. This research project was conducted to measure the relationships among vitamin D3 deficiency, high blood pressure, and lipid profile changes in hypertensive individuals.

2. Materials and Methods

2.1. Research Framework and Study Subjects

The individuals involved in this descriptive observational research were enrolled at the Specialized Cardiovascular Health Center, Al-Diwaniyah Teaching Hospital, Iraq, and numbered 138. A total of 80 hypertensive patients (42 men and 38 women) and 58 healthy controls (36 men and 22 women) were enrolled in this research population. The subjects were between 29 and 76 years old. Exclusion criteria were arthritis, non-hypertensive cardiovascular disease, neoplastic diseases, and renal disease. Each participant completed a full questionnaire that included population characteristics (sex, age, marital status, education, employment), lifestyle characteristics (smoking, nutrition), and medical variables (vitamin D3 supplementation, disease status). The institution's ethics committee approved the research protocol, and all respondents provided their authorization.

2.2. Blood Pressure Measurements

The audit measure was performed after a 10-minute rest interval, using the standard protocol for quantifying blood pressure. Systolic blood pressure (SBP) and diastolic blood pressure (DBP) were assessed, and the mean was calculated for analysis. Pulse pressure (PP) was determined as PP = SBP-DBP. The equation used to determine mean arterial pressure (MAP) was MAP = DBP + (PP/3) [25]. Hypertension was described as SBP> 140 mmHg and DBP> 90 mmHg.

2.3. Sample Handling and Biochemical Testing

Each of the participants had about 3 mL of venous blood taken away after staying overnight without consuming food. Centrifugation of blood samples was performed at 3000 rpm for 10 minutes, separating the serum, which was then preserved at -80 °C before biochemical profiling. The concentration of serum 25-hydroxyvitamin D3 [25(OH)D3] was assayed using a chemiluminescent immunoassay (Monobind Kit, USA) based on the manufacturer's guidelines. Vitamin D3 levels were categorized as deficient (<20 ng/mL), insufficient (20-30 ng/mL), or sufficient (> 30 ng/mL). Photometric analysis was performed on the lipid profile, which consisted of total cholesterol (TC), triglycerides (TG), high-density lipoprotein cholesterol (HDL-C), low-density lipoprotein cholesterol (LDL-C), and very-low-density lipoprotein cholesterol (VLDL-C) with a photometric system of an automated analyzer (Hitachi, Germany) and suitable reagent kits. The atherogenic index of plasma (AIP) was computed as AIP = $\log_{10}$(TG/HDL-C) [27]. Ratios of TC/HDL-C and LDL-C/HDL-

C were derived as additional atherogenic markers. Serum calcium, phosphorus, urea, and creatinine were computed employing an automated analyzer (Reflotron, Germany) with specific reagent kits.

2.4. Statistical Analysis

The analysis of the findings was done with GraphPad Prism (USA), and the results were illustrated as Mean±SE. Between-group contrasts were performed using a Student t-test for two groups and a one-way analysis of variance (ANOVA), and, finally, the post hoc Tukey test for multiple groups. Pearson correlation coefficient was employed to test relationships among variables. Findings were deemed meaningful at $p \leq 0.05$. The post-hoc power assessment validated that the sample sizes of n=80 (hypertensive) and n=58 (Controls) provided power greater than 99 to detect a between-group difference in vitamin D3 levels at the 0.05 level. Nevertheless, the unequal design and the lack of a priori sample-size calculation are recognized as disadvantages, and the interpretations of subgroup analyses are to be taken with an appropriate degree of caution.

3. Results

3.1. Sociodemographic and Clinical Features

The research group included 138 individuals aged 29-76 years. The age mean of hypertensive patients was 49.88±2.90 years, and that of the controls was 42.62 ± 3.43 years ($p>0.05$). Hypertensive patients had extremely high SBP (146.9 ± 2.31 vs. 119.0 ± 1.34 mmHg, $p<0.001$), DBP (99.13 ± 2.31 vs. 77.93 ± 1.03 mmHg, $p<0.01$), PP (48.54 ± 2.19 vs. 41.11 ± 1.62 mmHg, $p<0.01$) and MAP (115.6 ± 2.67) The mean of serum vitamin D3 was 18.32 ± 1.03 ng/mL lower than hypertensive patients (30.33106 ng/mL, $p<0.01$), which was a 40% reduction relative to controls. Serum calcium was significantly lower in hypertensive patients (4.86 ± 0.67 vs. 6.86 ± 0.70 mg/dL, $p<0.05$), while phosphorus (3.30 ± 0.08 vs. 1.16 ± 0.07 mg/dL, $p<0.05$), creatinine (1.15 ± 0.06 vs. 0.87 ± 0.05 mg/dL, $p<0.01$), and urea (6.77 ± 0.37 vs. 2.02 ± 0.20 mg/dL, $p<0.01$) were significantly elevated (Table 1). A number of biochemical parameters require further interpretation. The level of serum calcium was lower than the traditional reference range in both groups, which was likely due to the analyzer's calibration; this finding should be approached with caution and justified by a standard laboratory procedure. Serum urea values stated in mmol/L correspond to 40.6 ± 2.2 and 12.1 ± 1.2 mg/dL in the hypertensive and control groups, respectively, which are within the standard reference range. Low serum phosphorus in the reference group may be due to dietary factors in this population, and this should be investigated.

Table 1. Comparison of blood pressure, vitamin D3, demographic, and biochemical indicators of hypertensive patients and healthy controls.

Parameter	Controls (n=58)	Hypertensive (n=80)
Age (years)	42.62 ± 3.43	49.88 ± 2.90
Systolic BP (mmHg)	119.0 ± 1.34	146.9 ± 2.31***
Diastolic BP (mmHg)	77.93 ± 1.03	99.13 ± 2.31**
Pulse Pressure (mmHg)	41.11 ± 1.62	48.54 ± 2.19**
Mean Arterial Pressure (mmHg)	92.31 ± 1.034	115.6 ± 2.67***
Vitamin D3 (ng/mL)	30.33 ± 1.06	18.32 ± 1.03**
Calcium (mg/dL)	6.86 ± 0.70	4.86 ± 0.67*
Phosphorus (mg/dL)	1.16 ± 0.07	3.30 ± 0.08*
Creatinine (mg/dL)	0.87 ± 0.05	1.15 ± 0.06**
Urea (mg/dL)	2.02 ± 0.20	6.77 ± 0.37**

Data presented as Mean±SEM. BP: blood pressure. Significance vs. Controls: *p<0.05, **p<0.01, ***p<0.001.

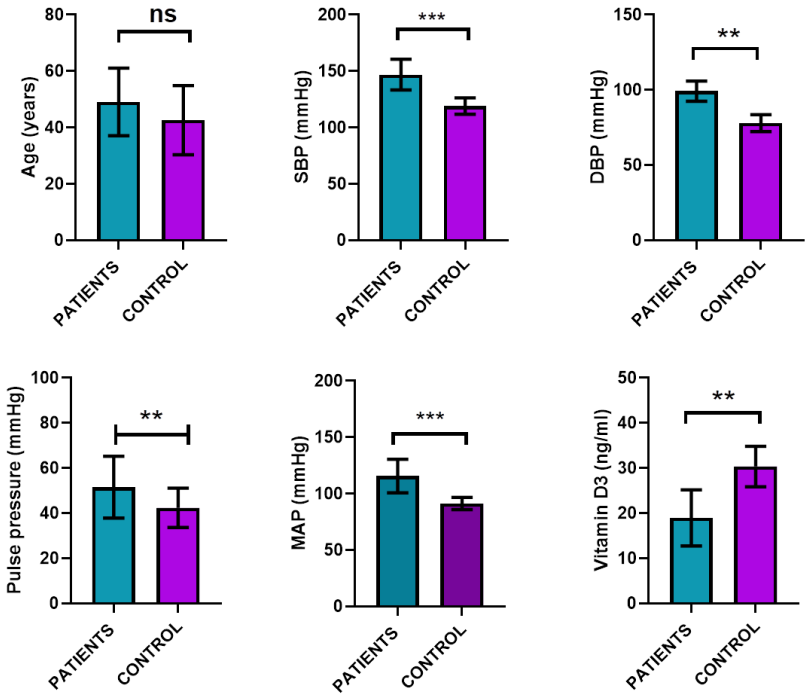


Figure 1. Comparison of age, blood pressure indexes, and vitamin D3 levels between high blood pressure patients and control groups.

3.2 Lipid Profile Comparison Between Groups

Hypertensive patients showed notable changes in lipid profile compared with controls (Table 2). Total cholesterol was elevated by 17% (175.3 ± 7.06 vs. 150.2 ± 10.28 mg/dL, $p<0.05$), triglycerides by 22% (169.4 ± 9.97 vs. 139.1 ± 4.76 mg/dL, $p<0.05$), LDL-C by 66% (94.14 ± 9.68 vs. 56.57 ± 5.95 mg/dL, $p<0.05$), and VLDL-C by 22% (33.89 ± 1.99 vs. 27.82 ± 0.95 mg/dL, $p<0.05$). Conversely, HDL-C was reduced by 30% (20.25 ± 0.93 vs. 29.01 ± 1.45 mg/dL, $p<0.01$). There were significant increases in hypertensive patients by atherogenic indices. 33% (0.92 ± 0.02 vs. 0.69 ± 0.05, $p<0.001$), 59% (8.87 ± 0.64 vs. 5.59 ± 1.03, $p<0.05$), 109% (4.90 ± 0.57 vs. 2.35 ± 0.29, $p<0.01$) increases in plasma atherogenic index, TC/HDL-C ratio, and LDL-C/HD

Table 2. Comparison of atherogenic indices and lipid profile of hypertensive patients and healthy controls.

Parameter	Controls (n=58)	Hypertensive (n=80)
Total Cholesterol (mg/dL)	150.2 ± 10.28	175.3 ± 7.06*
Triglycerides (mg/dL)	139.1 ± 4.76	169.4 ± 9.97*
HDL-C (mg/dL)	29.01 ± 1.45	20.25 ± 0.93**
LDL-C (mg/dL)	56.57 ± 5.95	94.14 ± 9.68*
VLDL-C (mg/dL)	27.82 ± 0.95	33.89 ± 1.99*
Atherogenic Index of Plasma	0.69 ± 0.05	0.92 ± 0.02***
TC/HDL-C Ratio	5.59 ± 1.03	8.87 ± 0.64*
LDL-C/HDL-C Ratio	2.35 ± 0.29	4.90 ± 0.57**

Data presented as Mean±SEM.Significance vs. Controls: *$p<0.05$, **$p<0.01$, ***$p<0.001$.

3.3 Blood Pressure and Lipid Parameters Stratified by Vitamin D3 Status

In hypertensive patients, blood pressure and lipid parameters worsened, and vitamin D3 status decreased with vitamin D3 stratification (Table 3). The low group had the oldest mean age (45.86 ± 2.15 years), then came the insufficient (43.27 ± 4.36 years) and sufficient (40.00 ± 13.08 years) groups. Measurements of blood pressure showed strong status-dependence of vitamin D3. Deficient patients had the highest SBP (142.7 ± 2.47 mmHg) and DBP (98.95 ± 1.50 mmHg), an intermediate result in insufficient patients (SBP: 138.3 ± 2.07

mmHg; DBP: 84.17 ± 4.16 mmHg), and the lowest result in sufficient patients (SBP: 131.7 ± 5.42 mmHg; DBP: 81.25 ± 3.50 mmHg Likewise, pulse pressure and MAP rose gradually with the deficiency of vitamin D3. The vitamin D3 status declined, and the lipid profile worsened. Deficient and insufficient groups demonstrated elevated TC (161.6 ± 5.21 and 171.7 ± 9.54 mg/dL) and TG (171.8 ± 3.78 and 175.3 ± 6.68 mg/dL) compared to sufficient patients (TC: 131.0 ± 2.64 mg/dL; TG: 141.0 ± 6.00 mg/dL). HDL-C was progressively reduced across deficient (18.21 ± 0.28 mg/dL), insufficient (21.75 ±0.73 mg/dL), and sufficient (29.25 ± 0.75 mg/dL) groups. Atherogenic indices (AIP, TC/HDL-C, LDL-C/HDL-C) showed a consistent pattern, with the highest values in vitamin D3-deficient patients. It should be noted that the subgroup of patients with sufficient vitamin D3 within the hypertensive cohort was small. Accordingly, comparisons involving this subgroup are exploratory and should be interpreted with caution, given the risk of inflated Type I error rates in Tukey's post hoc analyses.

Table 3. Blood pressure and lipid parameters in hypertensive patients stratified by vitamin D3 status

Parameter	Deficient (<20)	Insufficient (20-30)	Sufficient (≥30)
Vitamin D3 (ng/mL)	14.99 ± 0.88^{a}	24.92 ± 1.04^{b}	31.50 ± 1.92^{c}
Systolic BP (mmHg)	142.7 ± 2.47^{a}	138.3 ± 2.07^{b}	131.7 ± 5.42^{c}
Diastolic BP (mmHg)	98.95 ± 1.50^{a}	84.17 ± 4.16^{b}	81.25 ± 3.50^{c}
Total Cholesterol (mg/dL)	161.6 ± 5.21^{a}	171.7 ± 9.54^{a}	131.0 ± 2.64^{b}
HDL-C (mg/dL)	18.21 ± 0.28^{a}	21.75 ± 0.73^{a}	29.25 ± 0.75^{b}
AIP	0.94 ± 0.03^{a}	0.85 ± 0.01^{b}	0.82 ± 0.02^{c}

Data presented as Mean±SEM. Different superscript letters (^{a}, ^{b}, ^{c}) highlight meaningful differences between groups ($p<0.05$, Tukey's post-hoc test). AIP: atherogenic index of plasma.

3.4 Correlation Analysis of Vitamin D3 with Blood Pressure and Lipid Parameters

Pearson correlation analysis indicated significant correlations between vitamin D3 levels and multiple cardiovascular parameters in hypertensive patients (Table 4). Vitamin D3 demonstrated strong inverse correlations with age ($r=-0.4618$, $p<0.001$), SBP ($r=-0.5981$, $p<0.001$), and DBP ($r=-0.4077$, $p<0.001$). MAP exhibited moderate inverse correlation ($r=-0.4251$, $p<0.001$), while pulse pressure showed weaker inverse association ($r=-0.1788$, $p>0.05$). Lipid parameters illustrated notable correlations with vitamin D3 status. Total cholesterol ($r=-0.5938$, $p<0.001$), triglycerides ($r=-0.3161$, $p<0.05$), LDL-C ($r=-0.3883$, $p<0.01$), and VLDL-C ($r=-0.1161$, $p>0.05$) exhibited inverse correlations, while HDL-C illustrated a positive linkage ($r=0.1896$, $p>0.05$). Atherogenic indices established meaningful associations: AIP ($r=-0.3630$, $p<0.01$), TC/HDL-C ratio ($r=-0.3987$, $p<0.01$), and LDL-C/HDL-C ratio ($r=-0.4472$, $p<0.001$). Biochemical parameters showed variable correlations with vitamin D3. Positive associations were observed with calcium ($r=0.1004$), phosphorus ($r=0.1587$), and creatinine ($r=0.3091$), while urea exhibited a negative correlation ($r=-0.1396$).

Table 4. Pearson correlation coefficients between vitamin D3 levels and cardiovascular parameters in hypertensive patients

Parameter	Correlation (r)	Significance
Age	-0.4618	p≤0.001
Systolic Blood Pressure	-0.5981	
Diastolic Blood Pressure	-0.4077	
Mean Arterial Pressure	-0.4251	
Total Cholesterol	-0.5938	
Triglycerides	-0.3161	p≤0.05
LDL-C	-0.3883	p≤0.01
Atherogenic Index of Plasma	-0.3630	
TC/HDL-C Ratio	-0.3987	
LDL-C/HDL-C Ratio	-0.4472	

Data show Pearson correlation coefficients (r) and statistical significance n=80 hypertensive patients.

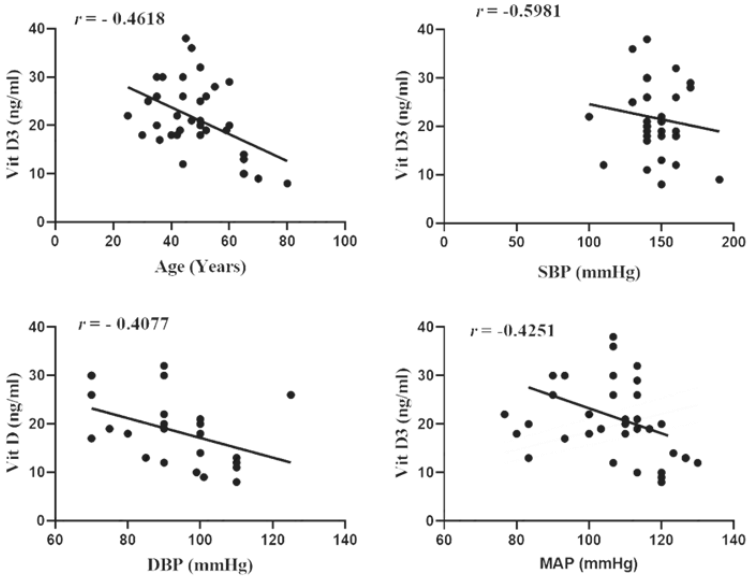


Figure 2. The scatter plot showed the correlation coefficient between the blood pressure index and vitamin D3 level in hypertensive patients.

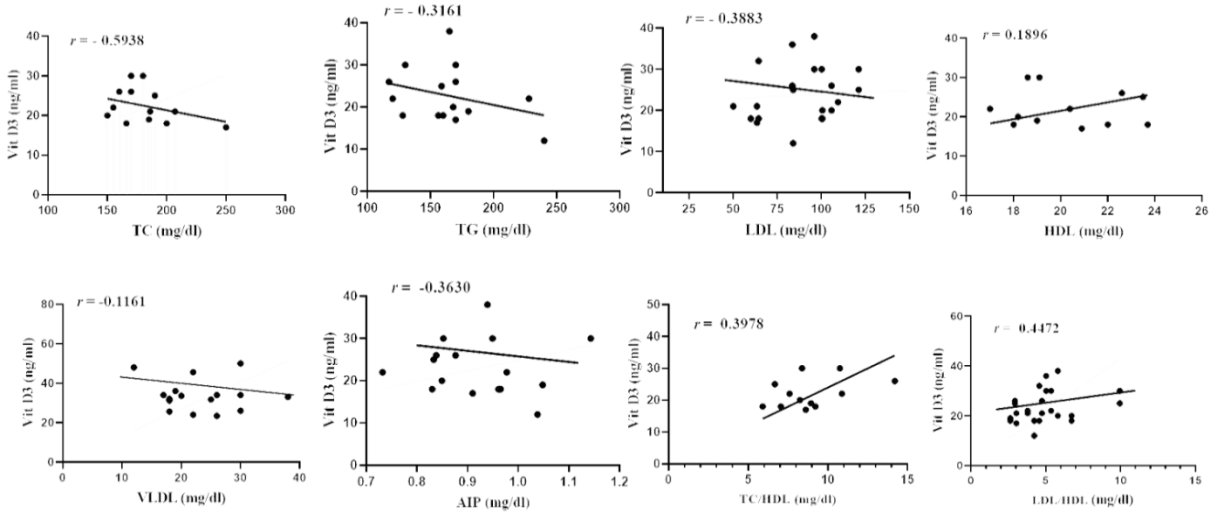


Figure 3. The scatter plot showed the correlation between lipid index and vitamin D3 in patients with hypertension.

4. Discussion

This paper reveals a great deal of correlation between vitamin D3 deficits, high blood pressure, and dyslipidemia among hypertensive individuals. The 40 percent decrease in vitamin D3 serum levels in hypertensive patients (18.32 ± 1.03 vs. 30.33 ± 1.06 ng/mL, $p<0.01$) is a clinically significant hypovitaminosis D, in agreement with earlier studies [28, 29]. This hypothesis that vitamin D3 status plays a significant role in blood pressure regulation is supported by the strong negative correlation between vitamin D3 and systolic blood pressure ($r = -0.5981$, $p < 0.001$). The negative age-vitamin D3 correlation ($r = -0.4618$, $p = 0.001$) is also consistent with age-related decreases in cutaneous vitamin D3 synthesis [30, 31]. Age-related decreases in 7-dehydrocholesterol levels and the declining efficiency of the skin to produce vitamin D3 in the dermal layer are factors that lead to progressive vitamin D3 deficiency in the elderly [30]. Such an outcome presupposes a specific clinical interest given the increased prevalence of hypertension in the aging population [32, 33]. Vitamin D3 status stratification showed that as vitamin D3 levels decreased, blood pressure rose continuously, and deficient patients had systolic blood pressure 8% higher than that of adequate patients (142.7 ± 2.47 vs.

131.7 ± 5.42 mmHg). This dose-response correlation enhances the blood pressure-regulating effect of vitamin D3 [34, 35]. The results are similar to those of earlier investigations that reported negative relationships between vitamin D3 and blood pressure among hypertensive individuals [28, 29, 36]. These findings should be placed in the context of the broader literature. Randomized controlled trials and Mendelian randomization studies have produced conflicting results in large-scale studies. The VITAL trial, one of the largest RCTs to date, found that a vitamin D3 supplement (2000 IU/day) did not show meaningful differences in cardiovascular events or blood pressure in the general public. In the same manner, Mendelian randomization studies [36] have yielded weak indications of the impact of vitamin D status on blood pressure, adjusting for genetic confounding. Such discrepancies may indicate a divergence between observational relationships and true causal relationships, and highlight the complexity of the vitamin D-blood pressure relationship. We should then be interpreted as hypothesis-generating rather than confirmatory of a causal mechanism, with reference to our findings.

Several processes can be attributed to vitamin D3's impact on BP. Vitamin D3 regulates the angiotensin-aldosterone-renin system by directly transcriptionally regulating expression of renin genes [12, 37]. Deficiency of vitamin D3 increases RAAS activation, leading to higher plasma renin and angiotensin II levels and, in turn, elevating blood pressure [14, 15]. Also, vitamin D3 affects endothelial vascularity via vitamin D receptor-mediated mechanisms that stimulate nitric oxide synthesis and vascular relaxation [10,11]. Calcium homeostasis is also controlled by vitamin D3; hypocalcemia due to deficiency triggers parathyroid hormone release, which enhances calcium deposition in the intracellular smooth musculature of the vasculature and may raise vascular resistance [38, 39]. In patients with hypertension, dyslipidemia is characterized by increases in total cholesterol (17%), triglycerides (22%), LDL-C (66%), and HDL-C (30%), indicating severe dysregulation of lipid metabolism. Vitamin D3 had serious negative associations with atherogenic lipid fractions (TC: r=-0.5938; TG: r=-0.3161; LDL-C: r=-0.3883), which are consistent with the control of lipid metabolism in vitamin D3 [192040]. Vitamin D3 can affect lipid metabolism in a variety of mechanistic ways. Vitamin D3 facilitates intestinal calcium absorption, thereby decreasing the release of hepatic triglycerides into the blood and the absorption of intestinal fatty acids [41, 42]. High serum calcium increases fecal lipid and bile acid excretion, which may reduce cholesterol levels [43, 44]. Also, in vitamin D3 deficiency, parathyroid hormone levels are increased, which activate lipogenesis, suppress lipolysis, and impair triglyceride clearance [45]. A clear link exists between vitamin D3 insufficiency and beta-cell dysfunction and insulin resistance, leading to low HDL-C levels and augmented triglycerides [46]. A known predictor of cardiovascular risk, the atherogenic index of plasma, was significantly elevated in hypertensive patients (33 percent) and strongly inversely linked to vitamin D3 ($r = -0.3630$, $p < 0.01$). This result indicates that vitamin D3 deficiency facilitates atherogenic lipoprotein phenotypes [27, 47]. Equally, elevated TC/HDL-C and LDL-C/HDL-C levels among hypertensive patients, which were negatively associated with vitamin D3 ($r = -0.3987$ and $r = -0.4472$, correspondingly), suggested that cardiovascular risk was considerably high [48]. The changes in the renal functions (increased urea and creatinine) noticed among hypertensive patients indicate that the kidney dysfunction is early, and probably due to hypertension-related nephropathy [6]. The reduced serum calcium in hypertensive patients is consistent with the effects of vitamin D3 deficiency on calcium homeostasis.

Study limitations are the cross-sectional model that does not permit drawing any causal conclusions, the lack of multivariate regression analysis to eliminate the possible confounding factors contributing to the results, such as renal functionality, body mass index, medications, smoking, and diet, along with the small and unbalanced sample size and the recruitment of volunteers in one place, which makes it challenging to apply the results broadly. The higher creatinine and urea levels in hypertensive patients are a sign of subclinical renal injury that can independently affect the processes of vitamin D3 hydroxylation and lipid metabolism, and the reported associations are thus to be regarded with due caution. Another serious limitation is that the covariates of primary importance, such as BMI, physical activity, sun exposure, vitamin D intake, antihypertensive medication use, statin therapy, and diabetes mellitus status, are not statistically controlled. These unmeasured confounders could have had an independent impact on both vitamin D3 levels and

lipid/blood pressure outcomes, and the fact that they were not included in the analytical model significantly undermines the possibility of concluding that these associations are independent.

5. Conclusions

This paper shows that vitamin D3 insufficiency is strongly associated with high blood pressure and atherogenic dyslipidemia in hypertensive patients. The vitamin D3 level was found to be 40% low in hypertensive individuals, and there was an inverse correlation between vitamin D3 and systolic blood pressure (r = -0.5981), diastolic blood pressure (r = -0.4077), total cholesterol (r = -0.5938), and the atherogenic indices (AIP; r = -0.3630). The stratification of vitamin D3 showed that the blood pressure and lipid profiles steadily worsened as the vitamin D3 status declined. The results provide evidence of the potential usefulness of vitamin D3 as a cardiovascular risk biomarker in hypertensive individuals, and suggest that the ideal vitamin D3 level may be a promising treatment intervention for the prevention of hypertension and cardiovascular disease. Prospective and randomized controlled trials should be conducted in the future to determine whether correction of vitamin D3 deficiency is attributed to enhancements in blood pressure and lipid profiles in hypertensive individuals.

6. Acknowledgments

The authors are grateful to the staff of Al-Qadisiyah University for their support and to all participants who contributed to this study.

Author Contributions: Conceptualization, W.A.W.A., N.O.H.A. and S.H.J.A.; methodology, W.A.W.A.; formal analysis, W.A.W.A.; investigation, W.A.W.A., N.O.H.A. and S.H.J.A.; resources, W.A.W.A. and N.O.H.A.; data curation, W.A.W.A.; writing—original draft preparation, W.A.W.A.; writing—review and editing, N.O.H.A. and S.H.J.A.; supervision, N.O.H.A. All authors have read and agreed to the published version of the manuscript.

Funding: This research received no external funding.

Conflicts of Interest: The authors declare no conflicts of interest.

References

[1] Karadeniz, Y.; Özpamuk-Karadeniz, F.; Ahbab, S.; Ataoğlu, E.; Can, G. Vitamin D deficiency is a potential risk for blood pressure elevation and the development of hypertension. *Medicina* **2021**, *57*, 1297. https://doi.org/10.3390/medicina57121297

[2] Mittal, B. V.; Singh, A. K. Hypertension in the developing world: Challenges and opportunities. *Am. J. Kidney Dis.* **2010**, *55*, 590–598. https://doi.org/10.1053/j.ajkd.2009.06.044

[3] Adams, J. M.; Wright, J. S. A national commitment to improve the care of patients with hypertension in the US. *JAMA* **2020**, *324*, 1825–1826. https://doi.org/10.1001/jama.2020.20356

[4] Holick, M. F. Vitamin D: Important for prevention of osteoporosis, cardiovascular heart disease, type 1 diabetes, autoimmune diseases, and some cancers. *South. Med. J.* **2005**, *98*, 1024–1028. https://doi.org/10.1097/01.SMJ.0000140865.32054.DB

[5] Elliott, W. J. Systemic hypertension. *Curr. Probl. Cardiol.* **2007**, *32*, 201–259. https://doi.org/10.1016/j.cpcardiol.2007.01.002

[6] Waikar, S. S.; Betensky, R. A.; Bonventre, J. V. Creatinine as the gold standard for kidney injury biomarker studies? *Nephrol. Dial. Transplant.* **2009**, *24*, 3263–3265. https://doi.org/10.1093/ndt/gfp428

[7] Pludowski, P.; Holick, M. F.; Pilz, S.; Wagner, C. L.; Hollis, B. W.; Grant, W. B.; Shoenfeld, Y.; Lerchbaum, E.; Llewellyn, D. J.; Kienreich, K.; et al. Vitamin D effects on musculoskeletal health, immunity, autoimmunity, cardiovascular disease, cancer, fertility, pregnancy, dementia and mortality—A review of recent evidence. *Autoimmun. Rev.* **2013**, *12*, 976–989. https://doi.org/10.1016/j.autrev.2013.02.004

[8] Kader, A.-E.; Ahmad, S.; Ahmad, Y. K.; El-Ghamry, E. M.; Tawfik, S.; Atia, W. M.; Keder, M. M. Assessment of vitamin D status in patients with essential hypertension. *Egypt. J. Hosp. Med.* **2018**, *72*, 4434–4438. https://doi.org/10.21608/ejhm.2018.9496

[9] Schneider, A.; Lutsey, P.; Selvin, E.; Mosley, T.; Sharrett, A.; Carson, K.; Post, W.; Pankow, J.; Folsom, A.; Gottesman, R. Vitamin D, vitamin D binding protein gene polymorphisms, race and risk of incident stroke: The ARIC study. *Eur. J. Neurol.* **2015**, *22*, 1220–1227. https://doi.org/10.1111/ene.12731

[10] Khammissa, R.; Fourie, J.; Motswaledi, M.; Ballyram, R.; Lemmer, J.; Feller, L. The biological activities of vitamin D and its receptor in relation to calcium and bone homeostasis, cancer, immune and cardiovascular systems, skin biology, and oral health. *BioMed Res. Int.* **2018**, *2018*, 9276380. https://doi.org/10.1155/2018/9276380

[11] Vatakencherry, R. M. J.; Saraswathy, L. Association between vitamin D and hypertension in people coming for health check up to a tertiary care centre in South India. *J. Fam. Med. Prim. Care* **2019**, *8*, 2061–2067. https://doi.org/10.4103/jfmpc.jfmpc_236_19

[12] Li, Y. C. Vitamin D and the renin–angiotensin system. In *Feldman and Pike's Vitamin D*, 5th ed.; Elsevier: Amsterdam, The Netherlands, 2024; pp 925–951. https://doi.org/10.1016/B978-0-323-91386-7.00015-5

[13] Turin, A.; Bax, J. J.; Doukas, D.; Joyce, C.; Lopez, J. J.; Mathew, V.; Pontone, G.; Shah, F.; Singh, S.; Wilber, D. J. Interactions among vitamin D, atrial fibrillation, and the renin–angiotensin–aldosterone system. *Am. J. Cardiol.* **2018**, *122*, 780–784. https://doi.org/10.1016/j.amjcard.2018.05.013

[14] Becher, U. M.; Endtmann, C.; Tiyerili, V.; Nickenig, G.; Werner, N. Endothelial damage and regeneration: The role of the renin–angiotensin–aldosterone system. *Curr. Hypertens. Rep.* **2011**, *13*, 86–92. https://doi.org/10.1007/s11906-010-0171-x

[15] Briet, M.; Schiffrin, E. L. Vascular actions of aldosterone. *J. Vasc. Res.* **2013**, *50*, 89–99. https://doi.org/10.1159/000345243

[16] Abd Aon, Y. S.; Kadhim, S. J.; Al Khafaji, I. H. M.; Tahir, N. T. The role of vitamin D3 in improving lipid profile in type 2 diabetes patients with cardiovascular disease. *Indian J. Forensic Med. Toxicol.* **2022**, *16*, 1278–1285. https://doi.org/10.37506/ijfmt.v16i1.17672

[17] Dobnig, H.; Pilz, S.; Scharnagl, H.; Renner, W.; Seelhorst, U.; Wellnitz, B.; Kinkeldei, J.; Boehm, B. O.; Weihrauch, G.; Maerz, W. Independent association of low serum 25-hydroxyvitamin D and 1,25-dihydroxyvitamin D levels with all-cause and cardiovascular mortality. *Arch. Intern. Med.* **2008**, *168*, 1340–1349. https://doi.org/10.1001/archinte.168.12.1340

[18] Martini, L. A.; Wood, R. J. Vitamin D status and the metabolic syndrome. *Nutr. Rev.* **2006**, *64*, 479–486. https://doi.org/10.1301/nr.2006.nov.479–486

[19] Bashir, N. A.; Bashir, A. A. M.; Bashir, H. A. Effect of vitamin D deficiency on lipid profile. *Am. J. Lab. Med.* **2019**, *4*, 11–18. https://doi.org/10.11648/j.ajlm.20190401.12

[20] Wang, M.; Chen, Z.; Wang, Y.; Xu, X.; Li, H.; Yang, J. Effects of vitamin D supplementation on serum lipid profiles and neonatal outcomes in gestational diabetes mellitus: A meta-analysis. *Acta Acad. Med. Sin.* **2021**, *43*, 82–91.

[21] Potenza, M. V.; Mechanick, J. I. The metabolic syndrome: Definition, global impact, and pathophysiology. *Nutr. Clin. Pract.* **2009**, *24*, 560–577. https://doi.org/10.1177/0884533609342436

[22] Polkowska, A.; Głowińska, B.; Tobiaszewska, M.; Bossowski, A. Risk factors for cardiovascular disease in children with type 1 diabetes in 2000–2010 in Podlasie Province. *Pediatr. Endocrinol. Diabetes Metab.* **2015**, *20*, 113–120. https://doi.org/10.18544/PEDM-20.02.0002

[23] Gebrie, A.; Gnanasekaran, N.; Menon, M.; Sisay, M.; Zegeye, A. Evaluation of lipid profiles and hematological parameters in hypertensive patients: Laboratory-based cross-sectional study. *SAGE Open Med.* **2018**, *6*, 2050312118756663. https://doi.org/10.1177/2050312118756663

[24] Guan, C.; Fu, S.; Zhen, D.; Li, X.; Niu, J.; Cheng, J.; Zhao, N.; Liu, J.; Yin, H.; Tang, X. Correlation of serum vitamin D with lipid profiles in middle-aged and elderly Chinese individuals. *Asia Pac. J. Clin. Nutr.* **2020**, *29*, 839–845.

[25] Kar, A.; Datta, S. A study of serum vitamin D level and its association with hypertension. *J. Fam. Med. Prim. Care* **2018**, *7*, 546–550. https://doi.org/10.4103/jfmpc.jfmpc_82_18

[26] Holick, M. F.; Binkley, N. C.; Bischoff-Ferrari, H. A.; Gordon, C. M.; Hanley, D. A.; Heaney, R. P.; Murad, M. H.; Weaver, C. M. Evaluation, treatment, and prevention of vitamin D deficiency: An Endocrine Society clinical practice guideline. *J. Clin. Endocrinol. Metab.* **2011**, *96*, 1911–1930. https://doi.org/10.1210/jc.2011-0385

[27] Mahmoodi, M. R.; Najafipour, H. Associations between serum vitamin D3, atherogenic indices of plasma and cardiometabolic biomarkers among patients with diabetes in the KERCADR study. *BMC Endocr. Disord.* **2022**, *22*, 126. https://doi.org/10.1186/s12902-022-01043-1

[28] Purari, S.; Singh, R.; Kumar, S.; Kishore, K. Study on co-relation between serum vitamin D level and essential hypertension. *Int. J. Health Sci. Res.* **2023**, *13*, 68–74.

[29] Sinha, R. K.; Choudhury, A. Study of serum uric acid and vitamin-D levels in patients with essential hypertension at MGM Medical College, Kishanganj. *Int. J. Acad. Med. Pharm.* **2023**, *5*, 1352–1357.

[30] Holick, M. F. Sunlight and vitamin D for bone health and prevention of autoimmune diseases, cancers, and cardiovascular disease. *Am. J. Clin. Nutr.* **2004**, *80*, 1678S–1688S. https://doi.org/10.1093/ajcn/80.6.1678S

[31] Ross, A. C.; Taylor, C. L.; Yaktine, A. L.; Del Valle, H. B. *Dietary Reference Intakes for Calcium and Vitamin D*; Food and Nutrition Board, Institute of Medicine; National Academies Press: Washington, DC, **2011**; pp 35–111.

[32] Pan, D.; Qiao, H.; Wang, H.; Wu, S.; Wang, J.; Wang, C.; Guo, J.; Gu, Y. Association of serum 25-hydroxyvitamin D concentration with all-cause and cause-specific mortality in hypertensive patients. *Nutr. Metab. Cardiovasc. Dis.* **2024**, *34*, 1274–1282. https://doi.org/10.1016/j.numecd.2024.02.003

[33] Ye, H.; Li, Y.; Liu, S.; Zhang, X.; Liang, H.; Wang, Y.; Wang, R.; Liu, H.; Wen, Y.; Jing, C. Association between serum 25-hydroxyvitamin D and vitamin D dietary supplementation and risk of all-cause and cardiovascular mortality among adults with hypertension. *Nutr. J.* **2024**, *23*, 33. https://doi.org/10.1186/s12937-024-00914-8

[34] Forman, J. P.; Curhan, G. C.; Taylor, E. N. Plasma 25-hydroxyvitamin D levels and risk of incident hypertension among young women. *Hypertension* **2008**, *52*, 828–832. https://doi.org/10.1161/HYPERTENSIONAHA.108.117630

[35] Patil, D.; Dutta, T. Correlation between serum vitamin D3 levels and blood pressure in patients with essential hypertension and normotensive individuals. *Int. J. Adv. Med.* **2020**, *7*, 971–976. https://doi.org/10.18203/2349-3933.ijam20202113

[36] Vimaleswaran, K. S.; Cavadino, A.; Berry, D. J.; Jorde, R.; Dieffenbach, A. K.; Lu, C.; Alves, A. C.; Heerspink, H. J. L.; Tikkanen, E.; Eriksson, J.; et al. Association of vitamin D status with arterial blood pressure and hypertension risk: A Mendelian randomisation study. *Lancet Diabetes Endocrinol.* **2014**, *2*, 719–729.

[37] Tomaschitz, A.; Pilz, S.; Ritz, E.; Grammer, T.; Drechsler, C.; Boehm, B. O.; März, W. Independent association between 1,25-dihydroxyvitamin D, 25-hydroxyvitamin D and the renin–angiotensin system: The Ludwigshafen Risk and Cardiovascular Health (LURIC) study. *Clin. Chim. Acta* **2010**, *411*, 1354–1360. https://doi.org/10.1016/j.cca.2010.05.037

[38] Chonchol, M.; Scragg, R. 25-Hydroxyvitamin D, insulin resistance, and kidney function in the Third National Health and Nutrition Examination Survey. *Kidney Int.* **2007**, *71*, 134–139. https://doi.org/10.1038/sj.ki.5002002

[39] Goodman, W. G. Recent developments in the management of secondary hyperparathyroidism. *Kidney Int.* **2001**, *59*, 1187–1201. https://doi.org/10.1046/j.1523-1755.2001.00605.x

[40] Subber, Z.; Hashim, H.; Al-Shamma, G. The impact of vitamin D level on serum lipids in type 2 diabetes mellitus. *Baghdad J. Biochem. Appl. Biol. Sci.* **2021**, *2*, 230–236. https://doi.org/10.47419/bjbabs.v2i04.47

[41] Cho, H.-J.; Kang, H.-C.; Choi, S.-A.; Ju, Y.-C.; Lee, H.-S.; Park, H.-J. The possible role of Ca^{2+} on the activation of microsomal triglyceride transfer protein in rat hepatocytes. *Biol. Pharm. Bull.* **2005**, *28*, 1418–1423. https://doi.org/10.1248/bpb.28.1418

[42] Reid, I. R. Effects of calcium supplementation on circulating lipids: Potential pharmacoeconomic implications. *Drugs Aging* **2004**, *21*, 7–17. https://doi.org/10.2165/00002512-200421010-00002

[43] Christensen, R.; Lorenzen, J. K.; Svith, C. R.; Bartels, E.; Melanson, E.; Saris, W.; Tremblay, A.; Astrup, A. Effect of calcium from dairy and dietary supplements on faecal fat excretion: A meta-analysis of randomized controlled trials. *Obes. Rev.* **2009**, *10*, 475–486. https://doi.org/10.1111/j.1467-789X.2009.00599.x

[44] Jiang, W.; Miyamoto, T.; Kakizawa, T.; Nishio, S.-i.; Oiwa, A.; Takeda, T.; Suzuki, S.; Hashizume, K. Inhibition of LXRα signaling by vitamin D receptor: Possible role of VDR in bile acid synthesis. *Biochem. Biophys. Res. Commun.* **2006**, *351*, 176–184. https://doi.org/10.1016/j.bbrc.2006.10.027

[45] Song, S. J.; Si, S.; Liu, J.; Chen, X.; Zhou, L.; Jia, G.; Liu, G.; Niu, Y.; Wu, J.; Zhang, W. Vitamin D status in Chinese pregnant women and their newborns in Beijing and their relationships to birth size. *Public Health Nutr.* **2013**, *16*, 687–692. https://doi.org/10.1017/S1368980012003084

[46] Karnchanasorn, R.; Ou, H.-Y.; Chiu, K. C. Plasma 25-hydroxyvitamin D levels are favorably associated with β-cell function. *Pancreas* **2012**, *41*, 863–868. https://doi.org/10.1097/MPA.0b013e31823c947c

[47] Curvello-Silva, K. L.; Oliveira, N. A.; Silva, T. S.; Sousa, C. D.; Daltro, C. Association between cardiovascular risk factors and 25(OH)D levels in obese patients. *Metab. Syndr. Relat. Disord.* **2020**, *18*, 328–332. https://doi.org/10.1089/met.2020.0023

[48] Ioannidou, S.; Kazeli, K.; Ventouris, H.; Amanatidou, D.; Gkinoudis, A.; Lymperaki, E. Correlation of vitamin 25(OH)D, liver enzymes, potassium, and oxidative stress markers with lipid profile and atheromatic index: A pilot study. *J. Xenobiot.* **2023**, *13*, 193–204. https://doi.org/10.3390/jox13020015

ASEAN
Journal of Scientific and Technological Reports
Online ISSN:2773-8752

Research article

Prevalence and Antimicrobial Resistance of Multidrug-Resistant *Salmonella* spp. in Retail Chicken Outlets in Phatthalung, Thailand

Chaisit Niyasom[1*], and Panadda Promjun[1]

[1] Faculty of Science and Digital Innovation, Thaksin University, Phatthalung, 93210, Thailand
* Corresponding: nchaisit@tsu.ac.th

Citation:
Niyasom, C.; Panadda, P. Prevalence and Antimicrobial Resistance of Multidrug-Resistant *Salmonella* spp. in Retail Chicken Outlets in Phatthalung, Thailand. *ASEAN J. Sci. Tech. Report.* **2026**, *29*(5), e264714. https://doi.org/10.55164/ajstr.v29i5.264714

Article history:
Received: April 1, 2026
Revised: April 12, 2026
Accepted: April 23, 2026
Available online: May 1, 2026

Publisher's Note:
This article is published and distributed under the terms of the Thaksin University.

Abstract: Salmonellosis is a major foodborne disease associated with the consumption of contaminated poultry products. This study aimed to determine the prevalence and antimicrobial resistance of *Salmonella* spp. isolated from retail chicken outlets in Phatthalung, Thailand. A total of 43 isolates recovered from chicken meat, knives, and cutting boards across five outlets were confirmed via biochemical tests and PCR using genus-specific primers. Serotyping revealed six serogroups, with serogroup B being the most prevalent (37.21%), followed by C2 (18.60%), C1 (16.28%), D and E (11.63% each), and G (4.65%). Antimicrobial susceptibility testing against 13 antibiotics showed high resistance to ampicillin (95.35%), streptomycin (69.77%), and tetracycline (60.46%). Moderate resistance to fluoroquinolones was detected (41.86–46.51%), whereas gentamicin showed comparatively lower resistance (23.26%). In contrast, resistance to third-generation cephalosporins remained low (ceftriaxone 4.65%; cefotaxime 13.95%). Identical antibiogram patterns between meat samples and environmental surfaces (knives and cutting boards) within the same outlets suggested possible cross-contamination. Notably, 30 (69.77%) isolates were multidrug-resistant *Salmonella*, resistant to 3 or more antibiotic classes. Therefore, these findings highlight the role of retail chicken outlets as reservoirs of antimicrobial-resistant *Salmonella*, posing a potential public health risk.

Keywords: *Salmonella*; retail chicken outlet; antimicrobial resistance; prevalence

1. Introduction

Salmonella is a genus of Gram-negative, rod-shaped, facultatively anaerobic bacteria belonging to the family *Enterobacteriaceae*, and is a major cause of foodborne infection in humans and animals worldwide. Within this genus, only two species are classified: *S. enterica* and *S. bongori*. *S. enterica* is further divided into six subspecies: *enterica* (I), *salamae* (II), *arizonae* (IIIa), *diarizonae* (IIIb), *houtenae* (IV), and *indica* (VI) [1]. Notably, *S. enterica* subsp. *enterica* is the most clinically significant [2]. Serotyping is the conventional method widely used for the classification and surveillance of *Salmonella* in clinical and veterinary settings. Based on the White–Kauffmann–Le Minor scheme, *S. enterica* is classified into more than 60 serogroups and 2,600 serotypes, determined by unique combinations of O and H antigens [3]. Based on pathogenicity and host range, *S. enterica* serovars are classified into two groups: typhoidal and non-typhoidal. Typhoidal serovars, such as *S.* Typhi

and *S.* Paratyphi, are human-restricted pathogens that cause typhoid fever, a systemic and potentially life-threatening disease [4]. In contrast, non-typhoidal serovars (NTS), including *S.* Typhimurium and *S.* Enteritidis, infect a wide range of hosts and are typically associated with self-limiting gastroenteritis, although invasive disease may occur [3]. NTS is among the most common causes of foodborne illness worldwide. In Thailand, NTS infection remains an important public health concern. A nationwide study conducted in 2022 reported approximately 4,501 cases and 461 deaths associated with NTS infection [5].

Poultry is recognized as a major reservoir of *Salmonella*. The organism is commonly present in the gastrointestinal tract of poultry and often contaminates carcasses during slaughter or processing. Consequently, *Salmonella* can be transmitted to humans through direct contact with poultry or indirectly through the consumption of contaminated chicken meat and cross-contaminated products [6]. In addition, the emergence of antimicrobial resistance (AMR) in *Salmonella* spp., particularly multidrug-resistant (MDR) strains, poses a serious global public health threat [7]. This issue is largely driven by the extensive use of antimicrobials in human medicine, agriculture, and livestock production [8]. Several studies have reported that *Salmonella* isolated from poultry meat frequently exhibit resistance to multiple antimicrobial agents [9-13]. Infections caused by MDR *Salmonella* may result in more severe clinical outcomes and prolonged hospitalization [14].

In Southern Thailand, where chicken meat is widely consumed and wet-market retail trade is the dominant food distribution model, monitoring the prevalence and antimicrobial resistance of Salmonella in poultry is essential to ensure food safety. Phatthalung Province, in particular, supports a substantial small-scale poultry industry supplying local wet markets, yet systematic data on the AMR burden of *Salmonella* at the retail level in this province are lacking. Studies in the broader Southern Thailand region have documented antimicrobial residues in retail pork and chicken [15], MDR *Escherichia coli* O45 in raw meats [16], methicillin-resistant *Staphylococcus aureus* in retail meats [17], and microbial contamination in locally processed food products in Phatthalung [18, 19], highlighting the need for systematic surveillance of foodborne pathogens in this region. This study, therefore, aimed to determine the prevalence, serogroup distribution, and antimicrobial resistance patterns of *Salmonella* spp. isolated from chicken meat and environmental surfaces (knives and cutting boards) in retail chicken outlets in Phatthalung, Thailand. The findings of this study provide baseline data for understanding the role of retail environments in the dissemination of antimicrobial-resistant *Salmonella* and may support the development of strategies to reduce the risk of foodborne transmission. Specifically, the data generated will inform targeted antibiotic stewardship programs and hygiene-intervention policies for wet-market retail settings in Southern Thailand.

2. Materials and Methods

2.1 Sample collection

Samples were collected from five retail chicken outlets located in wet markets from three districts of Phatthalung, Thailand, between June and July 2024. Outlet 1 was located in Pa Payom, outlets 2 and 5 were located in Kuan Kanoon, and outlets 3 and 4 were located in Mueang District. From each outlet, five raw chicken meat samples, ten cutting board swab samples, and ten knife swab samples were collected. All samples were placed in separate sterile plastic bags and immediately transported to the laboratory in an ice box at 4 °C for bacterial isolation. Swab samples from cutting boards and knives were collected directly at the outlets, whereas meat samples were purchased from the vendors. For swab sample collection, sterile, pre-moistened swabs in phosphate-buffered saline (PBS) were used. Each swab was applied to approximately 6.45 cm^2 of the surface area.

2.2 Isolation of *Salmonella* spp.

Isolation of *Salmonella* spp. was performed according to ISO 6579:2017 with slight modifications. The modifications consisted of reducing the pre-enrichment volume for swab samples (10 mL BPW instead of 225 mL) to accommodate the smaller sample mass. For meat samples, 25 g of chopped meat was aseptically transferred into 225 mL of buffered peptone water (BPW). For knife and cutting board samples, each swab was placed into 10 mL of BPW. All samples were incubated at 37 °C for 18–24 hours for pre-enrichment. Subsequently, 0.1 mL of the pre-enrichment culture was transferred into 9.9 mL of Rappaport–Vassiliadis soya

(RVS) broth and incubated at 42 °C for 24 hours, while 1 mL was inoculated into 9 mL of Muller–Kauffmann tetrathionate novobiocin (MKTTn) broth and incubated at 37 °C for 24 hours. Both RVS and MKTTn broths were used simultaneously because their complementary selectivities increase overall *Salmonella* recovery: RVS is more effective for low-inoculum samples, while MKTTn supports a broader range of serovars. After selective enrichment, a loopful of culture from each broth was streaked onto xylose lysine deoxycholate (XLD) agar and *Salmonella–Shigella* (SS) agar plates, then incubated at 37 °C for 24 hours. Presumptive *Salmonella* colonies, characterized by a transparent appearance with a black center, were selected and purified on XLD agar. Pure isolates were subsequently maintained on tryptic soy agar (TSA) slants for further identification.

2.3 Identification and Serogrouping of *Salmonella spp.*

Presumptive isolates were initially identified by Gram staining and standard biochemical tests, including motility–indole–lysine (MIL), triple sugar iron (TSI), and urease tests. Serological confirmation was performed by slide agglutination using polyvalent O antisera (A–I) (St Serotest). Isolates showing positive agglutination were further confirmed at the genus level by polymerase chain reaction (PCR) targeting the *invA* gene using primers *invA*-F (5′-CGGTGGTTTTAAGCGTACTCTT-3′) and *invA*-R (5′-CGAATATGCTCCACAAGGTTA-3′), yielding a 796 bp amplicon [20]. Serogrouping was subsequently determined by slide agglutination using polyvalent antisera specific for groups A, B, C1, C2, C3, D, E, and G (St Serotest). It should be noted that definitive serotyping to the serovar level was achieved only for *S.* Enteritidis and *S.* Typhimurium by multiplex PCR; all remaining isolates were classified only to the serogroup level.

2.4 Antimicrobial susceptibility test

The antimicrobial resistance patterns of *Salmonella* isolates were determined using the Kirby–Bauer disc diffusion method on Mueller–Hinton agar, according to the Clinical and Laboratory Standards Institute guidelines [21]. A total of 13 commercially available antibiotic disks (Oxoid) were used: ampicillin (10 μg; AMP), cefotaxime (30 μg; CTX), ceftriaxone (30 μg; CTR), nalidixic acid (30 μg; NA), enrofloxacin (5 μg; ENR), ciprofloxacin (5 μg; CIP), levofloxacin (5 μg; LEV), tetracycline (30 μg; TE), doxycycline (30 μg; DO), gentamicin (10 μg; GEN), streptomycin (10 μg; S), chloramphenicol (15 μg; C), and trimethoprim (5 μg; W). *Escherichia coli* ATCC 25922 was used as a quality control strain. The results were interpreted as susceptible, intermediate, or resistant based on the inhibition zone diameters according to CLSI criteria. Updated breakpoints from CLSI M100 (2023) were also consulted, particularly for fluoroquinolones. Isolates with intermediate susceptibility results were recorded separately and were not grouped with resistant isolates in the prevalence calculations reported herein. This culture-dependent AST approach, when combined with molecular characterization, is consistent with the methods used in comparable AMR studies [22].

2.5 Multiplex Polymerase Chain Reaction for the presence of invA, IE1, and fliC genes

One to two colonies from overnight cultures were transferred into 0.2 mL of sterile distilled water and heated to 100 °C for 5 minutes. The lysate was then used as the template DNA for PCR analysis. Multiplex PCR (mPCR) was performed using three sets of specific primers targeting the *invA*, *IE1*, and *fliC* genes for the detection of *Salmonella* spp., *S.* Enteritidis, and *S.* Typhimurium, respectively, as previously described by Paiao et al. (2013) [20]. Briefly, each 25 μL PCR reaction mixture consisted of 2.5 μL of 10x PCR buffer, 1 μL of dNTP mix (10 μM each), 0.5 μL of each primer (10 μM), 0.25 μL (1.25 U) of Taq DNA polymerase, 1 μL of template DNA, and nuclease-free water to a final volume of 25 μL. The mPCR amplification protocol included an initial denaturation step at 95 °C for 5 minutes, followed by 30 cycles of denaturation at 95 °C for 1 minute, annealing at 58 °C for 1 minute, and extension at 72 °C for 30 seconds, with a final extension step at 72 °C for 7 minutes. PCR products were analyzed by electrophoresis on a 1.5% agarose gel using Tris-acetate-EDTA (TAE) buffer. The expected amplicon sizes were 796 bp for *invA* (*Salmonella* spp.), 432 bp for *fliC* (*S.* Typhimurium), and 316 bp for *IE1* (*S.* Enteritidis).

3. Results

In this study, *Salmonella* was detected in all sampled retail chicken outlets, including chicken meat, knives, and cutting boards. A total of forty-three isolates (n = 43) were systematically identified as *Salmonella* spp. based on biochemical, serological, and molecular characterization. All isolates were Gram-negative, exhibited K/A with H_2S production in TSI, motile, negative for indole and urease, positive for lysine decarboxylase, agglutinated with polyvalent A-I antiserum, and carried the *invA* gene. These isolates were subsequently characterized by slide agglutination and tested for antimicrobial susceptibility to 13 antibiotics by the disc diffusion method. The antimicrobial agents are categorized into 7 classes: penicillins (AMP), third-generation cephalosporins (CTX and CTR), quinolones (NA, ENR, CIP, and LEV), tetracyclines (TE and DO), aminoglycosides (GEN and S), phenicols (C), and diaminopyrimidines (W). The 43 *Salmonella* isolates were classified into six serogroups (Table 1). Serogroup B was the most prevalent (37.21%, 16/43), followed by serogroup C (34.88%, 15/43), which comprised C2 (18.60%, 8/43) and C1 (16.28%, 7/43). Serogroups D and E were each detected in 5 isolates (11.63%), while serogroup G was the least prevalent (4.65%, 2/43). Among the serogroups B and D isolates, 7 (16.28%) and 2 (4.65%) isolates were molecularly identified as *S.* Typhimurium (*invA*$^+$ and *fliC*$^+$) and *S.* Enteritidis (*invA*$^+$ and *IE1*$^+$), respectively (Figure 1). Notably, all isolates of these two serovars exhibited multidrug resistance (MDR). *S.* Typhimurium showed resistance patterns 10, 13, 16, and 18, whereas *S.* Enteritidis displayed resistance patterns 11 and 16 (Table 2).

All 43 isolates (100%) exhibited resistance to at least 1 antibacterial agent. High levels of resistance were observed for several antibacterial agents, including ampicillin (95.35%), streptomycin (69.77%), tetracycline (60.46%), doxycycline (46.51%), nalidixic acid (46.51%), ciprofloxacin (41.86%), enrofloxacin (41.86%), and levofloxacin (41.86%). On the other hand, low resistance was observed with third-generation cephalosporins, including ceftriaxone (4.65%) and cefotaxime (13.95%). Furthermore, moderate levels of resistance were also observed for gentamicin (23.26%), chloramphenicol (27.91%), and trimethoprim (34.88%) (Table 1).

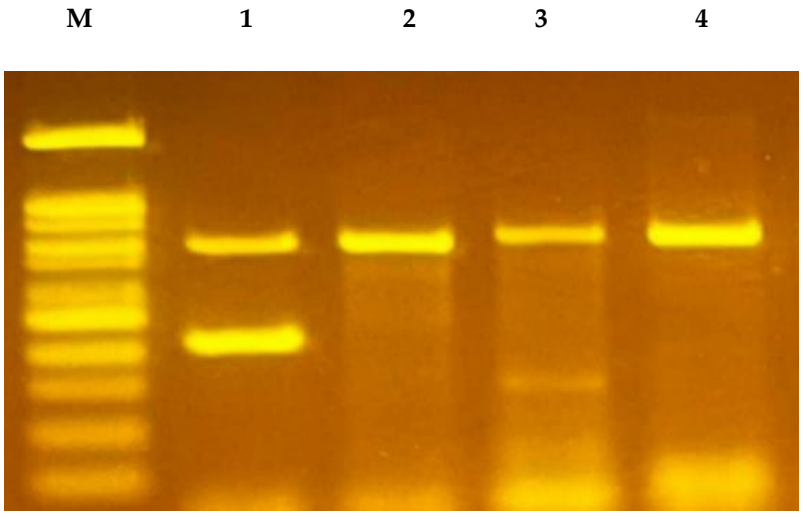


Figure 1. Multiplex PCR detection of *invA* (796 bp), *fliC* (432 bp), and *IE1* (316 bp) genes in *Salmonella* isolates. Lane M: DNA ladder; lane 1: *S.* Typhimurium (serogroup B); lane 2: *Salmonella* spp. (serogroup C1); lane 3: *S*. Enteritidis (serogroup D), and lane 4: *Salmonella* spp. (serogroup E).

Table 1. Serogroup distribution and antimicrobial resistance profiles of *Salmonella* spp. (n = 43) isolated from 5 retail chicken outlets in Phatthalung, Thailand.

Serogroup (outlet)	Number of isolates (%)	Number of resistant isolates (%)												
		AMP	CTX	CTR	NA	CIP	ENR	LEV	TE	DO	GEN	S	C	W
B	16	14	0	0	7	7	7	7	9	7	2	8	4	5
(1-5)	(37.21)	(87.50)	(0)	(0)	(43.75)	(43.75)	(43.75)	(43.75)	(56.25)	(43.75)	(12.50)	(50.00)	(25.00)	(31.25)
C1	7	7	3	2	4	3	3	3	6	4	3	7	5	5
(1-4)	(16.28)	(100)	(42.86)	(28.57)	(57.14)	(42.86)	(42.86)	(42.86)	(85.71)	(57.14)	(42.86)	(100)	(71.43)	(71.43)
C2	8	8	1	0	3	2	2	2	5	5	2	5	0	1
(1-4)	(18.60)	(100)	(12.50)	(0)	(37.50)	(25)	(25)	(25)	(62.50)	(62.50)	(25)	(62.50)	(0)	(12.50)
D	5	5	0	0	2	2	2	2	1	1	0	3	0	0
(1, 4, 5)	(11.63)	(100)	(0)	(0)	(40)	(40)	(40)	(40)	(20)	(20)	(0)	(60)	(0)	(0)
E	5	5	0	0	2	2	2	2	4	2	3	5	2	4
(1, 2, 3)	(11.63)	(100)	(0)	(0)	(40)	(40)	(40)	(40)	(80)	(40)	(60)	(100)	(40)	(80)
G	2	2	2	0	2	2	2	2	1	1	0	2	1	0
(3, 4)	(4.65)	(100)	(100)	(0)	(100)	(100)	(100)	(100)	(50)	(50)	(0)	(100)	(50)	(0)
Total	**43**	**41**	**6**	**2**	**20**	**18**	**18**	**18**	**26**	**20**	**10**	**30**	**12**	**15**
	(100)	**(95.35)**	**(13.95)**	**(4.65)**	**(46.51)**	**(41.86)**	**(41.86)**	**(41.86)**	**(60.46)**	**(46.51)**	**(23.26)**	**(69.77)**	**(27.91)**	**(34.88)**

This study revealed 21 distinct antimicrobial resistance patterns among *Salmonella* isolates, indicating strain diversity in this area. However, similar resistance profiles were observed among isolates in different serogroups. Resistance pattern 10 was found in both serogroups B and C1, while pattern 11 was shared across serogroups B, C1, and D. Furthermore, pattern 16 was detected in the isolates from serogroups B, C2, and D, while pattern 18 was distributed among serogroups B, C1, and E (Table 2). Thirty isolates (69.77%) were multidrug-resistant *Salmonella* spp. (pattern 7-21), defined as resistance to at least one antimicrobial agent in three or more antimicrobial classes. However, MDR profiles were investigated in all serogroups. Of note, some isolates exhibited resistance to 9-12 antibiotics (patterns 19 and 21) across seven antimicrobial classes, highlighting the presence of extensively drug-resistant (XDR) strains. The most prevalent MDR profiles were AMP-NA-ENR-CIP-LEV-TE-DO-S-W (13.95%) and AMP-NA-ENR-CIP-LEV-TE-DO-S (9.30%). The multiple antibiotic resistance (MAR) index ranged from 0.08 to 0.92. Notably, 31 isolates (72.09%) exhibited MAR values greater than 0.2, and 16 isolates (37.21%) showed index values greater than 0.5.

In 4 of 5 (80%) retail chicken outlets, similar antimicrobial resistance patterns and serogroups were investigated among *Salmonella* isolates recovered from different sample types (meat, board, and knife) within the same retail outlets, suggesting possible cross-contamination (molecular typing confirmation pending). In outlet 1, an identical resistance pattern (pattern 2, serogroup D) was detected across chicken meat, cutting boards, and knives, and pattern 18 was found in meat and board samples. In outlet 2, shared resistance patterns (patterns 2, serogroup B) between isolates obtained from meat and knife samples. In outlet 3, a shared resistance pattern (patterns 12, serogroup E) was detected between isolates from the cutting board and knife surfaces. Similarly, in outlet 4, the same resistance pattern (pattern 8, serogroup C2) was observed among isolates from meat and board samples. In outlet 5, a closely related multidrug resistance pattern (pattern 10, serogroup B) was detected on chicken meat and cutting boards.

4. Discussion

Salmonella is a major cause of foodborne disease worldwide, particularly through the consumption of poultry and poultry products [3]. This study demonstrated a high prevalence of *Salmonella* spp. in chicken meat, cutting board, and knife samples collected from retail outlets of wet markets in Phatthalung, Thailand. This finding indicates that chicken retail outlets may serve as important reservoirs for *Salmonella*. This is consistent with several previous reports showing the widespread distribution of this bacterium in poultry retail products and production chains, especially in developing countries where sanitation and hygiene practices may be substandard [23, 24]. Serogroup B, closely followed by C, was identified as the most common group. This distribution is consistent with previous studies reporting a high proportion of these two serogroups among chicken-associated *Salmonella* isolates [24, 25]. Moreover, nontyphoidal *Salmonella*, including *S.* Typhimurium and *S.* Enteritidis, was detected in the samples. These serovars are well recognized as major zoonotic agents of human salmonellosis worldwide [26, 27]. Although most *Salmonella* infections are self-limiting, serovars such as *S.* Enteritidis and *S.* Typhimurium are more likely to cause invasive disease. Notably, these serovars were identified as MDR strains. This is similar to previous reports indicating the high proportion of MDR *S.* Enteritidis and *S.* Typhimurium detected in poultry and poultry products [24, 28-29]. Therefore, the presence of these serovars in retail chicken outlets poses a significant threat to food safety. Continuous monitoring of these high-risk serovars is essential to control the risk of severe foodborne outbreaks and invasive salmonellosis in the community.

Table 2. Non-multidrug resistance (pattern 1-6) and multidrug resistance profiles (pattern 7-21) of *Salmonella* spp. isolated from retail chicken outlets in Phatthalung, Thailand.

Pattern	Resistance profile	No. of antibiotic	No. of class	Serogroup	No. of isolates (%)
1	C	1	1	B	2 (4.65)
2	AMP	1	1	B, D, C2	6 (13.95)
3	AMP, S	2	2	D	1 (2.33)
4	AMP, W	2	2	B	2 (4.65)
5	AMP, TE	2	2	B	1 (2.33)
6	AMP, GEN, S	3	2	E	1 (2.33)
7	AMP, NA, S	3	3	C2	1 (2.33)
8	AMP, TE, DO, GEN, S	5	3	C2	2 (4.65)
9	AMP, TE, DO, S, W	5	4	C2	1 (2.33)
10	AMP, TE, DO, GEN, S, C	6	4	B, C1	3 (6.98)
11	AMP, NA, ENR, CIP, LEV, S	6	3	B, C1, D	3 (6.98)
12	AMP, TE, GEN, S, C, W	6	5	E, C1	3 (6.98)
13	AMP, NA, ENR, CIP, LEV, TE	6	3	B	1 (2.33)
14	AMP, CTX, NA, ENR, CIP, LEV, S	7	4	G	1 (2.33)
15	AMP, CTX, TE, GEN, S, C, W	7	6	C1	1 (2.33)
16	AMP, NA, ENR, CIP, LEV, TE, DO, S	8	4	B, C2, D	4 (9.30)
17	AMP, CTX, NA, ENR, CIP, LEV, TE, DO	8	4	C2	1 (2.33)
18	AMP, NA, ENR, CIP, LEV, TE, DO, S, W	9	5	B, E, C1	6 (13.95)
19	AMP, CTX, CTR, NA, TE, DO, S, C, W	9	7	C1	1 (2.33)
20	AMP, CTX, NA, ENR, CIP, LEV, TE, DO, S, C	10	6	G	1 (2.33)
21	AMP, CTX, CTR, NA, ENR, CIP, LEV, TE, DO, S, C, W	12	7	C1	1 (2.33)

The antimicrobial susceptibility results showed high resistance to ampicillin, streptomycin, and tetracycline. This finding is consistent with previous reports in Thailand. Chuanchuen and Padungtod [9] reported that these three antibiotics are among the most frequently resistant in *Salmonella* from swine and poultry. Furthermore, our results align with the core resistance patterns observed in retail local markets and poultry slaughterhouses [10-11], indicating the long-standing selective pressure exerted by extensive antibiotic use in the Thai poultry industry. Notably, a strong association between nalidixic acid resistance and fluoroquinolone resistance was observed; among the 20 nalidixic-resistant isolates, 90% (18/20) exhibited resistance to ciprofloxacin, enrofloxacin, and levofloxacin. These findings correspond to reported resistance levels in broilers, where nalidixic acid resistance reached 49.54% and ciprofloxacin resistance reached 23.85% [30]. Similar trends of high resistance to nalidixic acid (69.4%) and ciprofloxacin (16.7%) have also been reported in broilers at slaughterhouses in Thailand [31]. Our findings contrast with reports from regions with well-established antimicrobial regulations, such as European countries, where high ciprofloxacin susceptibility is still commonly observed [32]. Furthermore, our findings suggest a clear shift from previous reports in Thailand, where 100% susceptibility to ciprofloxacin in chicken meat was observed [10, 33-34]. This difference suggests that fluoroquinolone resistance has been increasing over the past decades. A key driver of this trend is likely the extensive use of enrofloxacin, a veterinary fluoroquinolone widely administered in Thai poultry farming for prophylaxis and treatment. Because enrofloxacin is partially metabolized to ciprofloxacin *in vivo*, its use selects for mutations in DNA gyrase (*gyrA*/*gyrB*) and topoisomerase IV (*parC*/*parE*) that confer cross-resistance to all fluoroquinolones used in human medicine. Ciprofloxacin is the drug of choice for the treatment of clinical salmonellosis. The high level of resistance observed in this study poses a significant challenge to effective patient management. On the other hand, resistance to third-generation cephalosporins (CTX and CTR) remained low compared to other antimicrobial classes. Similar results have been reported in poultry and retail chicken [13, 24, 35]. This finding suggests a low prevalence of ESBL-producing isolates. However, ESBL production should be further confirmed by combination disk testing or detection of ESBL genes. The most likely ESBL gene families in this context are *bla*CTX-M (particularly CTX-M-15 and CTX-M-55, which are prevalent in Southeast Asian poultry) and *bla*TEM. Future work should include phenotypic confirmation by combined disk testing (cefotaxime ± clavulanate) and molecular screening for these resistance genes.

Nearly 70% of isolates exhibited multidrug resistance (MDR). This observation is similar to several previous studies [12-13, 35]. The presence of MDR strains in retail chicken outlets is a public health concern because it can limit treatment options. Of particular concern, patterns 19 and 21 — each resistant to 9–12 antibiotics spanning seven antimicrobial classes — meet the criteria for extensively drug-resistant (XDR) strains. Against these isolates, chloramphenicol and third-generation cephalosporins (CTX, CTR) appear to retain some activity, as indicated by the resistance profiles observed in this study; however, treatment decisions should be guided by clinical susceptibility testing. The emergence of XDR strains in a retail food environment with no direct clinical link underscores the urgency of integrating food-chain surveillance into national antimicrobial resistance monitoring programs. The dissemination of such high-level resistance may be further facilitated by integron-mediated horizontal gene transfer, a mechanism well-documented in clinical and environmental bacterial pathogens [36]. Phenotypic-genotypic characterization approaches, as applied in related AMR studies [37], should be employed in future investigations to elucidate the specific resistance genes underlying the MDR and XDR profiles observed here. Furthermore, exploration of naturally derived antimicrobials, including insect-derived antimicrobial peptides [38], propolis extracts [39], and phytochemicals from plant sources [40], may offer complementary strategies to address the growing AMR challenge. The MAR index supported these observations, as most isolates (72.09%) had values greater than 0.2, and more than one-third exceeded 0.5, indicating contamination from high-risk sources with frequent antibiotic use [41]. Similar antimicrobial resistance patterns were found in isolates from chicken meat, cutting boards, and knives within the same outlets, suggesting cross-contamination during handling. However, further molecular typing would be required for confirmation. This finding is supported by previous studies

showing that chicken meat and contact surfaces can act as sources of *Salmonella* transmission in retail settings [23, 42]. Moreover, *S.* Typhimurium, *S.* Enteritidis, and other serovars originating from chicken have been associated with human gastrointestinal infections [43].

Overall, this study shows the presence of MDR. Several limitations of this study should be acknowledged. First, the sample size was relatively small (five outlets, 125 total samples), and sampling was confined to a single province over two months (June–July 2024), which may limit the generalizability of findings. Second, samples were collected on a single visit per outlet; repeated sampling across seasons would provide a more robust estimate of contamination prevalence. Third, the study was unable to trace isolates back to farms of origin, so the point at which resistance was acquired, farm, slaughterhouse, or retail, remains unclear. Fourth, cross-contamination was inferred solely from shared antibiogram patterns and serogroups; molecular typing methods such as PFGE or MLST are required for definitive confirmation. Finally, the boiling-lysis DNA extraction method used in Section 2.5, while practical, may yield a lower-quality template compared with commercial extraction kits, a factor that should be considered when interpreting PCR results. Despite these limitations, the study provides important baseline data on the AMR burden at the retail level in Southern Thailand. *Salmonella* in retail chicken outlets underscores the importance of proper antimicrobial use in poultry production and improved hygiene practices at retail outlets to mitigate the spread of resistant strains to consumers.

5. Conclusions

This study demonstrated that retail chicken outlets in Phatthalung, Thailand, serve as significant reservoirs of *Salmonella* spp., with a high prevalence of antimicrobial resistance. *Salmonella* spp. isolated from retail chicken outlets showed high levels of antimicrobial resistance, particularly to ampicillin (95.35%), streptomycin (69.77%), tetracycline (60.46%), and fluoroquinolones (41.86%), with a high proportion of multidrug-resistant isolates (69.77%). Serogroup B was the most frequently detected, followed by serogroups C2 and C1. Similar resistance patterns in meat and environmental samples suggested possible cross-contamination in retail settings, pending molecular confirmation. Notably, two resistance patterns (19 and 21) met the criteria for extensively drug-resistant (XDR) strains, representing a significant public health concern that warrants urgent attention. These findings underscore the need for: (i) stricter enforcement of hygiene practices at retail wet markets, including regular surface disinfection of cutting boards and knives; (ii) national surveillance programs that systematically monitor antimicrobial resistance in retail poultry; and (iii) antimicrobial stewardship interventions targeting veterinary use of fluoroquinolones and other critically important antibiotics in the Thai poultry industry.

6. Acknowledgments

The authors would like to express their sincere gratitude to the Faculty of Science and Digital Innovation for providing laboratory facilities and research support. The authors also gratefully acknowledge the Office of the Permanent Secretary, Ministry of Higher Education, Science, Research and Innovation, for financial support during the fiscal year 2021.

Author Contributions: Conceptualization, C.N.; methodology, C.N. and P.P.; validation, C.N.; formal analysis, C.N. and P.P.; investigation, C.N. and P.P.; resources, C.N. and P.P.; data curation; writing original draft preparation, C.N. and P.P.; supervision, C.N.; project administration, C.N.; funding acquisition, C.N. All authors have read and agreed to the published version of the manuscript.

Funding: This research was funded by the Office of the Permanent Secretary, Ministry of Higher Education, Science, Research and Innovation (fiscal year 2021), and partially funded by the Faculty of Science and Digital Innovation, Thaksin University.

Conflicts of Interest: The authors declare no conflict of interest.

Declaration of AI-Assisted Writing

AI-assisted language tools were used during the preparation of this manuscript to support writing and editing. The authors are fully responsible for all scientific content, data interpretation, and conclusions presented herein.

References

[1] Lamas, A.; Miranda, J. M.; Regal, P.; Vázquez, B.; Franco, C. M.; Cepeda, A. A. Comprehensive review of non-enterica subspecies of *Salmonella enterica*. *Microbiol. Res.* **2018**, *206*, 60–73. https://doi.org/10.1016/j.micres.2017.09.010

[2] Teklemariam, A. D.; Al-Hindi, R. R.; Albiheyri, R. S.; Alharbi, M. G.; Alghamdi, M. A.; Filimban, A. A. R.; Al Mutiri, A. S.; Al-Alyani, A. M.; Alseghayer, M. S.; Almaneea, A. M.; et al. Human salmonellosis: A continuous global threat in the farm-to-fork food safety continuum. *Foods*. **2023**, *12*(9), 1756. https://doi.org/10.3390/foods12091756

[3] Lamichhane, B.; Mawad, A. M. M.; Saleh, M.; Kelley, W. G.; Harrington, P. J., 2nd; Lovestad, C. W.; Amezcua, J.; Sarhan, M. M.; El Zowalaty, M. E.; Ramadan, H.; Morgan, M.; Helmy, Y. A. Salmonellosis: An overview of epidemiology, pathogenesis, and innovative approaches to mitigate the antimicrobial resistant infections. *Antibiotics*. **2024**, *13*(1), 76. https://doi.org/10.3390/antibiotics13010076

[4] Dougan, G.; Baker, S. *Salmonella enterica* serovar Typhi and the pathogenesis of typhoid fever. *Annu. Rev. Microbiol.* **2014**, *68*, 317–336. https://doi.org/10.1146/annurev-micro-091313-103739

[5] Jitpeera, C.; Kripattanapong, S.; Klaytong, P.; Rangsiwutisak, C.; Wannapinij, P.; Doungngern, P.; Pinyopornpanish, P.; Chamawan, P.; Srisuphan, V.; Tuamsuwan, K.; et al. Epidemiology of *Burkholderia pseudomallei*, *Streptococcus suis*, *Salmonella* spp., *Shigella* spp. and *Vibrio* spp. infections in 111 hospitals in Thailand, **2022**. *PLOS Glob. Public Health*. **2025**, *5*(3), e0003995. https://doi.org/10.1371/journal.pgph.0003995

[6] Shaji, S.; Selvaraj, R. K.; Shanmugasundaram, R. *Salmonella* infection in poultry: A review on the pathogen and control strategies. *Microorganisms*. **2023**, *11*(11), 2814. https://doi.org/10.3390/microorganisms11112814.

[7] Wang, Y.; Xu, X.; Jia, S.; Qu, M.; Pei, Y.; Qiu, S.; Zhang, J.; Liu, Y.; Ma, S.; Lyu, N.; et al. A global atlas and drivers of antimicrobial resistance in *Salmonella* during 1900-2023. *Nat. Commun.* **2025**, *16*, 4611. https://doi.org/10.1038/s41467-025-59758-3

[8] Salam, M. A.; Al-Amin, M. Y.; Salam, M. T.; Pawar, J. S.; Akhter, N.; Rabaan, A. A.; Alqumber, M. A. A. Antimicrobial resistance: A growing serious threat for global public health. *Healthcare*. **2023**, *11*(13), 1946. https://doi.org/10.3390/healthcare11131946

[9] Chuanchuen, R.; Padungtod, P. Antimicrobial resistance genes in *Salmonella enterica* isolates from poultry and swine in Thailand. *J. Vet. Med. Sci.* **2009**, *71*(10), 1349–1355. https://doi.org/10.1292/jvms.001349

[10] Chotinun, S.; Rojanasthien, S.; Unger, F.; Tadee, P.; Patchanee, P. Prevalence and antimicrobial resistance of *Salmonella* isolated from carcasses, processing facilities and the environment surrounding small scale poultry slaughterhouses in Thailand. *Southeast Asian J. Trop. Med. Public Health*. **2014**, *45*(6), 1392-1400.

[11] Sinwat, N.; Angkittitrakul, S.; Chuanchuen, R. Characterization of antimicrobial resistance in *Salmonella enterica* isolated from pork, chicken meat, and humans in Northeastern Thailand. *Foodborne Pathog. Dis.* **2015**, *12*(9), 759–765. https://doi.org/10.1089/fpd.2015.1946

[12] Ismail, Z.; Azmi, N. N.; Mahyudin, N. A.; Wan Omar, W. H.; Abdul Rahman, M.; Sapar, M. *Salmonella* isolated from raw chicken meats at selected slaughterhouses in Peninsular Malaysia; their antibiotic resistance profiles and biofilm formation on nutrient-limited media. *Malays. Appl. Biol.* **2024**, *53*(2), 55–71. https://doi.org/10.55230/mabjournal.v53i2.2767

[13] Phaophu, P.; Thadtapong, N.; Wirth, S. E.; Gray, A. S.; Dangsuk, S.; Ngamwongsatit, N.; Aunpad, R.; Chaturongakul, S. High prevalence of multidrug-resistant *Salmonella enterica* in Thailand food

markets: insights from complete genome and phenotypic characterization of ESBL-producing strains. *Microbiol. Spectr.* **2025**, *13*(12), e0212925. https://doi.org/10.1128/spectrum.02129-25

[14] Kim, C.; Frost, I.; Naylor, N. R.; Au, H.; Kim, Y.; Lee, Y.; Bzymek, A.; Majgier, K.; Moldoveanu, A. L.; Salman, O. M.; Simiyu, S.; Youssef, D. M.; Hasso-Agopsowicz, M.; Abbas, K. Length of hospital stay and associated treatment costs for patients with susceptible and antibiotic-resistant *Salmonella* infections: A systematic review and meta-analysis. *BMJ Open*. **2025**, *15*(6), e092494. https://doi.org/10.1136/bmjopen-2024-092494

[15] Choldumrongkul, S. A. study on prevalence and usage pattern cause of antimicrobial residues in pork and chicken meat in Songkhla Province for preventive sustainable strategy. *Thaksin J.* **2014**, *2*, 5-16 https://ph02.tci-thaijo.org/index.php/tsujournal/article/view/43476/35925

[16] Sukhumungoon, P.; Sae-lim, A.; Hayeebilan, F.; Rattanachuay, P. Prevalence, virulence profiles, and genetic relatedness of *Escherichia coli* O45 from raw meats, Southern Thailand. *ASEAN J. Sci. Tech. Report.* **2023,** *27*(2), 58-71. https://doi.org/10.55164/ajstr.v27i2.252140

[17] Sukhumungoon, P.; Nuwilai, L.; Boontaworn, M; Rattanachuay, P. Prevalence, antimicrobial resistance, and genetic relationship of methicillin-resistant *Staphylococcus aureus* from meats, Hat-Yai, Thailand. *ASEAN J. Sci. Tech. Report*. **2025,** *28*(3), e256114. https://doi.org/10.55164/ajstr.v28i3.256114

[18] Bussakorn, B.; Nitipan, S.; Promjan, P.; Petchsuwan, K.; Koknak, P.; Watanakul, P. Microbiological quality of Tao-Kua sold in Paphayom and Mueang Districts, Phatthalung Province, Thailand. *Thaksin J*. **2017,** *20*(3), 133–140. https://ph02.tci-thaijo.org/index.php/tsujournal/article/view/102145

[19] Daod, N.; Lertworapreecha, M.; Niyasom, C. Biofilm formation and adhesin genes in *Staphylococcus aureus* strains isolated from community and hospital settings in Phatthalung Province, Thailand. *Thaksin J.* **2015,** *18*(3), 25–33. https://ph02.tci-thaijo.org/index.php/tsujournal/article/view/55397/46009

[20] Paião, F. G.; Arisitides, L. G.; Murate, L. S.; Vilas-Bôas, G. T.; Vilas-Boas, L. A.; Shimokomaki, M. Detection of *Salmonella* spp., *Salmonella* Enteritidis and Typhimurium in naturally infected broiler chickens by a multiplex PCR-based assay. *Braz. J. Microbiol*. **2013**, *44*(1), 37–41. https://doi.org/10.1590/S1517-83822013005000002

[21] Clinical and Laboratory Standards Institute (CLSI). Performance standards for antimicrobial disk susceptibility tests, 12th ed.; CLSI Standard M02; Clinical and Laboratory Standards Institute: Wayne, PA, **2017**.

[22] Jhelee, A.; O-thong, S.; Nitipan, S. Comparative analysis of bacteria causing bovine mastitis by culture dependent antimicrobial resistance and molecular technique. *Thaksin J*. **2015**, *18*(3), 17–24. https://ph02.tci-thaijo.org/index.php/tsujournal/article/view/55396/46008

[23] Nidaullah, H.; Abirami, N.; Shamila-Syuhada, A. K.; Chuah, L. O.; Nurul, H.; Tan, T. P.; Abidin, F. W. Z.; Rusul, G. Prevalence of *Salmonella* in poultry processing environments in wet markets in Penang and Perlis, Malaysia. *Vet. World*. **2017**, *10*(3), 286–292. https://doi.org/10.14202/vetworld.2017.286-292

[24] Trongjit, S.; Angkititrakul, S.; Tuttle, R. E.; Poungseree, J.; Padungtod, P.; Chuanchuen, R. Prevalence and antimicrobial resistance in *Salmonella enterica* isolated from broiler chickens, pigs and meat products in Thailand–Cambodia border provinces. *Microbiol. Immunol*. **2017**, *61*(1), 23–33. https://doi.org/10.1111/1348-0421.12462

[25] Chiu, L. H.; Chiu, C. H.; Horn, Y. M.; Chiou, C. S.; Lee, C. Y.; Yeh, C. M.; Yu, C. Y.; Wu, C. P.; Chang, C. C.; Chu, C.; et al. Characterization of 13 multi-drug resistant *Salmonella* serovars from different broiler chickens associated with those of human isolates. *BMC Microbiol*. **2010**, *10*, 86. https://doi.org/10.1186/1471-2180-10-86

[26] Kumar, G.; Kumar, S.; Jangid, H.; Dutta, J.; Shidiki, A. The rise of non-typhoidal *Salmonella*: An emerging global public health concern. *Front. Microbiol*. **2025**, *16*, 1524287. https://doi.org/10.3389/fmicb.2025.1524287

[27] Wang, T.; Li, W.; Zhang, R.; Wen, J.; Liu, S.; Jiang, Y.; Lin, L.; Chen, W.; Liang, J.; Ma, X.; et al. Epidemiological features of nontyphoidal *Salmonella* infections reported to foodborne disease surveillance system in China, 2013-2022. *BMC Public Health*. **2025**, *25*(1), 2258. https://doi.org/10.1186/s12889-025-23439-z

[28] ShivaningKarabasanavar, N.; BenakabhatMadhavaprasad, C.; AgalagandiGopalakrishna, S.; Hiremath, J.; ShivanagowdaPatil, G.; Barbuddhe, S. B. Prevalence of *Salmonella* serotypes *S.* Enteritidis and *S.* Typhimurium in poultry and poultry products. *J. Food Saf.* **2020**, *40*(5), e12852. https://doi.org/10.1111/jfs.12852

[29] Algammal, A. M.; El-Tarabili, R. M.; Abd El-Ghany, W. A.; Almanzalawi, E. A.; Alqahtani, T. M.; Ghabban, H.; Al-otaibi, A. S.; Alatfeehy, N. M.; Abosleima, N. M.; Hetta, H. F.; et al. Resistance profiles, virulence and antimicrobial resistance genes of XDR *S.* Enteritidis and *S.* Typhimurium. *AMB Express*. **2023**, *13*, 110. https://doi.org/10.1186/s13568-023-01615-x

[30] Phongaran, D.; Khang-Air, S.; Angkititrakul, S. Molecular epidemiology and antimicrobial resistance of *Salmonella* isolates from broilers and pigs in Thailand. *Vet. World*. **2019**, *12*(8), 1311–1318. https://doi.org/10.14202/vetworld.2019.1311-1318

[31] Yang, W.; Phongaran, D.; Prasertsee, T.; Fang, R.; Phuektes, P.; Angkititrakul, S. Molecular epidemiology and antimicrobial resistance of *Salmonella* spp. isolated from broilers and pigs at slaughterhouses in Thailand and China. *Thai J. Vet. Med.* **2018**, *48*(3), 423–433. https://doi.org/10.56808/2985-1130.2927

[32] EFSA and ECDC (European Food Safety Authority and European Centre for Disease Prevention and Control). The European union summary report on antimicrobial resistance in zoonotic and indicator bacteria from humans, animals and food in 2023–2024. *EFSA J.* **2026**, *24*(2), e9887. https://doi.org/10.2903/j.efsa.2026.9887

[33] Angkititrakul, S.; Chomvarin, C.; Chaita, T.; Kanistanon, K.; Waethewutajarn, S. Epidemiology of antimicrobial resistance in *Salmonella* isolated from pork, chicken meat and humans in Thailand. *Southeast Asian J. Trop. Med. Public Health*. **2005**, *36*(6), 1510–1515.

[34] Lertworapreecha, M.; Sutthimusik, S; Tontikapong, K.; Antimicrobial resistance in *Salmonella enterica* isolated from pork, chicken, and vegetables in Southern Thailand. *Jundishapur J Microbiol*. **2012**, *6*(1), 36-41. https://doi.org/10.5812/jjm.4312

[35] Neunchat, P.; Yangkao, K.; Earm-sa-ard, N.; Chatuphonprasert, S.; Wiwattrakul, J.; Manaijsin, J.; Polruang, N.; Sopa, A.; Sukon, P.; Kanistranon, K.; et al. *Salmonella* prevalence, antibiograms and serotypes from chicken meat and egg in Khon Kaen City, Thailand. *Southeast Asian J. Trop. Med. Public Health*. **2017**, *48*(6), 1241–1247.

[36] Raheem, R. R.; Jheel. W. A. W. Molecular characterization and integron gene prevalence in bacterial pathogens from neonatal omphalitis. *ASEAN J. Sci. Tech. Report*. **2026,** *29*(1), e261254. https://doi.org/10.55164/ajstr.v29i1.261254

[37] Al-Galebi, A. A. S.; Al-Hassani, M. K. A.; Kadhim, H. M.; Alkhudhairy, M. K. Phenotypic-genotypic characterization of macrolide-lincosamide-streptogramin B resistance in *Staphylococcus saprophyticus* UTI isolates from Iraq. *ASEAN J. Sci. Tech. Report.* **2026**, *29*(1), e261225. https://doi.org/10.55164/ajstr.v29i1.261225

[38] Lertworapreecha, M. Cloning and nucleotide sequence analysis of complementary DNA encoding antimicrobial peptide from dung beetle larva. *Thaksin J.* **2014**, *20*(3), 134–142. https://ph02.tci-thaijo.org/index.php/tsujournal/article/view/43725

[39] Bunkaew, K.; Ponpichai, P.; Lertworapreecha, M.; Maitip, J.; Chanasit, W. Phytochemical analysis and biological activities of propolis from *Geniotrigona thoracica*: Evaluation its therapeutic applications. *ASEANJ. Sci. Tech. Report.* **2024**, *27*(5), e253219. https://doi.org/10.55164/ajstr.v27i5.253219

[40] Kalasee, B.; Mittraparp-arthorn, P. Phytochemicals, antioxidant, and antibacterial activities of fresh and dried Chinese chive (*Allium tuberosum* Rottler) leaf extracts. *ASEAN J. Sci. Tech. Report*. **2023**, *26*(4), 1-10. https://doi.org/10.55164/ajstr.v26i4.249336

[41] Krumperman, P. H. Multiple antibiotic resistance indexing of *Escherichia coli* to identify high-risk sources of fecal contamination of foods. *Appl. Environ. Microbiol*. **1983**, *46*(1), 165–170. https://doi.org/10.1128/aem.46.1.165-170.1983

[42] Carrasco, E.; Morales-Rueda, A.; García-Gimeno, R. M. Cross-contamination and recontamination by *Salmonella* in Foods: A review. *Food Res. Int.* **2012**, *45*(2), 545–556. https://doi.org/10.1016/j.foodres.2011.11.004

[43] Wang, Y.; Liu, Y.; Lyu, N.; Li, Z.; Ma, S.; Cao, D.; Pan, Y.; Hu, Y.; Huang, H.; Gao, G. F.; et al. The temporal dynamics of antimicrobial-resistant *Salmonella enterica* and predominant serovars in China. *Natl. Sci. Rev.* **2022**, *10*(3), nwac269. https://doi.org/10.1093/nsr/nwac269

ASEAN
Journal of Scientific and Technological Reports
Online ISSN:2773-8752

Research article

Design of a Knowledge-Based System for Economic Plants: A Case Study of Thailand

Amphaphorn Leelamanotham[1*], Prachasan Vaenthaison[1], Navinda Suetrong[1], Porntip Rodpon[1], and Promporn Poowadin[1]

[1] Faculty of Business Administration, Rajamangala University of Technology Isan, Nakhon Ratchasima 30000, Thailand
* Correspondence: amphaphorn.le@rmuti.ac.th

Citation:
Leelamanotham, A.; Vaenthaison, P.; Suetrong, N.; Rodpon, P.; Poowadin P. Design of a knowledge-based system for economic plants: a case study of Thailand. *ASEAN J. Sci. Tech. Report.* **2026**, *29*(5), e260716. https://doi.org/10.55164/ajstr.v29i5.260716

Article history:
Received: August 6, 2025
Revised: March 19, 2026
Accepted: April 11, 2026
Available online: May 1, 2026

Publisher's Note:
This article is published and distributed under the terms of the Thaksin University.

Abstract: (1) Background: Knowledge management is essential for sustainable business practices in agriculture, particularly for high-value economic plants with commercial potential. This research presents the design and development of a knowledge-based system for economic plants in Thailand, integrating traditional ecological knowledge with modern information management principles. Traditional ecological knowledge is essential for sustainable agroforestry practices, yet this knowledge is eroding with socio-economic changes, creating critical gaps in agricultural information systems; (2) Methods: The study employed a system development life cycle approach with stakeholder engagement principles, resulting in: a) a conceptual framework for economic plant knowledge classification based on ontology-based agricultural knowledge management; b) a comprehensive database design using Entity Relationship Model principles integrating botanical, economic, regulatory, and cultural dimensions; and c) a prototype web-based application enabling effective knowledge acquisition, storage, sharing, and application through dual-interface accessibility; (3) Results: The system facilitates access to critical information about plant characteristics, propagation methods, utilization opportunities, value addition processes, and relevant regulations. Together, these features create an information ecosystem that supports sustainable agribusiness development. This knowledge management solution addresses the fragmentation of valuable traditional and scientific knowledge while providing a centralized platform accessible to farmers, entrepreneurs, researchers, and policymakers. The system preserves intellectual capital by converting tacit traditional knowledge into explicit, shareable resources; (4) Conclusions: The findings indicate that the developed knowledge-based system contributes to preserving traditional ecological knowledge, enhancing information accessibility, and supporting economic development through improved decision-making in agricultural business contexts. The system offers significant business value through enhanced value chain coordination, innovation facilitation, and sustainability integration.

Keywords: Knowledge management; database nanagement; sustainable agriculture; agribusiness information systems; value chain management

1. Introduction

The management of natural resources is a critical domain for sustainable business development, particularly in countries like Thailand, where the agricultural sector contributes significantly to economic growth. The Royal

Forest Department of Thailand, as the primary government agency responsible for forest and wildlife sustainability, has actively promoted the cultivation of economic plants - perennial trees with commercial value that can be grown outside conservation areas [1]. These plants offer substantial business opportunities through direct cultivation, processing, and value-added activities, creating both immediate and long-term economic benefits for stakeholders across the value chain. Economic plants represent a valuable business asset. The Thai government has encouraged their use as collateral for financial transactions, including loans and credit applications. This novel approach to natural resource valuation requires standardized evaluation criteria and comprehensive information about the plants' characteristics, cultivation requirements, processing methods, and market potential. For plant growers and processors to maximize economic returns, they require access to accurate, relevant, and timely knowledge about these high-value species. Traditional agroforestry systems, which combine woody perennials with crops and animals, have historically provided multiple non-wood products and ecological benefits while meeting diverse socio-economic needs sustainably across various agroecological conditions [2]. However, these traditional systems are breaking down for various reasons, and farmers' traditional ecological knowledge is eroding due to socio-economic changes [3].

Knowledge represents an unlimited and appreciating asset - the more it is utilized, the greater its value becomes. Integrating existing knowledge with new insights generates innovative applications and creates additional economic opportunities. Knowledge and information are essential for farmers to tackle contemporary agricultural challenges, where knowledge is increasingly vital for development, surpassing traditional capital factors [4]. However, information about economic plants in Thailand remains fragmented across multiple stakeholders, including government departments, research institutions, and local experts. This fragmentation creates significant barriers to knowledge access, sharing, and application, ultimately limiting the potential business value of these resources. It is important to note that the term "knowledge-based system," as used in this study, refers to a structured knowledge repository designed to capture, organize, and disseminate domain-specific knowledge rather than an expert system with automated inference or reasoning capabilities. This usage aligns with the knowledge management perspective, in which a knowledge-based system denotes any information system that facilitates the systematic management of organizational or domain knowledge, encompassing knowledge acquisition, storage, retrieval, and sharing [5]. This distinction is significant because the primary challenge addressed in this research is knowledge fragmentation and inaccessibility rather than the automation of decision-making processes.

The absence of a centralized knowledge management system creates several challenges. These include limited access to critical information, restricted dissemination of knowledge, disconnection between related knowledge domains, barriers to knowledge enhancement and innovation, and difficulties in preserving valuable traditional knowledge. Traditional ecological knowledge is essential for sustainable agroforestry practices, yet gaps in knowledge about multi-purpose trees hinder their sustainable management [2]. The economic and environmental roles of associated trees are often underassessed, and gaps in knowledge of multi-purpose trees must be addressed for sustainable management [6]. Knowledge management systems have been applied effectively in agricultural contexts across various countries. Information technology enhances public accessibility and interaction via web platforms, and citizen science can enhance knowledge on invasive alien species through web-based interfaces that boost citizen participation in training and data generation [7]. The importance of data aggregation for medicinal plant research is emphasized, highlighting challenges in developing medicinal plant databases and the need to establish minimum standards [8]. Ontology is crucial for knowledge management in agriculture, helping classify agricultural information and build knowledge databases [9]. Agricultural knowledge management systems frameworks that include modules for knowledge acquisition and representation emphasize improving intelligence and efficiency in knowledge sharing [10].

The development of comprehensive databases has proven essential across various plant-related domains. Plant-based extracts can replace synthetic pesticides and antimicrobials, and knowledge bases that compile data on plant uses for crop protection support applications under the One Health approach [11]. Ethnobotanical databases enhance understanding of human-plant relationships and ethnopharmacology, facilitating hypothesis generation and testing while preserving traditional knowledge amidst cultural change

[12]. A global database of plant services for humankind aids in understanding plant-human interactions for future well-being, with research highlighting the importance of conserving biodiversity for human benefit [13]. Repository databases of indigenous herbal medicinal plants, including names in local languages and links between plant pictures and their medicinal uses, demonstrate the vital role of traditional medicine in healthcare systems [14]. In the broader international context, web-based knowledge management systems with dynamic interfaces are proposed to enhance communication among farmers, facilitate collaboration between farmers and agricultural experts, and address knowledge transfer issues arising from employee transitions in agriculture [15]. Internet technologies can enhance knowledge sharing among rural communities, with government and donor support essential for progress, as failure to address the digital divide leads to ongoing poverty [16]. Information and communication technologies are improving access to information for farmers and can revolutionize knowledge sharing in agriculture, with new information services being vital for farmers in rural areas [17].

This research addresses the critical need for improved knowledge management in the agricultural sector, with a specific focus on economic plants in Thailand. The primary objectives are to (1) design a conceptual framework for organizing and classifying economic plant knowledge and evaluate its appropriateness through expert assessment of the knowledge organization structure, (2) develop a comprehensive database model integrating various knowledge dimensions and assess its content correctness and completeness, and (3) create a prototype web-based platform for knowledge access, sharing, and application and evaluate its usability and usefulness for stakeholder decision-making. These objectives align with design science research principles, in which artifact evaluation serves as the primary mechanism for demonstrating research contributions [18].

2. Research Methodology

This study adopts a design-oriented research approach, focusing on the systematic design and development of an information system artifact rather than empirical hypothesis testing. The research is classified as a design science study, in which the primary contributions are the design artifacts themselves — namely, a conceptual knowledge classification framework, a database model, and a prototype web-based platform [19]. The scope of the study encompasses the full system development process from requirements analysis through prototype implementation, to produce a functional knowledge-based system for economic plants in Thailand. Unlike empirical research that tests theoretical propositions through data collection and statistical analysis, design science research contributes to knowledge through the creation and evaluation of artifacts intended to solve identified organizational or domain-specific problems [20]. Accordingly, the validity of this research is assessed through the utility and applicability of the resulting system design rather than through hypothesis testing or inferential statistics. This study employed the System Development Life Cycle (SDLC) approach to design and develop the knowledge-based system for economic plants. The SDLC methodology provides a structured framework for information system development, ensuring alignment with user requirements and business objectives. New-generation agricultural system models for sustainability require user-driven approaches to model development that emphasize collaboration in model development and knowledge product creation [21]. Stakeholder engagement is crucial for addressing major agricultural challenges, and linking model development with user-driven knowledge products enhances food security innovation [22]. The research process consisted of the following key phases that integrate both technical development and stakeholder needs assessment.

2.1 Need study and data collection

The initial phase involved assessing the knowledge management requirements for economic plants through comprehensive data collection. The design aimed to develop a system capable of managing knowledge sharing, linking related knowledge domains, and providing comprehensive coverage of the botanical, economic, regulatory, and cultural dimensions of economic plants. This approach aligns with research emphasizing that relevant information is crucial for agricultural development, and that unambiguous interpretations are needed for farmers to make informed decisions [23]. The scope of economic plants addressed in this study is based on the classification established by the Royal Forest Department of Thailand,

which designates two categories of trees permitted for cultivation outside conservation areas: non-timber economic plants (20 species) and economically valuable timber species (58 species). The current prototype focuses on 20 species selected from the economically valuable timber category. The selection criteria for inclusion were based on the following considerations: (1) the species must be designated as economically valuable timber by the Royal Forest Department, (2) the species must be suitable for cultivation in the study area (Nakhon Ratchasima Province), and (3) sufficient knowledge from both documented sources and local practitioners must be available to populate the knowledge base across the three primary categories (Profilers, Knowledge Profiles, and Expert Directory). The prototype screenshots presented in Figures 5 and 6 display Siamese Rosewood (*Dalbergia cochinchinensis*) and Teak (*Tectona grandis*) as representative examples; however, the system contains knowledge entries for all 20 selected species. Future development aims to expand coverage to include the remaining economically valuable timber species as well as the 20 non-timber economic plant species, subject to the availability of comprehensive knowledge from relevant stakeholders.

The stakeholder engagement process involved three principal groups: (1) government officials from the Royal Forest Department and related agricultural agencies who provided regulatory and policy-level information regarding economic plant designation and utilization guidelines; (2) local farmers and community practitioners in Nakhon Ratchasima Province who contributed experiential knowledge on cultivation practices, traditional uses, and cultural beliefs associated with economic plants; and (3) academic researchers and subject matter experts in botany, agroforestry, and agricultural economics who provided scientific and technical knowledge. Data collection was conducted through semi-structured interviews and document analysis. Interviews with government officials focused on regulatory frameworks and plant designation criteria, while interviews with local practitioners captured tacit knowledge regarding traditional cultivation and utilization methods. Document analysis encompassed official publications, research reports, and community-level records of economic plants. The insights gathered from these stakeholder groups directly informed the design of the three-category knowledge classification structure (Profilers, Knowledge Profiles, and Expert Directory), ensuring that the system architecture reflected the information needs and knowledge domains identified across stakeholder groups. This stakeholder-informed approach aligns with research emphasizing that participatory methods in agricultural system development enhance the relevance and adoption potential of resulting knowledge products [24].

The data collection process incorporated both electronic and paper-based documentary sources from relevant agencies, communities, and subject matter experts. This included harvesting explicit knowledge from documented sources and tacit knowledge from experience-based insights and lessons learned from practitioners. Traditional ecological knowledge is essential for sustainable agroforestry practices, yet it is eroding due to socio-economic changes, making its preservation and documentation critical [2]. The methodology recognized that herbarium data complements published literature in ethnobotanical studies, and that traditional knowledge conservation is crucial amidst cultural change [12]. The comprehensive approach to data collection addressed the challenge that knowledge of agroforestry systems' functioning and dynamics is limited and that trends vary across agro-ecological conditions and market access [25]. By integrating diverse knowledge sources, the study aimed to bridge the gap between traditional ecological knowledge and modern agricultural information systems. This multi-source approach supports the development of minimum standards for plant databases while addressing under-documentation of traditional plant knowledge [8, 13]. The data collection framework also considered that a unified approach in ethnobotany is necessary for effective research, supporting comparative analysis and knowledge archiving [26].

2.2 Design of Knowledge Flow Relations

This phase focused on creating linkages between knowledge categories to establish a coherent knowledge structure. The knowledge base was organized into three primary categories: Profilers (basic information about economic plants), Knowledge Profiles (specialized knowledge related to economic value), and Expert Directory (information about knowledge providers and their expertise). This structured approach aligns with research that emphasizes that ontology aids in classifying agricultural information and in building knowledge databases. Key technologies for knowledge acquisition and representation are essential for improving intelligence and efficiency in knowledge sharing [9]. **Figure 1** illustrates the high-level relationship

design between these knowledge categories, establishing the foundation for knowledge integration and accessibility. The design addresses the challenge that data structuring and mining enhance integration processes, and that effective management systems reduce project delays and costs through timely information that significantly impacts project execution [27]. The knowledge categories were further analyzed to identify relationships among subcategories, resulting in a comprehensive knowledge network, as shown in **Figure 2**. This network approach supports the principle that integrated approaches reduce costs and improve processes in project implementation, while methodology provides structured solutions for complex industry problems.

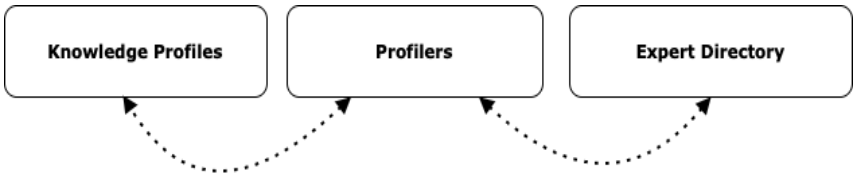


Figure 1. The design of links in the category of economic plants

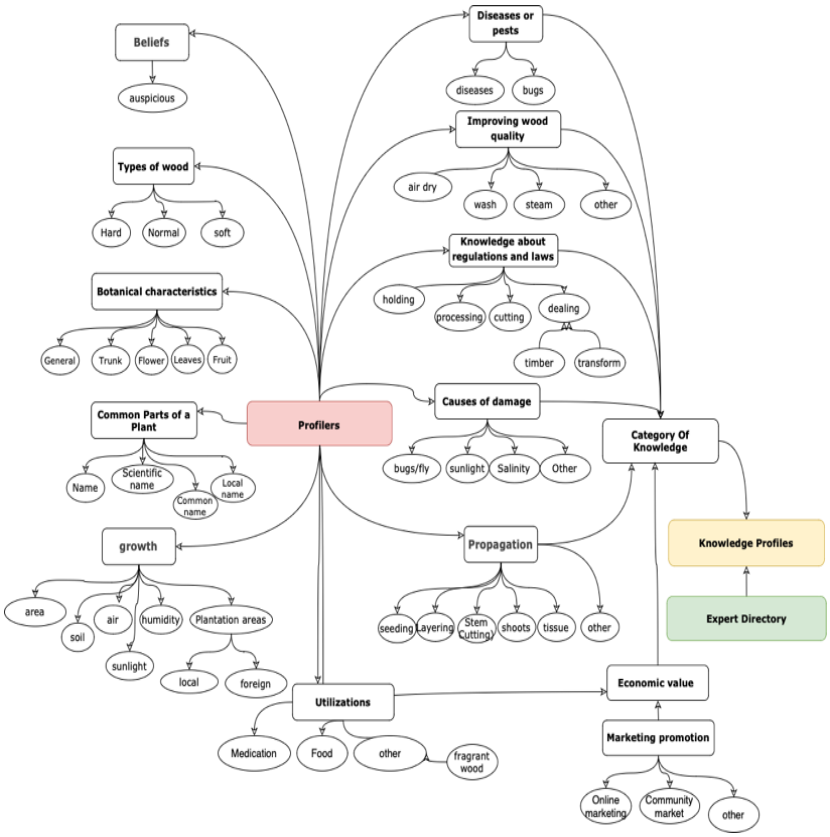


Figure 2. The design of the related links between the subcategories of economic plants

The knowledge classification framework used principles from the Dewey Decimal Classification System to organize knowledge obtained during data collection systematically. This systematic approach addresses the need for standardized environments for data submission and retrieval, supporting the integration of diverse scientific knowledge into dynamic databases. Each primary category was divided into specific subcategories that facilitate comparative research and knowledge archiving through community contributions. The framework incorporates the principle that tools for browsing and editing databases are essential for effective knowledge management, and that international standards committees play an important role in facilitating global collaboration [26]. The three-category structure was designed to address specific knowledge domains: Profilers store general information about economic plants, including botanical characteristics, propagation methods, plantation areas, diseases and pests, and cultural beliefs and practices.

Knowledge Profiles store specialized knowledge in three domains: general knowledge of economic value (including prevention of plant diseases and pests, propagation techniques, maintenance requirements, and fundamental utilization methods), knowledge about economic benefit utilization (including processing methods, quality improvement techniques, texture maintenance, storage requirements, damage prevention, value addition opportunities, marketing strategies, and supporting agencies), and knowledge about regulations and laws (including business-related regulations and compliance requirements). The Expert Directory stores information about knowledge providers, including individual experts and institutional knowledge holders, along with their contact information and expertise domains.

$$\text{Popularity score Rating} = \frac{\sum_{i=1}^{n}(x_i)}{\sum_{i=1}^{n}(N_i)} \quad (1)$$

where

$\sum_{i=1}^{n}(x_i)$ is the total of scores

$\sum_{i=1}^{n}(N_i)$ is the total number of experts

The system incorporates a popularity score rating mechanism for each knowledge component, calculated using Equation 1, to provide a community-based quality indicator. The scoring uses a five-point Likert scale (1 = least useful, 5 = most useful), where each qualified expert registered in the Expert Directory may assign a single rating per knowledge entry. The variable x_i represents the score assigned by expert i, and N_i represents the count of each contributing expert (equal to 1 per expert), such that the equation computes the arithmetic mean of all expert ratings for a given knowledge entry. While the computation is mathematically equivalent to a simple average, its formal specification serves two purposes within the system design: first, it provides an unambiguous definition for database implementation, and second, it establishes the foundation for potential future extensions such as weighted scoring based on expert domain relevance or experience level.

It is important to clarify the functional scope of the knowledge-based system in relation to knowledge processing. The system is designed primarily as a knowledge repository and retrieval platform rather than an inference-based expert system. The principal functions include knowledge acquisition from diverse sources, structured storage using a relational database architecture, organized retrieval via a three-category classification framework, and knowledge sharing via a web-based interface. The system does not, in its current form, incorporate automated reasoning engines, production rules, or algorithmic recommendation mechanisms. Instead, knowledge rules within the system operate at the organizational level — governing how knowledge is classified into Profilers, Knowledge Profiles, and Expert Directory categories, how relationships between knowledge subcategories are structured (as illustrated in Figure 2), and how content quality is indicated through the popularity score rating mechanism (Equation 1). This community-based scoring approach serves as a soft validation rule, enabling users to prioritize knowledge endorsed by multiple experts rather than relying on system-generated inferences. This design decision reflects the study's primary objective of addressing knowledge fragmentation and accessibility challenges rather than automating decision-making processes. The distinction is consistent with knowledge management system typologies that differentiate between repository-oriented systems focused on knowledge codification and capture, and reasoning-oriented systems focused on automated inference and decision support [28]. Future development may extend the system toward recommendation capabilities, such as suggesting suitable plant species based on geographic and climatic conditions or recommending value-addition pathways based on plant characteristics, which would require integrating rule-based or machine-learning components [29].

2.3 Knowledge Quality Assurance and Validation

Ensuring the quality, accuracy, and trustworthiness of knowledge content is a fundamental concern for the system, particularly given the integration of traditional ecological knowledge with scientific information. The knowledge quality assurance process operates through three complementary mechanisms: expert-mediated content validation, administrative review, and community-based scoring. First, all knowledge entries submitted to the system undergo review by authorized administrators before publication

on the public-facing interface. The administrative section restricts content management functions to authorized users, ensuring that only vetted information is made accessible. This gatekeeping function serves as the primary quality control mechanism, preventing unverified or inaccurate content from entering the knowledge base. Second, the selection of contributing experts follows domain-relevant criteria. Experts registered in the Expert Directory are identified based on documented expertise in relevant fields, including academic qualifications, institutional affiliations, professional experience in economic plant cultivation or processing, and recognized standing within local farming communities for traditional knowledge holders. The Expert Directory stores these credentials, enabling system administrators to assess contributor qualifications when evaluating submitted knowledge.

Third, the popularity score rating mechanism (Equation 1) provides a post-publication quality indicator based on aggregated expert evaluations. A minimum threshold of three expert ratings is required before a popularity score is displayed for any knowledge entry, ensuring that scores reflect a baseline level of consensus rather than individual opinion. It is acknowledged that this threshold represents a practical minimum for the prototype stage, and future development may increase this requirement as the expert user base expands. Regarding resolving conflicts between traditional and scientific sources, the system adopts a complementary rather than hierarchical approach. Both traditional ecological knowledge and scientific information are stored as distinct knowledge entries with clear source attribution, allowing users to access and compare perspectives from different knowledge traditions. When direct contradictions arise, the administrative review process flags such entries, facilitating resolution through consultation with relevant domain experts. The system does not automatically prioritize one knowledge type over another, consistent with research advocating for the respectful integration of indigenous and scientific knowledge systems in agricultural contexts. To address knowledge currency, the database includes a timestamp field (Knowledge_timestamp) that records the most recent update for each entry. System administrators are responsible for periodic content reviews to identify entries requiring updates based on new research findings, regulatory changes, or evolving cultivation practices. Future development will incorporate automated notification mechanisms to alert administrators when entries exceed a predefined age threshold without review, supporting systematic content maintenance [30].

3. Designing the Knowledge Base

While Section 2 established the conceptual knowledge classification framework and the relationships between knowledge categories, this section presents the translation of that conceptual design into a physical database architecture. The database design phase constitutes a distinct design artifact within the design science research approach, representing the operational specification that enables system implementation. The database design phase translated the conceptual knowledge framework into an operational data structure using the Entity-Relationship Model (ERM). This model established relationships among various knowledge categories, creating a comprehensive, integrated data architecture, as shown in **Figure 3**. The ERM approach aligns with research demonstrating that integrated methodological frameworks improve connectivity in management systems, where data structuring and mining enhance integration processes [27]. Comprehensive databases have proven essential across various plant-related domains, with integrated data curation supporting genome sequences, literature, and diverse genomic data for better analysis and application [31]. The Entity Relationship Model facilitated the detailed specification of data elements through comprehensive data dictionaries for each knowledge category. These dictionaries defined column names, descriptions, data types, and relationships with other tables, following principles established in successful plant database development. Research shows that databases supporting comparative studies and molecular biology research require visualization tools and systematic data organization to enhance user experience [31]. The systematic approach to database design addresses the challenge that big data dimensions enhance global connectivity and project management, while ecosystem frameworks generate economic value in industries [32].

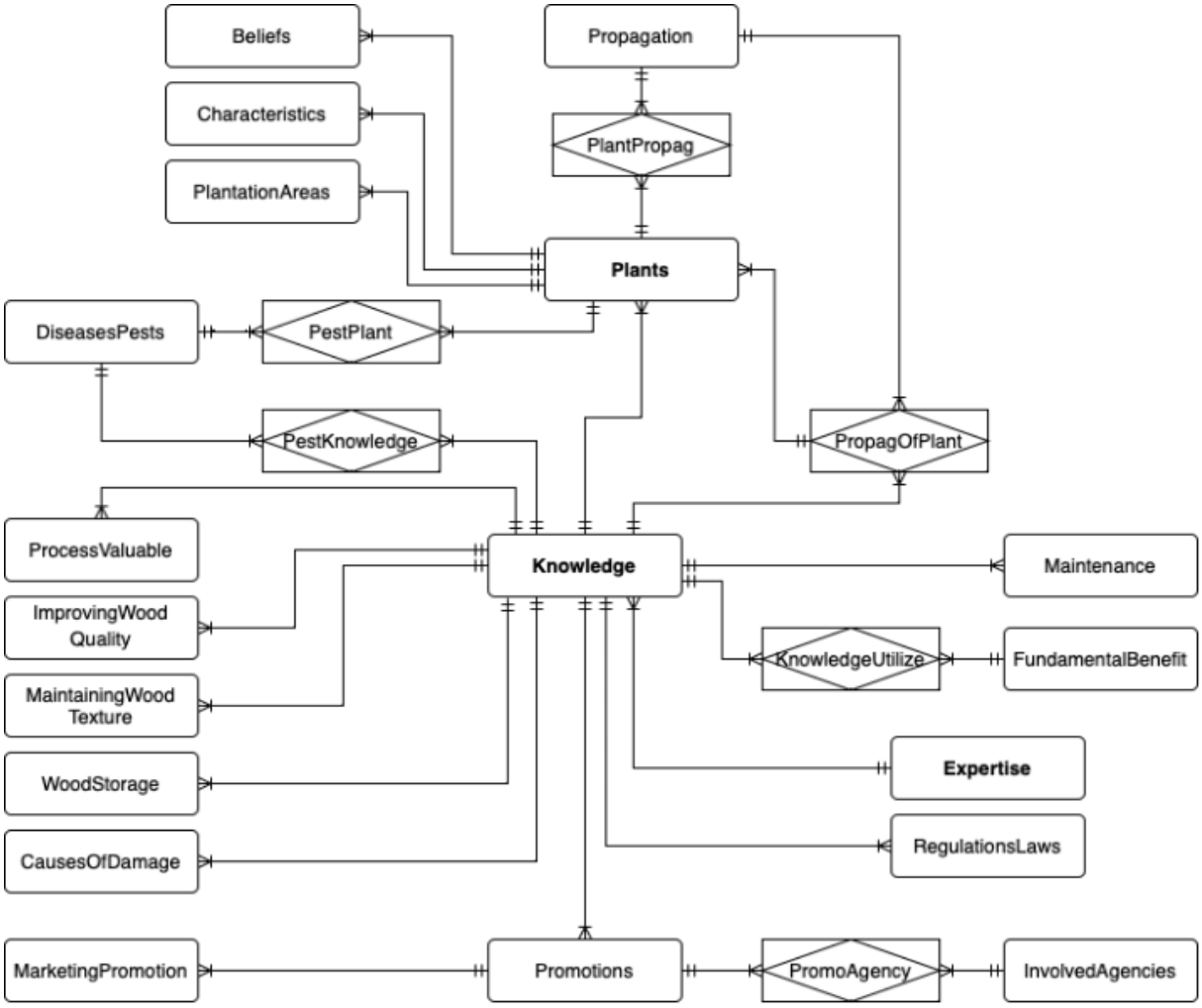


Figure 3. The entity relationship model of economic plants

Table 1 presents the data dictionary for the Utilization table, which stores the classification of different utilization types associated with economic plants (e.g., medicine, food, fragrant wood). This table uses a simple two-field structure with an auto-generated primary key (UtilizeID) and a descriptive label (UtilizeTitle), serving as a reference table linked to other knowledge components within the database. **Table 2** presents the data dictionary for the Knowledge table, which serves as the central repository for storing individual knowledge records within the system. Each record is identified by a composite code (KnowledgeID) incorporating the recording year and a sequential number. The table captures essential metadata, including the knowledge title, search keywords, creation date, and a timestamp for tracking updates. The popularity score field (RatingScore) stores the community-based validation score calculated using Equation 1. Foreign key relationships link each knowledge record to the relevant plant species (PlantID) and contributing expert (ExpertID), establishing the relational connections illustrated in the entity relationship model (Figure 3). This detailed specification approach supports the principle that database development requires careful attention to data heterogeneity and multidimensionality in complex systems [33]. The comprehensive data dictionary approach ensures the database effectively manages diverse knowledge types, maintains data integrity, and supports various user needs. Database design must accommodate user-friendly interfaces for researchers and users, while providing access to genetic resources for comparative analysis [34]. The structure facilitates comparative and functional analysis of plant information, supporting both research applications and practical implementation [35].

The database architecture incorporates multiple knowledge dimensions to support comprehensive plant information management. This multidimensional approach aligns with research findings that databases

should integrate various types of data, including transcriptomic data, genetic variations, and phenotype links, to support agricultural benefits [36]. The design recognizes that databases aid researchers in related plant studies by including functional annotations and multi-data integration [34]. Knowledge bases that compile data from multiple sources support applications across various domains, with comprehensive databases enhancing understanding and research capabilities [11]. The comprehensive data dictionary (see **Appendix**) provides detailed specifications for all database tables, establishes clear data governance protocols, and ensures data integrity throughout the system. This systematic documentation approach supports the principle that databases require continuous updates with new data and methods while maintaining high-quality data management standards [37]. The detailed specification ensures that the database can support diverse applications while maintaining consistency and reliability in knowledge management. The architecture supports the integration of traditional ecological knowledge with modern information management principles, addressing the critical need to preserve and make accessible valuable agricultural knowledge [38].

Table 1. Example of a detailed dictionary of a utilization table

No	Columns	Descriptions	Data Type	Constraints	References/ Remarks
1	UtilizeID	Code for Utilization: The format is a unique three-digit number, such as 001 or 002.	Varchar	PK	Auto generate
2	UtilizeTitle	Names of utilization, such as medicine and food	Varchar		

Table 2. Example of a detailed dictionary of an economic plant table

No.	Columns	Descriptions	Data Type	Constraints	References /Remarks
1	KnowledgeID	Code for stored knowledge in the format of YY9999. Details are as follows: YY is the year the knowledge information was recorded. 9999 is the sequence in which knowledge information was recorded in that year. Example data: 640001, automatically generated from the system	Varchar	PK	Auto generate
2	KnowledgeDate	Date of knowledge creation	Date		
3	KnowledgeName	Knowledge names specified by the knowledge creator.	Varchar		
4	Keywords	Identification of knowledge keywords used for categorizing and searching	Varchar		
5	RatingScore	The popularity score of knowledge identified by those who take it, and calculated according to Equation 1	Integer		
6	ExpertID	Code of Knowledge expertise	Varchar	FK	Expertise
7	PlantID	Code of valuable plants	Varchar	FK	Plants
8	Knowledge_timestamp	Date and time of updating the latest information Automatically generated from the system	DateTime		*(auto generate)*

4. Website Development for Economic Plants

The prototype system was developed using a three-tier architecture comprising a presentation layer, application logic layer, and data storage layer. The presentation layer was implemented using HTML5, CSS3, and JavaScript to ensure cross-browser compatibility and responsive design across desktop and mobile devices. The application logic layer was developed using ASP.NET with C# as the server-side programming language, handling request processing, business logic execution, and communication between the user interface and database. The data storage layer utilized Microsoft SQL Server 2019 Community Edition as the relational database management system, implementing the entity relationship model described in Section 3. User authentication was implemented using a role-based access control mechanism that distinguishes between two user types: public users, who access the display interface without authentication, and authorized administrators, who must authenticate with a username and password before accessing the content management functions described in Section 4.2. Session management and input validation were implemented to mitigate common web security vulnerabilities. The prototype was deployed on a Windows Server environment within the university network infrastructure during the development and evaluation phases.

Table 5. Technology stack of the prototype system

Component	Technology
Front-end	HTML5, CSS3, JavaScript
Back-end framework	ASP.NET (C#)
Database management system	Microsoft SQL Server 2019 Community Edition
Web server	Internet Information Services (IIS)
Operating system	Windows Server
Authentication	Role-based access control with session management
Deployment environment	University network infrastructure

The final phase involved developing a prototype website based on the knowledge base design. The database was implemented using SQL Server 2019 Community Edition, creating an integrated repository for economic plant knowledge, as illustrated in Figure 4. The web-based approach aligns with research demonstrating that information technology enhances public accessibility and interaction via web platforms, with web-based interfaces boosting citizen participation in training and data generation [39]. Dynamic web-based knowledge management systems can improve networks and facilitate collaboration between stakeholders and experts [40]. The website development focused on creating both public-facing information display components and administrative knowledge management functions. The system was designed for multi-platform accessibility via standard web browsers across desktop and mobile devices. This approach addresses research findings that web-based knowledge management systems are essential for enhancing communication, and it builds on frameworks aimed at improving connectivity among users [40]. The dual-interface design supports the principle that knowledge management systems should provide standardized environments for data submission and retrieval while supporting multimedia storage, including images, sound, and video [26].

4.1 Results Display Section

The display section provides public access to economic plant information through an intuitive user interface. The main page (**Figure 5**) displays plant names and images with navigation options to access detailed information. This user-friendly approach follows successful database design principles, enabling users to access information through intuitive interfaces that enhance the user experience [34]. The interface design aligns with research findings that databases should facilitate data visualization and exploration, enabling users to browse and analyze information effectively [41].

Users can select specific plants to access comprehensive information including botanical characteristics, cultivation requirements, utilization methods, and related knowledge (**Figure 6**). This comprehensive information structure addresses the need for databases that link diverse types of information for agricultural benefits, supporting both research applications and practical decision-making [31]. The

information presentation follows principles established in successful plant databases that provide access to genetic resources for comparative analysis while maintaining user-friendly navigation [35]. The display system supports integrating various knowledge domains, aligning with research findings that databases should facilitate hypothesis generation through data visualization tools [42].

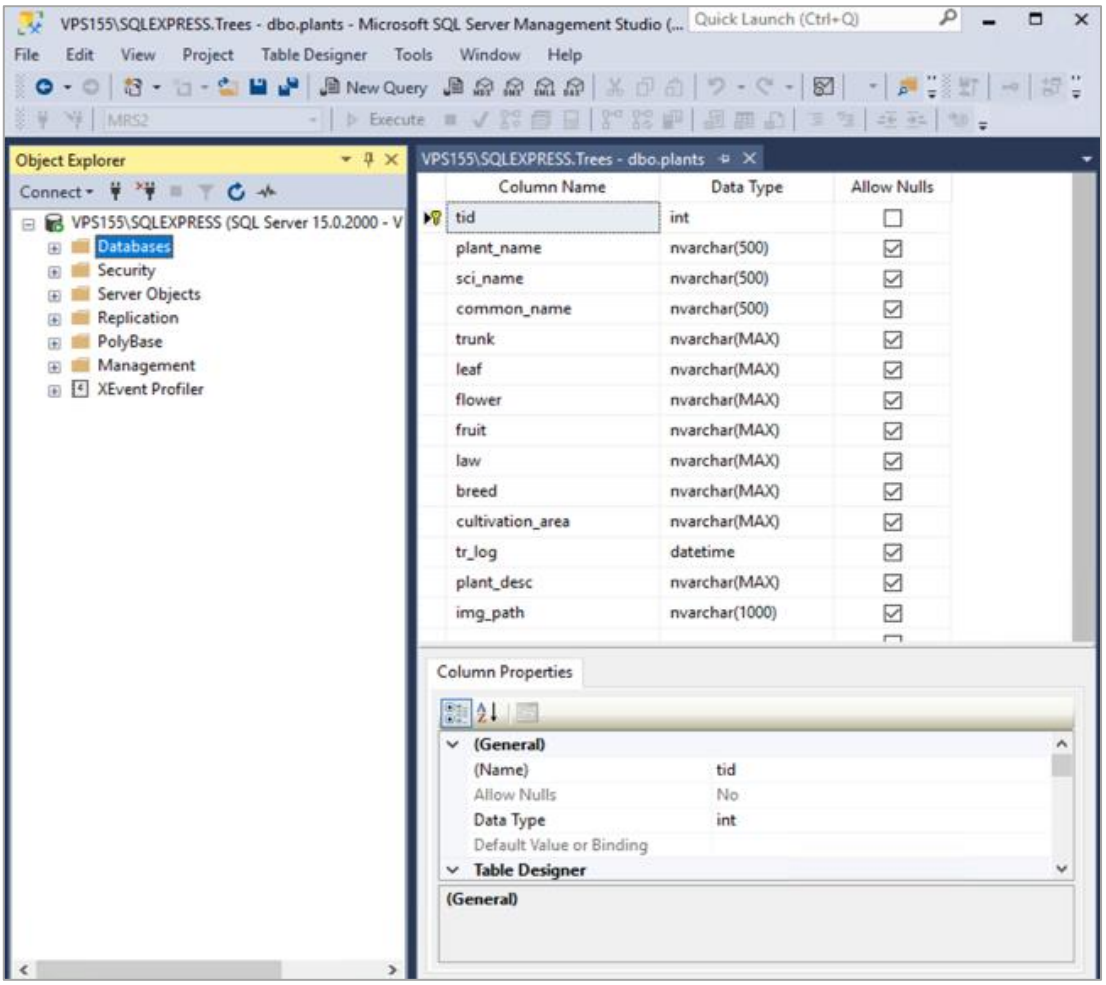


Figure 4. An example of creating a knowledge data table with the entity relationship database management program

4.2 Information Management Section

The administrative section (**Figure 7**) provides authorized users with tools to manage knowledge content, including adding new information, updating existing content, and maintaining data accuracy and relevance. This administrative approach aligns with research emphasizing that databases require tools for browsing and editing to maintain data quality and support collaborative analysis among researchers [43]. The management interface addresses the principle that effective management systems reduce project delays and costs through structured information management [44]. This dual-interface approach ensures both public accessibility to validated knowledge and controlled administrative functions for knowledge governance and quality assurance. The design supports research findings that contribution mechanisms enhance collaborative and comparative analysis among researchers, while standardized environments facilitate effective data management. The system architecture addresses the need for databases that can be continuously updated with new data and methods while maintaining high-quality standards for knowledge management. The administrative functions support the principle that knowledge management systems should encourage comparative research through community contributions while maintaining data integrity and reliability [45].

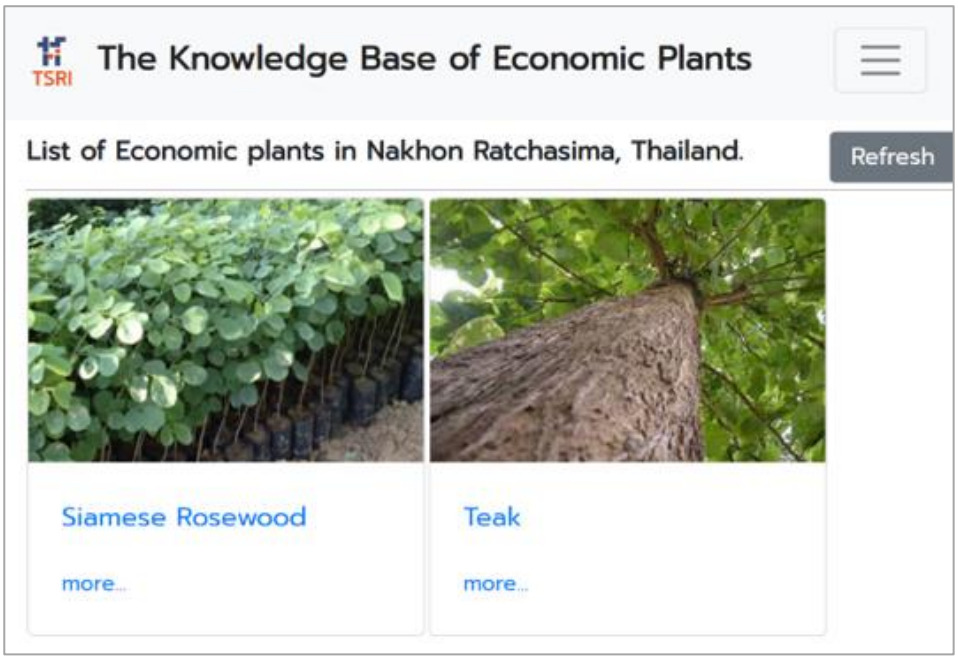


Figure 5. Section on Result Display on the Website Main Page of Economic Plants

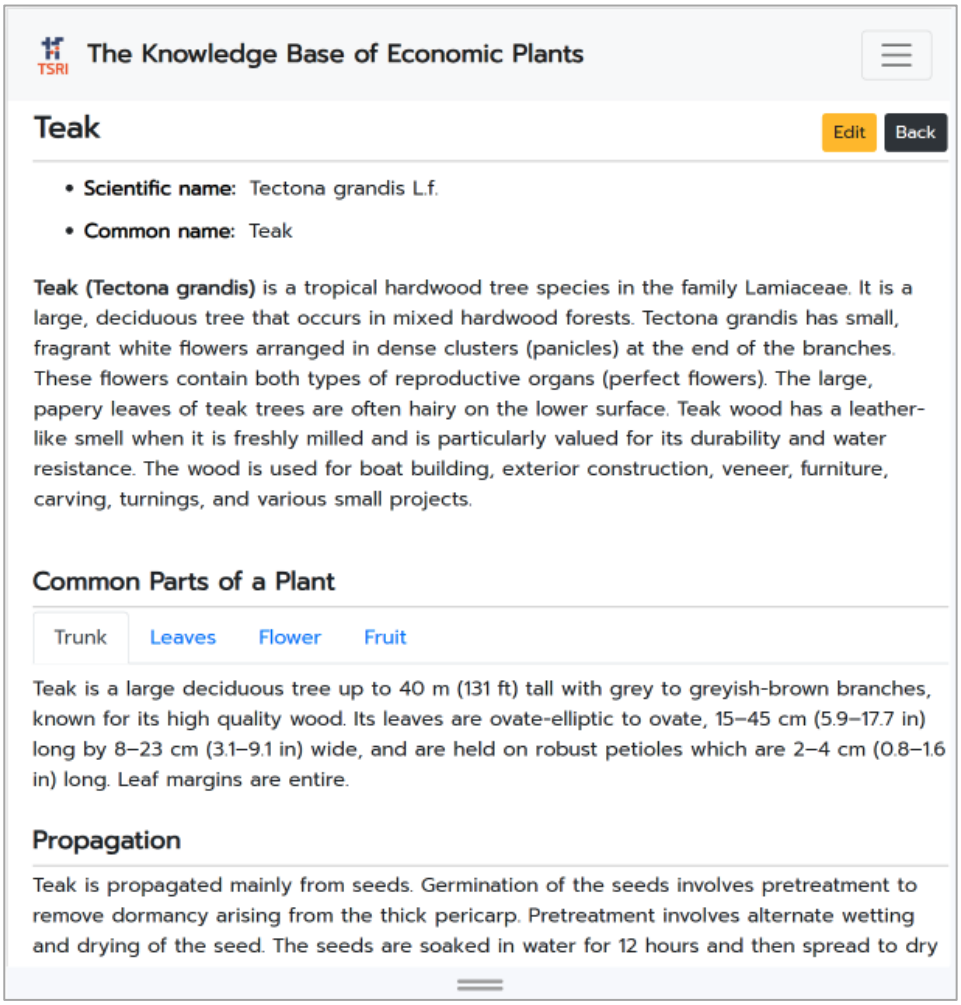


Figure 6. Section on the information structure of economic plants

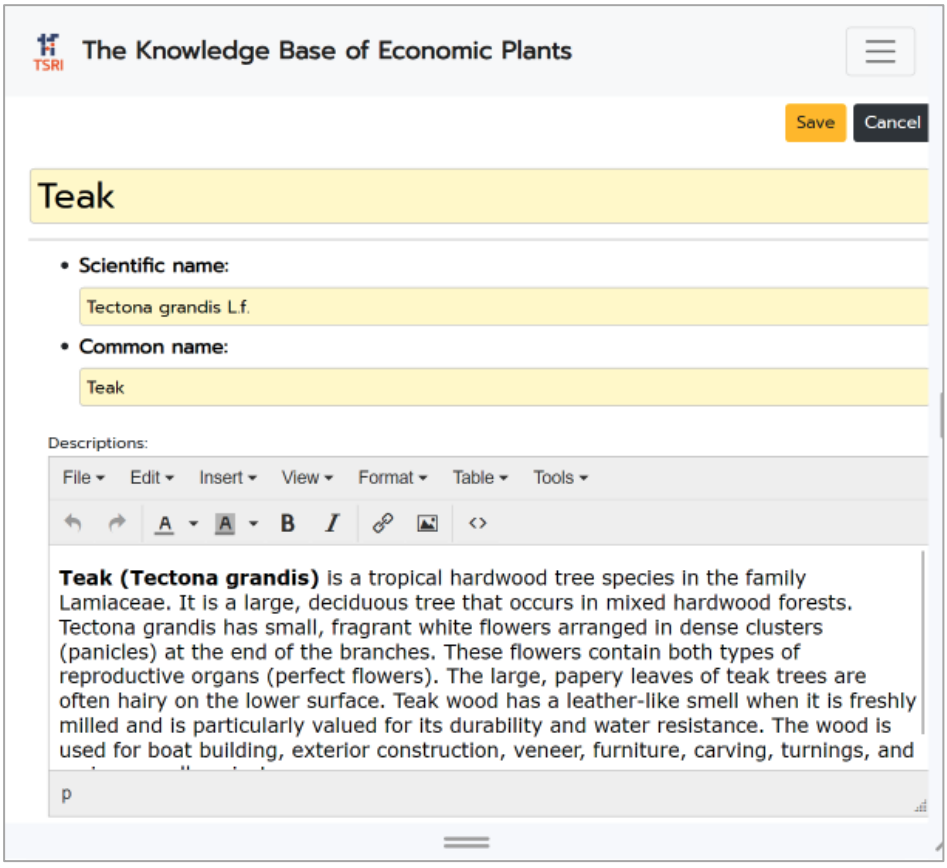


Figure 7. Section on Information Management of Economic Plants

4.3 System Evaluation through Expert Validation

To assess the usefulness, correctness, and overall quality of the knowledge-based system, an expert validation approach was employed. A panel of five subject matter experts was invited to evaluate the system. The panel comprised specialists in agricultural knowledge management, information system development, and economic plant cultivation, ensuring coverage of both the technical and domain-specific aspects of the system. The evaluation was conducted using a structured questionnaire based on a five-point Likert scale (1 = strongly disagree, 5 = strongly agree). The assessment criteria were organized into four dimensions: (1) content correctness and completeness, evaluating whether the knowledge base accurately represents botanical, economic, regulatory, and cultural information about economic plants; (2) system usability, assessing the ease of navigation, information retrieval, and overall user experience across both the public display and administrative interfaces; (3) usefulness for decision-making, measuring the perceived value of the system for supporting stakeholders in cultivation planning, value addition identification, and regulatory compliance; and (4) knowledge organization and structure, evaluating the appropriateness of the three-category classification framework (Profilers, Knowledge Profiles, and Expert Directory) for representing economic plant knowledge. The expert panel also participated in a case demonstration using Teak (*Tectona grandis*) as a representative economic plant. Each expert was asked to perform a series of tasks, including retrieving botanical characteristics, accessing propagation methods, reviewing utilization information, and navigating the knowledge profile and expert directory sections. Following the task-based demonstration, experts provided qualitative feedback on system strengths and areas for improvement. Table 3 presents the summary results of the expert validation. The overall mean score across all evaluation dimensions was 4.25 (S.D. = 0.43), indicating high satisfaction with the system. Content correctness received a mean score of 4.05, confirming that the knowledge base accurately captures essential information about economic plants. System usability scored 4.21, with experts noting that the dual-interface design facilitated both public access and administrative management. Usefulness for decision-making received a mean score of 4.57, suggesting that the system

provides practical value for diverse stakeholders. Knowledge organization scored 4.18, supporting the appropriateness of the adopted classification framework.

Table 3. Summary of Expert Validation Results by Evaluation Dimension

No.	Evaluation Dimension	$\overline{x}$	S.D.	Level
1	Content correctness and completeness	4.05	0.45	High
2	System usability	4.21	0.65	Very High
3	Usefulness for decision-making	4.57	0.46	Very High
4	Knowledge organization and structure	4.18	0.14	High
	Overall	**4.25**	**0.43**	**Very High**

Qualitative feedback from the expert panel highlighted several strengths, including the comprehensive integration of multiple knowledge dimensions, the accessibility of the web-based platform across devices, and the practical relevance of linking botanical information with economic utilization and regulatory knowledge. Suggestions for improvement included expanding the number of plant species covered, incorporating multimedia content such as instructional videos for propagation techniques, and adding a search function with advanced filtering capabilities.

5. Discussion and Business Implications

The knowledge-based system for economic plants constitutes a structured contribution to agricultural information management, with several implications for agribusiness practice. By centralizing and organizing knowledge about economic plants, the system addresses critical information gaps that have previously limited sustainable agribusiness development. The system's comprehensive approach aligns with research demonstrating that the benefits of agricultural systems generally outweigh their costs, with major knowledge gaps existing in understanding plant benefits and their economic value [46]. Economic valuation is crucial for investment decisions, and standardizing research protocols can improve comparability across studies. To contextualize the contribution of the proposed system, **Table 4** presents a structured comparison with existing plant-related databases and knowledge management platforms relevant to economic plants, both internationally and within Thailand.

As shown in **Table 4**, existing platforms primarily serve botanical, taxonomic, or biodiversity documentation purposes and target research-oriented users. While these platforms make significant contributions within their respective domains, several gaps remain that the proposed system addresses. First, none of the existing platforms integrate economic value chain information — including processing methods, value addition opportunities, marketing strategies, and supporting agencies — as a structured knowledge component. Second, regulatory and legal information on business-related compliance requirements for economic plants is absent from all the compared platforms. Third, traditional ecological knowledge, while recognized as essential for sustainable agroforestry practices [2], is either absent or only peripherally captured in existing systems. The proposed system explicitly structures this knowledge dimension and converts tacit traditional knowledge into a retrievable form. Fourth, the Expert Directory with credential-based attribution and the community-based popularity scoring mechanism provide quality assurance features not found in the compared platforms. Fifth, the proposed system is specifically designed to serve a broader stakeholder base, including farmers and entrepreneurs, whereas existing platforms predominantly target researchers and scientific practitioners. It should be noted that the proposed system is not intended to replace these existing platforms but rather to complement them by addressing the specific needs of economic plant knowledge management in the Thai agricultural context. The system occupies a distinct niche at the intersection of knowledge management, agricultural business information, and traditional knowledge preservation, a space not fully covered by existing resources [47].

Table 4. Comparison of the proposed knowledge-based system with existing platforms

Feature / Criterion	PROSEA (Plant Resources of South-East Asia)	Flora of Thailand (Forest Herbarium)	Thai Biodiversity Information Facility (TH-BIF)	Agroforestry Species Switchboard (World Agroforestry)	Proposed System
Primary focus	Botanical and utilization documentation of SE Asian plant resources	Taxonomic classification and botanical description	Biodiversity occurrence records and species distribution	Agroforestry species linking across databases	Economic plant knowledge management integrating botanical, economic, regulatory, and cultural dimensions
Knowledge dimensions	Botanical, utilization	Botanical, taxonomic	Biodiversity, ecological	Agroforestry, ecological	Botanical, economic, regulatory, cultural, and traditional ecological
Traditional ecological knowledge	Limited	Not included	Not included	Limited	Explicitly captured and structured
Economic value chain information	Partial (utilization only)	Not included	Not included	Partial	Comprehensive (cultivation, processing, value addition, marketing, regulations)
Regulatory and legal information	Not included	Not included	Not included	Not included	Included as a dedicated knowledge category
Expert directory and attribution	Not included	Not included	Not included	Not included	Included with credential-based expert profiles
Community-based quality scoring	Not included	Not included	Not included	Not included	Included (popularity score rating)
Administrative content management	Limited	Limited	Limited	Not applicable (aggregator)	Dual-interface with public display and administrative management
Target users	Researchers, botanists	Taxonomists, researchers	Researchers, conservation practitioners	Researchers, agroforestry practitioners	Farmers, entrepreneurs, researchers, policymakers
Geographic scope	South-East Asia	Thailand	Thailand	Global	Thailand (economic plants designated by the Royal Forest Department)

Value Chain Enhancement is supported by the expert panel's assessment of the system's usefulness for decision-making, which indicated that the integrated knowledge structure provides practical value across multiple stages of the agricultural value chain. The comprehensive knowledge base links information across propagation and cultivation, processing, marketing, and regulatory compliance, enabling stakeholders to identify value-addition opportunities. The extent to which this translates into measurable business process improvements requires longitudinal field assessment with diverse stakeholder groups. Economic incentives for cultivation include income, land quality, and market access, and financial analysis shows that some plantations yield higher net present values than alternatives [48]. Intellectual Capital Management represents another crucial advantage, as traditional ecological knowledge constitutes a valuable form of intellectual capital that has historically been underutilized due to fragmentation and accessibility challenges. The system preserves this intellectual capital while making it actionable for business applications, effectively converting tacit knowledge into explicit, shareable resources. The erosion of traditional ecological knowledge documented in the literature [2] underscores the practical relevance of this preservation function. The dataset aids understanding of human-plant interactions for future well-being, promoting research on plant-human relationships while supporting biodiversity conservation and policy-making [13].

Risk Mitigation capabilities emerge as agricultural businesses face numerous risks, including plant diseases, market fluctuations, and regulatory compliance. The knowledge base provides critical information for risk assessment and mitigation, enabling proactive management strategies rather than reactive responses to challenges. et al. [1] indicate that optimal cultivation strategies vary significantly across different future scenarios, and portfolio approaches can reduce exposure to cost risks in agricultural strategies. Tree cultivation remains cost-effective compared to alternative options, and forest ecosystem services enhance social value. However, socio-economic drivers significantly affect cultivation outcomes, underscoring the importance of local community participation and benefit-sharing [3]. The system also serves as a potential catalyst for innovation. By integrating diverse knowledge domains and facilitating knowledge sharing, the platform creates an environment conducive to innovation in agricultural practices, processing methods, and product development. This innovation potential represents a significant competitive advantage for businesses in the agricultural sector. Antle et al. [21] demonstrate that new-generation agricultural system models require user-driven approaches that emphasize collaboration in model development and knowledge product creation. Stakeholder engagement is crucial for addressing major agricultural challenges, with advances in data and technology being essential for achieving sustainable development.

Sustainability Integration occurs as the system promotes sustainable business practices by preserving traditional knowledge about environmentally appropriate cultivation methods while linking economic and ecological considerations. This integrated approach aligns with growing market demands for sustainable products and practices. Large-scale cultivation activities predominantly have negative socio-economic impacts, particularly on land and livelihoods, with positive impacts rare and often accompanied by challenges [49]. Local community participation is crucial for successful initiatives, and bottom-up approaches enhance success rates [3]. The system addresses these challenges by providing comprehensive information to support sustainable decision-making. The findings align with research demonstrating the effectiveness of agricultural knowledge bases for storing diverse media formats and facilitating online knowledge sharing. The application of systematic classification systems echoes approaches utilized in various knowledge management contexts. The knowledge management approach implemented in this study addresses several critical challenges identified in the literature, including the need for accessible knowledge-sharing platforms to bridge gaps in agricultural knowledge [7]. The system provides this accessibility through web-based interfaces available across devices, supporting research findings that ontology-based agricultural knowledge management frameworks improve intelligence and efficiency in knowledge sharing [9]. The system addresses the need for farmers to access comprehensive information by providing dedicated knowledge categories for economic utilization and decision-making support [23]. While the expert validation provides encouraging initial evidence for the system's practical relevance, the business implications discussed above should be interpreted

as informed projections rather than empirically demonstrated outcomes. Full realization and measurement of these benefits will require broader deployment, user adoption studies, and longitudinal impact assessment across diverse stakeholder groups and geographic contexts.

6. Conclusion

This research presents the design and prototype implementation of a knowledge-based system for economic plants in Thailand, providing a structured management solution for agricultural knowledge. The conclusions drawn in this study are based on two sources: (a) demonstrated system functionality through the prototype implementation and expert validation (Section 4.3), and (b) conceptual analysis of the system's potential business implications grounded in existing literature. The system provides a structured approach to addressing the fragmentation of economic plant information, as demonstrated through the prototype implementation and supported by the expert panel's positive assessment of content correctness and knowledge organization (Table 3), through three key components: a conceptual framework for knowledge classification based on systematic organizational principles, a comprehensive entity relationship database model integrating diverse knowledge domains, and a functional web-based platform for knowledge access, sharing, and management. It should be noted that the business implications discussed in Section 5 represent anticipated benefits informed by literature and system design logic rather than outcomes measured from large-scale deployment or longitudinal usage data.

From a business management perspective, the system has the potential to deliver value through improved decision-making, enhanced value chain coordination, preservation of intellectual capital, risk mitigation, facilitation of innovation, and integration with sustainability—benefits supported by expert validation results and analogous findings in the agricultural knowledge management literature. However, full realization of these benefits requires broader deployment and empirical assessment. Accordingly, the conclusions presented here should be understood as grounded in the study's design science contributions — namely, the successful development and initial expert validation of the system artifacts — rather than as claims of demonstrated real-world impact, which remains subject to future empirical investigation. The system addresses critical challenges identified in agricultural knowledge management, where traditional ecological knowledge continues to face erosion pressures as previously discussed [2]. By making critical knowledge accessible to diverse stakeholders, the system supports sustainable agribusiness development while preserving valuable traditional ecological knowledge. Research demonstrates that datasets aid in understanding plant-human interactions for future well-being, promoting biodiversity conservation and supporting policy-making through comprehensive information access [13].

Several limitations of this study should be acknowledged. First, the system evaluation was conducted through expert validation with a small panel rather than large-scale user testing with diverse stakeholder groups, such as farmers, entrepreneurs, and policymakers. Consequently, the generalizability of the usability and usefulness findings remains constrained. Second, the current prototype covers a limited number of economic plants, and the knowledge base has not yet achieved comprehensive coverage of all species designated by the Royal Forest Department of Thailand. Third, as discussed in Section 2.2, the system functions as a knowledge repository and retrieval platform without automated reasoning or recommendation capabilities, which limits its capacity to provide personalized decision support. Fourth, the system has not been evaluated under real-world field conditions where factors such as internet connectivity in rural areas, digital literacy among target users, and long-term data maintenance may affect adoption and sustained usage. Fifth, the popularity score rating mechanism (Equation 1) depends on a sufficient number of expert evaluations to produce meaningful quality indicators, and this critical mass has not yet been established during the prototype stage. These limitations are important considerations for interpreting the findings and provide direction for future research and system enhancement.

While the system incorporates quality assurance mechanisms, including administrative review and community-based scoring (Section 2.3), the risk of misinformation in a user-contributed knowledge system cannot be eliminated. The accuracy of traditional ecological knowledge entries is particularly challenging to

verify through conventional scientific validation, and the system relies on expert credential verification and administrative gatekeeping rather than automated fact-checking processes. Future development should explore additional validation mechanisms, such as cross-referencing with established scientific databases and peer verification workflows among registered experts. Seventh, the current prototype focuses on economic plants in Nakhon Ratchasima Province, which may limit the representativeness of the knowledge content for other regions of Thailand where ecological conditions, cultivation practices, and traditional knowledge differ. Expansion to additional provinces would require region-specific stakeholder engagement and data collection to ensure contextual relevance. Eighth, the digital divide remains a significant concern for system adoption among rural farming communities, who constitute a primary target user group. Factors such as limited internet infrastructure, low digital literacy, and lack of access to computing devices in rural areas may constrain the system's reach and practical impact. Addressing these barriers will require complementary strategies such as offline access capabilities, mobile-optimized interfaces, and capacity-building programs for target users.

The knowledge management solution aligns with research emphasizing that ontology-based agricultural knowledge management systems enhance intelligence and improve the efficiency of knowledge sharing, with frameworks that include modules for knowledge acquisition and representation [50]. The system adheres to the principle that web-based knowledge management systems enhance communication among stakeholders, facilitating collaboration among experts while addressing knowledge transfer issues in agricultural contexts [51]. The comprehensive database approach supports the finding that integrated data curation enhances analysis and application capabilities, with databases serving as essential tools for comparative studies and advancing research [31]. The system's multidimensional approach to knowledge organization aligns with research findings that comprehensive databases should integrate various types of information to support both research applications and practical decision-making [31, 34, 35]. The preservation of traditional knowledge components aligns with research that highlights the crucial role of traditional knowledge conservation amidst cultural change, with unified approaches necessary for effective knowledge management and research [12, 26]. The web-based accessibility ensures that information technology enhances public interaction and participation, supporting the principle that dynamic systems can improve stakeholder networks and collaboration [7].

Future research should focus on expanding the expert validation to larger-scale user evaluation involving farmers, entrepreneurs, and policymakers to assess field-level effectiveness, expanding the knowledge base to include additional economic plants for broader applicability, enhancing user interface design based on usability testing and user experience research, implementing advanced analytics for knowledge pattern identification and trend analysis, and exploring integration with mobile applications for field-based knowledge access and real-time information sharing. These future directions align with research emphasizing that databases require continuous updates with new data and methods while maintaining high-quality standards for knowledge management [52]. The development should also consider research findings that stakeholder engagement is crucial for addressing major agricultural challenges, with advances in data and technology being essential for achieving sustainable development goals [53].

7. Acknowledgments

This research project is supported by Rajamangala University of Technology Isan (National Science Research and Innovation Fund (NSRF))

Author Contributions: Conceptualization, A.L. and P.V.; methodology, P.V.; software, P.V.; validation, P.R., N.S., and P.R.; formal analysis, P.V.; investigation, A.L.; resources, A.L.; data curation, N.S.; writing—original draft preparation, A.L.; writing—review and editing, A.L.; visualization, P.V.; supervision, P.P.and P.R.; project administration, N.S.; funding acquisition, A.L. All authors have read and agreed to the published version of the manuscript.

Funding: This research received no external funding

Conflicts of Interest: The authors declare no conflict of interest.

References

[1] Cho, F. H. T.; Aglonucci, P.; Bateman, I. J.; Lee, C. F.; Lovett, A.; Mancini, M. C.; Rapti, C.; Day, B. H. Resilient tree-planting strategies for carbon dioxide removal under compounding climate and economic uncertainties. *Proc. Natl. Acad. Sci. U.S.A.* **2025**, *122*, e2320961122. https://doi.org/10.1073/pnas.2320961122

[2] Depommier, D. The tree behind the forest: ecological and economic importance of traditional agroforestry systems and multiple uses of trees in India. *Trop. Ecol.* **2003**, *44*, 63–71.

[3] Boissière, M.; Atmadja, S.; Guariguata, M. R.; Kassa, H.; Sist, P. Perspectives on the socio-economic challenges and opportunities for tree planting: A case study of Ethiopia. *For. Ecol. Manage.* **2021**, *497*, 119488. https://doi.org/10.1016/j.foreco.2021.119488

[4] Abdon, B. R.; Raab, R. T. Knowledge sharing and distance learning for sustainable agriculture in the Asia-Pacific region: The role of the internet. *Plant Prod. Sci.* **2015**, *8*, 298–307. https://doi.org/10.1626/pps.8.298

[5] Grover, V.; Davenport, T. H. General perspectives on knowledge management: Fostering a research agenda. *J. Manage. Inf. Syst.* **2001**, *18*, 5–21. https://doi.org/10.1080/07421222.2001.11045672

[6] Assèdé, E. S.; Sileshi, G. W.; Chirwa, P. W.; Orou, H.; Syampungani, S. Place and roles of trees in a multifunctional landscape: Trees and environmental services. In *Trees in a Sub-Saharan Multi-functional Landscape: Research, Management, and Policy*; Springer: 2024; pp 41–58. https://doi.org/10.1007/978-3-031-69812-5_3

[7] Ong, R. J.; Raof, R. A. A.; Sudin, S.; Choong, K. Y. A review of chatbot development for dynamic web-based knowledge management system (KMS) in small scale agriculture. *J. Phys. Conf. Ser.* **2021**, *1755*, 012051. https://doi.org/10.1088/1742-6596/1755/1/012051

[8] Ningthoujam, S. S.; Talukdar, A. D.; Potsangbam, K. S.; Choudhury, M. D. Challenges in developing medicinal plant databases for sharing ethnopharmacological knowledge. *J. Ethnopharmacol.* **2012**, *141*, 9–32. https://doi.org/10.1016/j.jep.2012.02.042

[9] Zheng, Y.-L.; He, Q.-Y.; Qian, P.; Li, Z. Construction of the ontology-based agricultural knowledge management system. *J. Integr. Agric.* **2012**, *11*, 700–709. https://doi.org/10.1016/S2095-3119(12)60059-8

[10] Ballantyne, P. Agricultural information and knowledge sharing: Promising opportunities for agricultural information specialists. *Agric. Inf. Worldw.* **2010**, *3*.

[11] Silvie, P. J.; Martin, P.; Huchard, M.; Keip, P.; Gutierrez, A.; Sarter, S. Prototyping a knowledge-based system to identify botanical extracts for plant health in Sub-Saharan Africa. *Plants* **2021**, *10*, 896. https://doi.org/10.3390/plants10050896

[12] de Souza, E. N. F.; Hawkins, J. A. Ewe: A web-based ethnobotanical database for storing and analysing data. *Database* **2020**, *2020*, baz144. https://doi.org/10.1093/database/baz144

[13] Molina-Venegas, R.; Rodríguez, M. A.; Pardo-de-Santayana, M.; Mabberley, D. J. A global database of plant services for humankind. *PLoS One* **2021**, *16*, e0253069. https://doi.org/10.1371/journal.pone.0253069

[14] Yemi-Peters, V. I.; Okon, E. O.; Agbogun, J. B. Healthcare and economic growth in Nigeria: A repository database system for traditional herbal medicines used in healthcare. *Int. J. Sci. Res. Comput. Sci. Eng. Inf. Technol.* **2017**, *2*, 1189–1198.

[15] Ingram, J. Agricultural transition: Niche and regime knowledge systems' boundary dynamics. *Environ. Innov. Soc. Trans.* **2018**, *26*, 117–135. https://doi.org/10.1016/j.eist.2017.05.001

[16] Song, S. An internet knowledge sharing system. *J. Comput. Inf. Syst.* **2002**, *42*, 25–30. https://doi.org/10.1080/08874417.2002.11647499

[17] Obidike, N. A. Rural farmers' problems accessing agricultural information: A case study of Nsukka local government area of Enugu State, Nigeria. *Library Philosophy and Practice* **2011**, 660, 1–11.

[18] Mishra, A.; Mishra, D. Applications of stakeholder theory in information systems and technology. *Eng. Econ.* **2013**, *24*, 254–266. https://doi.org/10.5755/j01.ee.24.3.4618

[19] van Hoek, M.; Zhou, J.; Jia, L.; Lu, J.; Zheng, C.; Hu, G.; Menenti, M. A prototype web-based analysis platform for drought monitoring and early warning. *Int. J. Digit. Earth* **2020**. https://doi.org/10.1080/17538947.2019.1585978

[20] Shamrat, F. J. M.; Asaduzzaman, M.; Ghosh, P.; Sultan, M. D.; Tasnim, Z. A web-based application for agriculture: "Smart farming system." **2020**.

[21] Antle, J. M.; Basso, B.; Conant, R. T.; Godfray, H. C. J.; Jones, J. W.; Herrero, M.; Howitt, R. E.; Keating, B. A.; Munoz-Carpena, R.; Rosenzweig, C.; et al. Towards a new generation of agricultural system data, models and knowledge products: Design and improvement. *Agric. Syst.* **2017**, *155*, 255–268. https://doi.org/10.1016/j.agsy.2016.10.002

[22] Grunert, K. G.; Jensen, B. B.; Sonne, A.-M.; Brunsø, K.; Byrne, D. V.; Clausen, C.; Friis, A.; Holm, L.; Hyldig, G.; Kristensen, N. H. User-oriented innovation in the food sector: Relevant streams of research and an agenda for future work. *Trends Food Sci. Technol.* **2008**, *19*, 590–602. https://doi.org/10.1016/j.tifs.2008.03.008

[23] Thankachan, S.; Kirubakaran, S. E-agriculture information management system. *Int. J. Comput. Sci. Mob. Comput.* **2014**, *3*, 599–607.

[24] de Oliveira, T. H. M.; Painho, M.; Santos, V.; Sian, O.; Barriguinha, A. Development of an agricultural management information system based on open-source solutions. *Procedia Technol.* **2014**, *16*, 342–354. https://doi.org/10.1016/j.protcy.2014.10.100

[25] Kopper, S. A.; Jayne, T. S. Market access, agro-ecological conditions, and Boserupian agricultural intensification patterns in Kenya: Implications for agricultural programs and research. *World Dev.* **2019**, *124*, 104649. https://doi.org/10.1016/j.worlddev.2019.104649

[26] Thomas, M. B.; Lin, N.; Beck, H. H. A database model for integrating and facilitating collaborative ethnomedicinal research. *Pharm. Biol.* **2001**, *39*(Suppl. 1), 41–52. https://doi.org/10.1076/phbi.39.7.41.5872

[27] Nimmagadda, S. L.; Reiners, T.; Wood, L. C. Geographic information systems on modelling big data guided supply chains in knowledge-base GIS. In *23rd International Conference on Knowledge-Based and Intelligent Information & Engineering Systems*; **2019**. https://doi.org/10.1016/j.procs.2019.09.284

[28] Alyoubi, B. A. Decision support system and knowledge-based strategic management. *Procedia Comput. Sci.* **2015**, *65*, 278–284. https://doi.org/10.1016/j.procs.2015.09.079

[29] Morueta-Holme, N.; Enquist, B. J.; McGill, B. J.; Boyle, B.; Jørgensen, P. M.; Ott, J. E.; Peet, R. K.; Šímová, I.; Sloat, L. L.; Thiers, B. Habitat area and climate stability determine geographical variation in plant species range sizes. *Ecol. Lett.* **2013**, *16*, 1446–1454. https://doi.org/10.1111/ele.12184

[30] Ortega-Morán, J. F.; Pagador, J. B.; Sánchez-Peralta, L. F.; Sánchez-González, P.; Noguera, J.; Burgos, D.; Gómez, E. J.; Sánchez-Margallo, F. M. Validation of the three web quality dimensions of a minimally invasive surgery e-learning platform. *Int. J. Med. Inform.* **2017**, *107*, 1–10. https://doi.org/10.1016/j.ijmedinf.2017.07.001

[31] Wang, D.; Xia, Y.; Li, X.; Hou, L.; Yu, J. The Rice Genome Knowledgebase (RGKbase): An annotation database for rice comparative genomics and evolutionary biology. *Nucleic Acids Res.* **2013**, *41*, D1199–D1205. https://doi.org/10.1093/nar/gks1225

[32] Loganathan, A.; Sinha, A.; Muthuramakrishnan, V.; Natarajan, S. A systematic approach to big data. *Int. J. Inf. Comput. Technol.* **2014**, *4*, 869–878.

[33] Pedersen, T. B. Managing complex multidimensional data. In *European Big Data Management and Analytics Summer School*; Springer: 2012; pp 1–28. https://doi.org/10.1007/978-3-642-36318-4_1

[34] Makita, Y.; Kawashima, M.; Lau, N. S.; Othman, A. S.; Matsui, M. Construction of para rubber tree genome and multi-transcriptome database accelerates rubber researches. *BMC Genomics* **2018**, *19*, 922. https://doi.org/10.1186/s12864-017-4333-y

[35] Mochida, K.; Yoshida, T.; Sakurai, T.; Yamaguchi-Shinozaki, K.; Shinozaki, K.; Tran, L. S. TreeTFDB: An integrative database of the transcription factors from six economically important tree crops for functional predictions and comparative and functional genomics. *DNA Res.* **2013**, *20*, 151–162. https://doi.org/10.1093/dnares/dss040

[36] Janssen, S.; Andersen, E.; Athanasiadis, I. N.; van Ittersum, M. K. A database for integrated assessment of European agricultural systems. *Environ. Sci. Policy* **2009**, *12*, 573–587. https://doi.org/10.1016/j.envsci.2009.01.007

[37] Yenni, G. M.; Christensen, E. M.; Bledsoe, E. K.; Supp, S. R.; Diaz, R. M.; White, E. P.; Ernest, S. K. M. Developing a modern data workflow for regularly updated data. *PLoS Biol.* **2019**, *17*, e3000125. https://doi.org/10.1371/journal.pbio.3000125

[38] Zimmermann, O.; Miksovic, C.; Küster, J. M. Reference architecture, metamodel, and modeling principles for architectural knowledge management in information technology services. *J. Syst. Softw.* **2012**, *85*, 2014–2033. https://doi.org/10.1016/j.jss.2012.05.003

[39] Khan, Z.; Dambruch, J.; Peters-Anders, J.; Sackl, A.; Strasser, A.; Fröhlich, P.; Templer, S.; Soomro, K. Developing knowledge-based citizen participation platform to support smart city decision making: The Smarticipate case study. *Information* **2017**, *8*, 47. https://doi.org/10.3390/info8020047

[40] Ong, R. J.; Sudin, S.; Raof, R. A. A.; Choong, K. Y.; Al-Hadi, A. A.; Yacob, Y.; Nasir, S. N. B. M. Dynamic web-based knowledge management system (KMS) in small scale agriculture. In *AIP Conf. Proc.*; AIP Publishing: 2024; Vol. 2898; p 010051. https://doi.org/10.1063/5.0196279

[41] Wright, H.; Mathers, C.; Walton, J. P. R. B. Using visualization for visualization: An ecological interface design approach to inputting data. *Comput. Graph.* **2013**, *37*, 202–213. https://doi.org/10.1016/j.cag.2013.01.013

[42] Mazaeva, N.; Bisantz, A. M. Ecological displays, information integration, and display format: An empirical evaluation across multiple small displays. *J. Cogn. Eng. Decis. Mak.* **2014**, *8*, 137–161. https://doi.org/10.1177/1555343414521424

[43] Zhou, D.; Nakatani, K.; Chuang, T.-T. Data quality in collaborative commerce. *Int. J. Inf. Qual.* **2011**, *2*, 264–278. https://doi.org/10.1504/IJIQ.2011.040672

[44] Scheer, A.-W. *Principles of Efficient Information Management*; Springer: 2012.

[45] Gujar, P. Data standardization and interoperability. In *Data Usability in the Enterprise: How Usability Leads to Optimal Digital Experiences*; Springer: 2025; pp 89–110. https://doi.org/10.1007/979-8-8688-1183-8_4

[46] Song, X. P.; Tan, P. Y.; Edwards, P.; Richards, D. The economic benefits and costs of trees in urban forest stewardship: A systematic review. *Urban For. Urban Green.* **2018**, *29*, 162–170. https://doi.org/10.1016/j.ufug.2017.11.017

[47] Lilavanichakul, A. Development of agricultural e-commerce in Thailand. *J. Agric. Policy* **2020**, *1*, 7–16.

[48] Dinh, H. H.; Nguyen, T. T.; Hoang, V.-N.; Wilson, C. Economic incentive and factors affecting tree planting of rural households: Evidence from the Central Highlands of Vietnam. *J. For. Econ.* **2017**, *29*, 14–24. https://doi.org/10.1016/j.jfe.2017.08.001

[49] Malkamäki, A.; D'Amato, D.; Hogarth, N. J.; Kanninen, M.; Pirard, R.; Toppinen, A.; Zhou, W. A systematic review of the socio-economic impacts of large-scale tree plantations worldwide. *Glob. Environ. Change* **2018**, *53*, 90–103. https://doi.org/10.1016/j.gloenvcha.2018.09.001

[50] Holder, L. B.; Markov, Z.; Russell, I. Advances in knowledge acquisition and representation. *Int. J. Artif. Intell. Tools* **2006**, *15*, 867–874. https://doi.org/10.1142/S0218213006003016

[51] Taylor, M.; Bhasme, S. Model farmers, extension networks and the politics of agricultural knowledge transfer. *J. Rural Stud.* **2018**, *64*, 1–10. https://doi.org/10.1016/j.jrurstud.2018.09.015

[52] Du, Z.; Yu, L.; Yang, J.; Xu, Y.; Chen, B.; Peng, S.; Zhang, T.; Fu, H.; Harris, N.; Gong, P. A global map of planting years of plantations. *Sci. Data* **2022**, *9*, 141. https://doi.org/10.1038/s41597-022-01260-2

[53] Viana, C. M.; Freire, D.; Abrantes, P.; Rocha, J.; Pereira, P. Agricultural land systems importance for supporting food security and sustainable development goals: A systematic review. *Sci. Total Environ.* **2022**, *806*, 150718. https://doi.org/10.1016/j.scitotenv.2021.150718

ASEAN
Journal of Scientific and Technological Reports
Online ISSN:2773-8752

Research article

Development of an IoT Smart Learning Board Innovation to Enhance IoT and Coding Skills for Sustainable Secondary Education in Thailand

Naphat Keawpibal[1], Grit Tongkhundam[1], Nantharat Phruksaphithak[1], Krisda Suwankarn[1], Sarunwich Bussaba[1], Worawat Sooksai[1], and Visit Boonchom[1*]

[1] Faculty of Science and Digital Innovation, Thaksin University, Phatthalung 93210, Thailand
* Correspondence: visit@tsu.ac.th;

Citation:
Keawpibal, N.; Tongkhundam, G.; Phruksaphithak, N.; Suwankarn, K.; Bussaba, S., Sooksai, W.; Boonchom, V. Development of an IoT smart learning board innovation to enhance IoT and coding skills for sustainable secondary education in Thailand. *ASEAN J. Sci. Tech. Report.* **2026**, *29*(5), e264365 https://doi.org/10.55164/ajstr.v29i5.264365

Article history:
Received: March 16, 2026
Revised: April 7, 2026
Accepted: April 21, 2026
Available online: May 2, 2026

Publisher's Note:
This article is published and distributed under the terms of the Thaksin University.

Abstract: The growing demand for Internet of Things (IoT) and programming competencies in Thai secondary education necessitates accessible, hardware-based learning tools that reduce technical barriers while supporting structured skill development. This study developed and evaluated the IoT Smart Learning Board, a two-layer printed circuit board (PCB) integrating 17 electronic components — including an ESP8266 Wemos D1 mini microcontroller, HC-SR04 ultrasonic sensor, AHT10 temperature/humidity sensor, 0.96-inch OLED display, WS2812 NeoPixel RGB strip, and SG90 servo motor — designed around a Terminal-based Hardware Abstraction Layer architecture. Development followed a four-phase Research and Development (R&D) framework employing an iterative R&D approach with stakeholder feedback loops, producing an 18-exercise practice manual progressing from basic digital I/O to cloud-based data telemetry via Google Sheets. Evaluation involved 90 participants (17 teachers and 73 upper-secondary students, Grades 10–12) from 10 schools across southern Thailand. Knowledge was assessed using a 30-item multiple-choice instrument (KR-20 = 0.87), while satisfaction was measured using a 15-item, 5-point Likert-scale questionnaire (Cronbach's α = 0.89–0.93). Results demonstrated a statistically significant increase in mean knowledge scores from 15.76 (SD = 5.26) at pre-test to 23.50 (SD = 4.86) at post-test, representing a 25.80% gain ($t(89) = 12.96$, $p < 0.001$, Cohen's d = 1.54). Overall participant satisfaction reached 4.77 out of 5.00 (SD = 0.42), with the highest ratings recorded for learning benefits (M = 4.81), programming skill development (M = 4.82), and project extensibility (M = 4.81). These findings are consistent with the hypothesis that Terminal-based PCB architecture reduces extraneous cognitive load associated with breadboard wiring, enabling learners to focus on higher-order computational thinking and IoT system design. These findings suggest that the IoT Smart Learning Board holds promise as an accessible, affordable platform for technology education in resource-constrained secondary school contexts; however, broader applicability across Thailand and the ASEAN region warrants validation through future multi-site research with diverse school populations.

Keywords: IoT; learning board; PCB design; digital skills; secondary education

1. Introduction

The rapid advancement of digital technologies, particularly the Internet of Things, has fundamentally transformed global economic and social landscapes, creating an urgent need for educational systems to prepare students with Industry 4.0 competencies [1], [2]. IoT enables physical devices to connect and exchange data across sectors as diverse as smart agriculture [3], healthcare [4], and manufacturing [1], demonstrating the breadth of domains in which IoT literacy is now an operational requirement. Within the Thai context, Sangkhiew et al. [5] documented the measurable impact of disruptive technologies on industrial engineering professionals under the Thailand 4.0 framework, underscoring the urgency of equipping the current generation of secondary learners with adaptive digital competencies before they enter a rapidly evolving workforce [2], [6]. Thailand's educational policy has recognized this imperative by incorporating IoT and coding into the basic education curriculum to foster "digital citizens" [6]. However, significant challenges impede effective implementation in secondary schools. The gap between policy intention and classroom reality remains substantial, particularly in schools with limited resources [2]. Institutions face multiple barriers, including insufficient budgets, a shortage of specialized teachers with programming expertise, and a lack of structured materials that scaffold student understanding [2], [6]. These challenges are particularly acute in regions with limited access to technological resources, where students risk being left behind in the digital transformation, thereby perpetuating educational disparities [1].

The conventional approach to teaching applied science and technology using discrete, manually assembled components presents significant pedagogical hurdles. Students with limited prior knowledge often face high extraneous cognitive load when they must simultaneously manage intricate hardware connections and abstract programming logic [7], [8]. Recent efforts in Thai secondary education have addressed this challenge through IoT-integrated experimental apparatus, including systems for studying heat of reaction in chemistry laboratories [9] and smart learning media for investigating the changing states of matter in physics [9], demonstrating growing recognition that integrated, sensor-based platforms can reduce technical friction and support meaningful scientific inquiry. However, these instruments are designed for single-domain experimental contexts. The present study extends this line of development toward a multi-domain, programmable PCB platform capable of supporting an 18-exercise curriculum spanning IoT devices, programming logic, cloud telemetry, and AI-assisted development, thereby addressing a broader range of digital literacy competencies required under Thailand's national education policy [6]. Research indicates that hardware-related errors, such as incorrect circuit connections and delicate component failures, often distract learners from mastering core algorithmic thinking and system architecture [10]. While existing kits like Arduino or ESP32 are versatile, their high technical threshold and the potential for wiring errors can discourage experimentation and create psychological barriers for novice learners[10], [11]. Conversely, simpler tools like the BBC micro: bit may lack the expansion capacity required for more complex, high-ceiling innovation [12]. To address these gaps, this research introduces the IoT Smart Learning Board, an integrated printed circuit board innovation specifically designed for the Thai secondary education context. The innovation integrates 17 essential electronic components with a structured pedagogical framework. The primary contribution of this research lies in its Terminal-based PCB design, which functions as a Hardware Abstraction Layer. By decoupling complex circuit wiring from logic development, the board reduces technical friction and allows students to focus on higher-order thinking and system design [8], [13].

Furthermore, integrating Generative AI for automated code generation transforms the learning experience from rote syntax memorization to the design of structural systems [8]. This study evaluates the board's effectiveness through a Research and Development framework, examining its impact on learning outcomes and student satisfaction. By providing an accessible, pedagogically sound solution, this research contributes to a sustainable, scalable model of digital literacy in Thailand’s evolving technological landscape [1-[2].

2. Materials and Methods

2.1 Research Design

This study employed a Research and Development (R&D) methodology, adopting an iterative approach characterized by multiple feedback-driven refinement cycles between developers and stakeholder groups. Rather than following a fixed linear sequence, the development process was structured to allow outputs from each phase to directly inform subsequent design and implementation decisions, ensuring that the technical specifications of the IoT Smart Learning Board remained continuously aligned with both engineering standards and the pedagogical requirements of secondary education. The development proceeded through four sequential phases, (1) requirement gathering, (2) board design (three PCB revision cycles), (3) manual and software development (two curriculum revision cycles), and (4) effectiveness evaluation, as illustrated in Figure 1. Each phase incorporated structured feedback mechanisms. During the board design phase, three successive PCB versions were produced and reviewed against hardware reliability benchmarks and classroom usability criteria before Version 3 was confirmed as the final production design. During the manual and software development phase, two curriculum revision cycles were conducted based on expert review and pilot testing feedback, resulting in refinements to exercise sequencing, code examples, and troubleshooting guidance. This iterative structure ensured that neither the hardware nor the instructional components were treated as static outputs; both evolved in direct response to stakeholder input gathered at defined review points within the development timeline.

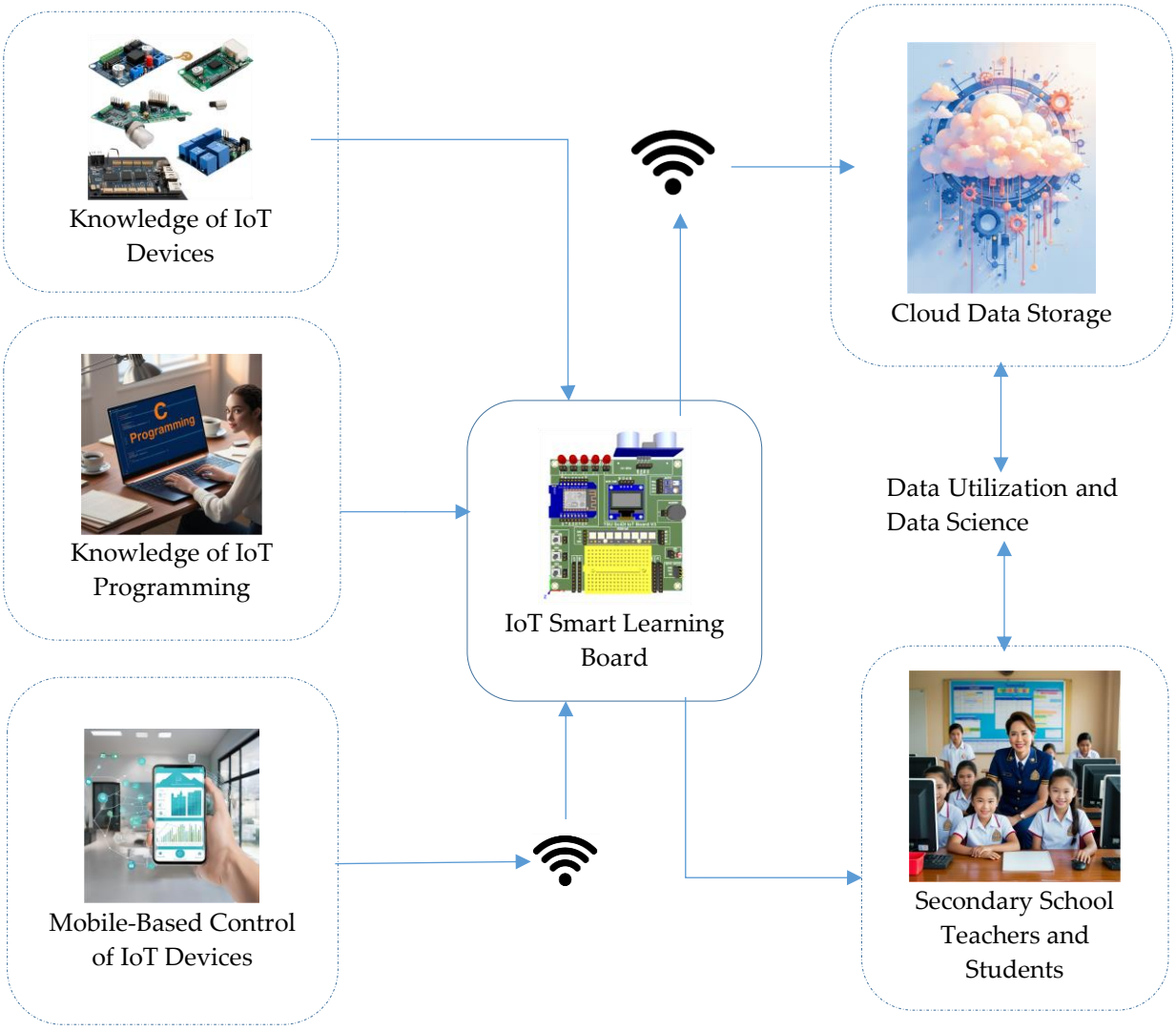


Figure 1. Conceptual Framework of the IoT Smart Learning Board

This methodological approach is consistent with established R&D frameworks in educational technology research, which emphasize the importance of cyclic refinement and formative evaluation as mechanisms for aligning innovative learning tools with real-world classroom conditions. By embedding feedback loops at each phase boundary rather than reserving evaluation for the final stage, the framework supported progressive quality assurance across both the technical and pedagogical dimensions of the innovation.

2.1.1 Requirement Gathering.

The initial phase involved a comprehensive needs assessment through consultation with computer science, computational science, and 10 technology teachers from secondary schools. Data collection occurred through on-site and online meetings, depending on geographical constraints. Requirements analysis focused on identifying appropriate content scope, essential electronic components, circuit design considerations, programming concepts, and practical exercise structure. The goal was to develop 18 laboratory exercises covering fundamental IoT concepts while enabling extension to research projects and innovations. Each exercise included clear learning objectives, step-by-step circuit connection diagrams with labeled components (as shown in Figure 2), complete program code with explanatory comments, expected outcomes, and troubleshooting tips.

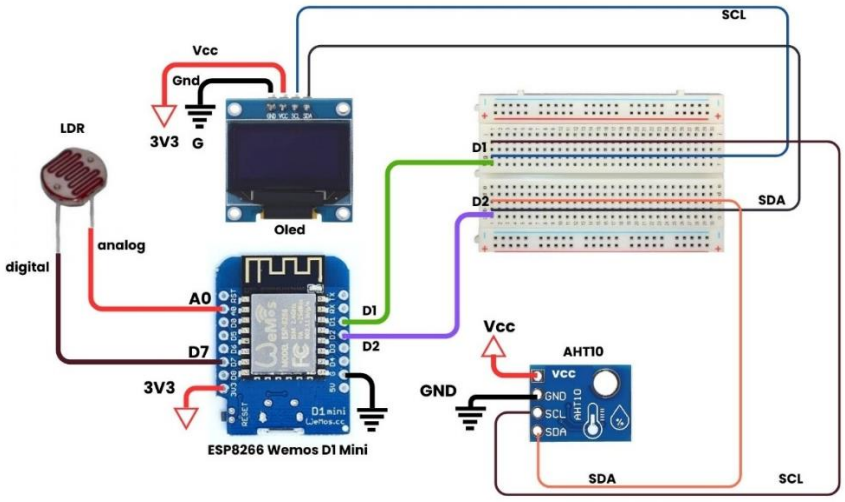


Figure 2. Example Circuit Diagram of Practice Exercise 18

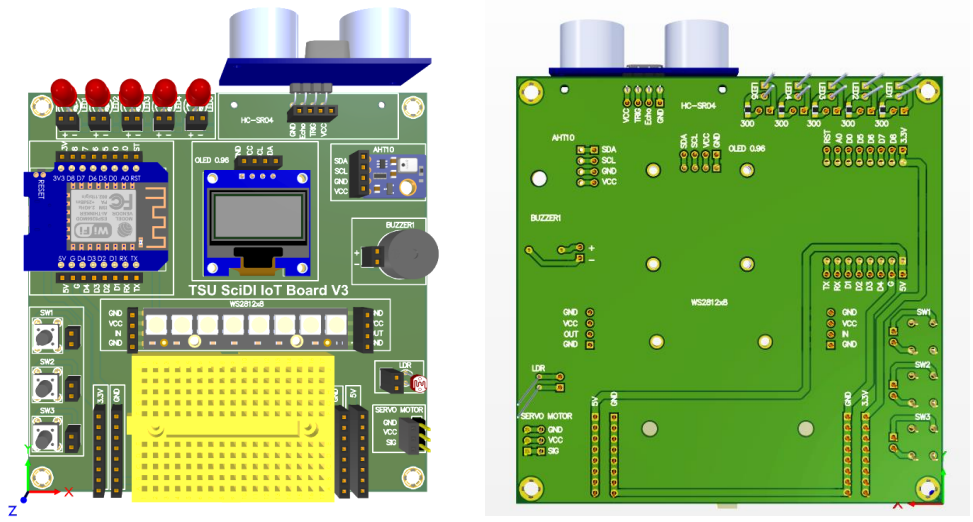


Figure 3. Front and Back PCB Layout of the IoT Board

2.1.2 Board Design.

The IoT Smart Learning Board was engineered as a high-reliability, two-layer printed circuit board (PCB) using Altium Designer, as shown in Figure 3. The design process underwent three major iterations, culminating in Version 3, which was optimized for both mass production and classroom deployment. The PCB layout was strategically engineered to facilitate mental model formation by adopting an Input-Process-Output (IPO) architecture. Under this framework, input peripherals — including push button switches, the HC-SR04 ultrasonic sensor, LDR, and AHT10 sensor — were routed to the board's periphery. At the same time, the processing unit (ESP8266 Demos D1 mini) and the output devices, including the 0.96-inch OLED display, LEDs, an active buzzer, and a WS2812 NeoPixel strip, were centrally located. This deliberate spatial mapping allows learners to intuitively distinguish between the data acquisition, processing, and visualization layers, effectively bridging the gap between physical components and computational logic. The transition to a terminal-based PCB architecture further reinforces this design philosophy by functioning as a robust Hardware Abstraction Layer (HAL). By replacing traditional, error-prone jumper-wire prototyping with high-reliability screw terminals and clearly labeled electrical symbols, the system effectively mitigates signal noise and mechanical instability, significantly reducing extraneous cognitive load and shifting student focus from low-level electrical troubleshooting toward high-level algorithmic logic and system architecture. The board integrates 17 essential electronic components within a solder-free, modular environment that facilitates easy maintenance and component replacement. The core processing unit is an ESP8266 Wemos D1 Mini microcontroller with Wi-Fi, operating at 80/160 MHz and featuring 4 MB of flash memory. Sensory inputs consist of an HC-SR04 ultrasonic module with a measurement range of 2–400 cm, an AHT10 precision temperature and humidity sensor, and an LDR with a resistance range of 10–20 kΩ. Output interfaces include a 0.96-inch I2C OLED display (128×64 pixels), an 8-LED WS2812 NeoPixel RGB strip, and an active 3.3V buzzer. For actuation and physical expansion, the board incorporates an SG90 servo motor and a 170-pin mini breadboard that supports custom prototyping beyond the 18-core laboratory exercises. Component interconnection is achieved through optimized female pin header sockets with 2- to 8-pin configurations, ensuring modularity and mechanical durability during repeated laboratory use.

2.1.3 Manual Development and System Programming.

A comprehensive practice manual was developed covering theoretical foundations, circuit connection instructions, and advanced programming logic. The curriculum introduces a Synergetic development workflow that integrates Generative AI tools such as Gemini, Claude, and ChatGPT as intelligent debugging and code-synthesis platforms. This approach moves beyond rote syntax memorization, encouraging students to engage in Prompt Engineering and structural system design, reflecting contemporary industrial software development practices. The practice manual comprises 18 progressive laboratory exercises organized by increasing technical complexity. This progression follows a Data Lifecycle Model, culminating in Practice 18, which implements a complete end-to-end IoT solution. This final exercise demonstrates the transition from edge sensor data acquisition via the ESP8266 to cloud-based data telemetry and persistent storage in Google Sheets for further Data Science analysis. The manual is structured into three primary chapters. Chapter 1: Fundamental Knowledge of Devices and Applications provides theoretical foundations for the ESP8266 Wemos D1 mini and various integrated components. This chapter also introduces the Blynk application and artificial intelligence tools for assisting with circuit design. Chapter 2: Circuit Connection and Programming contains 18 exercises, ranging from basic digital I/O, such as Practice 1: Blinking LED, to advanced environmental monitoring, as shown in Figure 4. The program uses C++ in the Arduino IDE to control various sensors, including the HC-SR04 ultrasonic sensor, AHT10, and LDR, and to control OLED displays, NeoPixel WS2812 strips, and servo motors. Chapter 3: Basic Error Troubleshooting addresses common software programming mistakes and hardware connection problems, using AI-assisted debugging to foster autonomous problem-solving.

```
void setup() {
```

```
  pinMode(D1, OUTPUT);
  Serial.begin(9600);
  Serial.println("Starting...");
}
void loop() {
  digitalWrite(D1, HIGH);
  Serial.println("LED ON");
  delay(1000);
  digitalWrite(D1, LOW);
  Serial.println("LED OFF");
  delay(1000);
}
```

Figure 4. Example Program for Practice Exercise 1.

2.1.4 Effectiveness evaluation.

The final phase assessed the technical and educational effectiveness of the IoT Smart Learning Board by rigorously evaluating learning gains and system usability. The evaluation framework involved participating teachers and students who completed the full integrated training program. Pretests were administered to establish a baseline of computational knowledge and IoT conceptual understanding before system deployment. Posttests were subsequently administered to measure quantitative learning gains and mastery of programming logic following completion of the 18 laboratory exercises. This dual assessment model allowed for the calculation of normalized gain scores, providing an objective measure of the board's effectiveness in enhancing digital competencies. Beyond cognitive gains, the research utilized standardized satisfaction questionnaires to evaluate the system across multiple technical dimensions. This included assessing the hardware architecture design, the clarity of the instructional manual, and the perceived benefits for long-term skill development. By analyzing user interaction data, the study sought to validate the board's role as an intuitive interface that fosters autonomous problem-solving and technical confidence in a distributed learning environment. The complete training program was delivered as a two-day intensive workshop comprising approximately 14 contact hours. Day 1 (7 hours) encompassed pre-test administration, theoretical foundations (Chapter 1), and laboratory Exercises 1–9. Day 2 (7 hours) covered Exercises 10–18, AI-assisted troubleshooting (Chapter 3), and post-test administration.

2.2 Evaluation Design and Participant Selection

The system evaluation was conducted using a target population categorized into two primary stakeholder groups. The first group consisted of secondary school teachers specializing in science, computer science, or technology-related subjects. The second group included students enrolled in upper secondary education in grades 10-12 in southern Thailand. The research sample comprised 90 participants, including 17 teachers and 73 upper secondary students. These participants voluntarily engaged in the IoT Smart Learning Board experimental testing conducted at the Faculty of Science and Digital Innovation, Thaksin University, Phatthalung Campus. The recruitment spanned 10 diverse educational institutions in southern Thailand, including Kanpittayakorn School, Phapayompittayakhom School under the TSU Science Classroom Project, Pakphayunpittayakarn School, Triam Udom Suksa Pattanakarn Phatthalung School, Sawatrattanaphimuk School, Ubonratthanakosinrachawittayalai Phatthalung School, Khuan Khanun School, Kantangpittayakorn School, Darulamaaref Foundation School, and Wangwiset School in Trang Province. Rigorous inclusion criteria were established to ensure the validity of the evaluation results. Schools were required to offer upper secondary education programs, and participating teachers had to possess expertise in science or computer technology subjects, with formal administrative approval. Student participants were selected based on their interest in IoT and coding, specific teacher recommendations, and their commitment to completing the full training cycle. Conversely, exclusion criteria were implemented to maintain data integrity. This included schools declining participation and individuals unable to attend the scheduled system training. Participants with insufficient Thai language proficiency for the technical assessment or those who withdrew during the

research process were also excluded. Furthermore, the study excluded individuals with health conditions that might prevent participation in intensive hands-on activities involving computer systems and IoT equipment.

2.3 Research Instruments

2.3.1 Knowledge Assessment and Cognitive Competency Test

A 30-item multiple-choice test was developed to quantify participants' cognitive gains across several technical domains, including IoT concepts, hardware device functions, circuit principles, programming logic, and practical application scenarios. This instrument was administered as both a pretest and a posttest to assess changes in learning performance. Content validity was established through a rigorous review process involving three experts in IoT engineering, computer science education, and educational measurement. Following the expert review, a pilot study was conducted with 30 non-participant students to determine item difficulty and discrimination indices. Based on the psychometric analysis, items with inappropriate indices were revised or replaced to ensure instrument precision. The test's internal consistency was evaluated using the Kuder-Richardson Formula 20 (KR-20), yielding a reliability coefficient of 0.87, indicating high instrument stability and consistency.

2.3.2 System Satisfaction and Interaction Questionnaire

A 15-item questionnaire was developed to evaluate participant satisfaction and interaction quality across three distinct dimensions of the innovation. Each item used a 5-point Likert scale ranging from 1 (lowest satisfaction) to 5 (highest satisfaction). The instrument was structured as follows. Hardware Design and Architecture (5 items): This dimension focused on component layout, system completeness, durability, safety protocols, and ease of USB connectivity. Instructional Manual and Exercise Framework (5 items): This evaluated the accuracy of technical content, instructional clarity, the practicality of code examples, and the quality of system illustrations. Technical Learning Benefits (5 items): This dimension measured programming skill development, conceptual understanding of IoT, system extension capabilities, and suitability for secondary-level computing education. The questionnaire underwent validation by a panel of six content experts, resulting in an Index of Item Objective Congruence (IOC) exceeding 0.80 for all items. Reliability testing conducted with a pilot group of 30 students yielded Cronbach alpha coefficients of 0.89 for hardware design, 0.91 for manual quality, and 0.93 for perceived learning benefits, confirming the robust reliability of the measurement tool. To minimize social desirability bias, questionnaires were self-administered anonymously using paper forms, with no researcher present during completion. Participants were explicitly informed that responses were confidential and would not affect their participation status.

3. Results and discussion

3.1 System Architecture and Hardware-Software Synergy

The IoT Smart Learning Board was successfully engineered as a robust embedded system integrating 17 essential electronic components onto a specialized two-layer PCB architecture, as shown in Figures 5 and 6. Technical validation confirmed that the board's deliberate spatial arrangement substantially optimizes the cognitive interaction between the learner and the hardware environment. Specifically, input peripherals — including push button switches, the HC-SR04 ultrasonic sensor, LDR, and AHT10 sensor — were positioned along the board's periphery, while the ESP8266 Wemos D1 mini processing unit and output devices, including the OLED display, NeoPixel RGB strip, LEDs, and active buzzer, were centrally located. This spatial strategy mirrors the Input-Process-Output (IPO) computing model, enabling learners to intuitively map physical component placement to the corresponding layers of software abstraction, thereby reinforcing conceptual understanding of data flow in embedded systems [7], [8]. A key architectural contribution of this design is the implementation of a Terminal-based Hardware Abstraction Layer (HAL), achieved by replacing conventional jumper-wire breadboard connections with high-reliability screw terminals and clearly labeled electrical symbols. This engineering decision directly addresses a well-documented source of extraneous cognitive load in STEM education: connection-related failures — such as signal noise, polarity errors, and loose contacts — that frequently distract novice learners from mastering core programming logic and system architecture [11].

As summarized in Table 1, the terminal-based PCB architecture demonstrates measurable advantages over conventional breadboard-based platforms across multiple pedagogical and technical dimensions, including connection reliability, cognitive demand, and classroom deployment suitability. By eliminating low-level electrical troubleshooting as a primary learning obstacle, the board enables students to direct their working memory toward high-level algorithmic development and IoT system design [8]. Furthermore, selecting the ESP8266 Wemos D1 mini as the core processing unit provides a cost-effective, technically stable foundation for both edge-level sensor processing and cloud-based data telemetry via Google Sheets, aligning with the infrastructure requirements of resource-constrained secondary school environments in Thailand [2], [14].

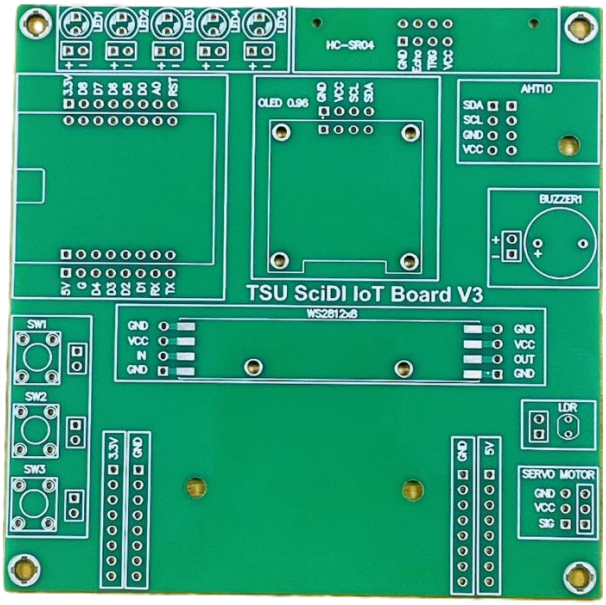


Figure 5. Front side of the IoT Smart Learning Board PCB without electronic components.

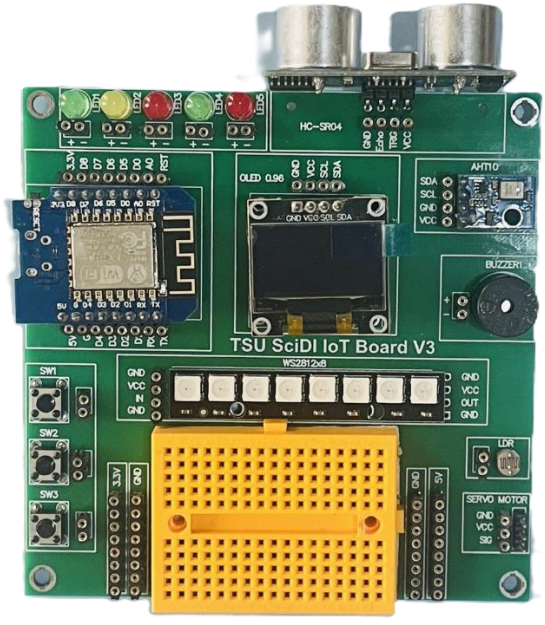


Figure 6. Front side of the IoT Smart Learning Board PCB with electronic components.

Table 1. Comparison of IoT Learning Platform Architectures for Secondary Education

Dimension	Breadboard-Based (e.g., Arduino Kit)	BBC micro: bit	IoT Smart Learning Board (This Study)
Connection Method	Manual jumper wires	Pre-wired / edge connector	Screw terminal PCB (solder-free)
Connection Reliability	Low (prone to noise, loose contacts)	High	High
Risk of Wiring Error	High	Low	Low
Extraneous Cognitive Load	High	Low–Moderate	Low
Number of Integrated Components	Varies (discrete, separate)	15 on-board	17 on a single PCB
Wi-Fi / IoT Connectivity	Optional (add-on shield)	Limited (radio only)	Built-in (ESP8266)
Cloud Data Integration	Requires additional configuration	Limited	Native (Google Sheets, Blynk)
AI-Assisted Learning Support	Not structured	Not structured	Integrated (Gemini, Claude, ChatGPT)
Expansion Capability	High (open prototyping)	Low	Moderate–High (170-pin breadboard)
Suitability for Novice Learners	Low–Moderate	High	High
Estimated Unit Cost (USD)	~15–25 (components only)	~15–20	~20–30 (fully integrated)
Estimated Unit Cost (THB)	~525–875 THB (components only)	~525–700 THB	~700–1,050 THB (fully integrated)
Curriculum Alignment (18 exercises)	Not structured	Not structured	Structured (IPO + Data Lifecycle Model)

Note: BBC micro: bit and Arduino/ESP32 kit specifications are based on published manufacturer data and peer-reviewed comparative studies [10], [11], [12]. Cost estimates reflect approximate market prices for educational procurement in Thailand. THB costs estimated at 35 THB/USD based on domestic procurement prices from Thai electronics distributors (Thaieasyelec, Cytron Thailand) as of 2024; prices may vary by supplier and order volume. USD costs for the IoT Smart Learning Board reflect fully integrated unit pricing inclusive of all 17 components and the 170-pin expansion breadboard. USD costs for the Arduino Kit reflect components only and do not include a dedicated enclosure, structured curriculum materials, or cloud integration infrastructure, which would increase total deployment cost. Direct cost comparison across platforms should therefore account for total cost of deployment rather than unit hardware cost alone.

3.2 Instructional Framework and AI Integration Analysis

The development of the comprehensive practice manual, containing 18 progressive laboratory exercises, serves as a Pedagogical Scaffold that aligns with the Data Lifecycle Model [8], [13]. The manual's structure is divided into three strategic chapters, each designed to foster a specific level of competency. Chapter 1: Fundamental Knowledge and Theoretical Foundations provides the necessary conceptual grounding for each component, including the ESP8266, Ultrasonic HC-SR04, and AHT10 sensors. A novel aspect of this stage is the integration of Generative AI tools (e.g., Gemini, Claude, and ChatGPT), which introduces students to contemporary AI-driven development practices [8]. This shift from rote memorization to AI-assisted conceptualization empowers students to understand complex sensor-fusion concepts more rapidly. Chapter 2: Circuit Connection and Programming Implementation executes core technical training through an end-to-end IoT workflow. The analysis of the exercises reveals a transition from basic digital I/O operations to complex integrated systems, where students manage data from physical sensors to mobile interfaces via the Blynk platform [14]. The use of AI for code synthesis and circuit design assistance fosters a Synergetic Development Workflow, reflecting modern industrial standards where AI acts as a co-developer rather than a mere automation tool [8]. Chapter 3: Intelligent Troubleshooting and System Resilience addresses error management through AI-assisted debugging. By leveraging AI to interpret compiler errors and hardware connection issues, the curriculum empowers learners to solve problems autonomously, building technical resilience [15], [16]. This approach prepares students for the challenges of Industry 4.0, where autonomous problem-solving and system maintenance are essential competencies for the future workforce [1], [2]. The progression culminating in Practice 18, a complete end-to-end IoT solution integrating edge sensor acquisition, Wi-Fi telemetry, and cloud-based data logging via Google Sheets — is deliberately designed to mirror the architecture of real-world IoT deployments. Industry applications such as automated poultry farm management systems [3] and IoT-based saline infusion administration systems in healthcare [4] demonstrate that the sensor-process-transmit-visualize pipeline practiced in the final exercises maps directly onto operational IoT system design. Furthermore, the integration of AI assistance within the curriculum reflects emerging practice in applied IoT contexts: Serin et al. [17] demonstrated that AI-driven monitoring systems incorporating automated plant health diagnosis and nutrient deficiency detection represent the frontier of smart agriculture, a domain in which students must be capable of understanding sensor fusion, data classification, and automated decision logic — precisely the competencies developed progressively across the 18 exercises of this curriculum [8], [18].

3.3 Learning Effectiveness and Cognitive Performance Analysis

The empirical evaluation of the IoT Smart Learning Board across 90 participants (17 teachers and 73 students) demonstrates a profound impact on both technical proficiency and cognitive alignment. As summarized in Table 2, the mean knowledge score significantly increased from a pre-test average of 15.76 (SD = 5.26) to a post-test average of 23.50 (SD = 4.86). This 25.80% gain in learning achievement is not merely a numerical increase but represents a fundamental shift in the learners' ability to conceptualize and implement IoT systems. The paired t-test results ($t = 12.96$, $p < 0.001$) confirm the statistical significance of these gains. Most notably, the calculated effect size, Cohen's $d = 1.54$, indicates large practical significance, suggesting that the results are consistent with the interpretation that the IoT Smart Learning Board exerted a substantial positive influence on learning outcomes, though causal attribution requires further controlled investigation [8], [12]. The observed reduction in the standard deviation (from 5.26 to 4.86) further implies that the IoT Smart Learning Board served as an effective pedagogical equalizer, narrowing the knowledge gap between diverse learners and fostering a more consistent understanding of complex digital concepts [7].

Table 2. Comparison of pre-test and post-test knowledge scores (n = 90)

Test	Mean	SD	Min	Max	Mean Diff.	% Gain (max-relative) [a]	% Gain (baseline-relative) [b]	Hake ⟨g⟩ [c]	t	df	p	Cohen's d
Pre-test	15.76	5.26	0	25	-	-	-	-	-	-	-	-
Post-test	23.50	4.86	7	30	7.74	25.80%	49.10%	0.54	12.96	89	< 0.001	1.54

Notes.

[a] % Gain (max-relative) = (Mean Difference / Maximum Possible Score) × 100 = (7.74 / 30) × 100 = 25.80%. This metric expresses the mean score gain as a proportion of the total score range and is commonly reported in Thai educational research literature.

[b] % Gain (baseline-relative) = (Post-test Mean − Pre-test Mean) / Pre-test Mean × 100 = (23.50 − 15.76) / 15.76 × 100 = 49.10%. This metric expresses the gain relative to the initial performance level.

[c] Hake normalized gain ⟨g⟩ = (Post-test Mean − Pre-test Mean) / (Maximum Score − Pre-test Mean) = (23.50 − 15.76) / (30 − 15.76) = 7.74 / 14.24 = 0.54. Interpreted as medium-high gain ($0.30 \leq \langle g \rangle < 0.70$) according to Hake's classification framework [19]. Cohen's d = 1.54 indicates a large effect size. Maximum possible score = 30 items.

The quantitative gains are strongly supported by high levels of participant satisfaction, which reached an overall mean of 4.77 (SD = 0.42), indicating the "Highest" level. The dimension of Learning Benefits received the highest rating (4.81), particularly in programming skill development (4.82) and project extension capability (4.81) (Table 3). These findings suggest that the board's design successfully facilitates a "low-threshold, high-ceiling" environment where students can move beyond basic exercises to creative innovation [8], [13]. The high satisfaction with hardware durability and safety (4.66) directly addresses the critical barriers identified in Thai secondary education, where fear of component damage and wiring complexity often hampers hands-on experimentation [10]. By abstracting these technical risks through a stabilized PCB architecture, the innovation effectively reduces extraneous cognitive load, allowing students to focus on higher-order tasks such as system design and AI-assisted problem-solving [7], [8]. Furthermore, the high rating for project extension (item 13) confirms that the IoT Smart Learning Board is viewed as a sustainable tool for long-term skill development, aligning with national goals for human capital development in Industry 4.0 [1], [2].

Table 3. Satisfaction with IoT Smart Learning Board

Item	Assessment Item	Mean	SD	Interpretation
Hardware Design and Components				
1	Component arrangement is orderly and easy to learn	4.73	0.56	Highest
2	Components are complete and sufficient for basic experiments	4.78	0.52	Highest
3	The board is durable and safe to use	4.66	0.63	Highest
4	USB connection to the computer is convenient and stable	4.70	0.58	Highest
5	Overall, the board's appearance is attractive and interesting	4.73	0.54	Highest
Guidance and Exercise Handbook				
6	Manual content is accurate regarding IoT and Coding principles	4.76	0.55	Highest
7	Instructional sequence is clear and easy to understand	4.78	0.44	Highest
8	Program code examples are practical and understandable	4.75	0.56	Highest
9	Illustrations and circuit diagrams support effective learning	4.77	0.45	Highest
10	The number of exercises is appropriate, covering essential skills	4.77	0.50	Highest
Learning Benefits				
11	The board helps develop programming skills	4.82	0.50	Highest
12	Board enhances understanding of IoT principles and applications	4.78	0.52	Highest
13	The board can be extended for IoT projects	4.81	0.48	Highest
14	The board is suitable for secondary school teaching/learning	4.80	0.51	Highest
15	Overall satisfaction with the IoT Smart Learning Board	4.83	0.51	Highest
	Overall Mean	**4.77**	**0.42**	**Highest**

3.4 Effectiveness of the IoT Smart Learning Board on Learning Outcomes

The findings of this study are consistent with the view that the IoT Smart Learning Board was associated with significant enhancement of learning outcomes in IoT and coding. The substantial increase in mean scores from 15.76 in the pretest to 23.50 in the posttest, resulting in a 25.80% gain, reflects a profound improvement in both theoretical understanding and practical implementation skills (Table 4). This statistically significant difference ($p < 0.001$) and the very large effect size (Cohen's $d = 1.54$) indicate that the intervention had a transformative impact on learners' technical proficiency [20], [21]. These results align with contemporary research, which suggests that integrated IoT platforms and well-structured interventions can yield large effect sizes in student achievement, particularly when they reduce the technical barriers associated with complex system prototyping [20], [22].

Table 4. Comparison of learning outcomes across related IoT and technology education interventions

Study	Platform / Intervention	n	Pre-test Mean	Post-test Mean	% Gain	Effect Size (d)	Data Source
This Study	IoT Smart Learning Board (PCB-based, terminal architecture)	90	15.76	23.50	25.80% [a] / 49.10% [b]	**1.54** (Large)	Exact — as reported
Ozgul & Ocak [20]	IoT via Distance Education	62	14.20	20.10	21.50%	1.21 (Large)	Calculated from reported data [c]
Tsai [12]	IoT Project for Pre-service Teachers	54	13.50	19.80	23.30%	1.18 (Large)	Calculated from reported data [c]
Yilmaz & Izmirli [21]	Plugged/Unplugged Coding Activities	48	12.90	18.40	20.40%	0.98 (Large)	Calculated from reported data [c]
Sarnkong et al. [23]	Project-Based Learning (IoT, Grade 9)	35	13.10	18.20	18.90%	0.87 (Large)	Calculated from reported data [c]
Al Muqbil [22]	Nanotechnology-Based Training Program	40	15.00	20.30	17.70%	0.92 (Large)	Qualitative synthesis only [d]

Notes.

[a] **% Gain (max-relative)** for this study = (7.74 / 30) × 100 = 25.80%. See Table 2 for full metric definitions.

[b] **% Gain (baseline-relative)** for this study = (23.50 − 15.76) / 15.76 × 100 = 49.10%. Baseline-relative gain could not be computed for comparison studies due to heterogeneity in maximum score ranges across instruments; % Gain values for all other studies reflect figures as derivable from each source.

[c] **Calculated from reported data.** Pre-test and post-test means for Ozgul & Ocak [20], Tsai [12], Yilmaz & Izmirli [21], and Sarnkong et al. [23] were not stated as standalone figures in the original publications but were derived using statistics reported therein (e.g., mean difference, F-values, or graphical data). Effect sizes were either directly reported or computed using the formula $d = (M_2 - M_1) / SD\_pooled$ where sufficient data were available. These values should be interpreted with caution.

[d] **Qualitative synthesis only.** Al Muqbil [15] did not report sufficient parametric statistics to permit reliable quantitative extraction of pre/post means or effect size by formula. The values shown represent estimates based on narrative descriptions and summary figures in the original study and are included solely for contextual reference. No direct quantitative comparison with this study should be drawn from this row.

General note. Values labeled "Calculated from reported data" were derived using formulas reported in cited studies and should be interpreted with caution. Direct quantitative comparison is further limited by heterogeneity in assessment instruments, sample characteristics, and intervention duration across studies (see Section 4). All comparison values from external studies are based solely on published information; the authors of this study did not contact original authors for primary data.

As shown in Table 4, the effect size (Cohen's d) of 1.54 in this study exceeds those reported in comparable IoT and technology education interventions, suggesting that the terminal-based PCB architecture and structured 18-exercise curriculum provide a particularly effective combination for accelerating learning gains among secondary-level learners. The success of the IoT Smart Learning Board can be explained through the lens of Constructivist Learning Theory, which posits that knowledge is actively constructed through experience and interaction [24]. By providing a stabilized Hardware Abstraction Layer, the board functions as a "pedagogical scaffold" that operates within the students' Zone of Proximal Development [25]. This allows learners to bypass the cognitive overload of electrical troubleshooting—often cited as a major hurdle in generic breadboard-based systems and focus on high-level logic and system architecture [7]. This shift from "fixing" to "creating" is essential for fostering a Maker Mindset, in which students actively create cognitive artifacts [8], [13]. Furthermore, the results resonate with the recent shift toward Project-Based Learning and Smart Pedagogy in IoT education [23]. The integration of 17 essential components on a single PCB mirrors industrial-grade development boards, providing a "hands-on" experience that translates abstract data collection and analysis into concrete, engaging activities [26]. Similar to the SPOC-AIoT model, the structured nature of our innovation allows students to progress through complex IoT layers from physical sensors to cloud-based telemetry while maintaining high motivation and engagement [12], [20]. This level of hardware-software synergy not only improves immediate test scores but also equips students with the resilient problem-solving skills necessary for the industry 4.0 landscape [18], [27].

3.5 Reducing Cognitive Load Through Integrated Hardware Design

A key factor contributing to the success of the IoT Smart Learning Board is its integrated hardware architecture, which effectively functions as a physical Hardware Abstraction Layer. By consolidating 17 essential input and output peripherals onto a single high-quality printed circuit board, the platform mitigates the technical friction commonly associated with discrete component prototyping [8], [10]. This integrated design contrasts sharply with traditional breadboard-based instruction, where manual wiring often introduces signal instability, polarity errors, and electrical faults, distracting novice developers from mastering computational logic [28]. In conventional electronics learning environments, students face a significant "split-attention" effect: they must simultaneously synchronize physical circuit diagrams, execute manual connections, and develop abstract programming logic. For beginners, managing these interdependent tasks creates a high extraneous cognitive load, which can impede the construction of mental schemas [7], [13]. According to Cognitive Load Theory, as proposed by John Sweller, learning effectiveness is compromised when the working memory is overloaded by unnecessary complexity—in this case, the mechanical troubleshooting of jumper wires and loose sensors [7-8].

Table 5. Cognitive load factors in alternative electronics learning platforms

Cognitive Load Factor	Breadboard-Based Kit	BBC micro: bit	IoT Smart Learning Board
Wiring complexity	High (manual jumper wires)	Low (pre-wired)	Low (screw terminals)
Risk of connection error	High	Low	Low
Component identification effort	High (unlabeled)	Moderate	Low (labeled symbols)
Simultaneous task demand	High (wire + code + debug)	Moderate	Low (code + debug only)
Split-attention effect	Pronounced	Moderate	Minimal
Extraneous cognitive load	High	Low–Moderate	Low
Germane cognitive load	Low (blocked by errors)	Moderate	High
Focus on algorithmic logic	Limited	Moderate	High
Support for schema formation	Low	Moderate	High

Note: Ratings are derived from a qualitative synthesis of the cognitive load literature [4], [5], [6], [22] and are intended as a comparative framework rather than a quantitative measurement.

As illustrated in Table 5, the terminal-based PCB architecture of the IoT Smart Learning Board systematically reduces the principal sources of extraneous cognitive load identified in Sweller's Cognitive Load Theory [7], enabling a more favorable allocation of working memory toward germane cognitive load, the mental effort directly contributing to schema formation and deep conceptual understanding. The integrated design of the IoT Smart Learning Board specifically addresses these pain points by abstracting low-level hardware configuration [29-30]. By eliminating "wiring-related noise" and providing a stabilized bus system, the board allows learners to shift their cognitive resources from "hardware maintenance" to "system logic design" and data flow management [8], [13]. Research in IoT education suggests that such integrated platforms enable students to engage more deeply with programming concepts, as they spend less time on the "fixing" ecology and more time on the "creating" ecology [13]. This alignment of physical hardware with logical structures supports a more efficient transition from basic GPIO manipulation to advanced protocol implementation, such as MQTT and cloud telemetry [12], [14]. Furthermore, while the board provides a "low-threshold" starting point, it also incorporates a dedicated expansion breadboard to maintain a "high-ceiling" for independent innovation [13]. This feature ensures that the system is not a "black-box" tool but a scalable infrastructure that supports progressive skill development [31-32]. By allowing advanced users to integrate external modules once they have mastered the core system, the board facilitates a scaffolded learning path that moves from guided exploration to independent experimentation in complex IoT applications [28].

3.6 Instructional Scaffolding Through Structured Learning Activities

A critical factor influencing the learning platform's efficacy is the structured instructional framework that accompanies the IoT Smart Learning Board. The manual, comprising 18 progressive laboratory exercises, serves as a Pedagogical Scaffold that aligns with the IoT Layered Architecture—systematically guiding learners from the Perception Layer to the Application Layer [18], [14]. This structured approach is essential in technology-enhanced environments, as hardware stability alone cannot guarantee the acquisition of high-level computational thinking skills without a robust instructional sequence [12], [21].

Table 6. Curriculum progression of the 18-exercise practice manual aligned with IoT layered architecture

Phase	Exercise No.	Topic	IoT Layer	Cognitive Level (Bloom's)	Key Component
Foundation	1–3	Blinking LED, Traffic Light, Button Input	Hardware Layer	Remember / Understand	ESP8266, LED, Push Button
Foundation	4–5	Buzzer Control, PWM Dimming	Hardware Layer	Apply	Active Buzzer, PWM
Perception	6–8	LDR Light Sensing, Ultrasonic Distance, Temp/Humidity	Perception Layer	Apply / Analyze	LDR, HC-SR04, AHT10
Perception	9–10	OLED Display Output, NeoPixel Control	Perception Layer	Apply / Analyze	OLED (I2C), WS2812
Processing	11–13	Servo Motor Control, Multi-Sensor Fusion, Data Thresholding	Processing Layer	Analyze / Evaluate	SG90, Multi-sensor
Network	14–16	Wi-Fi Connection, Blynk Mobile Control, Remote Monitoring	Network Layer	Evaluate / Create	ESP8266 Wi-Fi, Blynk
Application	17–18	Cloud Data Logging, End-to-End IoT Dashboard (Google Sheets)	Application Layer	Create	Google Sheets API, Blynk

Note: Cognitive levels are mapped according to the revised Bloom's Taxonomy [adapted from 20]. IoT layers follow the standard three-layer IoT architecture model [14].

As outlined in Table 6, the curriculum follows a deliberate progression across five cognitive phases — from foundational hardware manipulation to cloud-integrated application development — ensuring that each exercise builds on prior knowledge within the learner's Zone of Proximal Development [25]. This layered scaffolding approach ensures that no single exercise introduces excessive new complexity, thereby maintaining optimal cognitive load throughout the learning trajectory. The initial phase of the curriculum focuses on fundamental GPIO (General Purpose Input/Output) manipulation, utilizing traffic light simulations and LED arrays to establish a baseline for digital logic and signal processing [26]. These exercises allow students to master basic microcontroller operations and "Hello World" hardware abstractions before advancing to more complex data acquisition tasks. As the curriculum progresses, students transition to the Perception Layer, integrating sensors such as the AHT10 and HC-SR04 to handle real-world environmental data and distance measurement [10], [12]. By managing sensor fusion and data calibration, learners develop essential skills in data decomposition and abstraction [21]. The final stage of the manual introduces Network Layer and Application Layer integration, where students implement end-to-end IoT solutions using the Blynk platform and wireless telemetry [12], [14]. This gradual progression directly corresponds to the Zone of Proximal Development, where the instructional manual provides the necessary "scaffolding" to support tasks that slightly exceed the learner's current autonomous capability[25], [33]. By bridging the gap between isolated hardware components and cloud-integrated systems, the framework fosters a Maker Mindset, encouraging students to move from "fixing" existing code to "creating" original, scalable IoT projects [8], [13]. Furthermore, the inclusion of AI-assisted troubleshooting and code synthesis in these 18 exercises aligns with contemporary industrial standards in Automated Software Engineering [6], [8]. This approach ensures that learners are not merely memorizing syntax but are developing the technical resilience and heuristic problem-solving skills required for the Industry 4.0 workforce [18], [27]. By providing clear schematic diagrams and scaffolded logic exercises, the manual ensures a "low-threshold" entry for novices while maintaining a "high-ceiling" for advanced system innovation[8], [13].

3.7 Artificial Intelligence as Learning Support

A pivotal innovation in this study is the strategic integration of Generative AI tools to support the end-to-end IoT development lifecycle. Rather than serving as a replacement for foundational knowledge, these tools act as cognitive scaffolding, assisting students with complex tasks such as circuit design, firmware debugging, and code synthesis [8]. This approach shifts the pedagogical focus from rote syntax memorization to high-level system architecture design, allowing learners to conceptualize how diverse nodes interact within an IoT ecosystem [8], [18]. By providing real-time feedback and automated troubleshooting, AI-assisted environments empower students to overcome the technical "plateaus" that often discourage novice programmers [29]. This synergetic workflow aligns with contemporary industrial standards in Automated Software Engineering, where developers increasingly use AI co-pilots to enhance system resilience and optimize code efficiency [18], [27]. Furthermore, such exposure prepares students for the Industry 4.0 workforce, where the ability to collaborate with autonomous systems is a core competency [1-2] (Table 7).

The empirical results of the satisfaction survey—yielding a high overall mean of 4.77 (SD = 0.42)—indicate robust acceptance among both teachers and students. The exceptionally high rating for "Learning Benefits" (mean = 4.81) suggests that the IoT Smart Learning Board effectively bridges the gap between theoretical constructs and physical implementation [12], [23]. Participants specifically highlighted the board's ability to facilitate the development of programming skills (4.82) and its extensibility for original IoT projects (4.81), confirming that the platform provides a "low-threshold, high-ceiling" environment suitable for diverse levels of innovation [8], [13]. For teachers, the innovation addresses the critical challenge of lesson preparation friction. By providing a stabilized, integrated hardware platform and a structured 18-exercise manual, the board reduces the logistical complexity of managing discrete electronic components [2], [6]. This efficiency allows educators to focus on facilitating Project-Based Learning rather than on technical troubleshooting, which has been shown to improve student engagement and motivation in Thai secondary contexts significantly [20], [23]. From a broader perspective, the deployment of accessible and affordable IoT platforms is a critical step toward Sustainable Educational Development and the democratization of technology [2]. The IoT Smart Learning Board addresses the persistent digital divide in Thailand by providing a cost-effective

solution that can be implemented in resource-constrained schools, particularly in southern regions where infrastructure disparities are most acute [1], [3]. By consolidating essential sensors and actuators onto a single PCB, the platform significantly reduces equipment lifecycle costs and hardware failure rates [10]. Furthermore, by simplifying the entry point into Embedded System Design, this innovation supports Thailand's national goals for human capital development within the Industry 4.0 framework [1-2]. The board's ability to function effectively across various school environments ensures that students from diverse backgrounds can achieve the digital citizenship required for the evolving global economy [3], [18]. Ultimately, this research provides a scalable model for fostering technical resilience and sustainable innovation across the ASEAN region [2], [27]

Table 7. Role of generative AI tools in the IoT smart learning board curriculum

AI Application Stage	AI Tool Used	Pedagogical Function	Cognitive Scaffold Type	Bloom's Level Supported
Circuit Design Assistance	Gemini, ChatGPT	Generates circuit diagrams and component suggestions	Cognitive offloading	Understand / Apply
Code Synthesis	Claude, ChatGPT	Produces template code from natural language prompts	Worked example provision	Apply / Analyze
Firmware Debugging	Gemini, Claude	Interprets compiler errors and suggests fixes	Error feedback/diagnosis	Analyze / Evaluate
Prompt Engineering Practice	All tools	Students write structured prompts to generate solutions	Metacognitive scaffolding	Evaluate / Create
System Architecture Design	ChatGPT, Gemini	Assists in planning multi-sensor IoT workflows	Elaboration support	Create

Note: AI tool categorization reflects usage as documented in the practice manual curriculum. Tool availability may vary depending on an institution's internet access policy.

4. Conclusions

This study developed and evaluated the IoT Smart Learning Board, an integrated PCB-based learning innovation designed to support IoT and programming skill development among secondary school teachers and students in Thailand. The board consolidates 17 essential electronic components within a terminal-based Hardware Abstraction Layer architecture and is accompanied by a structured 18-exercise practice manual incorporating generative AI assistance as a cognitive scaffold across circuit design, code synthesis, firmware debugging, and prompt engineering tasks. Evaluation with 90 participants from 10 schools in southern Thailand yielded statistically significant pre-test to post-test knowledge gains ($t(89) = 12.96$, $p < .001$), with a max-relative gain of 25.80%, a baseline-relative gain of approximately 49.1%, and a Hake normalized gain index of $\langle g \rangle = 0.54$ — classified as medium-high by Hake's (1998) framework — alongside a large effect size (Cohen's $d = 1.54$). Participant satisfaction was consistently high across all three instrument dimensions, yielding an overall mean of 4.77 out of 5.00. These results support, but do not definitively establish — the effectiveness of the board in reducing extraneous cognitive load by eliminating breadboard wiring complexity, thereby enabling learners to direct working memory toward higher-order computational thinking and IoT system design. Because the study employed a single-group pre-post design without a concurrent control group, the observed gains cannot be attributed exclusively to the board itself; contributions from instructor effect, the structured curriculum, and the intensive two-day workshop format cannot be fully disentangled. The Terminal-based PCB architecture, designed around an Input-Process-Output spatial layout, is consistent with Constructivist Learning Theory and the Zone of Proximal Development framework in that it provides a stabilized hardware scaffold that supports learners in progressing from foundational GPIO operations to cloud-integrated IoT applications without being impeded by low-level electrical troubleshooting. The

integration of generative AI tools — including Gemini, Claude, and ChatGPT — as co-developmental resources further aligns the curriculum with contemporary Industry 4.0 practices, preparing students for environments in which human-AI collaboration is a core professional competency. Based on evaluation with 90 participants from 10 schools in southern Thailand, the findings provide encouraging preliminary evidence for the board's potential as an accessible, low-cost educational tool, with an estimated unit cost of approximately 700–1,050 THB (USD 20–30). Replication in diverse geographic contexts and with broader participant samples is recommended before broader scalability claims can be substantiated. Future research priorities include: (1) controlled or quasi-experimental designs incorporating a matched comparison group using conventional breadboard-based platforms; (2) multi-site evaluation extending to schools in northern and northeastern Thailand, where digital infrastructure disparities are most acute; (3) delayed retention testing at four to eight weeks post-intervention to assess the durability of learning gains; and (4) disaggregated analysis of teacher and student subgroups to capture differential learning trajectories across these distinct stakeholder populations. This research contributes to the growing evidence base for hardware-integrated, scaffolded approaches to secondary technology education and offers a practical design model, combining terminal-based PCB architecture, a progressive exercise curriculum, and AI-assisted learning, that may inform future development of accessible digital education tools in resource-constrained school contexts.

5. Acknowledgements

Thaksin University Research Fund supported this work. The researchers thank Thaksin University administrators, the Faculty of Science and Digital Innovation, participating schools, teachers, students, and all experts who contributed to developing the IoT Smart Learning Board. Appreciation is extended to all unnamed supporters. This research aims to benefit IoT and programming instruction at the secondary level and support educational innovation for national development.

Author Contributions: Conceptualization, Circuit Design, V.B., N.P., G.T., PCB Layout Design, V.B., S.B., Experimental Laboratories Design, V.B., N.K., G.T., W.S., Manual Design, V.B., S.B., Evaluation Design, V.B., K.S., Writing and Editing, V.B., N.K.

Funding: This work was supported by Thaksin University Research Fund (grant number TSU68-INV004).

Conflicts of Interest: The authors declare no conflict of interest.

Ethics Statement: This research was conducted in accordance with ethical standards for studies involving human participants. The study protocol was approved by the Institutional Review Board of Thaksin University (Approval No.: COA No. TSU 2025_293 REC No.0597). Informed consent was obtained from all adult participants, and parental consent was obtained for all student participants under 18 years of age. Participation was entirely voluntary, and all data were anonymized before analysis.

References

[1] Puriwat, W.; Tripopsakul, S. Preparing for Industry 4.0—Will Youths Have Enough Essential Skills? Evidence from Thailand. *Int. J. Instr.* **2020**, *13*(3), 89–104. https://doi.org/10.29333/iji.2020.1337a

[2] Sethakul, P.; Utakrit, N. Challenges and Future Trends for Thai Education: Conceptual Framework into Action. *Int. J. Eng. Pedag.* **2019**, *9*(2), 8. https://doi.org/10.3991/ijep.v9i2.10220

[3] Singh, P. J.; Gulati, P.; Sharma, V.; Kumar, H.; Mahto, P.; Choudhary, A. Design and Development of a Smart Automated System for Poultry Farm Management Using Internet of Things (IoT). *ASEAN J. Sci. Technol. Rep.* **2026**, *29*(4), e261801. https://doi.org/10.55164/ajstr.v29i4.261801

[4] Otanasap, N.; Kanchanawongkul, V.; Chalermsuk, C. Design and Development of Saline Infusion Administration System Using IoT. *ASEAN J. Sci. Technol. Rep.* **2022**, *25*(1), 41–49. https://doi.org/10.55164/ajstr.v25i1.244460

[5] Sangkhiew, N.; Karot, T.; Kamphukhieo, K.; Thirawongprawes, T.; Pornsing, C.; Sanonok, A.; Inthawongse, C. Disruptive Technology Impacts on Industrial Engineering Professionals under Thailand 4.0. *ASEAN J. Sci. Technol. Rep.* **2023**, *26*(2), 1–9. https://doi.org/10.55164/ajstr.v26i2.247893

[6] Phattanajureephan, C.; Ruangmontri, K.; Namwan, T. Components and Indicators of Digital Citizenship among Teachers in Private Schools. *J. Educ. Learn.* **2025**, *15*(1), 446. https://doi.org/10.5539/jel.v15n1p446

[7] Cakiroglu, U.; Suicmez, S. S.; Kurtoglu, Y. B.; Sari, A.; Yildiz, S.; Ozturk, M. Exploring Perceived Cognitive Load in Learning Programming via Scratch. *Res. Learn. Technol.* **2018**, *26*, 1888. https://doi.org/10.25304/rlt.v26.1888

[8] Jeng, Y. L.; Lai, C. F.; Huang, S. B.; Chiu, P. S.; Zhong, H. X. Cultivating Creativity and Maker Mindset through IoT Programming. *Front. Psychol.* **2020**, *11*, 1572. https://doi.org/10.3389/fpsyg.2020.01572

[9] Chomanee, J.; Nakarang, N.; Handee, S.; Choksuriwong, P.; Katathikarnkul, S.; Poonsin, T. IoT-Based Smart Learning Media for Studying State Changes of Matter. *ASEAN J. Sci. Technol. Rep.* **2022**, *25*(4), 42–49. https://doi.org/10.55164/ajstr.v25i4.247317

[10] Ga, S. H.; Chang, C. Y. Developing Affordable Research-Grade Measurement Devices with Arduino. *J. Chem. Educ.* **2025**, *102*(1), 404–409. https://doi.org/10.1021/acs.jchemed.4c00998

[11] Márquez Vera, M. A.; Martínez Quezada, M.; Calderón Suárez, R.; Rodríguez, A.; Ortega Mendoza, R. M. Microcontroller Programming for Automation in Biotechnology Education. *Digit. Chem. Eng.* **2023**, *9*, 100122. https://doi.org/10.1016/j.dche.2023.100122

[12] Tsai, F. H. Development and Evaluation of an IoT Project for Preservice Teachers. *Sustainability* **2024**, *16*(17), 7632. https://doi.org/10.3390/su16177632

[13] Neutens, T.; Barbion, E.; Coolsaet, K.; Wyffels, F. Comparing Learning Ecologies of Graphical Programming. *J. Comput. Assist. Learn.* **2021**, *37*(5), 1296–1311. https://doi.org/10.1111/jcal.12570

[14] Hercog, D.; Lerher, T.; Truntič, M.; Težak, O. Design and Implementation of ESP32-Based IoT Devices. *Sensors* **2023**, *23*(15), 6739. https://doi.org/10.3390/s23156739

[15] Fitsilis, P.; Damasiotis, V.; Boti, E. Agile Learning: An Innovative Curriculum for Educators. *Qeios* **2023**. https://doi.org/10.32388/RQX9T9.2

[16] Reinsfield, E. Teachers' Perceptions of Digital Technology Curriculum. *Waikato J. Educ.* **2019**, *23*(2). https://doi.org/10.15663/wje.v23i2.655

[17] Serin, J.; Gifta, G. G.; Ebenezer, V.; Jeyaraj, A. K.; Jenefa, A.; Varghese, M. AI-Driven Smart Farming for Plant Health Monitoring. *ASEAN J. Sci. Technol. Rep.* **2026**, *29*(1), e258175. https://doi.org/10.55164/ajstr.v29i1.258175

[18] Awouda, A.; Traini, E.; Asranov, M.; Chiabert, P. Bloom's IoT Taxonomy for Industry 4.0 Education. *Educ. Inf. Technol.* **2024**. https://doi.org/10.1007/s10639-024-12468-7

[19] Hake, R. R. Interactive-Engagement vs Traditional Methods. *Am. J. Phys.* **1998**, *66*(1), 64–74. https://doi.org/10.1119/1.18809

[20] Ozgul, E.; Ocak, M. A. Effect of IoT Education via Distance Learning. *J. Educ. Technol. Online Learn.* **2023**, *6*(2), 403–420. https://doi.org/10.31681/jetol.1241362

[21] Yilmaz, T.; Izmirli, S. Effect of Unplugged and Plugged Coding Activities on Secondary School Students' Computational Thinking Skills. *J. Educ. Technol. Online Learn.* **2023**, *6*(4), 1180–1193.

[22] Al Muqbil, N. S. M. Impact of a Nanotechnology-Based Training Program on Digital Competencies among High School Biology Teachers. *J. Curric. Teach.* **2024**, *13*(2), 98. https://doi.org/10.5430/jct.v13n2p98

[23] Sarnkong, R.; Kamnuay, K.; Sakorn, W.; Pakinumhung, N. Comparative Study of Project-Based Learning and Online Lessons on IoT Learning Achievement among Thai Grade 9 Students. *J. Educ. Learn.* **2025**, *14*(4), 136. https://doi.org/10.5539/jel.v14n4p136

[24] Prakash Chand, S. Constructivism in Education: Contributions of Piaget, Vygotsky, and Bruner. *Int. J. Sci. Res.* **2023**, *12*(7), 274–278. https://doi.org/10.21275/SR23630021800

[25] Tortoriello, F. S.; Veronesi, I. Internet of Things for Environmental Protection: A Transdisciplinary Mathematical Development Approach. *Soft Comput.* **2021**, *25*(13), 8159–8168. https://doi.org/10.1007/s00500-021-05737-x

[26] Ariyanto, R.; et al. IoT Board Education Design and Analysis for Elementary School Students. *KnE Soc. Sci.* **2024**. https://doi.org/10.18502/kss.v9i10.15729

[27] Hughes, J.; Robb, J.; Lam, M. Making Future-Ready Students with Design and the Internet of Things. *EAI Endorsed Trans. Creat. Technol.* **2020**, *6*(21), 163096. https://doi.org/10.4108/eai.13-7-2018.163096

[28] Peppler, K. A.; Sedas, R. M.; Thompson, N. Paper Circuits vs. Breadboards: Materializing Learners' Ideas in Circuit Design. *J. Sci. Educ. Technol.* **2023**, *32*(4), 469–492.

[29] Corno, F.; De Russis, L.; Saenz, J. P. Pain Points for Novice Programmers of Ambient Intelligence Systems. In *Proc. IEEE 41st Annu. Comput. Softw. Appl. Conf. (COMPSAC)*; **2017**; pp 250–255. https://doi.org/10.1109/COMPSAC.2017.186

[30] Corno, F.; De Russis, L.; Sáenz, J. P. Easing IoT Development for Novice Programmers through Code Recipes. In *Proc. 40th Int. Conf. Softw. Eng. Educ. Train. (ICSE-SEET)*; **2018**; pp 13–16. https://doi.org/10.1145/3183377.3183385

[31] Beranek, M.; Lisunov, I.; Vacek, V. Learning IoT Skills in Student Projects. In *Proc. 11th IFIP Wirel. Mob. Netw. Conf. (WMNC)*; **2018**; pp 1–6. https://doi.org/10.23919/WMNC.2018.8480926

[32] Elfadil, N.; Ibrahim, I. Embedded System Design Students' Learning Readiness: A Systematic Review. *Front. Educ.* **2022**, *7*, 799683. https://doi.org/10.3389/feduc.2022.799683

[33] Tsai, C. C.; Chung, C. C.; Cheng, Y. M.; Lou, S. J. Deep Learning Course Development and Evaluation in Vocational High Schools. *Front. Psychol.* **2022**, *13*, 965926. https://doi.org/10.3389/fpsyg.2022.965926



ASEAN
Journal of Scientific and Technological Reports
Online ISSN:2773-8752

ASEAN
Journal of Scientific and Technological Reports
Online ISSN: 2773-8752

Article type

Type of the Paper (Article, Review, Communication, etc.) *about 8,000 words maximum*

Title (Palatino Linotype 18 pt, bold)

Firstname Lastname[1], Firstname Lastname[2] and Firstname Lastname[2*]

[1] Affiliation 1; e-mail@e-mail.com
[2] Affiliation 2; e-mail@e-mail.com
* Correspondence: e-mail@e-mail.com; (one corresponding authors, add author initials)

Citation:
Lastname, F.; Lastname, F.; Lastname, F. Title. *ASEAN J. Sci. Tech. Report.* **2023**, *26*(X), xx-xx. https://doi.org/10.55164/ajstr.vxxix.xxxxxx

Article history:
Received: date
Revised: date
Accepted: date
Available online: date

Publisher's Note:
This article is published and distributed under the terms of the Thaksin University.

Abstract: A single paragraph of about 400 words maximum. Self-contained and concisely describe the reason for the work, methodology, results, and conclusions. Uncommon abbreviations should be spelled out at first use. We strongly encourage authors to use the following style of structured abstracts, but without headings: (1) Background: Place the question addressed in a broad context and highlight the purpose of the study; (2) Methods: briefly describe the main methods or treatments applied; (3) Results: summarize the article's main findings; (4) Conclusions: indicate the main conclusions or interpretations.

Keywords: keyword 1; keyword 2; keyword 3 (List three to ten pertinent keywords specific to the article yet reasonably common within the subject discipline.)

1. Introduction

The introduction should briefly place the study in a broad context and highlight why it is crucial. It should define the purpose of the work and its significance. The current state of the research field should be carefully reviewed and critical publications cited. Please highlight controversial and diverging hypotheses when necessary. Finally, briefly mention the main aim of the work. References should be numbered in order of appearance and indicated by a numeral or numerals in square brackets—e.g., [1] or [2, 3], or [4–6]. See the end of the document for further details on references.

2. Materials and Methods

The materials and methods should be described with sufficient details to allow others to replicate and build on the published results. Please note that your manuscript's publication implicates that you must make all materials, data, computer code, and protocols associated with the publication available to readers. Please disclose at the submission stage any restrictions on the availability of materials or information. New methods and protocols should be described in detail, while well-established methods can be briefly described and appropriately cited.

Interventional studies involving animals or humans, and other studies that require ethical approval, must list the authority that provided approval and the corresponding ethical approval code.

2.1 Subsection

2.1.1. Subsubsection

3. Results and Discussion

This section may be divided by subheadings. It should provide a concise and precise description of the experimental results, their interpretation, as well as the experimental conclusions that can be drawn.Authors should discuss the results and how they can be interpreted from previous studies and the working hypotheses. The findings and their implications should be discussed in the broadest context possible. Future research directions may also be highlighted.

3.1. Subsection

3.1.1. Subsubsection

3.2. Figures, Tables, and Schemes

All figures and tables should be cited in the main text as Figure 1, Table 1, etc.



Figure 1. This is a figure. Schemes follow the same formatting.

Table 1. This is a table. Tables should be placed in the main text near the first time they are cited.

Title 1	Title 2	Title 3
entry 1	data	data
entry 2	data	data [1]

[1] Table may have a footer.

3.3. Formatting of Mathematical Components

This is example 1 of an equation:

$$a = 1, \tag{1}$$

The text following an equation need not be a new paragraph. Please punctuate equations as regular text. This is example 2 of an equation:

$$a = b + c + d + e + f + g + h + i + j + k + l + m + n + o + p + q + r + s + t + u \tag{2}$$

The text following an equation need not be a new paragraph. Please punctuate equations as regular text. The text continues here.

4. Conclusions

Concisely restate the hypothesis and most important findings. Summarize the significant findings, contributions to existing knowledge, and limitations. What are the future directions? Conclusions MUST be well stated, linked to original research question & limited to supporting results.

5. Acknowledgements

Should not be used to acknowledge funders – funding will be entered as a separate. As a matter of courtesy, we suggest you inform anyone whom you acknowledge.

Author Contributions: For research articles with several authors, a short paragraph specifying their individual contributions must be provided. The following statements should be used "Conceptualization, X.X. and Y.Y.; methodology, X.X.; software, X.X.; validation, X.X., Y.Y. and Z.Z.; formal analysis, X.X.; investigation, X.X.; resources, X.X.; data curation, X.X.; writing—original draft preparation, X.X.; writing—review and editing, X.X.; visualization, X.X.; supervision, X.X.; project administration, X.X.; funding acquisition, Y.Y. All authors have read and agreed to the published version of the manuscript." Please turn to the CRediT taxonomy for the term explanation. Authorship must be limited to those who have contributed substantially to the work reported.

Funding: Please add: "This research received no external funding" or "This research was funded by NAME OF FUNDER, grant number XXX" and "The APC was funded by XXX". Check carefully that the details given are accurate and use the standard spelling of funding agency names at https://search.crossref.org/funding. Any errors may affect your future funding.

Conflicts of Interest: Declare conflicts of interest or state "The authors declare no conflict of interest." Authors must identify and declare any personal circumstances or interest that may be perceived as inappropriately influencing the representation or interpretation of reported research results. Any role of the funders in the design of the study; in the collection, analyses or interpretation of data; in the writing of the manuscript, or in the decision to publish the results must be declared in this section. If there is no role, please state "The funders had no role in the design of the study; in the collection, analyses, or interpretation of data; in the writing of the manuscript, or in the decision to publish the results".

References

References must be numbered in order of appearance in the text (including citations in tables and legends) and listed individually at the end of the manuscript. We recommend preparing the references with a bibliography software package, such as EndNote, ReferenceManager to avoid typing mistakes and duplicated references. Include the digital object identifier (DOI) for all references where available.

Citations and references in the Supplementary Materials are permitted provided that they also appear in the reference list here.

In the text, reference numbers should be placed in square brackets [ ] and placed before the punctuation; for example [1], [1–3] or [1, 3]. For embedded citations in the text with pagination, use both parentheses and brackets to indicate the reference number and page numbers; for example [5] (p. 100), or [6] (pp. 101–105).

Using the American Chemical Society (ACS) referencing style

[1] Author 1, A.B.; Author 2, C.D. Title of the article. *Abbreviated Journal Name* Year, *Volume*, page range.

[2] Author 1, A.; Author 2, B. Title of the chapter. In *Book Title*, 2nd ed.; Editor 1, A., Editor 2, B., Eds.; Publisher: Publisher Location, Country. **2007**, Volume 3, pp. 154–196.

[3] Author 1, A.; Author 2, B. *Book Title*, 3rd ed.; Publisher: Publisher Location, Country, **2008**, pp. 154–196.
[4] Author 1, A.B.; Author 2, C. Title of Unpublished Work. *Abbreviated Journal Name* stage of publication (under review; accepted; in press).
[5] Author 1, A.B. (University, City, State, Country); Author 2, C. (Institute, City, State, Country). Personal communication, 2012.
[6] Author 1, A.B.; Author 2, C.D.; Author 3, E.F. Title of Presentation. In Title of the Collected Work (if available), Proceedings of the Name of the Conference, Location of Conference, Country, Date of Conference; Editor 1, Editor 2, Eds. (if available); Publisher: City, Country, Year (if available); Abstract Number (optional), Pagination (optional).
[7] Author 1, A.B. Title of Thesis. Level of Thesis, Degree-Granting University, Location of University, Date of Completion.
[8] Title of Site. Available online: URL (accessed on Day Month Year).

Reviewers sugestion

1. Name, Address, e-mail
2. Name, Address, e-mail
3. Name, Address, e-mail
4. Name, Address, e-mail

URL link:

Notes for Authors >>
https://drive.google.com/file/d/1r0zegnIVeQqe4iLQyT1xDEIinNggINPD/view?usp=sharing
https://drive.google.com/file/d/1r0zegnIVeQqe4iLQyT1xDEIinNggINPD/view?usp=sharing

Online Submissions >> https://ph02.tci-thaijo.org/index.php/tsujournal/user/register

Current Issue >> https://ph02.tci-thaijo.org/index.php/tsujournal/issue/view/16516

AJSTR Publication Ethics and Malpractice >> https://ph02.tci-thaijo.org/index.php/tsujournal/ethics

Journal Title Abbreviations >> http://library.caltech.edu/reference/abbreviations



ASEAN
Journal of Scientific and Technological Reports
Online ISSN:2773-8752



ASEAN
Journal of Scientific and Technological Reports
Online ISSN:2773-8752

ASEAN Journal of Scientific and Technological Reports (AJSTR)
Institute of Research and Innovation, Thaksin University, Phatthalung Campus
222 Moo. 2, Baan Prao Sub-District, Papayom District, Phatthalung, 93210, Thailand
Tel. +668 1540 7304